

Technical Report N° 209020-00049-0000-GE-TEN-0001
Canadian Standard NI 43 – 101

DEFINITIVE FEASIBILITY STUDY OF MSB BLANCO LITHIUM CARBONATE PROJECT

Atacama Region, Chile

PREPARED FOR



SANTIAGO, CHILE

PREPARED BY



WorleyParsons
resources & energy



EFFECTIVE: 17-JAN-2019

TABLE OF CONTENTS

LIST OF ABBREVIATIONS	XV
1. SUMMARY	20
1.1 TERMS OF REFERENCE	20
1.2 PROPERTY LOCATION AND DESCRIPTION.....	20
1.3 HISTORY OF OWNERSHIP	21
1.4 PHYSIOGRAPHY, CLIMATE, AND ACCESS	22
1.5 EXPLORATION AND DRILLING	22
1.6 GEOLOGY AND MINERALIZATION	24
1.7 STATUS OF EXPLORATION, DEVELOPMENT AND OPERATIONS	25
1.8 BRINE RESOURCE ESTIMATES	25
1.9 BRINE RESERVE ESTIMATES	27
1.10 EXPLORATION TARGET	29
1.11 LITHIUM RECOVERY PROCESS FOR THE BLANCO PROJECT.....	29
1.12 CAPITAL AND OPERATING COST ESTIMATE	30
1.13 ECONOMIC ANALYSIS	33
1.14 PROJECTION CONCLUSIONS AND RECOMMENDATIONS	35
2. INTRODUCTION	39
2.1 TERMS OF REFERENCE.....	39
2.2 SOURCES OF INFORMATION AND DATA	39
3. RELIANCE ON OTHER EXPERTS	41
4. PROPERTY DESCRIPTION AND LOCATION	42
4.1 PROPERTY DESCRIPTION AND LOCATION.....	42
4.2 TENURE.....	42
4.3 PERMITS.....	46
4.4 ROYALTIES	46
4.5 ENVIRONMENTAL LIABILITIES.....	46
4.6 OTHER SIGNIFICANT FACTORS AND RISKS.....	46
5. ACCESSIBILITY, CLIMATE, LOCAL RESOURCES, INFRASTRUCTURE AND PHYSIOGRAPHY	48
5.1 ACCESSIBILITY	48
5.2 PHYSIOGRAPHY	49
5.3 CLIMATE	49
5.4 LOCAL RESOURCES.....	61
5.5 INFRASTRUCTURE	61
6. HISTORY	62
6.1 CORFO (1980's)	62
6.2 PRIOR OWNERSHIP AND OWNERSHIP CHANGES	62
6.3 BRINE EXPLORATION WORK BY PREVIOUS OWNERS	63

7.	GEOLOGICAL SETTING AND MINERALIZATION	70
7.1	REGIONAL GEOLOGY	70
7.2	LOCAL GEOLOGY	75
7.3	MINERALIZATION	92
8.	DEPOSIT TYPE	96
8.1	GENERAL	96
8.2	HYDROGEOLOGY	97
8.3	WATER BALANCE	101
8.4	DRAINABLE POROSITY	101
8.5	PERMEABILITY	102
9.	EXPLORATION	104
9.1	OVERVIEW	104
9.2	GEOPHYSICAL SURVEYS	104
9.3	TEST TRENCHING (2011)	108
10.	DRILLING	112
10.1	OVERVIEW	112
10.2	EXPLORATORY DRILLING	112
10.3	MONITORING - AND PRODUCTION WELL DRILLING	115
10.4	PUMPING TESTS (2015 AND 2017)	118
11.	SAMPLE PREPARATION, ANALYSIS, AND SECURITY	131
11.1	SAMPLING METHODS	131
11.2	BRINE ANALYSIS AND QUALITY CONTROL RESULTS	136
11.3	DRAINABLE POROSITY ANALYSIS AND QUALITY CONTROL RESULTS	147
12.	DATA VERIFICATION	165
13.	MINERAL PROCESSING AND METALLURGICAL TESTING	166
13.1	BACKGROUND – LI3 / MLE 2011 EXPLORATION PROGRAM	166
13.2	EXPERIMENTAL PROCEDURE	166
13.3	RESULTS OF THE EVAPORATION TESTS	167
13.4	POSCO PROCESS TESTS – 2012/13	171
13.5	2016 AND 2018 EVAPORATION POND TESTS	171
13.6	2017 AND 2018 SALT REMOVAL AND LITHIUM CARBONATE TESTS	175
14.	BRINE RESOURCE ESTIMATES	179
14.1	OVERVIEW	179
14.2	RESOURCE MODEL DOMAIN AND AQUIFER GEOMETRY	179
14.3	SPECIFIC YIELD	179
14.4	BRINE CONCENTRATIONS	180
14.5	RESOURCE CATEGORY	181
14.6	RESOURCE MODEL METHODOLOGY AND CONSTRUCTION	182

14.7	METHODOLOGY	183
14.8	UNIVARIATE STATISTICAL DESCRIPTION	183
14.9	SPATIAL DESCRIPTION AND VARIOGRAPH.....	189
14.10	GRADE ESTIMATE.....	195
14.11	RESOURCE ESTIMATE	200
15.	MINERAL RESERVE ESTIMATES	202
15.1	MODEL CONSTRUCTION	202
15.2	CALIBRATION METHODOLOGY.....	224
15.3	CALIBRATION RESULTS	234
15.4	BRINE RESERVE ANALYSIS	253
16.	MINING METHOD – BRINE EXTRACTION	266
16.1	GENERAL DESCRIPTION.....	266
16.2	WELLFIELD LAYOUT.....	266
17.	RECOVERY METHODS	267
17.1	OVERVIEW	267
17.2	OPERATION OF THE SOLAR EVAPORATION PONDS	268
17.3	SALT REMOVAL PLANT	269
17.4	LITHIUM CARBONATE PLANT	270
17.5	REAGENTS FOR THE PROCESS	272
17.6	WATER PURIFICATION.....	273
17.7	EQUIPMENT CLEANING.....	273
17.8	LITHIUM CARBONATE PLANT SOLID WASTE MANAGEMENT.....	273
18.	PROJECT INFRASTRUCTURE	275
18.1	OBJECTIVE.....	275
18.2	PROJECT ACCESS	277
18.3	TEMPORARY INSTALLATIONS.....	278
18.4	PERMANENT INSTALLATIONS	278
18.5	MINING CAMP	281
18.6	SERVICES	282
18.7	ENGINEERING DELIVERABLES	283
19.	MARKET STUDIES AND CONTRACTS	285
19.1	CONSUMPTION	285
19.2	PROCESSING AND RESOURCES	293
19.3	PRODUCTION	295
19.4	PRICES	300
19.5	COSTS.....	308
20.	ENVIROMENTAL STUDIES, PERMITTING AND SOCIAL OR COMMUNITY IMPACT	313
20.1	ENVIRONMENTAL STUDIES.....	313
20.2	ENVIRONMENTAL BASELINE STUDY	313

20.3	WASTE AND TAILING DISPOSALS	324
20.4	EVALUATIONS OF IMPACTS IDENTIFIED IN THE EIA	324
20.5	VOLUNTARY COMMITMENTS SPECIFIED IN THE EIA	325
21.	CAPITAL AND OPERATING COST	328
21.1	CAPITAL COST ESTIMATE	328
21.2	OPERATING COST ESTIMATE	335
22.	ECONOMIC ANALYSIS	340
22.1	EVALUATION CRITERIA	340
22.2	INCOME TAX AND ROYALTIES	341
22.3	CAPITAL EXPENDITURES	344
22.4	LITHIUM CARBONATE PRODUCTION AND RAMP UP	344
22.5	OPERATING COSTS	345
22.6	PRODUCTION REVENUES	345
22.7	CASH FLOW PROJECTION	346
22.8	ECONOMIC EVALUATION RESULTS	348
23.	ADJACENT PROPERTIES	356
24.	OTHER RELEVANT DATA AND INFORMATION	357
24.1	EXPLORATION POTENTIAL	357
24.2	GEA MESSO BASIC ENGINEERING	360
24.3	ENGINEERING DELIVERABLES	361
24.4	PROJECT SCHEDULE	362
25.	INTERPRETATION AND CONCLUSIONS	365
25.1	HYDROGEOLOGY, RESOURCE AND RESERVE ESTIMATE	365
25.2	PERMITS	368
25.3	PROCESS AND ECONOMICS	368
26.	RECOMMENDATIONS	370
26.1	HYDROGEOLOGY AND RESOURCE ESTIMATE	370
26.2	NEXT PHASE	370
26.3	ENERGY EXPENSES AND COGENERATION	372
27.	REFERENCES	373
28.	SIGNATURES PAGE AND QUALIFIED PERSONS CERTIFICATES	378
29.	APPENDIX 1 (LEGAL OPINION)	385
30.	APPENDIX 2: CORFO ALBEMARLE ROYALTY AGREEMENT	388

LIST OF TABLES

Table 1-1:	Maximum, average and minimum elemental concentrations of the Blanco Project brine	25
Table 1-2:	Drainable porosity values applied in the resource model	26
Table 1-3:	Measured, Indicated and Inferred Lithium and Potassium Resources for the Blanco Project	27
Table 1-4:	Blanco Project resources expressed LCE and potash	27
Table 1-5:	Brine Mining Reserve for pumping to ponds	28
Table 1-6:	Brine Production Reserve for Lithium Carbonate production (assuming 58% lithium process recovery efficiency)	28
Table 1-7:	Capital Cost Estimates Summary by Area (US\$ 000)	31
Table 1-8:	Production Cost per tonne of product.....	32
Table 1-9:	Base Case Economic Results (100% equity basis).....	33
Table 1-10:	Leveraged Case Economic Results	33
Table 1-11:	Project Summary Cash Flow	34
Table 4-1:	MSB mining concessions	42
Table 5-1:	Average Monthly Temperature at the Marte Lobo Project (°C).....	49
Table 5-2:	DGA Meteorological stations with long-term precipitation records	51
Table 5-3:	Selected PUC-DGA weather stations with partial precipitation records.....	51
Table 5-4:	Monthly solar radiation data (W/m ²) for the Marte and Lobo Stations	56
Table 5-5:	Evaporation Rates used for the Basin Water Balance.....	59
Table 5-6:	Climate data collected at the MSB weather station in Salar de Maricunga (December 2016 – August 2018).....	60
Table 6-1:	Estimated mineral resources for the Litio 1-6 claims – April 9, 2012	64
Table 7-1:	Maximum, average and minimum elemental concentrations of the Blanco Project brine	93
Table 7-2:	Average values (g/l) of key components and ratios for the Maricunga brine	93
Table 7-3:	Comparative chemical composition of various salars (weight %).....	95
Table 8-1:	Water Balance for the Salar de Maricunga Basin.....	101
Table 8-2:	Results of drainable porosity analyses (2011-2018).....	102
Table 8-3:	Summary of permeability values	103
Table 9-1:	Results of Trench pumping tests	109
Table 10-1:	Summary of 2011 - 2018 boreholes	114
Table 10-2:	Wells P1, P2 and P4 pumping test layout	118
Table 10-3:	P-1 Pumping Test Results	122
Table 10-4:	P-2 Pumping Test Results	125

Table 10-5:	P-2 pumping test results (2017)	127
Table 10-6:	P-4 pumping test results (2017)	130
Table 11-1:	List of analyses requested from the University of Antofagasta and Alex Stewart Argentina SA Laboratories	136
Table 11-2:	Standards analysis results from U. Antofagasta (2011).....	139
Table 11-3:	Check assays (U. Antofagasta vs. Alex Stewart): RMA regression statistics.....	140
Table 11-4:	Check assays between the University of Antofagasta and Alex Stewart	141
Table 11-5:	Duplicate analyses from the University of Antofagasta.....	141
Table 11-6:	Standards analysis results from U. Antofagasta (2016-2018), Lithium.....	144
Table 11-7:	Check assays between the University of Antofagasta and Alex Stewart	145
Table 11-8:	Duplicate analyses from the University of Antofagasta.....	146
Table 11-9:	Comparison of lithium concentrations in centrifuge and bailed brine samples ...	147
Table 11-10:	Results of laboratory specific yield (S_y) analyses	150
Table 11-11:	GSA laboratory tests performed	153
Table 11-12:	Sample lithology and GSA classification	153
Table 11-13:	Summary of total porosity and specific yield by lithological group and laboratory	161
Table 11-14:	Comparison of S_y values between GSA and Corelabs	163
Table 11-15:	Comparison of Total Porosity between GSA and Corelabs	164
Table 13-1:	Chemical composition (% weight) of brines used in the test work.....	167
Table 13-2:	Brine compositions during evaporation of the untreated brine	168
Table 13-3:	Salts compositions during evaporation of the untreated brine.....	168
Table 13-4:	Crystalized Salts in the harvest	169
Table 13-5:	Brine composition during evaporation of the treated brine	170
Table 13-6:	Wet salt compositions during evaporation of the treated brine.....	171
Table 14-1:	Porosity values applied in the resource model	180
Table 14-2:	Summary of brine chemistry composition.....	180
Table 14-3:	Summary of univariate statistics of potassium and lithium	184
Table 14-4:	Test of normality of potassium and lithium.....	184
Table 14-5:	Parameter for the calculation of the experimental variograms	189
Table 14-6:	Measured and Indicated Lithium and Potassium Resources for the Blanco Project	200
Table 14-7:	Blanco Project resources expressed LCE and potash	200
Table 15-1:	Hydrogeologic units.....	215
Table 15-2:	Unsaturated parameters.....	217
Table 15-3:	Effective porosity for transport simulations.....	218

Table 15-4:	Water level observations	225
Table 15-5:	Water balance components.....	230
Table 15-6:	Steady State calibration parameters – transfer coefficients.....	230
Table 15-7:	Summary of pumping tests.....	233
Table 15-8:	Observation wells for pumping tests	233
Table 15-9:	Calibrated hydraulic conductivities.....	235
Table 15-10:	Calibrated transfer rate coefficients	236
Table 15-11:	Observed and simulated water levels	244
Table 15-12:	Simulated water balance from calibrated model	246
Table 15-13:	Calibrated specific storage	247
Table 15-14:	Maximum simulated and observed drawdown values, P-1 Pumping Test	248
Table 15-15:	Maximum simulated and observed drawdown values, P-2 Pumping Test	251
Table 15-16:	Maximum simulated and observed drawdown values, P-4 Pumping Test	252
Table 15-17:	Summary of production well construction details	256
Table 15-18:	Simulated Blanco Project brine pumping schedule.....	258
Table 15-19:	Brine Mining Reserve for pumping to ponds	264
Table 15-20:	Brine Production Reserve for Lithium Carbonate production (assuming 58% lithium process recovery efficiency)	264
Table 17-1:	Annual generation of salts from evaporation ponds	269
Table 17-2:	Reagents used for the process.....	272
Table 17-3:	Annual generation of solid discards.....	274
Table 18-1:	WorleyParsons Engineering Deliverables	284
Table 18-2:	GEA Engineering Deliverables	284
Table 19-1:	Top five manufacturers in selected Li-ion battery components, 2017	291
Table 19-2:	Average annual contract and spot price forecast trend for lithium carbonate, 2017-2032 (US\$/t CIF)	306
Table 20-1:	Endangered Species	321
Table 20-2:	Significant Environmental Impacts	324
Table 20-3:	Mitigation and Compensation Plan.....	325
Table 20-4:	Voluntary Commitments	325
Table 21-1:	Total Capital Expenditure	329
Table 21-2:	Brine production wellfields and pipeline delivery system Cost Estimate	330
Table 21-3:	Evaporation Ponds Cost Estimate.....	331
Table 21-4:	Salt Removal Plant Cost Estimate.....	331
Table 21-5:	Lithium Carbonate Plant Cost Estimate.....	332
Table 21-6:	General Services Cost Estimate.....	333

Table 21-7: Infrastructure and Equipment Cost Estimate	333
Table 21-8: Operation Cost	335
Table 21-9: Ponds and Plants Reagents Costs	336
Table 21-10: Energy	337
Table 21-11: Maintenance Cost	337
Table 21-12: Salt Harvest and Transport Cost	338
Table 21-13: Manpower, Catering and Camp Services Cost	338
Table 21-14: Product Transportation Costs	339
Table 21-15: General & Administration	339
Table 22-1: CORFO Albemarle Royalty Agreement Summary	343
Table 22-2: Capex Schedule	344
Table 22-3: Production Capacity	344
Table 22-4: Production Ramp Up %	345
Table 22-5: Production Ramp Up Tonnes	345
Table 22-6: Production Revenues	345
Table 22-7: Project Summary Cash Flow Projection	347
Table 22-8: Base Case Economic Results	348
Table 22-9: Loan Disbursement and Repayment	350
Table 22-10: Economic Results	351
Table 22-11: Driver Variable, Sensitivity Analysis	351
Table 22-12: Project Before Taxes – NPV 8% Sensitivity Medium Scenario	351
Table 22-13: Project Before Taxes – IRR Sensitivity Medium Scenario	352
Table 22-14: Project After Taxes – NPV 8% Sensitivity Medium Scenario	353
Table 22-15: Project After Taxes – IRR Sensitivity Medium Scenario	353
Table 22-16: Sensitivity to Royalty Rate	354
Table 24-1: Blanco Project exploration target estimate	359
Table 24-2: Maximum Impurities in Li_2CO_3	361
Table 24-3: WorleyParsons Engineering Deliverables	362
Table 24-4: GEA Engineering Deliverables	362
Table 24-5: Summary for Blanco Project execution schedule	363
Table 24-6: Major Projects Milestones	364
Table 25-1: Summary of the average Blanco Project brine composition (g/l)	365
Table 25-2: Measured and Indicated Lithium and Potassium Resources of the Blanco Project	366
Table 25-3: Blanco Project resources expressed LCE and potash	366

Table 25-4:	Brine Production Reserve for Lithium Carbonate production (assuming 58% lithium process recovery efficiency)	367
Table 26-1:	Estimated costs for the deep exploration program	370
Table 30-1:	CORFO Albemarle Royalty Agreement	388

LIST OF FIGURES

Figure 1-1:	General Process Diagram	30
Figure 4-1:	Location map of the Blanco Project	44
Figure 4-2:	Location map of the MSB mining concessions	45
Figure 5-1:	Project Access	48
Figure 5-2:	Isotherm map for Salar de Maricunga	50
Figure 5-3:	Precipitation Data for the Maricunga Weather Station (PUC-DGA) for 2007/2008	52
Figure 5-4:	Precipitation Data for the Pedernales Sur Weather Station (PUC-DGA) for 2007/2008	52
Figure 5-5:	Precipitation Data from the Marte and Lobo Stations for 2009/2010	53
Figure 5-6:	Isohyet Map for Salar de Maricunga	54
Figure 5-7:	Weather Station at Maricunga Project	55
Figure 5-8:	Solar Radiation Distribution in Chile	57
Figure 5-9:	Average Hourly Solar Radiation Intensity at the Marte and Lobo Stations for 2009/2010	58
Figure 5-10:	Elevation versus Average Annual Pan Evaporation	58
Figure 5-11:	Monthly Distribution of Average Annual Pan Evaporation (% of total)	61
Figure 6-1:	Location map of wells installed by Compañía Mantos de Oro and Chevron 1988/1990	67
Figure 6-2:	Lithological logs of Compañía Mantos de Oro wells SP-2, SR-3 and SR-6	68
Figure 6-3:	Lithological Logs of Compañía Mantos De Oro Wells SR-1, SR-2, SR-4, SP-4 and Chevron Well Can-6	69
Figure 7-1:	Morphotectonic units of the Andean Cordillera in northern Chile	70
Figure 7-2:	Regional geology of the Maricunga Basin	71
Figure 7-3:	W-E Section showing the Maricunga geological model, looking north	75
Figure 7-4:	Photo of the Upper Halite	76
Figure 7-5:	N-S Section showing the distribution of the Upper Halite unit	77
Figure 7-6:	Isopach map on the Upper Halite	78
Figure 7-7:	N-S section showing the Clay Core, looking west	79

Figure 7-8:	Isopach map on the Clay Core	80
Figure 7-9:	Photo of the Clay Core unit	81
Figure 7-10:	Section between boreholes S-18 and C-2 showing the distribution of the Deep Halite	82
Figure 7-11:	Distribution of the East Alluvium	83
Figure 7-12:	Distribution of the NW Alluvium	85
Figure 7-13:	The NW Alluvium	86
Figure 7-14:	E-W section with the spatial distribution of the Lower Alluvium	86
Figure 7-15:	Drill core and cuttings of the Lower Alluvium	87
Figure 7-16:	Drill core of the Volcaniclastic material	87
Figure 7-17:	W-E section showing the spatial distribution of the Volcaniclastics	88
Figure 7-18:	Isopach map on the Volcaniclastics Unit	89
Figure 7-19:	Isopach map of the Lower Sand	91
Figure 7-20:	Drill cuttings of the Lower Sand (Borehole S-5)	92
Figure 7-21:	Comparison of brines from various salars in Janecke Projection	94
Figure 8-1:	Conceptual model for mature and immature salars showing the distribution of the facies and the main hydrogeological components	96
Figure 8-2:	W-E Hydrogeological cross section	99
Figure 8-3:	Salar de Maricunga hydrographic basin	100
Figure 9-1:	Location map of seismic refraction tomography, AMT and gravity profiles	106
Figure 9-2:	Seismic Tomography Line 1	107
Figure 9-3:	Test Trench T6 in the Upper Halite	109
Figure 9-4a – 9.4e:	Pumping test analyses for Trench pumping tests T1, T2, T3, T5 and T6	109
Figure 10-1:	Location map of the boreholes (2011 - 2018 programs)	113
Figure 10-2:	Collecting RC Airlift Flow Measurements (2011)	117
Figure 10-3:	Installation of surface casing in well P-1 (2011)	117
Figure 10-4:	Layout of pumping test P-1 and P-2	119
Figure 10-5:	Pumping test P-1 layout	120
Figure 10-6:	V-notch tank during P-1 constant rate test	120
Figure 10-7:	Water level responses P-1 constant rate test	121
Figure 10-8:	P-1 pumping test interpretation	122
Figure 10-9:	Pumping Test P-2 Layout	123
Figure 10-10:	Water level responses P-2 constant rate test	124
Figure 10-11:	P-2 pumping test interpretation	125
Figure 10-12:	Li and K concentrations during the P-1 and P-2 pumping tests	126
Figure 10-13:	Water level responses P-2 constant rate test (2017)	127

Figure 10-14: Pumping test P-4 layout	129
Figure 10-15: Water level responses P-4 constant rate test (2017).....	130
Figure 10-16: P-4 pumping test interpretation	130
Figure 11-1: Collection of field parameters of the brine samples at the wellhead.....	132
Figure 11-2: Porosity and brine samples	133
Figure 11-3: RC drill chip samples.....	133
Figure 11-4: Fluorescein tracer dye in the rotary drilling fluid	135
Figure 11-5: Comparison of lithium concentrations in centrifuge and bailed brine samples ...	147
Figure 11-6: DBSA laboratory specific yield (S_y) analyses against total porosity.....	150
Figure 11-7: Comparison of BGS and DBSA specific yield (S_y) analyses.....	151
Figure 11-8: Comparison of BGS and DBSA total porosity (P_t) analyses	152
Figure 11-9: Rejected core samples.....	154
Figure 11-10: Relative Solution Release Capacity (RSRC) HQ core sample testing	156
Figure 11-11: GSA specific yield vs GSA total porosity	158
Figure 11-12: Lithologically classified P_t and S_y distributions and statistics	159
Figure 11-13: Comparison of total porosity estimated by GSA using RSRC method and Core laboratory using the Centrifuge method	161
Figure 11-14: Comparison of specific yield estimated by GSA using RSRC method and Core laboratory using the Centrifuge method	162
Figure 11-15: Comparison of S_y values between GSA and Corelabs	163
Figure 11-16: Comparison of Total Porosity between GSA and Corelabs	164
Figure 13-1: General view of evaporation chambers	167
Figure 13-2: Evaporation curves plotted versus % Li in the brine.....	170
Figure 13-3: MSB evaporation ponds	172
Figure 13-4: MSB harvesting of salts.....	173
Figure 13-5: Evaporation curves plotted versus % Li of pilot ponds compared with test work realized in University of Antofagasta 2011 (UA)	174
Figure 13-6: Evaporation curves plotted versus % Li of pilot ponds compared with testwork realized at University of Antofagasta 2011 (UA)	175
Figure 13-7: Evaporation and cooling curves plotted in a Janecke projection of testwork realized at University of Antofagasta 2011 (UA)	178
Figure 14-1: Normal plots of the concentration of potassium and lithium	185
Figure 14-2: Histograms of the potassium and lithium and the best fitted normal distribution	186
Figure 14-3: Box plot of the specific yield	187
Figure 14-4: Scatter plot of the concentration of lithium versus potassium.....	188
Figure 14-5: Experimental semi-variograms of lithium in xy directions with theoretical model	190

Figure 14-6: Experimental semi-variogram of lithium in z-direction fitted with a theoretical model.....	190
Figure 14-7: Experimental semi-variograms of potassium in xy directions with theoretical model	191
Figure 14-8: Experimental semi-variogram of potassium in the z-direction with theoretical model.....	191
Figure 14-9: Lithium concentration distribution	193
Figure 14-10: Potassium concentration distribution	194
Figure 14-11: Boron concentration distribution	195
Figure 14-12: N-S section through the resource model showing the lithium grade distribution	196
Figure 14-13: W-E section through the resource model showing the lithium grade distribution	197
Figure 14-14: NW-SE section through the resource model showing the lithium grade distribution	198
Figure 14-15: Distribution of resource classification areas	199
Figure 15-1: Numerical model domain for brine reserve analysis.....	204
Figure 15-2: Schematic of “Smart-Layering” (left: standard rectangular mesh; right: optimized mesh to better represent 3D geology)	205
Figure 15-3: 3D view of reserve model mesh and typical Section A-A'	206
Figure 15-4: Reserve model boundary conditions for groundwater flow	207
Figure 15-5: Indirect, lateral recharge to Salar de Maricunga from surrounding catchments	208
Figure 15-6: Evapotranspiration and diffuse groundwater discharge zones	211
Figure 15-7: Pumping wells in reserve model domain.....	212
Figure 15-8: Surface hydrogeological units	214
Figure 15-9: Lithium concentration	219
Figure 15-10: Conceptualization of density-dependent flow processes at the Salar Blanco Project	221
Figure 15-11: Salar Blanco numerical reserve modeling approach	222
Figure 15-12: Implications of ignoring density-dependent flow effects.....	223
Figure 15-13: Monitoring wells in the Project area	229
Figure 15-14: Pumping test Locations	232
Figure 15-15: Calibrated evapotranspiration rates.....	237
Figure 15-16: Calibrated diffuse seepage rates	238
Figure 15-17: Simulated Steady State water table.....	240
Figure 15-18: Calibration residual map.....	241
Figure 15-19: Observed vs. simulated water levels – entire model domain.....	242
Figure 15-20: Observed vs. simulated water levels – reserve area	243

Figure 15-21: Simulated and observed drawdowns, P-1 Pumping Test	248
Figure 15-22: Simulated and Observed Drawdowns, P-2 Pumping Test	250
Figure 15-23: Simulated and observed drawdowns, P-4 Pumping Test	252
Figure 15-24: Brine production wellfield layout	255
Figure 15-25: Brine wellfield pumping rates.....	260
Figure 15-26: LCE contained in the brine wellfield production	261
Figure 15-27: Average lithium concentration of wellfield production.....	262
Figure 15-28: Predicted drawdown after 20 years of operation.....	263
Figure 17-1: General Process Diagram	267
Figure 17-2: Process Block Diagram	268
Figure 17-3: Simplified Salt Removal Plant Process Diagram	270
Figure 17-4: Simplified Lithium Carbonate Plant Process Diagram (1/2).....	271
Figure 17-5: Simplified Lithium Carbonate Plant Process Diagram (2/2).....	272
Figure 18-1: Location of Salar de Maricunga.....	275
Figure 18-2: Project location (magenta) showing the areas destined to the evaporation ponds and installation	276
Figure 18-3: Project Access.....	277
Figure 18-4: Transmission Line Route.....	282
Figure 19-1: The rise of rechargeable batteries in lithium consumption, 2000-2018f (000t LCE)	286
Figure 19-2: Consumption of lithium by country/region, 2002-2017 (000t LCE)	288
Figure 19-3: Li-ion battery consumption by end-use application, 2000-2017 (GWh).....	291
Figure 19-4: Simplified lithium-ion battery supply chain.....	291
Figure 19-5: Simplified overview of mine-to-product flow	294
Figure 19-6: Global lithium reserves and resources by country, 2018	295
Figure 19-7: Mine production of lithium by source type, 2000-2018p (000t LCE).....	296
Figure 19-8: World: Refined production of lithium by type, 2000-2018p (000t LCE).....	297
Figure 19-9: Mined and refined lithium output by producer, 2017 (%)	298
Figure 19-10: Forecast production and consumption, 2012-2032 (000t LCE).....	300
Figure 19-11: Average yearly contract and spot prices for lithium carbonate, 2000-2018 (US\$/t CIF)	302
Figure 19-12: Lithium cost curve progression, 2017-2027.....	303
Figure 19-13: Lithium price movement schematic	304
Figure 19-14: Forecast average yearly contract and spot price trend for lithium carbonate, 2017- 2032 (US\$/t CIF)	305
Figure 19-15: Cash cost breakdown for refined lithium production, 2017.....	309

Figure 19-16: Lithium carbonate cash cost curve, excluding royalties, 2027 (US\$/t)	310
Figure 19-17: Lithium carbonate cash cost curve, including royalties, 2027 (US\$/t)	311
Figure 19-18: Lithium carbonate production cost in Chile, including royalties, 2027 (US\$/t)	312
Figure 20-1: Weather and Air Quality Monitoring Station – MSB	314
Figure 20-2: Measurement Locations for Noise and Vibration for Humans	315
Figure 20-3: Measurement Locations for Noise and Vibration for Fauna	316
Figure 20-4: W-E Hydrogeological Cross-Section	317
Figure 20-5: Water Balance for the Maricunga Watershed	318
Figure 20-6: Landscape Units UP1 and UP2.....	319
Figure 20-7: Endemic Vegetation on Shore of Maricunga Lake	321
Figure 20-8: Vulnerable Reptiles	322
Figure 20-9: Endangered Mammals	322
Figure 22-1: Yearly Cash Flow.....	349
Figure 22-2: Cumulative Cash Flow	349
Figure 22-3: Project Before Tax NPV 8% Sensitivity Medium Scenario.....	352
Figure 22-4: Project Before Tax IRR Sensitivity Medium Scenario	352
Figure 22-5: Project After Tax NPV 8% Sensitivity Medium Scenario.....	353
Figure 22-6: Project After Tax IRR Sensitivity Medium Scenario	354
Figure 24-1: Schematic of the deep lithium exploration target (200-400 m)	357
Figure 24-2: Outline of the exploration target	358
Figure 24-3: Comparison of the Blanco Project with other lithium projects.....	360

LIST OF ABBREVIATIONS

The metric (SI system) units of measure is used in this report unless otherwise noted.

All currency in this report is US dollars (US\$) unless otherwise noted.

List of abbreviations

°C	degree Celsius
°F	degree Fahrenheit
A	ampere
a	annum
AMT	Audio-frequency Magnetotellurics
B	Boron
bbl	barrels
BLY	Boart Longyear
BSc	Bachelor of Science
Btu	British thermal units
C	Clay
C\$	Canadian dollars
C+H	Clay and halite
Ca	Calcium
CaCO ₃	Calcium carbonate
cal	calorie
CAPEX	Capital Expenditures
CChEN	Chilean Nuclear Commission
CEOL	Special Lithium Operation Contracts (Contratos Especiales de Operación de Litio)
cfm	cubic feet per minute
CG	Clayey gravel
CHP\$	Chilean pesos
CEOL	Special Operating Contracts (Contratos Especiales de Operación del Litio)
CIM	Canadian Institute of Mining, Metallurgy and Petroleum
Cl	Chloride
cm	centimetre
CODELCO	National Chilean Copper Corporation (Corporación Nacional del Cobre de Chile)
CORFO	Production Promotion Corporation (Corporación de Fomento de la Producción)
CPG	Certified Professional Geologist
CS	Clayey sand
d	Day



DIA	Environmental Impact Declaration (Declaración de Impacto Ambiental)
día	diameter
dmt	dry metric tonne
dwt	dead-weight tonne
EIA	Environmental Impact Study (Estudio de Impacto Ambiental)
ENAMI	National Mining Company (Empresa Nacional de Minería)
EV	Electric Vehicle
ft	foot
ft/s	foot per second
g	gram
G	giga (billion)
g/cm ³	grams per cubic centimetre
g/l	gram per litre
g/m ³	grain per cubic metre
g/t	grams per tonne
Gal	Imperial gallon
gpm	Imperial gallons per minute
GSA	Geo Systems Analysis
H	Halite
H+C	Halite and clay
H ₂ SO ₄	Sulfuric acid
ha	hectare
HDP	high density polyethylene
hp	horsepower
h	hour
HVAC	Heating, ventilation, and air conditioning
ICE	Internal combustion engine
in	inch
in ²	square inch
J	joule
JORC	Joint Ore Reserves Committee
k	kilo (thousand)
K	Potassium
K	Hydraulic conductivity
K/Ar	Potassium argon ratio
kcal	kilocalorie
KCl	Potassium chloride
KCl×MgCl ₂ ×6H ₂ O	carnallite
kg	kilogram

km	kilometre
km/h	kilometre per hour
km ²	square kilometer
km ³	cubic kilometer
kPa	kilopascal
kt	kilo tonne
kV	kilovolt
kVA	kilovolt-amperes
kW	kilowatt
kWh	kilowatt-hour
l	litre
l/s	litres per second
La/Yb	Lanthanum Ytterbium ratio
LCE	Lithium Carbonate Equivalent
Li	Lithium
Li ₂ CO ₃	Lithium carbonate
LiOH	Lithium hydroxide
LiOH·H ₂ O	Lithium hydroxide monohydrate
um	micron
m	metre
m	month
M	mega (million)
m/d	metres per day
m ²	square metre
m ² /d	square metre per day
m ³	cubic metre
m ³ /h	cubic metres per hour
m ³ /yr	cubic metres per year
Ma	Mega annus
MAIG	Member of the Australian Institute of Geoscientists
masl	metres above sea level
MAusIMM	Member of the Australasian Institute of Mining & Metallurgy
mbar	millibar
mbgs	Metres below ground surface
mE	meters East
mg	microgram
Mg	Magnesium
mg/l	miligrams per litre
Mg/Li	Magnesium lithium ratio
min	minute
MJV	Maricunga Joint Venture - Salar Blanco Project
mm	millimetre

mN	meters North
mph	miles per hour
us	microseconds
MSB	Minera Salar Blanco S.A.
MSc	Master of Science
Mt	million tonnes
MVA	megavolt-amperes
MW	megawatt
MWh	megawatt-hour
Na	Sodium
Na ₂ O	Sodium oxide
Na ₂ CO ₃	Soda ash
NaCl	sodium chloride
NFPA	National Fire Protection Association
NMC	Nickel-Manganese-Cobalt
NN	nearest-neighbor
OK	Ordinary Kriging
OPEX	Operating Expenses
opt, oz/st	ounce per short tonne
oz	Troy ounce (31.1035 g)
Pgeo	Professional Geoscientist
ppm	part per million
PS	Sectorial Permits (Permisos Sectoriales)
psi	pounds-force per square inch
psia	pound per square inch absolute
psig	pound per square inch gauge
P _t	Porosity
PWL	Pumping water level
QA/QC	Quality Assurance/Quality Control
QP	Qualified Person
R&D	Research and Development
RC	Reverse circulation
RL	relative elevation
RPG	Registered Professional Geologist
RSRC	Relative Solution Release Capacity
s	Second
S	Storativity
S	Sand
SC	Sandy clay
SEA	Environmental Evaluation Service (Servicio de Evaluación Ambiental)

SG	Sandy gravel
SGeMS	Stanford Geostatistical Modeling Software
SiO ₂	Silicon dioxide
SO ₄	Sulfate
SQM	Chilean Mining and Chemical Society (Sociedad Química y Minera de Chile)
Sr	Strontium
st/d	short tonne per day
Ss	Specific Storage
SS	Silty Sand
st	short tonne
st/y	short tonne per year
SWL	Static water level
SX	Solvent extraction
Sy	Specific Yield
ton	metric tonne
T	Transmissivity
TD	Total depth
TDEM	Time-domain electromagnetic
TDS	Total Dissolved Solids
TEM	Transient Electromagnetic Method
t/y	metric tonne per year
t/d	metric tonne per day
TPY	tonnes per year
U	Ulexite
US\$	United States dollar
US\$/tonne	United States dollar per tonne
USg	United States gallon
USgpm	US gallon per minute
UTM	Universal Transverse Mercator
V	volt
V	Volcaniclastic
W	watt
W/m ²	Watt per square metre
WGS	World Geodetic System
wmt	wet metric tonne
WP	WorleyParsons
WWTP	Wastewater Treatment Plant
yd ³	cubic yard
y	year

1. SUMMARY

1.1 TERMS OF REFERENCE

This report was prepared by WorleyParsons (WP) and FloSolutions for Minera Salar Blanco S.A. ("Minera Salar Blanco or MSB") to provide a National Instrument 43-101 ("NI 43-101") compliant Definitive Feasibility Study ("DFS") of its Blanco Project located in Salar de Maricunga in the Atacama Region of northern Chile. This report provides an independent updated Mineral Resource estimate, a Mineral Reserve Estimate and a technical appraisal of the economic viability of the production of 20,000 TPY of lithium carbonate from the lithium contained on the property, under the guidelines of NI 43-101 and in conformity with its standards. The Report includes technical judgment of appropriate additional technical parameters to accommodate certain specific characteristics of minerals hosted in liquid brine as outlined in CIM Best Practice Guidelines for Resource and Reserve Estimation for Lithium Brines and as discussed by Houston (Houston et al, 2011).

All items related to geology, hydrogeology, mineral resources and reserves were prepared by FloSolutions. Peter Ehren was responsible for preparing all technical items related to brine chemistry and mineral processing. Capital and Operating expenditures mentioned in this report were estimated by WP, relying on quotations requested from equipment, chemicals and other suppliers, as well as from its project data base. WP relied extensively on Minera Salar Blanco and its consultants as cited in the text of the study and the references, for information on future prices of lithium carbonate, legislation and tax in Chile, as well as for general project data and information.

1.2 PROPERTY LOCATION AND DESCRIPTION

The Blanco Project is located 170 km northeast of Copiapó in the Atacama Region of northern Chile at an elevation of 3,750 masl. The property is more particularly described as being centered at approximately 492,000 mE, 7,025,000 mN (WGS 84 datum UTM Zone 19). The Project covers some 2,563 ha of mineralized ground in Salar de Maricunga; 100 ha just to the northeast of the Salar for camp and evaporation test facilities, and an additional 1,800 ha some 8 km north of the Salar for the future construction of evaporation ponds, process and plant facilities.

The mineralized area of the Blanco Project is comprised of the following mining concessions: Litio 1-6 (1,438 ha), Cocina 19-27 (450 ha), Salamina, Despreciada, and San Francisco (675 ha). The Cocina 19-27, San Francisco, Despreciada and Salamina concessions were constituted under the 1932 Chilean mining law and have "grand-fathered" rights for the production and sale of lithium products; unlike the Litio 1-6 concessions which were constituted under the 1983 Chilean mining law and require additional government permits for the production and sale of lithium.



1.3 HISTORY OF OWNERSHIP

SLM Litio, a Chilean corporation, acquired the Litio 1-6 mining claims in 2004.

On May, 2011, Li3 Energy Inc. (Li3 – now Bearing Lithium) through its 100 % owned Chilean subsidiary Minera Li Energy (MLE) acquired its original interest in the Salar de Maricunga through the purchase of a 60 % interest in SLM Litio 1 through 6 (which are the legal entities holding the Litio 1-6 concessions).

On November 5, 2013, Li3 announced an agreement with BBL SpA (now MSB SpA) for BBL to acquire 51 % (a controlling stake) of MLE in return for specified funding for the company.

On April 16, 2013, MLE acquired 100% of Cocina 19-27 mining concessions.

On August 25, 2014, BBL purchased directly another 36 % interest in SML Litio 1-6 held by another third party. The remaining 4% interest in the Litio 1-6 claims is still held by a third-party individual.

On December 30, 2014, BBL acquired the option to buy the San Francisco, Despreciada and Salamina concessions from a local group (the Padilla Family).

On September 2, 2015, BBL changed its name to Minera Salar Blanco SpA. During December 2015, Minera Salar Blanco SpA acquired directly the Blanco and Camp mining concessions.

In 2016 MSB SpA (former BBL SpA), MLE and, Lithium Power International Ltd. agreed to form a new company, Minera Salar Blanco S.A, (MSB) to continue the development of the Blanco Project. At the same time, MSB SpA and Li3, shareholders of MLE, agreed to dissolve MLE. As a result, the ownership structure of MSB ended up with; LPI 50 %, Minera Salar Blanco SpA 32.3 %, and Li3 17.7 %. Through this agreement MSB holds 96 % interest in the Litio 1-6 concessions and 100 % in the Cocina, San Francisco, Despreciada and Salamina, Camp and Blanco concessions.

On December 11, 2016, Bearing Lithium Corp. announced a binding agreement to acquire 100 % of the common shares of Li3, and as a result, assumed Li3's 17.7 % interest in the MSB during 2017.

During August 2018, Minera Salar Blanco SpA. sold 1.3534% of its shares. Both LPI and Bearing Lithium exercised its preferential rights resulting on LPI acquiring 1.00% and Bearing Lithium 0.3534 %. As a result, the current ownership structure of MSB is; LPI 51 %, Minera Salar Blanco SpA. 30.98 %, and Bearing Lithium 18.02 %.

1.4 PHYSIOGRAPHY, CLIMATE, AND ACCESS

The hydrographic basin of Salar de Maricunga covers 2,195 km² in the Altiplano of the Atacama Region. The average elevation of the basin is 4,295 masl while the maximum and minimum elevations are 6,749 masl and 3,738 masl, respectively. The Salar itself is located in the northern extent of the hydrographic basin and covers 142 km² (DGA 2009). The elevation of the salar nucleus is approximately 3,750 masl.

The principal surface water inflow into the lower part of basin occurs from Rio Lamas which originates in Macizo de Tres Cruces. Average flow in Rio Lamas (at El Salto) is measured at 250 l/s approximately. All flows from the Rio Lamas infiltrate into the Llano de Cienaga Redonda (DGA 2009). The second largest surface water inflow (20 l/s) to the lower part of the basin occurs from Quebrada Cienaga Redonda and also infiltrates into the Llano de Cienaga Redonda (DGA 2009).

Laguna Santa Rosa is located at the southwest extent of the basin valley floor and is fed by a combination of surface and groundwater flows coming from the south and west. Laguna Santa Rosa drains north via a narrow natural channel into the Salar itself. Additional groundwater discharge occurs along the path of this channel and surface water flow has been recorded at 200-500 l/s (Fiosolutions, 2018). Nevado Tres Cruces National Park is located in the southern part of the Maricunga watershed and includes Laguna Santa Rosa.

Access to Maricunga from the city of Diego de Almagro is via a well-maintained gravel surface highway; this will be the main access of the project. Occasional high snowfalls in the mountains may close the highways for brief periods during the winter.

The climate at the property is that of a dry, cold, high altitude desert, which receives irregular rainfall from storms between December and March and snowfall during the winter months of late May to September. The average annual temperature in Salar de Maricunga is estimated at 5 to 6 °C. Average annual precipitation is estimated at 150 mm and average annual potential evaporation is estimated between 2,100 mm and 2,400 mm.

1.5 EXPLORATION AND DRILLING

The following exploration and drilling works were carried out on the MSB concessions between 2011 and 2018:

1.5.1 Geophysics

- ◆ A seismic tomography survey was carried out by GEC along six profiles (S1 though S6) for a total of 23 line-km to help define basin lithology and geometry.
- ◆ An AMT / TEM geophysical survey was completed by Wellfield Services along 6 profiles across the Salar covering a total of 75 line-km. 383 AMT sounding were collected at 200 m to 250 m station spacing; 15 TDEM soundings were carried out

at the end and center of each AMT profile. The purpose of the AMT survey was to help map the basin geometry and the fresh water / brine interface.

- ◆ A regional gravity survey was carried out along six profiles (parallel to the AMT survey) for a total of 75-line km across the Salar. The station spacing along the profiles varied between 250 m and 500 m. The objective of the gravity survey was to help define the geometry of the bedrock contact in the Salar.

1.5.2 Exploration drilling

- ◆ Twelve sonic boreholes were drilled between 2011 and 2018 as follows: C-1 through C-6 to 150 m depth; S-1A, S-2, S-18, S-23, and S-24 to 200 m depths and S-20 to 40 m depth. Undisturbed samples were collected from the sonic core at 3 m intervals for drainable porosity analyses and other physical parameters. Brine samples were collected during the sonic drilling at 3 m to 6 m intervals for chemistry analyses. All sonic boreholes were completed as observation wells on completion of drilling.
- ◆ A total of 915 m of exploration RC drilling was carried out for the collection of chip samples for geologic logging, brine samples for chemistry analyses and airlift data to assess relative aquifer permeability. The RC boreholes were completed as observation wells for use during future pumping tests.
- ◆ Eight exploration boreholes (S-3, S-3A, S-5, S-6, S-10, S-11 (or M2), S-13, and S-19) for a total of 1,709 m were drilled using the tricone rotary method at 3-7/8 and 5-1/2 inch diameter; HW-size casing was lowered during the drilling to selected depths as required to provide adequate borehole stability and facilitate brine sampling. Drill cuttings were collected at 2 m intervals. Brine samples were collected at 6 m intervals. Six of the nine exploration holes were completed as piezometers through the installation of 2-inch diameter blank and screened PVC casing.
- ◆ Six boreholes (S-8, S-12, S-15, S-16, S-17, and S-21) for a total of 205 m were drilled as monitoring wells using the rotary method at 5-1/2 inch diameter. Drill cutting were collected at 2 m intervals; brine sampling took place at selected depth intervals. All six holes were completed with 2-inch diameter blank and screened PVC casing.

1.5.3 Test production and monitoring well installations

- ◆ Two test production wells (P-1 and P-2) were drilled at 17-1/2 inch diameters to a total depth of 150 m using the flooded reverse method. The wells were completed with 12 inch diameter blank and screened PVC casing in the Upper Halite brine unit and lower semi-confined brine aquifer.
- ◆ One production well (P-4) was drilled at 17-1/2 inch diameter to a depth of 180 m using the flooded reverse method. The well was completed with 12 inch diameter PVC blank and screened production casing. The screened interval of the well was completed in the lower semi-confined to confined aquifer, below and isolated from the Upper Halite unit.

1.5.4 Pumping tests

- ◆ Two long-term pumping tests were carried out on production wells P-1 (14 days) and P-2 (30 days) at 37 l/s and 38 l/s, respectively. Water level responses were measured in four monitoring wells adjacent to each production well.
- ◆ One 30-day pumping test was carried on production well P-4 at a pumping rate of 25 l/s. Water level measurements were made in adjacent monitoring wells P4-1 (lower aquifer completion), P4-2 (upper halite), P4-3 (upper halite) and P4-4 (upper halite).
- ◆ One 7-day pumping test was carried out in production well P-2 at a flow rate of 45 l/s with a packer was installed at 40 m depth so that brine inflow during the pumping test was limited to the upper halite aquifer. Water level measurements were made in four adjacent monitoring wells during the 7-day pumping test.
- ◆ Six test trenches adjacent to the sonic boreholes (C-1 through C-6) were completed to a depth of 3 m and 24-hour pumping tests were carried out in each trench.

1.5.5 Laboratory brine and drainable porosity analyses

- ◆ 651 brine sample analyses (not including QA/QC check samples) were carried by the University of Antofagasta and Alex Steward Assayers in Argentina for laboratory chemistry analysis.
- ◆ 488 undisturbed sample analyses on sonic core for drainable porosity and other physical parameters were carried out by Daniel B Stephens & Associates (DBSA), Geosystems Analysis (GSA), and the British Geological Survey and Corelabs (for QA/QC).

1.6 GEOLOGY AND MINERALIZATION

1.6.1 Geology

Based on the drilling campaigns carried out in the Salar between 2011 and 2018, ten major geological units were identified and correlated from the logging of drill cuttings and undisturbed core to a general depth of up to 200 m. One deep borehole (S-19) was drilled to a depth of 360 m. No borehole reached bedrock. Salar de Maricunga is a mixed style salar, with a halite nucleus of up to 34 m in thickness in the central northern part. The halite unit is underlain by a clay core on the eastern and central part of the Salar. The clay is locally interbedded with silt and silty sands. The Salar is surrounded by relative coarse grained alluvial and fluvial sediments. These fans demark the perimeter of the actual salar and at depth grade towards the center of the Salar where they form the distal facies with an increase in sand and silt. At depth two unconsolidated volcanoclastic units have been identified that appear quite similar. These two volcanoclastic are separated by a relatively thin and continuous sand unit which may be reworked material of the lower volcanoclastic unit.

1.6.2 Mineralization

The brines from Maricunga are solutions saturated or close to saturation in sodium chloride with an average concentration of total dissolved solids (TDS) of 311 g/l. The average brine density is 1.20 g/cm³. Other components present in the Maricunga brine are: K, Li, Mg, Ca, SO₄, HCO₃ and B. Elevated values of strontium (mean of 359 mg/l) also have been detected.

Table 1-1 shows a breakdown of the principal chemical constituents in the Maricunga brine including maximum, average, and minimum values, based on the brine samples that were collected from the exploration drilling programs between 2011 and 2018.

Table 1-1: Maximum, average and minimum elemental concentrations of the Blanco Project brine

Analyte	HCO ₃ mg/l as CaCO ₃	B mg/l	Ca mg/l	Cl mg/l	Li mg/l	Mg mg/l	K mg/l	Na mg/l	SO ₄ mg/l	Density g/cm ³
Maximum	2,730	1,992	36,950	230,902	3,375	21,800	20,640	104,800	2,960	1.31
Average	471	596	12,853	190,930	1,146	7,462	8,292	85,190	709	1.20
Minimum	76	234	4,000	89,441	460	2,763	2,940	37,750	259	1.10

1.7 STATUS OF EXPLORATION, DEVELOPMENT AND OPERATIONS

This NI 43-101 technical report presents the results of the DFS which was started in March 2018. MSB contracted Stantec to prepare an EIA for the Blanco Project which was completed and presented to the Chilean authorities in September 2018. It is expected that the EIA permitting will be successfully completed during the second semester of 2019 and that a Project construction decision can be made immediately thereafter during 2019.

1.8 BRINE RESOURCE ESTIMATES

The brine resource estimate was determined by defining the aquifer geometry, the drainable porosity or specific yield (Sy) of the hydrogeological units in the Salar, and the concentration of the elements of economic interest, mainly lithium and potassium. Brine resources were defined as the product of the first three parameters.

The model resource estimate is limited to the MSB mining concessions in Salar de Maricunga and covers an area of 2,563 ha.

The resource model domain is constrained by the following factors:

- ◆ The top of the model coincides with the brine level that was measured in the monitoring wells installed in the Salar.
- ◆ The lateral boundaries of the model domain are limited to the area of the MSB mining concessions.
- ◆ The bottom of the model domain coincides with a total depth of 200 m.

The specific yield values used to develop the resources are based on results of the logging and hydrogeological interpretation of chip samples and recovered core of 8 rotary boreholes and 12 sonic boreholes, results of drainable porosity analyses carried out on 488 undisturbed samples from sonic core by Geosystems Analysis, Daniel B Stephens and Associates, Corelabs, BGC, and four pumping tests. The boreholes within the measured and indicated resource areas are appropriately spaced at a borehole density of one bore per 1.5 km². Table 1-2 shows the drainable porosity values assigned to the different geological units for the resource model.

Table 1-2: Drainable porosity values applied in the resource model

Unit	Sy
Upper Halite	0.04
Clay Core	0.02
NW Alluvium	0.18
Lower Alluvium	0.05
Volcaniclastic	0.11
Lower Sand	0.06
Lower Volcaniclastic	0.11

The distributions of lithium and potassium concentrations in the model domain are based on a total of 651 brine analyses (not including QA/QC analyses) mentioned in Section 1.6.2 above.

The resource estimation for the Project was developed using the Stanford Geostatistical Modeling Software (SGeMS) and the geological model as a reliable representation of the local lithology. The authors were closely involved with the block model development; all results have been reviewed and checked at various stages and are believed to be valid and appropriate for these resource estimates. Table 1-3 shows the Measured and Indicated Resources of lithium and potassium for the Blanco Project.

Table 1-3: Measured, Indicated and Inferred Lithium and Potassium Resources for the Blanco Project

	Measured (M)		Indicated (I)		M+I	
	Li	K	Li	K	Li	K
Property Area (km ²)	18.88		6.43		25.31	
Aquifer volume (km ³)	3.05		1.94		5	
Specific yield (Sy)	0.04		0.11		0.07	
Brine volume (km ³)	0.13		0.21		0.35	
Mean grade (g/m ³)	48	349	128	923	79	572
Concentration (mg/L)	1,175	8,624	1,153	8,306	1,167	8,500
Resource (tonnes)	146,000	1,065,000	244,000	1,754,000	389,000	2,818,000

Notes to the resource estimate:

- CIM definitions (2014) were followed for Mineral Resources.
- The Qualified Person for this Mineral Resource estimate is Frits Reidel, CPG
- No cut-off values have been applied to the resource estimate.
- Numbers may not add due to rounding.
- The Measured and Indicated Resources are inclusive of those Mineral Resources modified to produce the Mineral Reserves described in Section 15.
- The effective date is December 24, 2018

Table 1-4 shows the total resources of the Blanco Project expressed as lithium carbonate equivalent (LCE) and potash (KCL).

Table 1-4: Blanco Project resources expressed LCE and potash

	Measured and Indicated	
	LCE	KCL
Tonnes	2,070,000	5,380,000

- Lithium is converted to lithium carbonate (Li₂CO₃) with a conversion factor of 5.32.
- Potassium is converted to potash with a conversion factor of 1.9
- Numbers may not add due to rounding

1.9 BRINE RESERVE ESTIMATES

A three-dimensional finite element groundwater flow and transport model (FEFLOW code) was constructed and successfully calibrated to steady state pre-mining conditions and to transient pumping test responses. The calibrated model was used to simulate brine production scenarios of 20,000 TPY of LCE from the MSB concessions over a 20-year project life for the DFS. Additionally, the model predicts that the proposed brine wellfield can

extract an average of 16.7 kTPY of LCE for an additional 3 years which are not considered in the DFS economic analysis. These model simulations form the bases for the Blanco Project Lithium Mineral Reserve Estimate.

The Reserve Estimate was prepared in accordance with the guidelines of National Instrument 43-101 and uses the best practices methods specific to brine resources. The lithium reserves are summarized in Table 1-5 and Table 1-6. The effective date for the estimate is January 15, 2019.

Table 1-5: Brine Mining Reserve for pumping to ponds

Concession area	Category	Year	Brine Vol	Ave Li conc	Li metal	LCE
			(Mm3)	(mg/l)	(tonnes)	(tonnes)
Old code	Proven	1-7	21	1,051	22,000	115,000
	Probable	1-18	42	1,068	45,000	241,000
Litio 1-6	Proven	7-14	14	1,184	17,000	88,000
	Probable	14-23	48	1,170	56,000	298,000
Total 20y production	All	1-20	117	1,115	130,000	692,000
Mining Reserve	All	1-23	125	1,117	139,000	742,000

Table 1-6: Brine Production Reserve for Lithium Carbonate production (assuming 58% lithium process recovery efficiency)

Concession area	Category	Year	Brine Vol	Ave Li conc	Li metal	LCE
			(Mm3)	(mg/l)	(tonnes)	(tonnes)
Old code	Proven	1-7	21	1,051	13,000	67,000
	Probable	1-18	42	1,068	26,000	140,000
Litio 1-6	Proven	7-14	14	1,184	10,000	51,000
	Probable	14-23	48	1,170	32,000	173,000
Total 20y production	All	1-20	117	1,115	75,000	401,000
Mining Reserve	All	1-23	125	1,117	81,000	430,000

Notes to the Reserve Estimate:

1. Blanco Project brine production initiates in Year 1 on the mining concessions constituted under old Chilean mining code and include the Cocina, San Francisco, Salamina, Despreciada concessions (the "Old Code concessions"). In Year 7 brine production switches to the Litio 1-6 concessions that were constituted under the 1983 ("new") Chilean mining code and require a special operating license (CEOL) from the Chilean government. It is the opinion of the author that there is a reasonable

expectation that MSB will have obtained a CEOL by 2020, in advance of any brine production from the Litio 1-6 concessions.

2. The EIA for the Blanco Project was submitted to the Chilean Environmental Review Agency (SEA) in September 2018; it is the opinion of the author that there is a reasonable expectation that the final environmental approvals for the construction and operation of the Project will be obtained during 2019.
3. The Blanco Project Reserve Estimate includes an optimized wellfield configuration and pumping schedule to comply with environmental constraints and water level decline restrictions on the northeast side of the Salar over the total 23-year simulated brine production.
4. The total Mineral Reserves contain approximately four (4) percent of Li mass that is derived from outside of the Blanco Project property boundaries.
5. Lithium is converted to lithium carbonate (Li_2CO_3) with a conversion factor of 5.32.
6. The effective date for the Reserve Estimate is January 15, 2019.
7. Numbers may not add to due rounding effects.
8. Approximately 36 percent of the Measured and Indicated Resource are converted to Proven and Probable Reserves as brine feed from the production wellfield to the evaporation ponds without accounting for the lithium process recovery efficiency. The overall conversion from M+I Resources to Total Reserves including lithium process recovery efficiency is approximately 21 percent.

1.10 EXPLORATION TARGET

Based on the results of borehole S-19, an exploration target of 1.0 to 2.5 Mt of lithium carbonate equivalent (LCE) and 2.9 to 6.6 Mt of potassium chloride (KCl) has been identified (below the current resource) between a depth of 200 m and 400 m. The exploration target provides significant potential for resource expansion.

1.11 LITHIUM RECOVERY PROCESS FOR THE BLANCO PROJECT

The facilities have been designed to obtain lithium carbonate (Li_2CO_3) at a rate of 20,000 TPY.

The brine obtained from the production wells in the Salar is pumped to evaporation ponds, where it is concentrated through evaporation and chemical saturation, and different salts, such as halite, sylvinites and carnallite precipitate. All salts that precipitates are periodically harvested from the ponds and stored in stock piles defined for such purpose.

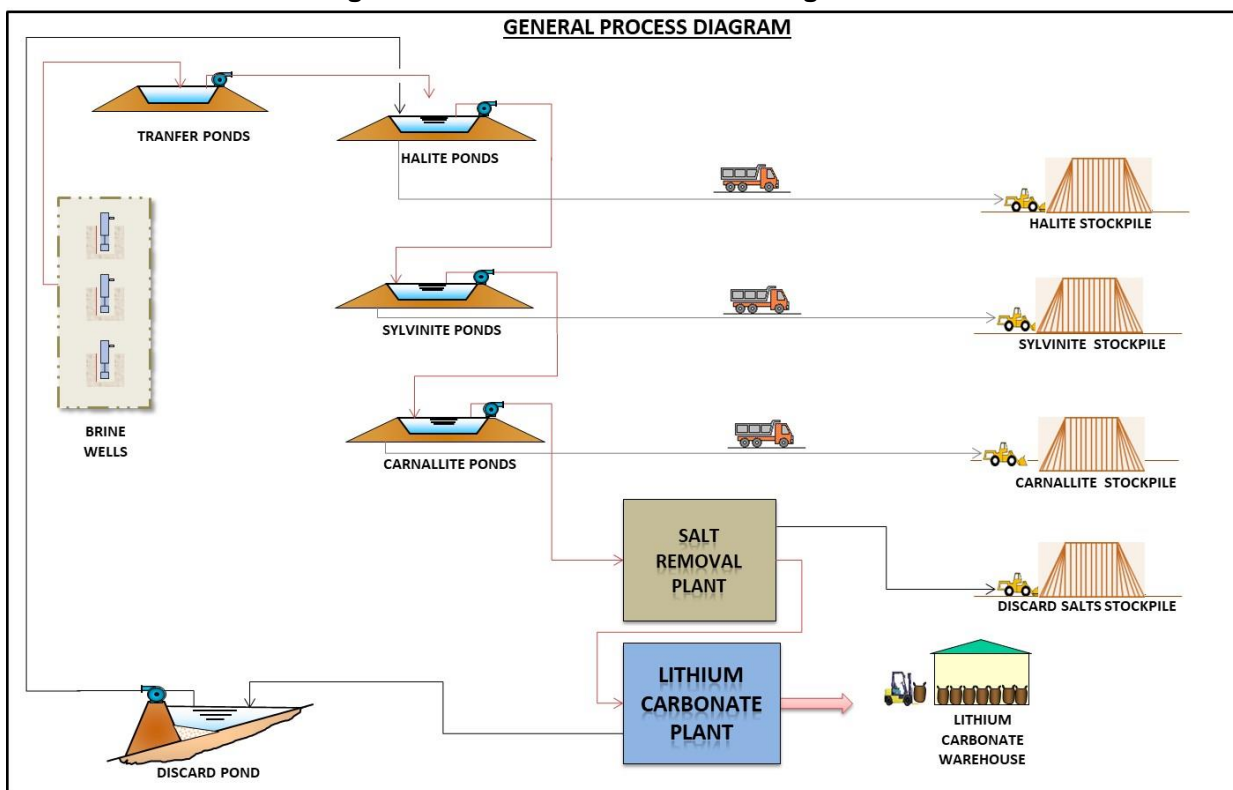
The concentrated lithium brine obtained from the evaporation ponds is pumped directly to reservoir ponds, which feed a Salt Removal Plant. This plant mainly removes Calcium impurities as calcium chloride and tachyhydrite from the brine. This is achieved through consecutive evaporation and crystallization steps. This process allows a higher concentration of the lithium in the brine.

The concentrated lithium brine obtained from the Salt Removal plant is subsequently fed to the lithium carbonate plant, where through processes of purification, solvent extraction, ionic exchange and filtration, impurities such as boron, calcium and magnesium are removed. The lithium concentrated brine is then fed to a carbonation stage, where through the addition of soda ash, lithium carbonate precipitates. This precipitated lithium carbonate is then fed to a centrifuge for water removal, and finally dried, reduced in size and packaged.

All impurities removed in the lithium carbonate plant are pumped directly to a discard pond, where through sedimentation, water is recovered and sent back to the evaporation ponds.

A simplified diagram of the process is presented on Figure 1-1 and a detailed description of the process is presented in Chapter 17.

Figure 1-1: General Process Diagram



1.12 CAPITAL AND OPERATING COST ESTIMATE

1.12.1 Capital Costs

Capital expenditures are based on an operating capacity of 20,000 TPY of lithium carbonate. Capital equipment costs have been determined based on over 150 quotes requested from

equipment manufacturers and construction companies. In house data was used for minor items. Considerable engineering progress has been achieved in the project. Given this, WorleyParsons expects the accuracy of this estimate to be within a +/- 15% range. Capital and operating costs estimates are expressed in fourth quarter 2018 US dollars.

The capital investment for the Blanco Project, including equipment, materials, indirect costs and contingencies during the construction period is estimated to be US\$ 563 million. Out of this total Direct Project Costs represent US\$ 456 million; Indirect Project Costs represent US\$ 45 million, and the Contingencies provision is US\$ 63 million. The former representing 8.0% of total project costs, while the latter is 11.1% of total project costs.

In addition, Sustaining Capital expenditures total US\$ 53 million over the 25-year evaluation period of the project, which includes a 3-year construction period and an operating life of 22 years. Working capital requirements over the project horizon averages US\$ 20 million.

Total capital expenditures are summarized on following Table 1-7.

Table 1-7: Capital Cost Estimates Summary by Area (US\$ 000)

Area	Total Project	Projected Budget 000 US\$
	Direct Costs	
1000	Brine Extraction Wells	39,374
2000	Evaporation Ponds	115,346
5000	Salt Removal Plant	66,438
6000	Lithium Carbonate Plant	71,622
8000	General Services	103,267
9000	Infrastructure	60,009
	Total Direct Cost	456,056
	Total Indirect Cost	44,831
	Contingencies (12,5%)	62,611
	Total	563,498

1.12.2 Operating Costs

An operating cost estimate for 20,000 TPY Li_2CO_3 facilities has been prepared. This estimate is based upon process definition, laboratory work, tests at equipment suppliers and reagents consumption rates all provided or determined by MSB. Vendor quotations have been used for reagents costs. Expenses estimates, as well as manpower levels are based on WP experience and information delivered by MSB.

Table 1-8: Production Cost per tonne of product

Description - Operation Costs	US\$ / Tonne Li ₂ CO ₃	Total 000 US\$
DIRECT COSTS		
Chemical Reactives and Reagents	1,040	20,799
Salt Removal	486	9,727
Energy	1,028	20,552
<i>Memo: - Electrical</i>	<i>370</i>	<i>7,398</i>
<i>- Thermal</i>	<i>658</i>	<i>13,154</i>
Manpower	458	9,160
Catering & Camp Services	105	2,100
Maintenance	295	5,899
Transport	237	4,740
DIRECT COSTS SUBTOTAL	3,649	72,977
INDIRECT COSTS		
General & Administration - Local	123	2,702
INDIRECT COSTS SUBTOTAL	123	2,702
TOTAL PRODUCTION COSTS	3,772	75,679

As indicated in Table 1-8, chemical reagents are the major operating cost of the project, closely followed by energy costs, of which fuel consumed by the Salt Removal Plant is the major component. Over 90% of the chemical costs correspond to soda ash costs, of which over 46,000 tonnes are required to produce 20,000 tonnes of Li₂CO₃. Other important expense items are salt harvesting or removal and manpower.

1.13 ECONOMIC ANALYSIS

Summary Base Case Project's economic results are presented on the following table:

Table 1-9: Base Case Economic Results (100% equity basis)

ECONOMIC RESULTS		BEFORE TAXES	AFTER TAXES
NPV 6%	MM US\$	1,738	1,248
NPV 8%	MM US\$	1,286	908
NPV 10%	MM US\$	949	653
IRR		23.8%	21.0%
PAYOUT		4 y, 1 m	4 y, 2 m

**Table 1-10: Leveraged Case Economic Results
(50/50 debt to equity project funding)**

ECONOMIC RESULTS		BEFORE TAXES	AFTER TAXES
NPV 6%	MM US\$	1,726	1,256
NPV 8%	MM US\$	1,302	940
NPV 10%	MM US\$	987	706
IRR		29.8%	26.7%
PAYOUT		3 y, 5 m	3 y, 5 m

The above tables show that the project's economic metrics are very attractive, with the IRR for the full equity case being 21.0% on an after-tax basis and a project NPV (8%) of MMUS\$ 908. In this same case, investment pay out occurs at 4 years and two months after the end of the investment period. Given the project's high rate of return, including debt in the capital structure further improves these results, as shown in Table 1-10. Table 1-11 shows the main items included in the project's cash flow and which produce the above shown results.

Table 1-11: Project Summary Cash Flow

SALAR BLANCO - SALAR DE MARICUNGA (20KTPA) PROJECT MINERA SALAR BLANCO S.A. DISCOUNTED CASH FLOW																		
Year	2020	2021	2022	2023	2024	2025	2026	2027	2028	2029	2030	2031	2032	2033	2034	2035	2036	2037
Period	1	2	3	4	5	6	7	8	9	10	11	12	13	14	15	16	17	18
Total																		
Revenues	-	-	-	83,888	168,175	280,179	289,566	298,455	308,488	317,989	328,537	338,523	349,464	349,464	349,464	321,564	6,928,935	
Li2CO3 Battery Grade	-	-	-	71,618	147,953	254,031	262,594	270,703	279,837	288,487	298,074	307,150	317,081	317,081	317,081	292,420	6,277,844	
Li2CO3 Battery Grade - OP	-	-	-	71,618	147,953	254,031	262,594	270,703	279,837	288,487	298,074	307,150	317,081	317,081	317,081	292,420	3,086,585	
Li2CO3 Battery Grade - NP	-	-	-	-	-	-	-	-	-	-	-	-	59,767	294,583	317,081	292,420	3,191,259	
Li2CO3 Technical Grade	-	-	-	12,270	20,222	26,148	26,972	27,752	28,651	29,503	30,463	31,373	32,383	32,383	32,383	29,145	651,092	
Li2CO3 Technical Grade - OP	-	-	-	12,270	20,222	26,148	26,972	27,752	28,651	29,503	30,463	31,373	32,383	32,383	32,383	29,145	325,895	
Li2CO3 Technical Grade - NP	-	-	-	-	-	-	-	-	-	-	-	-	6,104	30,085	32,383	29,145	328,434	
Expenses	-	-	-	(31,211)	(46,328)	(79,395)	(82,062)	(82,516)	(83,027)	(83,512)	(84,050)	(85,619)	(85,611)	(94,927)	(96,229)	(90,224)	(1,856,231)	
OPEX Li2CO3 Battery Grade	-	-	-	(24,973)	(38,726)	(65,702)	(67,890)	(67,890)	(67,890)	(67,890)	(67,890)	(67,890)	(67,890)	(67,890)	(67,890)	(64,049)	(1,415,473)	
OPEX Li2CO3 Technical Grade	-	-	-	(3,285)	(5,257)	(7,543)	(7,543)	(7,543)	(7,543)	(7,543)	(7,543)	(7,543)	(7,543)	(7,543)	(7,543)	(6,995)	(158,860)	
Royalties based on Sales	-	-	-	(2,000)	(985)	(4,117)	(4,539)	(4,939)	(5,391)	(5,818)	(6,293)	(8,002)	(7,729)	(17,044)	(18,346)	(16,899)	(232,483)	
Communities	-	-	-	(600)	(1,009)	(1,681)	(1,737)	(1,791)	(1,851)	(1,908)	(1,971)	(2,031)	(2,097)	(2,097)	(2,097)	(1,929)	(41,670)	
Mining Licenses & Water Rights	-	-	-	(352)	(352)	(352)	(352)	(352)	(352)	(352)	(352)	(352)	(352)	(352)	(352)	(352)	(7,744)	
Operating Margin	-	-	-	52,678	121,847	200,784	207,504	215,939	225,461	234,477	244,487	252,704	263,853	254,537	253,236	231,340	5,072,704	
Operating Margin %	-	-	-	61%	71%	72%	72%	72%	73%	74%	74%	75%	76%	73%	72%	72%		
Depreciation	-	-	-	(207,312)	(184,278)	(184,278)	-	-	-	(1,733)	(176)	(353)	(706)	(3,705)	(6,175)	(6,881)	(622,413)	
Amortization	-	-	-	(4,000)	(4,000)	(4,000)	(4,000)	(4,000)	(4,000)	(4,000)	(4,000)	(4,000)	(4,000)	(4,000)	(4,000)	(4,000)	(20,000)	
Remediation Allowance	-	-	-	(4,561)	(869)	(869)	(869)	(869)	(869)	(869)	(869)	(869)	(869)	(869)	(869)	(869)	(22,803)	
Remediation Guaranty Cost	-	-	-	(91)	(109)	(126)	(143)	(161)	(178)	(195)	(213)	(230)	(248)	(269)	(289)	(289)	(6,020)	
Operating Margin for Annual Royalty	-	-	-	(163,195)	(67,299)	11,637	202,635	211,070	224,592	231,876	243,442	251,483	262,279	249,964	246,192	223,591	4,407,488	
Additional royalty based on Operating Margin	-	-	-	0	0	0	0	0	0	0	0	0	0	(10,357)	(10,378)	(10,357)	(110,780)	
Profit Before Taxes	-	-	-	(163,286)	(67,407)	11,511	202,492	210,910	224,414	231,680	243,229	251,252	262,031	239,237	235,375	212,779	4,290,688	
Income Taxes	-	-	-	-	-	-	-	(52,439)	(60,592)	(62,554)	(65,672)	(67,838)	(70,748)	(64,594)	(63,551)	(57,450)	(1,158,486)	
Profit After Taxes	-	-	-	(163,286)	(67,407)	11,511	202,492	158,471	163,822	169,127	177,557	183,414	191,283	174,643	171,824	155,328	3,132,202	
Depreciation, Amortization & Allowance	-	-	-	215,873	189,146	189,146	4,869	4,869	869	2,602	1,045	1,222	1,574	4,574	7,044	7,749	665,216	
Operating After Tax Cash Flow	-	-	-	52,586	121,739	200,658	207,361	163,339	164,691	171,728	178,603	184,636	192,857	179,217	178,868	163,078	3,797,418	
Non Operating Cash Flow	(80,239)	(382,627)	(126,947)	1,779	(5,969)	(11,517)	(875)	(113)	(128)	(650)	(664)	(1,501)	(1,007)	(4,596)	(7,103)	(6,080)	(653,516)	
CAPEX & Sustaining Capital	(73,278)	(355,789)	(146,801)	-	-	(5,199)	-	-	-	(529)	(529)	(1,059)	(1,059)	(4,234)	(6,881)	(7,410)	(633,995)	
Working Capital Variation	-	-	-	(10,404)	(5,039)	(4,406)	(667)	(113)	(128)	(121)	(134)	(442)	52	(362)	(222)	1,001	(15,037)	
VAT (Net of refunds)	(6,961)	(26,839)	19,854	12,183	(930)	(1,912)	(208)	-	-	-	-	-	-	-	-	329	(4,484)	
Cash Flow Before Interest and Tax	(80,239)	(382,627)	(126,947)	54,457	115,878	189,267	206,629	215,826	225,333	233,827	243,823	251,203	262,847	249,941	246,133	225,260	4,419,188	
Remediation disbursement	-	-	-	-	-	-	-	-	-	-	-	-	-	-	-	(22,803)	(22,803)	
Before Tax Cash Flow	(80,239)	(382,627)	(126,947)	54,457	115,878	189,267	206,629	215,826	225,333	233,827	243,823	251,203	262,847	249,941	246,133	202,457	4,396,385	
Income Taxes (27%)	-	-	-	-	-	-	-	(52,439)	(60,592)	(62,554)	(65,672)	(67,838)	(70,748)	(64,594)	(63,551)	(57,450)	(1,158,486)	
After Tax Cash Flow	(80,239)	(382,627)	(126,947)	54,457	115,878	189,267	206,629	163,387	164,741	171,273	178,152	183,365	192,098	185,347	182,581	145,007	3,237,900	
Accumulated Cash Flow AfterTax	(80,239)	(462,866)	(589,814)	(535,357)	(419,479)	(230,212)	(23,583)	139,804	304,545	475,819	653,970	837,336	1,029,434	2,347,700	3,092,892	3,237,900		

1.14 PROJECTION CONCLUSIONS AND RECOMMENDATIONS

1.14.1 Conclusions

Based on the analyses and interpretation of the results of the exploration work carried out on the mining concessions of MSB in Salar de Maricunga between 2011 and 2018, as well as on laboratory work, tests with equipment suppliers and conceptual process and plant engineering, the following concluding statements are prepared:

- The entire Blanco Project area has been covered by exploratory drilling between 2011 and 2017 at an approximate borehole density of one exploration borehole per 1.5 km²; it is the opinion of the authors that such borehole density is appropriate for the mineral resource estimate described herein.
- It is the opinion of the authors that the Salar geometry, brine chemistry composition and the specific yield of the Salar sediments have been adequately defined to a depth of 200 m to support the Measured and Indicated Resource estimate described in Section 14 and shown in Table 1-3.
- The Blanco Project Lithium Mineral Reserve Estimate supports the feasibility of a 20,000 TPY lithium carbonate production facility with a 20-year Project life.
- Based on results of exploration borehole S-19 to a depth of 360 m, it is the opinion of the authors that a significant exploration target exists below the current resource defined to 200 m depth.
- The Salar de Maricunga brine due to its high calcium concentration is not fully suitable for conventional processing. The Blanco Project process principally consists of solar evaporation of the brine to a suitable concentration such that the brine can be treated in a salt removal plant –an addition to the conventional process– and finally in a lithium carbonate production plant. The concentrated Maricunga brine will require a boron, calcium and magnesium removal stages.
- A work program should be initiated to continue expanding the Blanco Project resource estimate by exploring the deeper portions of the Salar. It is recommended that the proposed work program includes the following components:
 - Deep drilling (7-10 holes) using a suitable drilling method to a depth of 400 m across the MSB properties. The drilling target will be the coarser grained sediments on the Lower Alluvium and Volcaniclastics.
 - Sampling protocols need to be developed to properly characterize the hydraulic parameters and the brine chemistry of these deeper units.
 - The estimated cost for the above exploration program is approximately US\$ 7 million.

- As indicated in Section 1.12, CAPEX for the Lithium Carbonate 20,000 TPY Salar Blanco Project is US\$ 563 million. This total is higher than for other similar size lithium carbonate projects due to the need to include a Salt Removal Plant. High Calcium content in the Salr de Maricunga brine makes this plant necessary. However, it also must be mentioned that the above referred plant has the following advantages:
 - It allows ending the solar pond evaporation stage with a comparatively low lithium concentration brine, (0.8% to 0.9%), given that in addition to Ca removal, substantial evaporation and concentration takes place at the above referred plant. Thus, if the Salt Removal Plant were not necessary, additional pond area would be required to obtain a concentrated brine suitable for the Lithium Carbonate Plant.
 - It allows recovery of part of the water contained in the brine, thus reducing the total water consumption.
 - It allows extracting impurities (mainly calcium) contained in the brine without the use of chemical reagents.
 - The above allows obtaining battery-grade lithium carbonate without adding a CO₂ purification stage.
- Table 1-8 indicates that total unit operating cost for the project is US\$ 3,772 per tonne of lithium carbonate. Again, this is somewhat higher than some comparably sized brine lithium project, the main reason being the energy cost associated with the Salt Removal Plant, but which has the advantages pointed out in the previous commentary.
- The project's economic results are very positive, with a full equity, after-tax base case that generates an IRR of 21,0 %, an NPV (8%) of over US\$ MM 908 and a pay out period of 4 years and two months. On a pre-tax basis, the NPV is US\$ MM 1,286 and providing a 23.8% IRR.
- Main reasons for the above results are the favourable outlook for lithium prices, as developed in Section 19, relatively low -27%- corporate income tax rate in Chile, as well as an expected low royalty rate regime for MSB, due mostly to the special "grandfathered" conditions affecting nearly half of the MSB mining properties.
- The project's sensitivity analysis carried out in sub section 22.8.2, analyzes its results when base case assumptions can deviate from expected values. The outcome of this analysis indicates that the project is quite sensitive to the expected price of lithium carbonate. In this way, if lithium prices were to be permanently only 75% of the base case projection¹, the project's IRR drops to 15% and NPV after-tax (8%) declines to US\$ MM 450. Conversely, the project's results improve very substantially -IRR 26% and NPV after-tax

¹ Supplied by mineral prices specialist Roskill Ltd.

(8%) US\$ MM 1,363- if lithium prices were to be permanently 125% of the base case projection.

- The project's sensitivity to other key variables, such as CAPEX and OPEX expenditures, is much less, with 25% changes in either variable causing only an 11% variation in NPV after-tax (8%). Variation in IRR is about 3.5 percentage points when CAPEX varies by 25%, while variation in IRR is only 1.5 percentage points when CAPEX varies by 25%. This indicates project resilience in face of possible negative CAPEX or OPEX scenarios.

1.14.2 Recommendations

- Final equipment selection with regards to the SX and drying plant sections must be made in the very near future, to maintain the proposed construction schedule. Proven technologies and suppliers exist for these items.
- Permits to modify the course of Highway C-173, whose current routing runs through the project's pond farm, must be given priority given that solar evaporation pond construction is the most critical element in the project's construction plan.
- For the same reason and given the very large pond surfaces that need to be covered with plastic film, it is advisable to enter as soon as possible, into a production contract with a reputable supplier of this critical material. This, considering that it may be possible that one, or more, additional lithium brine project might be in construction at the same time, straining plastic film production capacity.
- Continue and accelerate tests of the flexible bituminous sheet that might be used instead of the plastic film for pond lining. The main advantage of the bituminous sheet is that it may be installed even in very cold weather during winter. This would constitute another way to shorten the critical pond construction time.
- Continue obtaining further climatic data of the area, especially, evaporation rates rain and snow, records at the exact site of the project. Incorporate this data into final project design.
- As it was suggested in the PEA study, it is reasonable to postpone the investment in a KCI plant for a few years and reconsider the decision to build it, if there is a clear improvement of its expected long-term pricing outlook.
- It is recommended that a new risks evaluation workshop be conducted before the start of the detailed engineering. This workshop will address safety, environmental, brine production and process issues.
- It is recommended that for the project's next stage, an EPCM (Engineering, Procurement and Construction Management) contracting strategy be used. Another possible alternative would be a refundable type EPC (Engineering, Procurement and Construction) contract,

with the support of an Owner's Engineer. In either case, experience in lithium projects of the engineer/contractor is a recommended.

- The Maricunga Salar is a mid size salar and considering on the other hand that the mineral property in the salar is divided among four large holders (MSB being the one of the largest) and many other small holders, there will be a material advantage to the party that is able to progress its project faster, because the resource might not support another competitively sized lithium carbonate plant. Thus, if MSB can proceed quickly with this project, it may become “dominant” in the salar and might be in position to acquire additional resources at favourable conditions.

2. INTRODUCTION

2.1 TERMS OF REFERENCE

This report (the “Report”) was prepared by WorleyParsons Chile (“WP”), FloSolutions , and Peter Ehren at the request of Minera Salar Blanco S.A. (“MSB”) This report has been prepared in conformance with the requirements of National Instrument 43-101 – Standards of Disclosure for Mineral Projects and the associated Companion Policy 43-101CP and Form 43-101F1 of the Canadian Securities Administrators (modified June 24, 2011) and the associated Best Practice Guidelines for Industrial Minerals and Mineral Processing as issued by the Canadian Institute of Mining and Metallurgy (“CIM”). The Report also includes technical judgment of appropriate additional technical parameters to accommodate certain specific characteristics of minerals hosted in liquid brine as outlined in CIM Best Practice Guidelines for Resource and Reserve Estimation for Lithium Brines and as discussed by Houston (Houston et al, 2011).

2.2 SOURCES OF INFORMATION AND DATA

Previous technical reports prepared for the Project include:

- Estudio de Impacto Ambiental del Proyecto "Proyecto Blanco"; Minera Salar Blanco S.A.; preparado por Statec, Septiembre 2018.
- Modelo Hidrogeológico Conceptual Salar de Maricunga; Proyecto Blanco, Minera Salar Blanco, preparado por FloSolutions, Agosto 2018
- NI 43-101 Technical Report, Preliminary Assessment and Economic Evaluation of the Minera Salar Blanco Project, Atacama Region Chile. Prepared for: Minera Salar Blanco S.A. by: Worley Parsons, dated December 21, 2017.
- NI 43-101 Technical Report, Lithium & Potassium Resource Estimate Maricunga Joint Venture, III Region, Chile. Prepared for: Minera Salar Blanco S.A. by: Frits Reidel, BSc, CPG, Murray Brooker, MSc, RPG, MAIG and Peter Ehren, MSc, MAusIMM, dated August 25, 2017.
- NI 43-101 Technical Report, Lithium & Potassium Resource Estimate Maricunga Joint Venture, III Region, Chile. Prepared for: Minera Salar Blanco S.A. by: Frits Reidel, CPG, Murray Brooker, MSc, RPG, MAIG and Peter Ehren, MSc, MAusIMM, dated August 25, 2017.
- Maricunga Lithium Brine Project; 3.7 Fold Increase in Mineral Resource Estimate; JORC report dated 12 July 2017.

- Technical Report on the Maricunga Lithium Project, Region III, Chile. NI 43-101 Technical Report (update of 2012 NI 43-101 Technical Report) for Bearing Resources prepared by Don Hains March 20, 2017.
- Salar de Maricunga Desktop Study, prepared for Minera Salar Blanco Spa by Peter Ehren, MSc., October 2015
- Technical Report on the Maricunga Lithium Project, Region III, Chile. NI 43-101 Technical Report for Li3 Energy Inc. prepared by Don Hains and Frits Reidel, CPC April 17, 2012.
- Technical Report on the Salar de Maricunga Lithium Project, Northern Chile prepared for Li3 Energy Inc. NI 43-101 Technical report prepared by Donald H Hains, Amended May 26, 2011.

Chapters 1, 2 and 3 were prepared by WP and FloSolutions. Chapters 4 through 12, 14, 15, 16 and 23 have been prepared by Mr. Frits Reidel, CPG (Principal at FloSolutions), Chapters 13 was prepared by Mr. Peter Ehren, MSc, MAusIMM, Chapter 17 was prepared by Mr. Marek Dworzanowski and Mr. Peter Ehren. Chapter 18 was prepared by MSB. Chapters 19 and 20 were prepared by MSB. Chapter 21 and 22 were prepared by WorleyParsons.

This report was reviewed by Marek Dworzanowski, Pr. Eng., BSc (Hons), FSAIMM of WorleyParsons, Mr. Peter Ehren, MSc, MAusIMM and Frits Reidel, CPG. Mr. Dworzanowski, Mr. Peter Ehren and Mr. Frits Reidel are “qualified persons” (QP) and are independent of MSB as such terms are defined by NI 43-101.

3. RELIANCE ON OTHER EXPERTS

For the legal opinion on the status of the Project's mining claims the authors have relied on the following expert:

Mr. J.P. Bambach of the legal firm Philippi, Prietocarrizosa, Ferrero DU & Uria in Santiago, Chile.

For the purpose of this report, the authors have relied on ownership information provided by MSB. MSB has relied on a legal opinion by Philippi, Prietocarrizosa, Ferrero DU & Uria dated August 18, 2017 respecting legal title to the properties.

The authors also have relied on the topographic information regarding property locations provided by MSB and Philippi, Prietocarrizosa, Ferrero DU & Uria.

4. PROPERTY DESCRIPTION AND LOCATION

4.1 PROPERTY DESCRIPTION AND LOCATION

The Blanco Project is located approximately 170 km northeast of Copiapó in the III Region of northern Chile at an elevation of approximately 3,750 masl. Figure 4-1 shows the location of the Project. The property is more particularly described as being centered at approximately 492,000 mE, 7,025,000 mN (WGS 84 datum, UTM Zone 19). The Project covers 2,563 ha of mineralized ground in Salar de Maricunga, 100 ha just to the northeast of the Salar for camp and evaporation test facilities, and an additional 1,800 ha some eight km north of the Salar for the future construction of evaporation ponds, process and plant facilities.

4.2 TENURE

The mineralized area of the Blanco Project is comprised of the following mining concessions: Litio 1-6 (1,438 ha), Cocina 19-27 (450 ha), Salamina, Despreciada, and San Francisco (675 ha). Figure 4-2 shows the Blanco Project land tenure and concession boundaries in the northern part of Salar de Maricunga. Table 4-1 provides a detailed listing of the MSB concessions.

The Cocina 19-27, San Francisco, Despreciada and Salamina concessions were constituted under the 1932 Chilean mining law and have “grand-fathered” rights for the production and sale of lithium products; unlike the Litio 1-6 concessions which were constituted under the 1983 Chilean mining law and require additional government permits for the production and sale of lithium.

Table 4-1: MSB mining concessions

Property	Role Number	Area (ha)	Registered Owner	Mining Code
Litio 1, 1 al 29	03201-6516-4	131	SML Litio 1	1983
Litio 2, 1 al 30	0321-6517-2	143	SML Litio 2	1983
Litio 3, 1 al 58	03201-6518-0	286	SML Litio 3	1983
Litio 4, 1 al 60	03201-6519-9	300	SML Litio 4	1983
Litio 5, 1 al 60	03201-6520-2	297	SML Litio 5	1983
Litio 6, 1 al 60	03201-6521-0	282	SML Litio 6	1983
Cocina 19-27	03201-2110-19	450	MSB	1932
San Francisco 1 al 10	03201-0006-2	425	MSB	1932
Despreciada 6 al 7	03201-0007-0	100	MSB	1932
Salamina 1 al 3	03201-0005-4	150	MSB	1932
Blanco*	N/A	1,800	MSB	1983
Camp*	N/A	100	MSB	1983

* Note: Concessions not included in Mr. Bambach’s legal opinion.

Verification of the land titles and mining rights owned by MSB was conducted by Juan Paulo Bambach Salvatore of the legal firm Philippi Prietocarrizosa Ferrero DU & Uria in Santiago. Mr.

Bambach documented his legal opinion in a letter dated August 18, 2017 and concluded the following:

- Minera Salar Banco S.A. (MSB) has been duly incorporated and is a validly existing company under the laws of Chile and is in good standing.
- MSB owns 96 % of the shares over six mining legal companies (sociedades legales mineras) Litio 1 up to Litio 6, which in turn are respectively the exclusive owners of six Mining Exploitation Concessions, as shown in Table 4-1.
- Minera Salar Blanco S.A. (MSB) has all necessary corporate faculties and authority to carry on its business as now conducted by it and to own its properties and assets.
- Minera Salar Blanco S.A. (MSB) is duly licensed to carry on its business in Chile.
- The Company currently has a portfolio of 10 Mining Concessions (not including Blanco and Camp concessions), as follows:
 - 4 Old Legislation Concessions (pertenencias)
 - 6 1983 Exploitation Concessions (pertenencias)
- All titles of the Mining Concessions set out in Table 4-1 are in good standing and there are no encumbrances on such Mining Concessions.
- Minera Salar Blanco S.A. (MSB) is empowered to conduct exploration activities on the Exploration Concessions, and exploration and development activities on the Mining Claims.
- By means of the Old Mining Chilean Legislation, MSB is entitled to explore and exploit lithium, fulfilling all legal requirements provided by the Chilean legislation.
- The 1983 Exploitation Concessions do not allow to explore nor exploit lithium, unless a Special Operation Contract for Lithium, CEOL is obtained, but do permit the exploration and exploitation of any other mining substances, whether metallic or non-metallic, for example potassium, where lithium may be a sub product. In other words, the 1983 Exploitation Concessions do not entitle to appropriate the extracted lithium, but only other concessionable substances.
- According to the legal documentation reviewed, the Mining Concessions are valid and in force.
- To date, the granting processes of the applications under proceeding (the “Applications”) have been carried out according to the law, and they would not present defects that could lead to the expiration of the application.
- The Mining Concessions have no marginal records evidencing mortgages, encumbrances, prohibitions, interdictions or litigations.
- The Mining Concessions have all their last four periods of mining licenses duly paid.
- All the Mining Concessions have preferential rights over the relevant area. There are neither mining concessions nor mining rights held or filed by third parties challenging the rights and preference of the Mining Concessions.

- From a technical point of view and after having requested the review of the complete area by the expert in mining property Mr. Juan Bedmar, we can confirm that the location of the Mining Concessions is correct.

Figure 4-1: Location map of the Blanco Project

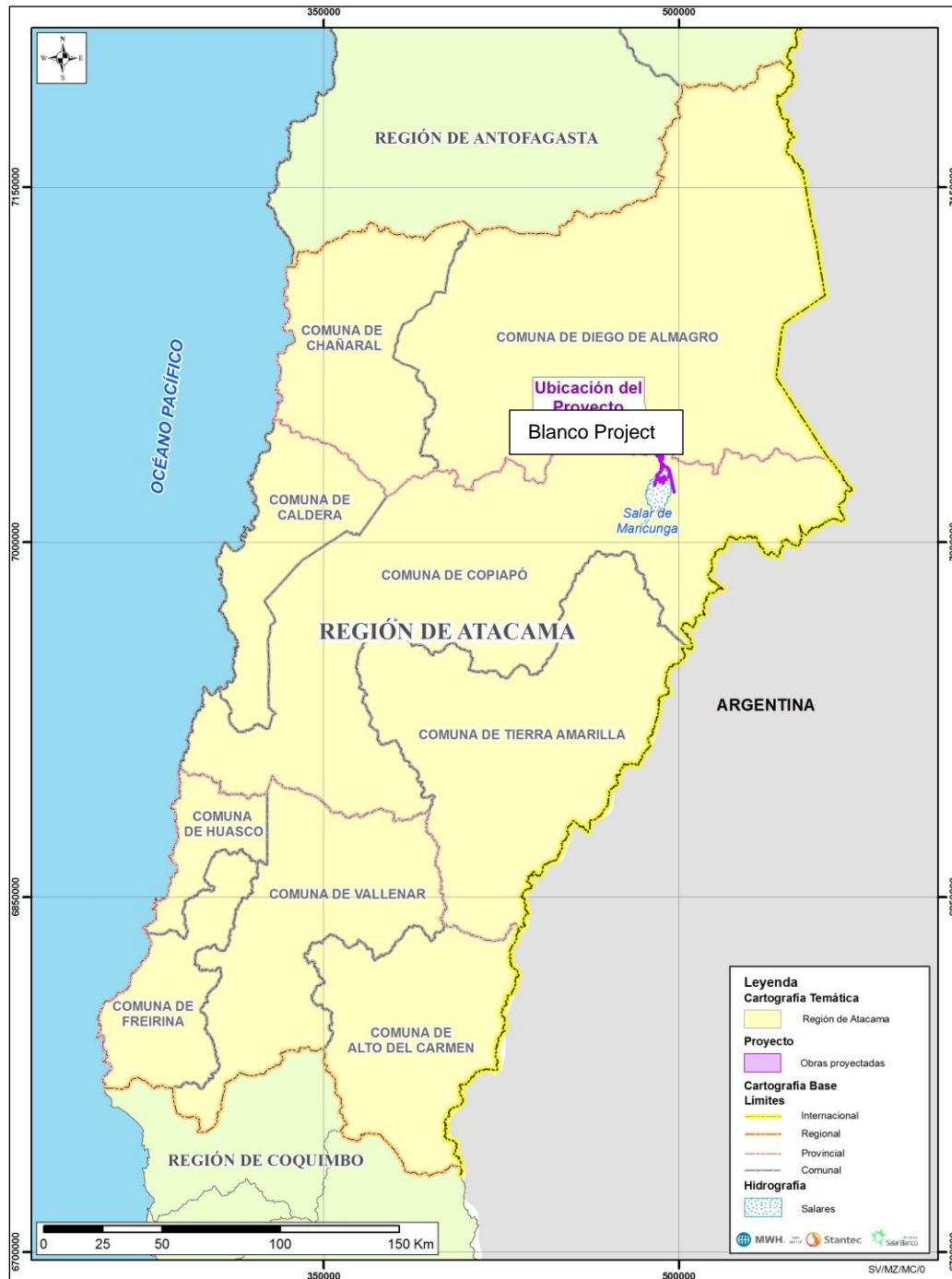
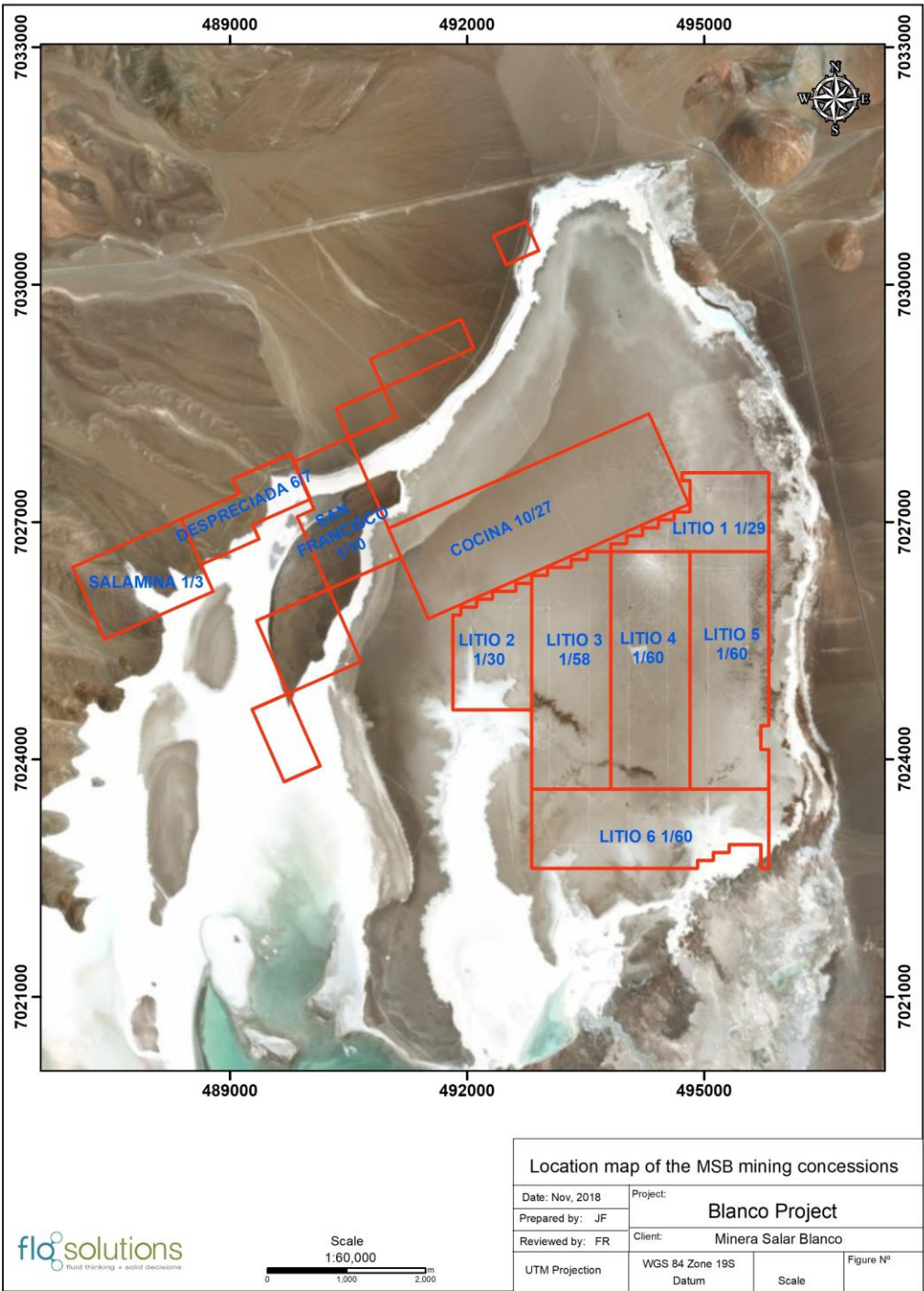


Figure 4-2: Location map of the MSB mining concessions



4.3 PERMITS

4.3.1 SEA Approval

MSB obtained all necessary environmental approvals through the Environmental Evaluation System (Sistema Evaluación Ambiental (SEA)) to carry out drilling, aquifer testing, road building and operate the evaporation test and camp facilities. The MSB concessions are located in a Tourist Interest Area (Zona de Interés Turístico (ZOIT)) and, therefore, SEA approvals are required to carry out exploration work. These approvals were obtained in 2013 through the filing and successful permitting of an Environmental Impact Declaration (Declaración de Impacto Ambiental (DIA)).

4.3.2 CChEN License

MSB was awarded a key regulatory license by the Chilean Nuclear Energy Commission (CChEN) to produce, market and export lithium products from Salar de Maricunga on March 9th, 2018. The CChEN license is for the production of an initial 88,885 t lithium metal or 472,868 t of LCE over a 30year term.

The permit is limited to the MSB's grandfathered mining concessions This permit allows MSB to request an increase on the initial quota under any of the following conditions:

- The current Indicated and Measured Mineral Resources are increased in grandfathered mining concessions
- The process recovery efficiency exceeds 40%.
- If MSB is awarded Special Operation Contract (CEOL) for the exploitation of lithium from the Litio 1-6 (new code) mining concessions. MSB is currently negotiating this contract with Chilean Government covering these mining concessions, i.e. those registered after 1979.

4.4 ROYALTIES

The Chilean government is currently reviewing a future royalty and permitting regime for lithium production. This matter is fully discussed on Section 22.2.

4.5 ENVIRONMENTAL LIABILITIES

The authors are not aware that the Blanco Project is subject to any material environmental liabilities.

4.6 OTHER SIGNIFICANT FACTORS AND RISKS

A few normal risk factors are associated with the Maricunga properties. These risks include but are not limited to the following. It is not anticipated they will affect access, title or the ability to perform work on the Salar de Maricunga:

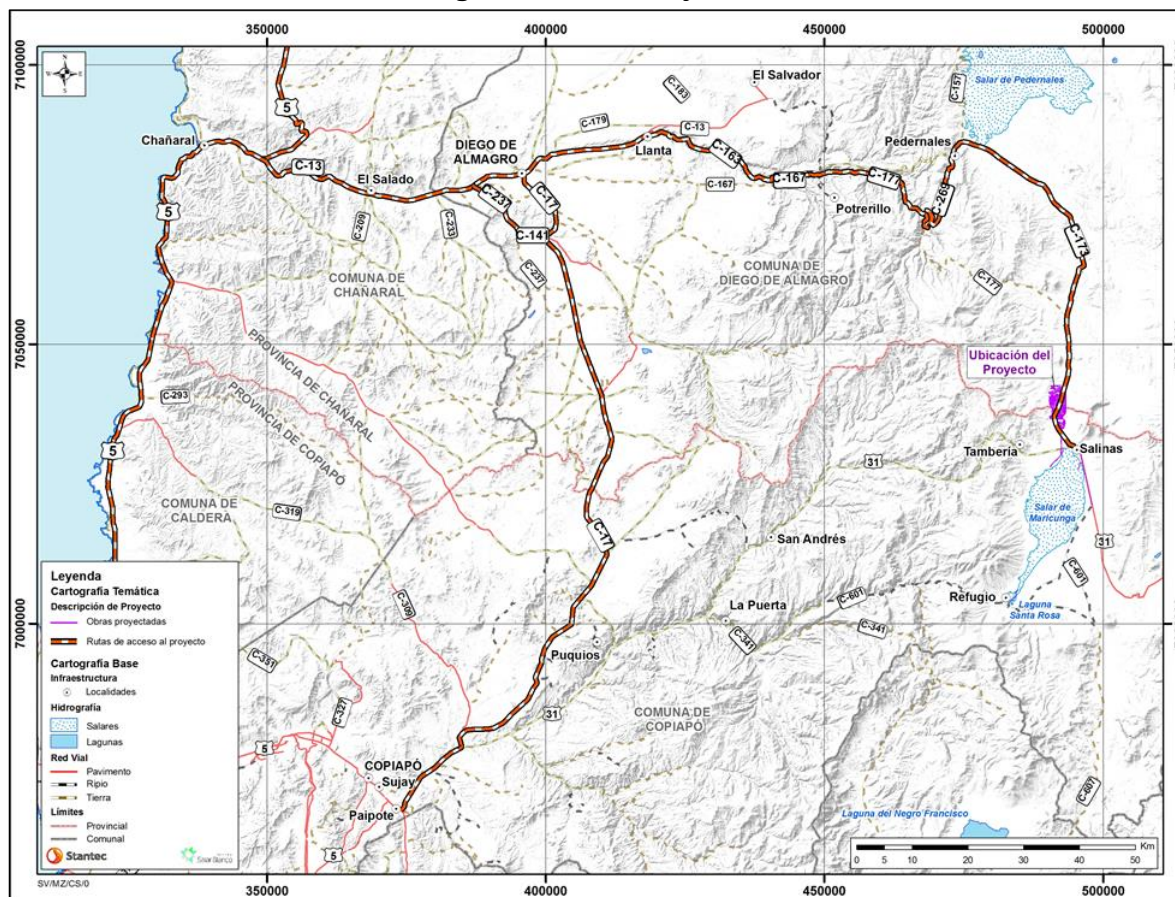
- The risk of obtaining final environmental approvals from the necessary authorities in a timely manner.
- The risk of obtaining all the necessary licenses and permits on acceptable terms, in a timely manner or at all.
- Risks associated with pending government regulation with respect to lithium exploitation, especially with regards to royalty rates.
- The risk of changes in laws and their implementation, impacting activities on the properties.
- The risk of activities on adjacent properties having an impact on the Maricunga project.
- The risk that the process, as currently defined, fails to produce the expected quantity and/or required quality of LCE. Nevertheless, extensive testing has been conducted and all individual process steps are conventional and commonly used in the industry.
- The risks of a high precipitation event, which can result in lower production, or an over estimation of evaporation rate, as the authors made the best estimate based on currently available information. MSB has been operating a weather station at the Project site to improve the understanding of the local climatic conditions.
- The risk of a faster lithium brine grade decline over time than that predicted by the hydro-geological model.

5. ACCESSIBILITY, CLIMATE, LOCAL RESOURCES, INFRASTRUCTURE AND PHYSIOGRAPHY

5.1 ACCESSIBILITY

The main road access to the Project corresponds to Route C-173, which is an existing, well maintained, mining road. Project tasks include the execution of a modification of this route, in an extension of approximately 8 km, for which authorizations will be requested. This route is accessed from Copiapó through Route C-17 to Diego de Almagro, and then taking Route C-13 in an eastern direction, then following Route C-163 East, until reaching Route C-173. The project location is 104 km away along this route.

Figure 5-1: Project Access



Source: Stantec Chile

Occasional high snowfalls in the mountains may close the highways for brief periods during the winter.

5.2 PHYSIOGRAPHY

The hydrographic basin of Salar de Maricunga covers 2,195 km² in the Altiplano of the III Region. The average elevation of the basin is 4,295 masl while the maximum and minimum elevations are 6,749 masl and 3,738 masl respectively. The Salar itself is located in the northern extent of the hydrographic basin and covers 142 km² (DGA 2009). The salar nucleus is at an elevation of approximately 3,750 masl.

The principal surface water inflow into the lower part of basin occurs from Rio Lamas which originates in Macizo de Tres Cruces. Average flow in Rio Lamas (at El Salto) is measured at 250 l/s approximately. All flows from the Rio Lamas infiltrate into the Llano de Cienaga Redonda (DGA 2009). The second largest surface water inflow (20 l/s) to the lower part of the basin occurs from Quebrada Cienaga Redonda and, infiltrates into the Llano de Cienaga Redonda (DGA 2009).

Laguna Santa Rosa is located at the southwest extent of the basin valley floor and is fed by a combination of surface and groundwater flows coming from the south and west. Laguna Santa Rosa drains north via a narrow natural channel into the Salar itself. Additional groundwater discharge occurs along the path of this channel and surface water flow has been recorded at 200-500 l/s (Flosolutions, 2018). Nevado Tres Cruces National Park is located in the southern part of the Maricunga watershed and includes Laguna Santa Rosa.

5.3 CLIMATE

5.3.1 Temperature

The climate at the property is a dry, cold, high altitude desert with cold, dry winters and dry summers. Summer temperatures range from 10 °C – 20 °C, with the winter daytime temperatures averaging approximately 4 °C – 0 °C. The average annual temperature at Salar de Maricunga is estimated at 5 °C – 6 °C as shown in Figure 5-2 (DGA 2009).

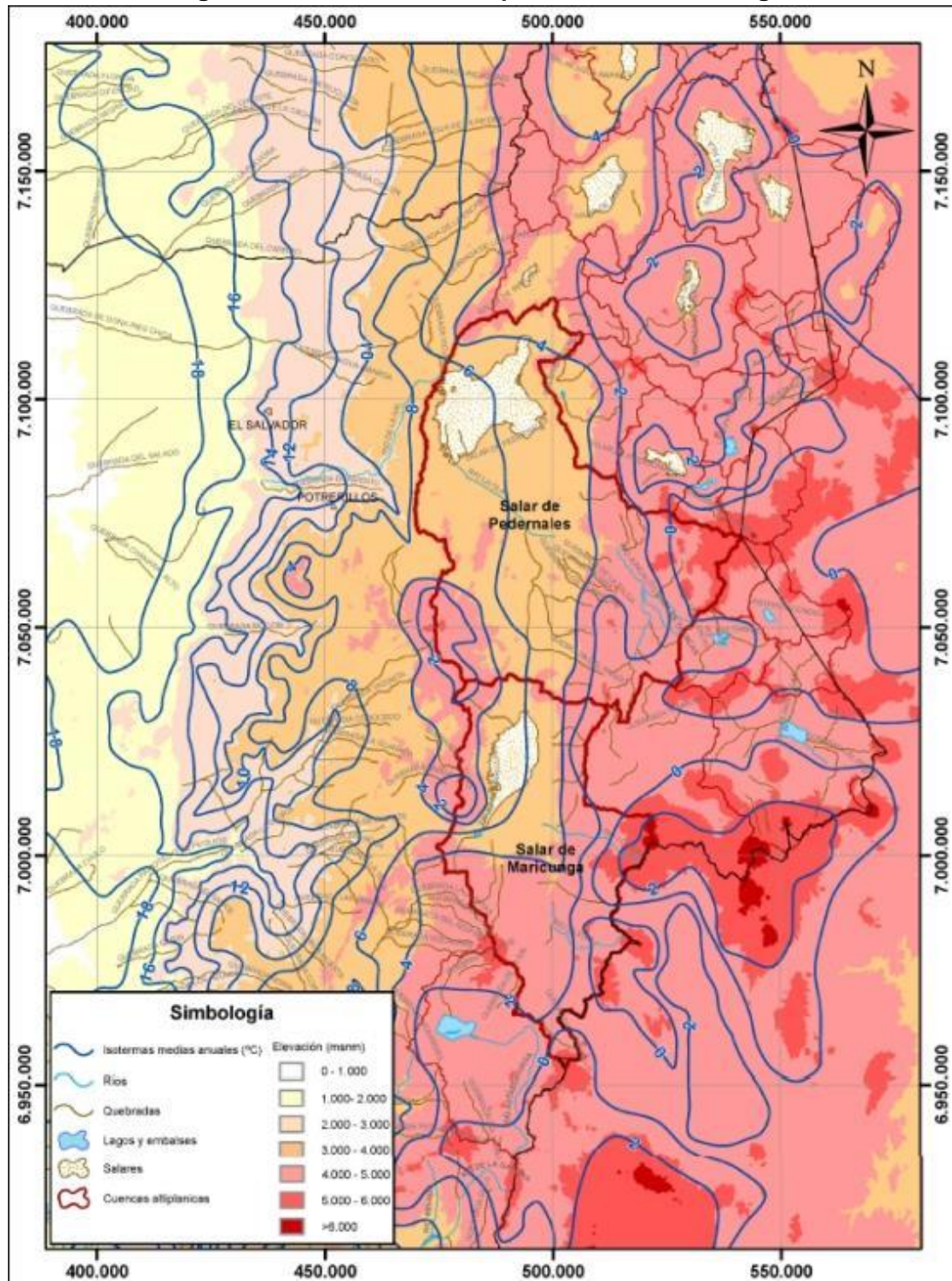
A weather station at the Marte Lobo Project site located in the southern extension of the Maricunga basin at an elevation of 4,090 masl, (30 km to the south of the Project) has average monthly temperature records available for the period between January 1997 and December 1998. Table 5-1 shows average monthly temperature data for the Marte Lobo Project (Golder Associates 2011) while Figure 5-2 provides an isotherm map for the salar de Maricunga region.

Table 5-1: Average Monthly Temperature at the Marte Lobo Project (°C)

Jan	Feb	Mar	Apr	May	Jun	Jul	Aug	Sep	Oct	Nov	Dec
8.5	6.6	6.5	2.5	-0.5	-5.0	-3.5	-2.5	-0.5	1.0	3.7	5.8

Source: re-elaborated after Golder Associates 2011

Figure 5-2: Isotherm map for Salar de Maricunga



Source: DGA 2009

5.3.2 Precipitation

Precipitation in Salar de Maricunga may occur during the months of January and February as a result of “Bolivian winter” effects. However, precipitation events are generally concentrated between the months of May through September. The intensity of these annual rainfall patterns is significantly influenced by the El Nino-Southern Oscillation.

The nearest long-term historical precipitation records for the Project are available from DGA maintained meteorological stations at Las Vegas (70 km northwest) at an elevation of 2,250 masl and Pastos Grandes (60 km WSW) at an elevation of 2,260 masl. No long-term historical precipitation records are available for the III Region above 2,500 masl elevation. Table 5-2 provides summary information of the Las Vegas and Pastos Grande stations.

Table 5-2: DGA Meteorological stations with long-term precipitation records

Station	BNA code	Basin	Elevation (masl)	Distance from Project	Record
Las Vegas	03210001-5	Rio Salado	2,250	70 km NW	1984 – to date
Pastos Grandes	03441001-1	Rio Copiapó	2,260	60 km WSW	1966 – to date

Source: DGA, 2009

Additional rainfall records are available from selected weather stations that are part of the “Pilot System for the III Region” operated by the Catholic University of Chile (PUC) in conjunction with the DGA. Table 5-3 provides summary information for the Maricunga and Pedernales Sur weather stations.

Table 5-3: Selected PUC-DGA weather stations with partial precipitation records

Station	Basin	UTM (WGS 84)		Elevation (masl)	Record
Maricunga	Maricunga	7,000,372 mN	486,326 mE	3,852	2007 – 2008
Pedernales Sur	Pedernales	7,049,016 mN	493,056 mE	3,774	2007 – 2008

Source: DGA, 2009

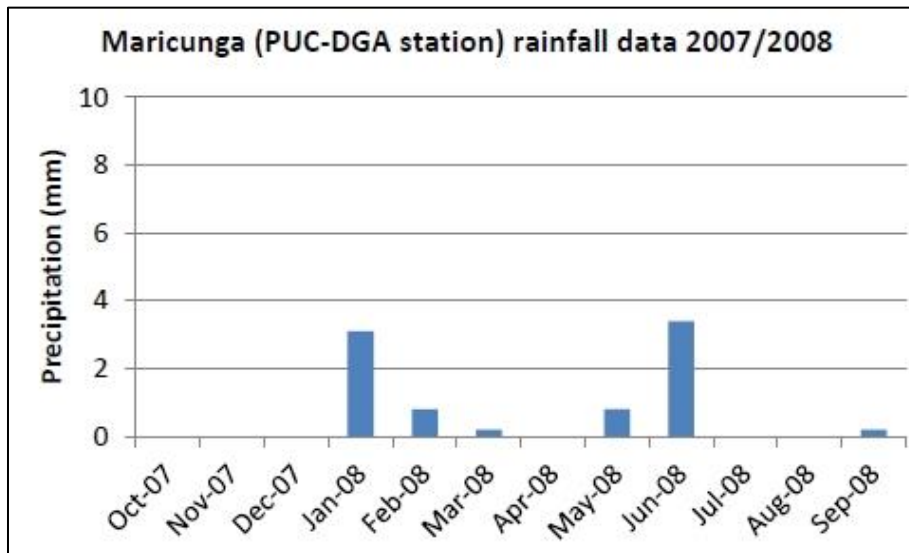
Figure 5-3 and Figure 5-4 shows monthly precipitation records for the Maricunga and Pedernales Sur weather stations for the 2007/8 period. It is believed that these data are representative of a relative dry year (DGA 2009).

Precipitation records collected at the Marte Lobo Project weather station during the 1997/1998 period show an annual cumulative precipitation (rainfall and snowfall water equivalent) of 451 mm (Golder Associates 2011). Further analyses of rainfall records of the III Region indicate that the 1997/8 cumulative precipitation coincides with a 100-year precipitation event. Additional precipitation data collected at the Marte and Lobo stations between 2009 and 2010 are shown in Figure 5-5.

Average annual precipitation estimates were prepared as part the “Balance Hídrico de Chile” (DGA 1987) and updated by DGA (2009). Figure 5-6 shows an isohyet map for the Salares de

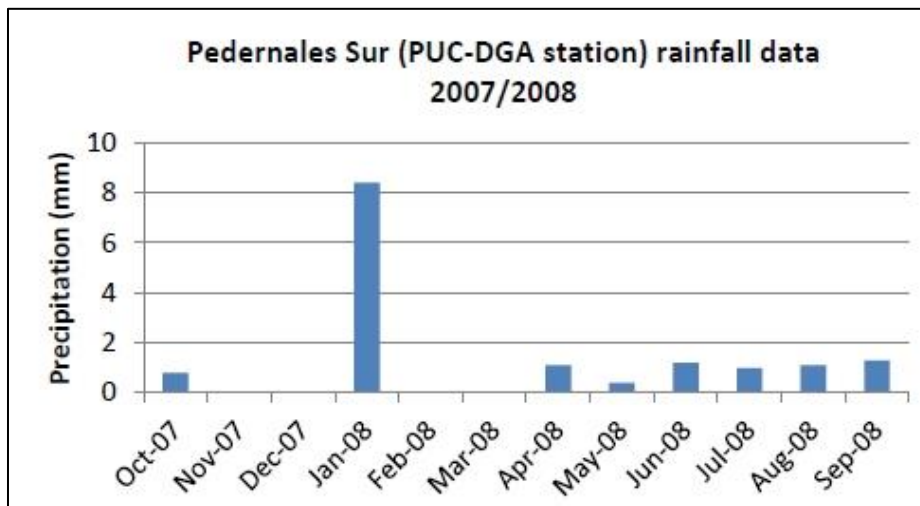
Maricunga and Pedernales (DGA, 2009). The map suggests that the average annual precipitation in Salar de Maricunga is 100 mm – 150 mm.

Figure 5-3: Precipitation Data for the Maricunga Weather Station (PUC-DGA) for 2007/2008



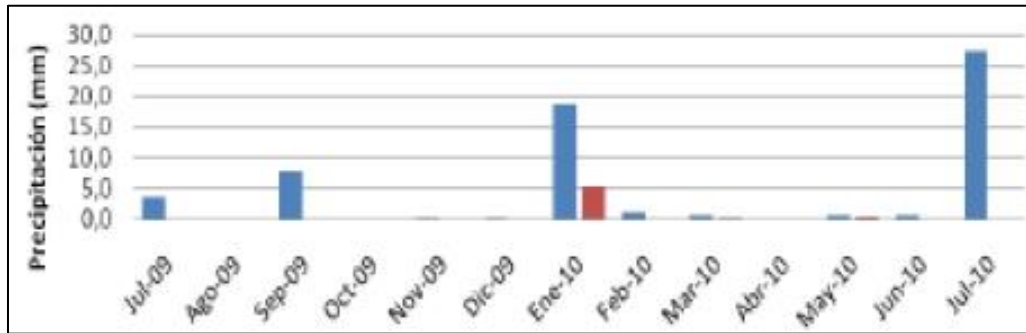
Source: DGA 2009

Figure 5-4: Precipitation Data for the Pedernales Sur Weather Station (PUC-DGA) for 2007/2008



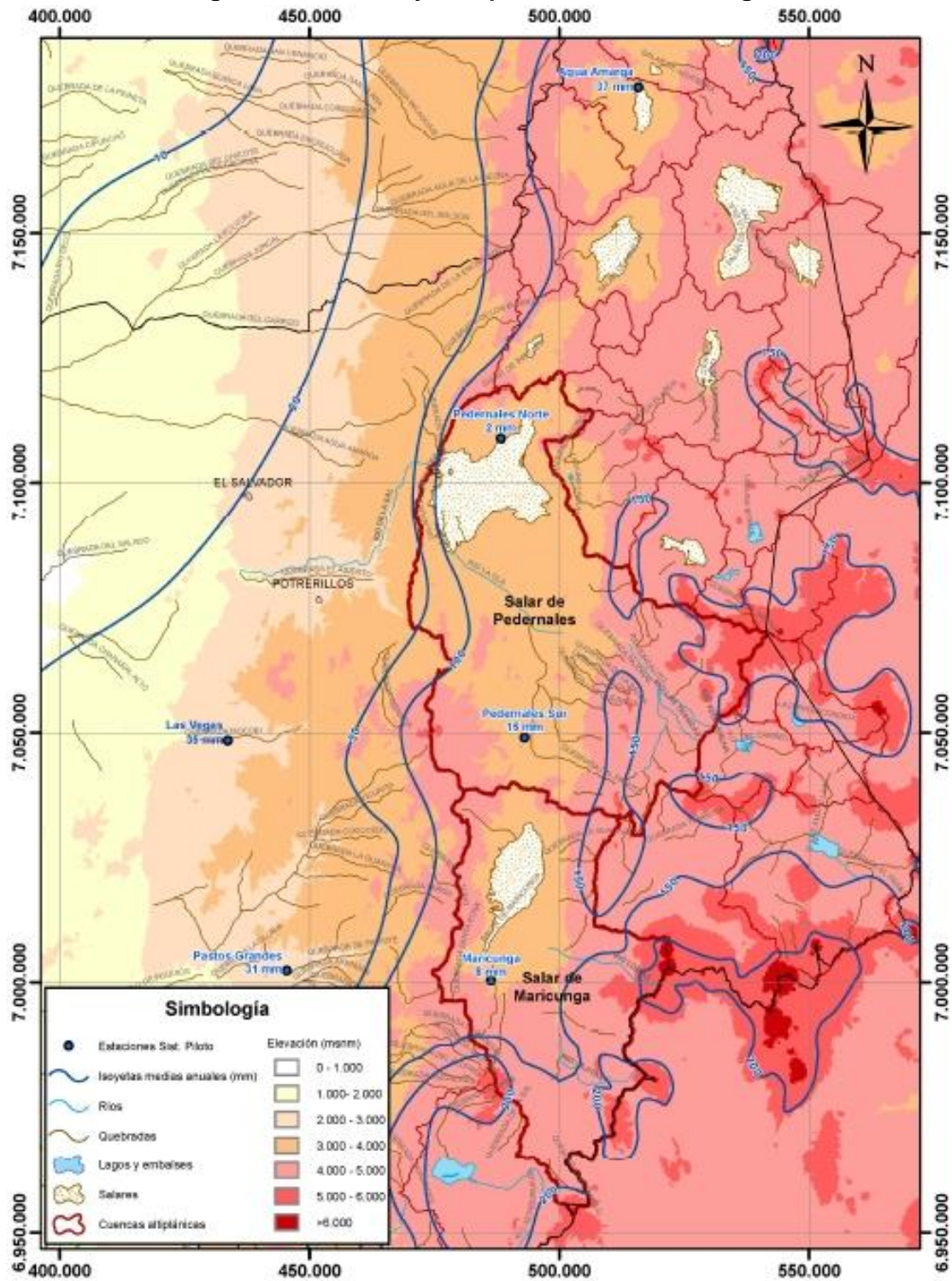
Source: DGA 2009

Figure 5-5: Precipitation Data from the Marte and Lobo Stations for 2009/2010



Source: AMEC 2011

Figure 5-6: Isohyet Map for Salar de Maricunga



Source: DGA 2009

The DGA (2006) carried out a hydrogeological investigation for Salar de Maricunga in which the following precipitation – elevation relationship was developed:

$$P = 0.1 \cdot H - 300$$

Where:

P is average annual precipitation (mm); and H is elevation (masl)

Using this correlation, for an average elevation of 3,750 masl, the average annual precipitation for Salar de Maricunga is estimated at 75 mm.

Finally, Hidromas (2017) produced an updated relationship of precipitation vs elevation:

$$P = 0.0287 \cdot H + 4.7237$$

Using this relationship, the average annual precipitation for Salar de Maricunga is estimated at 112 mm. This number is in accordance with the isohyet map of DGA (2009).

MSB installed a weather station in Salar de Maricunga in 2016 to validate the results of previous precipitation studies and third-party data sets (Figure 5-7). Figure 5-7 shows a summary of the data collected between November 2016 and August 2018.

Figure 5-7: Weather Station at Maricunga Project



Source: Hains site visit, Dec. 27, 2016

5.3.3 Solar Radiation

Solar radiation is the most important energy input for evaporation. Long-term solar radiation data are not available for Salar de Maricunga directly. Regional solar radiation estimates are shown in Figure 5-8 and suggest that solar radiation in Salar de Maricunga falls in the range of 1,700 –

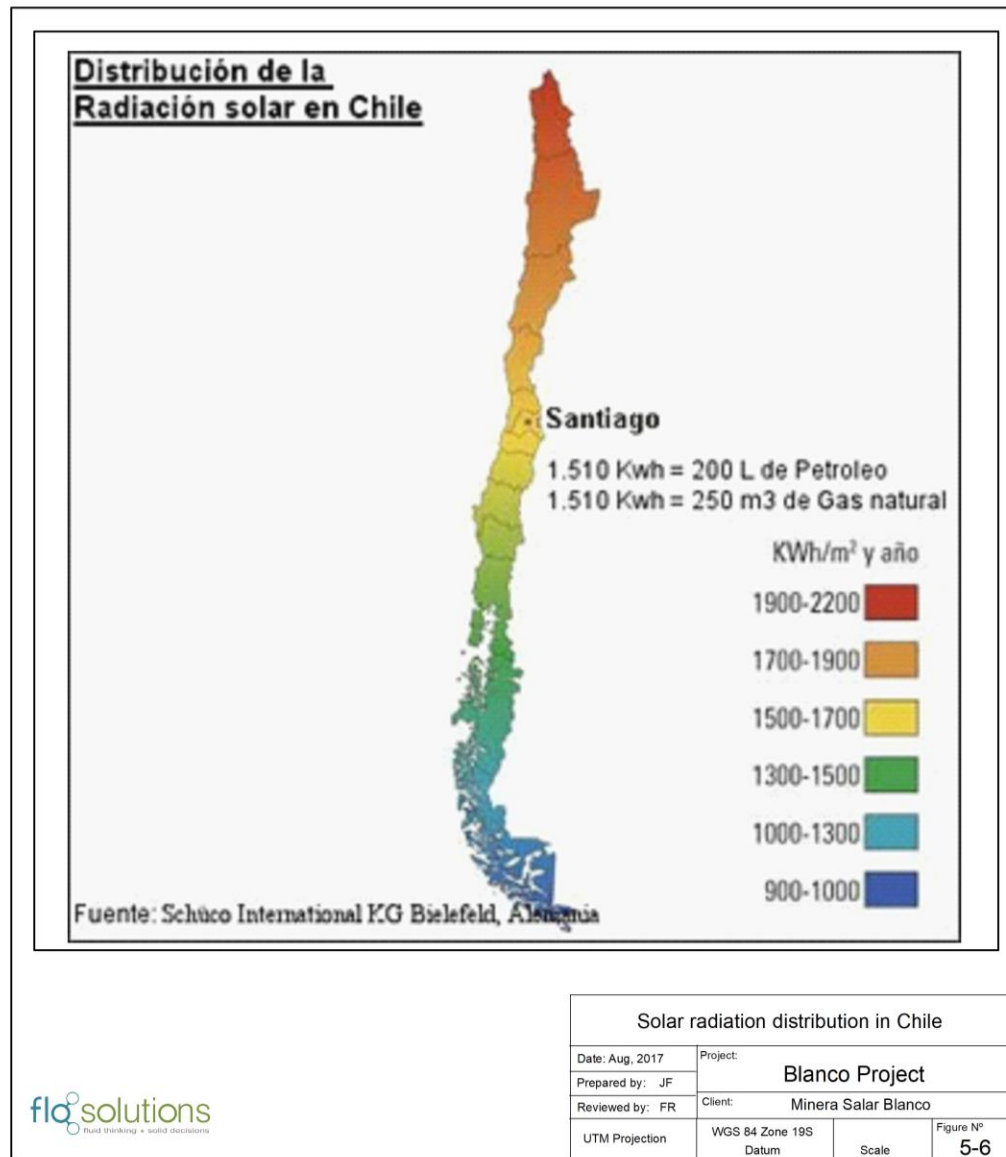
1,900 kWh/m² per year. Partial solar radiation data are available from the Marte Lobo Project site and are reported in Amec 2011. Table 5-4 shows monthly records solar radiation records in Watts/m² for the Marte and Lobo stations.

Table 5-4: Monthly solar radiation data (W/m²) for the Marte and Lobo Stations

Mes	Lobo			Marte		
	Minimo	Promedio	Máximo	Minimo	Promedio	Máximo
Jul-09	0.0	194.2	974.0	s/d	s/d	s/d
Ago-09	0.0	244.7	1078.7	s/d	s/d	s/d
Sep-09	0.0	324.0	1164.1	0.0	299.9	1019.2
Oct-09	0.0	374.3	1246.8	0.0	331.7	1157.6
Nov-09	0.0	394.7	1217.0	0.0	387.8	1171.0
Dic-09	0.0	417.6	1221.0	0.0	408.1	4981.0
Ene-10	0.0	397.4	1229.0	0.0	386.8	1154.0
Feb-10	0.0	375.8	1349.0	0.0	356.7	1156.0
Mar-10	0.0	328.0	1132.0	0.0	312.0	1019.0
Abr-10	0.0	259.6	1009.0	0.0	247.3	918.0
May-10	0.0	193.6	866.0	0.0	187.1	825.0
Jun-10	0.0	171.6	914.0	0.0	163.9	746.1

Source: AMEC 2011

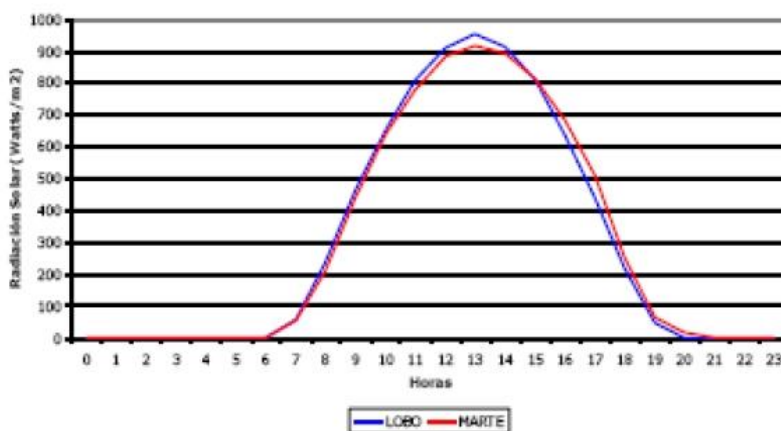
Figure 5-8: Solar Radiation Distribution in Chile



Source: Schüco International KG Bielefeld

Figure 5-9 shows the average hourly solar radiation intensity at the Marte and Lobo stations calculated for the 2009/2010 period.

Figure 5-9: Average Hourly Solar Radiation Intensity at the Marte and Lobo Stations for 2009/2010



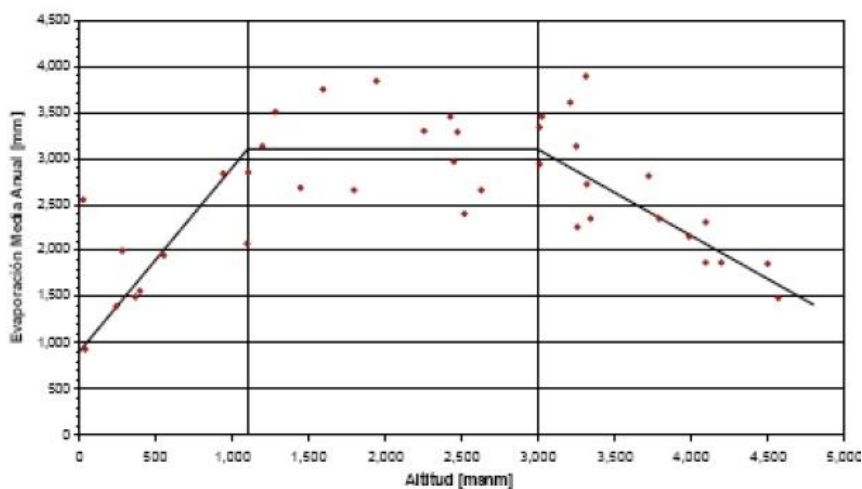
Source: AMEC 2011

The MSB weather station installed on site is collecting local suite-specific solar radiation data in support of the evaporation tests that are currently in progress.

5.3.4 Evaporation

The DGA (2009) has developed a relationship between elevation and average annual pan evaporation based on pan evaporation records from some 40 stations across the I, II, and III Regions of northern Chile as shown in Figure 5-10. Based on this correlation the annual average pan evaporation rate for Salar de Maricunga is estimated at 2,400 mm.

Figure 5-10: Elevation versus Average Annual Pan Evaporation



Source: DGA 2009

A similar relationship between elevation and average annual pan evaporation has been described by Houston (2006) as follows:

$MAE_{pan} = 4,364 - (0.59 \cdot A)$; where: MAE_{pan} is mean annual pan evaporation (mm) and A is elevation (m) for stations above 1,000 masl.

Using this correlation, the mean annual pan evaporation rate for Salar de Maricunga is estimated at 2,150 mm.

Houston (2006) further describes the effects of brine density on mean annual pan evaporation rates as:

$MAE_{pan} = 10,026 - 6,993 \cdot D$; where D is fluid density

Applying this to Maricunga brine ($D = 1.2$ g/ml), the annual average brine pan evaporation rate is estimated at 1,600 mm.

The DGA (2008) described the monthly distribution of average annual pan evaporation based on observations made from records (1977-2008) of the Linzor (4,096 masl) and Inacaliri (4,000 masl) stations in the II Region of northern Chile. Figure 5-11 summarizes this monthly distribution of the annual average pan evaporation (Golder Associates 2011).

The DGA (2009) carried out a detailed field investigation program in Salar de Maricunga to establish evaporation rates as a function of soil type and depth to groundwater. Table 5-5 summarizes the findings of this investigation.

Table 5-5: Evaporation Rates used for the Basin Water Balance

Type	Mean annual evaporation rate (mm)
Open water	6.1
Humid soil	4.1
Vegas	2.1
Salar crust	1.8

Source: DGA 2009 and Golder 2011

The Blanco project has installed several Class A evaporation pans (fresh water and brine) at the weather station and a series of test evaporation ponds adjacent to the camp site (Table 5-6). These test pans and ponds are designed to validate previous evaporation studies and confirm evaporation pathways for lithium brine concentration.

Table 5-6: Climate data collected at the MSB weather station in Salar de Maricunga (December 2016 – August 2018)

Month	Precipitation (mm)	Average Temperature (°C)	Freshwater Pan Evaporation (mm)	Brine Pan Evaporation (mm)
December 2016	17.00	6.60	323.61	236.60
January 2017	7.40	9.68	350.58	253.23
February 2017	8.20	6.68	243.00	185.00
March 2017	1.30	5.72	251.90	199.90
April 2017	11.10	1.86	137.30	191.30
May 2017	284.20*	1.90	40.40	35.40
June 2017	240.4*	1.90	0.00	0.00
July 2017	0*	-5.20	0.00	4.90
August 2017	23.00**	-2.70	40.60	44.20
September 2017	6.20**	0.60	104.30	184.80
October 2017	0.00	2.20	244.10	275.10
November 2017	0.00	4.70	306.30	289.90
December 2017	0.00	6.90	362.00	345.50
January 2018	1.40	6.70	280.10	282.30
February 2018	1.20	7.60	261.70	254.80
March 2018	0.00	4.90	277.60	267.50
April 2018	0.90	3.90	198.20	185.10
May 2018	0.00	0.10	54.8***	88.90
June 2018	0.00	-2.20	0.00***	117.00
July 2018	772*	-3.10	0.00***	62.60
August 2018	441*	-4.80	0.00***	39.50

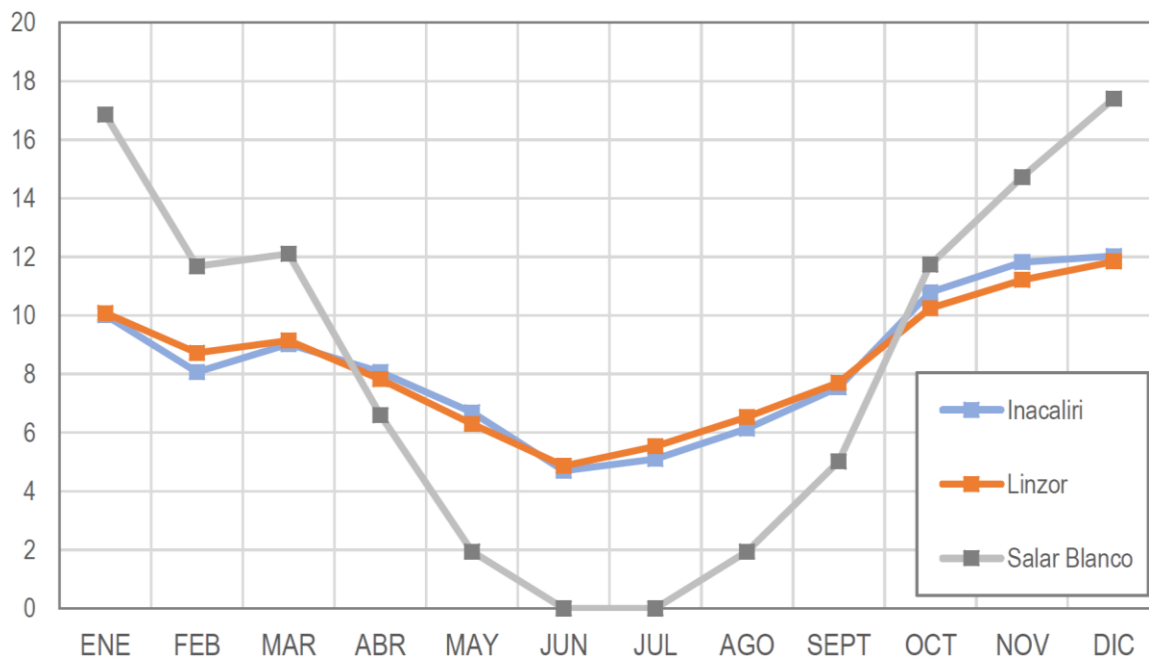
* Rain only, snow fell but was not registered.

**Fallen as snow, transformed at 0,1 ratio to liquid.

*** Freezed evaporimeter

Source: MSB

Figure 5-11: Monthly Distribution of Average Annual Pan Evaporation (% of total)



Source: Flosolutions (2018)

5.4 LOCAL RESOURCES

Local resources are absent at the salar. Copiapó is a major regional mining center and with a wide range of mining, machinery, construction and related services readily available.

5.5 INFRASTRUCTURE

Road infrastructure in the project area includes routes Ch - 31 and C - 173, but for environmental reasons, only the latter will be used by the Project. Route C -173 is a well-maintained road with heavy haul traffic and is mainly used by the Codelco Mine El Salvador. Other infrastructure in the area includes an electrical power line running parallel to route Ch-31, all the way to the border crossing with Argentina. At the northend of the salar there is a customs office that is staffed on a 24-hour basis.

Copiapó is a major city and provides a full range of services. Copiapó is serviced by multiple daily flights to Santiago and other major cities in Chile. The port of Caldera is located approximately 80 km west of Copiapó. The port has excellent docking facilities for general cargo, liquid fuel unloading and bulk cargo. The port of Chañaral is located approximately 250 km west from the salar.

6. HISTORY

6.1 CORFO (1980's)

CORFO, under the aegis of the Comité de Sales Mixtas, (CORFO, 1982) conducted a major study of the northern Chilean salars in the 1980s with the objective of determining the economic potential for production of potassium, lithium, and boron. CORFO undertook systematic hydrogeological and geological studies and sampling of the various salars. Exploration work at Salar de Maricunga consisting of sampling shallow pits (50 cm deep) covered the northern half of the Salar. It was determined that the phreatic level of the brine was at 15 cm below the Salar surface. Estimates of contained mineral resources were developed based on the assay results and assuming a constant porosity of 10 % down to a 30 m depth. CORFO estimated lithium metal resources in Salar de Maricunga at 224,300 tonnes. This estimate does not comply with NI 43-101 standards.

In spite of the above work, CORFO currently does not control any mineral rights in Salar de Maricunga but CODELCO, another Chilean Government owned entity, does have mineral rights in this Salar. This is discussed in Chapter 23.

6.2 PRIOR OWNERSHIP AND OWNERSHIP CHANGES

SLM Litio 1 through 6, Chilean corporations, acquired the Litio 1-6 mining claims in 2004.

On May, 2011, Li3 Energy Inc. (Li3 – now Bearing Lithium) through its 100 % owned Chilean subsidiary Minera Li Energy (MLE) acquired its original interest in the Salar de Maricunga through the purchase of a 60 % interest in SLM Litio 1 through 6 (which are the legal entities holding the Litio 1-6 concessions).

On November 5, 2013, Li3 announced an agreement with BBL SpA (now MSB SpA) for BBL to acquire 51 % (a controlling stake) of MLE in return for specified funding for the company.

On April 16, 2013, MLE acquired 100% of Cocina 19-27 mining concessions.

On August 25, 2014, BBL purchased directly another 36 % interest in SML Litio 1-6 held by another third party. The remaining 4% interest in the Litio 1-6 claims is still held by a third-party individual.

On December 30, 2014, BBL acquired the option to buy the San Francisco, Despreciada and Salamina concessions to a local group (the Padilla Family).

On September 2, 2015, BBL changed its name to Minera Salar Blanco SpA. During December 2015, Minera Salar Blanco SpA acquired directly the Blanco and Camp mining concessions.

In 2016 MSB SpA (former BBL SpA), MLE and, Lithium Power International Ltd. agreed to form a new company, Minera Salar Blanco S.A. (MSB) to continue the development of the Blanco Project. At the same time, MSB SpA and Li3, shareholders of MLE, agreed to dissolve MLE. As a result, the ownership structure of MSB ended up with; LPI 50 %, Minera Salar Blanco SpA 32.3 %, and

Li3 17.7 %. Through this agreement MSB holds 96 % interest in the Litio 1-6 concessions and 100 % in the Cocina, San Francisco, Despreciada and Salamina, Camp and Blanco concessions.

On December 11, 2016, Bearing Lithium Corp. announced a binding agreement to acquire 100 % of the common shares of Li3, and as a result, assumed Li3's 17.7 % interest in the MSB during 2017.

During August 2018, Minera Salar Blanco SpA. sold 1.3534% of its shares. Both LPI and Bearing Lithium exercised its preferential rights resulting in LPI acquiring 1.00% and Bearing Lithium 0.3534 %. As a result, the current ownership structure of MSB is: LPI 51%, Minera Salar Blanco SpA. 30.98%, and Bearing Lithium 18.02%.

6.3 BRINE EXPLORATION WORK BY PREVIOUS OWNERS

6.3.1 SLM Litio (2007)

SLM Litio carried out an initial exploration program on the Litio 1-6 concessions during February 2007 that consisted of the following components:

58 reverse circulation holes were drilled on a 500 m × 500 m grid to 20 m depth. Holes were 3.5" diameter and cased with either 40 mm PVC or 70 mm HDPE pipe inserted by hand to resistance. 232 brine samples were collected from these holes (using an airlift methodology) at 2 m to 10 m depth and 10 m to 20 m depth. The brine samples were analysed by Cesmec in Antofagasta.

No NI 43-101 compliant resource estimate was prepared by SML Litio.

6.3.2 MLE / Li3 - Resource Evaluation Program (2011/2)

Li3 carried out an initial brine resource investigation program on the *Litio 1-6* claims during 2011/2 that consisted of the following components:

- Six sonic boreholes (C-1 through C-6) were completed to a depth of 150 m. Undisturbed samples were collected from the sonic core at three-meter intervals for porosity analyses (318 samples). Brine samples were collected during the sonic drilling at three-meter intervals for chemistry analyses (431 primary samples and 192 QA/QC samples). All sonic boreholes were completed as observation wells on completion of drilling. Figure 10-1 shows the location of the six sonic boreholes
- A total of 915 m of exploration RC drilling was carried out for the collection of chip samples for geologic logging, brine samples for chemistry analyses and airlift data to assess relative aquifer permeability. The RC boreholes were completed as observation wells for use during future pumping tests. Two test production wells (P-1 and P-2) were installed to a total depth of 150 m each for future pumping trials.
- A seismic tomography survey was carried out by GEC along six profiles (S1 through S6) for a total of 23-line km to help define basin lithology and geometry.

- Six test trenches adjacent to the sonic boreholes were completed to a depth of 3 m and 24-hour pumping tests were carried out in each trench.
- Evaporation test work was initiated on the Maricunga brine at the University of Antofagasta to evaluate the suitability of conventional brine processing techniques. Test work was also initiated by Li3's strategic partner to evaluate the application of proprietary technology on the recovery of lithium.
- Environmental baseline monitoring of flora, fauna, surface water and groundwater were initiated by consultants GHD.
- A NI 43-101 Technical report (Technical Report on the Maricunga Lithium Project, III Region, Chile, prepared for Li3 Energy by D. Hains and F. Reidel, dated April 17, 2012) was prepared on the lithium and potassium resources of the Litio 1-6 mining claims based on the results of the 2011 work program. Table 6-1 summarizes the resource estimate therein.

Table 6-1: Estimated mineral resources for the Litio 1-6 claims – April 9, 2012

	Lithium		Potassium	
	Measured	Inferred	Measured	Inferred
Area (km ²)	14.38	7.06	14.38	7.06
Depth interval (m)	0-150	150-180	0-150	150-180
Aquifer volume (km ³)	2.157	0.212	2.157	0.212
Avg grade (g/m ³)	50	50	360	360
Lithium metal (tonne)	107,850	10,590		
Potassium (tonne)			776,250	76,320

6.3.3 BBL – AMT Geophysics and Pumping tests (2015)

BBL carried out a field program during 2015 that consisted of the following components:

- An AMT / TEM geophysical survey was completed by Wellfield Services along 6 profiles across the Salar covering a total of 75-line km. 383 AMT sounding were collected at 200 m to 250 m station spacing; 15 TDEM soundings were carried out at the end and center of each AMT profile. The purpose of the AMT survey was to help map the basin geometry and the fresh water / brine interface.
- Two long-term pumping tests were carried out on production wells P-1 (14 days) and P-2 (30 days) at 37 l/s and 38 l/s, respectively.

- The results of the 2015 program were reported in “Proyecto Blanco, Informe Técnico, Programa de Pruebas de Bombeo 2015, Análisis y Resultados”, prepared for BBL SpA by FloSolutions in October 2015.

The results of the field program are discussed in further detail in Sections 7 and 9 herein.

6.3.4 MSB - Resource Evaluation Program (2016-2018)

MSB initiated a phased work program in August 2016 to complete a FS and EIA for the Blanco Project. The first phase of this work program consisted of exploration drilling and well testing focused on the *Cocina, San Francisco, Salamina and Despreciada* mining claims. Sections 9 and 10 herein provide a detailed description of the MSB working program.

MSB drilled an additional two sonic holes to depth of 200 m in the Litio 1-6 claims as part of the DFS program in May 2018.

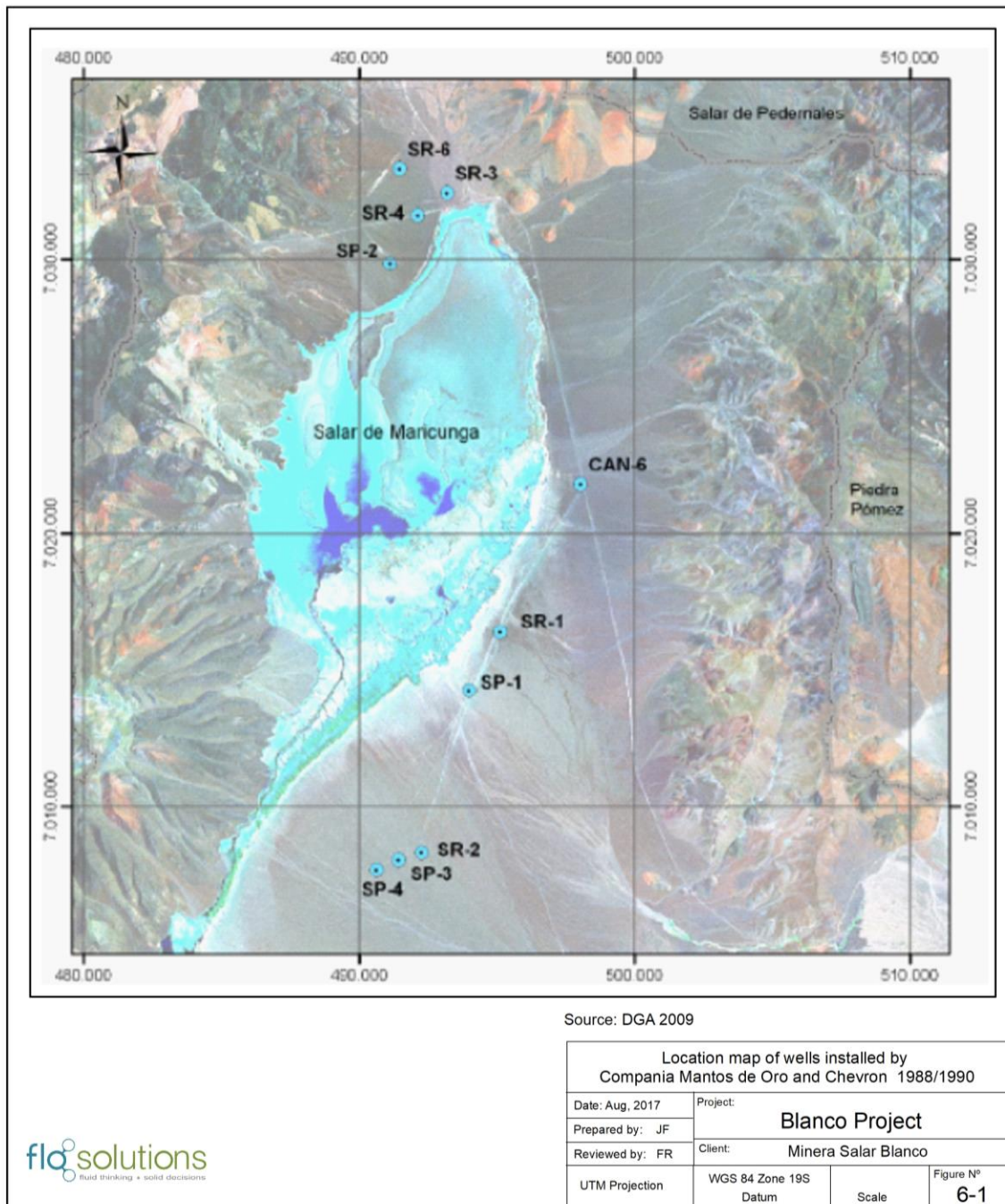
6.3.5 Previous Water Exploration in Salar de Maricunga

A significant amount of hydrogeological and water resources studies has been carried in the Maricunga basin in the past. Below is a list of work and references relevant to this investigation.

- Balance Hídrico de Chile, Dirección General de Aguas, 1987.
- Mapa hidrogeológico de la cuenca Salar de Maricunga: sector Salar de Maricunga, Escala 1:100.000, Región de Atacama. N° Mapa: M62.- Autor: Iriarte D., Sergio. SERNAGEOMIN, 1999.
- Mapa hidrogeológico de la Cuenca Salar de Maricunga: sector Ciénaga Redonda, escala 1:100.000, Región de Atacama. N° Mapa: M65. Venegas, M.; Iriarte, S. y Aguirre, I. SERNAGEOMIN, 2000.
- Geología del Salar de Maricunga, Región de Atacama, Escala 1:50.000. N° Mapa: M54.- Autor: Tassara O., Andrés. SERNAGEOMIN, 1997.
- Ref. 14 Mapa Hidrogeológico de la Cuenca Campo de Piedra Pómez-Laguna Verde.
- Región de Atacama, Escala 1:100.000. N° Mapa: M66.- Autor: Santibáñez I., Venegas M. Formato JPG. SERNAGEOMIN, 2005.
- Geoquímica de Aguas en Cuencas Cerradas: I, II y III Regiones de Chile, Volumen I, Síntesis. S.I.T N° 51, de los autores Risacher, Alonso y Salazar, Convenio de Cooperación DGA – UCN – IRD, 1999.
- Análisis de la Situación Hidrológica e Hidrogeológica de la Cuenca del Salar de Maricunga, III Región. DGA, Departamento de Estudios y Planificación (2006). S.D.T. N° 255.
- Hidrogeología Sector Quebrada Piedra Pómez. EDRA, 1999.

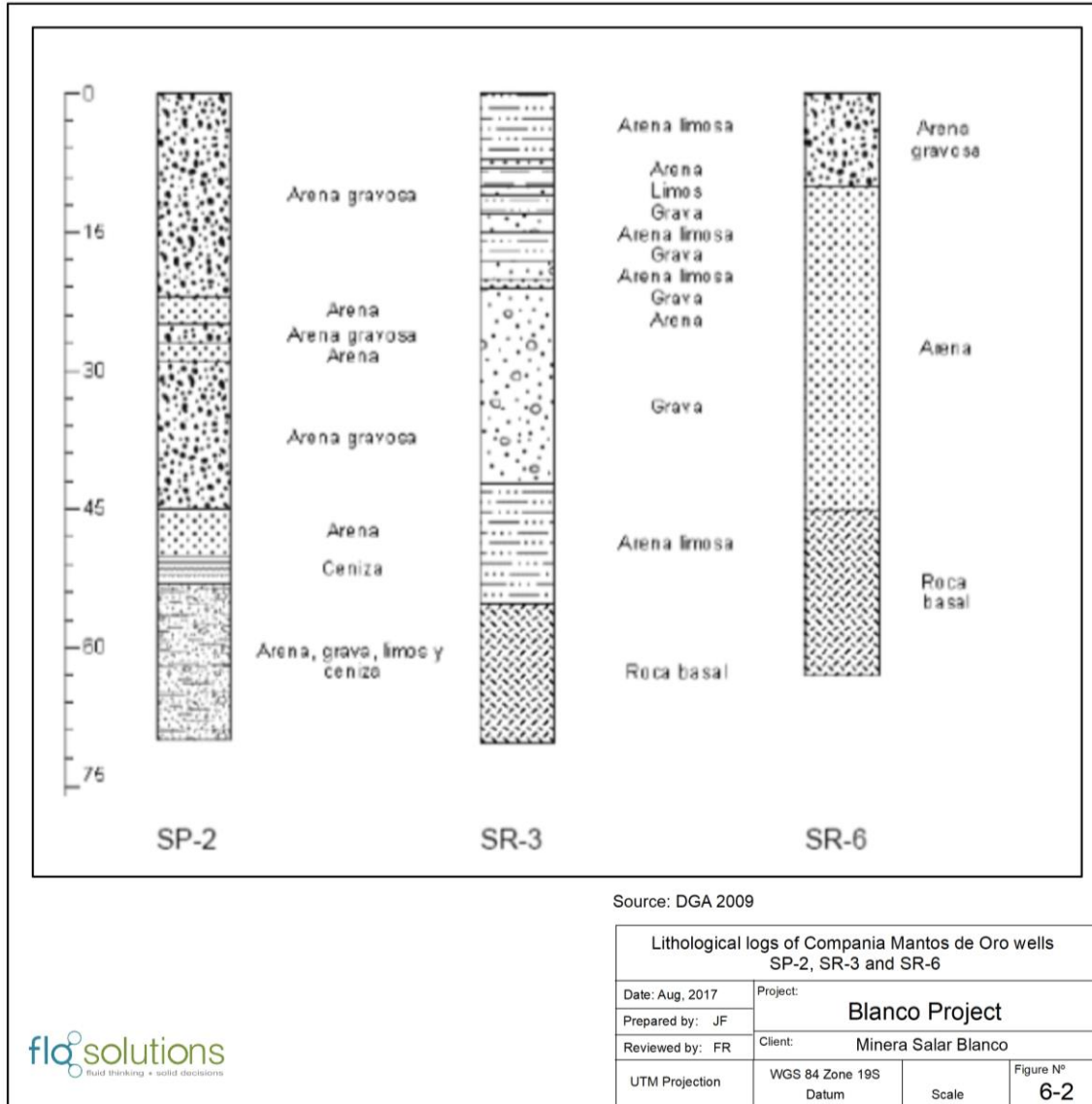
- Evaluation of the Hydrogeological Interconnection between the Salar de Maricunga and the Piedra Pomez Basins, Atacama Region, Chile; An Isotope and Geochemical Approach. Iriarte, Santibáñez y Aravena, 2001.
- Levantamiento Hidrogeológico para el Desarrollo de Nuevas Fuentes de Agua en Áreas Prioritarias de la Zona Norte de Chile, Regiones XV, I, II, y III. Etapa 2 Sistema Piloto III Región Salares de Maricunga y Pedernales. Realizado por Departamento de Ingeniería Hidráulica y Ambiental Pontifica Universidad Católica de Chile (PUC). SIT No. 195, Noviembre 2009.
- Hidrogeología Campo de Pozos Piedra Pómez- Compania Minera Casale; prepared by SRK Consulting; May 2011.
- Línea Base Hidrogeológica y Hidrológica Marte Lobo y Modelo Hidrogeológico Ciénaga Redonda – Kinross Gold Corporation; prepared by Golder Associates, June 2011.
- Compañía Mantos de Oro and Chevron Minera Corporation of Chile carried out several water well drilling campaigns between 1988 and 1990 during which a total of 10 wells were installed around the perimeter of Salar de Maricunga as shown in Figure 6-1. Figure 6-2 and Figure 6-3 show the available lithological logs for these wells.

Figure 6-1: Location map of wells installed by Compañía Mantos de Oro and Chevron 1988/1990



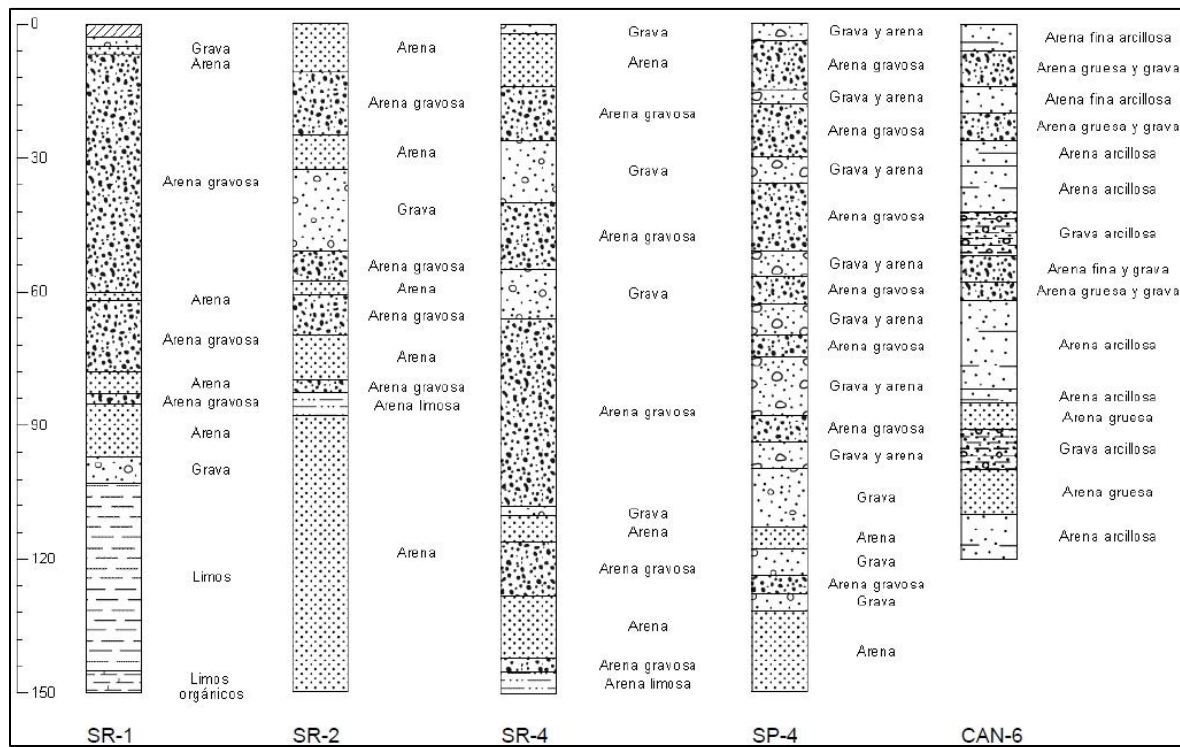
Source: DGA 2009

Figure 6-2: Lithological logs of Compañía Mantos de Oro wells SP-2, SR-3 and SR-6



Source: DGA 2009

Figure 6-3: Lithological Logs of Compania Mantos De Oro Wells SR-1, SR-2, SR-4, SP-4 and Chevron Well Can-6



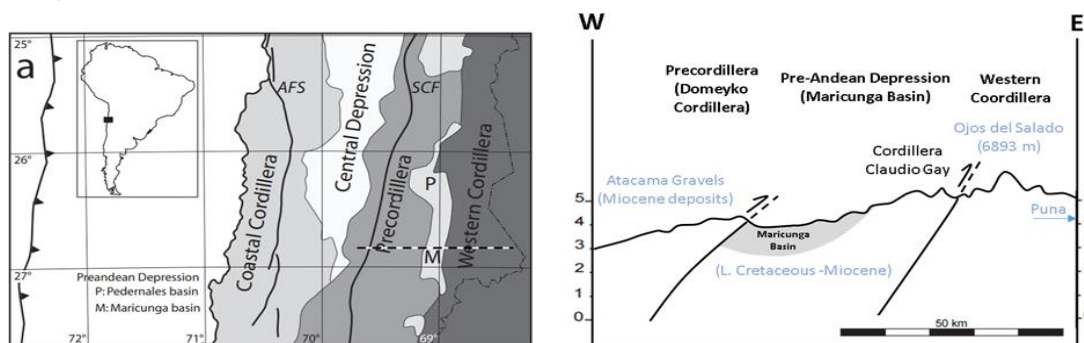
Source: DGA 2009

7. GEOLOGICAL SETTING AND MINERALIZATION

7.1 REGIONAL GEOLOGY

The Andean Cordillera in northern Chile is divided in five (Figure 7-1) well-defined morphotectonic units: The Coastal Cordillera and Central Depression, Precordillera (or Cordillera de Domeyko), Preandean depressions (Pedernales and Maricunga basins) and the Western Cordillera (where the Cordillera Claudio Gay separates the Western Cordillera from the Maricunga Basin). The Coastal Cordillera comprise the eroded remnants of Jurassic-early Cretaceous magmatic arc represented by large plutonic complexes, a Jurassic andesitic to basaltic volcanic sequence (La Negra Formation, Garcia, 1967), and Upper Jurassic-Early Cretaceous andesitic to dacitic lavas (Punta del Cobre Group Lara and Godoy, 1998). The main tectonic feature in the Coastal Cordillera is the Atacama Fault System, which originated in the Jurassic as a "trench-linked" structural system along the axis of the early Andean magmatic arc. Back-arc Jurassic-early Cretaceous marine and continental sedimentary units appear further east in the Precordillera overlying Late Paleozoic igneous basement units (Cornejo et al., 1993). To the east, in the Precordillera, the Mesozoic back-arc sediments are intruded by Eocene sub volcanic stocks and porphyries and deformed by the Eocene Sierra del Castillo-Agua Amarga fault and Potrerillos Fault and Thrust Belt (Tomlinson et al., 1994; Mpodozis et al., 1995; Tomlinson et al., 1999) which form part of the regionally important Domeyko Fault system. Finally, The Cordillera Claudio Gay is an uplifted basement block, covered by Eocene-Miocene sedimentary and volcanic sequences (Mpodozis and Clavero, 2002).

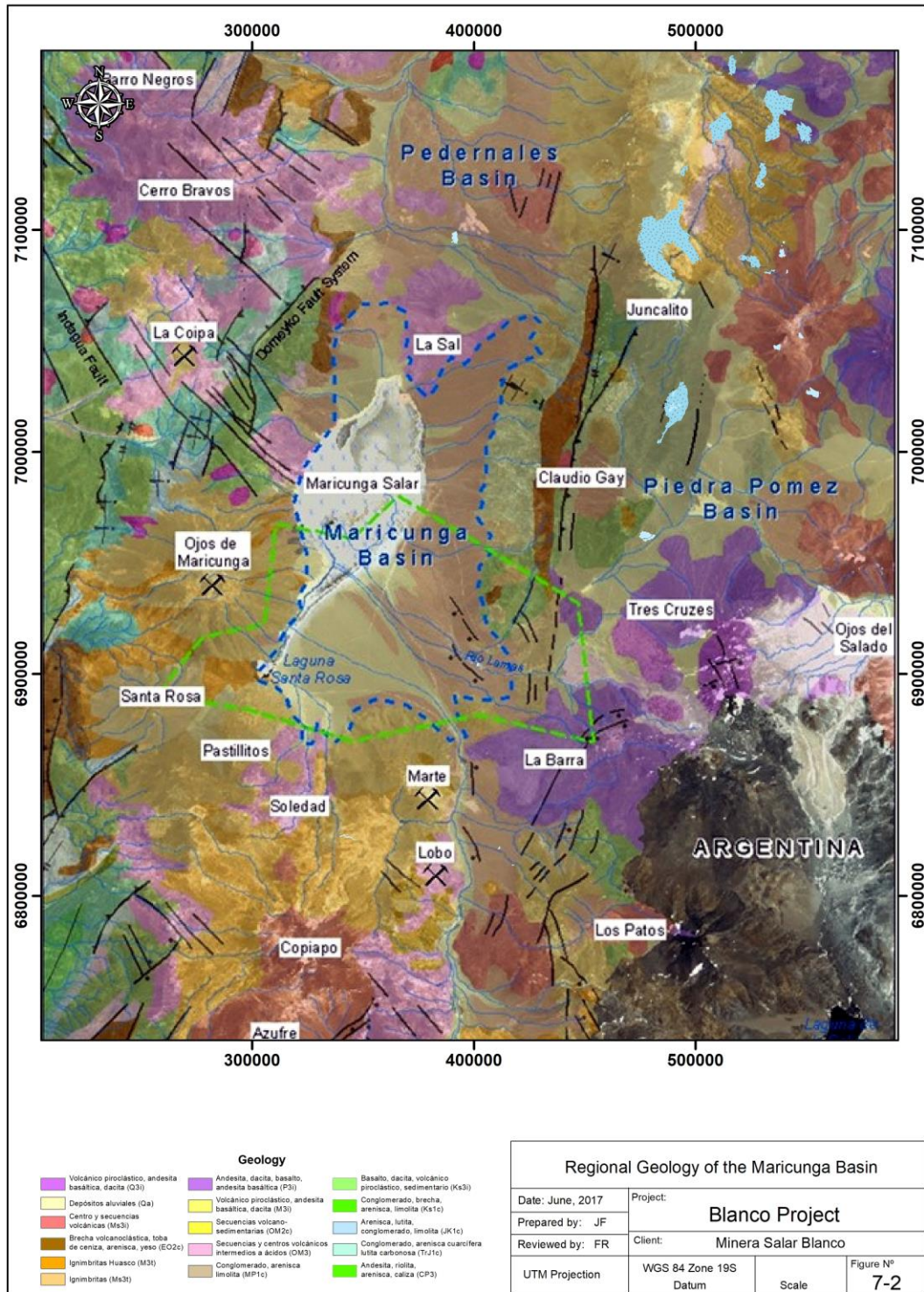
Figure 7-1: Morphotectonic units of the Andean Cordillera in northern Chile



Source: Modified from Nalpas (2008)

The Project is located in the Maricunga Basin within the pre-andean depression. Uplift and denudation should have produced a large amount of sediments during the Cenozoic era. Nevertheless, only the Maricunga and Pedernales Basins preserve a large amount of sediments while in the Precordillera and Central Depression only a thin blanket of Miocene sediments (Atacama Gravels) forms the infill of a Tertiary paleovalley network (Sillitoe et al., 1968; Mortimer 1980; Riquelme, 2003; Gabalda et al., 2005). The geodynamic framework and geological evolution that makes possible the formation, thickening and preservation of the Maricunga basin is presented and summarized in five stages inside the project area as shown in Figure 7-2.

Figure 7-2: Regional geology of the Maricunga Basin



7.1.1 First stage: Pre-Basin evolution (299 to 66 Ma)

The oldest outcrops near the Maricunga basin are related to a Late Paleozoic granitoids and rhyolites in the precordillera and the Claudio Gay cordillera (Mpodozis and Clavero, 2002), they are uplifted basement blocks that are overlain by Devonian to Carboniferous sandstones, shales and mudstones of the Chinchas Formation, abruptly covered by Triassic deposits corresponding to the continental El Mono Beds (Mercado 1982; Corneto et al. 1998), consisting of a thick succession of breccias and conglomerates with rhyolitic and andesitic clasts, and intercalations with huge boulders (1 m in diameter), laminated black carbonaceous lacustrine shale and sandstones containing Triassic fauna, and matrix-supported conglomerated and sandstones. This succession is continuous with Early Jurassic marine deposits of the Montandón Formation.

Other Mesozoic formations are described near as the Pantanoso Formation or El Leoncito sequence. The Mesozoic cover is formed by sedimentary rocks, mainly arkosic sandstones and carbonaceous black shales of the late Triassic La Ternera Formation (Brüggen, 1950), Jurassic marine limestone and volcanic rocks of the Lautaro Formation, sandstone of the late Jurassic to early Cretaceous Quebrada Monardes Formation, and volcanoclastic rocks of the late Cretaceous Quebrada Seca Formation. The Mesozoic cover is capped by andesitic breccias and agglomerates of late Cretaceous to early Tertiary age.

7.1.2 Second stage: Early volcanic episode (66 to 21 Ma)

During this stage occurred the earliest volcanic episode of the Maricunga arc. This volcanic event erupted over a moderately dipping subduction zone through a crust that was likely near 40 km thick. These centers mark the frontal arc west of the backarc basalt. This is seen in the Cerros Bravos–Barros Negros centers that are located along a NW-trending sinistral strike-slip faults that are part of the Domeyko Fault System (Cornejo et al., 1993; Mpodozis et al., 1995; Tomlinson et al., 1999). K/Ar ages from these centers range from 25 to 21.7 Ma (Mpodozis et al., 1995; Tomlinson et al., 1999). Many of the dome complexes and associated tuff and pyroclastic breccia rings are hydrothermally altered. Epithermal, high-sulfidation, gold-silver and porphyry-style gold mineralization occurred during this stage at La Coipa, Esperanza, and La Pepa (Vila and Sillitoe, 1991; Mpodozis et al., 1995; Muntean and Einaudi, 2001).

Activity at the Cerros Bravos–Barros Negros centers began with the eruption of small-volume rhyodacitic ignimbrites that were subsequently covered by main stage pyroxene and hornblende-andesitic lava and block and ash deposits. Crystal-rich hornblende and dacitic domes were then emplaced in the cores of the stratovolcanoes. A series of subcircular domes that host the Esperanza epithermal gold and silver deposit (Vila and Sillitoe, 1991; Moscoso et al., 1993) were emplaced in an 8-km long belt along a reactivated NW-trending fault zone (Cornejo et al. 1993) on the northeastern flank of Cerros Bravos. The domes at Esperanza are surrounded by rhyolitic lapilli tuffs with K/Ar ages ranging from 24 to 20 Ma. Alteration ages range from 23 to 19 Ma (Sillitoe et al. 1991; Moscoso et al. 1993). The northeastern most domes are intruded by unaltered dacitic porphyry dikes with biotite K/Ar ages of 22.5 and 22.4 Ma (Cornejo et al., 1993; Kay et al., 1994).

A few kilometers at the south of Cerro Bravos, a multistage dome complex was emplaced at La Coipa. This complex is located where west-verging, north-trending thrusts (Domeyko Fault System) intersect the sinistral northwest-trending (Quebrada Indagua fault). The La Coipa dome cluster K/Ar ages range from 24.6 to 22.9 Ma (Zentilli 1974; Moscoso et al., 1993). The domes are surrounded by an extensive coeval blanket of intensely altered, coarse pyroclastic breccias, and poorly welded lapilli tuffs with biotite K/Ar ages of 24.7 and 24.0 Ma. Volcanism in the La Coipa region ended with the emplacement of middle Miocene domes (Mpodozis et al., 1995).

7.1.3 Third stage: Compressional and crustal thickening (21 to 17 Ma)

This stage begins with a virtual volcanic lull during a period of compressional deformation and crustal thickening. Evidence for compressional deformation is seen in the Cordillera Claudio Gay (Mpodozis and Clavero, 2002). The depositional regime changed dramatically as east-verging, high-angle reverse faults uplifted the Late Paleozoic basement of the Cordillera Claudia Gay. Intense volcanism followed as large 20–19 Ma dome complexes with extensive block and ash-flow aprons erupted along the northern Cordillera Claudio Gay. These domes are covered by the widespread 18–19 Ma dacitic ignimbrite that has been correlated with the huge Rio Frio ignimbrite (Cornejo and Mpodozis, 1996). All these volcanic deposits are the base of the Maricunga basin.

In the middle Miocene, the Claudia Gay Cordillera was affected by the last compressional deformation in the region of the modern pre-Andean depression. Evidence for this deformation comes from the alluvial gravels interbedded with distal ignimbrites (K/Ar age of 15–16 Ma) in the Rio Lamas sequence. These gravels show progressive unconformities and intraformational folds indicative of synsedimentary deformation (Gardeweg et al., 1997; Mpodozis and Clavero, 2002).

7.1.4 Fourth stage: Stratovolcanic complexes (17 to 11 Ma)

The fourth stage was marked by the construction of voluminous, andesitic to dacitic stratovolcanic complexes along the length of the Maricunga arc. From north to south, these centers include the Ojos de Maricunga, Santa Rosa, Pastillitos volcanoes and which were emplaced during the initial stages at some centers. Most centers are little eroded and preserve much of their original form. The third stage ended with the emplacement of structurally controlled, shallow-level, quartz-dioritic stocks hosting gold and copper mineralization (Marte, and Lobo, gold porphyries; Vila and Sillitoe, 1991).

The largest group of middle Miocene volcanic centers in the Maricunga Belt is the cluster of stratovolcanoes to the west and south of the Salar de Maricunga. The northernmost of these centers is the well-preserved Ojos de Maricunga volcano (4,985 m) with a basal diameter of 15 km and a central crater filled by a dacite dome dated at 15.8 ± 0.9 Ma (whole-rock K/Ar; Mpodozis et al., 1995). The slopes of the volcano are covered by unconsolidated hornblende andesite block and ash deposits that have yielded K/Ar ages from 16.2 ± 0.6 to 15.1 ± 0.7 Ma (Zentilli, 1974; Mpodozis et al., 1995) and a $^{40}\text{Ar}/^{39}\text{Ar}$ age of 14.5 ± 0.1 Ma (McKee et al., 1994). The block and ash deposits overlie two ignimbrites of uncertain origin. The older is a welded red tuff (60 %–62 % SiO_2) that is up to 100 m thick and has a whole-rock K/Ar age of 15.8 ± 0.8 Ma. The younger, which

is exposed on the southwestern slope, is a slightly welded, pumice-rich biotite-bearing ignimbrite with biotite K/Ar ages of 14.3 ± 1.6 Ma and 13.7 ± 2.6 Ma (Zentilli, 1974).

Other middle Miocene volcanic centers to the south are principally made of hornblende- and pyroxene-bearing andesite. They include the Santa Rosa, Cerro Lagunillas, and Pastillitos volcanoes. Blocks from a coarse blanket of reworked pyroclastic block and ash deposits on the slopes of the Santa Rosa cone have K/Ar ages of 15.4 ± 0.55 Ma (hornblende, McKee et al., 1994) and 13.8 ± 0.6 Ma (whole rock, González-Ferrán et al., 1985). Whole-rock K/Ar ages from a Cerro Lagunillas lava, a block from the Pastillitos center, and a Cerro Las Cluecas lava range from 16.2 ± 0.6 to 15.9 ± 1.4 Ma (Mpodozis et al., 1995).

7.1.5 Fifth stage: Volcanic arc migration (11 to 4 Ma)

A radical change in the distribution of volcanic centers occurred during this stage as most of the volcanic activity at the north of Laguna Negro Francisco became concentrated in the silicic andesitic to dacitic Copiapó volcanic complex. Volcanic activity in the Maricunga Belt from 11 to 7 Ma was largely restricted to the Copiapó volcanic complex at the intersection of the northwest-trending Valle Ancho– Potrerillos fault system with the Maricunga Belt. The silicic andesitic to dacitic pyroclastic flows, domes, and lavas that make up the Copiapó complex cover an area of more than 200 km².

The Ojos del Salado volcanic region is located near the southern termination of the modern Central Volcanic Zone near 27°S latitude. This region is home to the Central Volcanic Zone arc and the late Oligocene to Miocene volcanic centers that erupted in the backarc of the Maricunga arc, which is over 40 km to the west. Between 9 and 6 Ma, the Maricunga arc volcanic activity dramatically decreased and then ceased as volcanism increased significantly in the backarc. By 4 Ma, the main frontal volcanic arc was essentially in the Ojos del Salado region. The distribution, age, and geochemistry of the Ojos del Salado region volcanic rocks reflect complex magmatic-tectonic interactions associated with arc migration, crustal thickening, and uplift (Mpodozis et al., 1996; Kay et al., 2006). Considering the modern subduction geometry and assuming that the magmatic front of the Maricunga arc was located around 100 km above the subducting Nazca slab, a significant portion of the forearc crust and frontal arc lithosphere should have been removed from below this region after 8 Ma (Kay and Mpodozis, 2002; Kay et al., 2006).

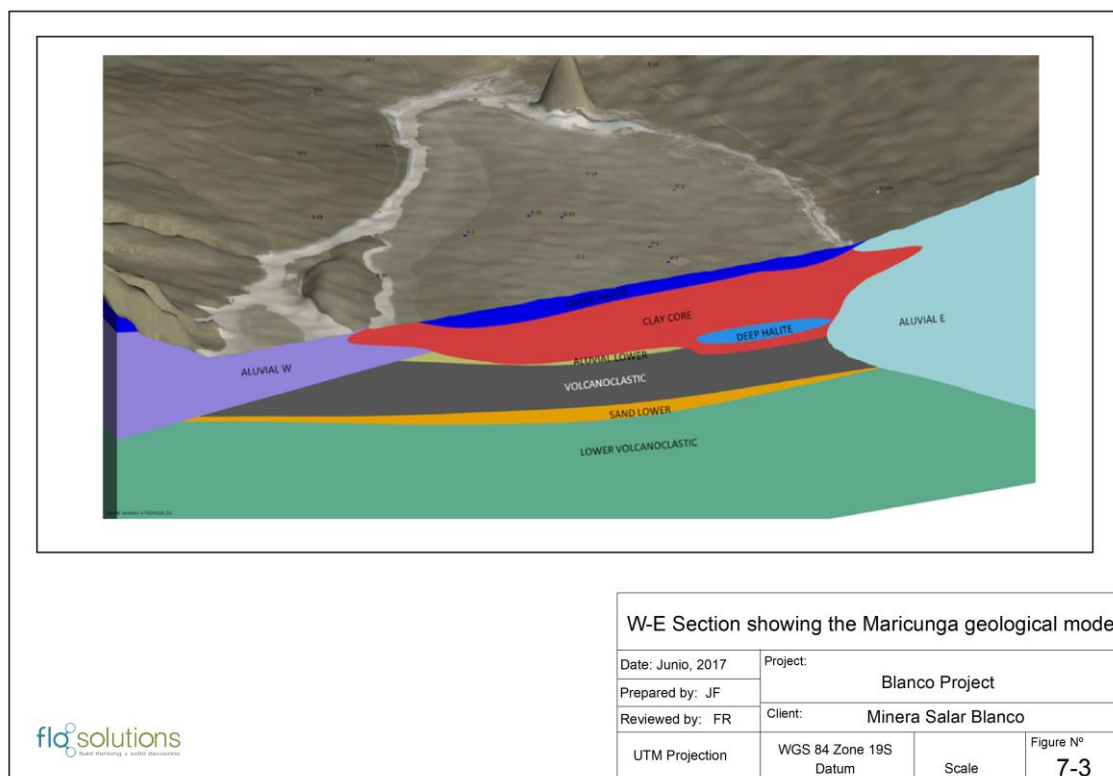
The late Miocene to Pliocene is marked by the eruption of small-volume bimodal centers at the southern end of the Maricunga arc. These eruptions include ignimbrites associated with the fault-controlled Jotabeche rhyodacitic caldera and glassy mafic andesitic to andesitic Pircas Negras lavas emplaced along faults (Mpodozis et al., 1995; Kay et al., 1994). The chemistry (very high La/Yb ratios and Na₂O and Sr contents) of these magmas are uncommon in the central Andes and have been associated with a very thick crust and contamination of the mantle wedge by crustal material removed from the forearc by subduction erosion. Climatic conditions change from 9 to 10 Ma to a hyper-arid climate (Hartley and May, 1998), both sedimentation and erosion came to a halt. This is also attributed to an important change on the mass transfer regime that occurred

between the Oligocene when all the sediments are exported out of the drainage system towards the ocean, and the Miocene, when the sediments started to accumulate along the drainage network (Nalpas et al., 2008).

7.2 LOCAL GEOLOGY

Based on the drilling campaigns carried out in the Salar between 2011 and 2018, ten major geological units were identified and correlated from the detailed geological logging of drill cuttings and undisturbed core to a general depth of 200 m. One deep borehole (S-19) was drilled to a depth of 360 m. No boreholes reached bedrock. Salar de Maricunga is a mixed style salar, with a halite nucleus of up to 34 m in thickness in the central northern part. The halite unit is underlain by a clay core on the eastern and central part of the Salar. The clay is locally interbedded with silt and silty sands. The Salar is surrounded by relative coarse grained alluvial and fluvial sediments. These sedimentary fans demarcate the perimeter of the actual salar and at depth grade towards the center of the Salar where they form the distal facies with an increase in sand and silt. At depth two un-consolidated volcanoclastic units have been identified that appear quite similar. These two volcanoclastics are separated by a relatively thin and continuous sand unit which may be reworked material of the lower volcanoclastic unit. Figure 7-3 is a W-E Section through the Salar schematically showing the geological model.

Figure 7-3: W-E Section showing the Maricunga geological model, looking north



7.2.1.1 Upper Halite

The nucleus of the Salar is comprised of a halite crust. This unit is characterized by coarse translucent crystals (1 to 10 mm) of euhedral halite as shown in Figure 7-4. Locally it has traces of interstitial clay and /or ulexite and minor thin strings of clay with halite.

The halite crust thickens towards the center and north. The halite has a thickness of 30 m in borehole C-2 and 34 m in P-2. Halite pinnacles of up to 60 cm height have developed in the central part of the Salar (Rugosa crust) showing an absence of flooding in this area. In the south (holes S-8 and C-5) the halite unit has a thickness of approximately 1 m; and in the north (holes S-1A, C-1, S-10 and S-19) a thickness of approximately 6 m. Towards the edges of the Salar the crust thins, until it is a saline efflorescence surface that includes areas of re-resolution and precipitation from rainwater or recent flooding. Figure 7-5 is a North-South section through the Salar showing the distribution of the Upper Halite. Figure 7-6 is an isopach map on the Upper Halite showing the thickness of this unit.

Figure 7-4: Photo of the Upper Halite

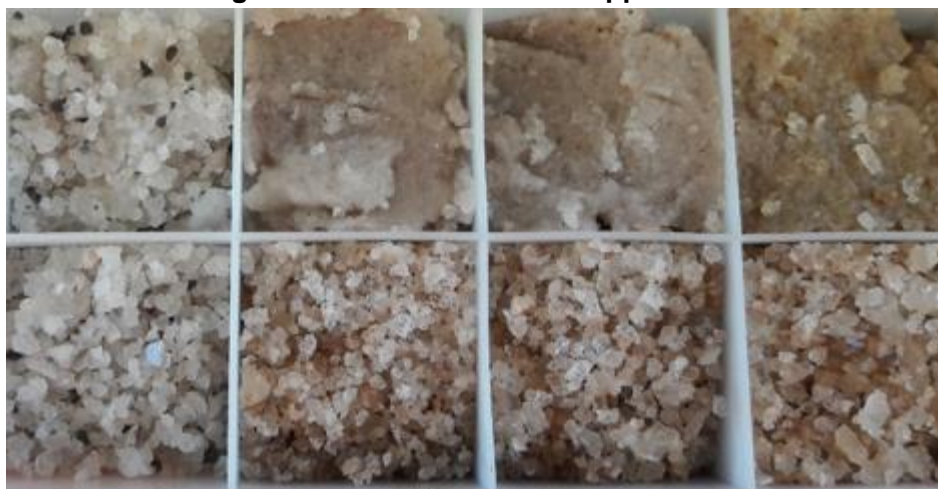


Figure 7-5: N-S Section showing the distribution of the Upper Halite unit

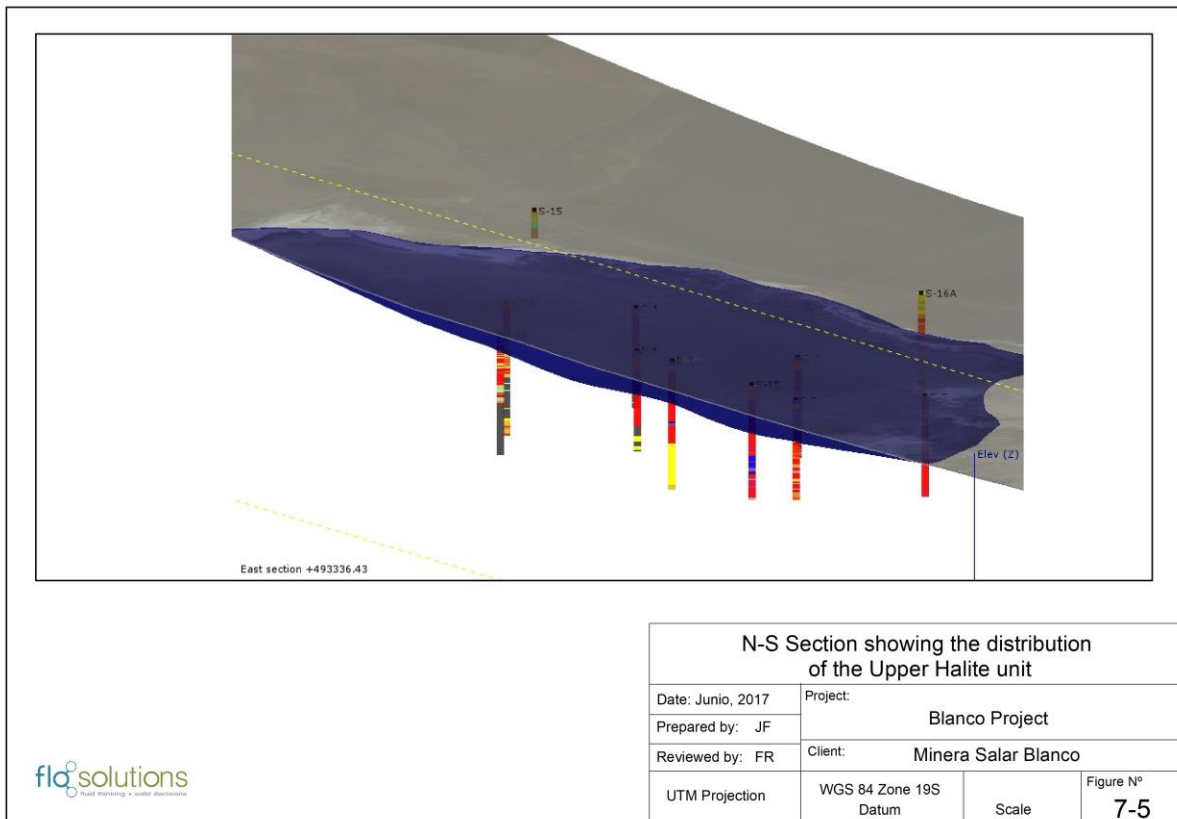
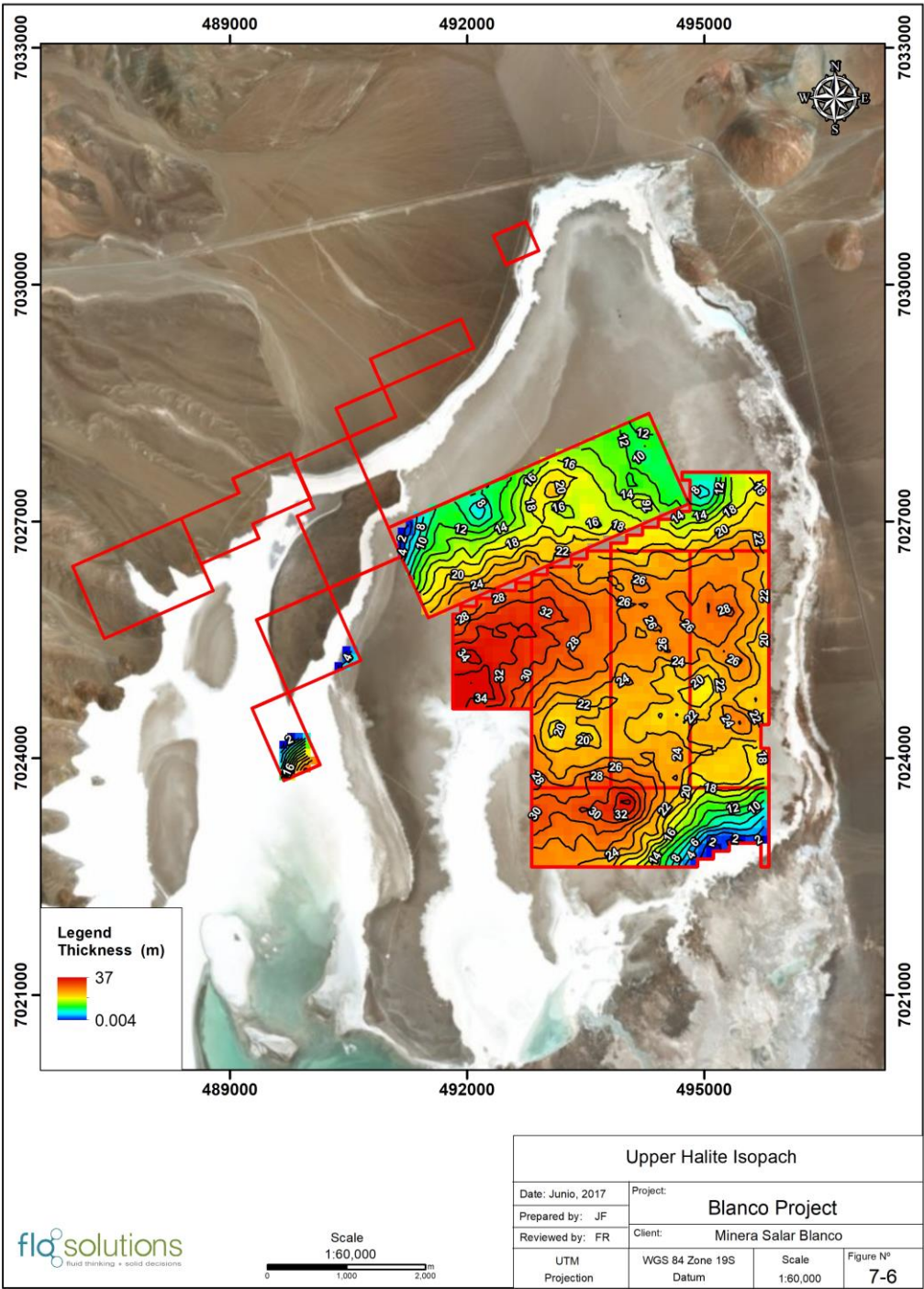


Figure 7-6: Isopach map on the Upper Halite



7.2.1.2 Clay Core

Immediately beneath the Upper Halite unit, a thick clay unit was identified with a thickness of up to 140 m (Hole S-18) and which thins towards the edges of the Salar (Figure 7-7). This Clay Core unit extends below the alluvial sediments on the east side of the basin (the East Alluvium unit as further described below) as identified in hole S-16. Geological logs of previously drilled boreholes (by Minera Mantos de Oro) MDO-08, MDO-10, MDO-24 and CAN-6 suggest that the Clay Core continues as far south as under the Rio Llamas fluvial fan. Figure 7-8 shows an isopach map on the Clay Core.

The clay core is well defined by the sonic boreholes C-1 through C-6 and S-24 in the *Litio 1-6* concessions, although not all holes penetrated the full thickness of the Clay Core. The unit is characterized by reddish, green, brown and in small amounts black clays in horizontal parallel layers with occasional 1 m interbedded layers of ulexite (Figure 7-9). Locally and near the edges of the Salar the Clay Core is intercalated locally with fine layers of sand and towards the center of the Salar with thin layers of halite. At the contact with the overlying Upper Halite the Clay Core contains abundant disseminated halite crystals (up to 50 %).

Figure 7-7: N-S section showing the Clay Core, looking west

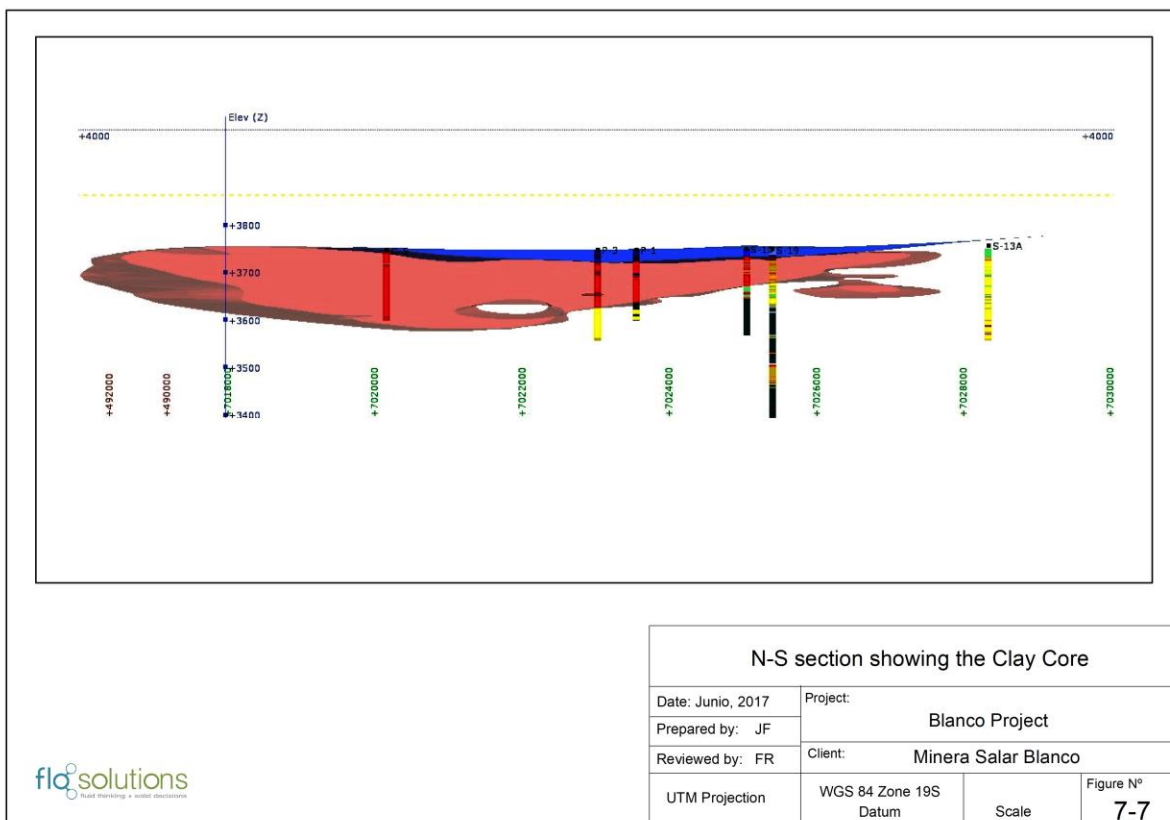


Figure 7-8: Isopach map on the Clay Core

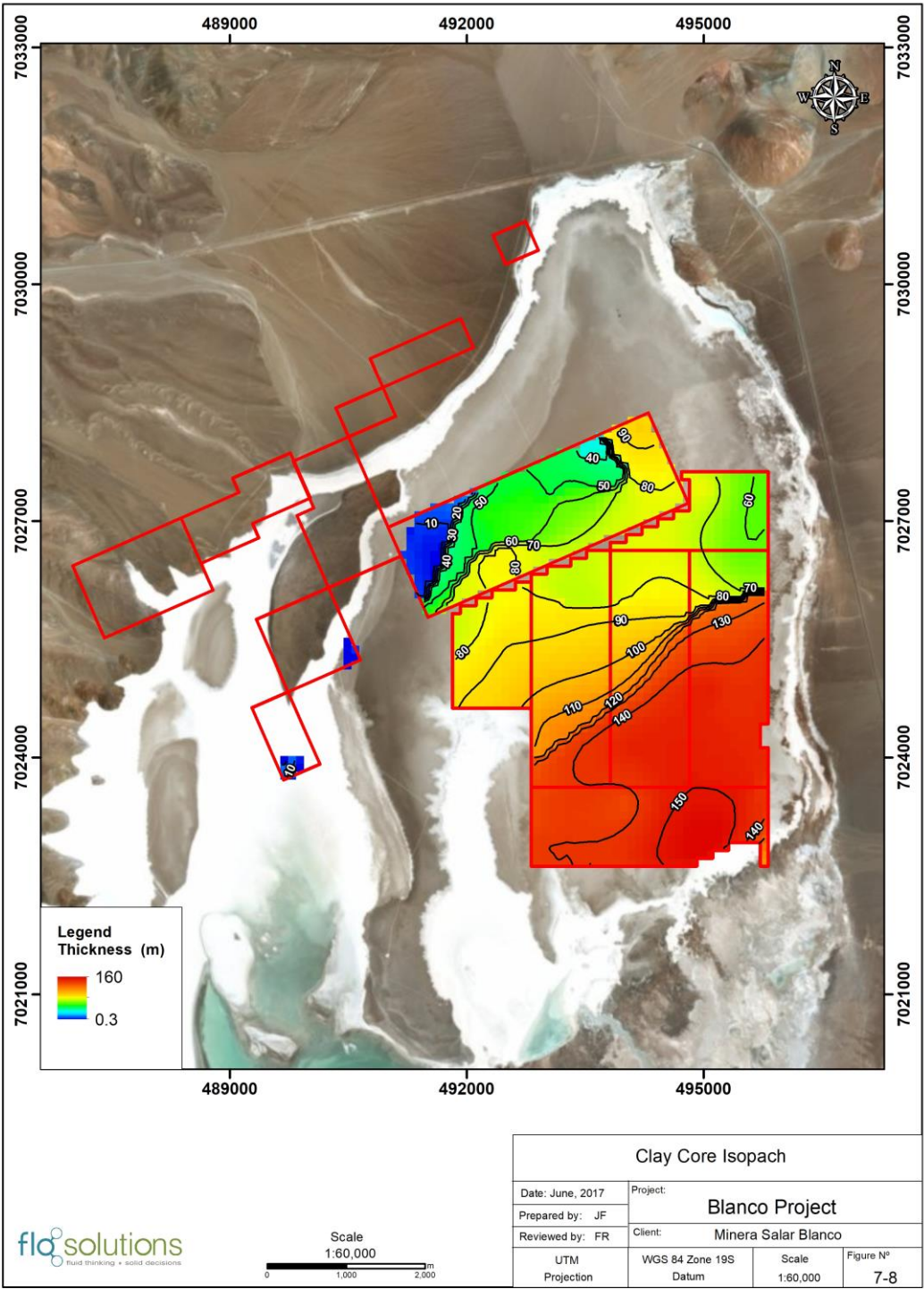


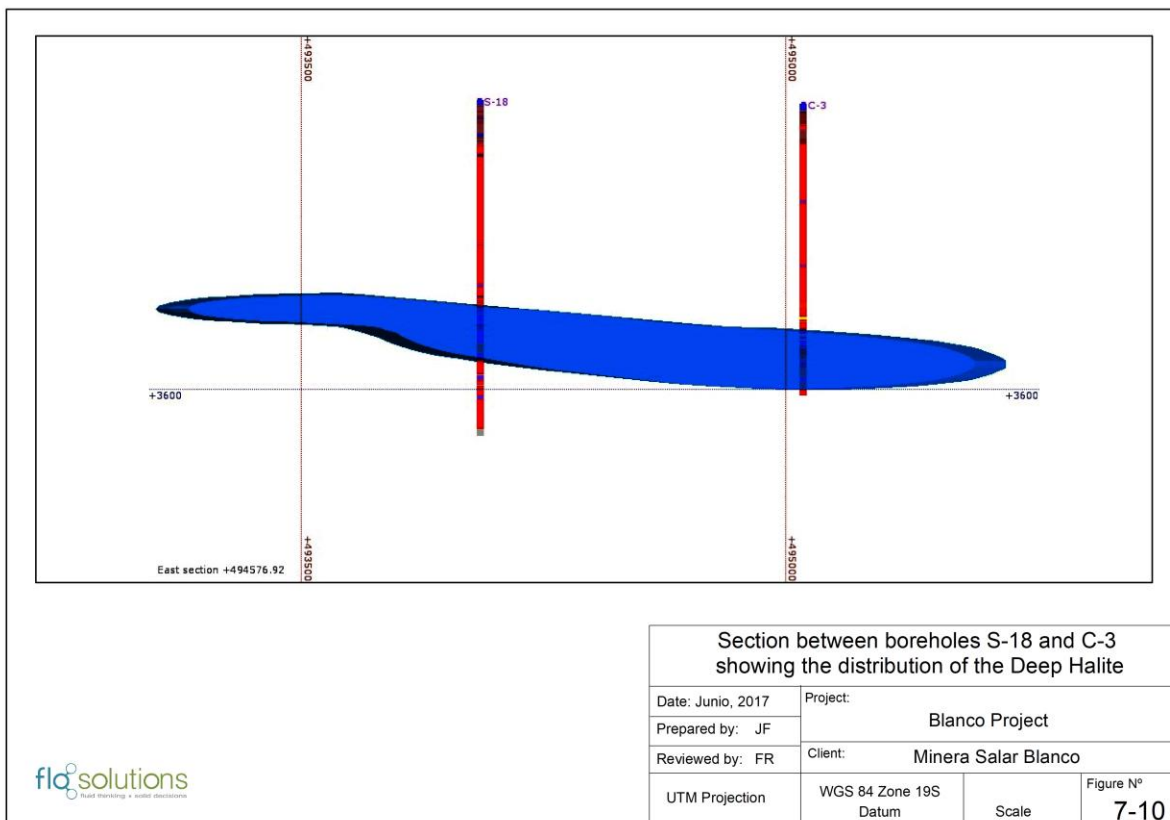
Figure 7-9: Photo of the Clay Core unit



7.2.1.3 Deep Halite

A Deep Halite unit was identified between boreholes S-18 and C-3. This Deep Halite unit has a thickness of up to 20 m and was intersected at a depth of around 110 m; it is entirely contained within the Clay Core unit (Figure 7-10). This unit is characterized by whitish, massive compacted halite with crystals of between 1 to 5 mm with interstitial clay and ulexite. A fine layer of black clay and some ulexite with a thickness of approximately 1 m was also identified in these two boreholes.

Figure 7-10: Section between boreholes S-18 and C-3 showing the distribution of the Deep Halite

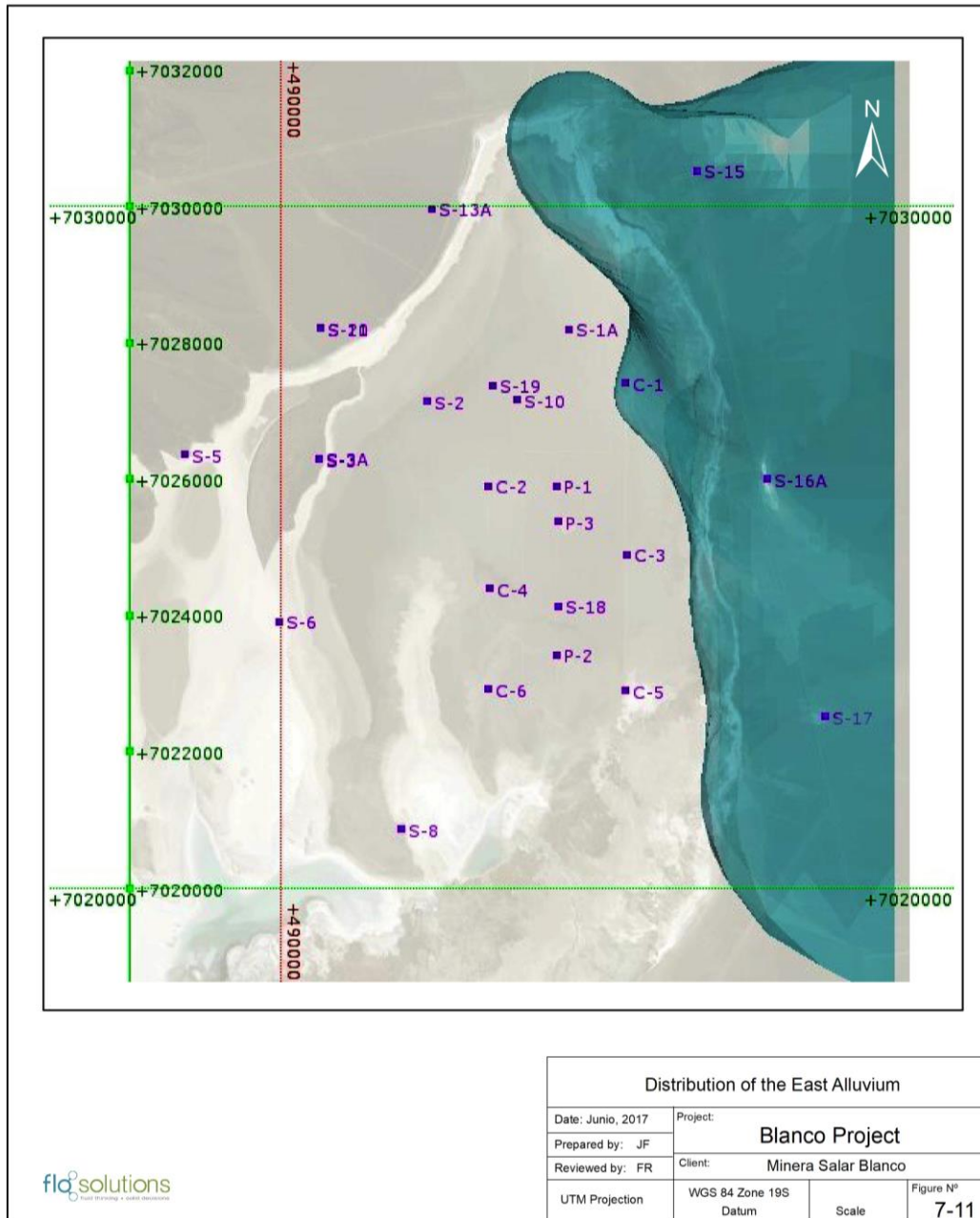


7.2.1.4 East Alluvium

The unit was identified in the boreholes S-15, S-16, S-17 drilled on the east side of the Salar. The East Alluvium is present along the entire eastern side of the Salar and is interbedded with layers of sand. It forms the foothills of the Claudio Gay Range (the eastern limit of the basin). Figure 7-11 shows the lateral distribution of the East Alluvium. In the area of borehole S-16 it is inter-fingered with clays and sands of the Salar's nucleus.

The unit is characterized by a heterogeneous sequence of clayey gravels made up of many sub-rounded clasts of up to 5 cm in a matrix of brown clayey-silty sand and grading at depth into finer-grained layers of brown silty- and clayey sands. At the surface one can find sands (S-16A) and gravels (S-15).

Figure 7-11: Distribution of the East Alluvium



7.2.1.5 NW Alluvium

The northwestern part of the Salar is characterized by a series of W-E fluvial/alluvial fans, associated with recent intermittent drainages and older drainage systems that form the limit of the basin in the area around Quebrada Caballo Muerto. Figure 7-12 shows the lateral extent of the NW Alluvium.

The unit was encountered and correlated between boreholes S-11 [M2], S-13A, S-3A and S-10. The Lower Alluvium (described below) is interpreted as the distal and deep facies of the NW Alluvium. The NW Alluvium is characterized by a sequence of gravels and sandy gravels with rounded and sub-rounded clasts. Locally it can contain layers of coarse- to very coarse sands. Figure 7-13 shows the texture of the NW alluvium.

Figure 7-12: Distribution of the NW Alluvium

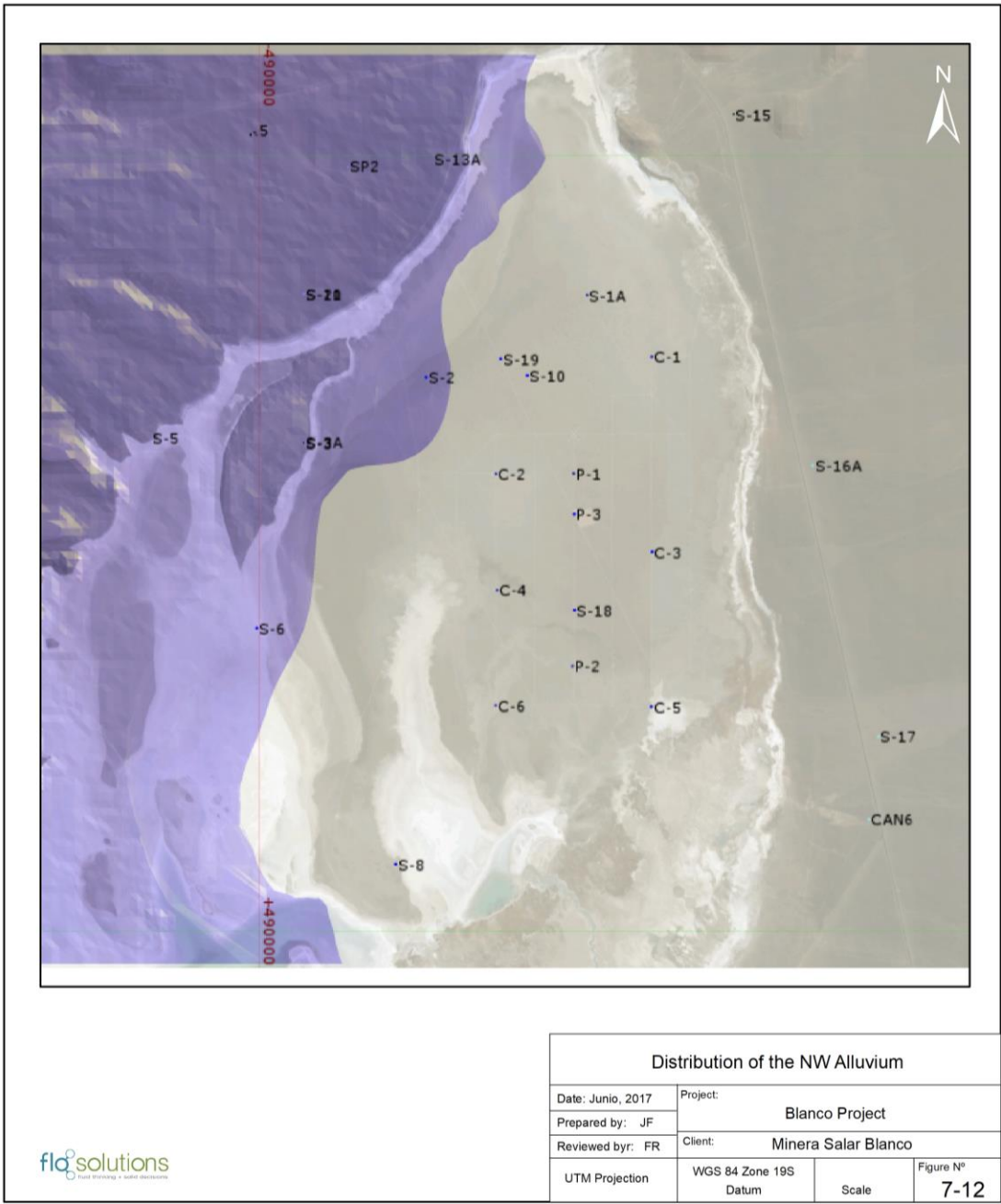


Figure 7-13: The NW Alluvium



7.2.1.6 Lower Alluvium

The Lower Alluvium consists of gravels, sands and silty sands and is spatially interpreted as the distal part of NW Alluvium system that enters the Salar from the northwest. This unit is inter-fingered with the Clay Core further east in the Salar. The Lower Alluvium is interpreted in part as reworked material of the underlying volcanoclastic sequences. The Lower Alluvium was encountered in boreholes S-1A [M1A], S-2, S-10, S-19, C-1, C-2, S-23 y C-4. Figure 7-14 shows the spatial distribution of the Lower Alluvium and Figure 7-15 shows drill cuttings of the Lower alluvium.

Figure 7-14: E-W section with the spatial distribution of the Lower Alluvium

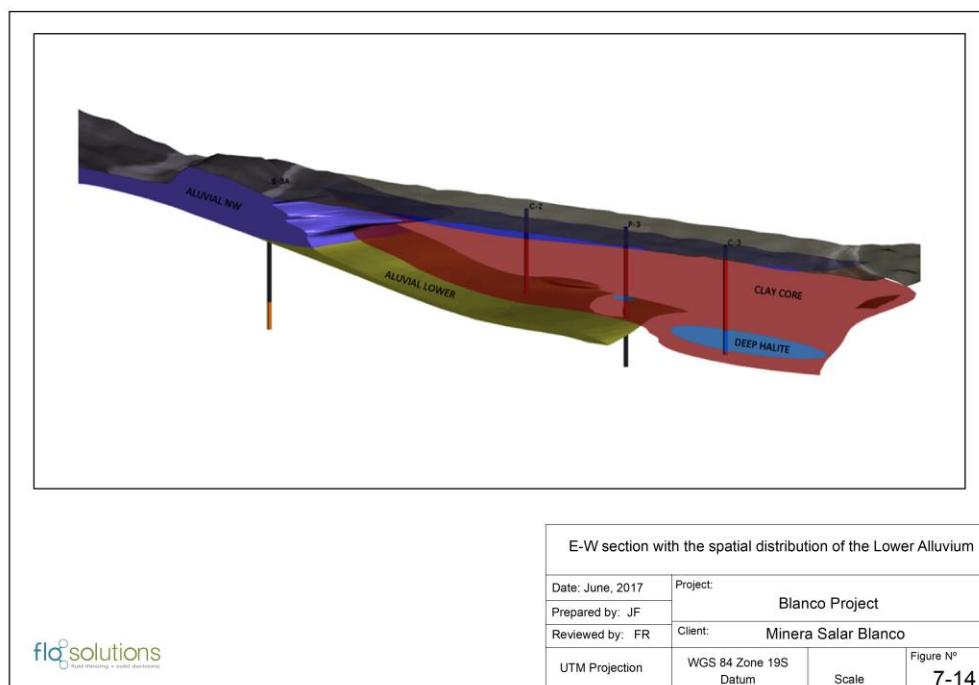


Figure 7-15: Drill core and cuttings of the Lower Alluvium



7.2.1.7 Volcaniclastic

This Volcaniclastics unit is found in numerous wells (C-1, C-2, S-23, S-24, P-1, S-1A, S-2, S-3A, S-5, S-6, S-10, S-11, S-13A and S-19). It is comprised of an array of friable volcaniclastic material, matrix supported, with some 1 to 15 mm isolated grey, brown and reddish sub-angular aphanitic clasts (3-5 %) and abundant whitish pumice fragments in a light brown silty matrix (volcanic ash) as shown in Figure 7-16. The unit is unconsolidated, and it interpreted as a volcanic air-fall deposit.

The unit has a tilted wedge shape distribution with the greatest thickness to the west (borehole S-11: 139 m) and deepening to the east. The spatial distribution of the unit is shown in Figure 7-17 and Figure 7-18 shows an isopach map for the unit.

Figure 7-16: Drill core of the Volcaniclastic material



Figure 7-17: W-E section showing the spatial distribution of the Volcaniclastics

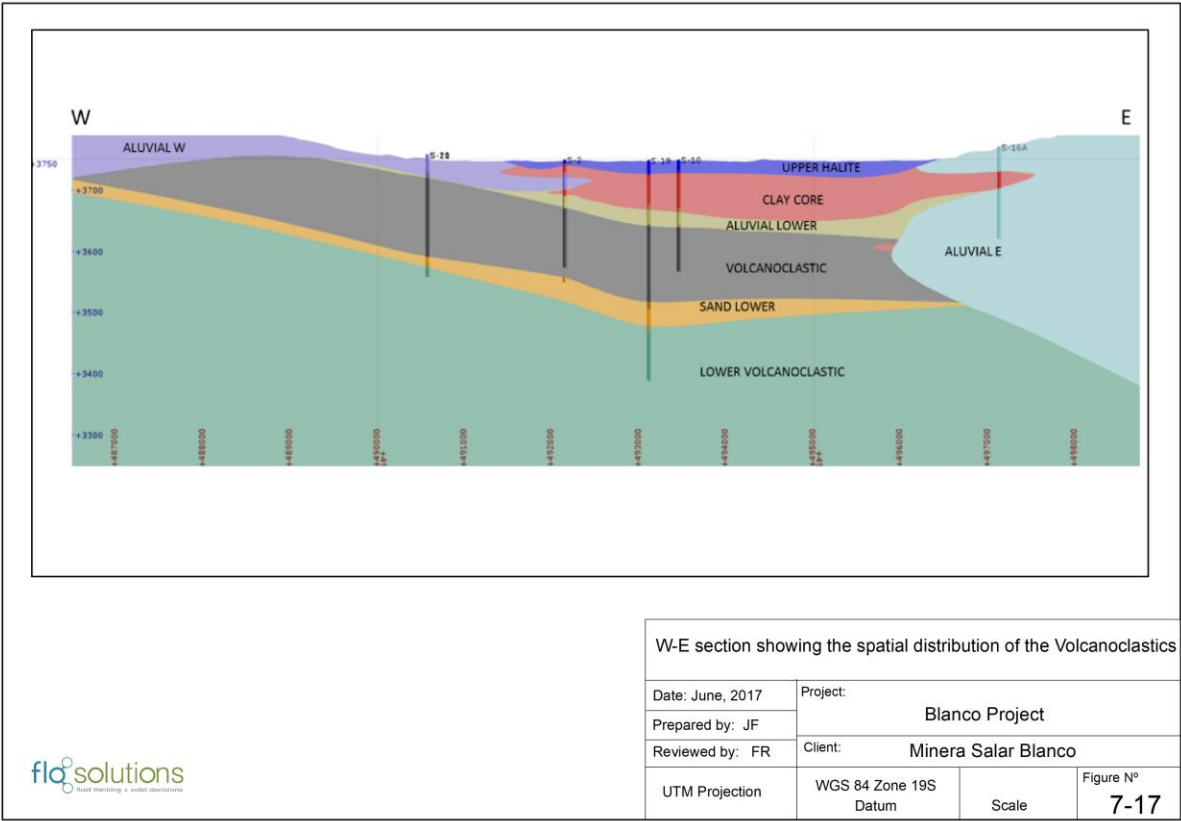
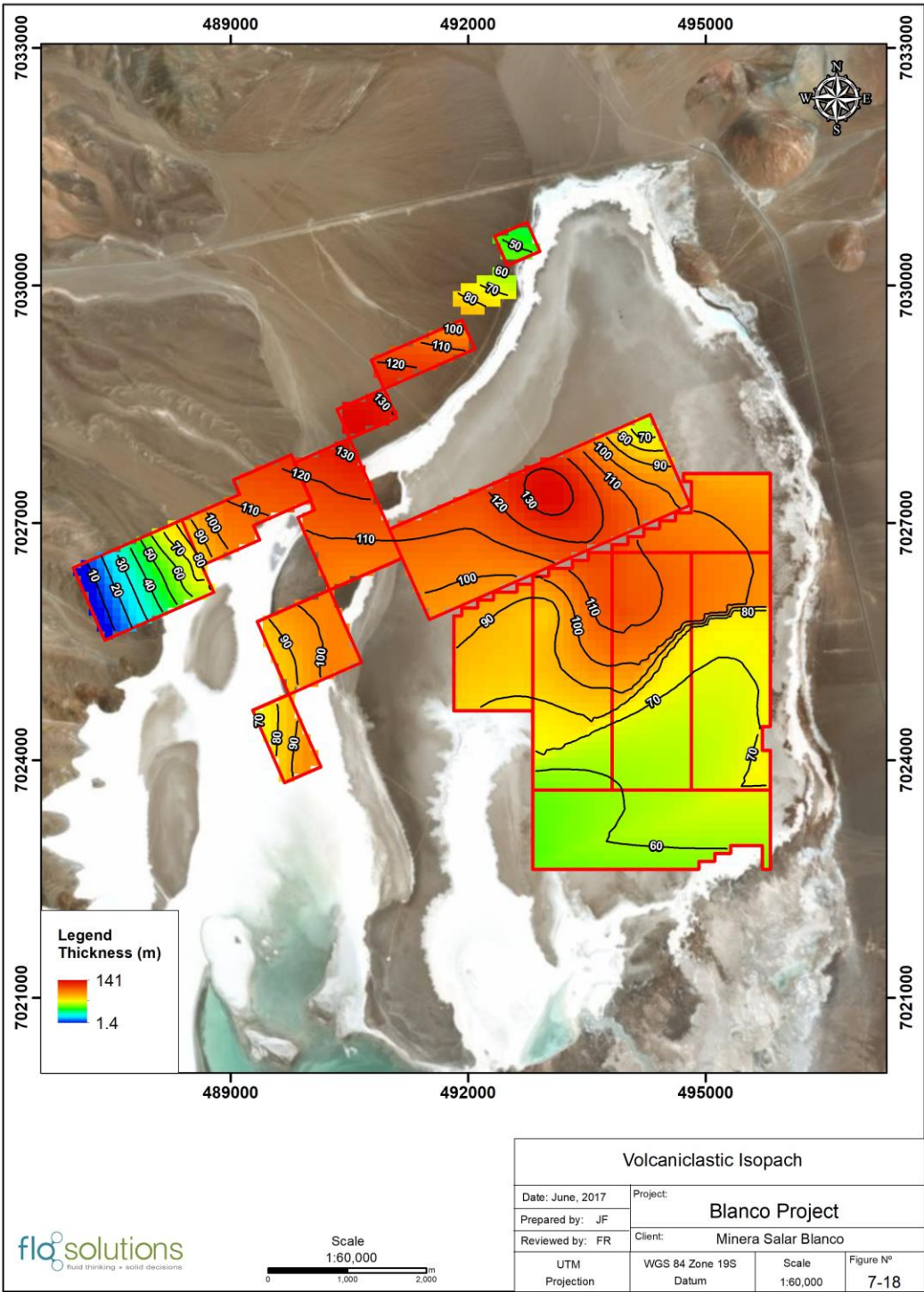


Figure 7-18: Isopach map on the Volcaniclastics Unit



7.2.1.8 Lower Sand

The Lower Sand is a well-defined unit that separates the overlying Volcaniclastic from the Lower Volcaniclastic (describe below). The Lower Sand was identified in boreholes S-1A [M1A], S-3A, S-5, S-6, S-11, S-13A and S-19 and can be interpreted as reworked material of the underlying volcaniclastic sequence, indicating a gap in the eruption. Figure 7-19 shows the spatial distribution and isopach contours on the Lower Sand. The unit consists of fine to medium grained sand and locally it can include fine to coarse sand with traces of silt. Figure 7-20 shows drill cutting of the Lower Sand.

Figure 7-19: Isopach map of the Lower Sand

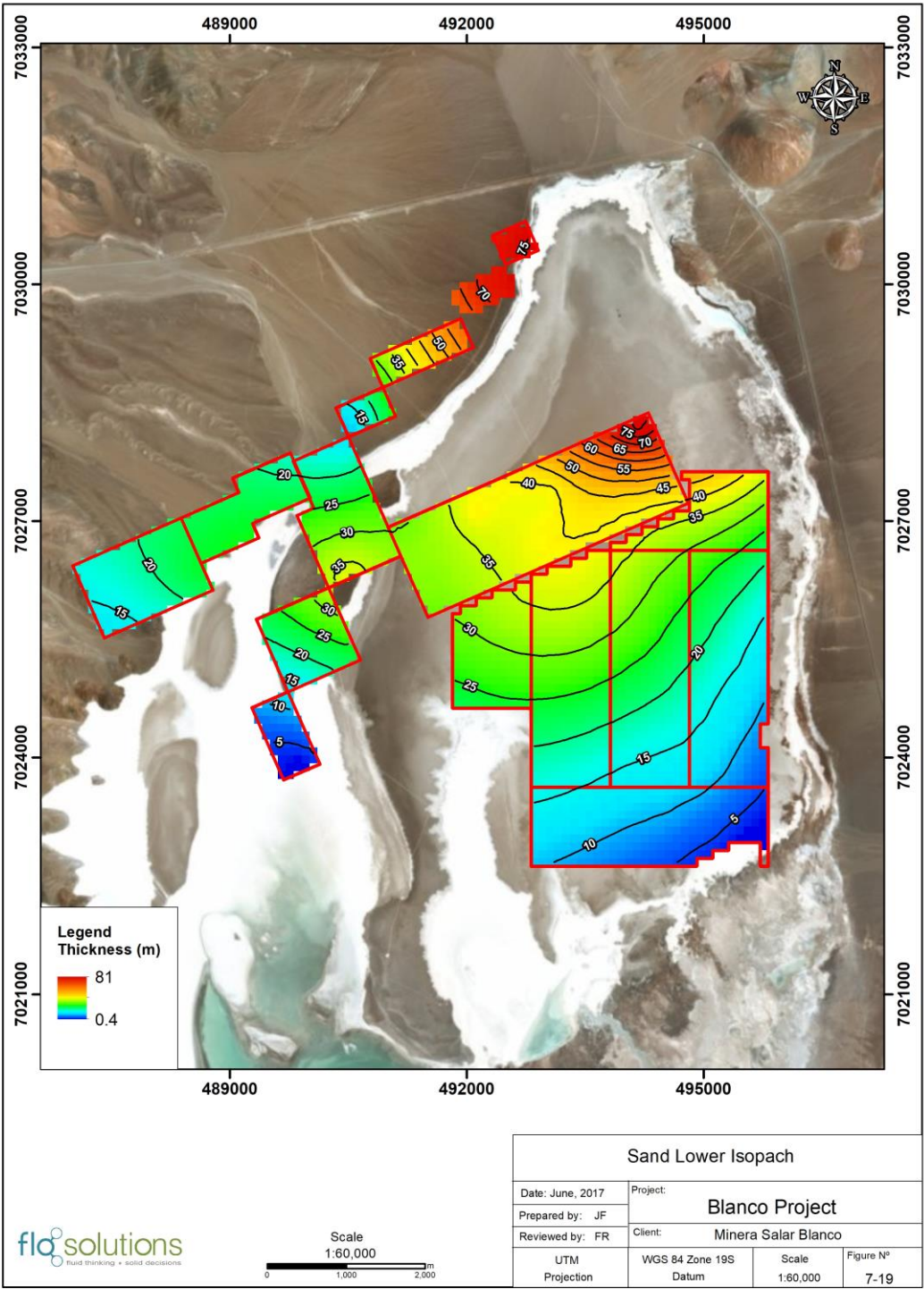


Figure 7-20: Drill cuttings of the Lower Sand (Borehole S-5)



7.2.1.9 Lower Volcaniclastic (LV)

The oldest and deepest unit identified in the Salar consists of volcaniclastics in boreholes S-5, S-6, S-11 and S-19. The unit has a thickness of 78 m in borehole S-19. No borehole has penetrated the full thickness of the LV and therefore its thickness is not known. This LV unit is characterized by a homogeneous sequence of friable volcaniclastics and is very similar in composition to the upper volcaniclastics unit.

7.3 MINERALIZATION

The brines from Maricunga are solutions nearly saturated in sodium chloride with an average concentration of total dissolved solids (TDS) of 311 g/l. The average density is 1.20 g/cm³. The other components present in the Maricunga brine are K, Li, Mg, Ca, SO₄, HCO₃ and B. Moderated values of strontium (mean of 359 mg/l) also have been detected and have been considered in process development.

Table 7-1 shows a breakdown of the principal chemical constituents in the Maricunga brine including maximum, average, and minimum values, based on 651 brine samples used in the brine resource estimate herein that were collected from the drilling programs between 2011 and 2018 and analyzed at the University of Antofagasta.

Table 7-1: Maximum, average and minimum elemental concentrations of the Blanco Project brine

Analyte	HCO ₃ mg/l as CaCO ₃	B mg/l	Ca mg/l	Cl mg/l	Li mg/l	Mg mg/l	K mg/l	Na mg/l	SO ₄ mg/l	Density g/cm ³
Maximum	2,730	1,992	36,950	230,902	3,375	21,800	20,640	104,800	2,960	1.31
Average	471	586	12,853	190,930	1,146	7,462	8,292	85,190	706	1.20
Minimum	76	234	4,000	89,441	460	2,763	2,940	37,750	259	1.10

Figure 14-9 and Figure 14-10 show the kriged lithium and potassium concentration distribution in the Salar at approximate 30 m, 70 m and 130 m depth. Typically, high and low concentrations of lithium and potassium are correlated. The kriged three-dimensional distribution of lithium and potassium concentrations were used in the updated resource model as further described in Section 14.

Brine quality is evaluated through the relationship of the elements of commercial interest, such as lithium and potassium, with those components that in some respect constitute impurities, such as Mg, Ca and SO₄. The calculated ratios for the averaged chemical composition are presented in Table 7-2.

Table 7-2: Average values (g/l) of key components and ratios for the Maricunga brine

K	Li	Mg	Ca	SO ₄	B	Mg/Li	Ca/Li	K/Li
8.23	1.12	7.34	13.49	0.71	0.60	6.55	12.04	7.35

As indicated in Table 7-2, the brines from Maricunga have a Mg/Li ratio (6.6) very similar to the Atacama brine (6.4). However, Maricunga has a low sulfate content, which is also influenced by relatively high calcium content. The advantage of low sulfate brine is that will reduce lithium losses as lithium sulfate salts in the ponds when a conventional solar evaporation process is used to recover the lithium. Treatment of the brine to remove the calcium would make the process similar to that utilized by SQM and Albemarle at Salar de Atacama.

The known phase diagram (Janecke projection) of the aqueous quinary system (Na⁺, K⁺, Mg⁺⁺, SO₄⁼, Cl⁻) at 25 °C and saturated in sodium chloride (equilibrium data in the technical literature) can be used when adjusted for the presence of lithium in the brines. The Janecke projection of MgLi₂-SO₄-K₂ in mol % is used to make this adjustment. The Maricunga brine composition has been represented in this diagram (field of KCl), as shown in Figure 7-21 along with brine compositions from other salars. The Maricunga brine composition is compared with those of Silver Peak, Salar de Atacama, Salar del Hombre Muerto, Salar de Cauchari, Salar de Rincon and Salar de Uyuni in Table 7-3. This indicates that the salts that will crystalize during solar evaporation process are mainly halite, sylvinite and carnallite.

Figure 7-21: Comparison of brines from various salars in Janecke Projection

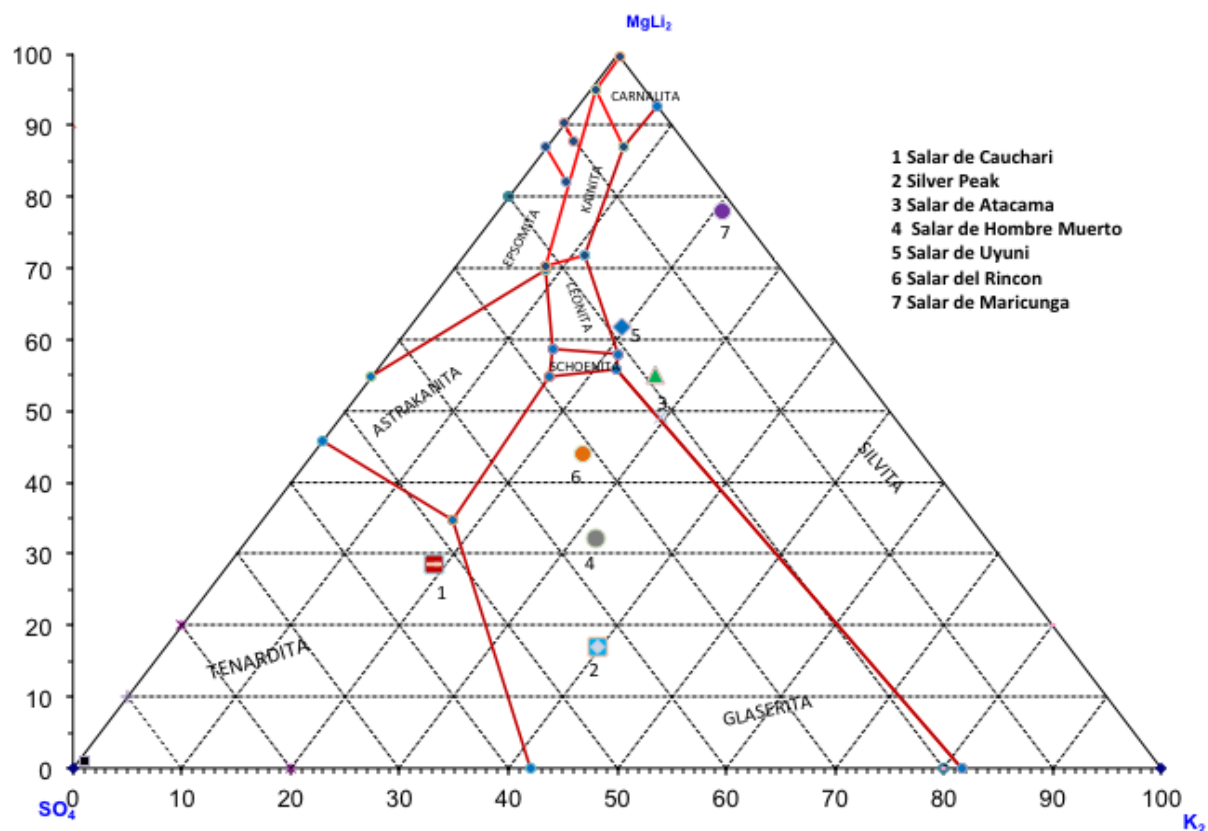


Table 7-3: Comparative chemical composition of various salars (weight %)

	Salar de Maricunga (Chile)	Silver Peak (USA)	Salar de Atacama (Chile)	Hombre Muerto (Argentina)	Salar de Cauchari (Argentina)	Salar del Rincon (Argentina)	Salar de Uyuni (Bolivia)
Na	7.10	6.20	7.60	9.79	9.55	9.46	8.75
K	0.686	0.53	1.85	0.617	0.47	0.656	0.72
Li	0.094	0.023	0.150	0.062	0.052	0.033	0.035
Mg	0.61	0.03	0.96	0.085	0.131	0.303	0.65
Ca	1.124	0.02	0.031	0.053	0.034	0.059	0.046
SO ₄	0.06	0.71	1.65	0.853	1.62	1.015	0.85
Cl	15.91	10.06	16.04	15.80	14.86	16.06	15.69
HCO ₃	0.039	n.a.	Traces	0.045	0.058	0.030	0.040
B	0.050	0.008	0.064	0.035	0.076	0.040	0.020
Density	1.200	n.a.	1.223	1.205	1.216	1.220	1.211
Mg/li	6.55	1.43	6.40	1.37	2.52	9.29	18.6
K/Li	7.35	23.04	12.33	9.95	9.04	20.12	20.57
SO ₄ /Li	0.64	30.87	11.0	13.76	31.06	31.13	24.28
SO ₄ /Mg	0.097	23.67	1.72	10.04	12.33	3.35	1.308
Ca/Li	9.5	0.87	0.21	0.86	0.65	1.79	1.314

Source: Published data from various sources

8. DEPOSIT TYPE

8.1 GENERAL

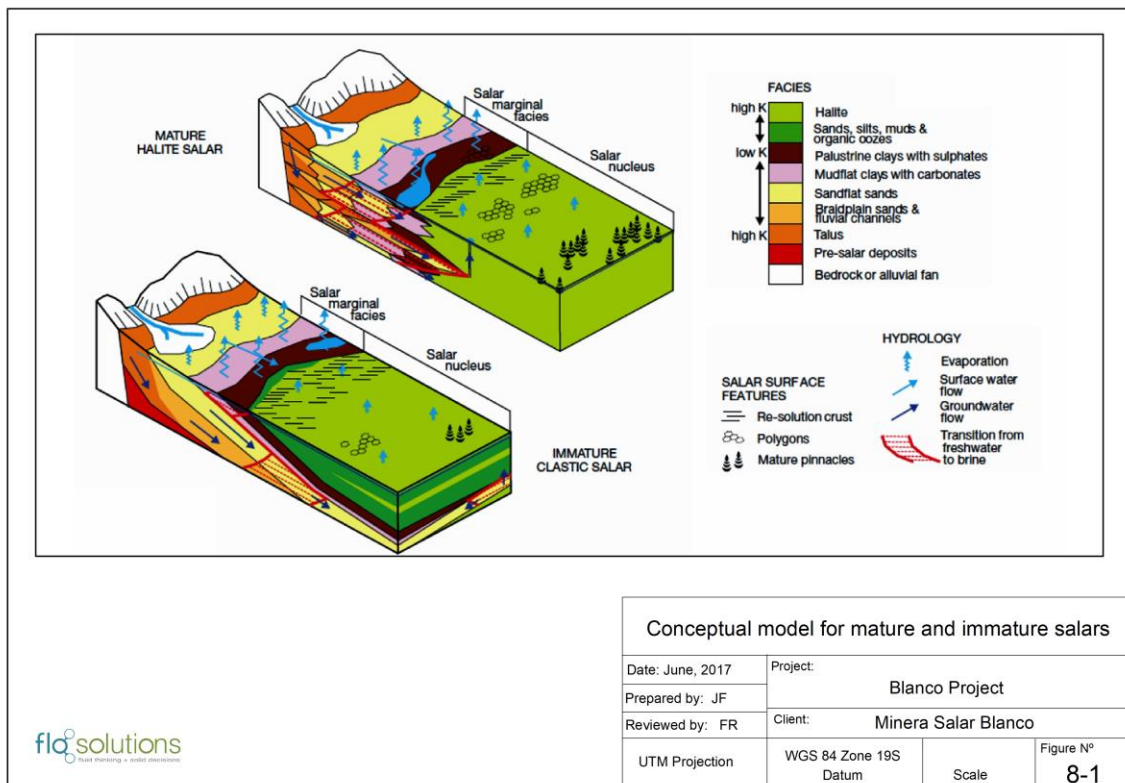
Salars occur in closed (endorheic) basins without external drainage, in dry desert regions where evaporation rates exceed stream and groundwater recharge rates, preventing lakes from reaching the size necessary to form outlet streams or rivers. Evaporative concentration of surface water over time in these basins leads to residual concentration of dissolved salts (Bradley et al., 2013) to develop saline brines enriched in one or more of the following constituents: sodium, potassium, chloride, sulfate, carbonate species, and, in some basins, metals elements such as boron and lithium.

Houston et al., 2011 identified two general categories of salars:

1. mature, halite dominant, and
2. immature, clastic dominant.

Figure 8-1 shows the general conceptual model for each salar type.

Figure 8-1: Conceptual model for mature and immature salars showing the distribution of the facies and the main hydrogeological components.



Source: Houston, et al., 2011.

Immature salars are characterized by increased humidity (increased precipitation, less evaporation) and are more frequent at higher elevations and in the wetter northern and eastern parts of the region. They are characterized by alternate sequences of fine-grained sediments and evaporitic beds of halite and/or ulexite, indicating the changes in sediment supply due to variable tectonic and climate history (Houston, et al., 2011). Immature salars include Olaroz, Cauchari, Diablillos and Centenario.

Mature salars are less humid and tend to be more common in lower and drier areas of the region. They are characterized by a relative thick and uniform sequence of halite deposits in variable sub-aquatic and sub-aerial conditions. Nevertheless, ancient floods leading to widespread silty clay deposits and volcanic fallout have led to thin intercalated beds that can be recognized in drill core and geophysical surveys. The central portion of Salar de Atacama is a typical mature setting.

Salar de Maricunga, is a mixed type. The northern part of Salar de Maricunga has a well-developed halite crust with a thickness of up to 34 m. This halite unit is underlain by clastic sediments. Brine is saturated in respect to halite. Progressively to the south clastic facies become dominant (Tassara, 1997). As described in Section 7.2, drilling within the MSB properties has been able to identify the geometry of the clastic and halite dominant units. Pumping tests have been carried out to characterize the hydraulic behavior of both the clastic and halite units as further described in Sections 9 and 10 below.

8.2 HYDROGEOLOGY

The salar is the topographic low point within the Maricunga Basin. The Salar itself is surrounded by alluvial fans which drain into the salar. The floor of the Salar in the north and northeast is composed of chloride facies consisting of flat halite crust (more recently flooded) and coarse irregular- and pinnacle shaped halite blocks (absence of recent flooding). The floor of the Salar in the southeast is composed of boric and sulphate facies. In the nucleus of the Salar the water table can be within approximately 5 cm of the surface.

Interpretation of drilling and testing results in the Salar and the surrounding alluvial fans by the MSB and other companies previously exploring for fresh water resources suggests the occurrence of several hydrogeological units of importance. Figure 8-2 is a hydrogeological section through the Salar showing the principal units and which are summarized as follows:

- Alluvial fans surrounding the salar. These are coarse grained and overall highly permeable units that drain towards the salar. Groundwater flow is unconfined to semi-confined; specific yield (drainable porosity) is high. Water quality in the fans on the east side of the Salar is fresh to brackish.
- An unconfined to semi-confined Upper Halite aquifer can be identified in the northern part of the Salar. This unit is limited in areal extent to the visible halite nucleus as observed in satellite images. This Upper Halite unit is highly permeable; has a medium drainable porosity; and contains high concentration lithium brine.

- The clay core underlies the upper halite aquifer in the center of the Salar and extends to the east below the alluvial fans. This clay unit has a very low permeability and forms a hydraulic barrier for flow between the Upper Halite aquifer and the underlying clastic units (deeper sand gravel and Volcaniclastics aquifer). On the east side of the Salar fresh water in the alluvial fans sits on top of this clay core; while brine is encountered in the clastic sediments underlying the clay. In the nucleus of the Salar the clay unit contains high concentration lithium brine.

A deeper brine aquifer occurs in the gravel, sand and Volcaniclastics units underlying the clay core. Below the nucleus of the Salar this deeper aquifer is overlain by the Clay Core and groundwater conditions are confined. On the west side of the Salar, in absence of the Clay Core, groundwater conditions become semi-confined to unconfined. The deeper brine aquifer is relatively permeable and has a relatively high drainable porosity.

A groundwater monitoring network has been installed across the Maricunga basin and is part of the baseline monitoring program for the EIA. An updated conceptual hydrogeological model, including a water balance, has been completed for the Maricunga basin and is further described in Section 15 below. This conceptual model forms the basis for the three-dimensional numerical groundwater / brine flow model used to estimate brine reserves, optimize the configuration of the future brine wellfield and evaluate potential effects of the future proposed brine abstraction for the EIA.

Figure 8-2: W-E Hydrogeological cross section

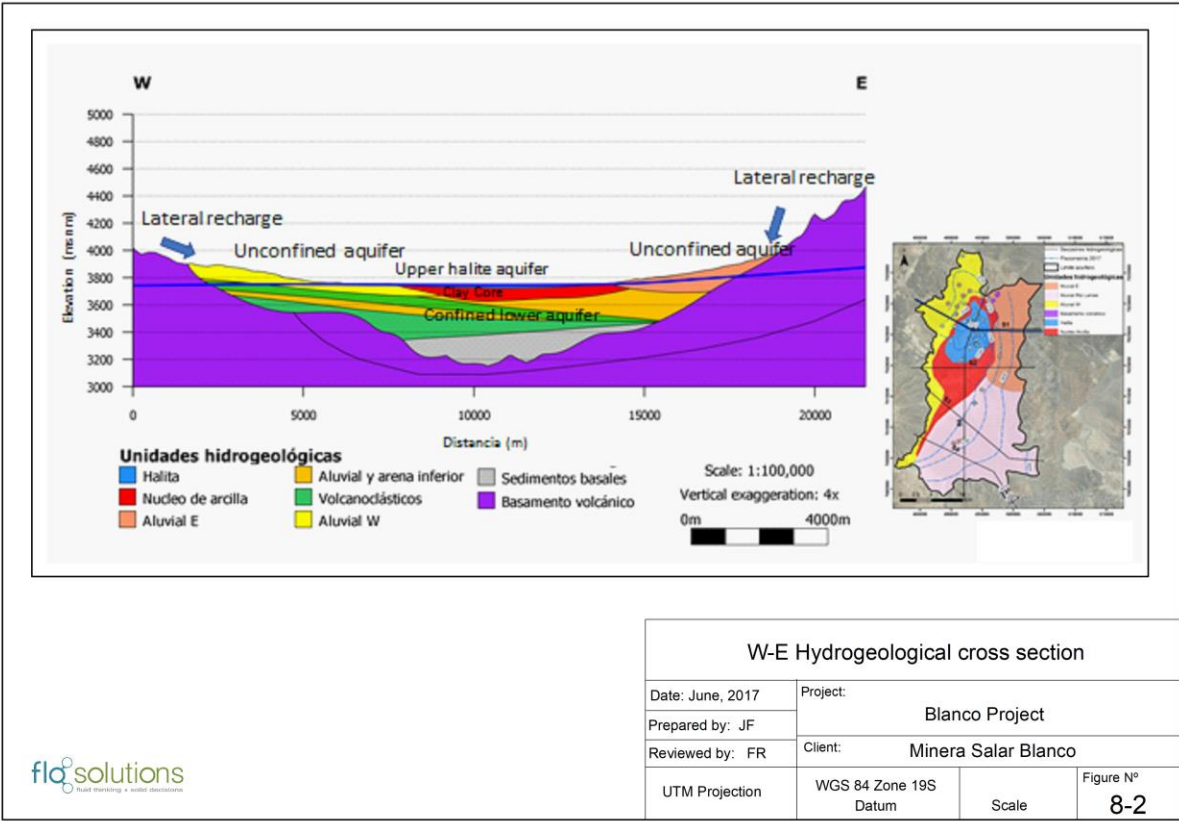
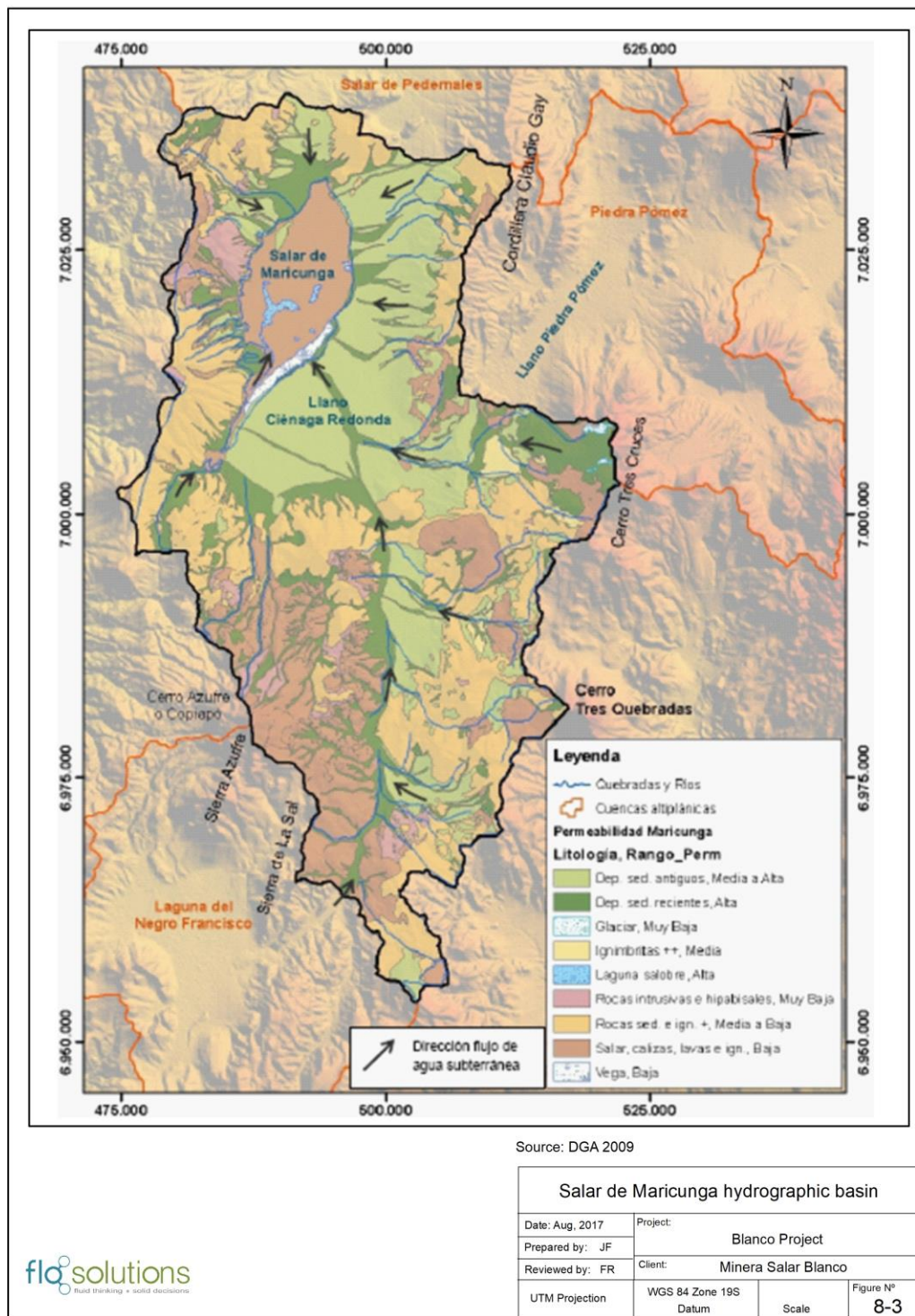


Figure 8-3: Salar de Maricunga hydrographic basin



Source: DGA 2009

8.3 WATER BALANCE

A water balance for Salar de Maricunga was prepared by Flosolutions (2018) as part of a new conceptual hydrogeological model for the EIA which is summarized in Table 8-1. Figure 8-3 shows the general surface and groundwater flow patterns in the Salar de Maricunga watershed. Surface water flow generally only occurs at higher ground and infiltrates into the more permeable alluvial and fan sediments surrounding the Salar before reaching the Salar floor itself. The only surface water flow that occurs on the Salar floor is the natural discharge from Laguna Santa Rosa north towards the center of the Salar. There is no surface water outflow from the Maricunga watershed. Groundwater flow patterns follow closely the surface water flow patterns. There are no known groundwater outflows from the Maricunga watershed.

Recharge to the Maricunga basin occurs through the direct infiltration of precipitation (709 l/s) and through lateral recharge from Río Lamas (264 l/s) and Ciénaga Redonda (436 l/s) catchments. The total average annual recharge to the Maricunga basin is estimated at 1,409 l/s or 44.5 million m³.

Discharge from the Maricunga basin is through seepage to streams and lakes, evaporation, evapotranspiration and groundwater pumping. The total average annual discharge through evaporation has been estimated at 1,348 l/s or 42.5 million m³.

According to DGA records, existing granted water rights in the Salar de Maricunga basin amount to 845 l/s, but actual authorized usage by the Environmental Evaluation System (SEA) is estimated at 153 l/s.

Table 8-1: Water Balance for the Salar de Maricunga Basin

INFLOWS (l/s)		
Direct recharge (Pp)		709
Lateral recharge	Río Lamas (surface flow)	264
	Cienaga Redonda (groundwater flow)	436
Total inflows		1,409
OUTFLOWS (l/s)		
Evaporation	seepage to streams and lakes	488
	Evapotranspiration	370
	Soil evaporation	450
Groundwater pumping	Wells	40
Total outflows		1,348

Source: FloSolutions 2018

8.4 DRAINABLE POROSITY

Porosity is highly dependent on lithology. Total porosity is generally higher in finer grained sediments, whereas the reverse is true for drainable porosity or specific yield since finer grained sediments have a high specific retention. The lithology within the Salar is variable with halite and

halite mixed units, clay and gravel-sand-silt-clay sized mixes spanning the full range of sediment types.

Based on the results of drainable porosity analyses carried out on 488 undisturbed samples from sonic core by GeoSystems Analysis, Daniel B Stephens and Associates, Corelabs, and the British Geological Survey it was possible to assign drainable porosity values to the specific lithological units encountered during the various drilling programs in the Salar. Table 8-2 summarizes the results of the porosity analysis. The analysis of drainable porosity is further discussed in Section 11.

Table 8-2: Results of drainable porosity analyses (2011-2018)

Lithology	Drainable Porosity		
	Average	Min	Max
Halite	0.09	0.01	0.15
Gypsum	0.01	0.01	0.02
Clay	0.025	0.01	0.03
Clay with Halite	0.04	0.01	0.11
Silty Clay	0.06	0.01	0.25
Sand	0.09	0.037	0.16
Clayey sand	0.045	0.01	0.08
Silty sand	0.08	0.01	0.30
Clayey gravel	0.09	0.02	0.19
Sandy gravel	0.19	0.01	0.31
Volcaniclastics	0.15	0.06	0.31

8.5 PERMEABILITY

Permeability (or hydraulic conductivity) is also a parameter that is highly dependent of lithology. Generally finer grained and well-graded sediments have a lower permeability than coarser grained poorly graded sediments. The permeability of halite can be enhanced though fracturing and solutions features. MSB has carried out four pumping tests within the Salar and third parties have carried out numerous other pumping tests in the alluvial sediment surrounding the Salar. The results of the permeability calculations from these pumping tests integrated with third party data (Flosolutions, 2018) are summarized in Table 8-3. The analysis of the pumping tests is further discussed in Sections 10 and 15 below.

Table 8-3: Summary of permeability values

Unit	Description	K (m/d)
Halite	Confined and fractured	100 - 640
Clay core	Clay with sands and gravels - confined	0.001 - 0.01
East Alluvium	Semi-confined to confined	0.1 - 40
West Alluvium	Unconfined to semi-confined	0.1 - 40
Lower alluvium	Confined	0.1 - 1.0
Volcaniclastic	Confined	0.1 - 1.0

9. EXPLORATION

9.1 OVERVIEW

This section provides a description of the exploration work that has been carried out on the MSB properties between 2011 and 2017 by the various owners.

The following work was carried out on the Litio 1-6 claims by MLE in 2011

- Seismic refraction tomography survey along 6 profiles for a total of 23 km to map lithological units and basin geometry.
- Construction of six test trenches to carry out 24-hour pumping trials to determine hydraulic parameters.

The following work was carried out by BBL in 2015:

- AMT / TEM survey along 6 profiles for a total of 75 km across the Salar to map basin geometry and the interface between freshwater and brine.
- Topographic survey between Laguna Rosa and the Project area to map hydraulic gradients.

The following work was carried out by MSB in 2016/7:

- Gravity survey along 6 profiles for a total of 75 km across the Salar to map basin geometry and bedrock topography.

9.2 GEOPHYSICAL SURVEYS

9.2.1 Seismic refraction tomography (2011)

Geophysical Exploration and Consulting S.A. (GEC) from Mendoza Argentina was contracted to carry out a Seismic Refraction Tomography Survey to map lithological units and structure in the northern part of the Salar. A total of 23 line km of seismic tomography data were collected along six lines as shown in Figure 9-1. Prior to the seismic data collection all lines were surveyed using a differential GPS system. All data collection work was completed in the field between September and December 2011.

A 24-bit, ultra-high resolution 20 kHz bandwidth (8 to 0.02 ms sampling), low distortion (0.0005 %), low noise (0.2 uV) GEODE Acquisition System was used for the collection of the seismic tomography data. Geophone (14 Hz Geospace) spacing was 5 m; inline source spacing was 15 m and outline offsets were 30 m, 60 m, 90 m, 150 m, 250 m and 500 m. The spread data acquisition layout included 48 active channels. The seismic source for the surveys was a 150 kg trailer-mounted accelerated drop-weight. Recording length was 250/500 ms with a 1.0 ms sampling rate.

During the seismic data acquisition, data quality control and pre-processing of the geophysical data were carried out in the field with PC based processing and interpretation packages called

“*Firstpix*” / *Gremix 15*” and “*Rayfract 32*”. Final data processing with the “*Rayfract 32*” software included tomography inversion techniques *Delta TV* and WET or *Wave Eikonal Traveltime* as follows:

- Delta T-V method (after Gebrande and Mille, 1985): The Delta TV method is a pseudo 2D Inversion method that delivers a continuous 1D velocity versus depth model for all geophone stations. The method handles geological situations such as velocity gradients, linear increasing of velocity with depth, velocity inversions, pinching out layers and outcrops, faults and local velocity anomalies.
- WET or Wave Eikonal Travel time Tomography processing. Wave propagation is modelled in a physically meaningful way with ray paths, using the output from the Delta-TV inversion as starting model. It handles geological situations, such as discontinuities velocity distributions and sharp vertical or horizontal velocity gradients. Quality control of geological models is performed by direct graphical comparison of the measured travel time data to those calculated from the model solution.

Figure 9-2 shows as an example of the result of the WET processing and inversion with the geological interpretation below along Profile 1 and is considered representative of the overall seismic survey results obtained. Data from the 2011 sonic and RC boreholes were included in the final interpretation. The seismic tomography survey provided valuable information on the vertical distinction and lateral continuity of lithological layers, however bedrock was not clearly detected along any of the profiles.

Figure 9-1: Location map of seismic refraction tomography, AMT and gravity profiles

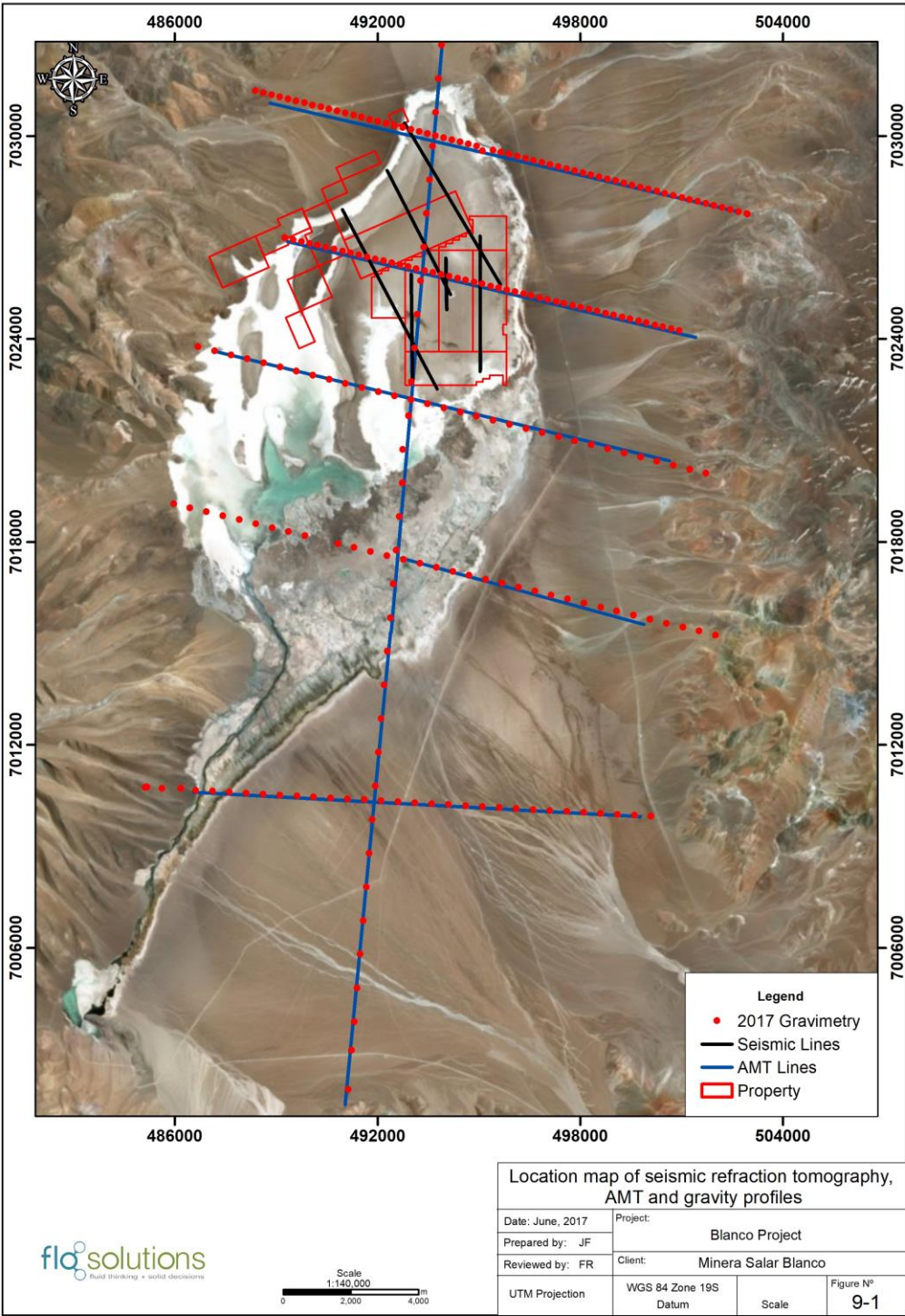
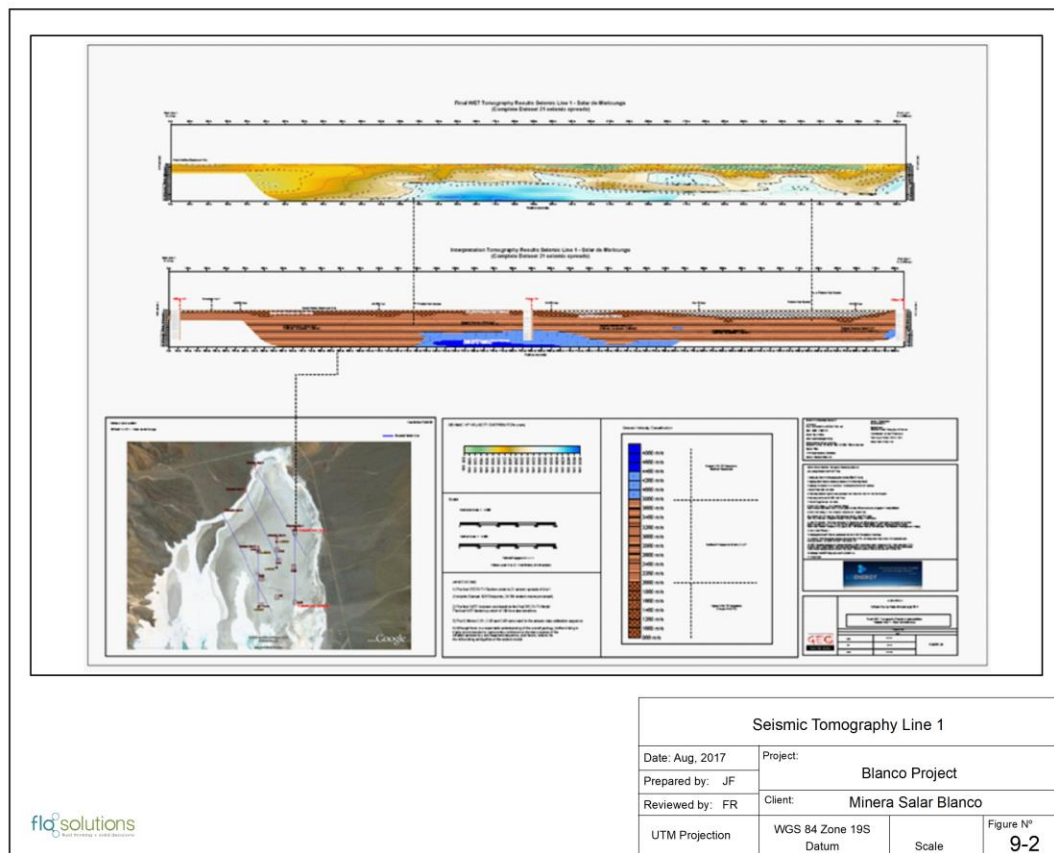


Figure 9-2: Seismic Tomography Line 1



9.2.2 AMT / TEM (2015)

Six profiles of Audio Magnetotellurics were carried out across Salar de Maricunga to map the bedrock geometry and identify the interface between freshwater and brine along the perimeter of the Salar. The work was carried out by Wellfield Services Ltda. The survey consisted of 60.8 km of AMT profiles with a station spacing of 200 m and 14 km with a station spacing of 250 m. 360 stations were measured with scalar methodology and 23 stations were measured with the tensorial array. 15 TEM soundings were carried out at the ends of the AMT lines and at the intersection with Line 6. Figure 9-1 shows the location of the AMT profiles.

AMT data were collected in the range of 10,000 – 1 Hz and MT data in the range of 4 – 0.01 Hz to include the deeper portion of the frequency spectrum. Seven GPS synchronized systems were operated by two teams with data collection taking place overnight for a period of 15-18 hours at each station.

Due to logistical and climatic conditions (partial flooding of the Salar) the survey was carried out in 3 stages during March and April 2015. The AMT data were inverted into 2D resistivity models using the software WinGLink.

9.2.3 Gravimetry

A gravity survey was carried out in the Salar along Prolifes 1 – 6 (immediately over the AMT lines) as shown in Figure 9-1. Station spacing along Line 1 and 2 was 250 m, while station spacing along lines 3 to 6 was 500 m. Each station was surveyed in with a differential GPS with a precision of ± 5 cm. The gravity data was collected with a Scintrex micro-gravimeter Model CG-5 with resolution of 0.001 mgals and with an automatic drift correction.

Data processing included the Free Air, Simple Bouguer, and Total Terrain corrections; the final product included final Bouguer anomaly maps and 2D inversion models. An average density contrast of 0.45 g/cm^3 was used between the bedrock and the Salar basin fill sediments to prepare depth-to-bedrock models along each of the gravity profiles. The density contrast was based on results of laboratory (Universidad de Chile) density measurements on 18 rock samples collected in outcrop at the end of Lines 1 – 6 and the density measurements carried out by GSA on the basin fill sediments. The geological model described in Section 7 was used to constrain the geometry of the lithological units within the gravity interpretation. The gravity profiles were also overlain by the AMT resistivity sections to aid in the final depth-to-bedrock model. The final bedrock topography was kriged based on interpolation from the line profiles.

9.3 TEST TRENCHING (2011)

Six test trenches (T1 through T6) were constructed in 2011 on the Lito 1-6 tenements to test the feasibility of brine production from trenches as an alternative to brine production from production wells. One trench was installed adjacent to each sonic borehole C-1 through C-6. The trenches were dug at 3 m width to a depth of 2.5 m. Each trench was completed in generally massive (relatively competent) halite and the trench walls did not encounter stability problems as shown in Figure 9-3.

A 24-hour pumping test was carried out in each trench at a flow rate of 5 l/s using a sump pump. Water level responses during each pumping test were observed in a shallow monitoring well (36 m depth) adjacent to each trench that allowed for the calculation of aquifer parameters.

Figure 9-4a through Figure 9-4e show the water level response in each observation well and the associated pumping test analyses. Table 9-1 summarizes the results of the pumping test analyses. The relatively high S_y values obtained from the pumping tests are representative of the halite mix sediments and suggest enhanced porosity in the halite through dissolution and fracture features.

Figure 9-3: Test Trench T6 in the Upper Halite



Table 9-1: Results of Trench pumping tests

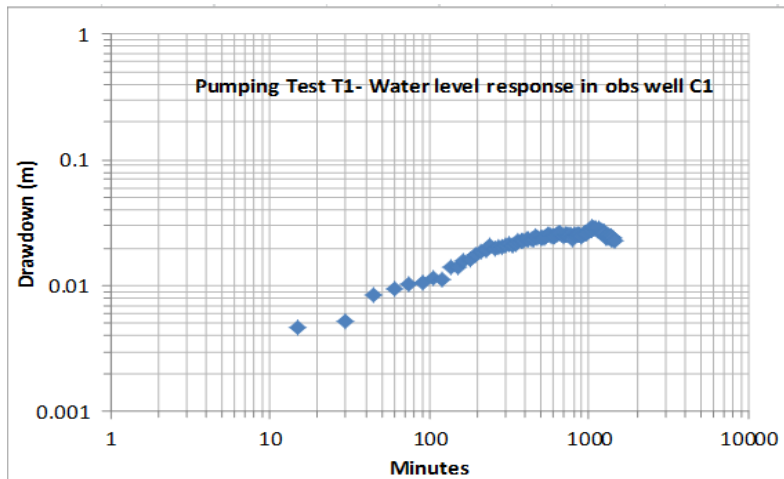
Trench	Hydraulic Conductivity (K) m/d	Specific Yield (S_y)
T1	208	0.24
T2	84	0.28
T3	145	0.24
T4	No water level response in piezometer	
T5	15	0.12
T6	45	0.04

The results of these tests indicate that the upper halite is highly permeable and that brine production from trenches is a feasible alternative to production wells from the upper metres of the upper halite.

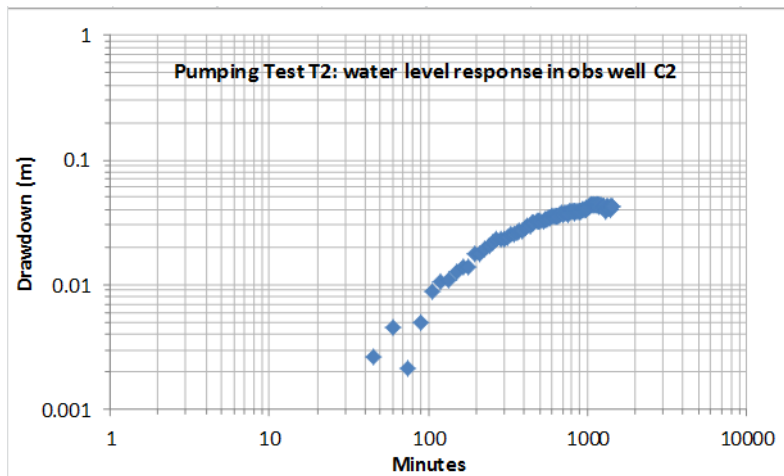
Figure 9-4a – 9.4e: Pumping test analyses for Trench pumping tests T1, T2, T3, T5 and T6

After Papadopoulos 1967

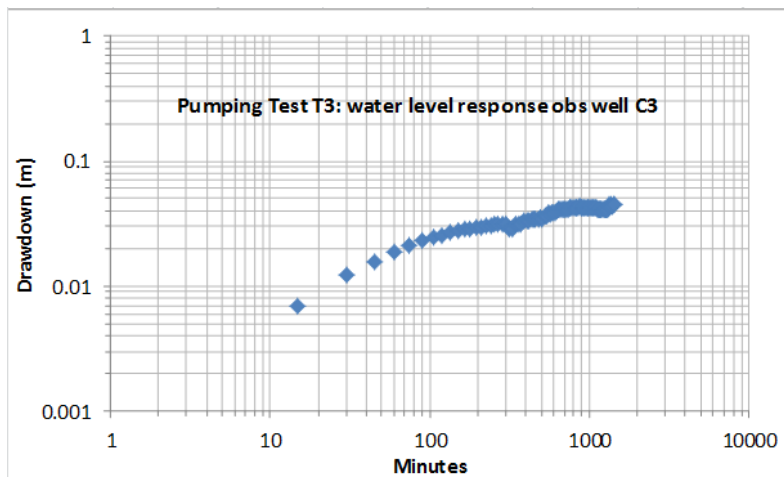
a 0.01
1/u 100



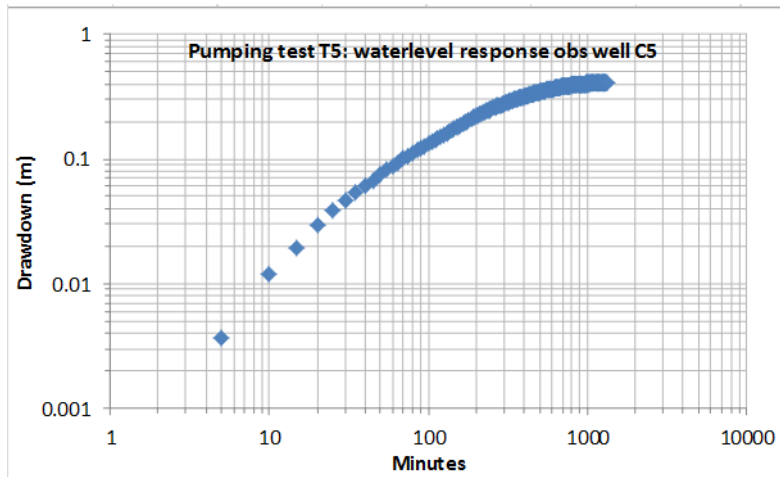
F(u)	1
t	190 min
s	0.055 m
r	12.9 m
Q	529 m ³ /d
KD	7,513 m ² /d
Sy	0.24



After Papadopoulos 1967	
a	0.1
1/u	10
F(u)	1
t	350 min
s	0.015 m
r	32.47 m
Q	529 m ³ /d
KD	7,513 m ² /d
Sy	0.24

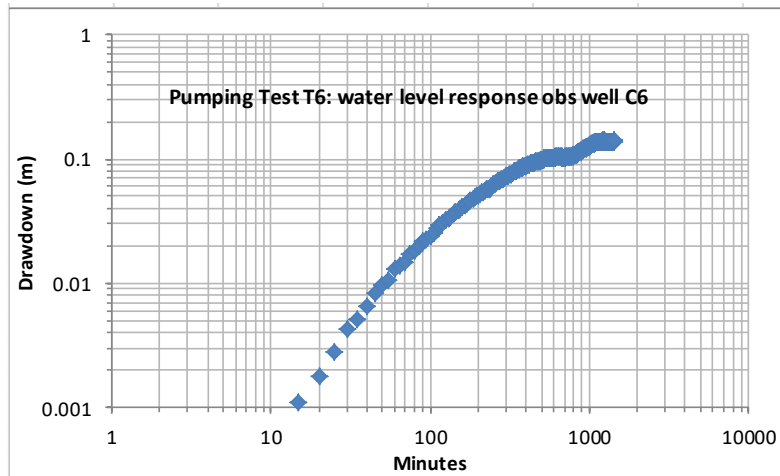


After Papadopoulos 1967	
a	0.1
1/u	10
F(u)	1
t	35 min
s	0.009 m
r	14.6 m
Q	593 m ³ /d
KD	5,237 m ² /d
Sy	0.24



After Papadopoulos 1967

a	0.01
1/u	100
F(u)	1
t	300 min
s	0.085 m
r	6 m
Q	562 m ³ /d
KD	526 m ² /d
Sy	0.12



After Papadopoulos 1967

a	0.01
1/u	100
F(u)	1
t	410 min
s	0.025 m
r	22.6 m
Q	518 m ³ /d
KD	1,650 m ² /d
Sy	0.04

10. DRILLING

10.1 OVERVIEW

Two principal drilling campaigns were carried out the first in 2011 on the Litio 1-6 claims and a second on the MSB properties between 2016 and 2018.

The objectives of each drilling campaign can be broken down into three general categories:

- Exploration drilling on a general grid basis to allow the estimation of “in-situ” brine resources. The drilling methods were selected to allow for 1) the collection of continuous cores to prepare “undisturbed” samples at specified depth intervals for laboratory porosity analyses and 2) the collection of depth-representative brine samples at specified intervals without the possibility of contamination by drilling fluids. The 2011 campaign included six (6) sonic boreholes (C-1 through C-6) on the Litio 1-6 claims. The 2016 campaign included four (4) sonic boreholes (S-1[M1], S-2, S-18 and S-20) and eight (8) tricone /HWT boreholes (S-3, S-3A, S-5, S-6, S-10 [M-10], S-11[M2], S-13, and S-19). Two additional sonic boreholes S-23 and S-24 were completed immediately adjacent to C-2 and C-5, respectively during 2018. Figure 10-1 shows the location of the exploration boreholes.
- Production- and monitoring well drilling. Test production wells were installed to carry out pumping tests to determine the hydraulic parameters of the Salar sediments and investigate the behavior of the brine aquifer under pumping stress. Monitoring wells were installed adjacent to production wells to observe water levels changes during the pumping tests and in other locations to monitor baseline groundwater conditions around the Salar. Monitoring wells were drilled using the reverse circulation (air) drilling method (RC) to allow hydraulic test work. Production wells were installed using conventional rotary methods at large diameter. Production wells P-1 and P-2 along with piezometers P1-1, P1-2, P1-3, P1-4, P2-1, P2-2, P2-3, P2-5 and P-3 were installed in the 2011 campaign. Production well P-4 and monitoring wells S-7, S-8, S-12, S-15, S-16A, S-17, and S-21 were installed during the 2016/7 campaign. The analytical results of brine samples collected during the production and monitoring well drilling were not used in the resource model.
- Pumping tests. Long-term pumping tests were carried out on wells P-1 and P-2 during 2015 and on wells P-4 and P-2 (shallow) in 2017.

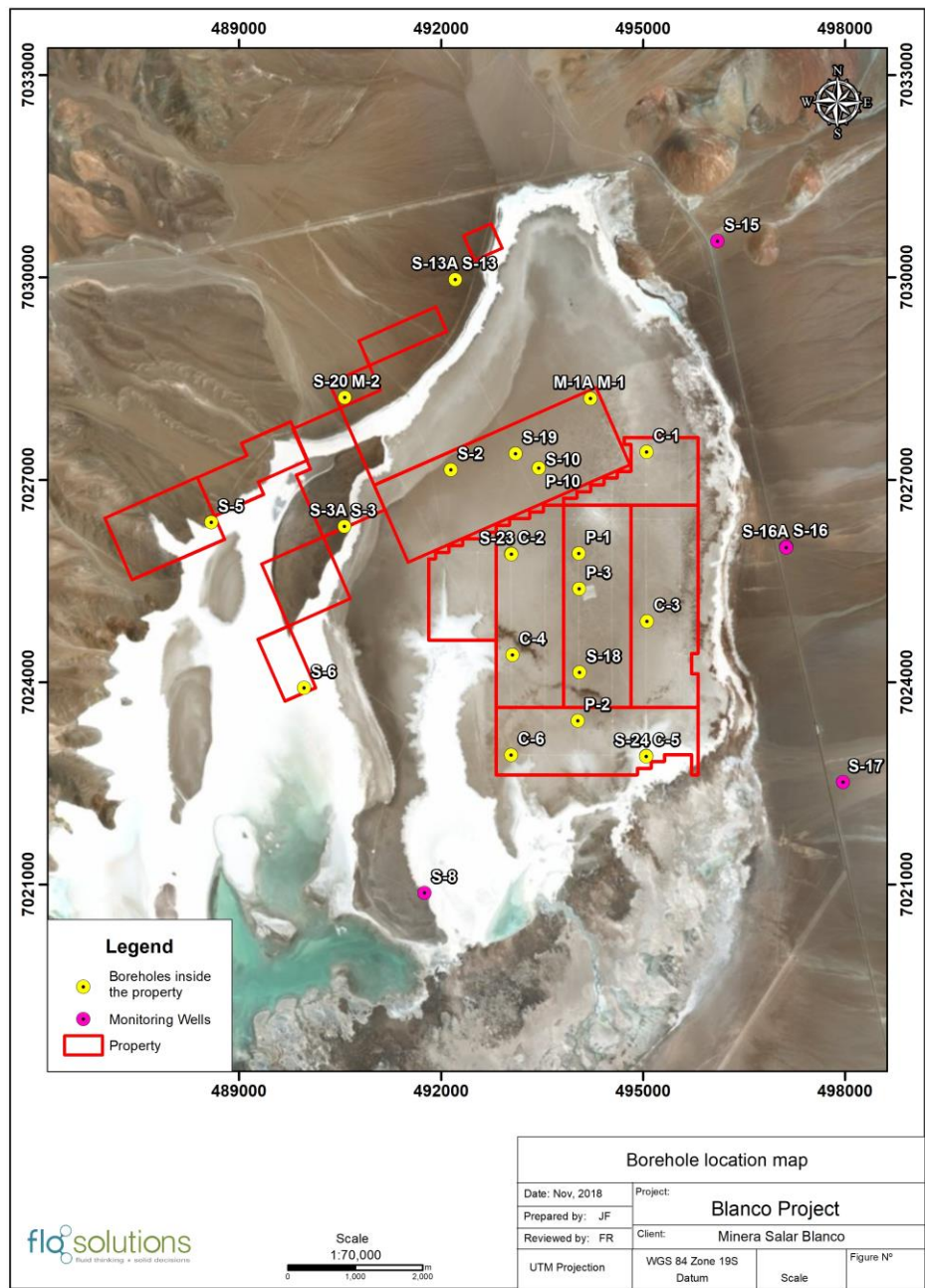
10.2 EXPLORATORY DRILLING

10.2.1 Sonic Drilling

Boart Longyear (BLY) was contracted to carry out sonic drilling for the collection of continuous core and brine samples for all 2011 / 2018 programs. Sonic boreholes C1 through C6 were drilled to a depth of 150 m in 2011 and S-1A, S-2, S-18, S-23, and S-24 to depths of up to 200 m in 2016 and

2018. Sonic hole S-20 was drilled as a twin hole to S-11 to a depth of 40 m to correlate porosity information. Core recovery was consistently high and exceeded 90%.

Figure 10-1: Location map of the boreholes (2011 - 2018 programs)



The drilling equipment consisted of a BLY (SR-162 SRF 600T) sonic rig and support equipment utilizing a 4-inch diameter coring by 6-inch casing system. No drilling additives/fluids were used thereby preventing possible brine sample contamination. All holes were drilled vertically. The drilling was carried out in 1.5 m runs and core was collected in alternating plastic bags (1.5 m) and lexan core barrel liners (1.5 m). The retrieved lexan core liners were capped and sealed with tape at each end. All retrieved core was labeled with its borehole number and the drilling depth interval and stored in wooden core boxes. The 6-inch diameter casing was advanced at the end of each core run.

Brine samples were collected at 3 m intervals during the 2011 program and at 6 m intervals during 2016 and 2018. Brine level measurements were made inside the drill casing to calculate the required volume of brine to be bailed from the hole prior to obtaining a brine sample. Up to three well volumes were bailed prior to collecting the final brine sample from the bottom of the hole. This procedure was repeated to total depth (TD).

On completion of drilling, each sonic borehole was completed as a monitoring well with 2-inch diameter PVC blank and slotted casing, gravel pack and cement seal. S-23 and S-24 were completed with 3-inch diameter PVC slotted casing and geomembrane material (without gravel pack).

Table 10-1: Summary of 2011 - 2018 boreholes

Borehole	North	East	Elevation	TD (m)	Method	Year	Objective	Screened interval	SWL
C1	7,027,408	495,052	3,747.51	150	Sonic	2011	Resource	Abandoned	na
C2	7,025,899	493,041	3,747.35	150	Sonic	2011	Resource	06-34	0.11
C3	7,024,895	495,056	3,746.86	150	Sonic	2011	Resource	03-26	0.12
C4	7,024,400	493,058	3,747.35	150	Sonic	2011	Resource	06-29	0.24
C5	7,022,900	495,045	3,746.58	150	Sonic	2011	Resource	06-11	0.15
C6	7,022,918	493,039	3,746.78	150	Sonic	2011	Resource	06-11	0.23
P1	7,025,904	494,043	3,747.25	150	Rotary	2011	Production	6-24;60-144	0.18
P1.1	7,025,891	494,032	3,747.59	150	DTRC	2011	Monitoring	60-149	0.72
P1.2	7,025,894	494,061	3,747.34	30	DTRC	2011	Monitoring	06-24	0.18
P1.3	7,025,905	494,032	3,747.69	70	DTRC	2011	Monitoring	54-66	0.37
P1.4	7,025,915	494,032	3,747.74	30	DTRC	2011	Monitoring	06-24	0.12
P2.1	7,023,393	494,035	3,746.44	113	DTRC	2011	Monitoring	102-108	0.26
P2.3	7,023,410	494,03	3,746.38	30	DTRC	2011	Monitoring	12-30	0.2
P2.4	7,023,403	494,034	3,746.44	150	DTRC	2011	Monitoring	60-145	0.27
P2.5	7,023,397	494,061	3,746.60	150	DTRC	2011	Monitoring	60-145	0.77
P3	7,025,380	494,052	3,747.62	192	DTRC	2011	Monitoring	127-185	-0.37
P2	7,023,422	494,03	3,746.22	150	Rotary	2011	Production	6-24; 66-144	0.25
S 1A	7,028,201	494,22	3,748.95	200	Sonic	2016	Resource	29-119	0.23
S 2	7,027,141	492,143	3,748.84	200	Sonic	2016	Resource	184-190	1.43
S-3	7,026,300	490,56	3,751.54	40	Tricone/HWT	2016	Resource	Abandoned	na
S-3A	7,026,306	490,563	3,751.53	200	Tricone/HWT	2016	Resource	Abandoned	na
S-5	7,026,366	488,59	3,750.17	200	Tricone/HWT	2016	Resource	182-188	1.55
S-6	7,023,913	489,964	3,749.09	200	Tricone/HWT	2016	Resource	184-195	3.09

Borehole	North	East	Elevation	TD (m)	Method	Year	Objective	Screened interval	SWL
S-8	7,020,871	491,753	3,748.72	40	Rotary	2016	Monitoring	28-34	1.18
S-11	7,028,215	490,569	3,757.61	200	Tricone/HWT	2016	Resource	144-150	8.95
S-12	7,013,856	493,74	3,769.28	40	Rotary	2016	Monitoring	22-28	na
S-13	7,029,964	492,213	3,755.88	200	Tricone/HWT	2016	Resource	194-200	9.18
S-15	7,030,533	496,104	3,781.23	40	Rotary	2016	Monitoring	34-40	25.11
S-17	7,022,516	497,969	3,789.94	40	Rotary	2016	Monitoring	32-38	29.8
S-16A	7,026,005	497,122	3,769.89	150	Tricone/HWT	2016	Monitoring	50-62	11.3
S-16B	7,025,991	497,123	3,769.99	18	Tricone/HWT	2016	Monitoring	09-15	14.72
S-18	7,024,141	494,054	3,748.64	173	Sonic	2016	Resource	1160-172	2.58
S-19	7,027,381	493,104	3,748.17	360	Tricone/HWT	2016	Resource	196-208	2.98
S-20	7,028,217	490,569	3,757.64	40	Sonic	2016	QA/QC	Abandoned	na
S-21	7,037,751	491,855	3,863.06	85	Rotary	2016	Monitoring	72-84	dry
S-22	NA	NA			Not drilled				
S-23	7,025,899	493,041	3,747.35	200	Sonic	2018	Resource	0-200	0.10
S-24	7,022,900	495,045	3,746.58	200	Sonic	2018	Resource	0-200	0.15
P-4.1	7,027,224	493,194	3,748.81	200	Tricone/HWT	2016	Monitoring	160-172	2.26
P-4.2	7,027,242	493,172	3,748.65	2	Auger	2016	Monitoring	0-2	0.1
P-4.3	7,027,250	493,16	3,748.70	2	Auger	2016	Monitoring	0-2	0.12
P-4.4	7,027,265	493,139	3,748.74	2	Auger	2016	Monitoring	0-2	0.11

10.2.2 Rotary tricone/HWT drilling

Eight (8) tricone /HWT boreholes (S-3, S-3A, S-5, S-6, S-10 or M-10, S-11, S-13, and S-19) were drilled as part of the 2016 program. Rotary drilling with HWT casing (flush jointed drilling casing with 114.3mm outer diameter) was substituted for conventional diamond drilling as core recovery of the coarse grained sediments on the western side of project area did not prove to be successful. The rotary drilling was carried out by AK drilling using an EDM rig. Rotary drilling was carried out using a 3½ inch tricone bit, with sample recovery through the HWT casing to surface. Cuttings were collected at surface in cloth bags with representative sub-samples at 2 m intervals stored in labelled chip trays. Brine samples were collected at 6 m intervals during the rotary drilling. The brine sampling methodology is further described in Section 11. Selected boreholes were completed as monitoring wells with blank and slotted PVC.

10.3 MONITORING - AND PRODUCTION WELL DRILLING

10.3.1 Reverse circulation (RC) drilling and piezometer installations (2011)

A total of 915 m of DTRC (dual tube reverse circulation) drilling (P1-1, P1-2, P1-3, P1-4, P2-1, P2-2, P2-3, P2-5 and P-3) was carried out for the collection of chip samples for geologic logging, brine samples for chemistry analyses and airlift data. Rock Drilling S.A. provided an Ingersoll Rand T3-W reverse circulation rig equipped with a 350 psi, 1000 cfm air compressor and support equipment. The exploration drilling was carried out at 5½ inch diameter using dual tube reverse circulation pipe and air; no additives/fluids were used during the drilling. Exploration drilling depths ranged from 30 m to 192 m. Chip samples were collected at 2 m intervals for geological logging,

brine samples were collected at 3 m intervals (directly from the cyclone) and airlift tests were completed at 6 m intervals. The RC exploration boreholes were completed as monitoring wells for use during the future pumping tests. The distance between each monitoring well and the associated production well ranges from 10 m to 35 m. Table 10-2 shows the details of the RC exploration drilling completed.

10.3.2 Production well drilling (2011 and 2016)

Drilling of production wells P1 and P2 was carried out by Rock Drilling S.A. using an Ingersoll Rand T3-W rig in 2011. The wells were drilled in two passes at 11-inch and 17-inch diameter to a final total depth of 150 m using flooded reverse circulation (rotary) drilling. The wells were completed with a 10-inch diameter PVC production casing string in both the upper halite aquifer and the lower gravel and volcanoclastics aquifer. The annulus of each test well was completed with gravel pack. Well development was carried out over a 72-hour period in each well using a double swab/airlift system. Table 10-2 shows the construction details of P-1 and P-2.

Production well P-4 was drilled by Hellema Holland Engineering using a Prakla rig. The well was drilled using conventional rotary drilling at 17-1/2 inch diameter to a depth of 180 m. The well was completed with screened 12-inch diameter PVC production casing in the lower aquifer between 70 m and 180 m depth. A bentonite / cement seal was installed (on top of the gravel pack) from ground surface to a depth of 56 m. Well development was carried out over a 48-hour period using a double swab/airlift system. Table 10-2 shows the construction details of P-4.

10.3.3 Piezometer installations (2016)

Piezometers S-7, S-8, S-12, S-15, S-16A, S-17, and S-21 were installed as part of the 2016 campaign. These monitoring wells were drilled using conventional rotary methodology to depths of up to 150 m. Fluid samples were taken at selected intervals during the drilling of the monitoring wells. The wells were completed with 2-inch diameter schedule 80 blank and screened PVC casing. A geomembrane filter was placed over the screened casing to prevent silting. No materials were installed in the annulus. Table 10-1 shows the completion details of each of these installations.

Figure 10-2: Collecting RC Airlift Flow Measurements (2011)

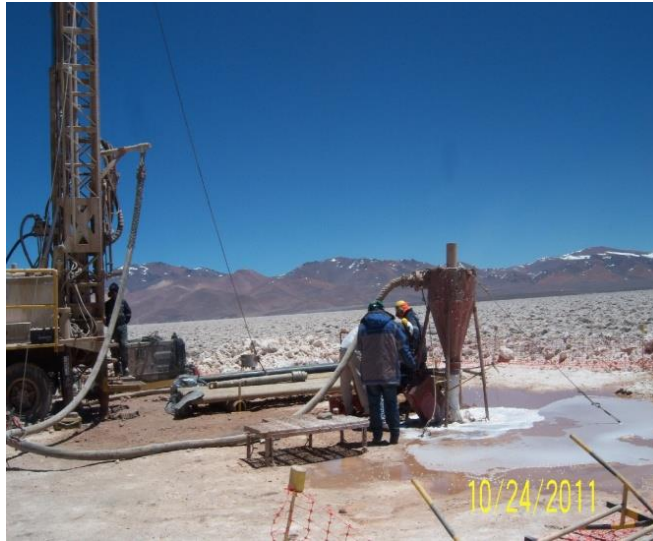


Figure 10-3: Installation of surface casing in well P-1 (2011)



10.4 PUMPING TESTS (2015 AND 2017)

Pumping tests were carried out on wells P-1, P-2, and P-4 between 2015 and 2017. Table 10-2 summarizes the construction details of each pumping test.

Table 10-2: Wells P1, P2 and P4 pumping test layout

Well	Type	UTM E	UTM N	Screened interval (mbgs)	Unit
P-1 Test					
P-1	Pumping	494,043	7,025,903	0-12,18-24, 60-144	Upper Halite and Lower Alluvium
P1-1	Observation	494,032	7,025,890	60-149	Clay Core and Lower Alluvium
P1-2	Observation	494,061	7,025,893	7-24	Upper Halite
P1-3	Observation	494,032	7,025,905	55-66	Clay Core
P1-4	Observation	494,031	7,025,915	7-24	Upper Halite
P-2 Test					
P-2	Pumping	494,030	7,023,422	0-16, 62-141	Upper Halite and Lower Alluvium
P2-1	Observation	494,034	7,023,392	102-108	Clay core
P2-3	Observation	494,030	7,023,409	11-28	Upper Halite
P2-4	Observation	494,033	7,023,402	58-140	Clay Core and Lower Alluvium
P2-5	Observation	494,060	7,023,397	55-144	Clay core and Lower Alluvium
P-4 Test					
P-4	Pumping	493,040	7,025,899	70-180	Lower alluvium
P4-1	Monitoring	495,055	7,024,994	170-182	Lower alluvium
P4-2	Monitoring	493,057	7,024,400	0-2	Upper halite
P4-3	Monitoring	495,045	7,022,900	0-2	Upper halite
P4-4	Monitoring	493,038	7,022,917	0-2	Upper halite

10.4.1 P-1 Pumping Test (2015)

Production well P-1 has two completion intervals: the upper completion between 6 and 24 m depth in the Upper Halite aquifer and the lower completion between 60 m and 144 m depth in the lower part of the Clay Core and the under-laying Lower Alluvium. Four monitoring wells (P1-1, P1-2, P1-3 and P1-4) are installed adjacent to well P-1 at radial distances from 11 m to 20 m as shown in Figure 10-4 and Figure 10-5. Piezometers P1-2 and P1-4 are completed in the Upper Halite unit. Piezometer P1-3 is completed in a deeper halite layer within the Clay Core and Piezometer P1-1 is completed in the lower part of the Clay Core and the Lower Alluvium.

A 14-day constant rate test was conducted at 38 l/s between May 31 and June 13, 2015, followed by recovery. Pumped brine was piped through a 1,200 m plastic line to a V-notch tank where final discharge took place on to the Salar as shown in Figure 10-6. The pumping rate was measured by an inline flow meter, manual measurements and in the V-notch tank. Pressure transducers were installed in all piezometers and the V-notch tank to record water level responses during the test in addition to manual measurements. Observed water level responses to the test are shown in Figure

10-7. The curve fitting and interpretation results of the P-1 constant rate test are shown in Figure 10-8 and Table 10-3.

Figure 10-4: Layout of pumping test P-1 and P-2

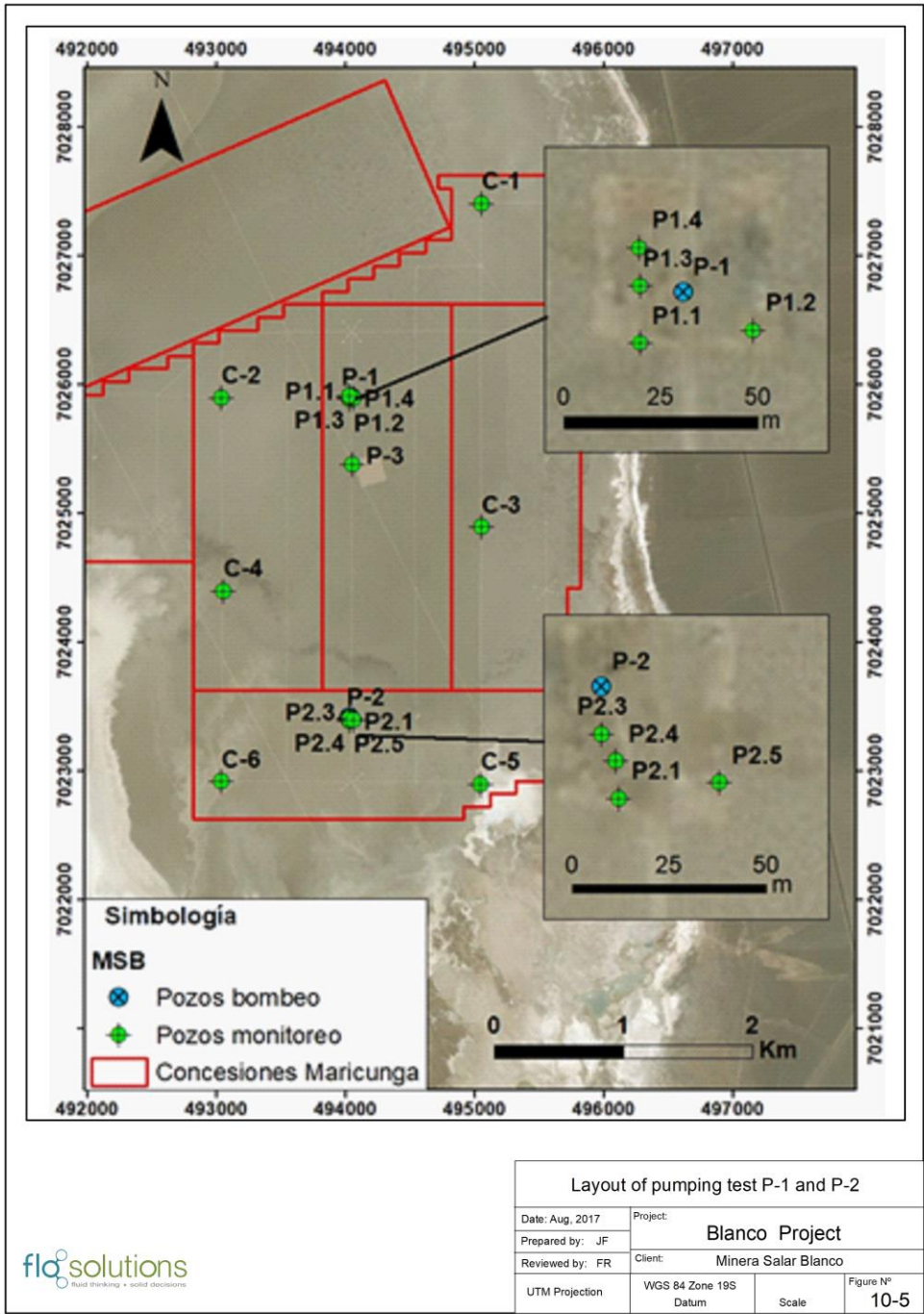


Figure 10-5: Pumping test P-1 layout

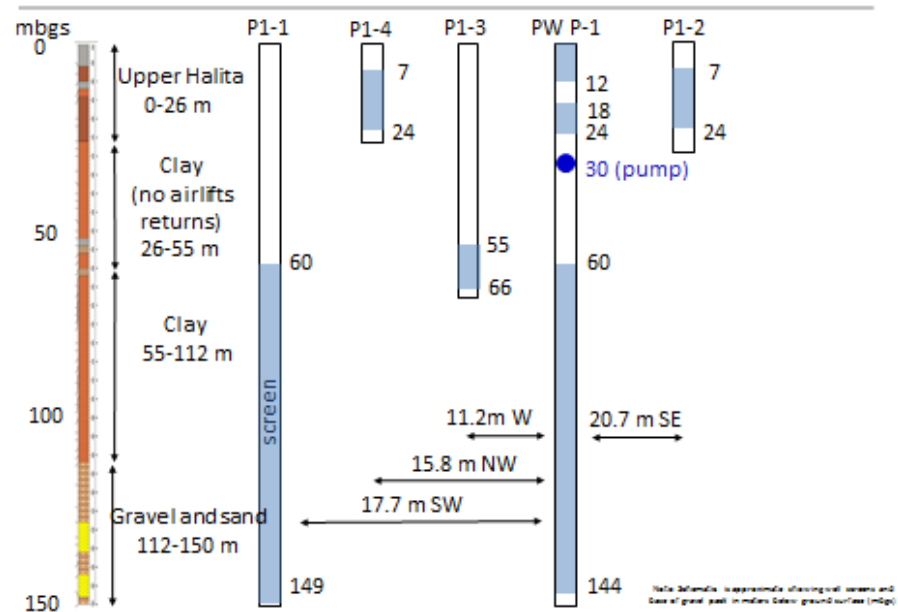


Figure 10-6: V-notch tank during P-1 constant rate test

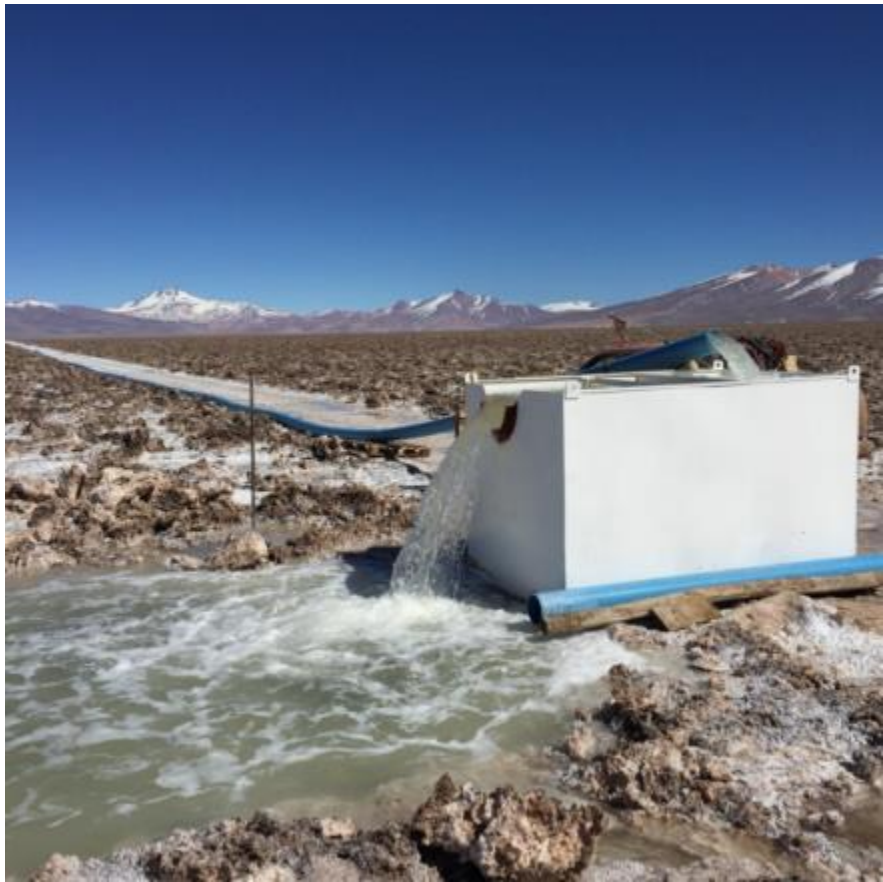
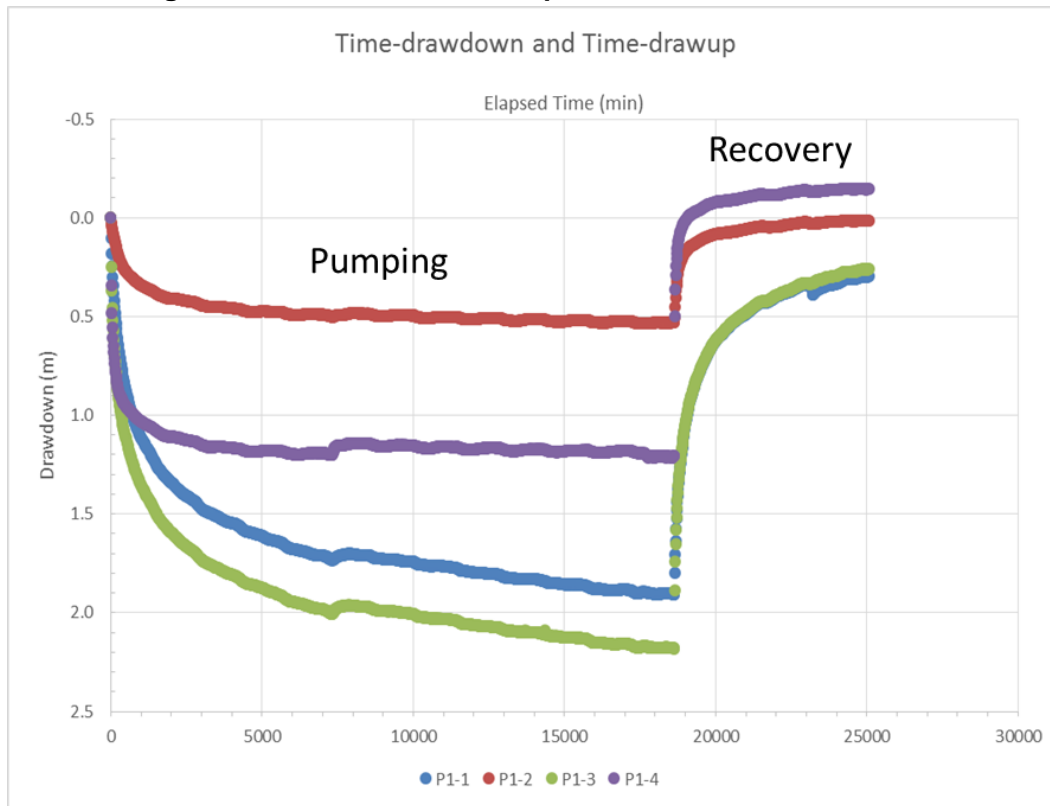


Figure 10-7: Water level responses P-1 constant rate test



Source: FloSolutions 2015b

Figure 10-8: P-1 pumping test interpretation

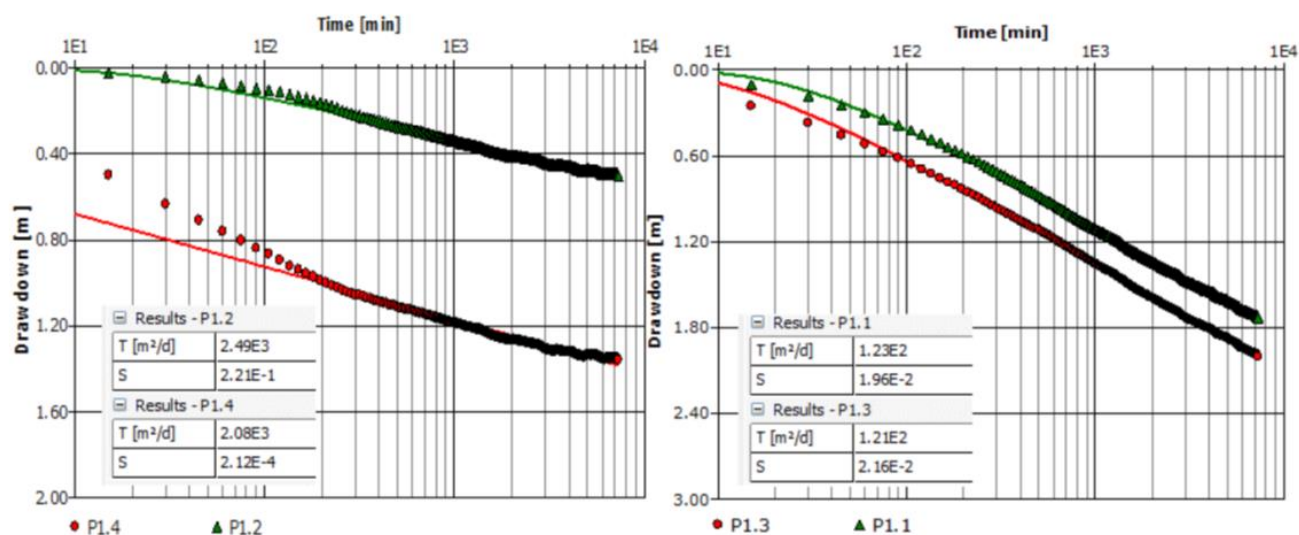
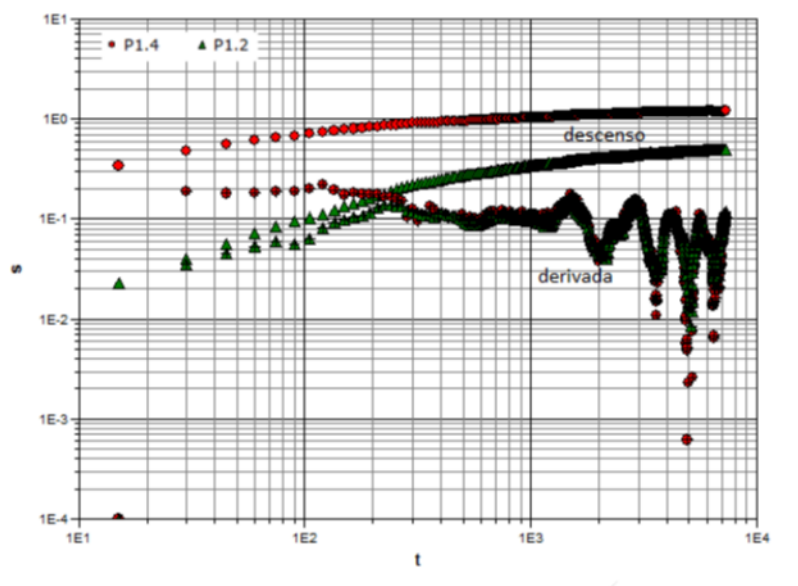


Table 10-3: P-1 Pumping Test Results

Well	Unit	Max Drawdown (m)	Fit	T (m ² /d)	S(-)	K (m/d)*	Ss (1/m)
P-1.2	Upper Halite	0.531	Theis	2,490	2.21E-01	146.5	1.3E-02
P-1.4	Upper Halite	1.362	Theis	2,080	2.12E-04	122.4	1.2E-05
P-1.1	Lower aquifer	1.906	Theis	123	1.96E-02	1.4	2.2E-04
P-1.3	Lower aquifer	2.181	Theis	121	2.16E-02	11.0	2.0E-03

10.4.2 P-2 Pumping test (2015)

Production well P-2 has two completion intervals: the upper completion between 0 and 16 m depth in the Upper Halite aquifer and the lower completion between 60 m and 144 m depth in the lower part of the Clay Core and the underlying Lower Alluvium. Four monitoring wells (P2-1, P2-3, P2-4 and P2-5) are installed adjacent to well P-2 at radial distances from 12 m to 40 m as shown in Figure 10-5 and Figure 10-9. Piezometer P2-3 is completed in the Upper Halite unit. Piezometer P2-1, P2-4 and P2-5 are completed within the lower part of the Clay Core and the Lower Alluvium.

A 30-day constant rate test was conducted at 37 l/s during July/ August 2015, followed by recovery. Pumped brine was piped through a 1,200 m plastic line to a V-notch tank where final discharge took place on to the Salar. The pumping rate was measured by an inline flow meter, manual measurements and in the V-notch tank. Pressure transducers were installed in all piezometers and the V-notch tank to record water level responses during the test in addition to manual measurements. Observed water level responses to the test are shown in Figure 10-10. The curve fitting and interpretation results of the P-2 constant rate test are shown in Figure 10-11 and Table 10-4.

Figure 10-12 shows the variation of lithium and potassium concentrations during the P-1 and P-2 pumping tests, which is within the range of laboratory analytical variability.

Figure 10-9: Pumping Test P-2 Layout

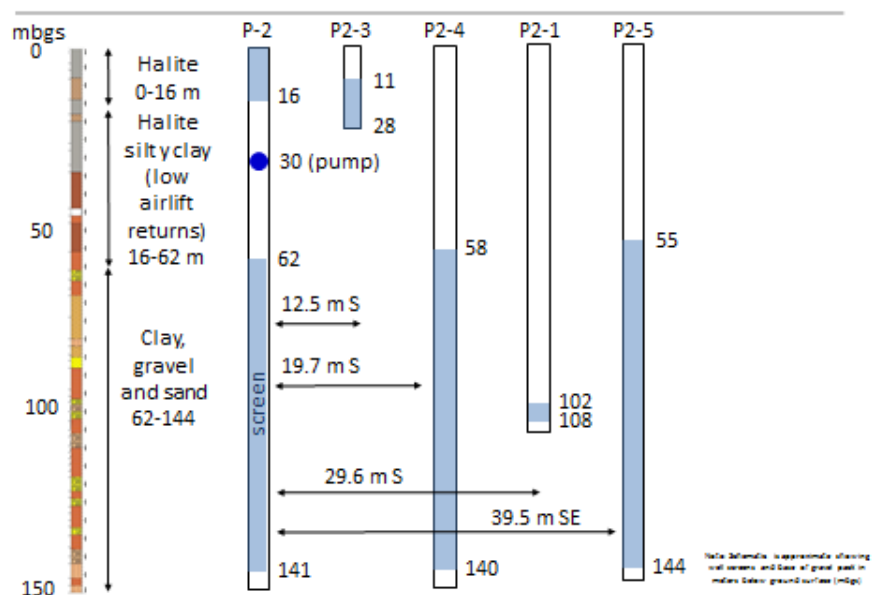


Figure 10-10: Water level responses P-2 constant rate test

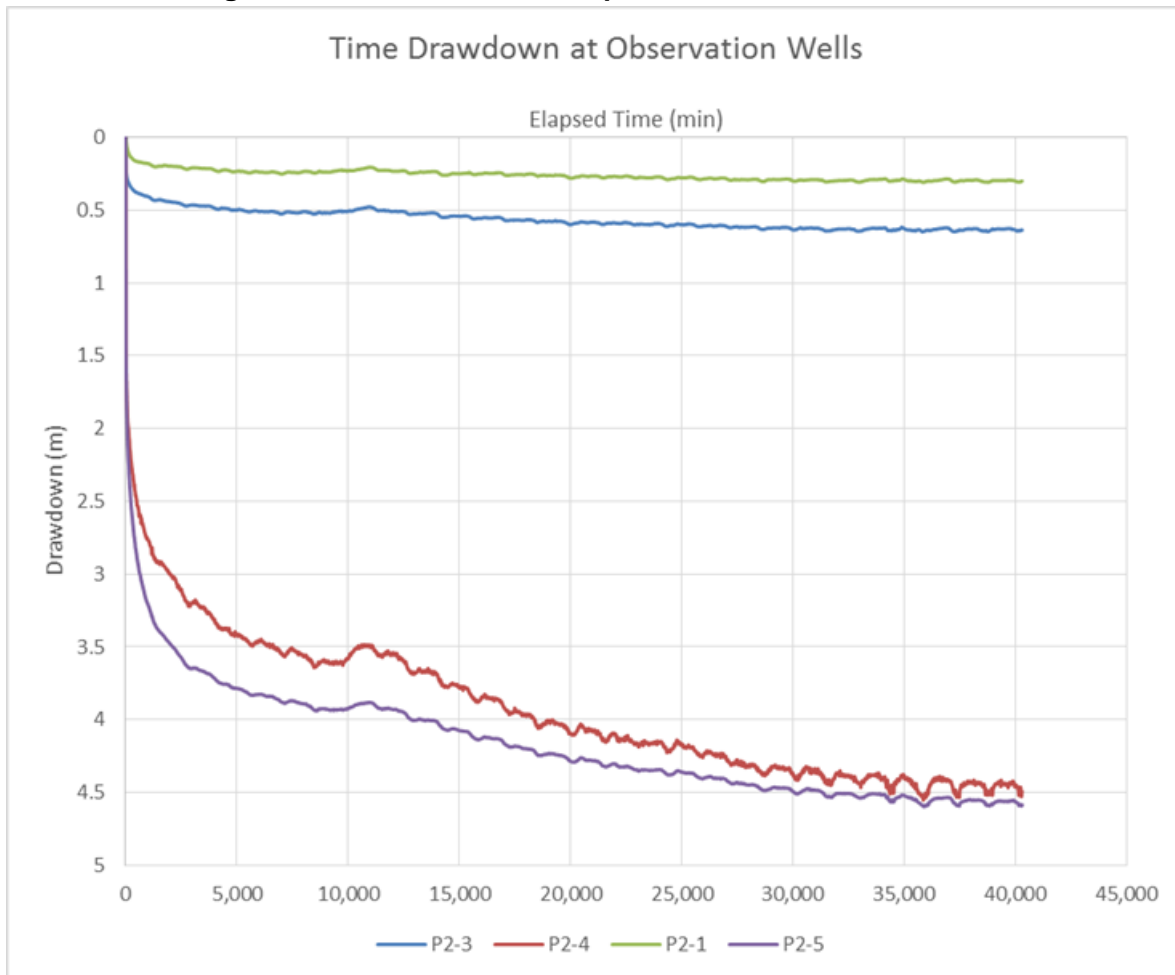


Figure 10-11: P-2 pumping test interpretation

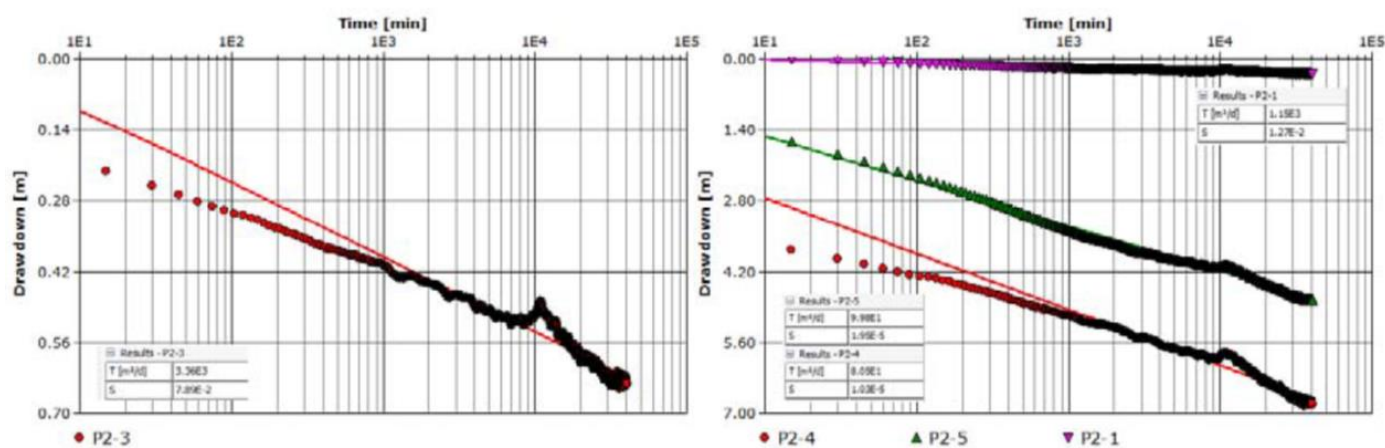
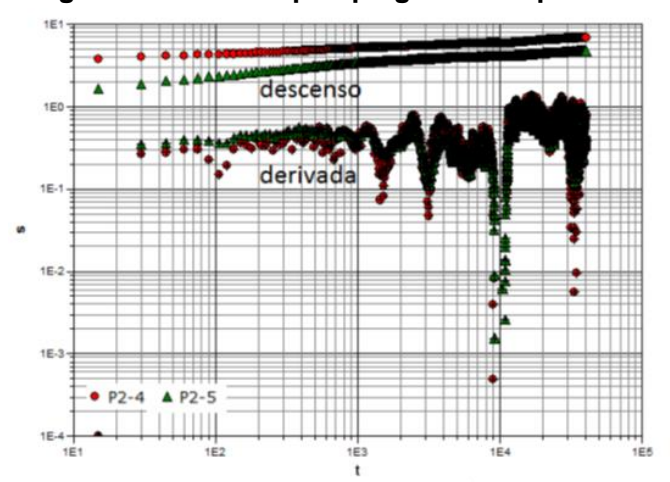
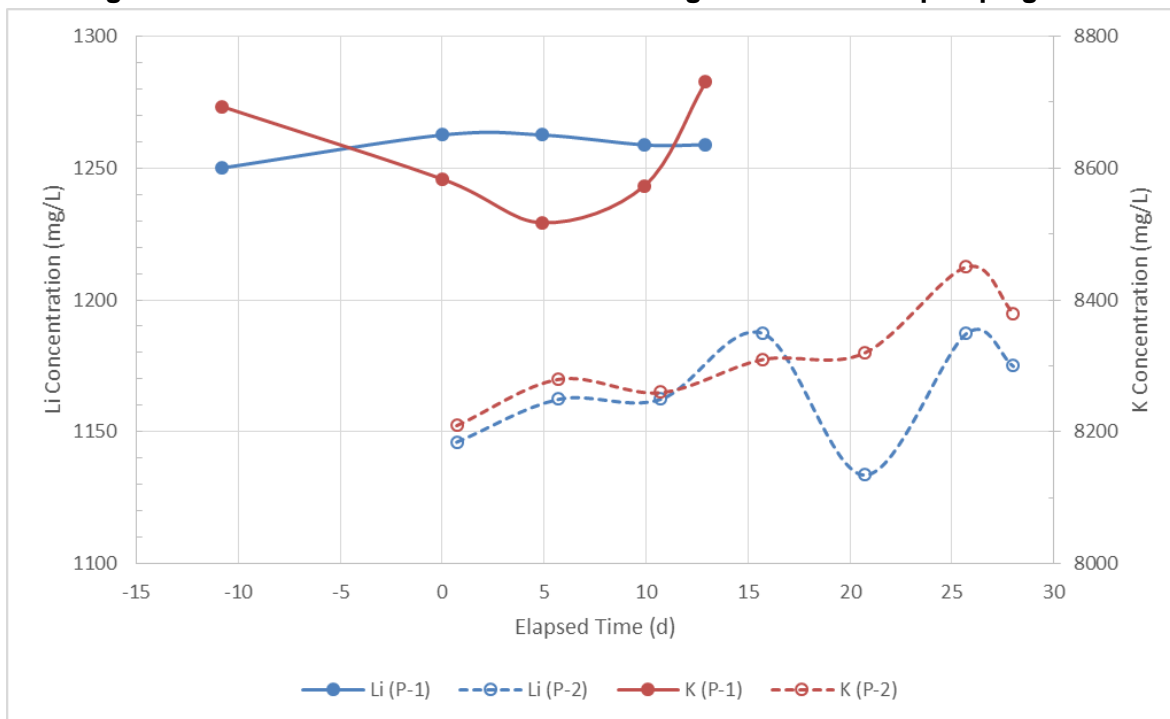


Table 10-4: P-2 Pumping Test Results

Well	Unit	Max Drawdown (m)	Fit	T (m ² /d)	S(-)	K (m/d)	Ss (1/m)
P-2.3	Upper Halite	0.637	Theis	3,360	7.89E-02	197.6	4.64E-03
P-2.1	Upper Halite-clay	0.299	Theis	1,150	1.27E-02	191.7	2.12E-03
P-2.5	Clay core/ lower alluvium	4.723	Theis	99.8	1.95E-05	1.1	2.19E-07
P-2.4	Clay core/ lower alluvium	6.795	Theis	80.5	1.03E-05	0.9	1.17E-07

Figure 10-12: Li and K concentrations during the P-1 and P-2 pumping tests



Source: FloSolutions 2015

10.4.3 P-2 Pumping test – shallow (2017)

A second pumping test was carried out on production well P-2 during 2017. During this test a packer was installed in the well at 40 m depth to isolate the deeper screened interval of the well and pump brine from just the Upper Halite unit. As expected, some brine still entered the upper section of the well via upward vertical flow through the gravel pack. This second test was carried out at 45 l/s over a 7-day period during February 2017. Water level responses were measured in the adjacent monitoring wells (P2-1, P2-3, P2-4 and P2-5). The pumping rate was measured by an inline flow meter, manual measurements and in the V-notch tank. Pressure transducers were installed in all piezometers and the V-notch tank to record water level responses during the test in addition to manual measurements. Observed water level responses to the test are shown in Figure 10-13. The curve fitting and interpretation results of the second P-2 constant rate test are shown in Table 10-5.

Figure 10-13: Water level responses P-2 constant rate test (2017)

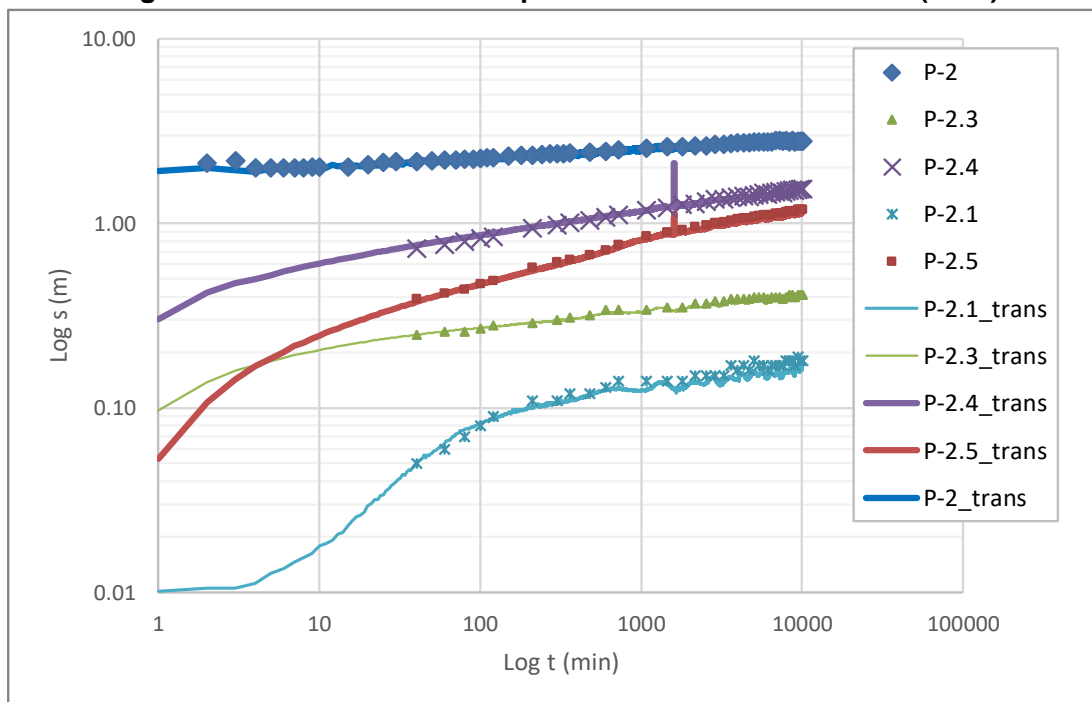


Table 10-5: P-2 pumping test results (2017)

Well	Unit	Max Drawdown (m)	Fit	T (m ² /d)	S(-)	K (m/d)	Ss (1/m)	Sy
P-2.1	Upper Halite	0.17	Neuman	287	7.00E-03	47.8	1.17E-03	19%
P-2.3	Upper Halite and clay	0.4	Theis	10,830	6.00E-04	637.1	3.53E-05	
P-2.4	Clay Core / Lower Alluvium	2.12	Theis	96	1.00E-04	1.1	1.14E-06	
P-2.5	Clay Core / Lower Alluvium	1.14	Theis	95	3.80E-04	1.1	4.27E-06	

10.4.4 P-4 Pumping test (2017)

Production well P-4 is completed with screened casing from 70 and 180 m depth in sands and gravels of the Lower Alluvium (lower aquifer). A bentonite and cement seal were installed in the annulus of the well between 57 m depth and ground surface so that no water from the upper aquifer (Upper Halite) could enter the well. Four monitoring wells (P4-1, P4-2, P4-3 and P4-4) are installed adjacent to well P-4 at radial distances from 10 m to 40 m as shown in Figure 10-14. Piezometer P4-1 is completed in the Lower Alluvium, while piezometers P4-2, P4-3 and P4-4 are all shallow completions in the Upper Halite.

A 30-day constant rate test was conducted at 25 l/s during January / February 2017, followed by recovery. Pumped brine was piped through a 1,200 m plastic line to a V-notch tank where final discharge took place on to the Salar. The pumping rate was measured by an inline flow meter, manual measurements and in the V-notch tank. Pressure transducers were installed in all piezometers and the V-notch tank to record water level responses during the test in addition to manual measurements.

Observed water level responses to the test are shown in Figure 10-15. It should be noted that no water level responses were observed in shallow monitoring wells P4-2, P4-3 and P4-4. The curve fitting and interpretation results of the P-4 constant rate test are shown in Figure 10-16 and Table 10-6.

Figure 10-14: Pumping test P-4 layout

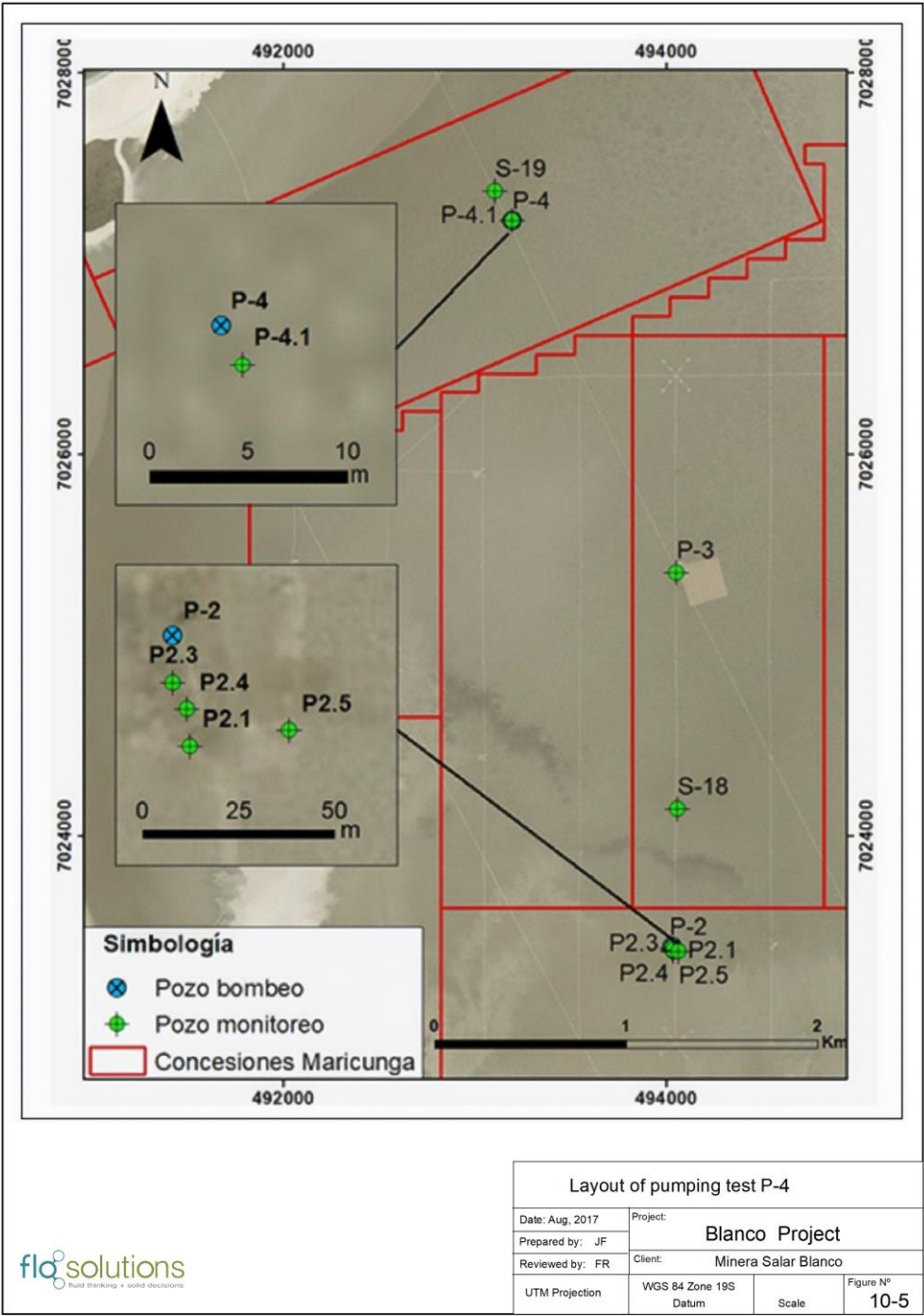


Figure 10-15: Water level responses P-4 constant rate test (2017)

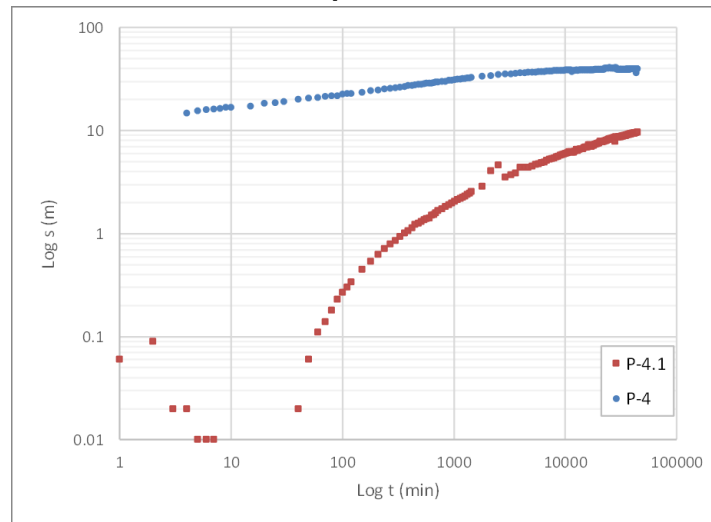


Figure 10-16: P-4 pumping test interpretation

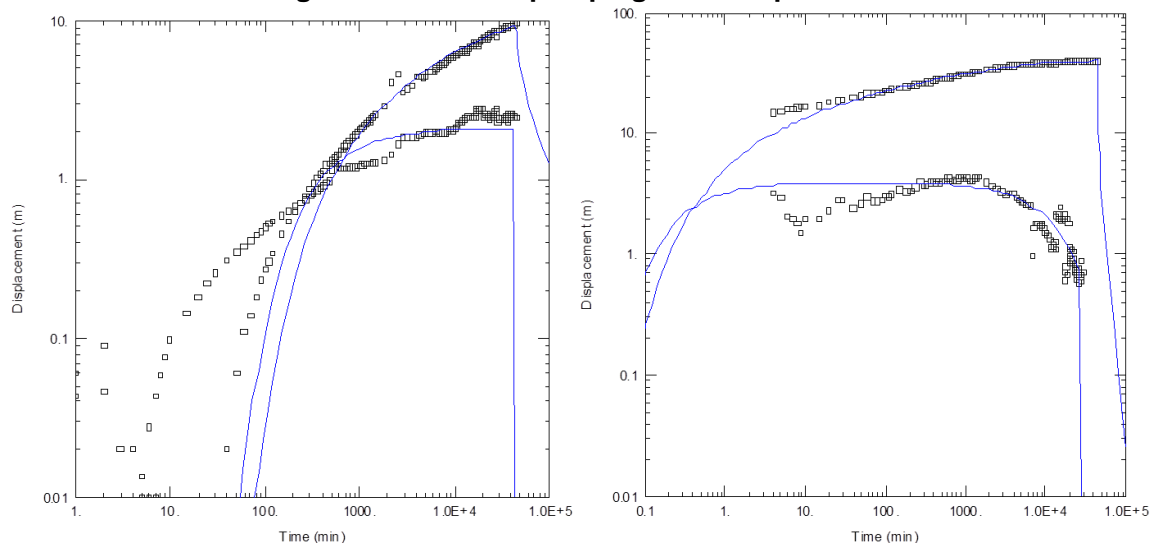


Table 10-6: P-4 pumping test results (2017)

Well	Unit	Max Drawdown (m)	Fit	T (m ² /d)	S(-)	K (m/d)	Ss (1/m)
P-4	Lower aquifer	40.73	Hantush	44		0.4	
P-4.1	Lower aquifer	9.58	Theis	82	4.00E-01	0.9	4.44E-03

11. SAMPLE PREPARATION, ANALYSIS, AND SECURITY

11.1 SAMPLING METHODS

Sampling and sample preparation protocols for the sonic drilling and RC drilling programs in 2011 were developed by Frits Reidel, CPG, Don Hains, P.Geo, and Pedro Pavlovic, Chem Eng. All protocols were implemented at the start-up of the drilling programs in October 2011 under the supervision of Frits Reidel, CPG and included extensive day to day training and supervision of Li3 field staff and experienced MWH hydrogeologists and field technicians. Frits Reidel, CPG was present throughout the drilling program on regular intervals to review the day to day execution of these protocols.

Sampling and sample preparation protocols for the 2016-2018 drilling programs were developed by Frits Reidel, CPG and Murray Brooker, RPGeo. All protocols were implemented at the start-up of the drilling programs in October 2016 under the supervision of Frits Reidel, CPG. Both QP's were present throughout the drilling program on regular intervals to review the day to day execution of these protocols.

11.1.1 Sonic drilling sampling procedures

11.1.1.1 Porosity samples

Sonic core was collected in 1.5 m lexan core liners in alternating 1.5 m intervals as described in Section 10 above. A 10 cm sub-sample was cut from the lexan core liner; caps were placed on each end of the porosity sub-sample and taped to prevent any fluid loss. The samples were labelled with the borehole number and depth interval. Each day the porosity samples were transferred to the workshop in the on-site camp where the samples were labelled with a unique sample number. Prior to shipping each sample was wrapped in bubble plastic to prevent disturbance during shipping.

285 porosity samples were shipped to Daniel B Stephens and Associates (DBS&A) Laboratory in the USA in 2011

32 porosity check samples were shipped to the British Geological Survey (BGS) in the UK in 2011

208 core samples were shipped to Geosystems Analysis (GSA) during the 2016-2018 drilling programs 6 from which 28 samples were analysed by Corelabs as check samples.

11.1.1.2 Brine Samples

Brine samples were collected at three-meter intervals during the 2011 sonic drilling where possible. Based on the experience from the 2011 program the brine sampling interval for the 2016-2018 programs was 6 m. In some cases where the formation permeability was low, it was not possible to collect a brine sample after a one hour waiting period. The borehole was purged by bailing up to three well volumes of brine from the drill casing as calculated from the water level measurement prior to collecting the final brine sample from the bottom of the hole. The final brine

sample was discharged from the bailer into a 20-liter clean bucket from which three one-liter sample bottles were rinsed and filled with brine. Each bottle was taped and marked with the borehole number and depth interval. A small sub-sample from the bucket was used to measure field parameters (density, electric conductivity, pH and temperature) at the wellhead (Figure 11-1).

Figure 11-1: Collection of field parameters of the brine samples at the wellhead



The samples were moved from the drill site to secure storage at the camp on a daily basis. All brine sample bottles are marked with a unique label. One sample bottle was stored as a permanent back-up sample in the on-site warehouse. One sample bottle was prepared for shipment and the third bottle was either used as a duplicate or discarded. No filtration was carried out on the brine samples prior to shipment to laboratories. Figure 11-2 illustrates the porosity samples and brine samples.

Figure 11-2: Porosity and brine samples



11.1.2 RC Drilling Sampling Procedures

11.1.2.1 RC Drill Cuttings (2011)

During RC drilling, rock chip and brine were collected directly from the cyclone. Drill cuttings were collected over two-meter intervals in plastic bags that were marked with the borehole number and depth interval. Sub-samples were collected from the plastic bag by the site geologist to fill chip trays (also at two-meter interval). At the end of each borehole all chip trays were removed to storage in the on-site office (Figure 11-3). All plastic sample bags were stored in a secure on-site warehouse.

Figure 11-3: RC drill chip samples



11.1.2.2 RC Brine Sampling (2011)

Brine samples were collected at three-meter intervals during the RC drilling from the cyclone where possible. In some cases where the formation permeability was low, it was not possible to collect a brine sample. Brine samples were collected in three one-liter (rinsed) sample bottles. Each bottle was taped and marked with the borehole number and depth interval. A small sub-sample from the cyclone was used to measure field parameters (density, electric conductivity, pH and temperature) at the wellhead.

11.1.3 Rotary /HWT brine sampling procedures 2017

11.1.3.1 Rotary Drill Cuttings (2017)

During the rotary drilling, cuttings were collected directly at the head of the borehole in cloth, flow-through bags that minimize the loss of fines but allow fluid to drain at 2 m intervals. The cloth bags were marked with the borehole number and depth interval. Sub-samples were collected from the bags by the site geologist to fill chip trays (also at two-meter interval). At the end of each borehole all chip trays were removed to storage in the on-site office. All sample bags were moved and stored in a secure warehouse in Copiapo.

196 rotary chip samples were shipped to Geosystems Analysis (GSA) in 2017 for GSA classification and consolidation tests.

11.1.3.2 Rotary Brine Sampling (2017)

A plug-type device connected to the wireline cable was used to purge the hole, rather than using a bailer. This consists of a very stiff rubber plug on a steel tool which is lowered down the hole. When this tool is pulled up from the base of the hole the rubber plug expands to flush with inside of the drill rods, drawing brine up the drill rods above the plug, with the brine flowing out of the rods at surface. This works in a similar fashion to the bailer, but in a continuous mode, rather than numerous repetitions of lowering and raising a bailer.

In the case of the rotary drilling it was not possible to lower the HWT casing to a meter above the base of the hole in many cases and consequently inflows from around the sides to the base of the hole could occur. The raising of the plug is likely to have had a suction effect around the base of the hole, stimulating inflows into the hole over a larger area than with the sonic drill holes.

Drilling fluids (in this case brine) are required during the rotary drilling to lift the cuttings out of the hole. The drilling fluid was mixed with a rhodamine / fluorescein tracer dye in portable tanks adjacent to the rig to distinguish the drilling fluid from the natural formation brine (Figure 11-4). Purging of the drill hole was continued until no tracer dye was observed in the purged brine. Any trace of dye observed in brine samples was noted to indicate the potential for contamination with drilling fluid. Brine samples were collected in duplicate at every sampling interval and in triplicate at every fifth sampling interval.

Figure 11-4: Fluorescein tracer dye in the rotary drilling fluid



11.2 BRINE ANALYSIS AND QUALITY CONTROL RESULTS

11.2.1 Analytical methods

The University of Antofagasta in northern Chile was selected as the primary laboratory to conduct the assaying of the brine samples collected as part of the 2011 – 2018 drilling programs. The laboratory of the University of Antofagasta is not ISO certified, but it is specialized in the chemical analysis of brines and inorganic salts, with extensive experience in this field since the 1980s, when the main development studies of the Salar de Atacama were begun. Other clients include SQM, FMC, LAC and Orocobre.

Alex Stewart Argentina in Mendoza, Argentina was used for the analysis of external check samples during the 2011 drilling campaign, while NOA Alex Stewart Argentina in Jujuy was used for external check samples during 2016 – 2018 campaigns. This laboratory is accredited to ISO 9001 and operates according to Alex Stewart Group standards consistent with ISO 17025 methods at other laboratories.

Table 11-1 lists the basic suite of analyses requested from both laboratories. Both used the same analytical methods based on the Standard Methods for the Examination of Water and Wastewater, published by American Public Health Association (APHA) and the American Water Works Association (AWWA), 21st edition, 2005, Washington DC. The University of Antofagasta used Atomic Absorption Spectrometry (AAS) was used for the determination of lithium, potassium, magnesium and calcium. Alex Stewart (Mendoza) employed Inductively Coupled Plasma (ICP), which is generally used for a large suite of elements (multi-elemental analysis), including the detection of trace metals. ASA included 10 elements in the determination with this analytical technique: B, Ba, Ca, Fe, K, Li, Mg, Mn, Na and Sr.

Table 11-1: List of analyses requested from the University of Antofagasta and Alex Stewart Argentina SA Laboratories

Analysis	University of Antofagasta	Alex Stewart	Method
Chemical-Physical Parameters			
Total Dissolved Solids	SM 2540-C	SM 2540-C	Total Dissolved Solids Dried at 180°C
PH	SM 4500-H+B	SM 4500-H+B	Electrometric Method
Density	CAQ – 001DS	IMA-28	Pycnometer
Alkalinity	SM 2320-B	SM 2320-B	Acid-Base Titration
Inorganic Parameters			
Boron (B)	CAQ – 005 BS	ICP - OES	Acid-Base Titration
Chlorides (Cl)	SM 4500-Cl+B	SM 4500-Cl+B	Argentometric Method
Sulfates (SO ₄)	SM 4500 ² -D (Drying of Residue)	SM 4500 ² -C (Ignition of Residue)	Gravimetric Method

Analysis	University of Antofagasta	Alex Stewart	Method
Dissolved metals			
Sodium (Na)	SM 3111 B	ICP-OES 10	Direct Aspiration-AA or ICP Finish
Potassium (K)	SM 3111 B	ICP-OES 10	Direct Aspiration-AA or ICP Finish
Lithium (Li)	SM 3111 B	ICP-OES 10	Direct Aspiration-AA or ICP Finish
Magnesium (Mg)	SM 3111 B	ICP-OES 10	Direct Aspiration-AA or ICP Finish
Calcium (Ca)	SM 3111 D	ICP-OES 10	Direct Aspiration-AA or ICP Finish

11.2.2 Analytical Quality Assurance and Quality Control (“QA/QC”) 2011 Program

A full QA/QC program for monitoring accuracy, precision and potential contamination of the entire brine sampling and analytical process was implemented. Accuracy, the closeness of measurements to the “true” or accepted value, was monitored by the insertion of standards, or reference samples, and by check analysis at an independent secondary laboratory.

Precision of the sampling and analytical program, which is the ability to consistently reproduce a measurement in similar conditions, was monitored by submitting blind field duplicates to the primary laboratory. Contamination, the transference of material from one sample to another, was measured by inserting blank samples into the sample stream at site. Blanks were barren samples on which the presence of the main elements undergoing analysis has been confirmed to be below the detection limit.

Approximately 31 % of the 623 samples submitted for chemical analysis during the 2011 campaign were quality control samples. The QA/QC procedures adopted for the Project are discussed below, and included the following:

Three standards (A, B and C) were inserted at a frequency of 1 in 15 samples (1/3 of each type of standard, randomly inserted). The specially prepared samples were submitted to five laboratories as a Round Robin (each analyzing five 1-L sub-samples from each type of standard) to establish an accepted mean and standard deviations for the analytical variables. These three standards were prepared from Maricunga brine and each with a different dilution factor.

The University of Antofagasta made an internal check on overall analytical accuracy for the primary constituents of the brine by using ion balance. This calculation was checked and the ratio of measured to calculated TDS was added as another procedure for checking the correctness of analyses.

Duplicate samples at a frequency of 1 in 10 samples in the analysis chain were submitted to the University of Antofagasta as unique samples (blind duplicates) to monitor precision.

Stable blank samples (distilled water) were inserted at a frequency of 1 in 30 samples to measure cross contamination.

Duplicates at a frequency of 1 in 10 samples and including blind control samples (a total of 70 samples), were submitted to the secondary laboratory (Alex Stewart in Mendoza) as check samples (external duplicates).

11.2.3 Analytical accuracy 2011 Program

11.2.3.1 Anion-Cation Balance

The anion-cation balance was used as a measure of analytical accuracy. The anion and cation sums, when expressed as equivalents or milliequivalents per liter, must balance in an ideally perfect analysis, because mixtures of electrolytes are electrically neutral. The term meq/L is defined as:

$$\text{Meq/L} = (\text{mg/l} * \text{valence number} / \text{molecular weight of ion})$$

The charge balance is expressed as a percentage, as follows:

$$\% \text{ Difference} = ((\sum \text{Cations} - \sum \text{Anions}) / (\sum \text{Cations} + \sum \text{Anions})) * 100,$$

Although this test does not monitor individual elements, it is recommended by APHA-AWWA-WPCF in their Standard Methods, 21st edition, 2005 (1030 E) as a procedure for checking correctness of water analyses. The typical criterion for acceptance is a maximum difference of 5 %, which is used by the University of Antofagasta as well as by Alex Stewart.

The performance of the University of Antofagasta in the analyses of 431 primary samples and 61 duplicates show a balance within 2 %, i.e. much less than the maximum acceptable difference of 5 %. All the check samples analyzed by Alex Stewart had a balance within a value of 5 %.

11.2.3.2 Measured versus Calculated TDS

Measured versus calculated Total Dissolved Solids (TDS) was used as a second evaluation test of analytical accuracy. The recommended ratio according to the APHAA/AWWA/WPCF Standard Method should be between 1.0 and 1.2. Results for the submitted samples to the University of Antofagasta (431 primary samples plus 61 duplicates) ranged from 0.983 to 1.043, with 10 % of the samples below the acceptable ratio (1.0) and most of these between 0.994 and 1.0. This is considered as a very good performance given the high dissolved solids content of the brine.

Based on the results detailed above, the authors are of the opinion that the sample analytical results are reliable and accurate.

11.2.3.3 Certified Analytical Standards

Three standard reference samples, prepared at site with original brine (Standard A, 100% natural brine; Standard B, 80 %; Standard C, 60 %, dilution with distilled water) were used in the sampling program. Sets of randomized replicates were sent in a Round Robin analysis program to five laboratories (15 sub-samples to each lab) to determine the certified values used to monitor the accuracy of analyses. Statistics were done on the Round Robin assay results and

the standard reference samples certified for the elements that met the criteria of having a global Relative Standard Deviation (RSD) of near 5 % or less.

The results of the standards analyses for Li, K and Mg are summarized in Table 11-2. This table lists the statistics, number of samples exceeding the acceptable failure criteria of the mean \pm 2 standard deviations, and the relative standard deviation (RSD) for each standard. Standard analyses at the University of Antofagasta indicate very acceptable accuracy. There are only two exceptions: one failure for potassium analysis of the Standard A and one failure for Mg analysis of the Standard B. Each of these failures is not significant. From Table 11-2 the relative standard deviation values (measure of precision) for the University of Antofagasta analyses range from 1.36 to 2.67, indicating very good analytical reproducibility for the standard analyses conducted at the primary laboratory. Based on the analysis detailed above, the authors are of the opinion that the lithium, potassium and magnesium analyses are accurate. There is also a good reproducibility or precision in the assay values reported by the University of Antofagasta for these three elements.

Table 11-2: Standards analysis results from U. Antofagasta (2011)

Standard	A	B	C
Statistics	Li (mg/l)		
Count	14	14	14
Min	1095	855	675
Max	1150	950	725
Mean	1128	914	699
Standard Deviation	15.3	21.9	14.2
Mean \pm 2 Standard Deviation			
Mean + 2SD	1159	958	728
Mean - 2SD	1098	870	671
No of Failures >2SD	0	0	0
Relative Standard Deviation			
RSD	1.36	2.40	2.04
Statistics	K (mg/l)		
Count	14	14	14
Min	7896	6291	4883
Max	8510	6830	5215
Mean	8090	6533	5033
Standard Deviation	157.8	142.7	87.3
Mean \pm 2 Standard Deviation			
Mean + 2SD	8405	6818	5207
Mean - 2SD	7774	6247	4858
No of Failures >2SD	1	0	0
Relative Standard Deviation			
RSD	1.95	2.18	1.74
Statistics	Mg (mg/l)		

Standard	A	B	C
Count	14	14	14
Min	6875	5588	4275
Max	7450	6225	4600
Mean	7169	5915	4487
Standard Deviation	148.4	157.7	101.8
Mean ± 2 Standard Deviation			
Mean + 2SD	7466	6231	4691
Mean - 2SD	6872	5600	4284
No of Failures >2SD	0	1	0
Relative Standard Deviation			
RSD	2.07	2.67	2.27

11.2.3.4 Check Analyses

Checks analyses were conducted at Alex Stewart located in Mendoza, Argentina. About 15 % of external duplicates (61 samples) were submitted. In addition, some blanks and standard control samples were inserted to monitor accuracy and potential laboratory bias. The total number of samples in the batch was 70. The standards indicated acceptable accuracy and precision for Li and K.

Statistical analysis of the 61 pairs of check sample assay values was conducted using Reduction-to-Major-Axis ("RMA") multiple linear regressions for Li, K and Mg. StatGraphics software was used for this analysis. The results are summarized in Table 11-3.

Table 11-3: Check assays (U. Antofagasta vs. Alex Stewart): RMA regression statistics

Maricunga Project - RMA Parameters							
Element	R ²	Pairs	m	Error (m)	B	Error (b)	Bias
Li (mg/l)	0.98223	61	0.8598	0.01511	832.787	192.822	14.02%
K (mg/l)	0.98675	61	10.207	0.01539	521.422	141.618	-2.07%
Mg (mg/l)	0.97183	61	10.978	0.02433	-217.714	206.109	-9.78%

The R-squared statistic is the indicator of the quality of the fit. High values of this coefficient reflect a good fit and low values a poor fit.

The bias, which is a measure of accuracy (the higher the bias, the lower the accuracy), is calculated as Bias (%) = 1 – RMA where RMA is the slope (m) of the Reduction-to-Major-Axis regression line of the secondary laboratory ICP values (ASA) versus the primary laboratory AAS values (University of Antofagasta) for each element. Because of different analytical finish, in general the University of Antofagasta obtained a little higher assay values for lithium and a little lower for potassium and magnesium, as shown in Table 11-4.

Table 11-4: Check assays between the University of Antofagasta and Alex Stewart

Statistics	UA Li (mg/l)	ASA Li (mg/l)	UA K (mg/l)	ASA K (mg/l)	UA Mg (mg/l)	ASA Mg (mg/l)
Count	61	61	61	61	61	61
Min	470	447	3,828	4,123	2,838	3,030
Max	1,850	1,697	13,750	14,396	13,200	14,574
Mean	1,240	1,149	8,946	9,654	8,199	8,783
Std Dev	304	264	2,152	2,209	2,146	2,390
Precision		7.5		7.8		7.6
% Bias		14.02		-2.07		-9.78
Correlation		0.98		0.99		0.97
%<10%		88		85		87
%<15%		98		100		98

Precision in Table 11-4 was assessed through the Relative Percent Difference or Relative Error, defined as the absolute value of the difference between two similar analyses, and divided by the average between these two assays. Precision of the external duplicate analyses is acceptable for Li, K and Mg. Eighty-eight per cent of the Li assays are within $\pm 10\%$ of one another (ASA considers acceptable 10% RPD for check samples analyzed in the same lab).

Based on the analysis detailed above, the authors are of the opinion that the check assays indicate that the lithium and potassium concentrations determined for the primary sample assays are suitable for use in a resource calculation.

11.2.3.5 Sample Duplicate Analyses

Sixty-one duplicate samples were collected in the field to confirm the overall sampling precision and shipped also to the University of Antofagasta laboratory. Table 11-5 lists the statistics, as well as the calculated precision, bias, correlation and percent of duplicate analyses with results within 5% of one another. The bias and correlation were calculated through RMA plots, constructed with StatGraphics software. The duplicate analysis repeated exceedingly well, as was shown in these RMA plots.

Table 11-5: Duplicate analyses from the University of Antofagasta

Statistics	Li (mg/l)	Duplicate Li (mg/l)	K (mg/l)	Duplicate (mg/l)	Mg (mg/l)	Duplicate Mg (mg/l)
Count	61	61	61	61	61	61
Min	470	470	3,853	3,918	3,031	3,006
Max	1,938	1,950	13,506	13,519	14,425	14,250
Mean	1,261	1,265	9,098	9,090	8,444	8,445
Std Dev	298	299	2,159	2,134	2,107	2,090
Precision		1.17		1.25		1.31
% Bias		0.03		1.42		1.07

Statistics	Li (mg/l)	Duplicate Li (mg/l)	K (mg/l)	Duplicate (mg/l)	Mg (mg/l)	Duplicate Mg (mg/l)
Correlation		0.99		0.99		0.99
%<5%		100		100		95

Assay results for duplicate samples at the U. Antofagasta indicate excellent precision (within 5 % or less) for Li, K and Mg. Bias between duplicates and main samples are within 2 % and correlation is high ($R^2=0.9938$ to 0.9950) for the three elements.

11.2.3.6 Sample Contamination

Potential sources of sample contamination are related to sample mis-ordering errors or insufficient washing of analytical equipment between samples. A field blank consisting of distilled water was inserted into the sample stream 20 times. New plastic bottles were used in all the cases to avoid eventual contamination with brine samples.

Results reported by the University of Antofagasta indicate <0.05 mg/l (detection limit for lithium) in most blank samples. However, there are four results, corresponding to the last two sample batches with 0.07 (2), 0.08 and 0.09 mg/l for lithium. This reveals that some small contamination with brine was produced in the manipulation of the plastic bottles, either at the project site, or in the lab. This issue is not considered to detract from the validity of the overall sampling and assay results and the use of the assay results in resource estimates.

11.2.4 Analytical Quality Assurance and Quality Control (“QA/QC”) 2016-2018 Program

A total of 363 primary brine samples were analyzed from the 2016-2018 drilling campaigns. An additional 133 brine samples from pumping tests and baseline monitoring were analyzed. These primary analyses were supported by a total 1669QA/QC analyses consisting of:

- 49 standard samples (7 %),
- 89 duplicates (13 %) and
- 28 blank samples (4 %).

In addition to evaluation of standards, field duplicates and blanks the ionic balance (the difference between the sum of the cations and the anions) was evaluated for data quality. Balances are generally considered to be acceptable if the difference is < 5 % and were generally < 1 %. No samples were rejected as having > 5 % balances. The results of standard, duplicate and blank samples analyses are considered to be adequate and appropriate for use in the resource estimation described herein.

11.2.5 Analytical accuracy 2016-2018 Program

11.2.5.1 Anion-Cation balance

The performance of the University of Antofagasta in the analyses of 328 main samples and 32 duplicates show a balance within 3 %, i.e. less than the maximum acceptable difference of 5 %. All the check samples analyzed by Alex Stewart had a balance within a value of 2 %.

11.2.5.2 Measured versus Calculated TDS

Measured versus calculated Total Dissolved Solids (TDS) was used as a second evaluation test of analytical accuracy. The recommended ratio according to the APHAA/AWWA/WPCF Standard Method should be between 1.0 and 1.2. Results for the submitted samples to the University of Antofagasta (308 main samples plus 30 duplicates) ranged from 0.97 to 1.02, with 9 % of the samples below the acceptable ratio of 1.0, and most of these between 0.99 and 1.0. This is considered as a very good performance given the high dissolved solids content of the brine.

Results for the submitted samples to the external laboratory (30 duplicate samples) ranged from 0.98 to 1.14, with only one sample below the acceptable ratio of 1.0, and most of these between 1.02 and 1.14. This is considered as a good performance given the high dissolved solids content of the brine.

Based on the results detailed above, the authors are of the opinion that the sample analytical results are reliable and accurate.

11.2.5.3 Certified Analytical Standards

Two standard reference samples, SRM-1 and SRM-2 were used in the sampling program. Sets of randomized replicates were sent in a Round Robin analysis program to five laboratories to determine the certified values used to monitor the accuracy of analyses. Statistics were done on the Round Robin assay results and the standard reference samples certified for the elements that met the criteria of having a global Relative Standard Deviation (RSD) of near 5 % or less. Overall the performance of University of Antofagasta laboratory and the external laboratory were satisfactory.

The results of the standards analyses for Li, K and Mg, are summarized in Table 11-6. This table lists the statistics, number of samples exceeding the acceptable failure criteria of the mean ± 2 standard deviations, and the relative standard deviation (RSD) for each standard. Standard analyses at the University of Antofagasta indicate an acceptable accuracy. There is one failure for Li and K analysis, and 2 failures for Mg analysis of the Standard SRM-1, and there is no failure for Li analysis and one failure for K and Mg analysis of Standard SRM-2. Overall these failures are not significant. From Table 11-6 the relative standard deviation values (measure of precision) for the University of Antofagasta analyses range from 1.3 to 2.4, indicating very good analytical reproducibility for the standard analyses conducted at the primary laboratory. Based on the analysis detailed above, the authors are of the opinion that the lithium, potassium and magnesium

analyses are accurate. There is also a good reproducibility or precision in the assay values reported by the University of Antofagasta for these three elements.

Table 11-6: Standards analysis results from U. Antofagasta (2016-2018), Lithium

Statistics	Li (mg/l)	
Standard	SRM-1	SRM-2
Count	16	15
Min	476	1,040
Max	500	1,087
Mean	486	1,059
Standard Deviation	7	15
Mean \pm 2 Standard Deviation		
Mean + 2SD	499	1,090
Mean - 2SD	473	1,029
No of Failures >2SD	1	0
Relative Standard Deviation		
RSD	1.4	1.4

Statistics	K (mg/l)	
Standard	SRM-1	SRM-2
Count	16	156
Min	6,150	7,760
Max	6,630	8,540
Mean	6,341	7,986
Standard Deviation	123	195
Mean \pm 2 Standard Deviation		
Mean + 2SD	6,588	8,377
Mean - 2SD	6,094	7,596
No of Failures >2SD	1	1
Relative Standard Deviation		
RSD	1.9	2.4

Statistics	Mg (mg/l)	
Standard	SRM-1	SRM-2
Count	16	15
Min	4,415	5,915
Max	4,730	6,250
Mean	4,557	6,052
Standard Deviation	69	81
Mean \pm 2 Standard Deviation		
Mean + 2SD	4694	6214
Mean - 2SD	4420	5890
No of Failures >2SD	2	1
Relative Standard Deviation		
RSD	1.5	1.3

11.2.5.4 Check Analyses

Checks analyses were conducted at Alex Stewart located in Mendoza, Argentina. A total of 28 samples were submitted. In addition, some blanks and standard control samples were inserted to monitor accuracy and potential laboratory bias. The total number of samples in the batch was 35. The standards indicated acceptable accuracy and precision for Li and K.

Statistical analysis of the 28 pairs of check sample assay values was conducted using Reduction-to-Major-Axis ("RMA") multiple linear regressions for Li, K and Mg. StatGraphics software was used for this analysis. The results are summarized in Table 11-7.

In general, there is an acceptable correlation between the main samples and the external duplicates, with R^2 ranging from 0.919 to 0.955.

The bias is below 5 % with the highest bias (0.55 %) for lithium, lower bias (-3.79 and -3.23) for potassium and magnesium, indicating that the UoA obtained a little higher assay values for lithium and a little lower for potassium and magnesium, as shown in Table 11-7.

Precision of the external duplicate analyses is acceptable for Li, K and Mg. Eighty-three per cent of the Li assays are within ± 15 % of one another.

Table 11-7: Check assays between the University of Antofagasta and Alex Stewart

Statistics	UA Li (mg/l)	ASA Li (mg/l)	UA K (mg/l)	ASA K (mg/l)	UA Mg (mg/l)	ASA Mg (mg/l)
Count	28	28	28	28	28	28
Min	660	566	4,520	4,446	3,880	3,456
Max	1,626	1,517	12,620	12,833	11,000	10,675
Mean	1,015	931	7,744	7,642	6,308	6,064
Std Dev	248	246	1,982	2,053	1,702	1,755
Precision		9.43		5.83		5.94
% Bias		0.55		-3.79		-3.23
Correlation		0.955		0.919		0.955
%<10%		63		77		80
%<15%		83		83		90

Based on the analysis detailed above, the authors are of the opinion that the check assays indicate that the lithium and potassium concentrations determined for the primary sample assays are suitable for use in a resource calculation.

11.2.5.5 Sample Duplicate Analyses

Thirty-two (32) duplicate samples were collected in the field to confirm the overall sampling precision and shipped also to the University of Antofagasta laboratory. Table 11-8 lists the statistics, as well as the calculated precision, bias, correlation and percent of duplicate analyses

with results within 5 % of one another. The bias and correlation were calculated through RMA plots, constructed with StatGraphics software. The duplicate analysis repeated exceedingly well.

Table 11-8: Duplicate analyses from the University of Antofagasta

Statistics	Li (mg/l)	Duplicate Li (mg/l)	K (mg/l)	Duplicate K (mg/l)	Mg (mg/l)	Duplicate Mg (mg/l)
Count	32	32	32	32	32	32
Min	523	516	2,940	2,940	3,215	3,300
Max	3,375	3,342	20,640	20,020	21,800	21,760
Mean	1,123	1,121	8,079	8,101	7,074	7,101
Std Dev	511	511	3,220	3,120	3,370	3,351
Precision		1.79		1.96		1.47
% Bias		0.15		-3.21		-0.58
Correlation		0.997		0.995		0.998
%<5%		93		93		97

Assay results for duplicate samples at the U of Antofagasta indicate excellent precision (within 5 % or less) for Li, K and Mg. Bias between duplicates and main samples are within 3 % and correlation is high ($R^2=0.995$ to 0.998) for the three elements.

11.2.5.6 Sample Contamination

A field blank consisting of distilled water was inserted into the sample stream 21 times. New plastic bottles were used in all the cases to avoid eventual contamination with brine samples. Results reported by the University of Antofagasta indicate <0.05 mg/l (detection limit for lithium) in all of the blank samples. This indicates no lithium contamination during all the sampling and analysis stages.

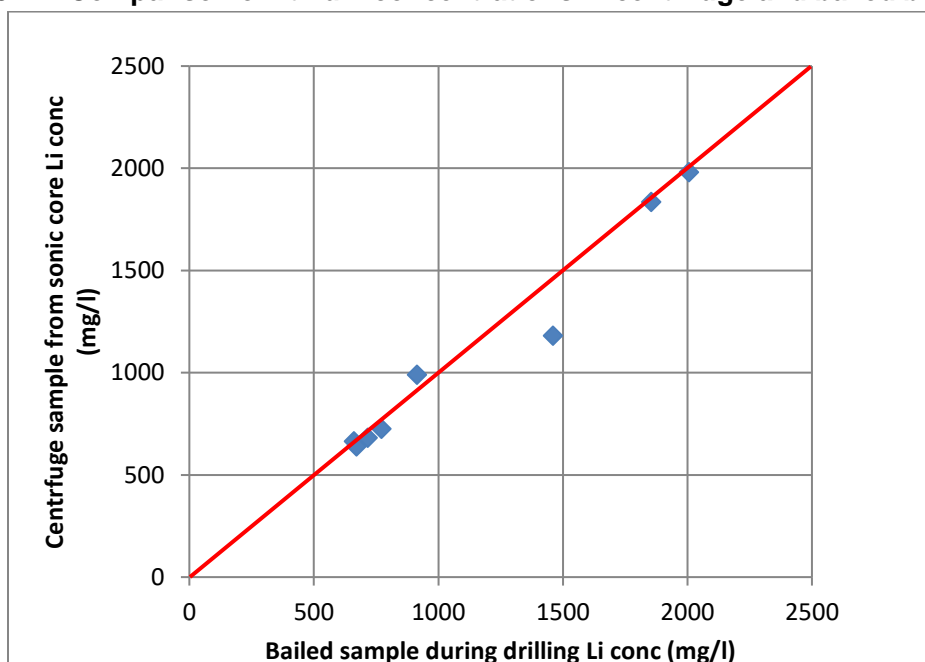
11.2.6 Additional QA/QC analysis 2016-2018 Program

A comparison was carried out between centrifuged brine samples from sonic core and bailed brine samples collected during sonic drilling. Eight sonic cores were centrifuged at 1/3 bar by Corelabs and the released brine was collected and shipped to University of Antofagasta in small sealed glass containers for Li concentration analysis. Table 11-9 shows the selected core samples (borehole and depth interval) with the analysis of the Li concentration of the centrifuged brine and the Li concentration of the bailed brine sample during the sonic drilling at the same depth interval. Figure 11-5 shows the comparison between the bailed and the centrifuged brine samples. The two methodologies show a good correlation.

Table 11-9: Comparison of lithium concentrations in centrifuge and bailed brine samples

Borehole	Depth (m)	Centrifuge Li (mg/l)	Bailed Li (mg/l)
S-1	5	1,834	1,854
S-1	11	990	913
S-1	19	1,980	2,006
S-2	11	1,180	1,460
S-2	89	664	660
S-2	110	725	770
S-2	134	639	670
S-2	152	681	716

Figure 11-5: Comparison of lithium concentrations in centrifuge and bailed brine samples



11.3 DRAINABLE POROSITY ANALYSIS AND QUALITY CONTROL RESULTS

11.3.1 DBSA 2011

Daniel B. Stevens & Associates Inc. in Albuquerque, New Mexico (DBSA) was selected as the prime laboratory for determination of drainable porosity (or specific yield) on the 2011 sonic core samples from boreholes C-1 through C-6. DBSA also undertook analysis of particle size, density and other physical properties of the core samples. DBSA received a total of 285 core samples which had been initially prepared by Li3 staff at the field camp on the Salar. All samples were prepared and shipped to DBSA as detailed in section 11.1 of this report. On receipt of samples at DBSA, the samples were treated in one of three ways in preparation for determination of Relative Brine Release Capacity. These were:

- the entire intact sample was used,
- an intact sub-sample was obtained by cutting the original sample acetate sleeve with a chop saw,
- an intact sub-sample was obtained by pushing a smaller diameter testing ring into the original sample.

All but six samples received were subject to RBRC testing. The six samples not used for RBRC testing were considered to be too brittle or crumbly to obtain an appropriate sub-sample. Thirty-four (34) verification tests (duplicates) were also performed, for a total of 313 RBRC tests. After completion of RBRC tests, 30 samples were selected for particle size analysis.

11.3.1.1 Relative Brine Release Capacity Test

The Relative Brine Release Capacity test predicts the volume of solution that can be extracted from an unstressed geologic sample which is equivalent to drainable porosity. The test method is briefly described below:

Undisturbed samples from the site are saturated in the laboratory using site specific brine solution. The bottom of the samples are then attached to a vacuum pump using tubing and permeable end caps and are subjected to a suction of 0.2 to 0.3 bars for 18 to 24 hours. The top end cap is fitted with a one-gallon air bladder which allows enough drainage while inhibiting continuous atmospheric air flow. The vacuum system permits testing multiple samples simultaneously in parallel. The samples are then oven dried at 60 °C.

Based on the density of the brine, the sample mass at saturation, and the sample mass at 'vacuum dry', the volumetric moisture (brine) contents of the samples are calculated. The difference between the volumetric moisture (brine) content of the saturated sample and the volumetric moisture (brine) content of the 'vacuum dry' sample is the "relative brine release capacity".

This methodology has been widely accepted by companies involved in the lithium brine exploration activities and is regarded as being a suitable method for determination of Specific Yield (Houston, 2011).

DBSA also undertook several verification tests related to RBRC testing. These included the following:

- "Remolded" samples in cases where there was insufficient intact original material for secondary testing. Samples were prepared for testing by remolding the material to target the initial density after the initial testing was performed.
- Samples designated as 'Sub-sample #2' were prepared for testing by obtaining a separate intact sub-sample from the original core.
- Samples designated as 'Day 1' and 'Day 2' are the same sub-sample, only the time the sample was subjected to vacuum suction was varied (18-24 hours and 36-28 hours, respectively).

11.3.1.2 Particle Size Analysis

After RBRC testing, thirty (30) of the samples were chosen to be used for particle size analysis (PSA). The samples were chosen with the intent to represent each of the material types present in the sample batch. Several of the sample results indicate discontinuity between the physical particle size analysis and the hydrometer analysis due to high clay and/or salt content.

DBSA employed the following standard test methods for determination of other physical properties of the samples:

- Dry Bulk Density: ASTM D7263
- Moisture Content: ASTM D7263
- Calculated Porosity: ASTM D7263
- Particle Size Analysis: ASTM D422
- USDA Classification: ASTM D422, USDA Soil Textural Triangle

DBSA relied upon the brine solution density (1.20) provided by Li3 in calculating the volumetric moisture (brine) content. Particle densities of the samples were calculated based on the assumption that the samples were 100% saturated after the saturation stage of the test procedure. The calculated particle density was then used to calculate the total porosity of each of the samples. Volume measurements for each sample were obtained at the “as received”, “saturated”, and “vacuum dry” conditions. It is noted that due to irregularities on the sample surfaces, volume measurements should be considered as estimates.

A total of 20 samples tested were noted to have questionable integrity (QI) relative to the in-situ conditions described by Li3. For sands, silts, and clays a ‘questionable integrity’ designation indicates that the sample may, or may not, accurately represent in-situ conditions (material appeared loose initially) relative to presumed in-situ conditions. For halite cores a ‘questionable integrity’ designation indicates that the sample core had grooves, pits, or other void spaces that may, or may not, be a result of the sampling technique employed. For halite cores a ‘questionable integrity’ may indicate that some dissolution has occurred during testing.

11.3.1.3 RBRC test results

Drainable porosity is largely dependent on lithology which is highly variable as observed from the drilling results. Figure 11-10 shows a plot of total porosity vs drainable porosity based on the results of the DBSA analyses. Therefore, based on visual inspection and particle size analyses the samples were grouped in three types as follows: 1) a halite mix, 2) a silt-clay mix and 3) a sand mix.

Table 11-10 shows the results of the laboratory drainable porosity analyses.

Figure 11-6: DBSA laboratory specific yield (S_y) analyses against total porosity

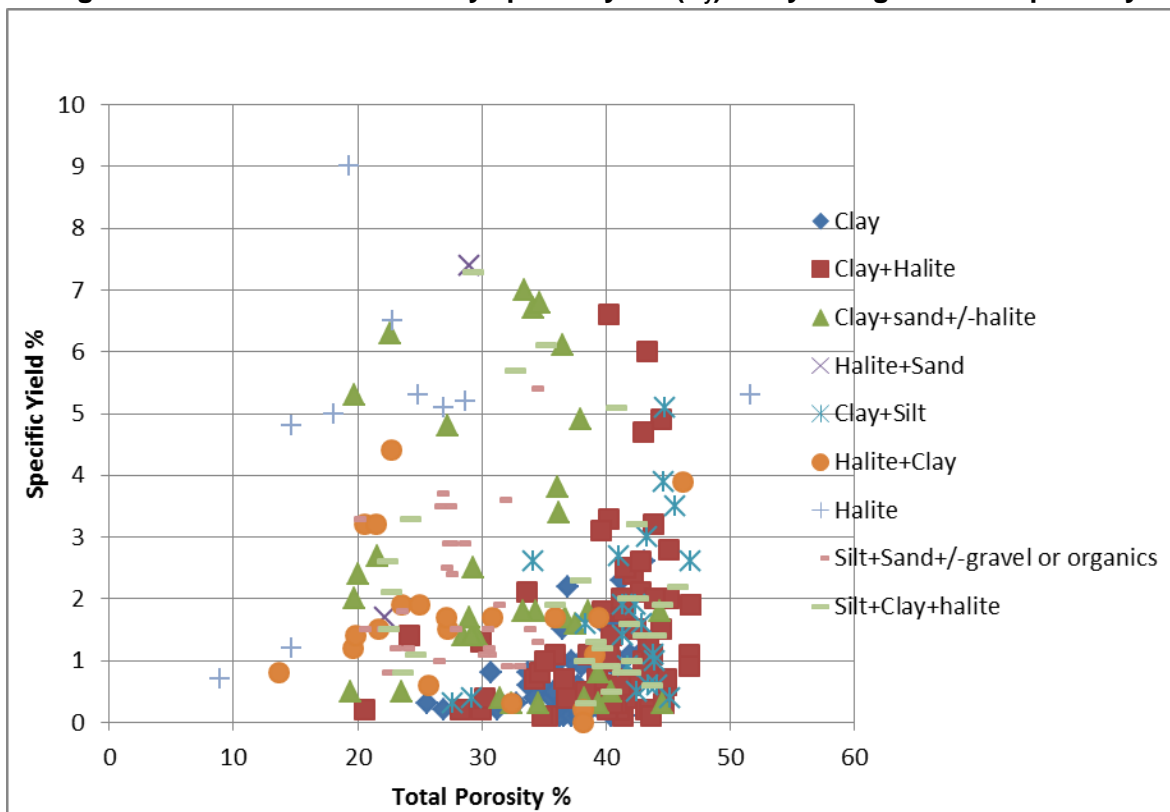


Table 11-10: Results of laboratory specific yield (S_y) analyses

	S_y - Halite mix	S_y - Silt-clay mix	S_y - Sand mix
Number of samples	56	195	29
Max	0.203	0.066	0.310
Min	0.002	0.001	0.015
Mean	0.034	0.012	0.061
Standard Deviation	0.038	0.011	0.058

11.3.1.4 British Geological Survey QA/QC tests 2011

Thirty (30) sonic core samples were shipped to the British Geological Survey (BGS) for determination of porosity and specific yield as a check against the DBSA results. The samples were duplicates of samples shipped to DBSA for RBRC testing. Samples were initially centrifuged to release pore fluid to determine S_y in "as received conditions". The chemistry of released pore fluid was analyzed as a double check against UoA and ASA results and found to be similar. The samples were then re-saturated and allowed to drain (similar to the RBRC test) and then oven dried to obtain total porosity values

Results of the BGS test work showed significantly higher drainable porosity values than reported by DBSA, as shown in Figure 11-11, however DBSA shows significantly higher total porosity values (Figure 11-12). It is possible that the DBSA testing methodology systematically underestimates drainable porosity for finer grained sediments (clay and silt).

Figure 11-7: Comparison of BGS and DBSA specific yield (S_y) analyses

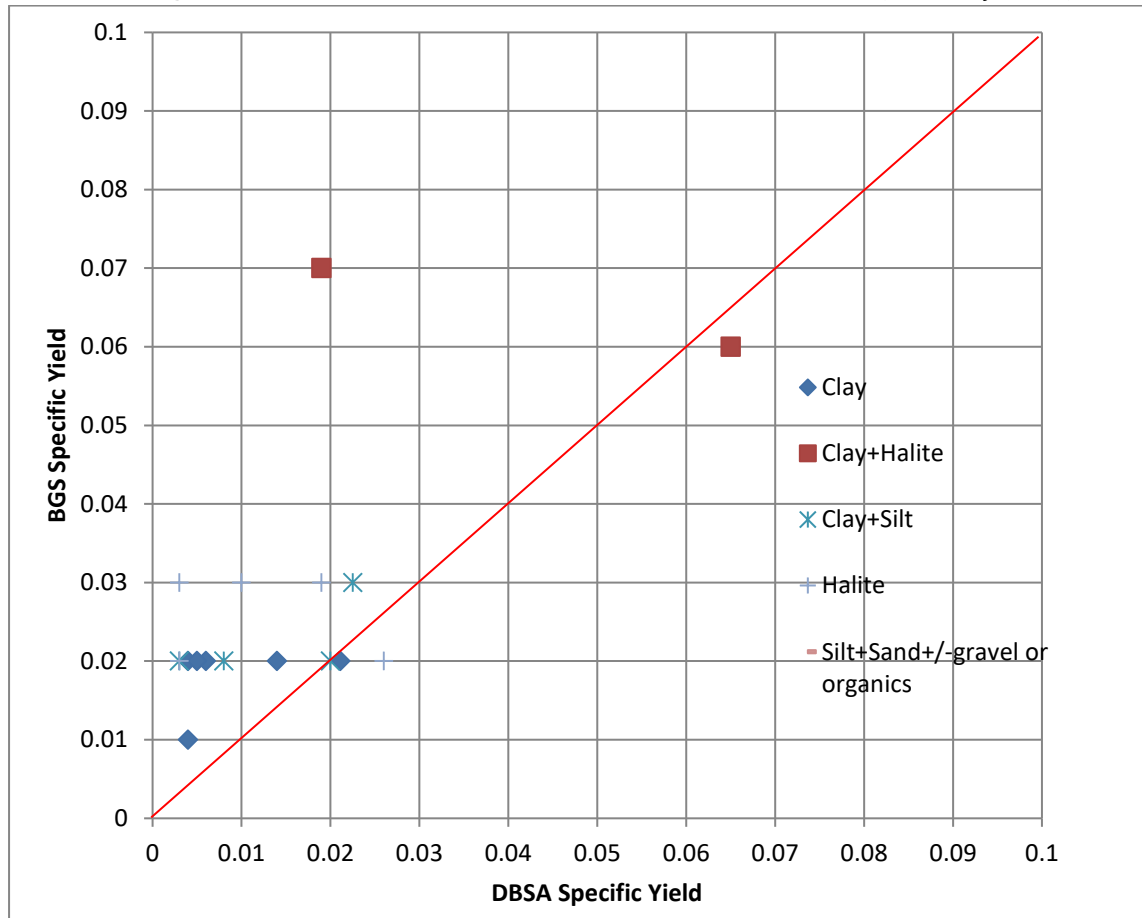
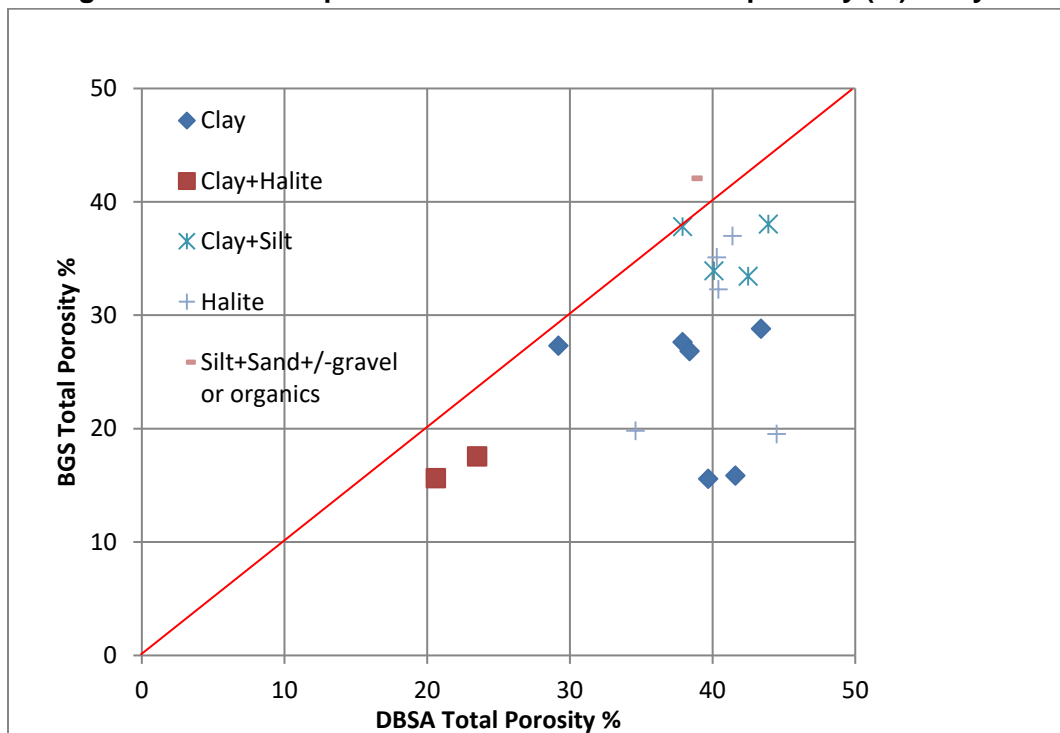


Figure 11-8: Comparison of BGS and DBSA total porosity (P_t) analyses



11.3.2 GSA 2016-2018

The Relative Solution Release Curve (RSRC) method was used by the GSA Laboratory (Tucson, AZ) to determine S_y and P_t . A subset of paired samples was tested using the Centrifuge Moisture Equivalent of Soils (Centrifuge) method by Core Laboratories (Houston, TX). The goals of the test work were to provide S_y and P_t values for each sample and summary statistics of S_y and P_t values by lithological group; to compare the results from the core and tri-cone samples; and to compare the S_y and P_t values for paired sonic core samples derived from the RSRC and Centrifuge methods. Table 11-11 shows an overview of the laboratory test work performed by GSA.

190 10-cm diameter sonic drill intact core samples (core) from boreholes S-1A, S-2, S-18, S-20, S-23, and S-24 and 196 unconsolidated tri-cone samples from boreholes S-3A, S-5, S-6, S-11, S-13, and S-19 were received by GSA. The core samples which ranged in length from 10 to 20 cm, were received wrapped in cellophane and bubble-wrap in a re-sealable bag or in a clear, lexan sleeve with end caps duct-taped; the tri-cone rotary samples were in plastic bags. Table 11-12 lists the lithology of the samples received. For interpretation of RSRC and Centrifuge method results, samples were classified into the following categories: clay-dominated, sand-dominated, gravel-dominated, halite, ulexite, and volcanoclastic material.

Table 11-11: GSA laboratory tests performed

Test Type	Sample Type and Number	Test Method	Testing Laboratory	Standard
Physical	184 Core samples 49 Tri-cone samples	Bulk Density	GSA Laboratory, (Tucson, AZ)	ASTM D2937-10
	29 Tri-cone samples	1-D Consolidation	Pattison Engineering and Geo-Logic Associates, (Tucson, AZ)	ASTM D2435
Hydraulic	28 Core samples	Centrifuge Moisture Equivalent of Soils	Core Laboratories (Houston, TX)	Modified ASTM D425-17
	184 Core samples 49 Tri-cone samples	Estimated Total Porosity Estimated Field Water Capacity Relative Solution Release Capacity (RSRC)	GSA Laboratory (Tucson, AZ)	MOSA Part 4 Ch. 2, 2.3.2.1 MOSA Part 4 Ch. 3, 3.3.3.2 Modified ASTM D6836-02 MOSA Part 4 Ch. 3, 3.3.3.5

Table 11-12: Sample lithology and GSA classification

Lithology Code	Lithology	Number of Sonic Core Samples	Number of Tri-cone Samples	GSA Material Classification
C	Clay	51	1	Clay dominated
C+H	Clay and halite	4		Clay dominated
SC	Sandy clay	5		Clay dominated
S	Sand	4	92	Sand dominated
SS	Silty sand	10	9	Sand dominated
CS	Clayey sand	7	4	Sand dominated
CG	Clayey gravel	7		Gravel dominated
SG	Sandy gravel	15	7	Gravel dominated
H	Halite	8	3	Halite
H+C	Halite and clay	12		Halite
U	Ulexite	5		Ulexite
V	Volcaniclastic	42	80	Volcaniclastic

11.3.2.1 Sample Preparation

Undisturbed 10 cm diameter by 10 to 20 cm length sonic core samples were prepared to fit into HQ (6.35 cm diameter by 2.5 cm length) stainless steel liners by driving the liners into the in-tact sonic cores using a hydraulic press in order to maintain the core sample bulk density. The soil cores were carefully trimmed to the same height and width as the liners. Care was taken to reduce core handling that could modify the physical structure of the core and effect porosity and drainage

measurements. The core samples were prepared using identical procedures for the RSRC and Centrifuge methods, except the samples for the Centrifuge method were prepared in 3.8 cm diameter and 5 cm length stainless steel sleeves. Seventeen core samples appeared to contain a significant amount of material greater than 0.63 cm in diameter. The bulk density of these in-tact cores were measured (ASTM D2937-10) and then the material was re-packed into a 15 cm diameter Tempe cell for RSRC testing.

It was not possible to test six of the S-18 borehole core samples: 2 H, 1 V, and 1 H+C cores from 120 m to 127 m depth and 1 U and 1 C core from 152 m to 155 m depth, because these cores were dominated by solid salt crystals and could not be prepared for testing. Figure 11-9 shows the rejected samples.

Figure 11-9: Rejected core samples



To seal the stainless steel liner of the HQ samples, a pre-wetted micro-pore membrane (rated 760 mbar air entry) was placed into a bottom PVC cap and top cap was added and the sample was sealed air-tight with gaskets and connectors between both PVC caps as shown in Figure 11-14.

The HQ core assembly was then saturated with a brine solution prepared to mimic the Maricunga brine solution (specific gravity = 1.2 g/cm³). Saturation was achieved by repetitively applying solution from the bottom of the assembly and then applying vacuum (30 to 50 mbar) from the top of the core to assist the saturation. The core samples for the Centrifuge method were prepared by immersing the core samples into brine solution for 24 hours and allowing the solution to saturate from the bottom. The 15 cm cells and HQ core assemblies packed with tri-cone samples were slowly injected with the brine solution from the bottom of the assembly until the material was saturated. The 15-cm cells and HQ core assemblies packed with tri-cone samples saturated quickly, so no vacuum was needed. Any standing brine solution was carefully removed prior to starting the test.

11.3.2.2 Relative Solution Release Capacity (RSRC) Sample Testing

HQ core samples and the 15-cm diameter repacked core samples were tested in the GSA laboratory using the RSRC method to measure the amount of brine that may be released under gravity drainage conditions from saturated porous media (i.e. the specific yield, S_y). The RSRC is based on the moisture retention characteristic method using the Tempe cell design (Modified ASTM D6836-02). Total porosity (P_t) is also measured in the RSRC method.

Each core assembly was transferred to a test rack for the pressure extraction procedure as shown in Figure 11-10. Three pressure steps were applied to each core assembly: the first step was applied without pressure for a day and any free water due to over saturation was removed from this step. Two sequential pressure steps, 120 mbar and 333 mbar (estimated field water capacity, MOSA Part 4 Ch. 3, 3.3.3.2), were used to approximate brine solution release at 120 mbar and 333 mbar of the brine solution. The 120 mbar pressure step was maintained for two days and the 333 mbar was continued for another two to four days. Core assemblies were weighed prior to saturation, after saturation, and then two to three times daily to determine loss of brine solution content over time. Samples were oven dried after the final step to determine P_t (MOSA Part 4 Ch. 2, 2.3.2.1). P_t was calculated as:

$$1 - (\text{Bulk density} / \text{Particle density})$$

Brine solution release volumes at the 120 mbar and at 333 mbar pressure steps were estimated as the difference of the brine weight divided by the brine specific gravity (1.2 g/cm^3) between the initial cell assembly mass and the mass after each pressure plate step (MOSA Part 4 Ch3, 3.3.3.5). The solution release volume (specific yield) from saturation to 333 mbar can be considered to approximate the maximum solution drainage under gravity/pumping conditions and was calculated as follows:

$$S_y = (w_s - w_{333 \text{ mbar}}) / (A * L * B_{sg})$$

Where: w_s is the saturated weight, $w_{2 \text{ mbar}}$ is the weight at 333 mbar, A is sample area, L is sample length, and B_{sg} is the specific gravity of the brine solution.

One hundred and eighty-four (184) core samples were measured for P_t and S_y using the RSRC method.

Figure 11-10: Relative Solution Release Capacity (RSRC) HQ core sample testing



11.3.2.3 Centrifuge Moisture Equivalent of Soils Sample Testing

The repeatability of S_y and P_t measurements was assessed by testing 28 paired samples using the RSRC method by GSA and the Centrifuge Moisture Equivalent of Soils (Centrifuge) method by Core Laboratories (Houston, TX). GSA packed all of the samples in stainless steel sleeves, saturated them with a brine solution prepared to mimic the Maricunga brine solution, and shipped to Core Laboratories. The sample pairs were of adjacent sections of the same core section and thus reflect similar lithologies as closely as possible, although there is no way of repeating the analysis on exactly the same sample.

Saturated samples were weighed, placed in a low-speed centrifuge for four hours, and then removed from the centrifuge and weighed for a second time. The centrifuge speed was selected to produce suction on the samples equivalent to 330 mbar. Specific yield was calculated as described in Section 11.3.3 Cores were oven dried at a low temperature for five days to determine the residue brine content and bulk density. Particle density was measured using Boyle's Law on oven-dried samples. P_t was calculated as above.

11.3.2.4 GSA Drainable Porosity Results

In order to assess the relationship between the porosity parameters (P_t and S_y) and lithology, samples were classified into the following categories: clay-dominated, sand-dominated, gravel-dominated, halite, ulexite, and volcanoclastic material as shown in Table 11-12 and Figure 11-1. Histograms and normal distributions for the GSA core data are shown in Figure 11-2 by category and a summary of all of the data is given in Table 11-13. Figure 11-3 and Figure 11-4 compare all of the P_t and S_y data, respectively, by borehole as measured by GSA and Core Laboratories.

P_t generally increases from gravel-dominated material (lowest porosity) to sand and then clay-dominated material (highest porosity). Volcanoclastic material also had high P_t values, similar to the gravel-dominated material. The halite material had low P_t values, similar to gravel-dominated material, but three halite samples could not be tested because they contained cemented salt crystals. Only five ulexite samples were tested; these also had low porosity (mean= 0.35). Mean values were in good agreement with literature values for these types of sediments (Morris and Johnson, 1967).

In contrast, S_y increased with increasing particle size; therefore, the gravel-dominated material showed the highest S_y values, followed by sand and then clay-dominated material with the lowest S_y values. The volcanoclastic material showed similar S_y values to the gravel-dominated material. The halite samples had intermediate S_y values similar to the sand-dominated material, but not all of the halite samples could be tested because some were cemented and solid, and therefore would have little to no S_y . Ulexite material had lower S_y values than the sand-dominated material.

Mean values for S_y were in good agreement with literature values for these types of sediments (Johnson, 1967). The halite samples showed a relatively wide range of P_t values. There was a relatively wide range of S_y values for the gravel-dominated, volcanoclastic, and halite material. The gravel-dominated material included clayey-gravels, which had lower S_y values than the sandy gravels.

Figure 11-11: GSA specific yield vs GSA total porosity

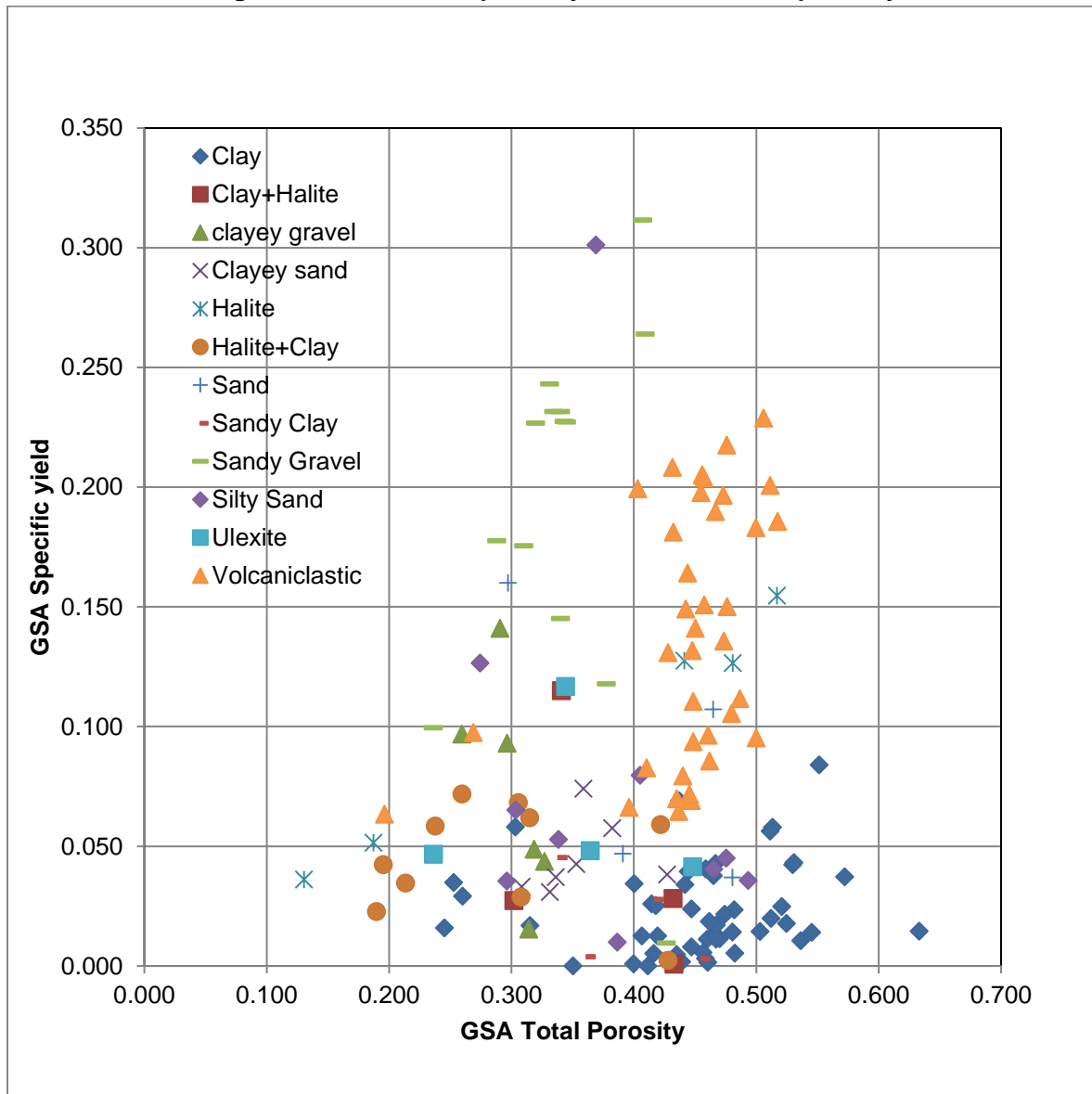
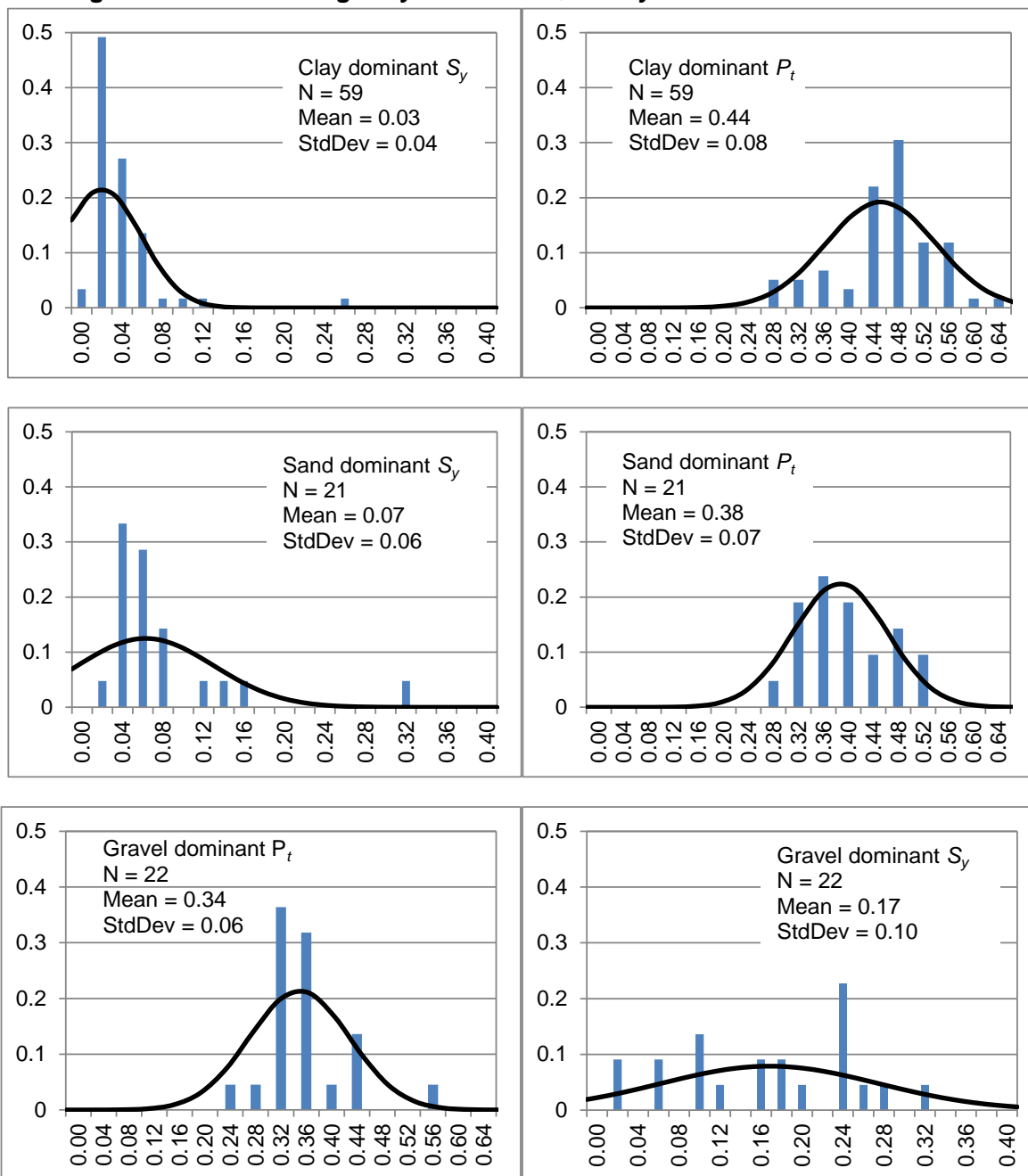


Figure 11-12: Lithologically classified P_t and S_y distributions and statistics



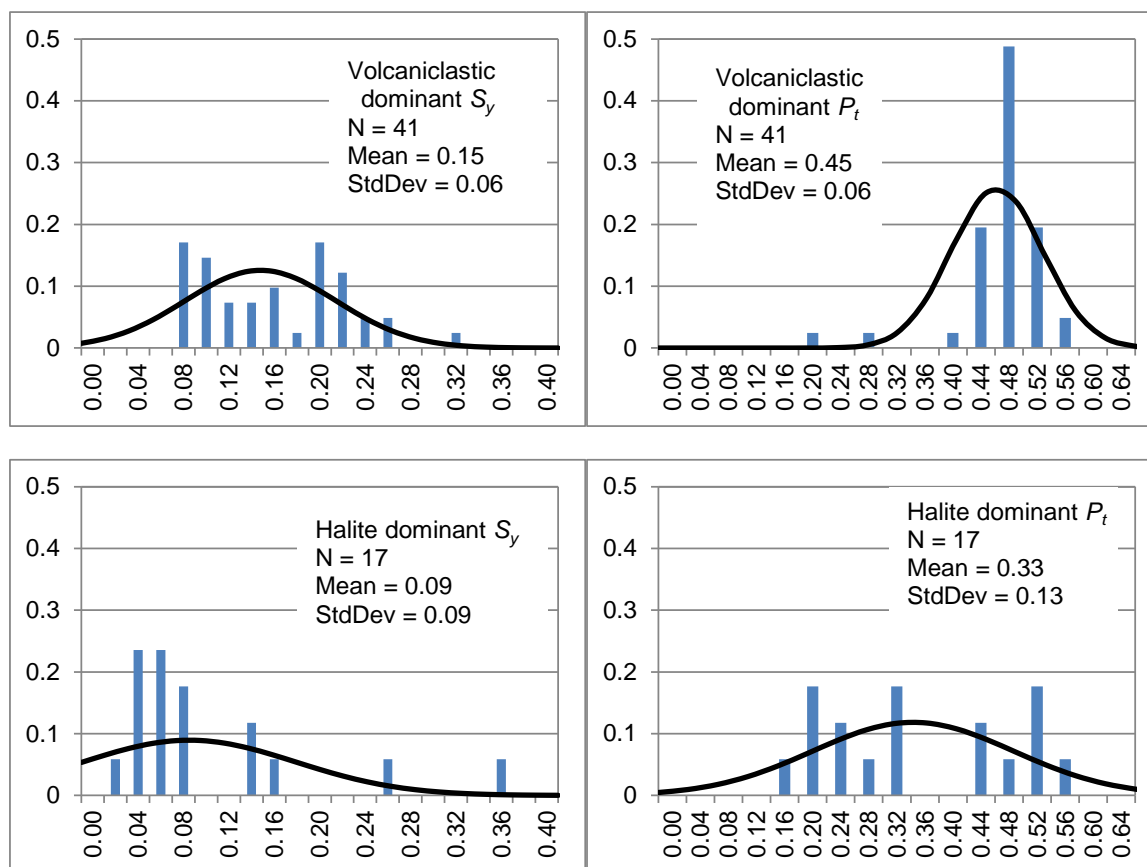


Table 11-13: Summary of total porosity and specific yield by lithological group and laboratory

Lithological Group	Core Lab Total Porosity (P _t)			GSA Total Porosity (P _t)			Core Lab Specific Yield (S _y)		GSA Specific Yield (S _y)	
	N	Mean	StdDev	N	Mean	StdDev	Mean	StdDev	Mean	StdDev
Clay dominated	6	0.53	0.05	59	0.44	0.08	0.02	0.03	0.03	0.04
Sand dominated	3	0.45	0.08	21	0.38	0.07	0.05	0.04	0.07	0.06
Gravel dominated	3	0.32	0.02	22	0.34	0.06	0.10	0.07	0.17	0.10
Volcaniclastic	13	0.46	0.05	41	0.45	0.06	0.13	0.05	0.15	0.06
Halite	2	0.35	0.08	17	0.33	0.13	0.07	0.05	0.09	0.09
Ulexite	1	0.49	N/A	5	0.35	0.09	0.04	N/A	0.05	0.04

Figure 11-13: Comparison of total porosity estimated by GSA using RSRC method and Core laboratory using the Centrifuge method

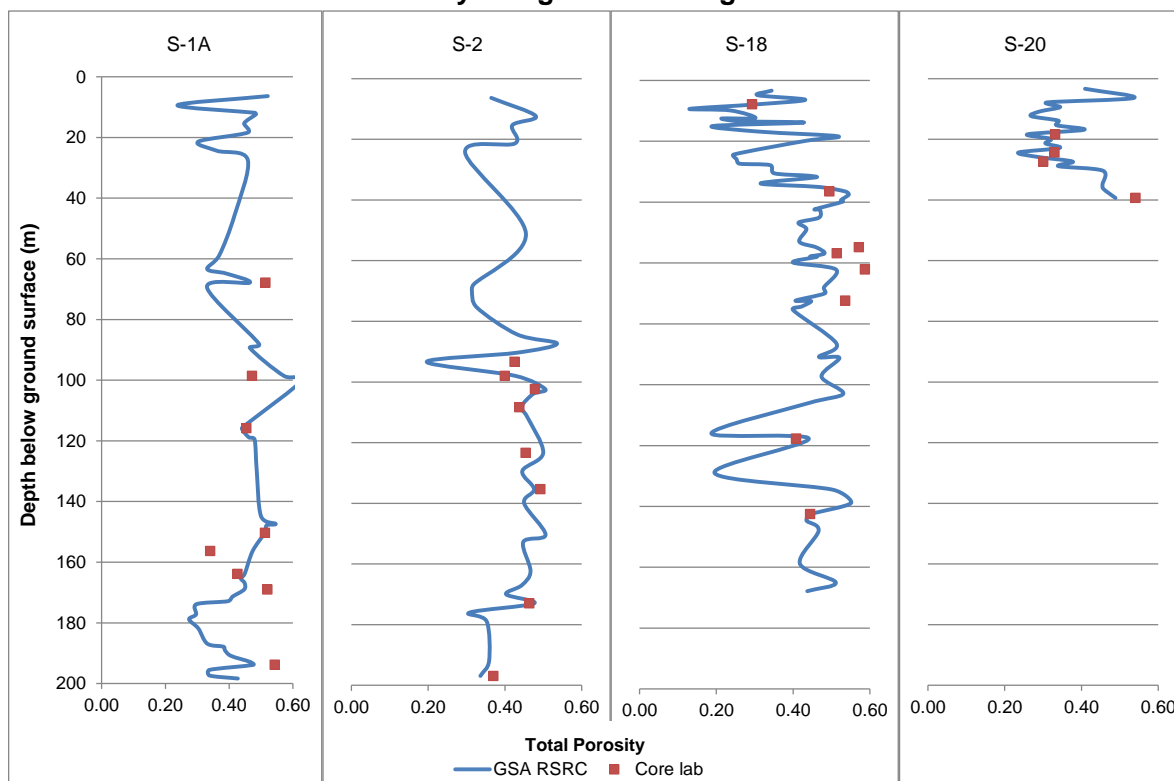
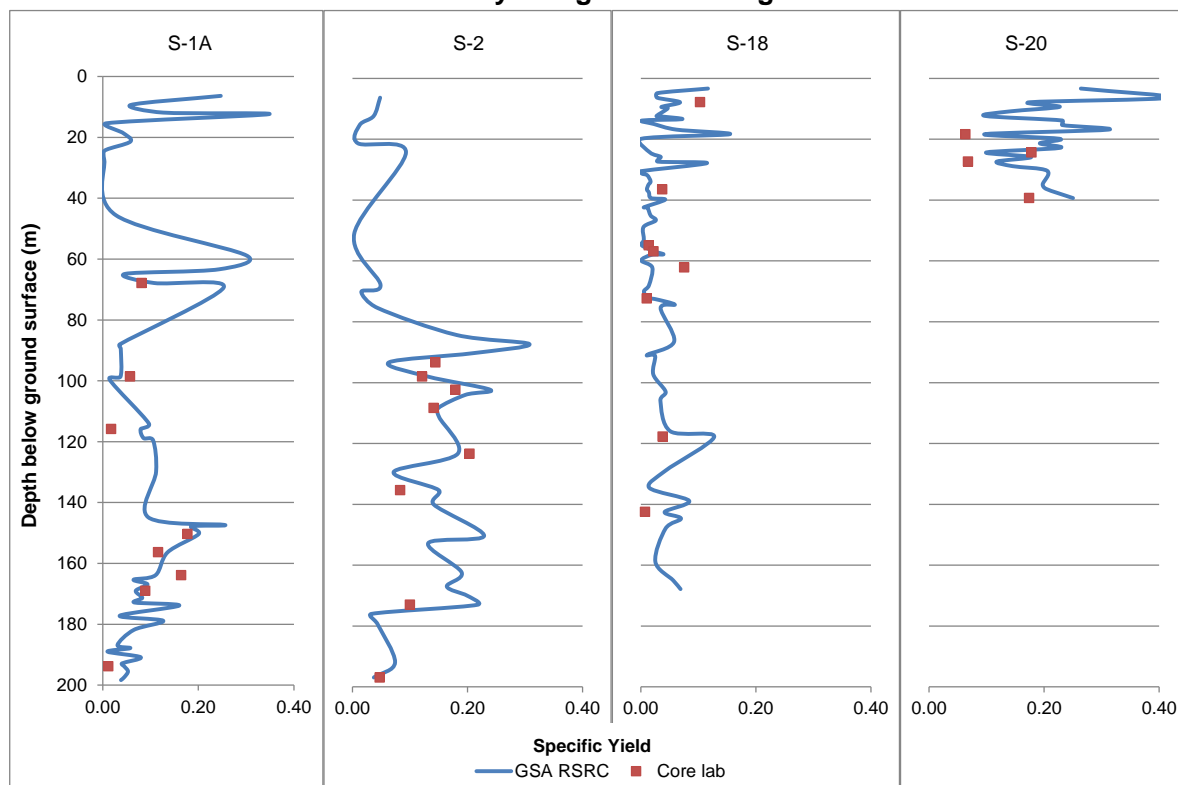


Figure 11-14: Comparison of specific yield estimated by GSA using RSRC method and Core laboratory using the Centrifuge method



11.3.3 Quality Control – GSA and Core Laboratory Determinations of S_y and P_t

Table 11-14 provides summary statistics and Figure 11-15 compares the measured S_y (drainable porosity) values by lithological category between the laboratories. There is good agreement between the specific yield data ($R^2 = 0.62$); correlation is lower between the total porosity data ($R^2 = 0.39$). The S_y values measured by GSA are in general similar or slightly higher than the S_y measured by Core Laboratories, except for the clay samples, where the results from GSA were slightly lower than the Core Laboratories results. The largest difference in the paired results was for volcanoclastic material.

Table 11-15 provides summary statistics and Figure 11-16 compares the measured total porosity P_t values by lithology between the laboratories. The P_t was frequently higher measured by Core Laboratories compared to GSA.

Table 11-14: Comparison of S_y values between GSA and Corelabs

	Clay Dominated		Sand Dominated		Gravel Dominated		Halite		Ulexite		Volcaniclastic	
	Core	GSA	Core	GSA	Core	GSA	Core	GSA	Core	GSA	Core	GSA
N	7	7	3	3	3	3	1	1	1	1	13	13
Mean	0.03	0.02	0.05	0.06	0.10	0.10	0.10	0.13	0.04	0.04	0.13	0.15
Standard Deviation	0.02	0.02	0.04	0.04	0.07	0.01	N/A	N/A	N/A	N/A	0.05	0.06
Average Relative % Difference	3%		21%		1%		21%		11%		13%	

Figure 11-15: Comparison of S_y values between GSA and Corelabs

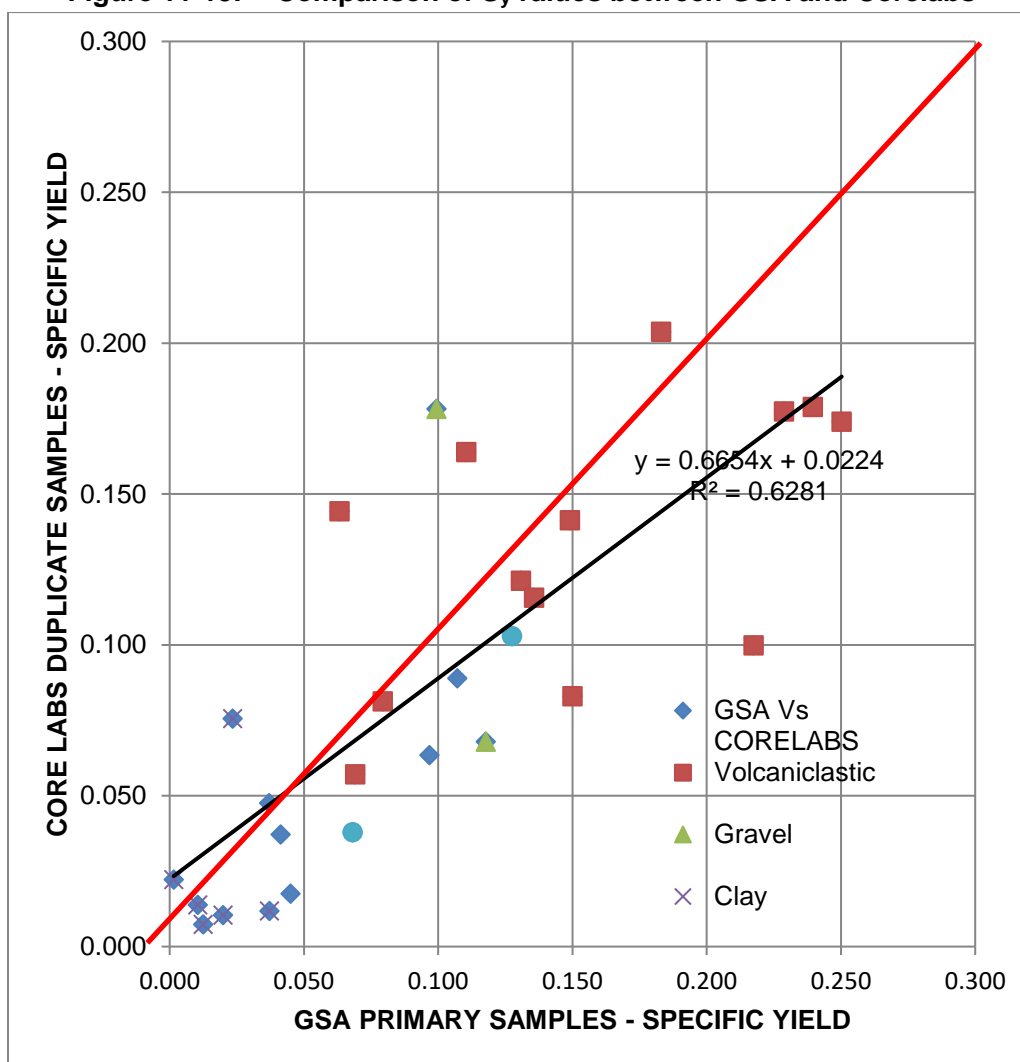
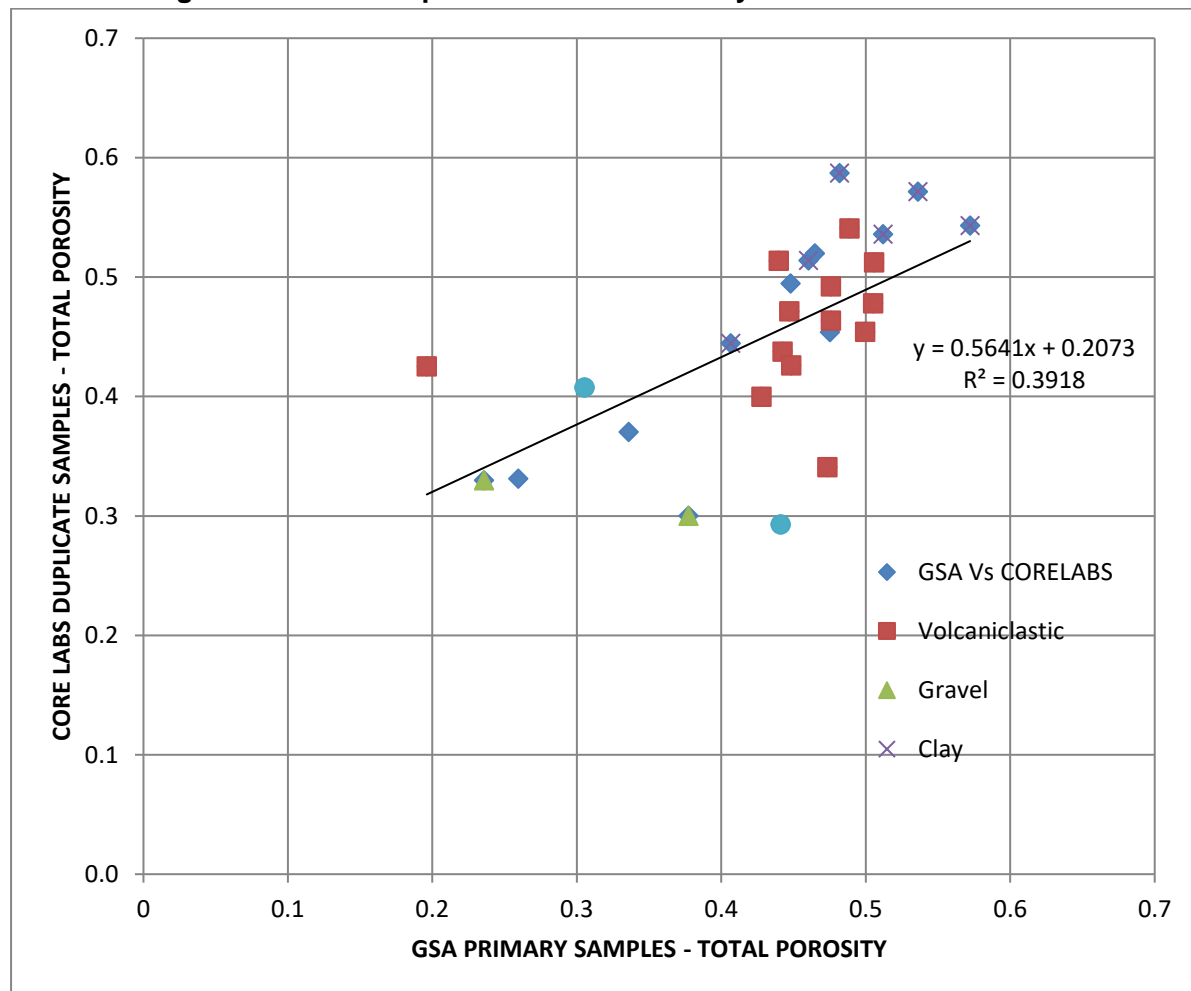


Table 11-15: Comparison of Total Porosity between GSA and Corelabs

	Clay Dominated		Sand Dominated		Gravel Dominated		Halite		Ulexite		Volcaniclastic	
	Core	GSA	Core	GSA	Core	GSA	Core	GSA	Core	GSA	Core	GSA
N	7	7	3	3	3	3	1	1	1	1	13	13
Mean	0.51	0.47	0.45	0.43	0.32	0.29	0.29	0.44	0.49	0.45	0.46	0.45
Standard Deviation	0.07	0.09	0.08	0.08	0.02	0.08	N/A	N/A	N/A	N/A	0.05	0.08
Average Relative % Difference	10%		5%		10%		40%		10%		2%	

Figure 11-16: Comparison of Total Porosity between GSA and Corelabs



12. DATA VERIFICATION

The author, Frits Reidel was involved with the planning, execution and oversight of the 2011, 2015, and 2016-2018 drilling and testing programs in Salar de Maricunga. The author was responsible for developing drilling and sampling methodologies and the implementation of field sampling protocols. The author spent a significant amount of time in the field during each of 2011, 2015 and 2016-18 field campaigns overlooking the implementation and execution of drilling, testing, and sampling protocols. The second QP; Murray Brooker also spent time on site during the 2016 drilling and testing program. QP Mr. Peter Ehren has visited the site periodically since 2011.

The author was responsible for the oversight and analysis of the QA/QC programs related to brine sampling and laboratory brine chemistry analysis as well as the laboratory porosity analysis. A significant amount of QA/QC protocols were implemented for the brine chemistry and drainable porosity analysis programs that allowed continuous verification of the accuracy and reliability of the results obtained. As described in Section 11 no issues were found with the results of the brine and porosity laboratory analysis. It is the opinion of the author that the information developed and used for the brine resource and reserve estimate herein is adequate, accurate and reliable.

13. MINERAL PROCESSING AND METALLURGICAL TESTING

13.1 BACKGROUND – LI3 / MLE 2011 EXPLORATION PROGRAM

In order to study the phase chemistry of the Maricunga brine, the initial step for designing a lithium recovery process, a simulated lab solar evaporation test work was conducted at the University of Antofagasta, northern Chile. Two batch wise evaporation tests at laboratory scale were carried out at a relatively constant temperature of 20 °C. The natural brine was used in the first test and in the second one a treated brine with sodium sulfate, to remove most of the high calcium content that characterizes the Maricunga brine. Both tests provided information on the nature of the crystallized salts along the different stages of an evaporation process, which has been useful for process simulations.

A summary of the experimental procedure and the main results of both tests are presented below:

13.2 EXPERIMENTAL PROCEDURE

A total brine feed of 192.04 kg was used in the first test (natural brine), distributed in four fiberglass glass reinforced plastic pans, each of 75.5 cm diameter and 12.3 cm height. The brine evaporation takes place at a temperature of 20 °C into a thermally insulated chamber (3.5 m long by 1 m wide by 0.8 m high), where a fan with variable speed propels air. Temperature, air speed and relative humidity, are measured through a data acquisition system to monitor the evaporation. This evaporation chamber operates continuously (24 hours) with air having relative humidity of 60 % to 75 %.

The amount of salt deposited in the pans, weighed by a digital scale, was used to define each stage (harvest) of evaporation, as well as determining the cumulative percentage of evaporated water. Samples of the solution and the salts after filtration were collected from every stage for chemical analysis and X-ray diffraction.

When the concentration of the Maricunga brine increases and the brine volume has diminished significantly, the evaporation is continued in another insulated chamber (1.18 m long by 0.70 m wide by 0.46 m high). The concentrated brine has a much lower brine activity (vapor pressure of the brine divided by the vapor pressure of the water), which results in lower evaporation rates.

The second chamber operates continuously with dehumidified air, which circulates through three PVC columns containing silica gel as drying agent. Under these conditions, the air can reach a relative humidity of the order of 40 %. When the silica gel gets saturated, heating in a dryer at 120 °C activates it for re-use.

As per the brine treated previously with anhydrous sodium sulfate (10 % excess was used to precipitate 88.7 % of Ca⁺⁺), a total of 156.04 kg, distributed in three pans, was fed to the evaporation system. Table 13-1 shows the composition of the natural brine and treated brine used in the evaporation test work.

Table 13-1: Chemical composition (% weight) of brines used in the test work

Brine	Na	K	Li	Ca	Mg	Cl	SO ₄	H ₃ BO ₃	HCO ₃	Density
Natural	7.81	0.676	0.0933	0.743	0.616	16.44	0.059	0.216	0.044	1.20761
Treated	8.59	0.547	0.0927	0.102	0.578	16.10	0.440	0.234	0.040	1.20787

A general view of the two evaporation chambers is shown in Figure 13-1.

Figure 13-1: General view of evaporation chambers



13.3 RESULTS OF THE EVAPORATION TESTS

The natural brine was concentrated up to 0.925 % lithium and 3.95 % magnesium in twelve stages of evaporation, being 69.1 % the cumulative evaporation. The treated brine was concentrated up to 1.98 % lithium and 6.08 % magnesium in nine stages of evaporation, with a cumulative evaporation of 68 %. Due to the low activity of the concentrated brine, it was necessary to increase the evaporation temperature to 30 °C during the last stages of both tests. Table 13-2 and Table 13-3 show the changes in the chemical composition of the untreated brine as well as the wet salt composition after every harvest (12) of the pans. Table 13-3 also shows a mass balance (crystallized salts, solution and evaporated water) referred to the initial weight of brine for each evaporating stage at 20 °C. The brine has been concentrated until the end of the carnallite field.

Table 13-2: Brine compositions during evaporation of the untreated brine

Brine									Density 20°C kg/l	Activity, 20°C (Vpbrine /Vpwater)
Mg %	Ca %	Na %	K %	Li %	Cl %	SO ₄ %	B %	H ₂ O %		
0.616	0.743	7.810	0.676	0.093	16.440	0.059	0.038	73.525	120.761	0.775
1.080	1.300	6.150	1.220	0.167	16.560	0.062	0.069	73.392	121.768	*
1.280	1.710	5.370	1.490	0.204	17.600	0.040	0.090	72.216	122.526	*
1.790	2.340	4.030	1.990	0.280	18.220	0.040	0.114	71.196	123.663	*
2.500	3.160	1.900	2.620	0.394	20.260	0.010	0.158	68.998	126.965	*
2.650	3.520	1.480	2.430	0.423	20.390	0.010	0.169	68.928	126.902	0.606
2.690	3.580	1.480	2.380	0.431	20.500	0.020	0.171	68.748	127.017	0.618
3.130	4.110	0.868	1.910	0.508	22.220	0.020	0.204	67.030	128.485	0.570
3.389	4.540	0.506	1.500	0.561	22.940	0.037	0.216	66.311	*	*
3.417	5.165	0.366	0.907	0.655	24.040	0.022	0.245	65.183	132.527	0.398
3.263	5.550	0.347	0.873	0.685	24.660	0.005	0.247	64.370	131.376	0.518
3.570	5.670	0.299	0.679	0.709	25.120	0.018	0.257	63.678	132.864	0.404
3.950	7.630	0.086	0.088	0.925	30.670	0.000	0.268	56.383	137.405	0.292

* No measurements

The density and activity of the brine along the concentration process is also indicated. Additionally, the moisture of the crystallized salts after harvesting and filtration of the solution is included in Table 13-3.

Table 13-3: Salts compositions during evaporation of the untreated brine

	Salts kg	Brine kg	Evapor kg	Mg %	Ca %	Na %	K %	Li %	Cl %	SO ₄ %	B %	H ₂ O %	Mois %
Brine feed		192.04											
Harvest 1	19.91	117.91	54.22	0.069	0.122	36.210	0.082	0.009	57.890	0.136	0.008	5.47	4
Harvest 2	8.85	84.09	26.10	0.135	0.296	35.430	0.282	0.016	56.520	0.360	0.014	6.95	4
Harvest 3	6.04	61.23	16.76	0.182	0.248	35.670	0.312	0.021	56.600	0.170	0.018	6.78	5
Harvest 4	5.05	41.43	14.74	0.220	0.351	34.970	1.815	0.033	57.690	0.250	0.013	4.66	4
Harvest 5	0.74	39.00	1.58	0.080	0.109	37.230	0.128	0.013	58.920	0.380	0.016	3.12	3
Harvest 6	0.12	37.46	1.35	0.378	0.528	20.560	16.940	0.060	50.790	0.110	0.026	10.61	9
Harvest 7	1.29	31.92	4.98	0.426	0.536	17.940	21.440	0.066	50.960	0.150	0.035	8.45	8
Harvest 8	0.78	17.78	2.70	5.556	0.709	6.890	11.830	0.042	40.100	0.092	0.041	34.74	5
Harvest 9	2.68	21.22	4.30	6.410	0.665	6.480	10.590	0.037	40.730	0.058	0.069	34.96	4
Harvest 10	0.24	6.21	1.39	7.425	0.779	2.370	10.670	0.089	37.770	0.034	0.054	40.81	8
Harvest 11	0.97	16.64	3.16	5.660	3.090	2.580	7.010	0.263	33.040	0.129	0.919	47.31	3
Harvest 12	1.64	12.27	2.72	6.670	3.920	1.730	5.060	0.362	36.420	0.001	0.173	45.66	14

Table 13-4 shows the main estimated crystallized salts in each harvest according to mineralization calculated by chemical assay and X-ray diffraction analysis.

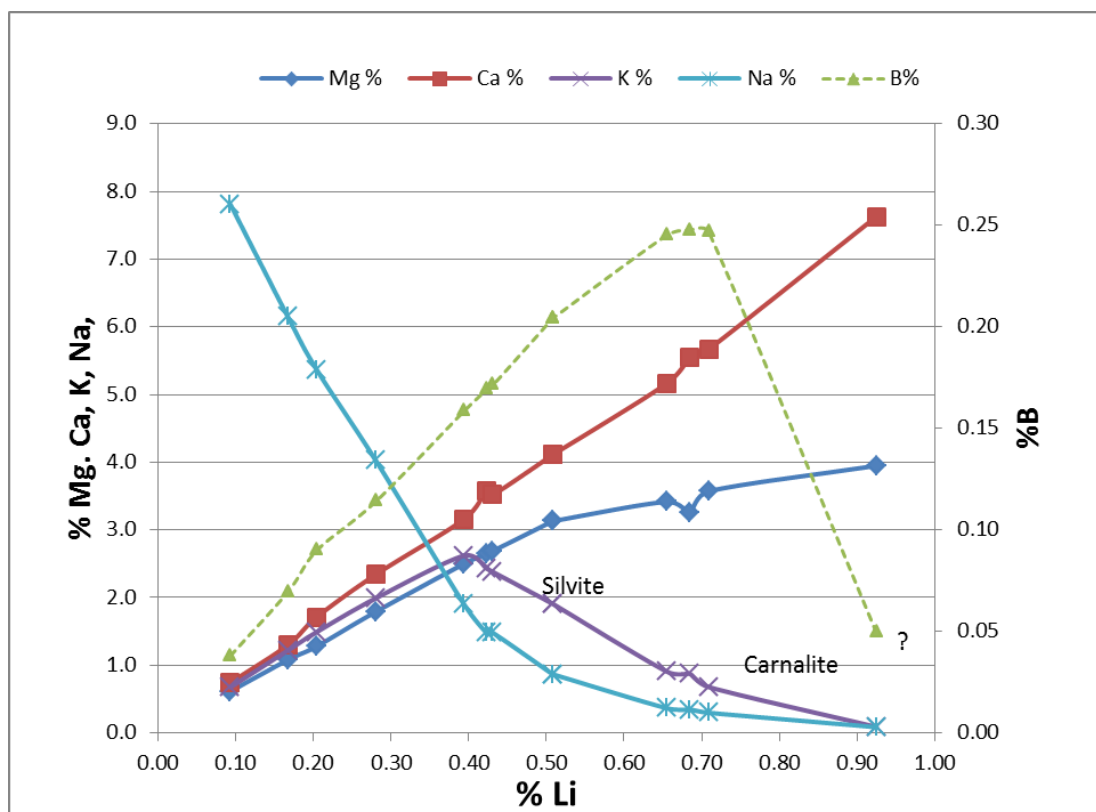
Table 13-4: Crystallized Salts in the harvest

	NaCl	KCl	CaSO ₄ .2H ₂ O and/or Na ₂ Ca(SO ₄) ₂	KCl*MgCl ₂ *H ₂ O	CaCl ₂ *2MgCl ₂ *12H ₂ O	CaB ₆ O10*6H ₂ O
Harvest 1	1		1			
Harvest 2	1		1			
Harvest 3	1		1			
Harvest 4	1		1			
Harvest 5	1	1	1			
Harvest 6	1		1			
Harvest 7	1	1	1			
Harvest 8	1		1			
Harvest 9	1	1	1			
Harvest 10	1		1	1		
Harvest 11	1		1	1	1	
Harvest 12	1		1	1	1	1

According to the salt composition, harvests 11 and 12 should have tachyhydrite; however, analyzing the brine evaporation curves of the ions presented by K/Li and Ca/Mg pairs, it is expected that this salt has not yet been crystallized, and the author suspects that the calcium and lithium are still entrained in the brine within the harvested salts.

Figure 13-2 illustrates the complete evaporation curve for the untreated brine.

Figure 13-2: Evaporation curves plotted versus % Li in the brine



The results of the brine evaporation, after treatment with sodium sulfate to remove most of the calcium, are presented in Table 13-5 and Table 13-6.

Table 13-5: Brine composition during evaporation of the treated brine

Brine									Density 20 °C Kg/l	Activity 20 °C (Vpbr /Vpwater)
Mg	Ca	Na	K	Li	Cl	SO ₄	B	H ₂ O		
%	%	%	%	%	%	%	%	%	%	
0.578	0.102	8.590	0.547	0.093	16.100	0.440	0.041	73.509	1.20787	*
0.984	0.108	7.910	1.110	0.154	16.590	0.510	0.062	72.572	1.21019	*
1.240	0.127	7.160	1.404	0.199	16.910	0.600	0.079	72.281	1.2273	0.664
1.540	0.077	6.270	1.800	0.261	16.980	0.650	0.101	72.321	1.21899	0.706
1.920	0.088	5.140	2.250	0.325	17.230	0.730	0.129	72.188	1.22507	0.693
2.600	0.141	3.910	3.000	0.428	18.130	0.860	0.168	70.763	1.23517	0.535
3.130	0.030	2.730	3.007	0.514	18.510	1.000	0.178	70.901	1.23518	0.443
4.705	0.013	1.050	2.007	0.764	20.620	1.380	0.305	69.156	*	*
6.771	0.016	0.160	0.133	1.130	25.960	0.466	0.571	64.793	1.31812	0.248
6.080	0.012	0.093	0.062	1.980	28.080	0.084	0.721	62.888	1.32492	*

Table 13-6: Wet salt compositions during evaporation of the treated brine

	Salts kg	Brine kg	Evap kg	Mg %	Ca %	Na %	K %	Li %	Cl %	SO ₄ %	B %	H ₂ O %	Moist %
Brine feed		156.24											
Harvest 1	16.87	95.42	43.90	0.070	0.592	36.410	0.088	0.010	57.630	0.740	0.006	4.454	3
Harvest 2	6.27	70.38	18.60	0.139	0.290	35.020	0.171	0.021	55.670	0.770	0.012	7.907	8
Harvest 3	3.92	47.28	19.10	0.128	0.241	36.510	0.160	0.020	56.730	0.730	0.016	5.465	5
Harvest 4	2.94	30.84	6.40	0.791	1.052	20.540	13.51	0.127	49.740	0.620	0.066	13.55	2
Harvest 5	1.43	23.39	6.00	0.141	0.318	37.120	11.55	0.022	59.230	0.990	0.019	1.943	1
Harvest 6	2.34	15.24	5.80	0.259	0.338	30.180	7.820	0.020	56.000	0.950	0.027	4.406	2
Harvest 7	2.10	4.15	1.80	5.556	0.709	6.890	11.83	0.042	40.100	0.092	0.041	34.74	3
Harvest 8	0.56	6.36	4.00	6.004	0.088	2.830	8.430	1.840	31.670	0.217	0.085	37.50	3
Harvest 9	2.51	2.56	1.29	9.910	0.009	0.247	0.230	0.599	32.380	0.836	0.605	55.18	12

13.4 POSCO PROCESS TESTS – 2012/13

Pilot plant evaluation of the POSCO direct extraction process was undertaken in late 2012 – early 2013. The POSCO process is a proprietary process for direct extraction and recovery of lithium from brine. Details of the process were not made available to MSB. The test work used brine recovered from trenches on the Litio 1-6 claims, with the brine being processed in a pilot plant established at Copiapo. POSCO reported the process test work was successful but did not provide details of the results to MSB. Subsequent to 2013, POSCO decided not to pursue further evaluation of the use of the process at Maricunga. The reasons for the POSCO decision are unknown.

13.5 2016 AND 2018 EVAPORATION POND TESTS

A series of evaporation pond tests were initiated by MSB in late 2016 using brine from Well P1. During the Q4/16 a total of ten trial evaporation ponds were constructed in series in order to measure the precipitation of salts, the evolution of brine, and evaporation rates over a minimum one-year period to determine the optimal processing methodology and process flow sheet for the extraction of lithium, potassium, and other by-products. The evaporation pond test site is illustrated below.

Figure 13-3: MSB evaporation ponds



The average grade of the brine fed from the pump well to the first of the evaporation test ponds was 1,260 mg/l lithium and over an initial 9-month period, the brine concentration increased seven-fold to 8,600 mg/l lithium on a continuous way and up sixteen-fold to 20,460 mg/l batch wise. In addition, sodium chloride (NaCl), potassium chloride (KCl) and carnallite ($\text{KCl} \cdot \text{MgCl}_2 \cdot 6\text{H}_2\text{O}$) and in small fraction of calcium chloride hexahydrate ($\text{CaCl}_2 \cdot 6\text{H}_2\text{O}$) crystalized as by-products. In all ponds very small amounts of gypsum ($\text{CaSO}_4 \cdot \text{H}_2\text{O}$) are identified. The behaviour of the ions in the brine is given in Figure 13-5. and confirms the test work at the University of Antofagasta in 2011. The potassium solubility is lower as the ponds at 4000 m operates at a significant lower temperature than test work done at Antofagasta carried out at 20°C. At higher lithium concentration boron get saturated as most likely calcium borates and slowly the values are reduced or maintained constant, strontium is crystalized as a salt and very strongly reduces its solubility.

Figure 13-4: MSB harvesting of salts



Sampling and assay procedures for the pond evaporation tests incorporated the following:

- Collection of brine samples on a periodic basis to measure brine properties such as chemical analysis, density, brine activity, etc. Samples were assayed at the University of Antofagasta using the same methods and QA/QC procedures as for brine samples collected from drill holes and from pumping tests;
- Collection of precipitated salts from the ponds for chemical analysis to evaluate the evaporation pathways, brine evolution and physical and chemical properties of the salts.

Figure 13-5: Evaporation curves plotted versus % Li of pilot ponds compared with test work realized in University of Antofagasta 2011 (UA)

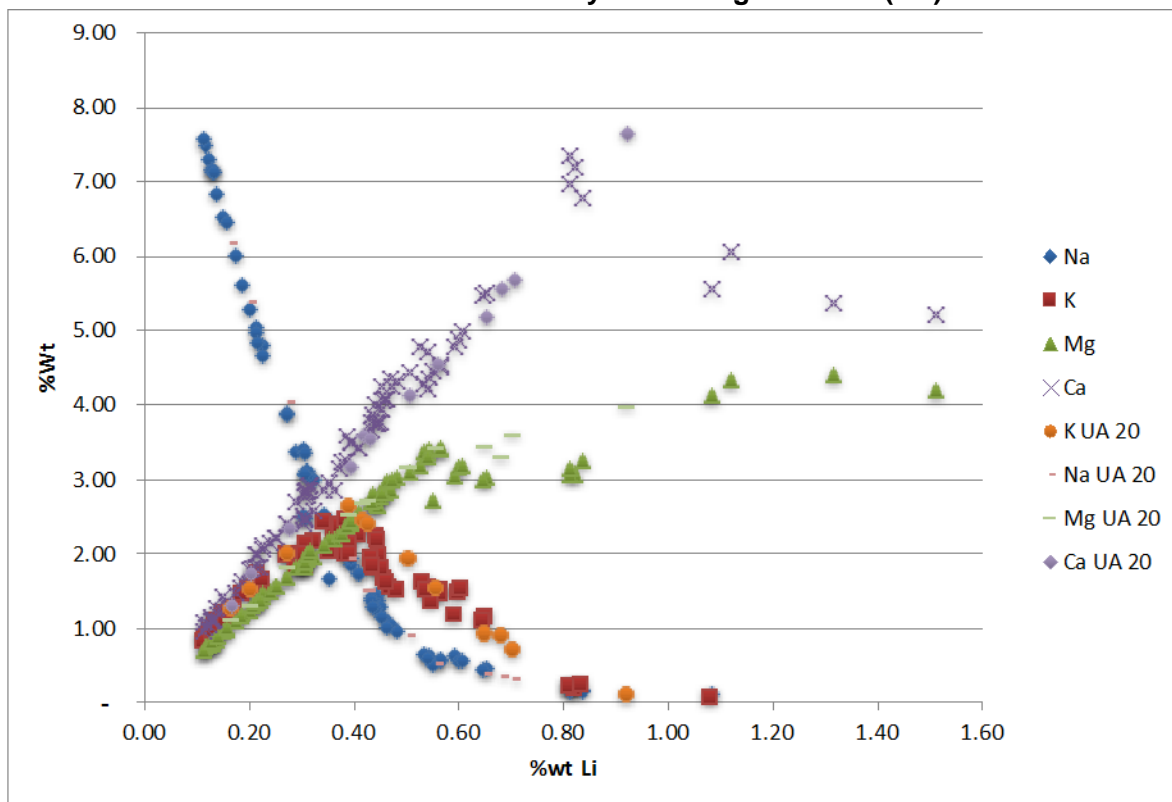
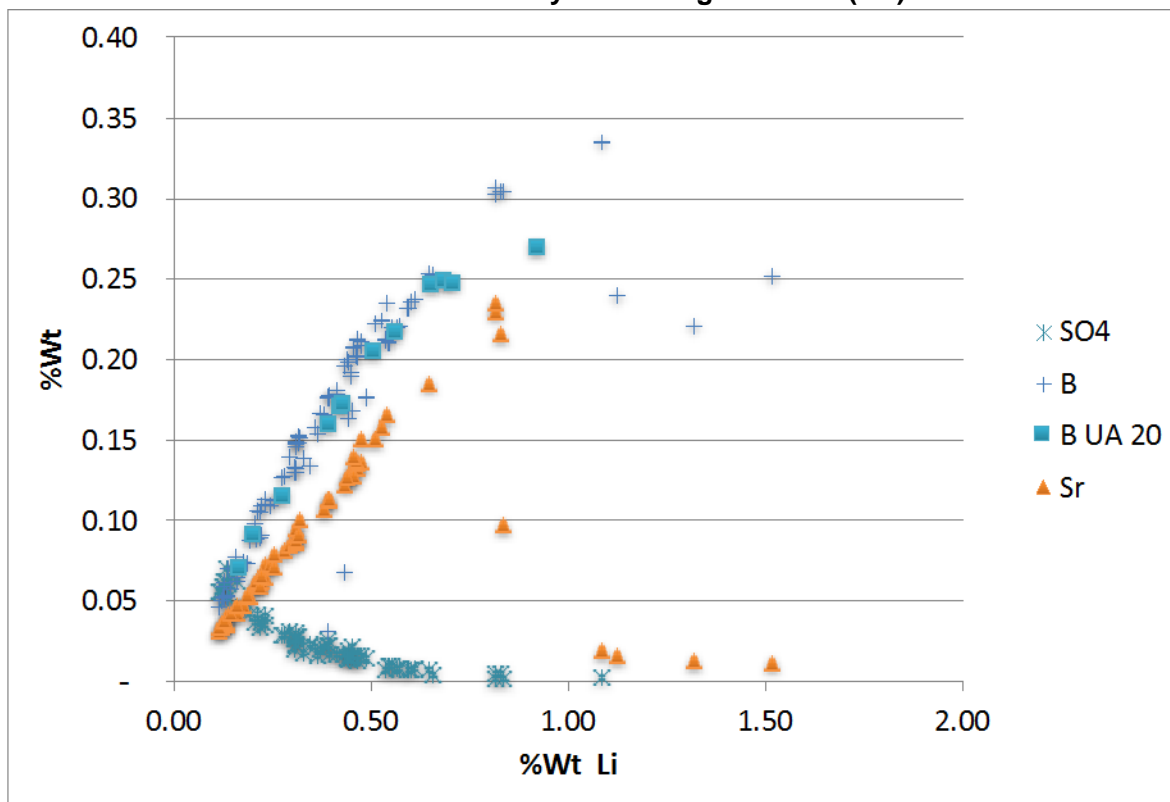


Figure 13-6: Evaporation curves plotted versus % Li of pilot ponds compared with testwork realized at University of Antofagasta 2011 (UA)



13.6 2017 AND 2018 SALT REMOVAL AND LITHIUM CARBONATE TESTS

The concentrated brine that was produced in the pilot ponds was tested at the University of Antofagasta through processes of evaporation and crystallization, which allows the concentration of the lithium contained in the brine, and at the same time enables the elimination of impurities from the brine in the form of tachyhydrite and calcium chloride.

In the Janecke diagram below (Figure 13-7) some of test results are represented and it can be observed how lithium is concentrated by evaporation and cooling as it moves in the direction that represents the lithium chloride concentration. Lithium can be concentrated with values above 4.5%Li, with Ca lower than 3% and Mg lower 1.5%.

Based on this concept, for detailed process design and equipment specification the concentrated lithium brine was tested by the technology provider GEA to concentrate the brine up to slightly above 4% lithium and subsequently remove boron, calcium and magnesium by precipitation as calcium carbonate and magnesium hydroxide. Then from the purified lithium brine, lithium carbonate solids are precipitated by the addition of soda ash.

Further optimization testing was done by GEA with brine produced from the pilot ponds at the Salar de Maricunga.

The testwork was divided in the Salt Removal Plant:

1. Two stage preconcentration (Falling film evaporator)
2. Cooling crystallization of tachhydrite (Vacuum cooling unit)
3. Crystallization of tachhydrite and $\text{CaCl}_2 \times 2 \text{H}_2\text{O}$ (Evaporation and crystallization unit)
4. Acidification and cooling crystallization of $\text{CaCl}_2 \times 6\text{H}_2\text{O}$ and boric acid (Surface cooling crystallization)

and the Lithium Carbonate Plant:

1. Solvent extraction of boron
2. Precipitation CaCO_3
3. Precipitation of $\text{Mg}(\text{OH})_2$ and CaCO_3
4. Final removal of calcium, magnesium and heavy metals by ion exchange resins
5. Li_2CO_3 precipitation crystallization (Li_2CO_3 crystallizer)
6. Li_2CO_3 resuspension and solid- liquid separation unit including washing

13.6.1 Results of Salt removal Plant

It was observed that there is no danger of tachhydrite crystallization in the falling film evaporator up to a solution composition at 100°C of 5.9 wt.-% LiCl 23.4 wt.-% CaCl_2 15.8 wt.-% MgCl_2 .

Up to 11.3 wt.-% lithium chloride, the flash cooling stages produce only tachhydrite and traces of sodium chloride and strontium chloride at 40°C. The saturation concentrations are 31.0 wt.-% for CaCl_2 and 6.4 wt.-% for MgCl_2 were at a level of 11.4 wt.-% LiCl. To minimize lithium losses, crystal washing with saturated or almost saturated wash solution is absolutely necessary. tachhydrite from vacuum cooling crystallization contained 7.3 wt.-% adherent mother liquor. This product was washed with 17 wt.-% wash solution (referred to the wet crystals) on the centrifuge (refer to the amount of wet crystals), so that the amount of adherent mother liquor could be reduced down to 2.6 wt.-%.

The evaporation stage at 57°C produces tachhydrite and calcium chloride dihydrate. During the tests it was found out that dewatering of tachhydrite is much easier than dewatering of $\text{CaCl}_2 \times 2\text{H}_2\text{O}$. The amount of adhering mother liquor of tachhydrite was around 7 wt.-%. For $\text{CaCl}_2 \times 2\text{H}_2\text{O}$ plus tachhydrite about 17 wt.-% were determined. To minimize the lithium losses the evaporation stage will be divided into two crystallization and separation steps. One stage should crystallize tachhydrite and the second stage should crystallize a mixture of tachhydrite plus $\text{CaCl}_2 \times 2\text{H}_2\text{O}$. Due to co-crystallization exact splitting of them is not possible.

Both products should be washed with 40 wt.-% wash liquor (refer to the wet crystals) on the centrifuge.

It was noticed that the condensates of this test work had high conductivities as well as high pH values. With increasing concentration factor this effect became stronger. The analysis showed that the condensates contained some hydrochloric acid.

For a safe process control is absolutely necessary to adjust the lithium concentration in the evaporation stage to a fixed level. Large derivation in the ratio between lithium, calcium and magnesium can cause co-crystallization of lithium chloride in the surface cooling stage. Small derivations can be compensated by the amount of added water.

Before the cooling crystallization of $\text{CaCl}_2 \cdot 6\text{H}_2\text{O}$ the solution was slightly diluted to provide the water for the calcium chloride crystals avoiding co- crystallization of lithium chloride and also acidified to remove the boron as boric acid.

At 30 wt.-% LiCl only 7.3 wt.% CaCl_2 and 1.2 wt% MgCl_2 were soluble. Also, the solubility of boric acid was reduced to approx. 0.9 wt.%. Boric acid crystallized as fine solids and it was not possible to separate them completely by centrifugation. Here an additional filtration step is required for fines removal. The low magnesium concentration is also very positive for further processing in the lithium carbonate plant.

Until now washing is not foreseen, a recrystallization step of the calcium chloride can increase still significantly the lithium yield.

13.6.2 Results of Lithium Carbonate Testing

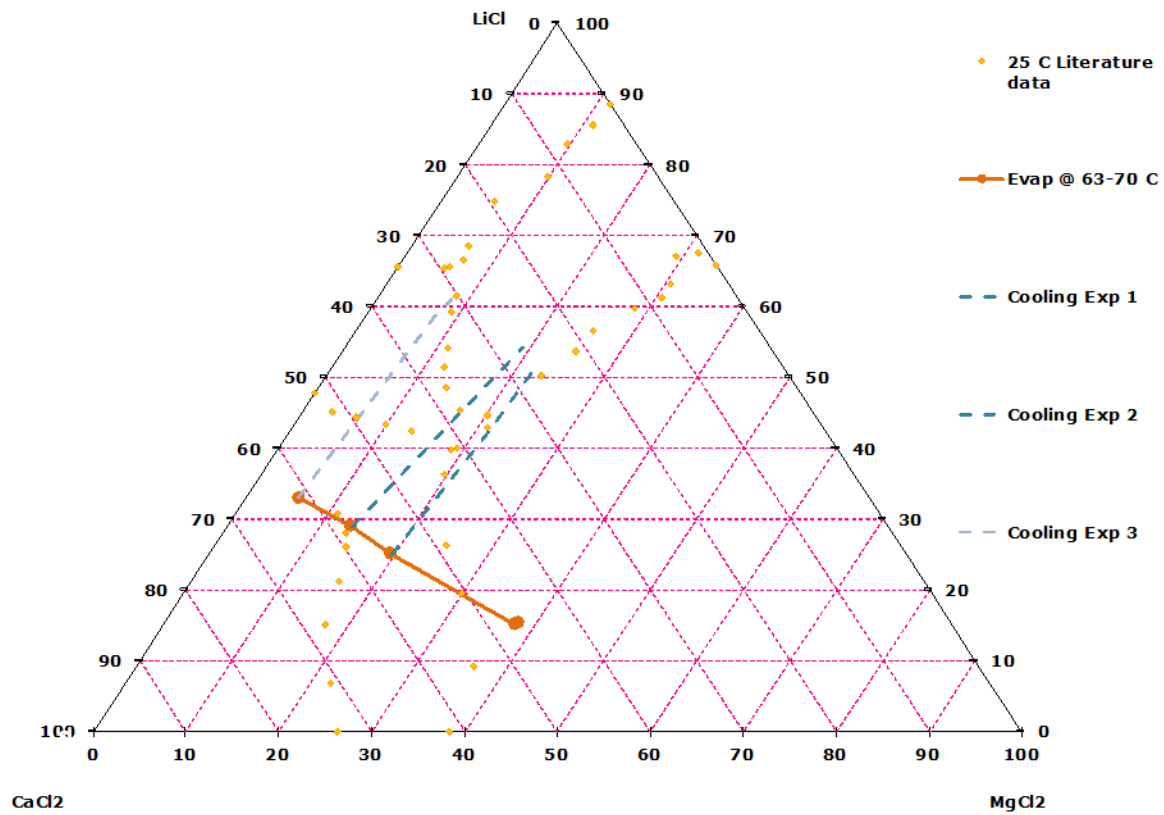
Several process routes were tested, which turned out that based on chemical consumptions, the best process steps are those mentioned above. Solvent extraction tests were executed by SGS, GEA and Technoforce. All tests confirmed that boron can easily be removed with iso-octanol as extractant and kerosene as carrier.

First the precipitation of calcium and magnesium was executed in two steps at 40 and 80 °C.

Finally, it was concluded that in the best approach is to remove the calcium as calcium carbonate in a first batch stage and magnesium in a secondary stage with slaked lime, followed up by ion exchange to remove final calcium and magnesium values

The treated solution was so pure that the Li_2CO_3 precipitation crystallization can follow. The process was simulated by semi-continuous operation in order to add the calculated Na_2CO_3 solution (102% - stoichiometric-) dropwise at 85°C. After the retention time of two hours followed the separation of the suspension took place. The crystals were washed 4 times with water (100 % refer to the amount of wet filter cake) on the filter at ambient temperature resulting in very high-grade lithium carbonate solids fulfilling completely the target set by MSB.

Figure 13-7: Evaporation and cooling curves plotted in a Janecke projection of testwork realized at University of Antofagasta 2011 (UA)



14. BRINE RESOURCE ESTIMATES

14.1 OVERVIEW

The essential elements of a brine resource determination for a salar are:

- Definition of the aquifer geometry,
- Determination of the drainable porosity or specific yield (Sy) of the hydrogeological units in the salar, and
- Determination of the concentration of the elements of interest.

Resources may be defined as the product of the first three parameters. The use of specific yield allows the direct comparison of brine resources from the widest range of environments.

Aquifer geometry is a function of both the shape of the aquifer, the internal structure and the boundary conditions (brine / fresh water interface). Aquifer geometry and boundary conditions can be established by drilling and geophysical methods. Hydrogeological analyses are required to establish catchment characteristics such as ground and surface water inflows, evaporation rates, water chemistry and other factors potentially affecting the brine reservoir volume and composition in-situ. Drilling is required to obtain samples to estimate the salar lithology, specific yield and grade variations both laterally and vertically.

14.2 RESOURCE MODEL DOMAIN AND AQUIFER GEOMETRY

The model resource estimate is limited to the MSB mining concessions in Salar de Maricunga that cover an area of 2,563 ha as shown in Figure 4-2.

The resource model domain is constrained by the following factors:

- The top of the model coincides with the brine level in the Salar that was measured in the monitoring wells shown in Table 10-1.
- The lateral boundaries of the model domain are limited to the area of the MSB mining claims in the Salar.
- The bottom of the model domain coincides with a total depth of 200 m.

14.3 SPECIFIC YIELD

Specific yield is defined as the volume of water released from storage by an unconfined aquifer per unit surface area of aquifer per unit decline of the water table.

The specific yield values used to develop the resources are based on results of the logging and hydrogeological interpretation 10 sonic boreholes, results of drainable porosity analyses carried out on 488 undisturbed valid samples from sonic core by GeoSystems Analysis, Daniel B Stephens and Associates, Corelabs, BGC, and four pumping tests. The boreholes within the measured and indicated resource areas are appropriately spaced at a borehole density of one bore per 1.5 km². Table 14-1 shows the drainable porosity values assigned to the different geological units for the resource model and summarizes the statistics of specific yield classified in terms of the corresponding lithology of the core sample. Most of the core samples were taken from the clay (285), volcanoclastic (81), and upper halite (51) units. The mean of the specific yield associated with the alluvial and volcanoclastic units is 0.18 and 0.11, respectively. These values are one order of magnitude larger than the rest of the units, which show specific yield values ranging between 0.02 and 0.06. The degree of variability in each unit is relatively high with coefficients of variations that range between 0.4 and 1.0 except for the upper halite and lower sand unit (coefficient of variation of 0.09 and 0.06, respectively).

Table 14-1: Porosity values applied in the resource model

Geological Unit	Count	Sy Ave	Sy Low	Sy Max	Sy Std. Dev
Upper Halite	51	0.04	0	0.15	0.04
Clay Core	285	0.02	0	0.09	0.02
NW Alluvium	17	0.18	0.09	0.31	0.07
Lower Alluvium	39	0.05	0	0.3	0.06
Volcaniclastics	81	0.11	0	0.31	0.07
Lower Sand	15	0.06	0.01	0.16	0.04
Lower Volcaniclastics*		0.11			

* The Volcanoclastic drainable porosity has been assigned to the Lower Volcanoclastic unit due to geological similarities.

14.4 BRINE CONCENTRATIONS

The distributions of lithium and potassium concentrations in the model domain are based on a total of 651 valid brine analyses (not including QA/QC analyses). Table 14-2 shows a summary of the brine chemical composition.

Table 14-2: Summary of brine chemistry composition

Variable	Average	Low	Max	Std. Dev
Li (mg/L)	1,146	24	3,375	364
K (mg/L)	8,292	85	20,640	2,527
Mg (mg/L)	7,462	161	21,800	2,548
Ca (mg/L)	12,853	521	36,950	4,666
SO ₄ (mg/L)	706	259	2,960	308
B (mg/L)	586	16	1,992	186

14.5 RESOURCE CATEGORY

The CIM Council (May 10, 2014) adopted the following definition standards for minerals resources:

Inferred Mineral Resource

An Inferred Mineral Resource is that part of a Mineral Resource for which quantity and grade or quality are estimated on the basis of limited geological evidence and sampling. Geological evidence is sufficient to imply but not verify geological and grade or quality continuity.

An Inferred Mineral Resource has a lower level of confidence than that applying to an Indicated Mineral Resource and must not be converted to a Mineral Reserve. It is reasonably expected that the majority of Inferred Mineral Resources could be upgraded to Indicated Mineral Resources with continued exploration.

An Inferred Mineral Resource is based on limited information and sampling gathered through appropriate sampling techniques from locations such as outcrops, trenches, pits, workings and drill holes. Inferred Mineral Resources must not be included in the economic analysis, production schedules, or estimated mine life in publicly disclosed Pre- Feasibility or Feasibility Studies, or in the Life of Mine plans and cash flow models of developed mines. Inferred Mineral Resources can only be used in economic studies as provided under NI 43-101.

There may be circumstances, where appropriate sampling, testing, and other measurements are sufficient to demonstrate data integrity, geological and grade/quality continuity of a Measured or Indicated Mineral Resource, however, quality assurance and quality control, or other information may not meet all industry norms for the disclosure of an Indicated or Measured Mineral Resource. Under these circumstances, it may be reasonable for the Qualified Person to report an Inferred Mineral Resource if the Qualified Person has taken steps to verify the information meets the requirements of an Inferred Mineral Resource.

Indicated Mineral Resource

An Indicated Mineral Resource is that part of a Mineral Resource for which quantity, grade or quality, densities, shape and physical characteristics are estimated with sufficient confidence to allow the application of Modifying Factors in sufficient detail to support mine planning and evaluation of the economic viability of the deposit.

Geological evidence is derived from adequately detailed and reliable exploration, sampling and testing and is sufficient to assume geological and grade or quality continuity between points of observation.

An Indicated Mineral Resource has a lower level of confidence than that applying to a Measured Mineral Resource and may only be converted to a Probable Mineral Reserve.

Mineralization may be classified as an Indicated Mineral Resource by the Qualified Person when the nature, quality, quantity and distribution of data are such as to allow confident interpretation of the geological framework and to reasonably assume the continuity of mineralization. The Qualified Person must recognize the importance of the Indicated Mineral Resource category to the advancement of the feasibility of the project. An Indicated Mineral Resource estimate is of sufficient quality to support a Pre-Feasibility Study which can serve as the basis for major development decisions.

Measured Mineral Resource

A Measured Mineral Resource is that part of a Mineral Resource for which quantity, grade or quality, densities, shape, and physical characteristics are estimated with confidence sufficient to allow the application of Modifying Factors to support detailed mine planning and final evaluation of the economic viability of the deposit.

Geological evidence is derived from detailed and reliable exploration, sampling and testing and is sufficient to confirm geological and grade or quality continuity between points of observation.

A Measured Mineral Resource has a higher level of confidence than that applying to either an Indicated Mineral Resource or an Inferred Mineral Resource. It may be converted to a Proven Mineral Reserve or to a Probable Mineral Reserve.

Mineralization or other natural material of economic interest may be classified as a Measured Mineral Resource by the Qualified Person when the nature, quality, quantity and distribution of data are such that the tonnage and grade or quality of the mineralization can be estimated to within close limits and that variation from the estimate would not significantly affect potential economic viability of the deposit. This category requires a high level of confidence in, and understanding of, the geology and controls of the mineral deposit.

14.6 RESOURCE MODEL METHODOLOGY AND CONSTRUCTION

The resource estimation for the Project was developed using the Stanford Geostatistical Modeling Software (SGeMS) and the geological model as a reliable representation of the local lithology. The following steps were carried out to calculate the lithium and potassium resources:

- Generation of histograms, probability plots and box plots for the Exploratory Data Analysis (EDA) for lithium and potassium. No outlier restrictions were applied, as distributions of the different elements do not show anomalously high values. Calculation of the experimental variograms with their respective variogram models for lithium and potassium in three orthogonal directions;
- Definition of the block model (34,560,000 blocks) and block size ($x=50$ m, $y=50$ m, $z=1$ m). The block size has been chosen for being representative of the fine units inside the geological model;

- Interpolation of lithium and potassium concentrations for each block in mg/l using ordinary kriging with the variogram models shown Figure 14-5 to Figure 14-8. The presence of brine is not necessarily followed by the lithologies. Therefore, hard boundaries are not considered inside the geological units for the estimation;
- Calculation of total resources using the average drainable porosity value for each geological unit, based on the boreholes data. Each geological unit will represent a particular drainable porosity value as shown in Table 14-1. The total resources are shown in Table 14-6.

14.7 METHODOLOGY

The method used to describe the data is based on the following two observations: (1) the lithium and potassium concentration in the system are orders of magnitude larger than the variability in the specific yield. The interquartile range of the specific yield is 0.37, whereas the interquartile range of potassium and lithium is 17,700 mg/L and 2,915 mg/L, respectively. Therefore, it is more important to represent the variability of the concentrations than that of the specific yield; (2) there is not enough information to estimate the correlation structure associated with the different lithological units. Therefore, the specific yield is described by a discrete random function and assumed constant within each unit; and the concentrations are defined by a continuous random function described by a correlation function that includes the information of all units.

14.8 UNIVARIATE STATISTICAL DESCRIPTION

The univariate statistical description of lithium and potassium concentrations are based on histograms, probability plots and box plots. Table 14-3 presents a summary of the univariate statistics of potassium and lithium. As described in the methodology, these statistics contain the information of all geological units. The mean concentration of potassium is 7.2 times of the lithium. Both exhibit the same degree of variability with a coefficient of variation of 0.29 and 0.30 for the potassium and lithium, respectively. Distributions are positively skewed. The concentrations of potassium range between 2,940 mg/L and 20,640 mg/L, and the concentrations of lithium range between 460 mg/L and 2,275 mg/L.

Table 14-3: Summary of univariate statistics of potassium and lithium

	K (mg/l)	Li (mg/l)
N Valid	647	647
Mean	8,342	1153
Median	8,220	1145
Std. Deviation	2,453	354
Skewness	0.662	0.886
Std. Error of Skewness	0.096	0.096
Kurtosis	0.653	2.487
Std. Error of Kurtosis	0.192	0.192
Range	17,700	2,915
Minimum	2,940	460
Maximum	20,640	3,375

Table 14-4: Test of normality of potassium and lithium

	K (mg/l)	Li (mg/l)
N Valid	647	647
Mean	8,342	1153
Median	8,220	1145
Std. Deviation	2,453	354
Skewness	0.662	0.886
Std. Error of Skewness	0.096	0.096
Kurtosis	0.653	2.487
Std. Error of Kurtosis	0.192	0.192
Range	17,700	2,915
Minimum	2,940	460
Maximum	20,640	3,375

Table 14-4 summarizes the test of normality of the distribution of lithium and potassium. Results show that the data do not strictly follow a normal distribution. However, the normal plots shown in Figure 14-1 permit to identify a clear straight line, indicating that even though the data does not pass the normality tests, the distribution is close to a Gaussian shape. This gives confidence to the kriging estimation of the concentrations. Kriging is known to be the best estimator (linear and not linear) when the data follows a multivariate normal distribution.

Figure 14-1: Normal plots of the concentration of potassium and lithium

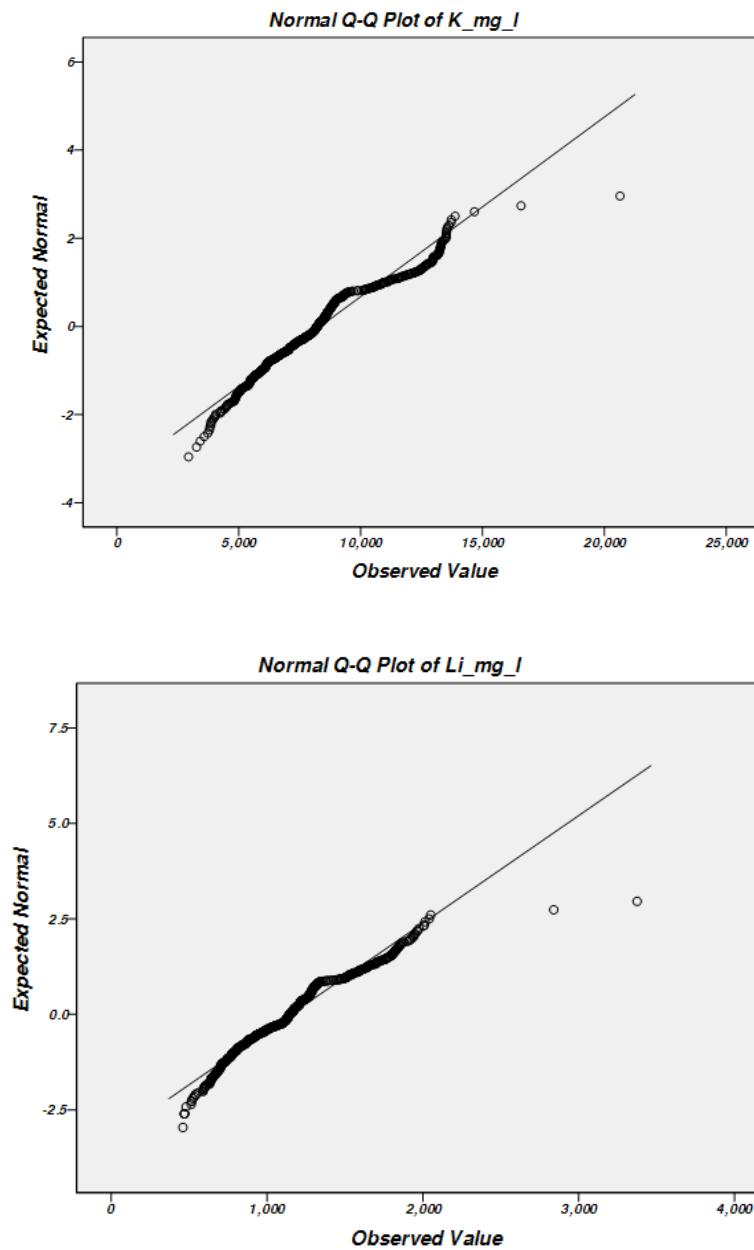


Figure 14-2: Histograms of the potassium and lithium and the best fitted normal distribution

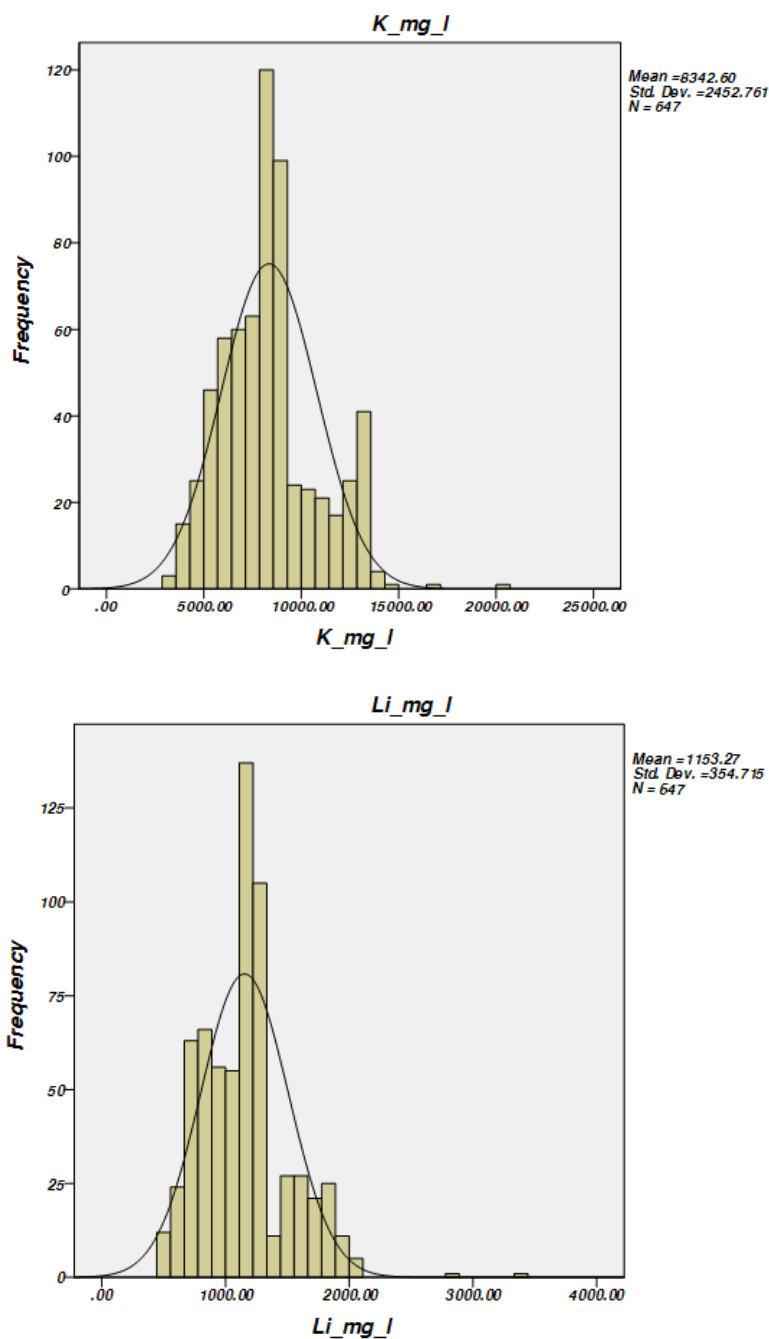
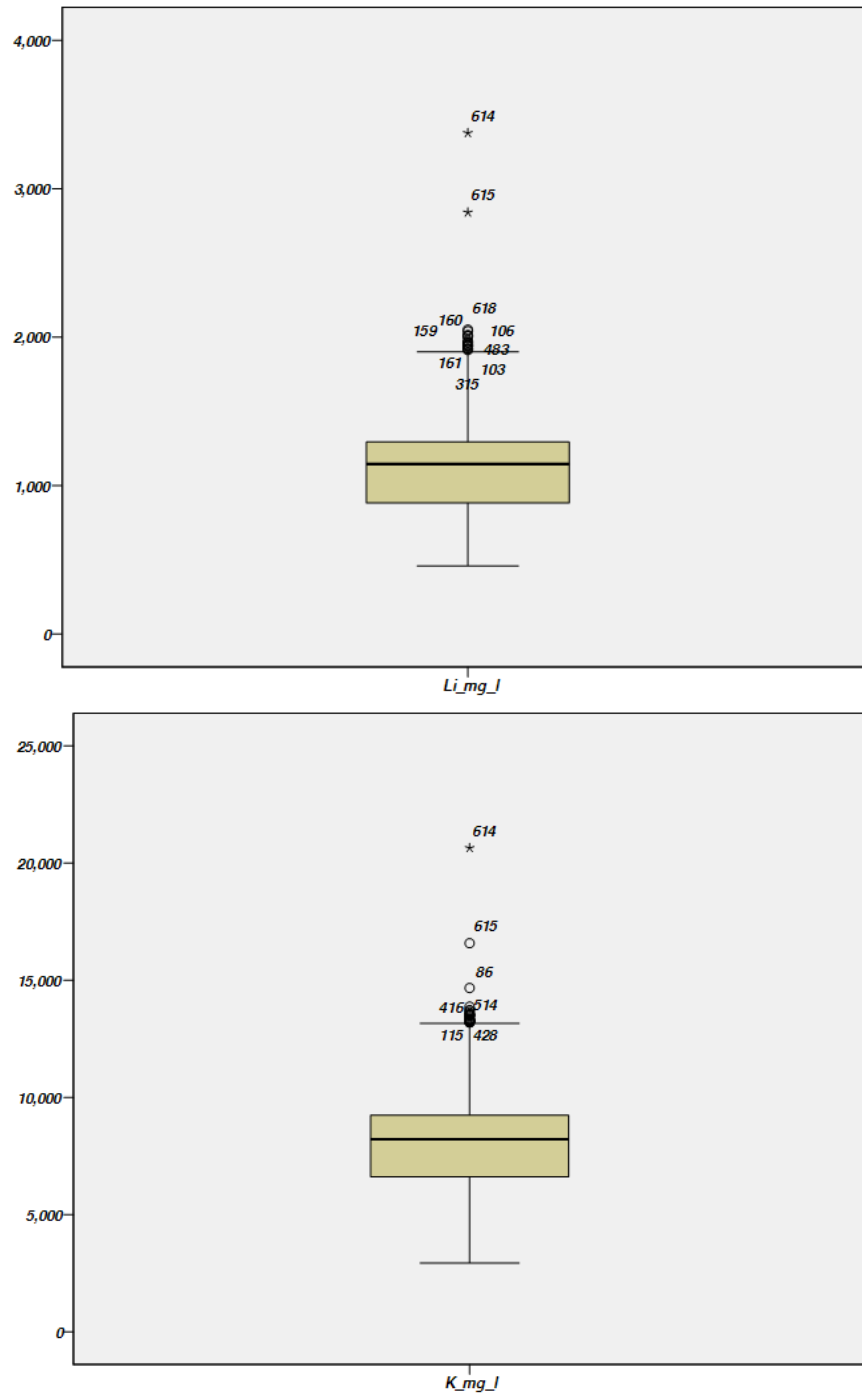


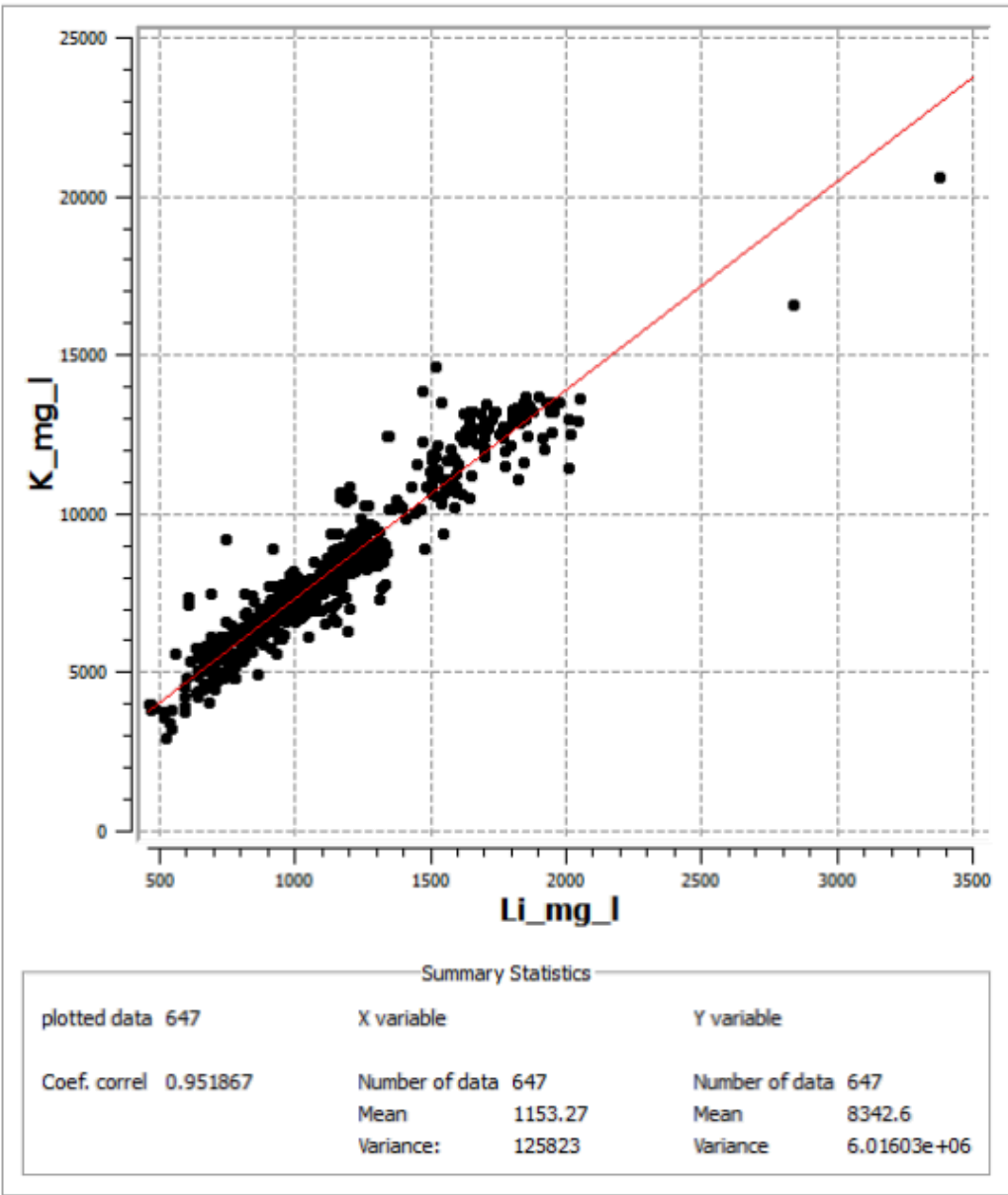
Figure 14-2 shows the histogram of the concentrations of potassium and lithium. The distribution is slightly bimodal, but close to a Gaussian shape in overall. The boxplot of the concentrations of potassium and lithium is shown in the distribution is quite symmetric but with noticeable extreme values that deviate from the general structure.

Figure 14-3: Box plot of the specific yield



In terms of a bivariate statistical description it is important to note that the concentrations of potassium and lithium are highly correlated. Figure 14-4 exhibits the scatterplot of the concentrations of lithium against potassium. The graph depicts a clear correlation between both concentrations, with a coefficient of correlation of 0.95 obtained with 647 data pairs.

Figure 14-4: Scatter plot of the concentration of lithium versus potassium



14.9 SPATIAL DESCRIPTION AND VARIOGRAPH

The spatial variability of lithium, potassium and boron concentrations were characterized by the semi-variogram, $\gamma(\mathbf{h})$. The semivariogram is a function that measures the variability between pairs of variables separated by a distance \mathbf{h} . Very often, the correlation between two variables separated by a certain distance disappears when $|\mathbf{h}|$ becomes too large. At this instant, $\gamma(\mathbf{h})$ approaches a constant value. The distance beyond which $\gamma(\mathbf{h})$ can be considered to be a constant value is known as the range, which represents the transition of the variable to the state of negligible correlation. Experimental semi-variograms obtained with the parameters shown in Table 14-5 along multiple directions revealed that the random function model can be characterized with an axisymmetric model; symmetric semi-variogram with respect to the z-direction.

Table 14-5: Parameter for the calculation of the experimental variograms

Variogram Parameters				Tolerance	
Lag (m)	Max. No. Of Lags	Azimuth (°)	Dip (°)	Bandwidth (m)	Angular (°)
500	50	-45	0	1,000	45
500	50	-30	0	1,000	45
500	50	0	0	1,000	45
500	50	0	0	1,000	90
6	26	0	90	100	45

This type of correlation function model can be observed in sedimentary geological formations such as an evaporitic system. Based on this, the experimental semi-variograms were fitted with a theoretical model consisting of two correlation structures, i.e., the combination of an exponential model with a Gaussian model. This composite structure is necessary in this case to properly represent the small-scale correlation observed along the z-direction compared to a larger correlation observed in the xy plane directions. The experimental variograms for lithium and potassium with their respective variogram models are shown in the following figures.

Figure 14-5: Experimental semi-variograms of lithium in xy directions with theoretical model

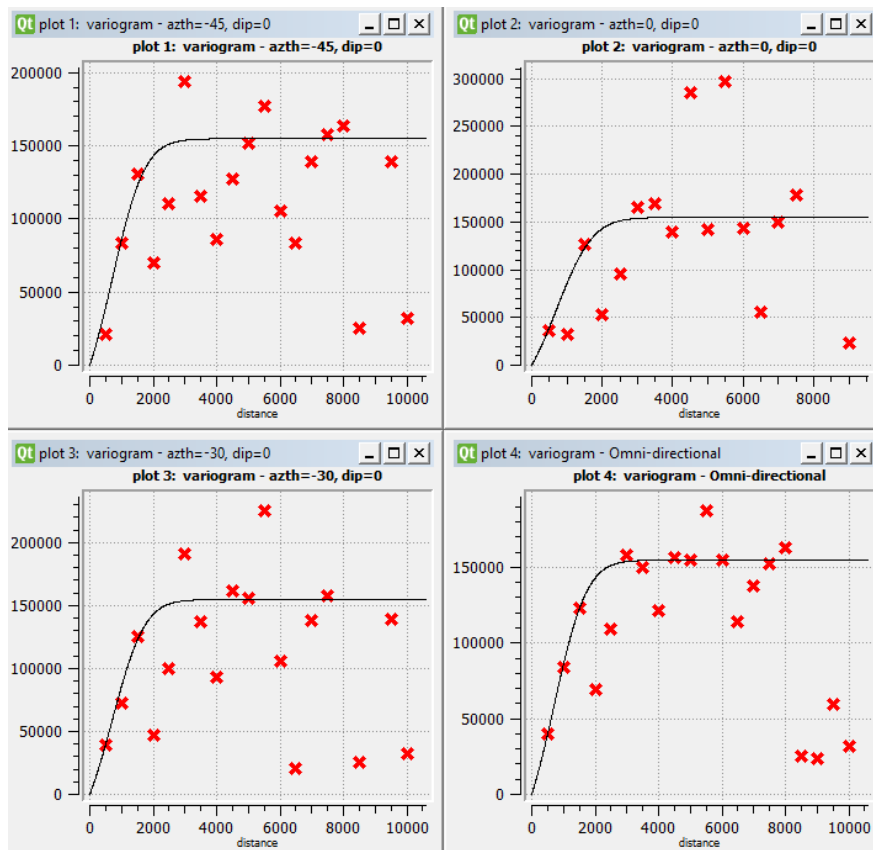


Figure 14-6: Experimental semi-variogram of lithium in z-direction fitted with a theoretical model

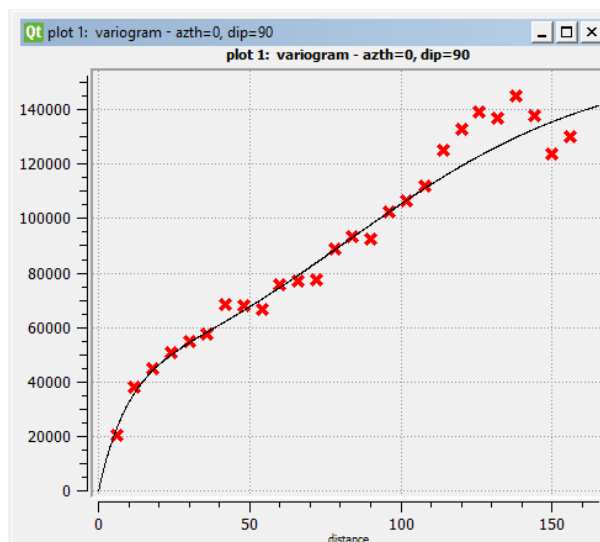


Figure 14-7: Experimental semi-variograms of potassium in xy directions with theoretical model

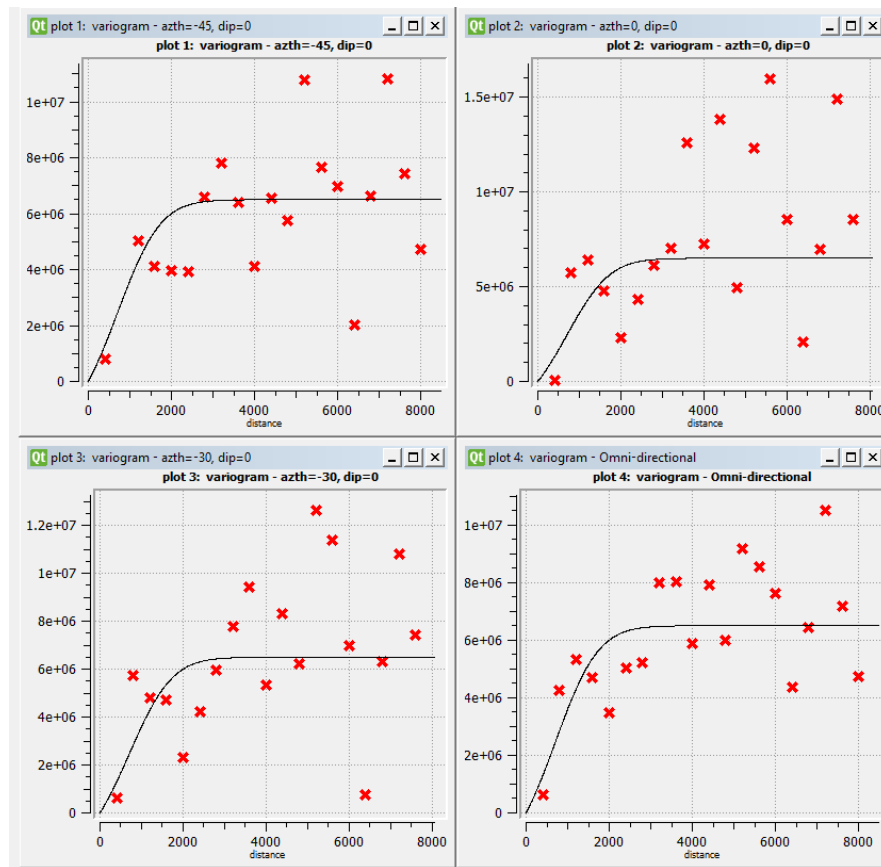
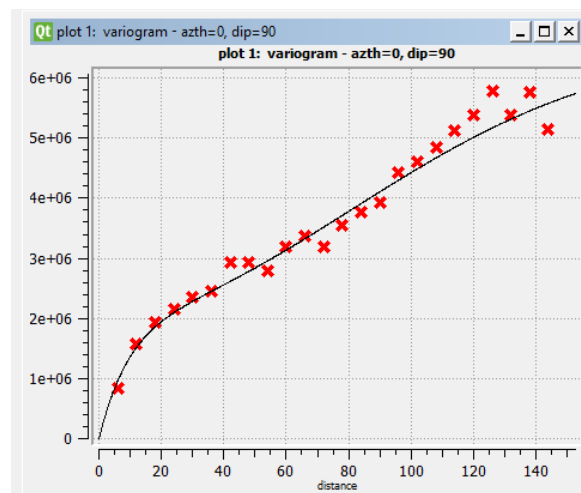


Figure 14-8: Experimental semi-variogram of potassium in the z-direction with theoretical model



The semi-variogram is expressed in mg^2/L^2 and the range in units of meters. Thus, the correlation structure in the xy plane has a range of 2,200 meters, whereas the correlation structure in the z-direction has one structure with a range of 30 meters and another with a range of 200 meters. This means that in overall the system is highly stratified with lenses that extend laterally several kilometers but with limited thickness of few meters. Experimental semi-variogram data shown in the graphs correspond to semi-variogram point estimates with more than 50 pair samples. Formally, the correlation function of lithium and potassium can be written as:

$$\begin{aligned}\gamma_{Li}(\mathbf{h}) &= 50000 \times \gamma_{exp}(a_x = 2200, a_y = 2200, a_z = 30) \\ &\quad + 105000 \times \gamma_{Gauss}(a_x = 2200, a_y = 2200, a_z = 200) \\ \gamma_K(\mathbf{h}) &= 2100000 \times \gamma_{exp}(a_x = 2200, a_y = 2200, a_z = 30) \\ &\quad + 4410000 \times \gamma_{Gauss}(a_x = 2200, a_y = 2200, a_z = 200)\end{aligned}$$

The total contribution (variability) of lithium and potassium are $155,000 \text{ mg}^2/\text{L}^2$ and $6,510,000 \text{ mg}^2/\text{L}^2$. The correlation structure of the different ion concentrations is similar because these properties are highly correlated between each other, i.e., the coefficient of correlation between lithium and potassium is 0.95.

The interpolation methodology for estimating lithium and potassium was Ordinary Kriging (OK), which assumes that the mean is locally constant but unknown. The estimation was carried out separately for each parameter using their respective variogram models as appropriate. The final distribution is shown in the following figures.

Figure 14-9: Lithium concentration distribution

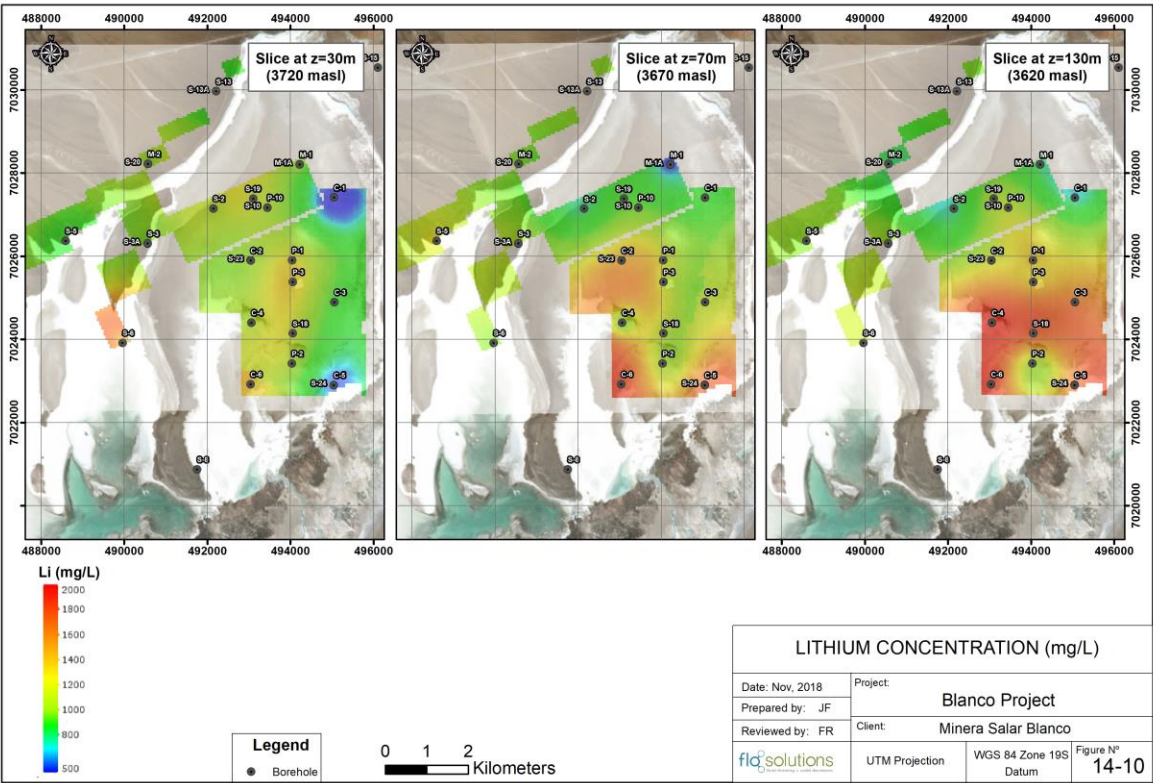
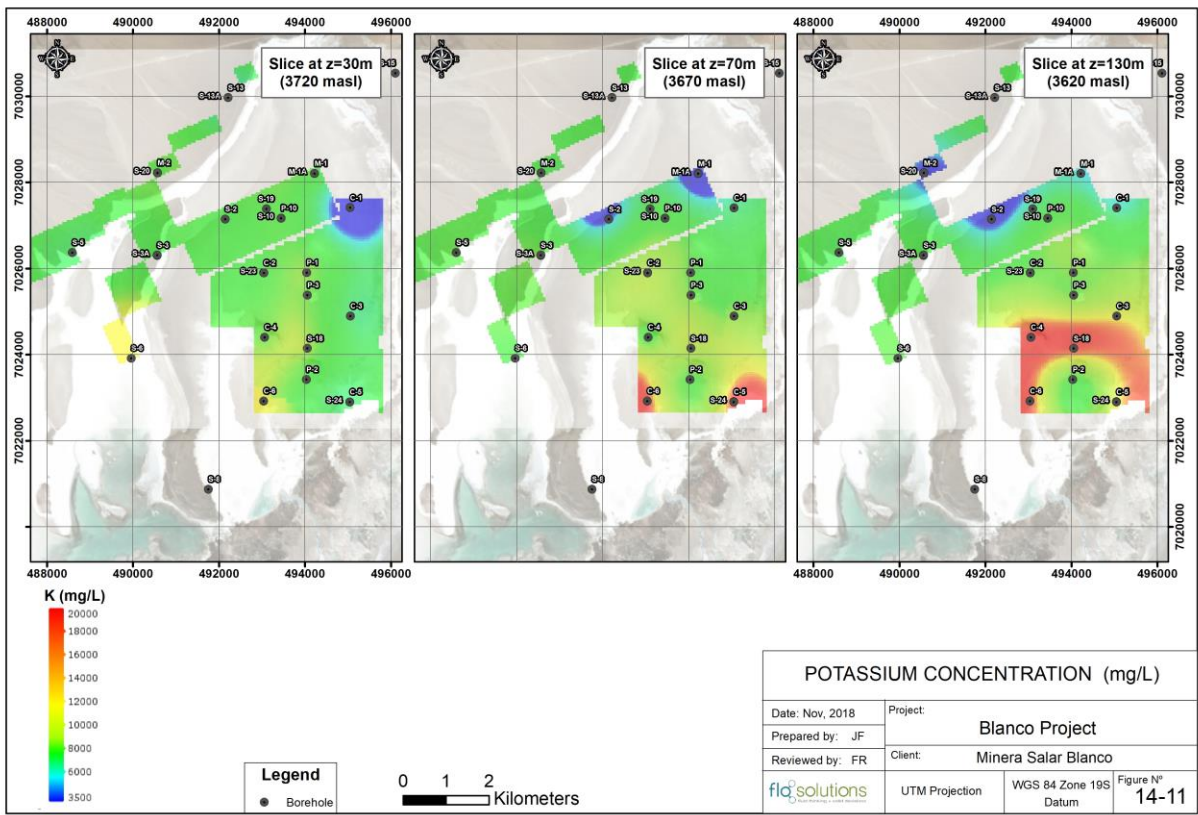
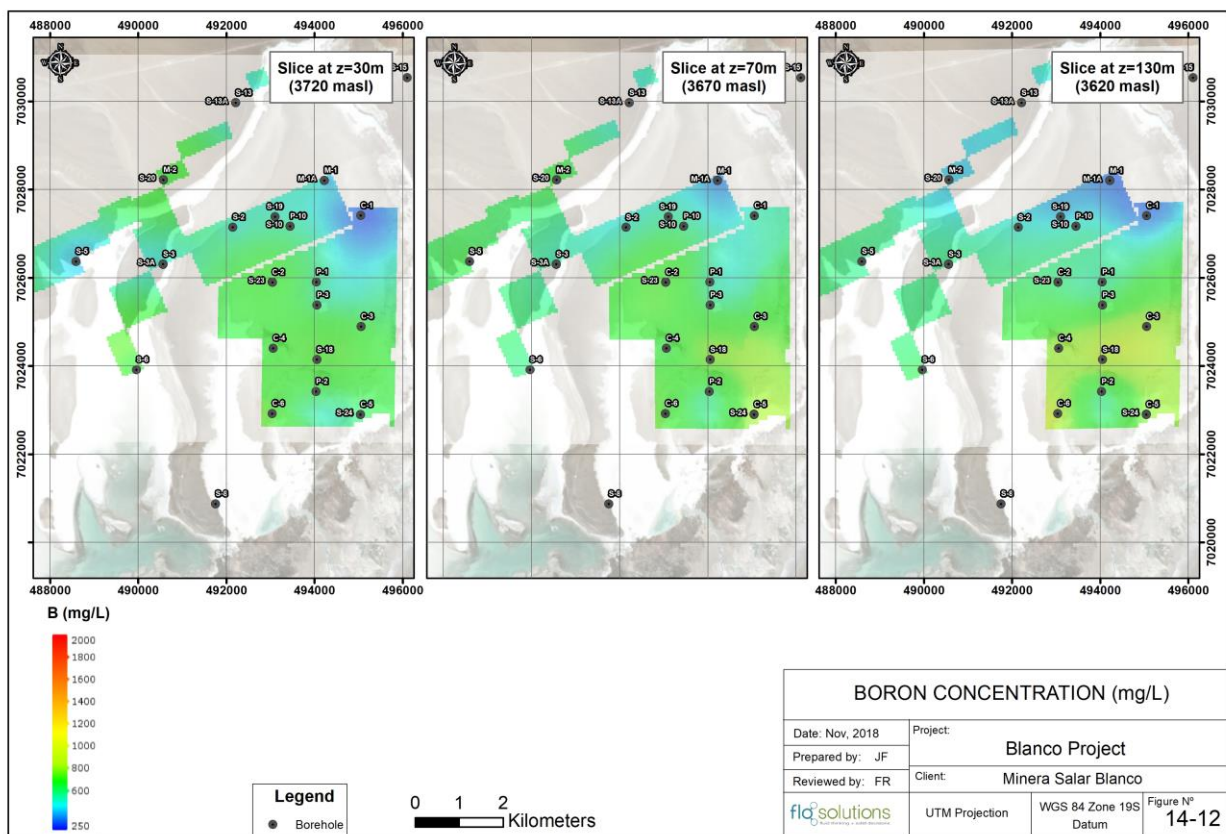


Figure 14-10: Potassium concentration distribution



Scale

Figure 14-11: Boron concentration distribution



14.10 GRADE ESTIMATE

The grade estimates of lithium and potassium in each block inside the model were calculated applying the following operation:

$$R_i = C_i \cdot S_{y_i}$$

Where: i is the indice of the block, going from 1 to 34,560,000

R_i : Grade value to be assigned (g/m^3)

C_i : Concentration value assigned from the estimation (mg/L)

S_{y_i} : Drainable porosity value assigned from the estimation (-)

V_i : Block volume (m^3)

The total resource in the reservoir is estimated as the sum of all blocks in the model,

$$R_T = \sum_i R_i V_i$$

Figure 14-12 through Figure 14-14 show N-S, W-E, and NW-SE sections through the resource model showing lithium grade distributions in g/m^3 . All the resource classification was made in the limits of the block model. The measured and indicated resource areas are shown in Figure 14-15.

Figure 14-12: N-S section through the resource model showing the lithium grade distribution

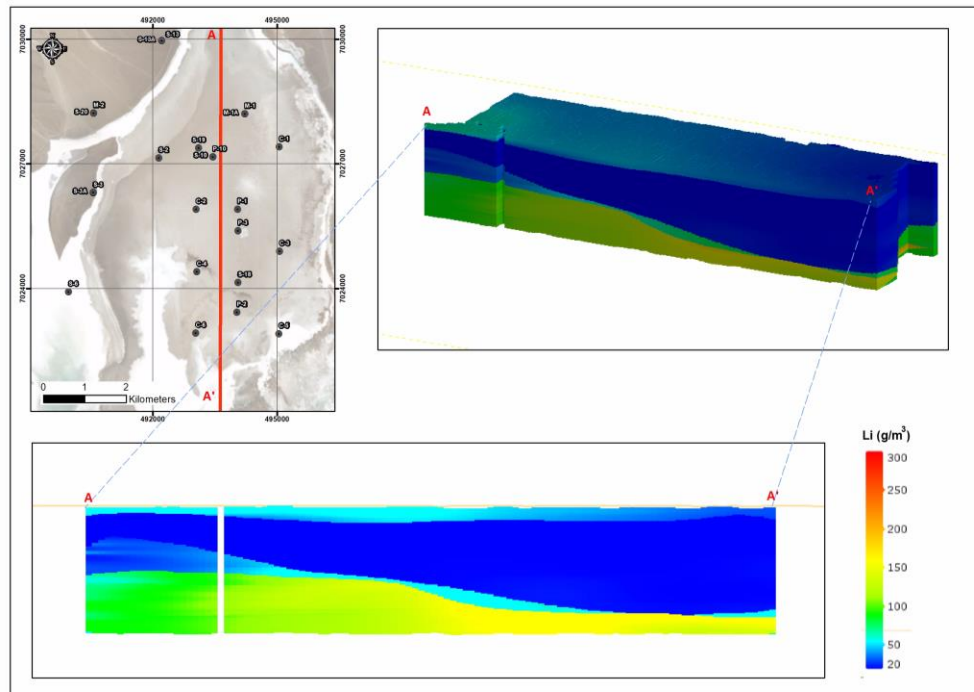


Figure 14-13: W-E section through the resource model showing the lithium grade distribution

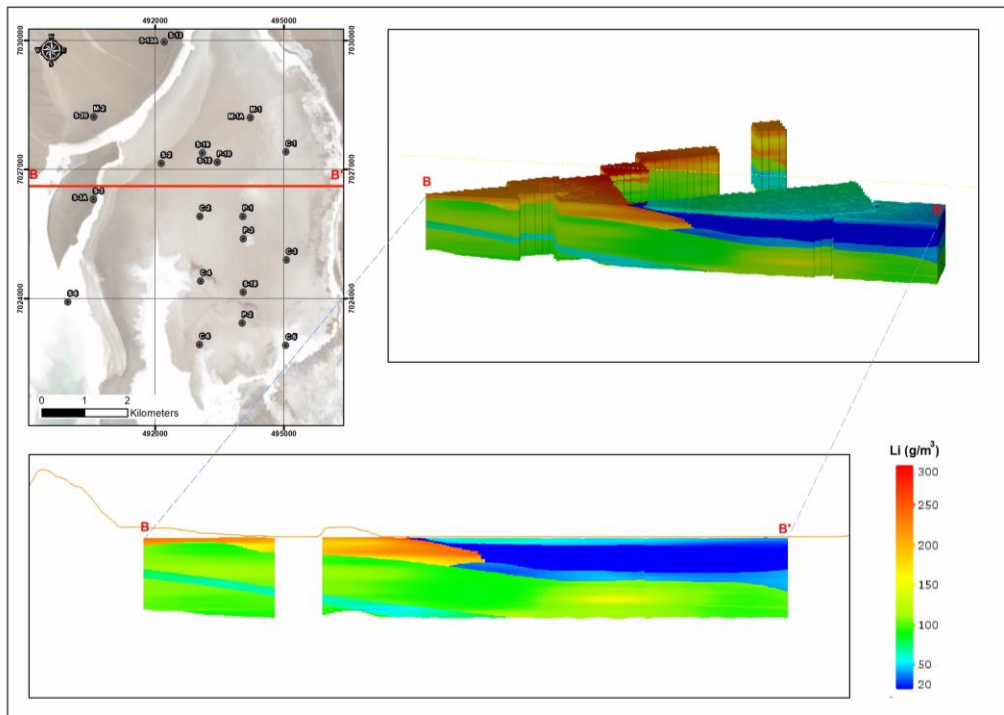


Figure 14-14: NW-SE section through the resource model showing the lithium grade distribution

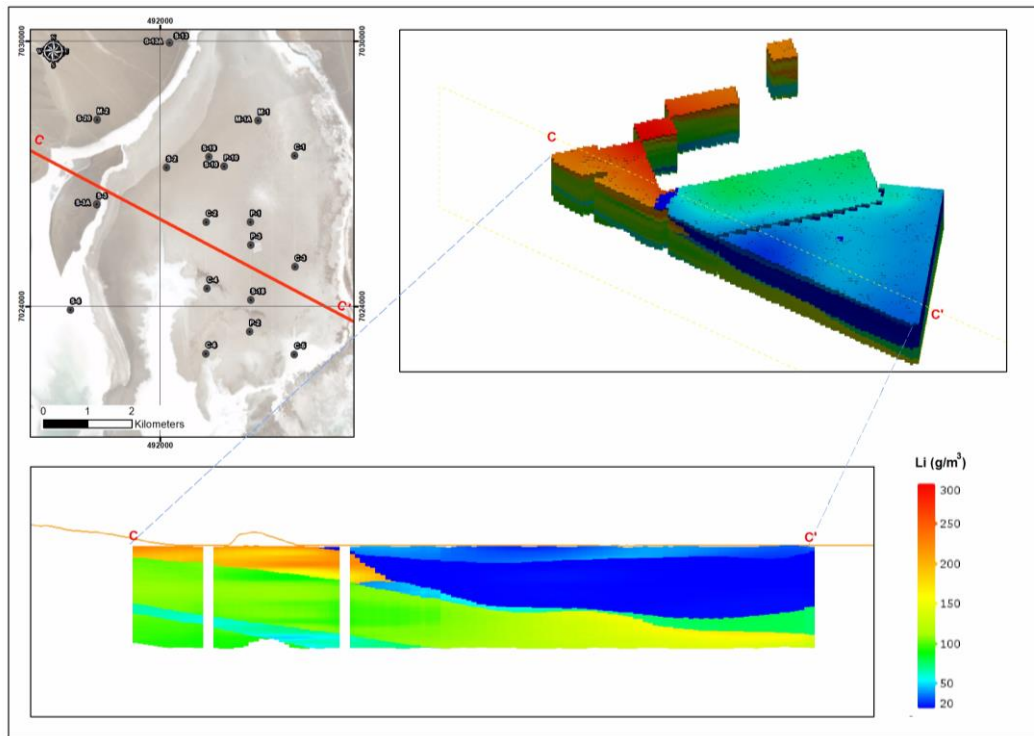
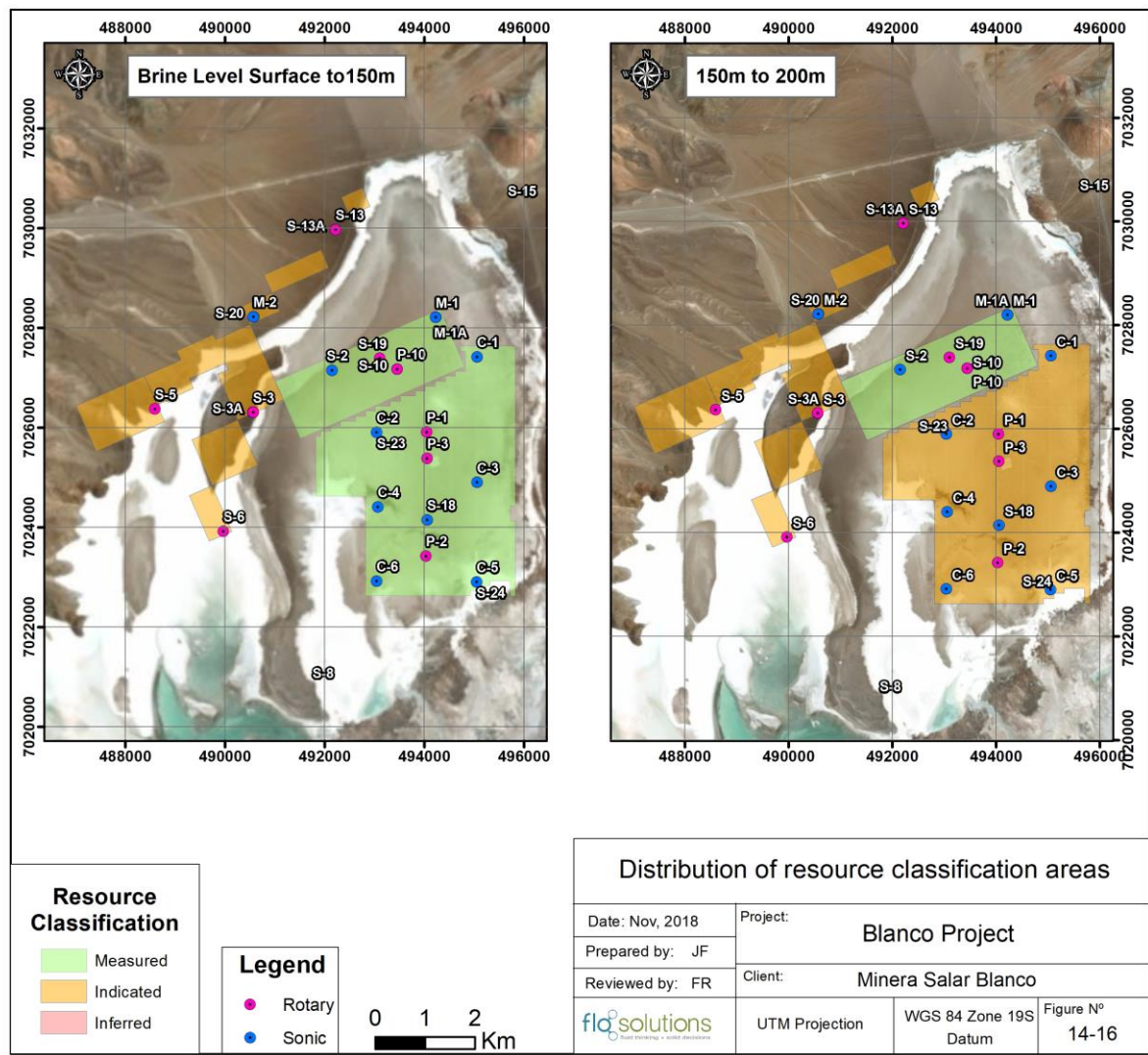


Figure 14-15: Distribution of resource classification areas



14.11 RESOURCE ESTIMATE

The resource estimate for the Blanco Project was prepared in accordance with the guidelines of National Instrument 43-101 and uses the best practices methods specific to brine resources. The lithium and potassium resources are summarized in Table 14-6. The effective date for the estimate is December 24, 2018.

Table 14-6: Measured and Indicated Lithium and Potassium Resources for the Blanco Project

	Measured (M)		Indicated (I)		M+I	
	Li	K	Li	K	Li	K
Property Area (Km ²)	18.88		6.43		25.31	
Aquifer volume (km ³)	3.05		1.94		5	
Mean specific yield (Sy)	0.04		0.11		0.07	
Brine volume (km ³)	0.13		0.21		0.35	
Mean grade (g/m ³)	48	349	128	923	79	572
Concentration (mg/L)	1,175	8,624	1,153	8,306	1,167	8,500
Resource (tonnes)	146,000	1,065,000	244,000	1,754,000	389,000	2,818,000

Notes to the resource estimate:

1. CIM definitions were followed for Mineral Resources.
2. The Qualified Person for this Mineral Resource estimate is Frits Reidel, CPG
3. No cut-off values have been applied to the resource estimate.
4. Numbers may not add due to rounding.
5. The Measured and Indicated Resources are inclusive of those Mineral Resources modified to produce the Mineral Reserves described in Section 15.
6. The effective date is December 24, 2018.

Table 14-7 shows the mineral resources of the Blanco Project expressed as lithium carbonate equivalent (LCE) and potash (KCl).

Table 14-7: Blanco Project resources expressed LCE and potash

Product	Total Resource (M+I)	
	LCE (Li ₂ CO ₃)	Potash (KCl)
Tonnes	2,070,000	5,383,000

1. Lithium is converted to lithium carbonate (Li₂CO₃) with a conversion factor of 5.32.
2. Potassium is converted to potash with a conversion factor of 1.91
3. Numbers may not add due to rounding

It is the opinion of the author that the Salar geometry, brine chemistry composition and the specific yield of the Salar sediments have been adequately characterized to support the Measured and Indicated Resource estimate for the Project herein.

It is the opinion of the authors that the resource estimated and described in the current report meet the requirements of reasonable prospects for eventual economic extraction, as defined in Form 43-101F1. The resource described herein has similar lithium concentrations, chemical composition and hydraulic parameter values (drainable porosity values between 0.05 and 0.11, and hydraulic conductivities values between 0.5 m/d and 300 m/d) to resources currently in commercial production such as those in Salar de Atacama or Salar de Olaroz located in the Puna region of Northern Argentina. The hydraulic parameters of the resource area determined from the results of the pumping tests suggests that it is reasonable to expect brine extraction by a conventional production wellfield at a commercially viable rate, while the geochemical characteristics of the brine suggest that conventional processing techniques may be employed to produce saleable lithium products in an economically profitable manner.

These conventional processing techniques are employed in most lithium brine operations, including the two operations at Salar de Atacama (Chile), one at Salar de Olaroz (Argentina), and one at Clayton Valley (USA)

15. MINERAL RESERVE ESTIMATES

This section presents a numerical groundwater flow and transport model developed for the Blanco Project to evaluate the brine mineral reserve. The majority of the modeling work was carried out by DHI in Lima, Peru under close supervision of Flosolutions and the QP. The essential elements of a brine reserves determination for a Salar are:

- Construction of a three-dimensional groundwater flow and transport model
- Steady state and transient calibration of the model
- Predictive simulation of brine extraction

The calibrated reserve model is used to simulate a brine extraction system that will meet the brine feed requirements for the evaporation ponds for an annual lithium carbonate (LCE) production target of 20,000 TPY over a 20 year project life. It is assumed that the Project has a lithium process recovery efficiency of 58%. Therefore, to meet the target LCE production rate of 20 kilo tonnes per year (kTPY), the brine abstraction from the production wellfield in the Salar needs to be at a rate of 34.6 kTPY. The reserve model predicts that the proposed brine wellfield can extract a cumulative average of 34.6 kTPY of LCE for 20 years in support of the DFS. Additionally, the model predicts that the proposed brine wellfield can extract a cumulative average of 16.7 kTPY of LCE for an additional 3 years, but which were not included in the economic evaluation of the DFS.

This Section describes the construction and calibration of the numerical model and summarizes the results of the brine production simulations and the reserve estimate.

15.1 MODEL CONSTRUCTION

15.1.1 Model domain

The Figure 15-1 shows the model domain. The boundary was defined to encompass the unconsolidated sediments of the Maricunga basin and extends from the Salar de Maricunga, in the west central portion of the domain, to the upper reaches of the alluvial fans in the catchments feeding the Salar.

The topographic elevation of the model domain ranges from 3,749 meters above sea level (masl) at the Salar to 4,230 masl in the northeast corner of the domain. The base of the model has an elevation of 3,545 m, for a total simulated sediment thickness beneath the Salar of 200m.

15.1.2 Meshing and layering

The stratigraphic units in the model domain were exported from 3D Geomodeller using the Smart Layering Approach, in which the stratigraphic units are exported into a 3D Feflow mesh, making adjustments so that the layers are generally horizontal. Figure 15-2 shows the generalized approach.

The model has a total of 2,489,422 nodes, 4,744,425 elements, and 25 layers (see Figure 15-3). Elements located where bedrock is present are inactive in the flow and transport simulations. Therefore, the total number of active elements is 3,823,317. All elements are triangular prisms with elemental diameters ranging from approximately 50 m in the center of the Salar to approximately 230 m at the outer edges of the model domain. The layer thickness ranges from 0.1 m to 51 m. The thinnest elements were defined during the Smart-Layering process, when the contact between dipping stratigraphic units was pinched off in order to keep the layers relatively horizontal. The thickest elements are also due to the Smart Layering process.

Figure 15-1: Numerical model domain for brine reserve analysis

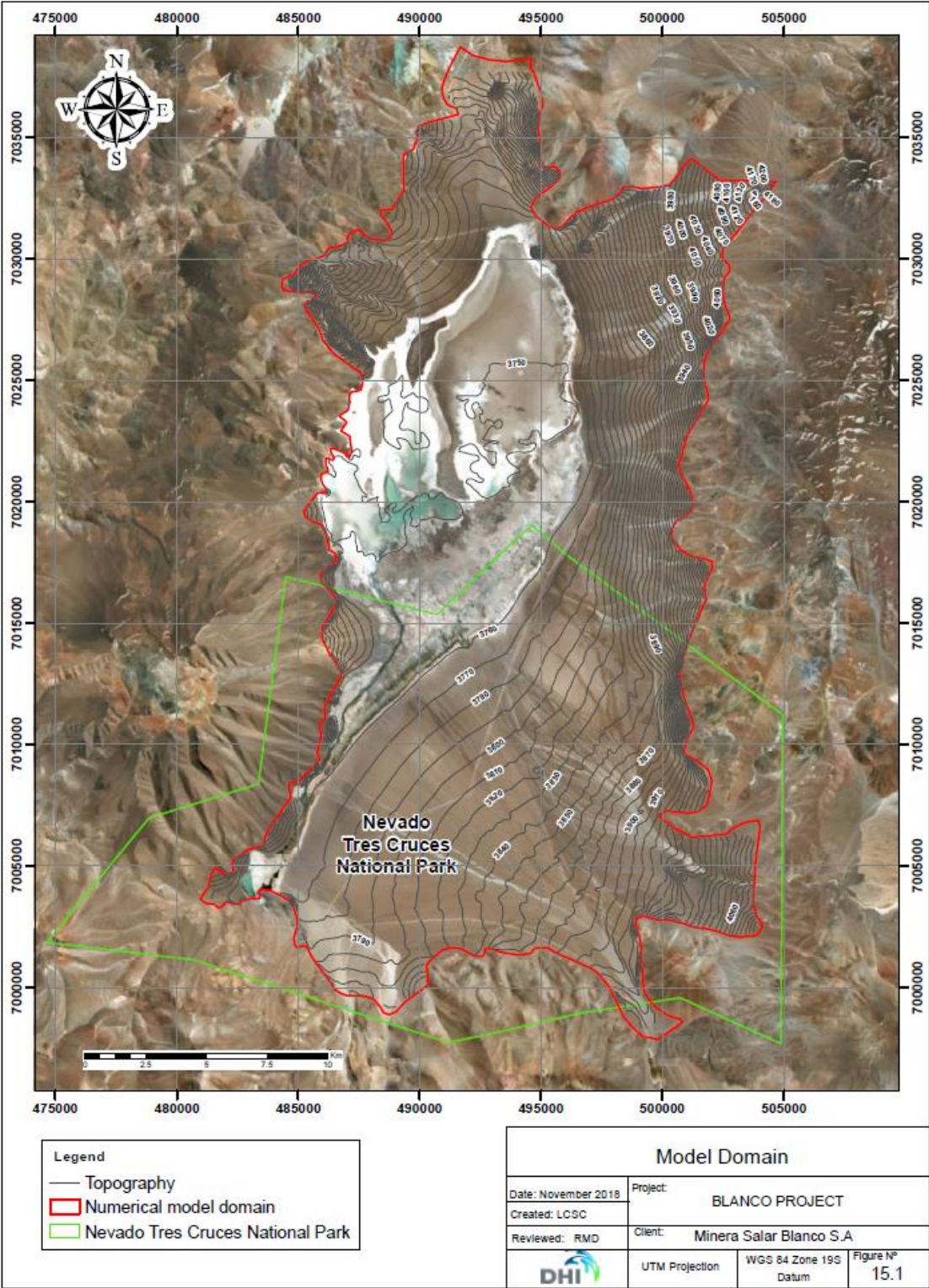


Figure 15-2: Schematic of “Smart-Layering” (left: standard rectangular mesh; right: optimized mesh to better represent 3D geology)

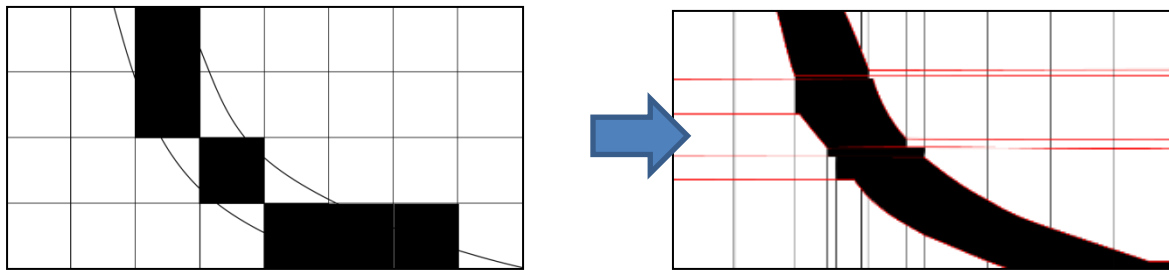
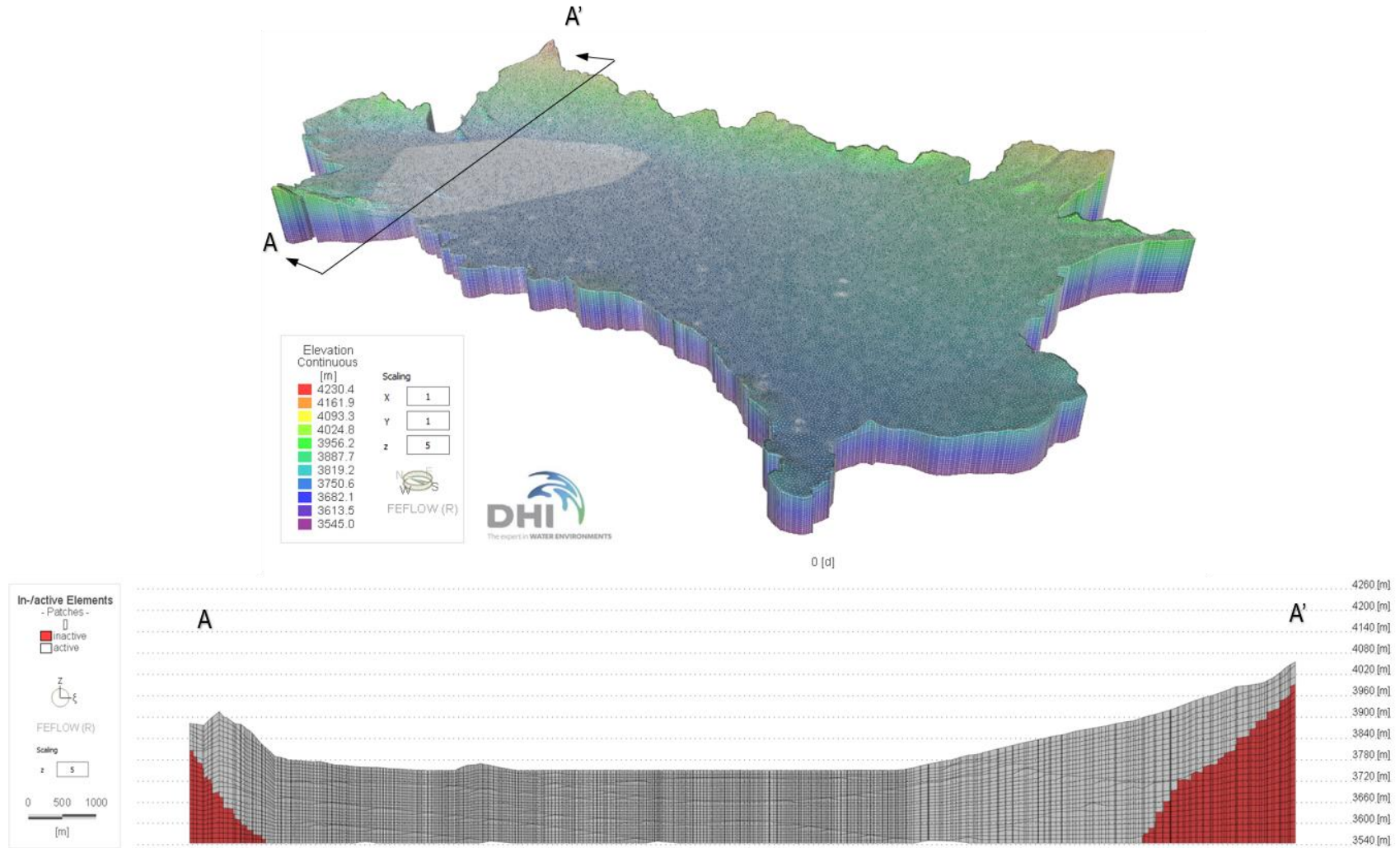


Figure 15-3: 3D view of reserve model mesh and typical Section A-A'

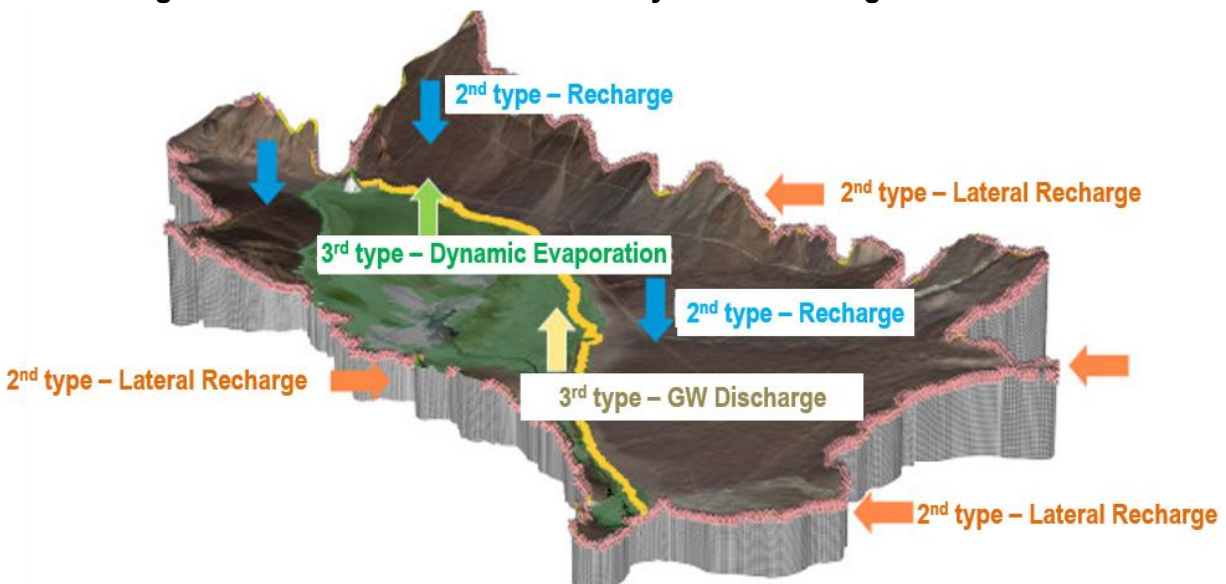


15.1.3 Flow boundary conditions

There are two primary groundwater inflow processes at the Salar de Maricunga: recharge by direct precipitation and indirect recharge on catchments surrounding the Salar. Groundwater discharges at lower elevations via evapotranspiration and diffuse seepage to surface water. A schematic of the key boundary condition types is presented in Figure 15-4. The boundary condition zones will be discussed later in this section.

The bottom of the model domain was treated as a no-flow boundary. Evapotranspiration and recharge boundary conditions were applied to Layer 1. The lateral recharge boundary conditions were applied to the outer boundaries in Slices 1 to 3 of the model. Where a lateral recharge boundary is not defined, the model edge is treated as a no-flow boundary.

Figure 15-4: Reserve model boundary conditions for groundwater flow



15.1.3.1 Recharge

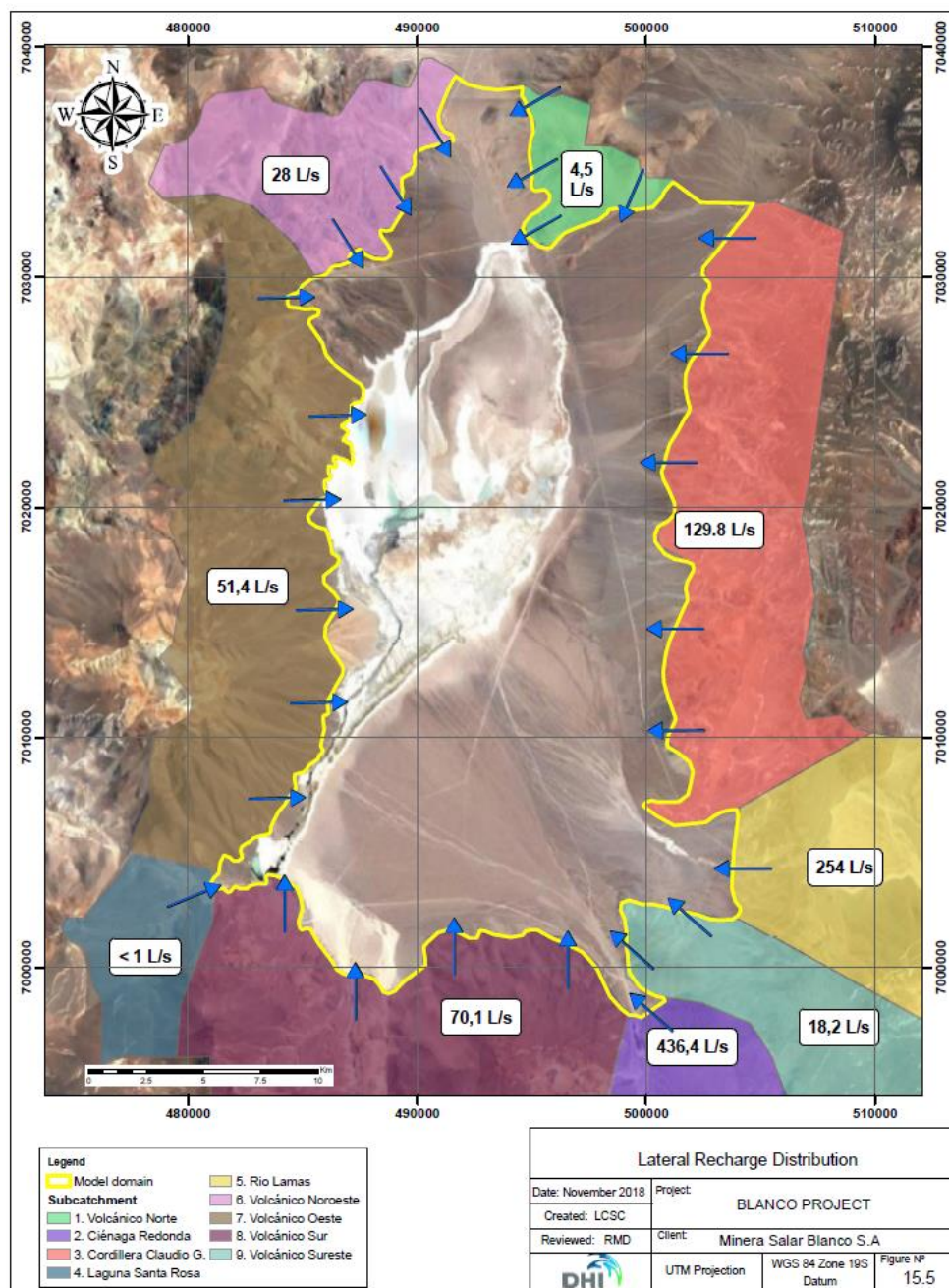
Recharge was applied only to the alluvial fan materials, at a rate of 32.9 mm/y, for a total of 405 L/s, consistent with the conceptual model (Flosolutions, 2018). This area is shown in Figure 15-4. No recharge was applied to the Salar which is assumed to be an area of net groundwater discharge.

15.1.3.2 Catchment inflows

In addition to direct recharge, the Salar de Maricunga receives indirect recharge at higher elevations within the catchments that surround the Salar. Figure 15-5 shows the eight catchments that generate lateral groundwater inflow into the Maricunga Basin and the annual average flow rates for each catchment. The catchment inflows were treated as flux (second type) boundary

conditions. As much as possible, the flux boundary nodes were set to be below the water table, and the boundary nodes were applied to Slices 1 to 3 of the model. Inflow rates range from 4.5 l/s from the North Volcanic basin located north of the Salar to 436 L/s from the Ciénaga Redonda catchment located southeast of the Salar.

Figure 15-5: Indirect, lateral recharge to Salar de Maricunga from surrounding catchments



15.1.3.3 Evapotranspiration and diffuse groundwater discharge

A significant groundwater discharge process at the Salar de Maricunga is evapotranspiration. Figure 15-6 illustrates the distribution of the evapotranspiration function in the model. In all cases, the evapotranspiration rate was defined as a linear function of water table depth from ground surface. When the water table was at ground surface, the applied evapotranspiration rate was a maximum value. The evapotranspiration rate decreased linearly with depth from ground surface to a depth of 2 m, at which point, the evapotranspiration rate was set to equal zero.

The magnitude of the maximum evapotranspiration zone was calibrated using target evapotranspiration fluxes from the water balance (Flosolutions, 2018). Saline water from the center of the Salar was assigned a lower maximum evapotranspiration rate, consistent with the well-established reduction in evaporation of saline waters compared to fresh water.

Four evapotranspiration zones were defined, as shown Figure 15-6. The four zones are designed to simulate:

- Two brine evapotranspiration zones within the clay core of the Salar
 - one at the lowest elevations within the Salar, where the salt lake exists, and
 - one zone in areas where there is no surface pond
- Two freshwater evapotranspiration zones were also defined
 - one at the margins of the Salar, at the contact between the brine and the alluvial fans and
 - one in the southern portion of the model domain, where vegetation extracts groundwater via transpiration through the roots.

Each of these zones was treated as a series of Feflow transfer boundary nodes, corresponding to Cauchy or third-type boundary conditions. The value of maximum evapotranspiration transfer rate in each zone was adjusted during the calibration such that the total evapotranspiration distribution matched the conceptual water budget.

The Salar de Maricunga has areas of surface water during the wet season. These areas are located along the eastern and southern margin of the Salar, where brine and freshwater come in contact at the downgradient edge of the alluvial fans. Conceptually, freshwater discharge is driven by the presence of the Clay Core unit, at the Salar margins. Three groundwater discharge zones were defined, as shown in Figure 15-6. These boundaries were simulated using Feflow transfer boundary nodes. However, unlike the evapotranspiration boundaries, in which the transfer rate coefficient is a function of depth from ground surface, the transfer rate coefficient for discharge is constant.

15.1.3.4 Pumping wells

The model domain includes pumping wells that intercept both freshwater and brine. Pumping tests were completed in three Project pumping wells, P-1, P-2, and P-4, located within the Salar de Maricunga. These wells were simulated as multi-level wells in the numerical model.

There are two existing water supply wells, MDO-23 and MDO-24, in the south central area of the model domain, as shown in Figure 15-7, that operated in the past as part of the Mantos de Oro water supply system; currently they are not under operation. Given that the water levels have practically recovered to pre-pumping levels (Golder, 2016), these wells were not part of the steady state or transient calibration runs. However, for the reserve assessment, these wells pump at a combined annual average rate of 66 L/s for 7.5 years. They are simulated as multiple-nodes well boundary conditions.

In addition, MSB has proposed a freshwater supply well at CAN-6 shown in Figure 15-7. CAN-6 was simulated as a series of seven vertically-stacked well boundary nodes within the FEFLOW model in the predictive simulations. The flow rate from CAN-6 is 35 L/s over the duration of the mine life, including 20 years of brine extraction and two years post-production. The simulations in this reserve analysis do not include groundwater predictions for the two post-production years, when water levels in the brine resource area will recover.

The brine extraction system was simulated as 44 well boundary conditions, each located in the center of the either the Upper Halite aquifer or the Lower Alluvial aquifer. These wells and their pumping rates are discussed in the reserve analysis presented in Section 15.4.

Figure 15-6: Evapotranspiration and diffuse groundwater discharge zones

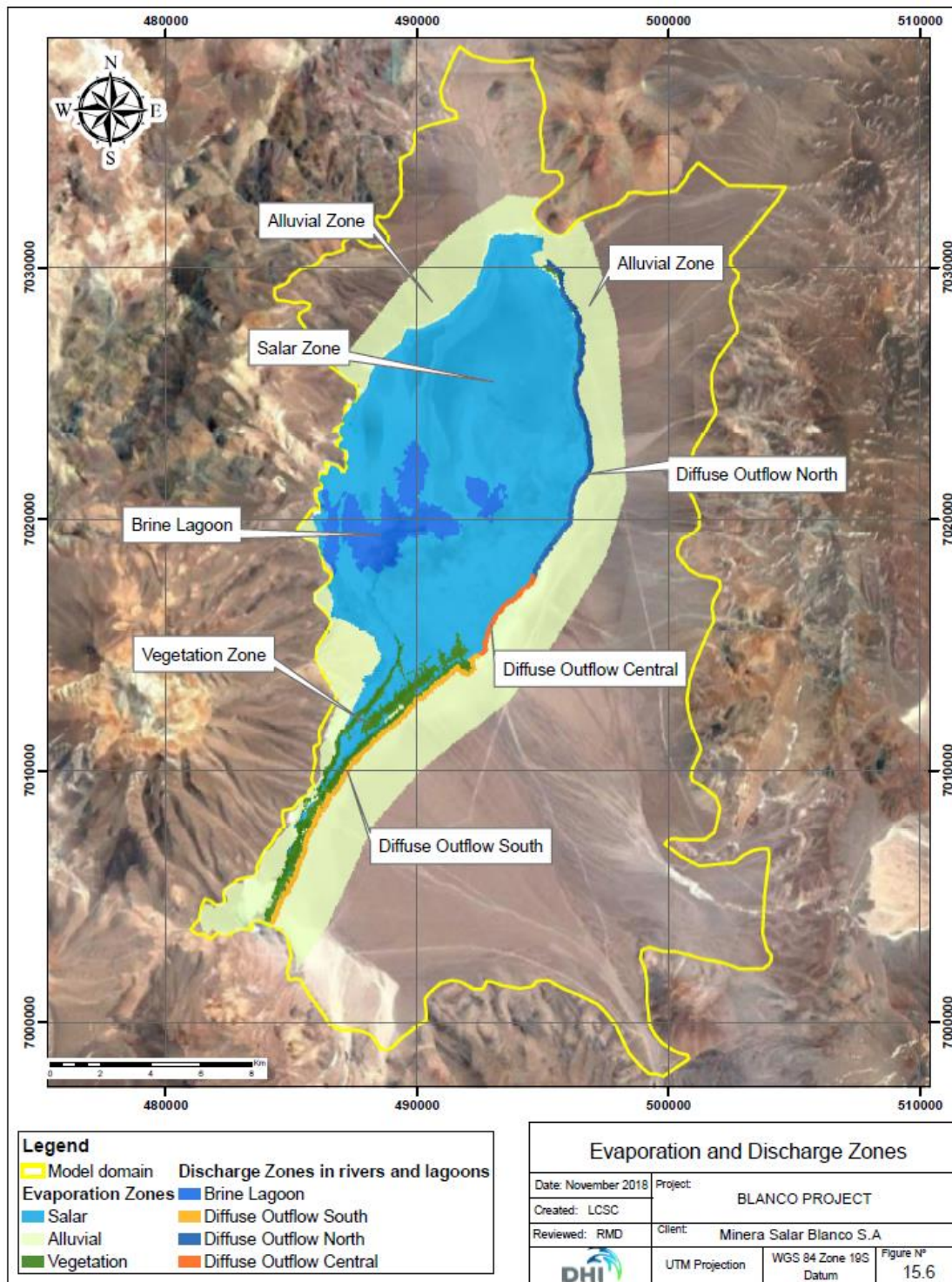
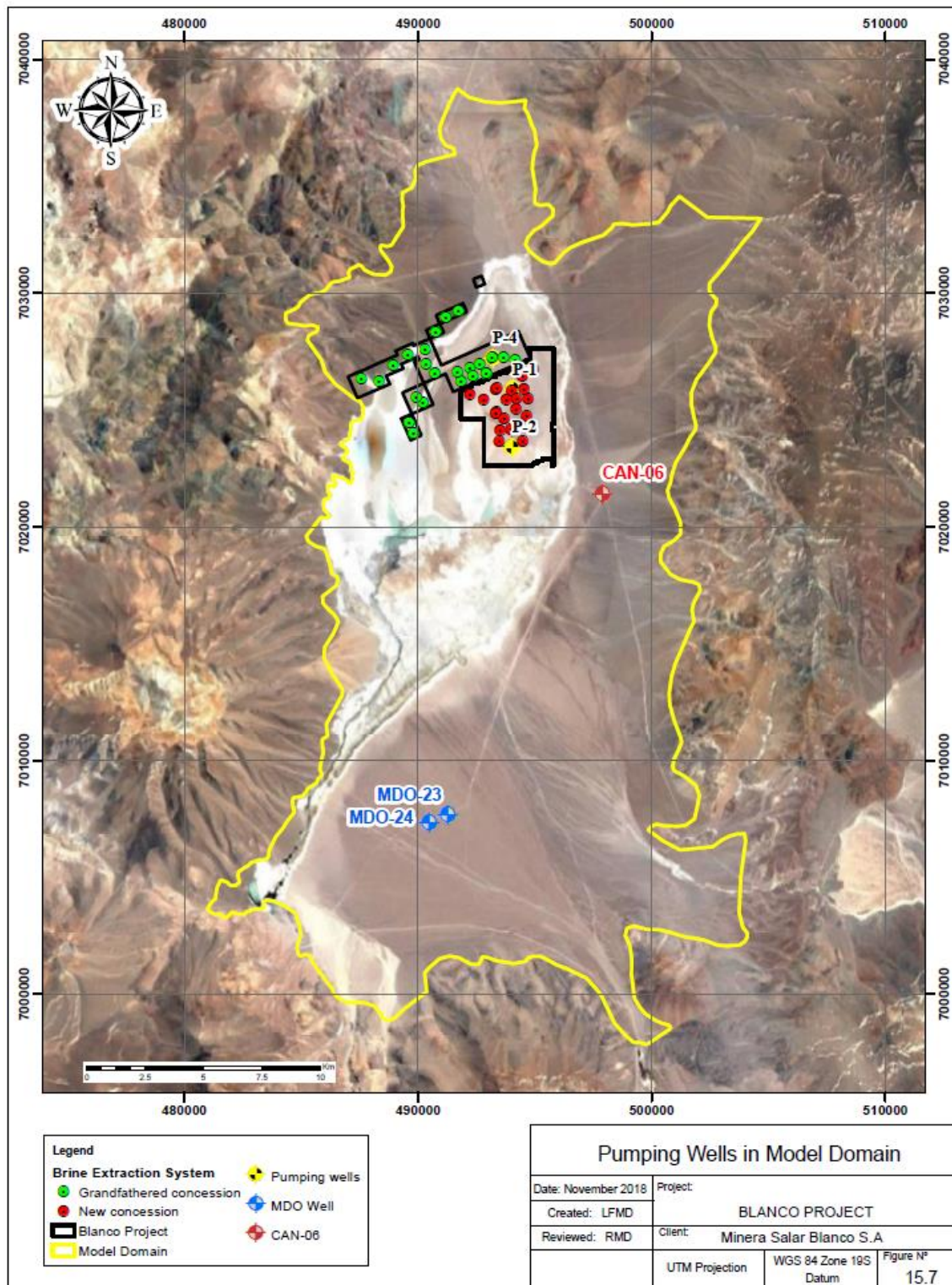


Figure 15-7: Pumping wells in reserve model domain



15.1.4 Hydrogeological units and parameters

15.1.4.1 Main Hydrogeological Units

As discussed above in Section 15.1.1, the hydrogeological units were derived from the stratigraphic model via 3D Geomodeller. Six primary hydrogeological units were defined for the reserve model, as shown in Table 15-1. These six units are as follows:

- UH-1: Upper Halite is a shallow permeable unit associated with the Salar.
- UH-2: Alluvial fans surround the Salar. The alluvial fan responsible for most of the lateral recharge—that associated with Río Lamas—is treated separately from the other alluvial fans, as presented in Table 15-1. UH-2B comprises the Río Lamas alluvial fan subunits. All other surficial alluvial units are included in UH-2A.
- UH-3: The Clay Core is a fine-grained unit that underlies the core of the Salar, including the Upper Halite. It serves as a confining unit for the two final units, and also as a barrier to lateral groundwater flow into the Salar.
- UH-4: The Lower Alluvium includes confined or semiconfined sands and volcanoclastics of low to moderate hydraulic conductivity.
- UH-5: The Basin Fill Sediments underlie the alluvial fans
- UH-6: Basement bedrock.

The conceptual model of the reserve is that there are two brine aquifers at the Salar Blanco project: a shallow aquifer (UH-1) comprising the Upper Halite and a deep aquifer (UH-4) comprising the Lower Alluvium, Lower Sand and the two Volcanoclastic units. The two aquifers are separated by the Clay Core (UH-3) aquitard. Outside the Salar, the alluvial fans (UH-2) transmit recharge from the catchments that feed the Salar. Below the alluvial fans, the Basin Fill Sediments (UH-5) form a zone of lower hydraulic conductivity. Bedrock (UH-6) underlies the entire model domain. Elements containing UH-6 are inactivated in the Feflow mesh and do not form a part of the reserve analysis.

During the calibration, subunits were defined to improve the match between the observed and simulated response. A total of 28 hydrogeological property zones are defined. The main hydrogeological zones that exist at ground surface—i.e., in Layer 1 of the model—are shown in Figure 15-8. A full list of the 28 hydrogeologic units is presented in Table 15-1, along with conceptual hydraulic conductivity and storage values.

The specific storage values presented in Table 15-1 are based on the analysis by Flosolutions (2018).

Figure 15-8: Surface hydrogeological units

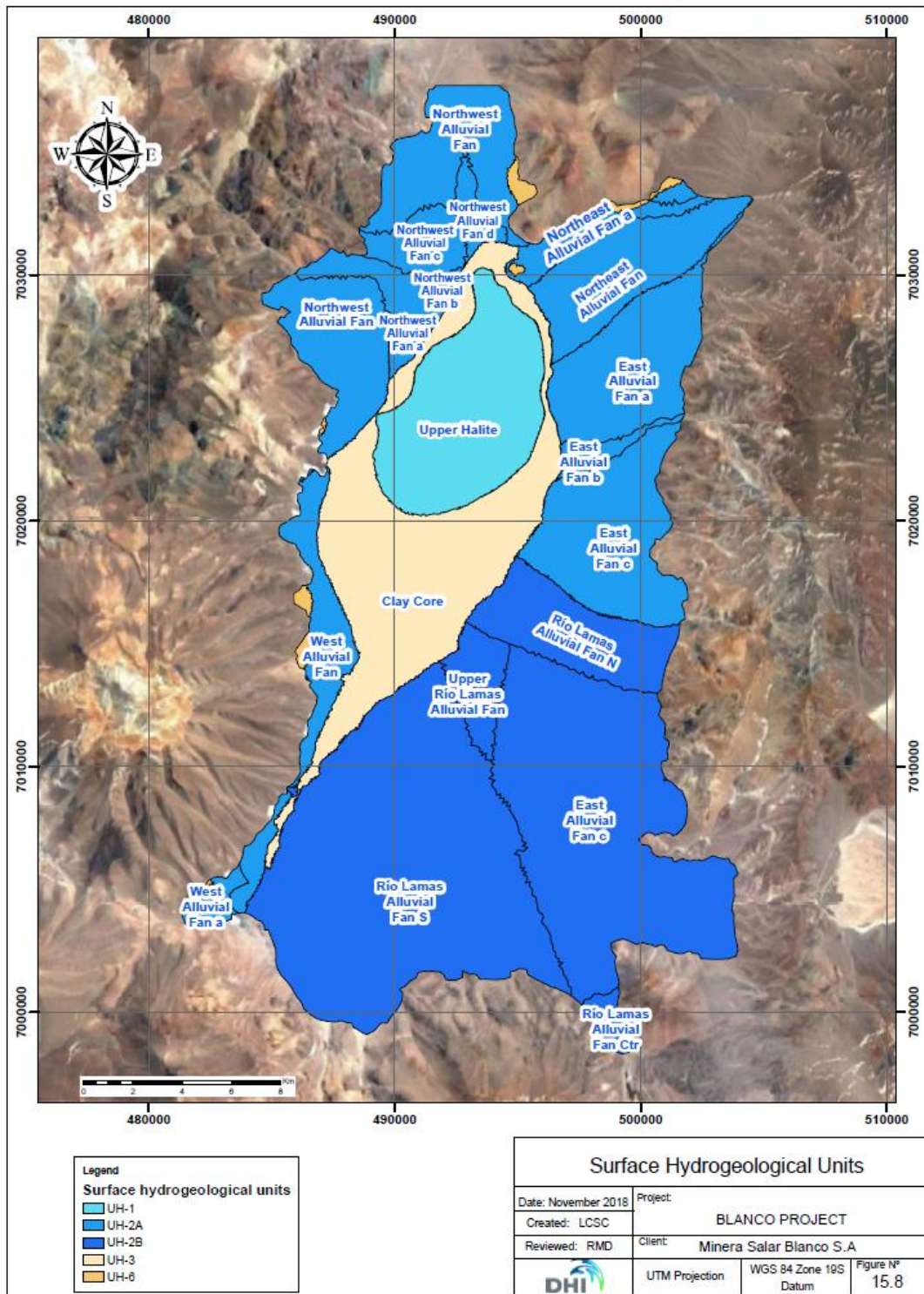


Table 15-1: Hydrogeologic units

UH	Sub-unit	Description	Layers of Model	Conceptual Hydraulic Conductivity (m/d)	Conceptual Ss (1/m)	Conceptual Sy
UH-1	Upper Halite	Shallow permeable unit associated with Salar	1 – 6	100 – 640	10^{-5} - 10^{-3}	0.07
UH-2A	Northwest Alluvial Fan	Unconfined, moderate-permeability materials associated with alluvial catchments surrounding Salar	1 – 25	0.1 – 40	10^{-5} - 10^{-3}	0.15
	Northwest Alluvial Fan a		1 – 22	0.1 – 40	10^{-5} - 10^{-3}	0.15
	Northwest Alluvial Fan b		1 – 25	0.1 – 40	10^{-5} - 10^{-3}	0.15
	Northwest Alluvial Fan c		1 – 25	0.1 – 40	10^{-5} - 10^{-3}	0.15
	Northwest Alluvial Fan d		1 – 25	0.1 – 40	10^{-5} - 10^{-3}	0.15
	Northeast Alluvial Fan		1 – 14	0.1 – 10	10^{-5} - 10^{-3}	0.10
	Northeast Alluvial Fan a		1 – 12	0.1 – 20	10^{-5} - 10^{-3}	0.10
	East Alluvial Fan		1 – 16	0.1 – 10	10^{-5} - 10^{-3}	0.10
	East Alluvial Fan a		1 – 16	0.1 – 10	10^{-5} - 10^{-3}	0.10
	East Alluvial Fan b		1 – 14	0.1 – 10	10^{-5} - 10^{-3}	0.10
	East Alluvial Fan c		1 – 19	0.1 – 10	10^{-5} - 10^{-3}	0.10
	West Alluvial Fan		1 – 23	0.1 – 40	10^{-5} - 10^{-3}	0.15
	West Alluvial Fan a		1 – 7	0.1 – 40	10^{-5} - 10^{-3}	0.15
UH-2B	Río Lamas Alluvial Fan N	Unconfined, high-permeability materials of Río Lamas alluvial fan	1 – 23	30 – 280	10^{-5} - 10^{-3}	0.10
	Río Lamas Alluvial Fan		1 – 15	30 – 280	10^{-5} - 10^{-3}	0.10
	Río Lamas Alluvial Fan S		1 – 19	30 – 280	10^{-5} - 10^{-3}	0.10
	Río Lamas Alluvial Fan Ctr		1 – 22	30 – 300	10^{-5} - 10^{-3}	0.10
	Upper Río Lamas Alluvial Fan		1 – 8	10 – 280	10^{-5} - 10^{-3}	0.10
UH-3	Clay Core	Fine-grained sediments (aquitar) underlying Salar, intercalated with sands and gravels	1 – 23	0.0001-0.01	10^{-7} - 10^{-3}	0.02
	Clayey Sand		10 - 11	0.01 – 10	10^{-7} - 10^{-3}	0.02
	Clayey Gravel		13	0.01 – 10	10^{-7} - 10^{-3}	0.02
	Sandy Clay		13	0.01 – 10	10^{-7} - 10^{-3}	0.02
UH-4	Lower Alluvium		2 – 25	0.1 – 1	10^{-7} - 10^{-3}	0.06

	Lower Sand	Confined or semi-confined lower alluvial deposits	12 – 25	0.1 – 2.5	10^{-7} - 10^{-3}	0.06
	Upper Volcaniclastic	Confined, low-permeability volcanoclastic materials	4 - 25	0.1 – 2	10^{-7} - 10^{-3}	0.10
	Lower Volcaniclastic		5 – 25	0.1 – 1	10^{-7} - 10^{-3}	0.10
UH-5	Basin Fill Sediments	Confined or semi-confined lower alluvial deposits	2 – 25	0.01 – 2.5	10^{-7} - 10^{-5}	0.01

15.1.4.2 Unsaturated parameters

The Feflow model was run using a variably saturated configuration. Feflow's modified van Genuchten parameterization was used. This formulation makes use of this pressure-saturation relationship:

$$S_e = \left(\frac{\theta - \theta_r}{\theta_s - \theta_r} \right) = \left[\frac{1}{1 + (\alpha\psi)^n} \right]^m \quad (1)$$

where S_e is the effective saturation, θ is the volumetric moisture content; θ_s is the volumetric moisture content at the water table ($\theta_s = S_{sat}\phi$, where S_{sat} is the saturation fraction at zero pressure, and ϕ is the porosity); ψ is the matric pressure head, or the negative pressure head; and θ_r , α , n and m are fitting parameters. The first fitting parameter, θ_r , is called the residual moisture content and denotes a theoretical minimum moisture state. The second fitting parameter, α , is approximately equal to the “air entry pressure head”, the matric head at which a saturated soil begins to desaturate. The other two fitting parameters are exponents.

The modified van Genuchten relative hydraulic conductivity relationship is as follows:

$$K_r = \left(\frac{\theta - \theta_r}{\theta_s - \theta_r} \right)^\delta = \left[\frac{1}{1 + (\alpha\psi)^n} \right]^{m\delta} \quad (2)$$

where K_r is the relative hydraulic conductivity and δ is an exponent. The decoupling of m and n and the addition of δ adds flexibility to the modified van Genuchten model relative to the van Genuchten (1980) relationship. In addition, the modified relationship does not possess a portion of the pressure- hydraulic conductivity curve in which hydraulic conductivity becomes constant with pressure under very dry conditions. The parameters used in the Feflow model are shown in Table 15-2. Also shown in the table are the effective specific yield values for each hydrogeological unit.

Table 15-2: Unsaturated parameters

Hydrogeologic Unit	Porosity	Sr *	α (m-1)	n	m	δ	Effective Sy**	Conceptual Sy
Upper Halite	0.35	0.25	0.50	1.35	0.25	4.0	0.07	0.07
Clay Core	0.40	0.10	0.15	1.19	0.15	7.0	0.02	0.02
Grava	0.25	0.00	0.80	1.45	0.28	2.0	0.10	0.10-0.15
Río Lamas Alluvial Fan	0.25	0.15	0.90	1.50	0.33	2.5	0.10	0.10
Lower Alluvial & Sand	0.25	0.30	0.50	1.50	0.33	2.0	0.06	0.06
Basin Fill Sediment	0.20	0.00	0.50	1.50	0.33	2.0	0.07	0.01
Volcaniclastics	0.25	0.00	0.80	1.40	0.29	2.0	0.10	0.10

Notes:

*S_r = θ_r/ϕ , or the residual saturation

** Effective Sy (specific yield) is the amount water released from storage due to a water table drop of 1 m from a soil column extending from the final water table elevation to a height of 3 m above the initial water table elevation, using Equation 1.

15.1.5 Lithium transport parameters

In addition to groundwater flow, the FEFLOW model was configured to simulate the mass transport of lithium in support of the reserve calculation. In these simulations, the longitudinal dispersivity was set to a constant value of 30 m, and the horizontal and vertical transverse dispersivity values were set to 3 m.

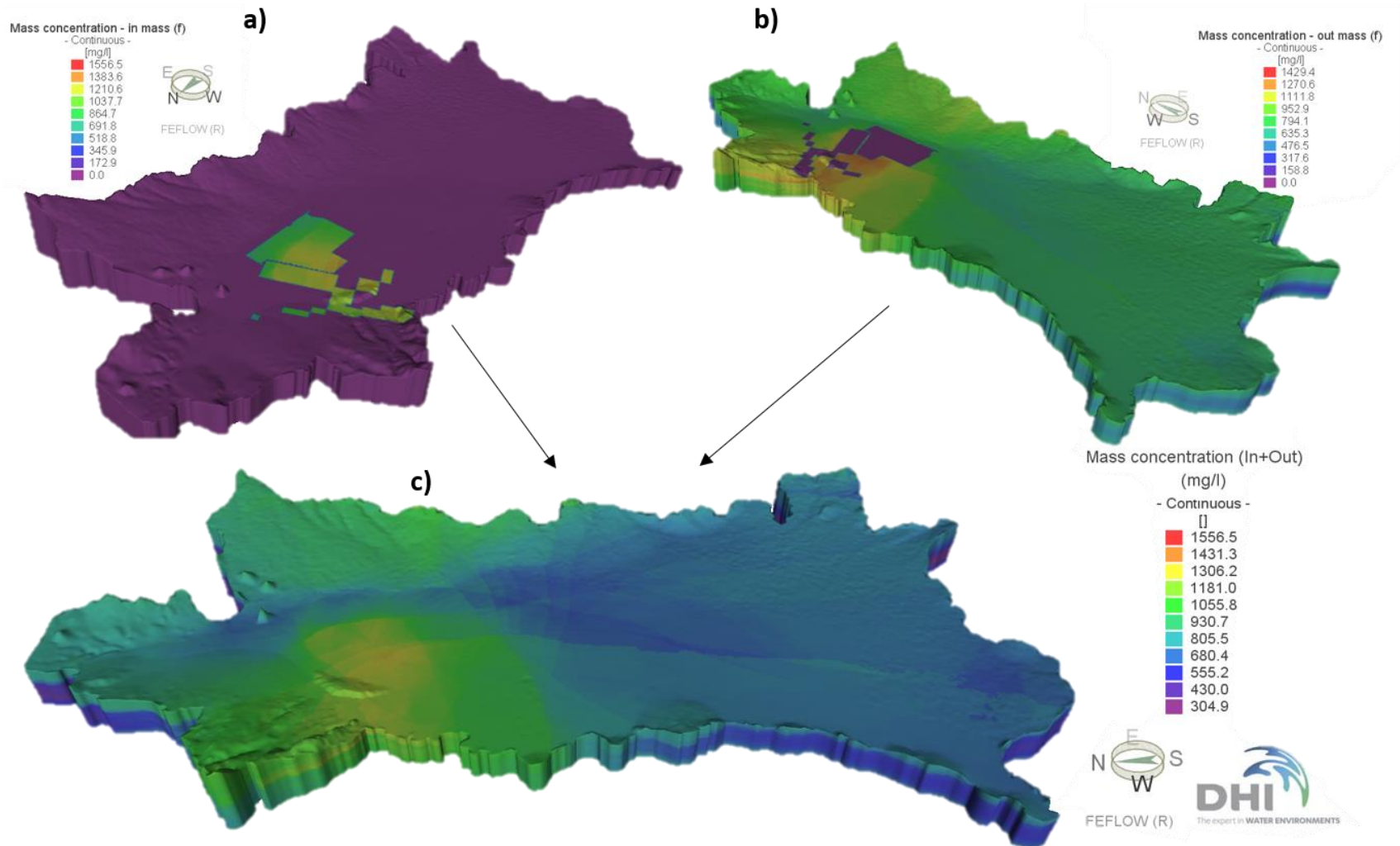
The initial concentration of lithium for the reserve estimate simulations was based on the Measured and Indicated resources as described in Section 14. This information was derived from the Leapfrog database. In the reserve assessment, the lithium present under the MSB project boundary was treated separately from brine present at the start of operations outside of the property boundary. The initial concentration distribution is shown Figure 15-9. The figure shows how on-property lithium (Figure 15-9a) and off-property lithium (Figure 15-9b) are treated as separate solutes in the FEFLOW transport simulation. The concentrations of both of these solutes can be summed to compute a total mass of lithium (Figure 15-9c).

The effective porosity for the mass transport simulations was based on the conceptual specific yield and is shown in Table 15-3.

Table 15-3: Effective porosity for transport simulations

UH	Subunit	Effective Porosity
UH-1	Upper Halite	0.07
UH-2A	all units (Alluvial Fans exc. Río Lamas)	0.16
UH-2B	all units (Río Lamas Alluvial Fan)	0.11
UH-3	all units (Clay Core)	0.02
UH-4	Lower Alluvium	0.07
	Lower Sand	0.06
	Upper Volcaniclastic	0.11
	Lower Volcaniclastic	0.11
UH-5	Basin Fill Sediments	0.11

Figure 15-9: Lithium concentration



15.1.6 Density considerations

Fluid density is an important factor in the movement of groundwater in and around a lithium-brine Salar. Key flow processes related to the MSB project are illustrated in Figure 15-10. Groundwater is recharged by fresh rainfall primarily at higher elevations and on the alluvium surrounding the Salar, as shown in Figure 15-4. Freshwater flows through the alluvium around the Salar and discharges via evapotranspiration near the freshwater-brine interface and, to a lesser degree, within the Salar itself.

The computational burden of simulating variable-density groundwater flow is significant. For the purposes of the reserve calculation, the three-dimensional groundwater flow and transport model was configured to assume single-density groundwater. Figure 15-11 illustrates the generalized approach to simulating the flow processes in the three-dimensional model. As in the variable-density system shown in Figure 15-10, groundwater recharges at higher elevations and on the alluvium surrounding the Salar. This freshwater from recharge flows toward the Salar and discharges at approximately the location of the freshwater-brine interface due to the change in topographic slope that coincides with the brine-freshwater interface. Due to the lower evapotranspiration rate of brine compared to freshwater, additional groundwater (brine) discharges in the center of the Salar, but the magnitude of this flow is lower than that which discharges at the margins of the Salar.

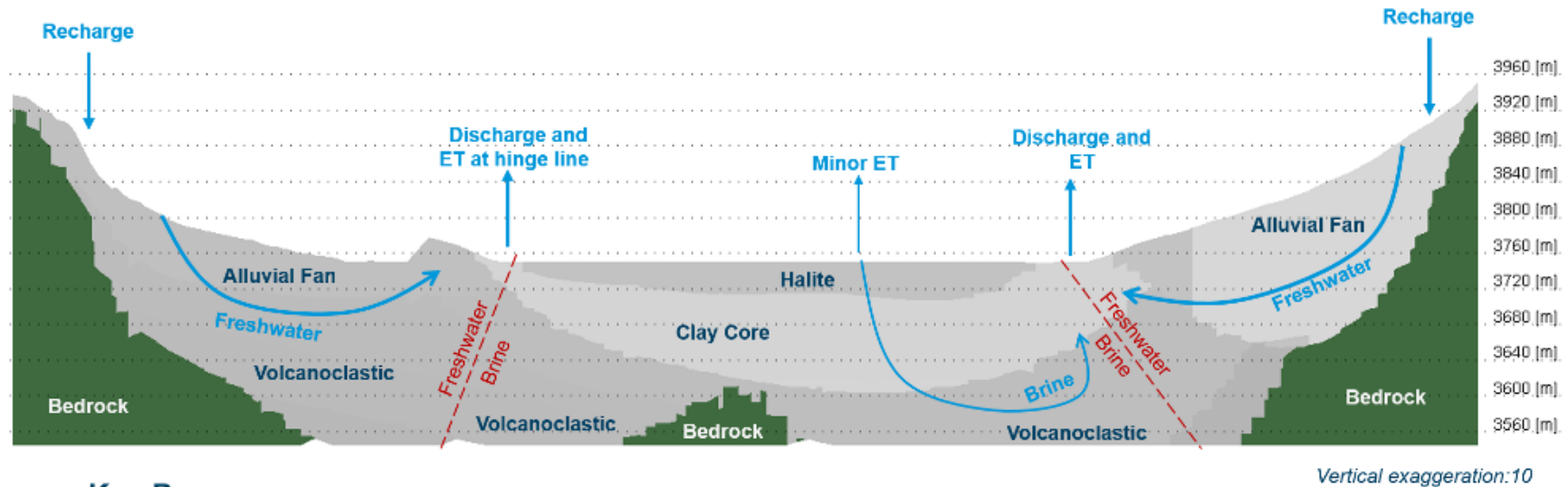
Figure 15-12 presents in graphical form the implications of simulating the Salar de Maricunga as a single-density system.

As a general observation, ignoring density effects will result in greater groundwater mixing and dilution. Therefore, the use of a single-density model for the reserve estimate, especially given the relatively uniform brine density distribution, will provide a conservative estimate of the reserve.

15.1.7 Solver and convergence criteria

The flow solver used in the FEFLOW runs is the Algebraic Multigrid Methods for Systems (SAMG) solver with a maximum of 50 AMG cycles and 200 PCG iterations. The transport equation was also solved with the SAMG solver with these settings. A root mean squared (RMS) Euclidian L2 error tolerance of 1×10^{-5} , with a maximum of 12 outer iterations. Mass matrices were computed using a lumped mass configuration. The convective form of the transport solution was applied.

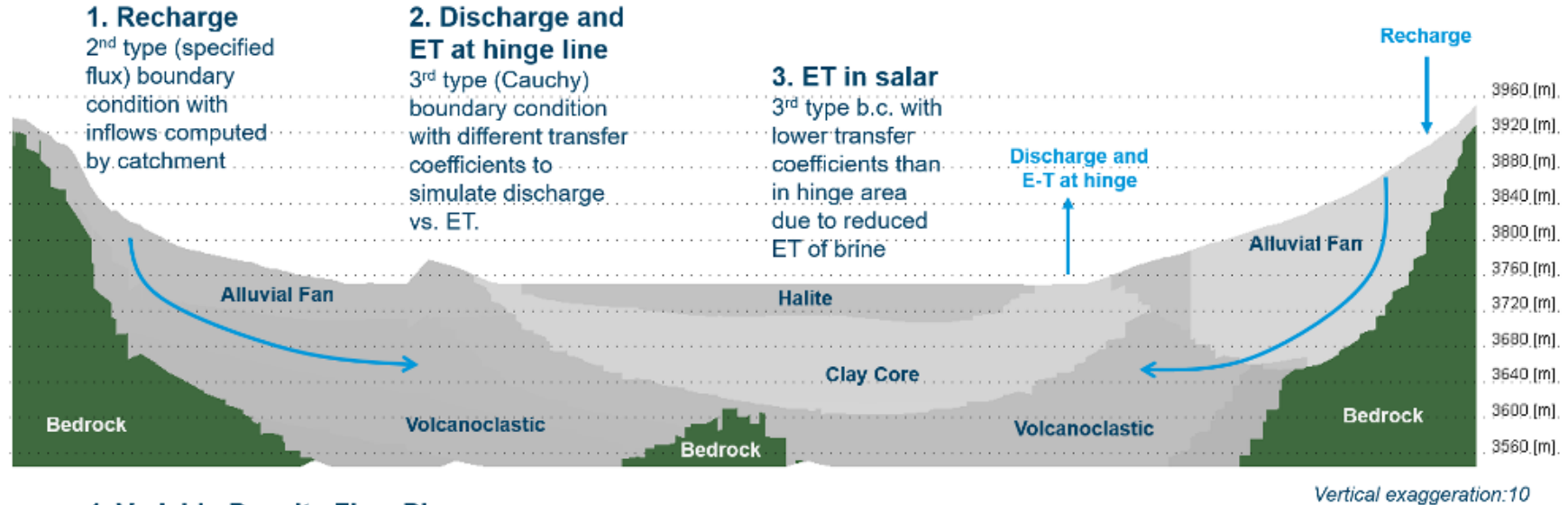
Figure 15-10: Conceptualization of density-dependent flow processes at the Salar Blanco Project



Key Processes:

1. Recharge of freshwater occurs at higher elevations and flows toward the salar.
2. At the edge of the salar, freshwater encounters saltwater and flows to the surface due to density effects, causing both groundwater discharge to the surface and enhanced evaporation. This area is sometimes called the "hinge" line.
3. Evaporation also occurs, *though to a lesser extent*, within the salar itself. Small variations in density caused by evaporation that is not balanced by groundwater flow or precipitation can lead to free convection (i.e., downward flux of higher-density groundwater). One free convection cell is shown above.

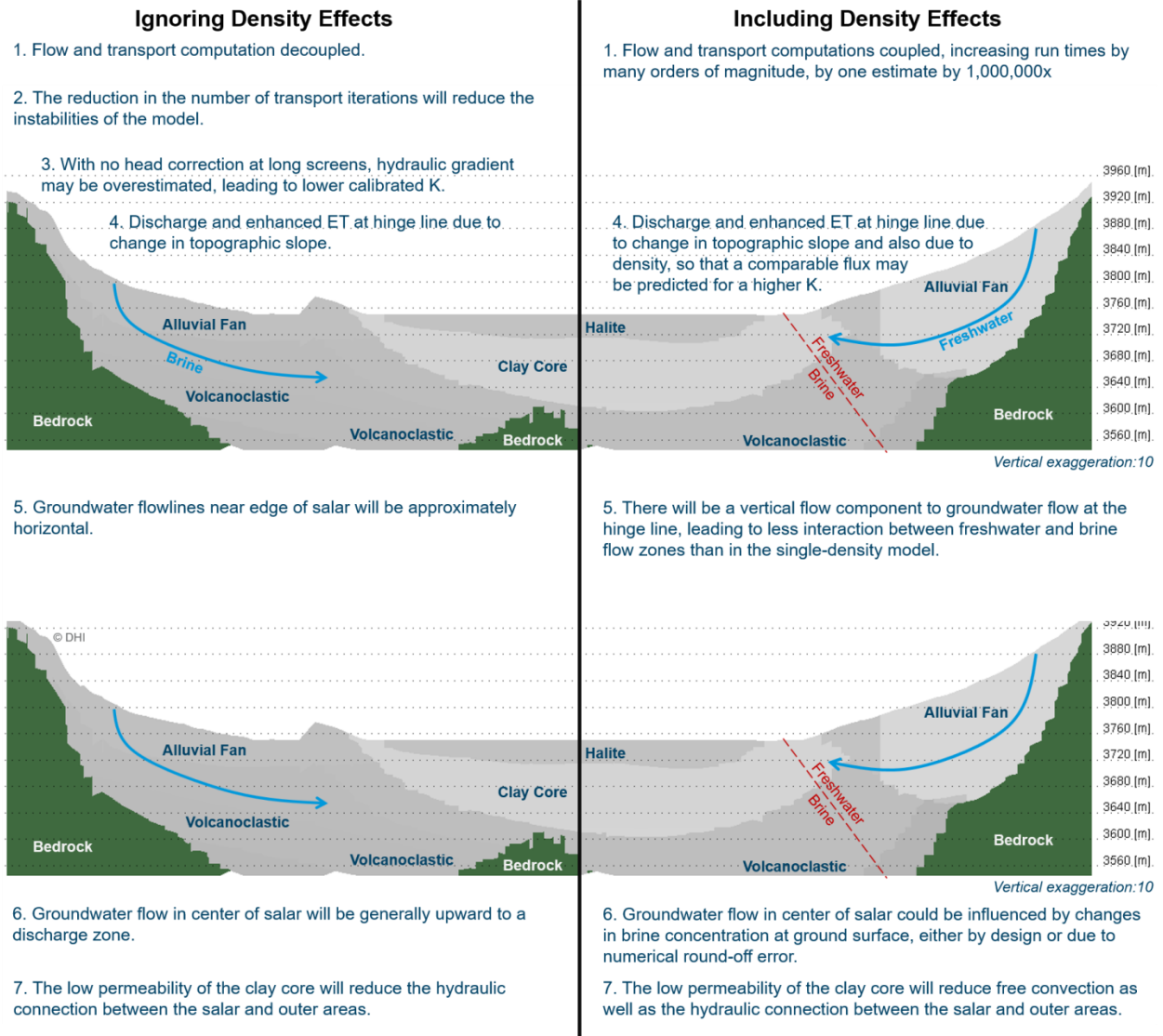
Figure 15-11: Salar Blanco numerical reserve modeling approach



4. Variable-Density Flow Phenomena

In the 3D model, a single density is assumed, corresponding to 1.2 g/cm³ the typical brine density at Salar de Maricunga. No correction for freshwater density was made for long-screened wells. In the handful of wells with short screens, the head was converted to an equivalent brine head.

Figure 15-12: Implications of ignoring density-dependent flow effects



15.2 CALIBRATION METHODOLOGY

The flow model was calibrated under steady state and transient conditions to (1) fit the static water levels in project area wells, (2) match the conceptual water balance, and (3) simulate three pumping tests completed in the Salar. A combination of manual and automated calibration was completed under both steady state and transient conditions. This section describes the calibration methodology. Calibration results are presented in Section 15.3.

15.2.1 Steady State calibration

In the steady state calibration step, the hydraulic conductivities and the transfer coefficients used to simulate evapotranspiration and diffuse groundwater discharge (Section 15.1.3.3) were calibrated to fit the field data. Manual and automated calibration were completed. For the automated calibration, Feflow's built-in version of the PEST parameter optimization program, FePest, was applied.

15.2.1.1 Calibration targets

Water level measurements are available in 53 monitoring wells and 25 mini-piezometers within the active elements of the model domain. Of these, five wells have measurements that could not be used as calibration targets. Three of these wells are the pumping wells, P-1, P-2 and P-3, which had higher resolution water level measurements from 12 observation wells (P-1.1, P-1.2, P-1.3, P-1.4, P-2.1, P-2.3, P-2.4, P-2.5, P-4.1, P-4.2, P-4.3 and P-4.4) in their vicinity. The shallow well S-16B which is screened in a thin saturated zone above a confining clay that may be perched. Its deeper well couplet, S-16A was used. Well S-12 was excluded because of its proximity to MDO-10. The 73 water level targets that were used in the steady state model calibration are shown in Figure 15-13, along with the observed water table configuration. Table 15-4 lists these wells and the target water level for the well.



Table 15-4: Water level observations

Well	Water Type	Easting (WGS84)	Northing (WGS84)	Top of Casing Elevation (DEM)	Period	Maximum Static Water Level (mbtc)	Minimum Static Water Level (mbtc)	Average Static Water Level (mbtc)	Range in Water Level (m)	Piezometric Head Target (masl)
C-2	Brine	493,044.62	7,025,902.64	3,750.44	15/02/17 - 19/04/18	0.64	0.47	0.58	0.17	3,749.86
C-3	Brine	495,056.61	7,024,897.72	3,750.68	31/01/18 - 19/04/18	0.79	0.75	0.77	0.04	3,749.91
C-4	Brine	493,059.76	7,024,405.59	3,750.79	31/01/18 - 19/04/18	1	0.97	0.98	0.03	3,749.81
C-5	Brine	495,050.60	7,022,904.26	3,750.57	31/01/18 - 19/04/18	0.83	0.6	0.65	0.23	3,749.93
C-6	Brine	493,039.33	7,022,924.26	3,750.89	31/01/18 - 19/04/18	1.06	0.99	1.03	0.07	3,749.86
P-1.1	Brine	494,034.91	7,025,893.63	3,750.71	15/02/17 - 19/04/18	1.6	1.34	1.22	0.26	3,749.49
P-1.2	Brine	494,063.94	7,025,896.31	3,750.71	20/12/12 - 19/04/18*	0.85	0.81	0.82	0.04	3,749.88
P-1.3	Brine	494,034.85	7,025,907.94	3,750.80	20/12/12 - 19/04/18*	1.16	0.76	1.07	0.4	3,749.73
P-1.4	Brine	494,034.98	7,025,917.77	3,750.83	20/12/12 - 19/04/18*	0.91	0.72	0.86	0.19	3,749.97
P-2.1	Brine	494,060.99	7,023,400.92	3,750.71	05/08/17 - 19/04/18	0.96	0.73	0.8	0.23	3,749.91
P-2.3	Brine	494,033.40	7,023,407.49	3,750.63	05/08/17 - 31/01/18	0.77	0.63	0.71	0.14	3,749.92
P-2.4	Brine	494,034.97	7,023,397.81	3,750.64	05/08/17 - 19/04/18	0.85	0.59	0.73	0.26	3,749.91
P-2.5	Brine	494,061.03	7,023,401.60	3,750.81	02/09/17 - 19/04/18	1.35	1.05	1.21	0.3	3,749.59
P-3	Brine	494,054.41	7,025,382.67	3,750.70	15/02/17 - 19/04/18	0.5	0.21	0.35	0.28	3,750.34
P-4.1	Brine	493,193.91	7,027,224.49	3,750.71	05/08/17 - 19/04/18	2.56	2.35	2.48	0.21	3,748.24
P-4.2	Brine	493,172.29	7,027,241.94	3,750.23	15/04/17 - 19/04/18*	0.37	0.3	0.34	0.07	3,749.89
P-4.3	Brine	493,159.83	7,027,250.82	3,750.23	15/04/17 - 19/04/18*	0.37	0.34	0.36	0.03	3,749.88
P-4.4	Brine	493,139.56	7,027,265.13	3,750.34	15/04/17 - 19/04/18*	0.47	0.42	0.45	0.05	3,749.89
S-11	Brine	490,569.36	7,028,216.96	3,759.57	02/05/17 - 19/04/18	9.74	9.46	9.62	0.28	3,749.95
S-13A	Brine	492,212.92	7,029,964.14	3,757.79	05/05/17 - 19/04/18	10.51	9.45	9.76	1.05	3,748.04
S-15	Brine	496,103.46	7,030,533.98	3,783.09	05/05/17 - 18/04/18	25.72	25.34	25.59	0.37	3,757.50
S-16A	Fresh	497,122.21	7,026,004.87	3,771.74	05/05/17 - 18/04/18	9.47	9.14	9.36	0.32	3,762.38
S-17	Fresh	497,968.45	7,022,516.03	3,792.02	05/05/17 - 18/04/18	30.05	29.84	30	0.2	3,762.01

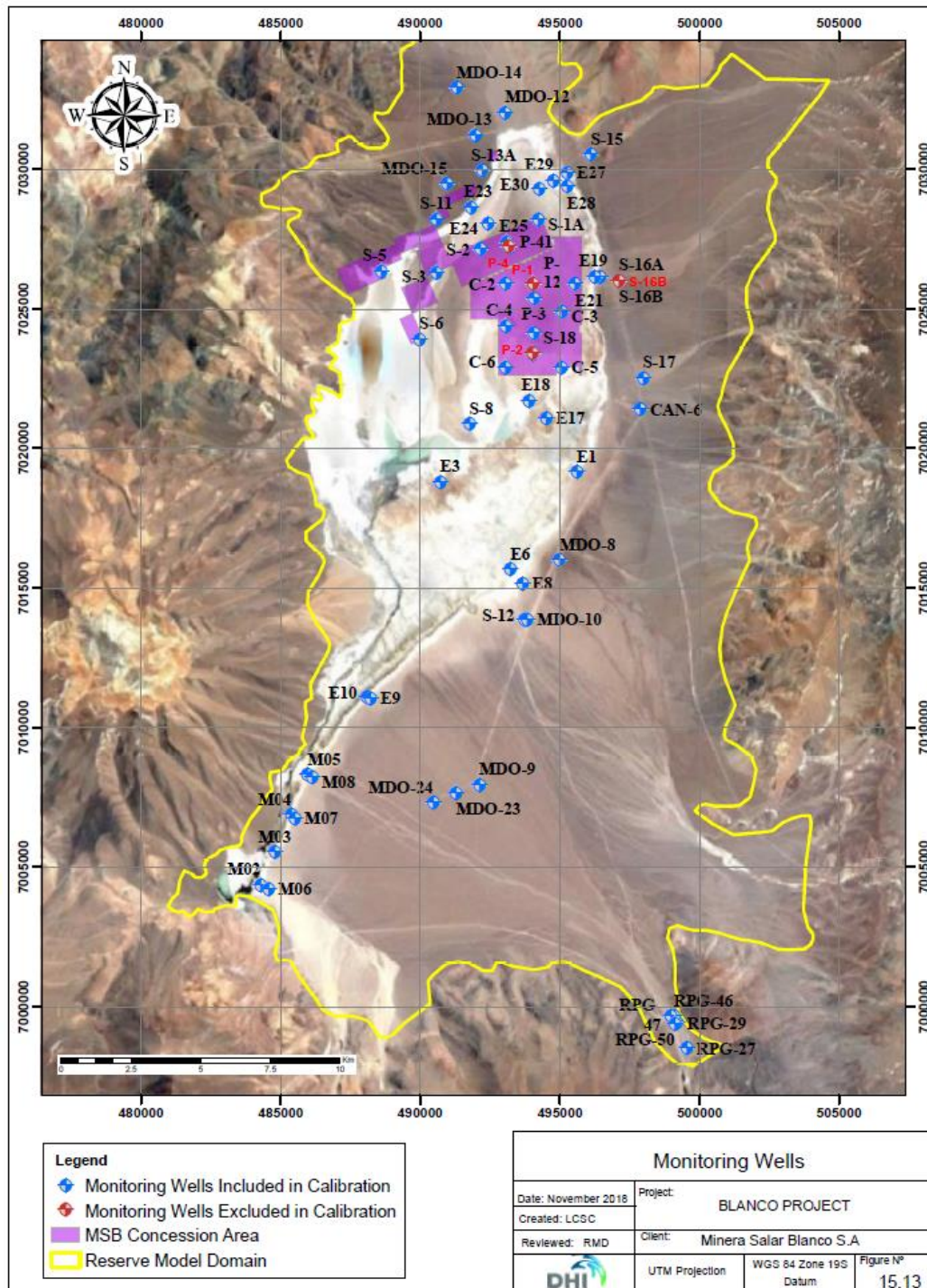
Well	Water Type	Easting (WGS84)	Northing (WGS84)	Top of Casing Elevation (DEM)	Period	Maximum Static Water Level (mbtc)	Minimum Static Water Level (mbtc)	Average Static Water Level (mbtc)	Range in Water Level (m)	Piezometric Head Target (masl)
S-18	Fresh	494,054.31	7,024,141.55	3,749.98	02/05/017 - 02/09/17	4.79	4.26	4.34	0.53	3,745.64
S-19	Brine	493,104.55	7,027,380.64	3,750.71	05/05/17 - 19/04/18	3.25	2.73	2.86	0.52	3,747.85
S-1A	Brine	494,219.92	7,028,201.32	3,750.25	05/05/17 - 19/04/18	0.99	0.76	0.9	0.23	3,749.36
S-2	Brine	492,143.45	7,027,141.30	3,750.75	05/05/17 - 19/04/18	4.01	2.61	2.99	1.4	3,747.76
S-5	Brine	488,590.38	7,026,366.35	3,752.06	05/05/17 - 19/04/18	2.26	2.11	2.19	0.16	3,749.87
S-6	Brine	489,964.01	7,023,912.39	3,750.68	05/05/17 - 19/04/18	4.66	4.35	4.44	0.32	3,746.23
S-8	Brine	491,753.61	7,020,871.40	3,750.72	05/05/17 - 19/04/18	2.38	0.55	1.29	1.83	3,749.43
S-3	Brine	490,563.49	7,026,306.08	3,753.01***	05/05/17 - 19/04/18	3.35	3.21	3.27	0.14	3,749.74
RPG-27	Fresh	499,528***	6,998,523***	3,927.59***	06/07/10 – 04/11/13	47.53	46.72	47.02	0,81	3,880.70***
RPG-29	Fresh	499,190***	6,999,427***	3,919.47***	07/07/10 – 16/11/13	45.39	44.7	44.97	0,69	3,874.50***
RPG-46	Fresh	499,074***	6,999,670***	3,917.40***	25/01/12 – 15/05/12	47.56	45.63	46.14	1,93	3,871.30***
RPG-47	Fresh	498,977***	6,999,649***	3,917.86***	27/01/12 – 03/05/12	53.85	48.75	50.45	5,1	3871.00***
RPG-48	Fresh	499,111***	6,999,494***	3,919.31***	13/12/11 – 16/11/13	47.38	45.46	45.97	1,92	3873.30***
RPG-49	Fresh	498,978***	6,999,669***	3,916.91***	11/03/12 – 18/11/13	45.84	45.57	45.73	0,27	3871.20***
RPG-50	Fresh	499,101***	6,999,421***	3,919.32***	01/03/12 – 18/11/13	45.89	45.14	45.58	0,75	3873.30***
MDO-8	Brine	494,966.12	7,016,017.88	3,769.61	23/05/88 - 26/12/90**	8.15	7.5	7.67	0.65	3,761.94
MDO-10	Brine	493,815.15	7,013,872.21	3,771.89	21/05/88 - 03/12/90**	8.5	8.09	8.29	0.41	3,763.60
MDO-24	Fresh	490,468.00	7,007,320.24	3,803.30	20/05/88 - 19/12/90**	38.43	37.58	38.02	0.85	3,765.28
MDO-9	Fresh	492,108.88	7,007,955.82	3,812.23	14/05/88 - 14/12/90**	47.71	46.79	47.33	0.92	3,764.90
MDO-12	Brine	493,021.21	7,032,048.36	3,759.50	20/05/88 - 18/12/90**	7.43	6.73	7.14	0.7	3,752.36
MDO-13	Brine	491,961.26	7,031,234.96	3,772.43	21/05/88 - 27/12/90**	19.72	18.52	18.76	1.2	3,753.67
MDO-14	Fresh	491,306.01	7,032,924.99	3,777.25	01/06/88 - 29/11/90**	23.07	22.47	22.65	0.6	3,754.60
MDO-23	Fresh	491,275.30	7,007,666.15	3,807.73	18/05/88 - 11/12/90**	43.1	42.69	42.89	0.41	3,764.84
MDO-15	Brine	490,947.92	7,029,481.77	3,774.87	20/05/88 - 14/12/90**	23.44	22.94	23.08	0.5	3,751.79
M02	Fresh	484,288	7,004,376	3,760.40	01/07/10 - 01/03/16	0.48	0.27	0.39	0.21	3,762.98

Well	Water Type	Easting (WGS84)	Northing (WGS84)	Top of Casing Elevation (DEM)	Period	Maximum Static Water Level (mbtc)	Minimum Static Water Level (mbtc)	Average Static Water Level (mbtc)	Range in Water Level (m)	Piezometric Head Target (masl)
M03	Fresh	484,789	7,005,534	3,761.36	01/07/10 - 01/03/16	0.54	0.17	0.29	0.37	3,761.80
M04	Fresh	485,384	7,006,873	3,761.51	01/07/10 - 01/03/16	0.27	0.03	0.13	0.24	3,761.42
M05	Fresh	485,956	7,008,319	3,762.67	01/07/10 - 01/03/16	0.22	0.07	0.22	0.15	3,759.89
M06	Fresh	484,559	7,004,241	3,762.46	01/07/10 - 01/03/16	1.67	1.55	1.62	0.12	3,763.61
M07	Fresh	485,504	7,006,753	3,763.07	01/07/10 - 01/03/16	0.85	0.62	0.77	0.23	3,761.89
M08	Fresh	486,122	7,008,223	3,764.29	01/07/10 - 01/03/16	0.97	0.15	0.72	0.82	3,760.47
CAN-6	Fresh/Brine	497,869	7,021,411	3,782.71	14/12/90 - 20/07/17	20.15	19.52	19.76	0.63	3,762.474****
E27	Fresh	495,248	7,029,884	3,752.26	30/10/2017	n/a	n/a	0.13	n/a	3,752.13
E28	Fresh	495,243	7,029,390	3,750.07	31/10/2017	n/a	n/a	0.00	n/a	3,750.07
E29	Fresh	494,761	7,029,606	3,750.17	1/11/2017	n/a	n/a	0.00	n/a	3,750.17
E30	Fresh	494,247	7,029,313	3,750.24	3/11/2017	n/a	n/a	0.10	n/a	3,750.14
E23	Fresh	491,826	7,028,648	3,750.99	5/11/2017	n/a	n/a	0.29	n/a	3,750.70
E24	Fresh	492,421	7,028,065	3,750.28	4/11/2017	n/a	n/a	0.08	n/a	3,750.20
E25	Fresh	493,084	7,027,415	3,750.24	2/11/2017	n/a	n/a	0.08	n/a	3,750.16
E19	Fresh	496,435	7,026,152	3,752.19	21/11/2017	n/a	n/a	0.38	n/a	3,751.81
E20	Fresh	496,245	7,026,138	3,750.08	22/11/2017	n/a	n/a	0.48	n/a	3,749.60
E21	Fresh	495,532	7,025,902	3,749.58	23/11/2017	n/a	n/a	0.10	n/a	3,749.48
E18	Fresh	493,876	7,021,712	3,750.12	26/11/2017	n/a	n/a	0.88	n/a	3,749.24
E17	Fresh	494,507	7,021,081	3,750.88	25/11/2017	n/a	n/a	0.13	n/a	3,750.75
E1	Fresh	495,596	7,019,150	3,755.06	24/11/2017	n/a	n/a	0.03	n/a	3,755.03
E3	Fresh	490,720	7,018,799	3,750.78	6/11/2017	n/a	n/a	1.60	n/a	3,749.18
E6	Fresh	493,219	7,015,682	3,755.58	29/10/2017	n/a	n/a	0.05	n/a	3,755.53
E8	Fresh	493,662	7,015,155	3,761.63	28/10/2017	n/a	n/a	0.99	n/a	3,760.64

Well	Water Type	Easting (WGS84)	Northing (WGS84)	Top of Casing Elevation (DEM)	Period	Maximum Static Water Level (mbtc)	Minimum Static Water Level (mbtc)	Average Static Water Level (mbtc)	Range in Water Level (m)	Piezometric Head Target (masl)
E10	Fresh	488,097	7,011,084	3,758.65	28/11/2017	n/a	n/a	0.00	n/a	3,758.65
E9	Fresh	488,219	7,011,050	3,759.78	27/11/2017	n/a	n/a	0.79	n/a	3,758.99

Notes: mbtc: meters below top of casing
masl: meters above mean sea level
n/a: Mini-piezometer water level information based on manual measurements
**Data obtained from EDRA (1998)
*** Data obtained from Golder (2016)
****Initial water level reported in Expediente DGA ND-0302-208

Figure 15-13: Monitoring wells in the Project area



In addition to head calibration targets, water flux targets from the conceptual water balance were introduced to the FePest run. Table 15-5 lists the approximate flux calibration targets. The

catchment recharge from the Río Lamas and Ciénaga Redonda basins account for 700 L/s, or half of the groundwater inflows to the Maricunga basin. The combined lateral inflows from all other catchments plus direct recharge of precipitation on the model domain provides the other half of the recharge, or 709 L/s, for a total inflow of 1,409 L/s.

The primary groundwater outflow is diffuse discharge to surface water in and around the Salar. These surface water features are evident during the wet season, and are groundwater derived. An estimated 488 L/s of groundwater seepage feeds these surface water features. Evaporation from bare soil plus evapotranspiration in vegetated areas together account for an estimates 820 L/s of groundwater losses in the Maricunga basin. As evident in Table 15-5, there remains uncertainty in the water balance computation. The total estimated groundwater inflow based on the available data is 1,410 L/s, and the total estimated groundwater outflow is 1,310 L/s.

Table 15-5: Water balance components

Component	Flow Target (L/s)
Direct recharge of precipitation and indirect, lateral recharge from subcatchments except Río Lamas and Ciénaga Redonda	709
Indirect, lateral recharge from Río Lamas and Ciénaga Redonda catchments	700
Evapotranspiration from vegetated areas around Salar	370
Evaporation from bare soil	450
Diffuse groundwater discharge into surface water in and around Salar	488

15.2.1.2 Calibration parameters

A total of 62 parameters were calibrated to the steady state head solution: 28 hydraulic conductivity zones and 6 transfer coefficient zones. The seventh transfer coefficient associated with evaporation from the salt lake, was specified manually. These parameters are listed in Table 15-5 and Table 15-1.

Table 15-6: Steady State calibration parameters – transfer coefficients

Transfer Coefficient Zone	Location
Evaporation in Clay Core around Salt Lake	Within Salar
Evaporation from Alluvial Fans	Around Salar
Evapotranspiration from Vegetation	Southern portion of Salar
Diffuse Discharge to Surface Water	Northeastern edge of Salar
Diffuse Discharge to Surface Water	East central edge of Salar
Diffuse Discharge to Surface Water	Southeastern edge of Salar

15.2.2 Transient calibration

15.2.2.1 Mesh refinement

The mesh of the numerical model was refined to incorporate the pumping test well locations. The mesh at the wells in which pumping tests were conducted was discretized to a node spacing of approximately 5 m at P-1 and P-2 and a spacing of approximately 2.5 m at P-4. A node spacing of 2.5 m is insufficient to resolve turbulent well losses, and the observed hydraulic head from the pumping wells themselves were not used for the transient calibration. Therefore, this section will describe the goodness of fit of the numerical model to the drawdowns observed in the observation wells surrounding the pumping well.

15.2.2.2 Transient calibration approach

Data obtained from three pumping tests conducted by Flosolutions (2018)), and as described in Section 10.4, were used in the transient calibration of the reserve model. The locations of the wells used in the pumping tests are shown in Figure 15-14. The pumping rates, duration and observation well locations are shown in Table 15-7 and Table 15-8.

The P-1 and P-2 pumping tests were conducted in December 2015, and the P-4 pumping test was conducted in December 2016 through January 2017. The pumping test durations were 13 days for P-1, 28 days for P-2 and 31 days for P-4 (Table 15-7). The flow rates ranged from 25 L/s in the P-4 pumping test to 38 L/s in the P-1 test. The P-1 pumping test occurred in the Upper Halite (UH-1), Clay Core (UH-3) and Lower Alluvium (UH-4) units. The P-2 pumping test occurred in the Upper Halite and Clay Core units, and the P-4 pumping test was designed to measure the hydraulic properties of the Lower Alluvium and Upper Volcaniclastic (UH-4) units.

The pumping test data indicate that there are intercalations of fine- and coarser-grained sediments within the Clay Core, and the P-1 and P-2 pumping tests were designed to discriminate these zones. As a consequence, the Clayey Sand, Clayey Gravel and Sandy Clay subunits were defined within the Clay Core (see Table 15-1).



Figure 15-14: Pumping test Locations

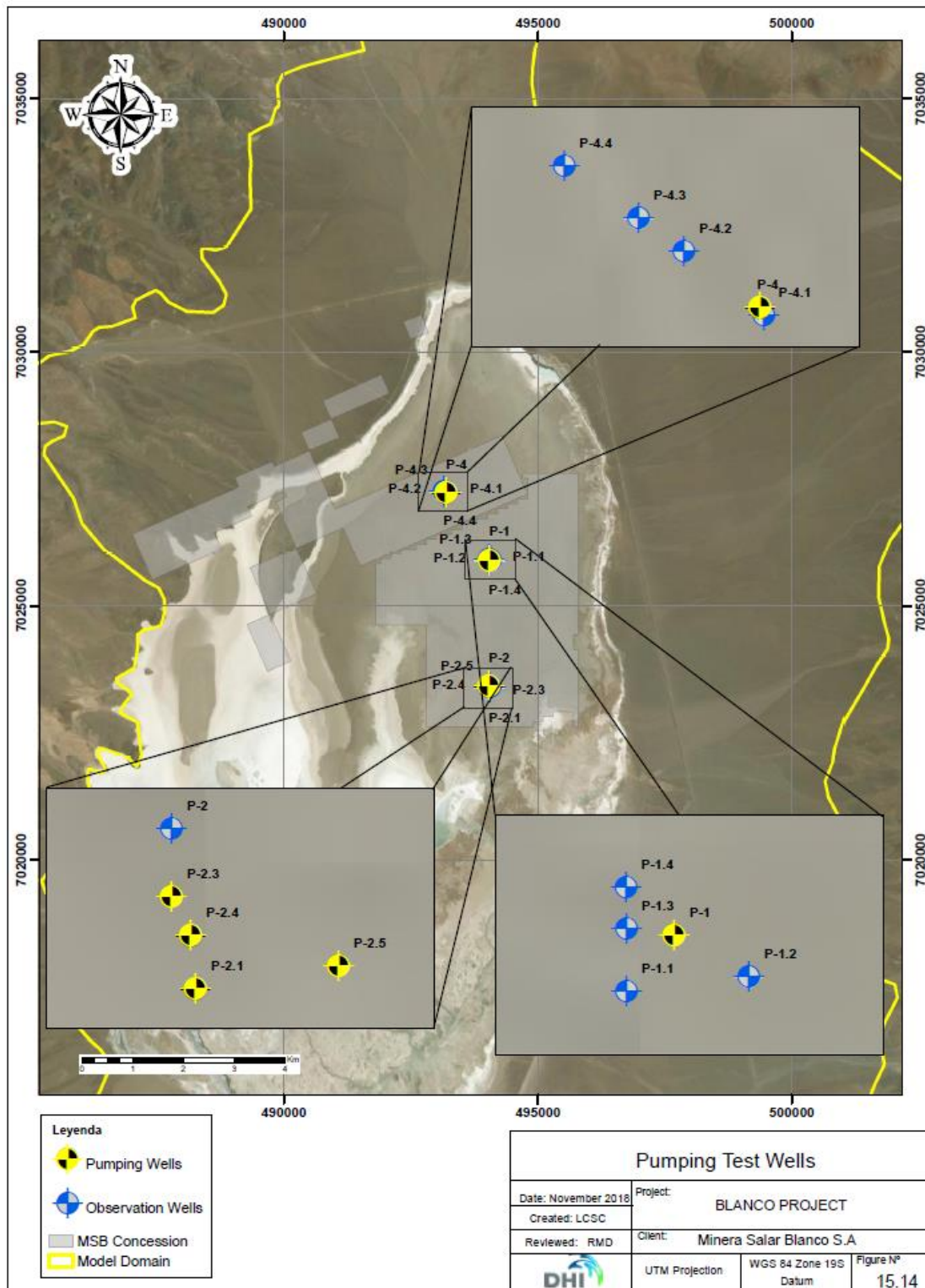


Table 15-7: Summary of pumping tests

Pumping Well	Pumping Rate (L/s)	Start of Test	End of Test	Duration (days)
P-1	38	2015/05/31 09:15	2015/06/13 08:30	13
P-2	37	2015/07/06 13:45	2015/08/03 14:00	28
P-4	25	2016/12/20 15:30	2017/01/20 15:30	31

Table 15-8: Observation wells for pumping tests

Pumping Well	Observation Well	Screened Interval (mbgs)	Hydrogeologic Unit	Distance from Pumping Well (m)
P-1	P-1.1	60 - 149	UH-3 Clay Core	17.0
	P-1.2	6 - 24	UH-1 Upper Halite	20.6
	P-1.3	54 - 66	UH-3 Clay Core	11.0
P-2	C2	6 - 34	UH-1 Upper Halite	2667.1
	C3	3 - 26	UH-1 Upper Halite	1795.1
	C4	6 - 29	UH-1 Upper Halite	1378.9
	C5	6 - 11	UH-1 Upper Halite	1141.4
	C6	6 - 11	UH-1 Upper Halite	1111.8
	P-1.1	60 - 149	UH-3 Clay Core	2482.0
	P-1.2	6 - 24	UH-1 Upper Halite	2498.0
	P-1.3	54 - 66	UH-3 Clay Core	2484.2
	P-1.4	6 - 24	UH-1 Upper Halite	2502.0
	P-2.3	12 - 30	UH-1 Upper Halite	12.0
	P-2.4	60 - 145	UH-3 Clay Core	19.4
	P-2.5	60 - 145	UH-3 Clay Core	39.8
	P-3	127 - 185	UH-3 Clay Core	1958.1
P-4	P-4.1	160 - 172	UH-4 Lower Alluvium	17.8
	P-4.2	0 - 2	UH-1 Upper Halite	10.6

15.2.2.3 Transient calibration parameters

The pumping test simulations were used to calibrate the hydraulic parameters in the units screened by the pumping and observation wells. These are the Upper Halite (UH-1), Clay Core (UH-3), Lower Sand (UH-4) and Upper Volcaniclastic (UH-4) units. Both the hydraulic conductivity and the specific storage values were calibrated using the pumping tests.

15.3 CALIBRATION RESULTS

15.3.1 Steady State calibration

15.3.1.1 Calibrated parameters

Table 15-9 presents the final calibrated hydraulic conductivity values. The calibrated hydraulic conductivities are within the conceptual range specified in the calibration. The optimum hydraulic conductivity equals the maximum value from the conceptual model for the Clay Core, central Río Lamas Alluvial Fan, Lower Sand, Basin Fill Sediment and Lower Volcaniclastic units. For all other values, the optimum hydraulic conductivity falls inside the conceptual range.

The lowest transfer rate coefficient for evapotranspiration is $1.00 \times 10^{-4} \text{ d}^{-1}$ for the Salar halite nucleus, (Table 15-10). In the Clay Core around the Salar, the calibrated evapotranspiration transfer rate coefficient is $2.79 \times 10^{-4} \text{ d}^{-1}$. The evapotranspiration rate coefficient for the alluvial fan areas is from $8.92 \times 10^{-4} \text{ d}^{-1}$, and the calibrated evapotranspiration rate coefficient for the vegetated zone in the southwestern portion of the model domain is $2.35 \times 10^{-3} \text{ d}^{-1}$. Figure 15-15 presents the zonally averaged evaporation rate from the calibrated model, using the transfer rate coefficients in Table 15-10.

The calibrated transfer rate coefficients for diffuse groundwater discharge are higher than the transfer rate coefficients for evapotranspiration, as shown in Table 15-10. The portion of the Salar margin with the highest transfer rate coefficient is the central zone that coincides with the alluvial fan from the Río Lamas (see Figure 15-16, Figure 15-5 and Figure 15-8). The Lamas alluvial fan transmits some of the lateral recharge the three of the main recharge catchments—Cordillera Claudio Gay, Río Lamas, and Ciénaga Redondo. As a consequence, the hydraulic conductivity and the diffuse seepage from the Río Lamas alluvial fan is higher than that of other alluvial fans in the model domain.

Table 15-9: Calibrated hydraulic conductivities

Hydrogeologic Unit	Calibrated Hydraulic Conductivity (m/d)			
	Subunit	K _H	K _V	Conceptual Range
UH-1	Upper Halite*	116	16.6	100 – 640
UH-3	Clay Core*	0.01	0.01	0.0001 – 0.01
	Clayey Sand (P-2)*	0.500	0.500	0.01 – 10
	Clayey Gravel (P-2)*	0.500	0.500	0.01 – 10
	Sandy Clay (P-1)*	2.75	1.19	0.01 – 10
UH-2A	Northwest Alluvial Fan	10.4	20	0.1 – 40
	Northwest Alluvial Fan a	20	0.862	0.1 – 40
	Northwest Alluvial Fan b	20	4.96	0.1 – 40
	Northwest Alluvial Fan c	6.36	0.150	0.1 – 40
	Northwest Alluvial Fan d	20	0.145	0.1 – 40
	Northeast Alluvial Fan	3.00	1.06	0.1 – 10
	Northeast Alluvial Fan a	16.1	0.490	0.1 – 20
	East Alluvial Fan	1.00	4.07	0.1 – 10
	East Alluvial Fan a	1.00	3.49	0.1 – 10
	East Alluvial Fan b	0.770	0.279	0.1 – 10
	East Alluvial Fan c	1.39	0.001	0.1 – 10
	West Alluvial Fan	20.0	13.2	0.1 – 40
UH-2B	West Alluvial Fan a	16.0	2.48	0.1 – 40
	Río Lamas Alluvial Fan N	157	0.103	30 – 280
	Río Lamas Alluvial Fan	52.5	0.171	30 – 280
	Río Lamas Alluvial Fan Ctr	300	2.14	30 – 300
	Río Lamas Alluvial Fan S	47.4	8.67	30 – 280
UH-4	Upper Río Lamas Alluvial Fan	14.5	0.580	10 – 280
	Lower Alluvium*	0.900	0.031	0.01 – 1
	Lower Sand	2.50	0.094	0.01 – 2.5
	Basin Fill Sediments	2.00	1.16	0.01 – 2
	Upper Volcaniclastic*	0.200	0.100	0.01 – 1
	Lower Volcaniclastic	2.50	0.766	0.01 – 2.5

Note:

*These units are screened by the pumping and observation wells and were included in the transient calibration.

Table 15-10: Calibrated transfer rate coefficients

Evapotranspiration Zone	Transfer Rate (1/d)
Salar Halite Nucleus	1.00×10^{-4}
Clay Core around Salar	2.79×10^{-4}
Vegetation Zone	2.35×10^{-3}
Alluvial Fan	8.92×10^{-4}
Groundwater Diffuse Discharge Zone	Transfer Rate (1/d)
North	1.65×10^{-2}
Central	1.00×10^{-1}
South	1.36×10^{-2}

Figure 15-15: Calibrated evapotranspiration rates

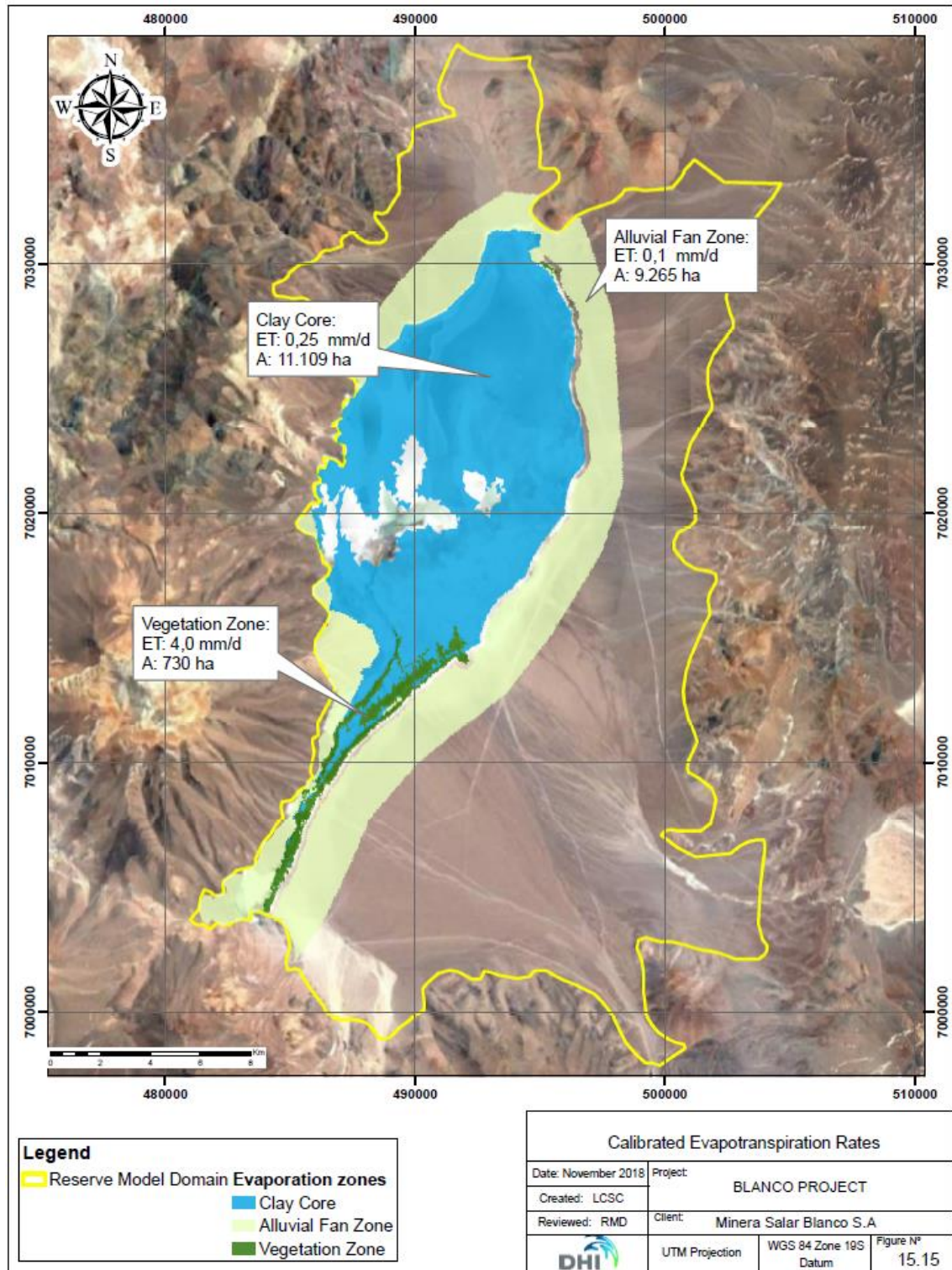
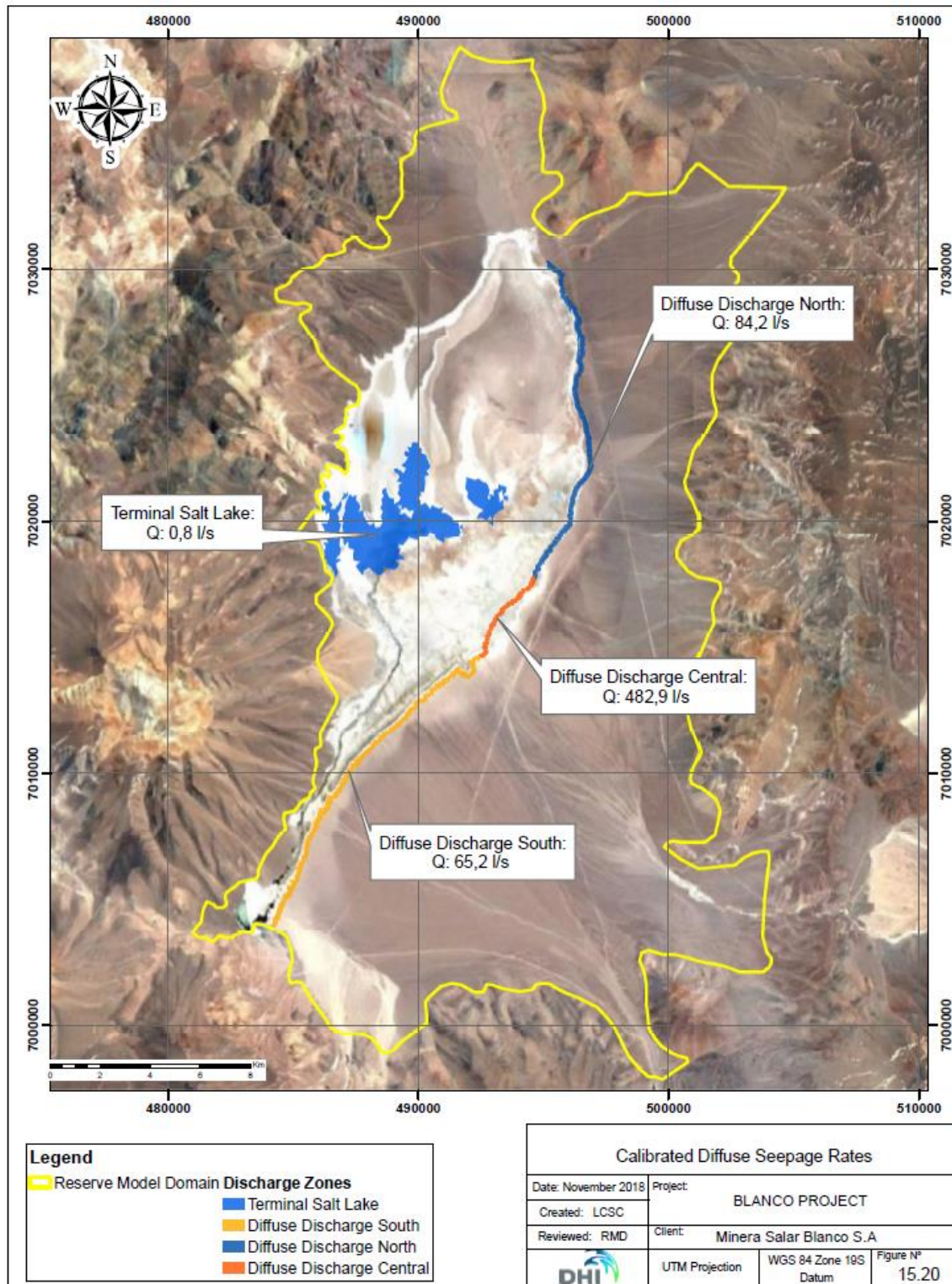


Figure 15-16: Calibrated diffuse seepage rates



15.3.1.2 Calibration to heads

Figure 15-17 shows the simulated initial steady state water table. Figure 15-18 presents a map-view of the calibration residuals, and Figure 15-19 and Figure 15-20 display the calibration statistics. The simulated and observed hydraulic head values are shown in Figure 15-19 and Figure 15-20. The residual mean of the calibrated model is -1.1 m, and the absolute residual mean is 2.4 m, for a normalized root mean squared error (NRMSE) of 3.9%. Within the salar, the residual mean is -0.2 m, and the absolute residual mean was 1.1 m, for a normalized root mean squared error (NRMSE) of 5.9%.

The majority of the monitoring points have an absolute residual that is less than 1.7 m. There are seven wells with higher residuals. Within the Salar, the maximum residuals are at S-13A, where the head is overpredicted by 4.3m; at S-18, where the head is overpredicted by 3.2 m, S-6, where the head is overpredicted by 2.7 m, and S-2, where the head is overpredicted by 2.2 m. All four of these wells are located in one of the UH-4 Lower Sand or Alluvium units below the Clay Core. As discussed above in Section 15.1.1, the thickness of the Maricunga basin sediments was defined based on the borehole data, and the sediments therefore is not assumed to extend to the depth inferred from the geophysical surveys. The overestimation of hydraulic head in layers at the bottom of the model is therefore due to the presence of a no-flow boundary at the base of the model, located 200 m below ground surface. The water level data therefore corroborate the thicker hydrogeologically active sediment zone determined from the geophysical surveys. The net result is that the model underestimates the transmissivity of the deep sediments and the potential lithium reserve and overestimates drawdowns in the deeper sediments.

The wells with the greatest underprediction of head are S-16A, CAN-6 and SP-1/MDO-10, where the head is underpredicted by 2.3 m, 2.3 m, and 2.2 m, respectively. All three of these wells are located in the alluvial fan deposits east of the Salar. The underpredicted head at these locations is due partly to the flow calibration targets and partly due to higher heads in these deep wells than in the shallow mini-piezometers in their vicinity. As a general rule, lower hydraulic heads in the alluvial fans implies that the hydraulic conductivity may be overestimated in the reserve model, which in turn would tend to overstate the dilution of the brine by freshwater during production. Therefore, the calibration misfit at these locations will be conservative with respect to the reserve calculation.



Figure 15-17: Simulated Steady State water table

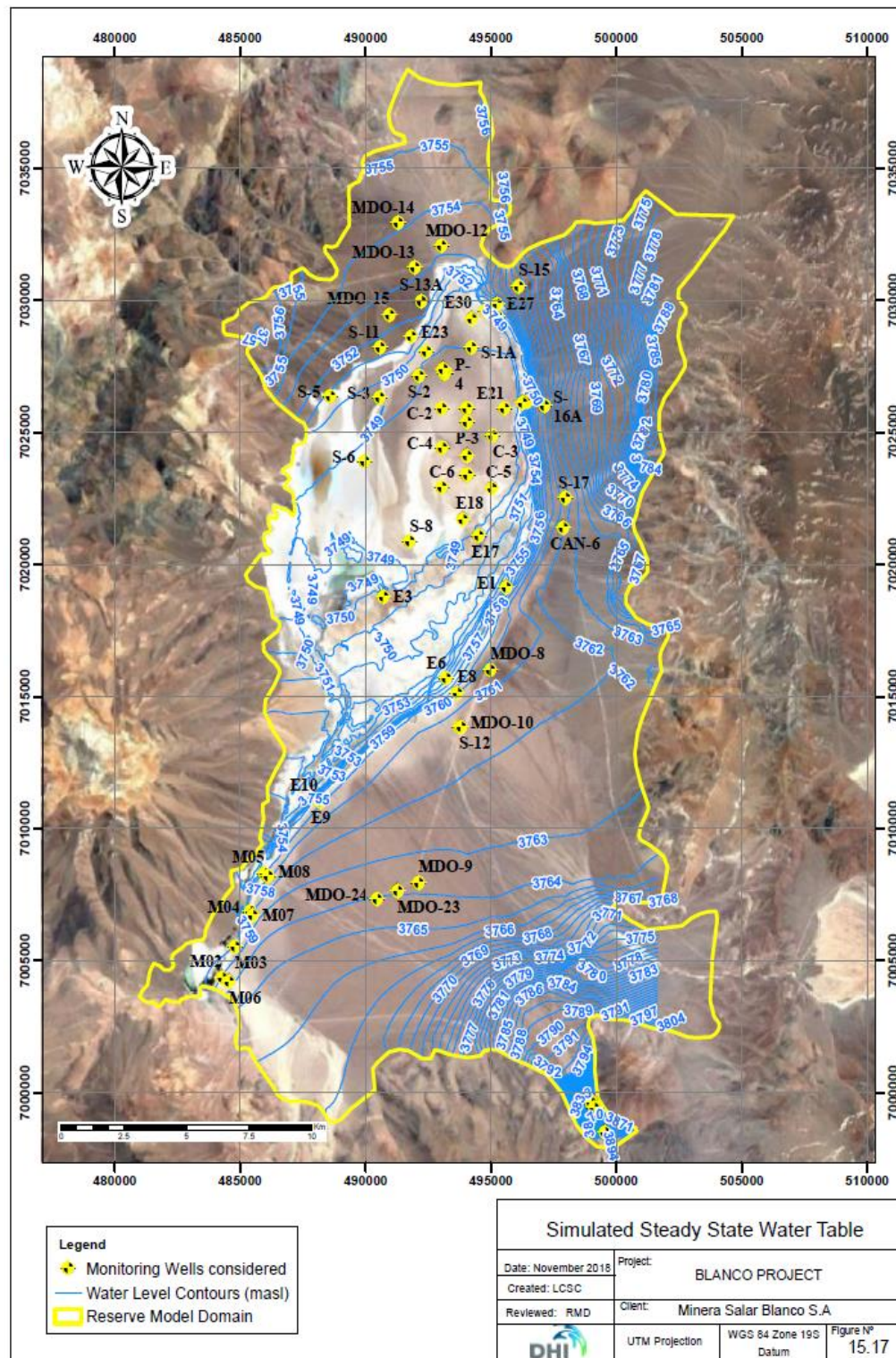


Figure 15-18: Calibration residual map

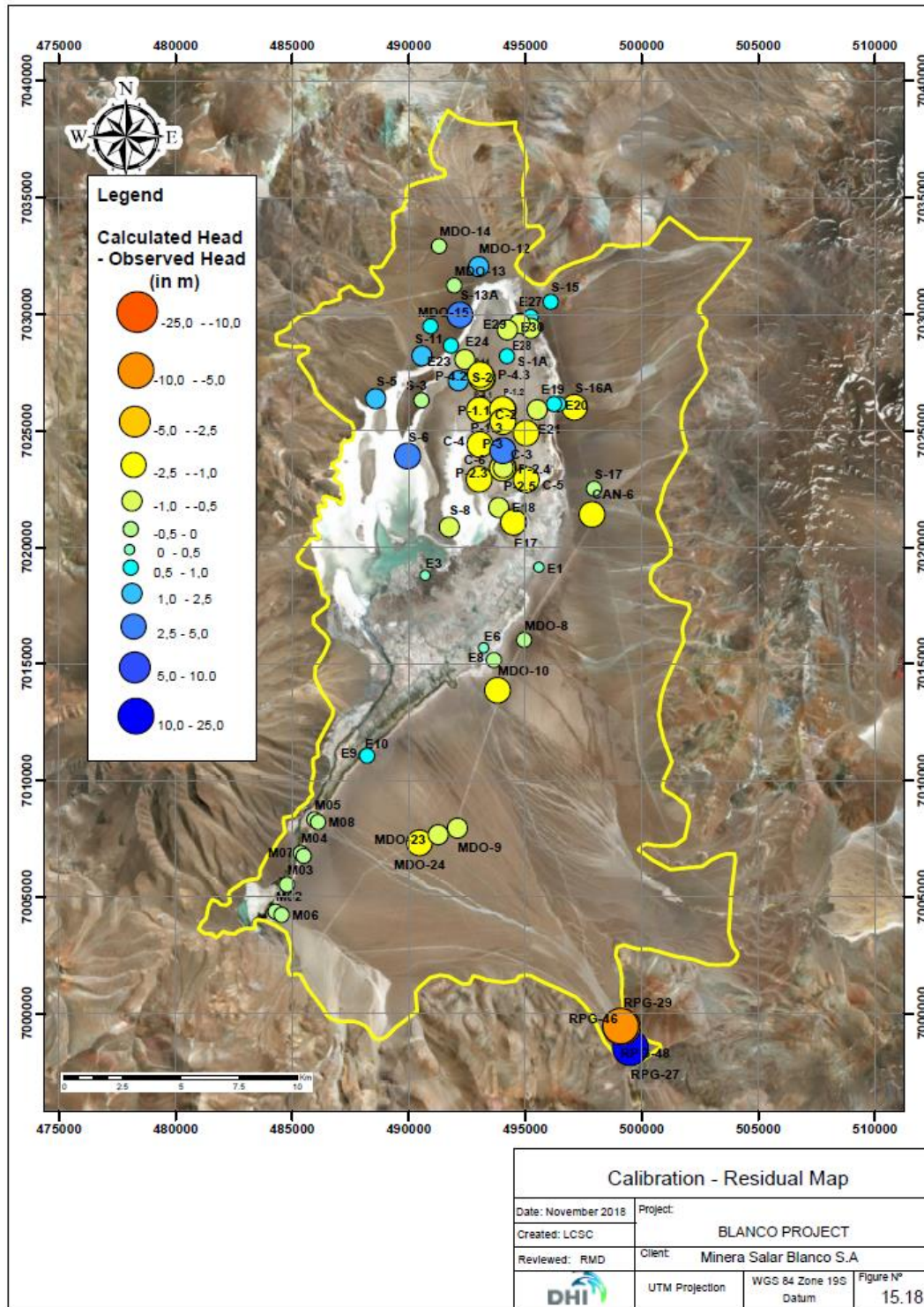
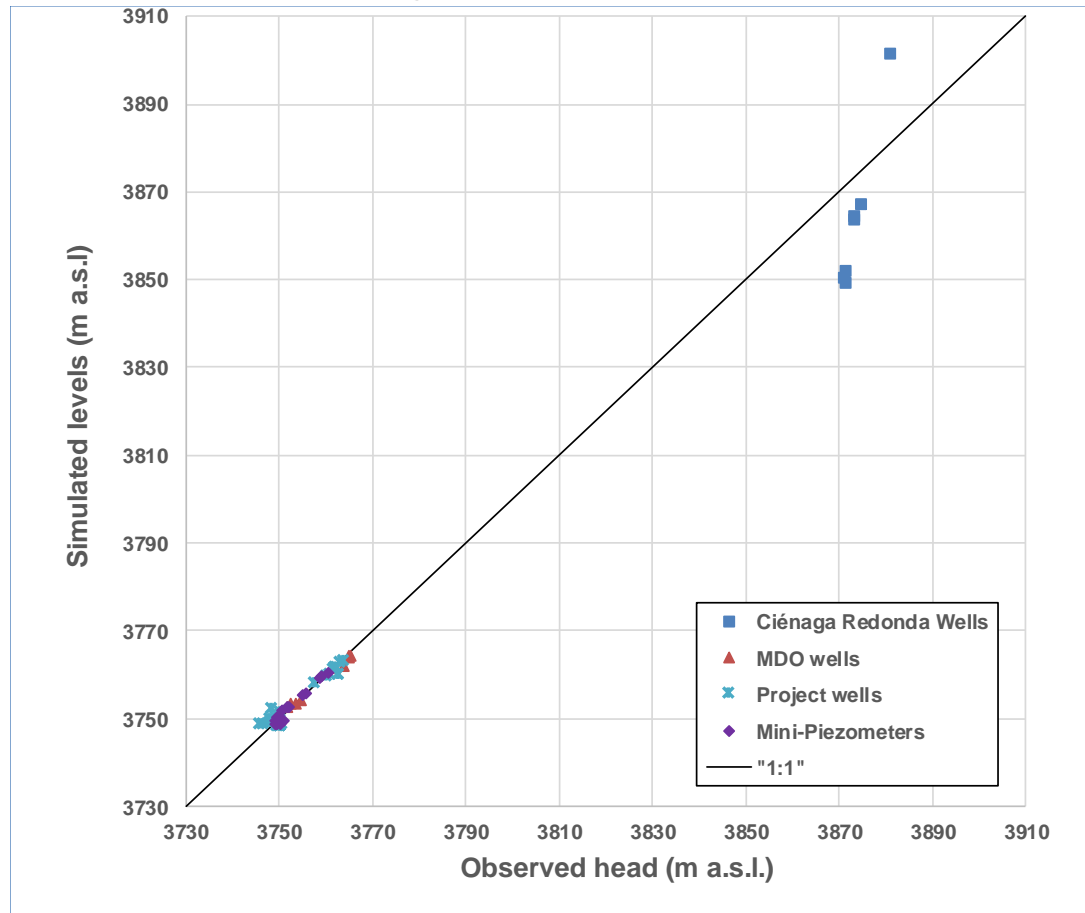
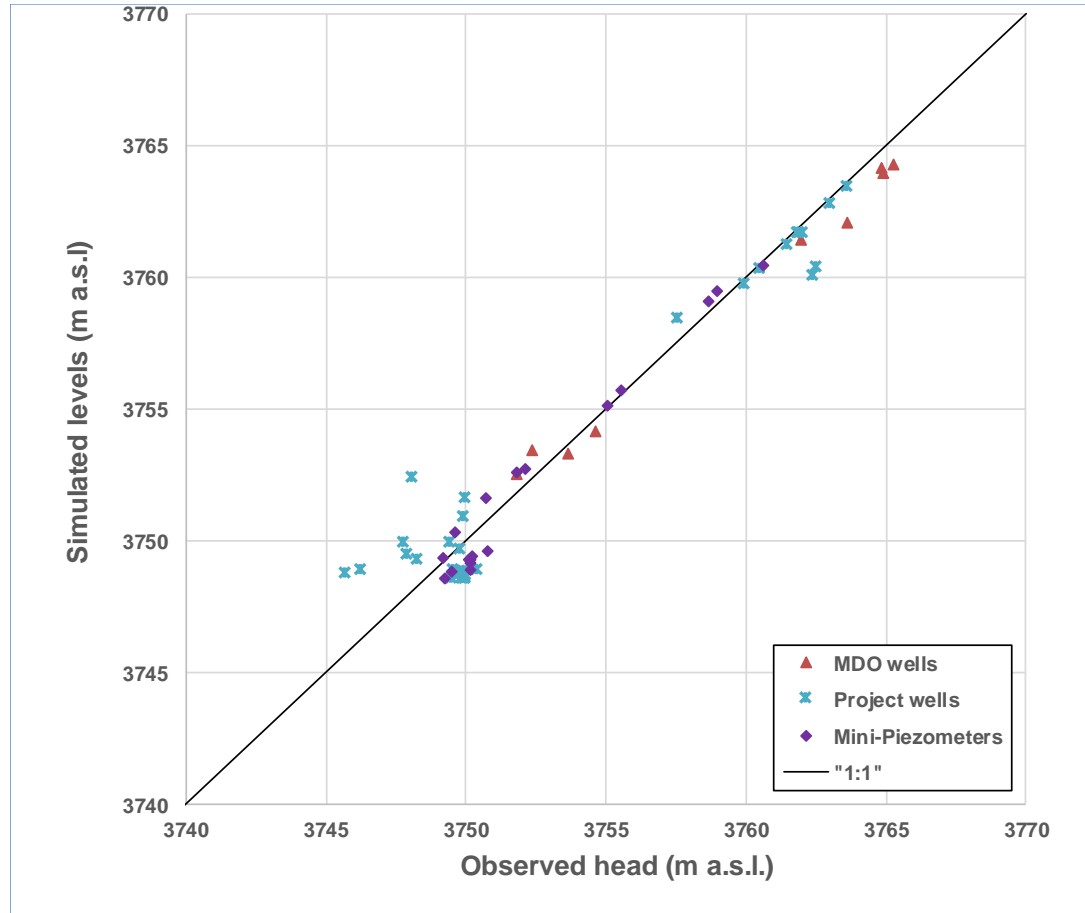


Figure 15-19: Observed vs. simulated water levels – entire model domain



Summary of Calibration Statistics	
73	Number of Wells
-1.1	Residual Mean (m)
2.36	Absolute Residual Mean (m) [MAE]
5.3	Root mean square
3.9%	Normalized Root Mean Squared [NRMS]

Figure 15-20: Observed vs. simulated water levels – reserve area



Summary of Calibration Statistics	
66	Number of Wells
-0.2	Residual Mean (m)
1.08	Absolute Residual Mean (m) [MAE]
1.2	Root mean square
5.9%	Normalized Root Mean Squared [NRMS]

Table 15-11: Observed and simulated water levels

Well	Well Group	Measured Water Level (masl)	Simulated Water Level (masl)	Residual (m)	Absolute Residual (m)
RPG-27	Ciénaga Redonda	3880.70	3901.63	20.93	20.93
RPG-29	Ciénaga Redonda	3874.50	3867.25	-7.25	7.25
RPG-46	Ciénaga Redonda	3871.30	3852.18	-19.12	19.12
RPG-47	Ciénaga Redonda	3871.00	3850.38	-20.62	20.62
RPG-48	Ciénaga Redonda	3873.30	3864.49	-8.81	8.81
RPG-49	Ciénaga Redonda	3871.20	3849.36	-21.84	21.84
RPG-50	Ciénaga Redonda	3873.30	3863.56	-9.74	9.74
MDO-8	MDO	3761.94	3761.47	-0.47	0.47
MDO-10	MDO	3763.60	3762.06	-1.54	1.54
MDO-24	MDO	3765.28	3764.27	-1.01	1.01
MDO-9	MDO	3764.90	3763.98	-0.92	0.92
MDO-12	MDO	3752.36	3753.46	1.10	1.10
MDO-13	MDO	3753.67	3753.33	-0.34	0.34
MDO-14	MDO	3754.60	3754.15	-0.45	0.45
MDO-23	MDO	3764.84	3764.16	-0.68	0.68
MDO-15	MDO	3751.79	3752.55	0.76	0.76
C-2	Project	3749.86	3748.77	-1.09	1.09
C-3	Project	3749.91	3748.70	-1.21	1.21
C-4	Project	3749.81	3748.64	-1.17	1.17
C-5	Project	3749.93	3748.61	-1.32	1.32
C-6	Project	3749.86	3748.59	-1.27	1.27
P-1.1	Project	3749.49	3748.93	-0.57	0.57
P-1.2	Project	3749.88	3748.75	-1.13	1.13
P-1.3	Project	3749.73	3748.84	-0.89	0.89
P-1.4	Project	3749.97	3748.75	-1.22	1.22
P-2.1	Project	3749.91	3748.72	-1.19	1.19
P-2.3	Project	3749.92	3748.59	-1.33	1.33
P-2.4	Project	3749.91	3748.72	-1.19	1.19
P-2.5	Project	3749.59	3748.72	-0.87	0.87
P-3	Project	3750.34	3748.94	-1.40	1.40
P-4.1	Project	3748.24	3749.34	1.10	1.10
P-4.2	Project	3749.89	3748.87	-1.02	1.02
P-4.3	Project	3749.88	3748.87	-1.01	1.01
P-4.4	Project	3749.89	3748.87	-1.02	1.02
S-11	Project	3749.95	3751.64	1.69	1.69
S-13A	Project	3748.04	3752.42	4.38	4.38
S-15	Project	3757.50	3758.47	0.97	0.97

Well	Well Group	Measured Water Level (masl)	Simulated Water Level (masl)	Residual (m)	Absolute Residual (m)
S-16A	Project	3762.38	3760.10	-2.28	2.28
S-17	Project	3762.01	3761.72	-0.29	0.29
S-18	Project	3745.64	3748.83	3.19	3.19
S-19	Project	3747.85	3749.51	1.66	1.66
S-1A	Project	3749.36	3749.95	0.59	0.59
S-2	Project	3747.76	3749.95	2.19	2.19
S-5	Project	3749.87	3750.97	1.10	1.10
S-6	Project	3746.23	3748.90	2.67	2.67
S-8	Project	3749.43	3748.62	-0.81	0.81
CAN-6	Project	3762.47	3760.42	-2.06	2.06
S-3	Project	3749.74	3749.71	-0.03	0.03
M02	Project	3762.98	3762.85	-0.13	0.13
M03	Project	3761.80	3761.73	-0.07	0.07
M04	Project	3761.42	3761.31	-0.11	0.11
M05	Project	3759.89	3759.81	-0.08	0.08
M06	Project	3763.61	3763.46	-0.15	0.15
M07	Project	3761.89	3761.77	-0.12	0.12
M08	Project	3760.47	3760.37	-0.10	0.10
E27	Mini-Piezometer	3752.13	3752.80	0.67	0.67
E28	Mini-Piezometer	3750.07	3749.32	-0.75	0.75
E29	Mini-Piezometer	3750.17	3749.33	-0.84	0.84
E30	Mini-Piezometer	3750.14	3749.18	-0.96	0.96
E23	Mini-Piezometer	3750.70	3751.66	0.96	0.96
E24	Mini-Piezometer	3750.20	3749.44	-0.76	0.76
E25	Mini-Piezometer	3750.16	3748.88	-1.28	1.28
E19	Mini-Piezometer	3751.81	3752.60	0.79	0.79
E20	Mini-Piezometer	3749.60	3750.33	0.73	0.73
E21	Mini-Piezometer	3749.48	3748.81	-0.67	0.67
E18	Mini-Piezometer	3749.24	3748.59	-0.65	0.65
E17	Mini-Piezometer	3750.75	3749.62	-1.13	1.13
E1	Mini-Piezometer	3755.03	3755.21	0.18	0.18
E3	Mini-Piezometer	3749.18	3749.33	0.15	0.15
E6	Mini-Piezometer	3755.53	3755.71	0.18	0.18
E8	Mini-Piezometer	3760.64	3760.44	-0.20	0.20
E10	Mini-Piezometer	3758.65	3759.11	0.46	0.46
E9	Mini-Piezometer	3758.99	3759.51	0.52	0.52

15.3.1.3 Calibration to flows

The calibrated water balance components are shown in Table 15-12. The simulated direct recharge and lateral recharge from the alluvial basins are within 2 L/s of the calibration targets. The simulated total inflow is essentially equal to the conceptual target--i.e., the simulated flow of 1,397 L/s simulated is within 1% of the conceptual target of 1,409 L/s.

Table 15-12: Simulated water balance from calibrated model

Water Balance Component		Simulated Flow (L/s)	Conceptual Target (L/s)
Inflow	Direct recharge of precipitation and indirect, lateral recharge from sub-catchments except Río Lamas and Ciénaga Redonda	707	709
	Indirect, lateral recharge from Río Lamas and Ciénaga Redonda catchments	690	700
Outflow	Evapotranspiration from vegetated areas around Salar	369	370
	Evaporation from bare soil	446	450
	Diffuse groundwater discharge into surface water in and around Salar	583	488

The sum of evapotranspiration and diffuse discharge exactly equals the sum of the direct and indirect (lateral) recharge. The evaporation from bare soil and the evapotranspiration from vegetated areas match the conceptual values. As noted in Section 15.2.1.1, the field data and conceptual model were not able to account for 100% of the groundwater discharges. In the calibrated numerical model, the shortfall in groundwater discharge was derived primarily via diffuse groundwater discharge at the brine-freshwater contact, where intermittent surface water is observed. The reserve model predicts 95L/s more diffuse groundwater discharge than accounted for in the conceptual water balance.

The majority of the additional groundwater discharge occurs in the Río Lamas alluvial fan area, southeast of the Minera Salar Blanco project. The volume of groundwater discharge in this area does not affect the reserve computation.

15.3.2 Pumping test calibration

15.3.2.1 Calibrated Parameters

Table 15-9 presents the final calibrated hydraulic conductivity values and indicates the hydraulic conductivities with calibrated values based on the pumping test runs. The calibrated specific storage values are listed in Table 15-13.

Table 15-13: Calibrated specific storage

Unit	Hydrogeological Subunit	Calibrated Specific Storage (1/m)
UH-1	Upper Halite	1.00×10^{-3}
UH-3	Clay Core	4.75×10^{-6}
UH-3	Clayey Sand (P-2 pumping test)	5.00×10^{-7}
UH-3	Clayey Gravel (P-2 pumping test)	5.84×10^{-7}
UH-3	Sandy Clay (P-1 pumping test)	1.00×10^{-7}
UH-4	Upper Volcaniclastic	1.00×10^{-5}
UH-4	Lower Alluvium	1.30×10^{-4}
UH-4	Lower Alluvium (around P-4)	2.90×10^{-3}

15.3.2.2 Pumping Test P-1

The observed and simulated drawdowns at the three observation wells are shown on Figure 15-21. The maximum simulated drawdowns at the end of the pumping period match closely the observed drawdowns. The maximum simulated drawdown is 4 cm less than the maximum observed drawdown at observation point P-1.2 in the Upper Halite (UH-1) (Table 15-14). The maximum simulated drawdown is 5 cm less than the minimum observed drawdown at observation point P-1.1 in the Clay Core unit and the minimum simulated drawdown is 18 cm greater than the observed drawdown at observation point P-1.3 in the Clay Core unit. The simulated drawdown and recovery show the same pattern as the observed values. The more rapid observed recovery at P-1.2 and the lower observed drawdown at P-1.3 are the most obvious differences when compared to the simulated drawdowns.

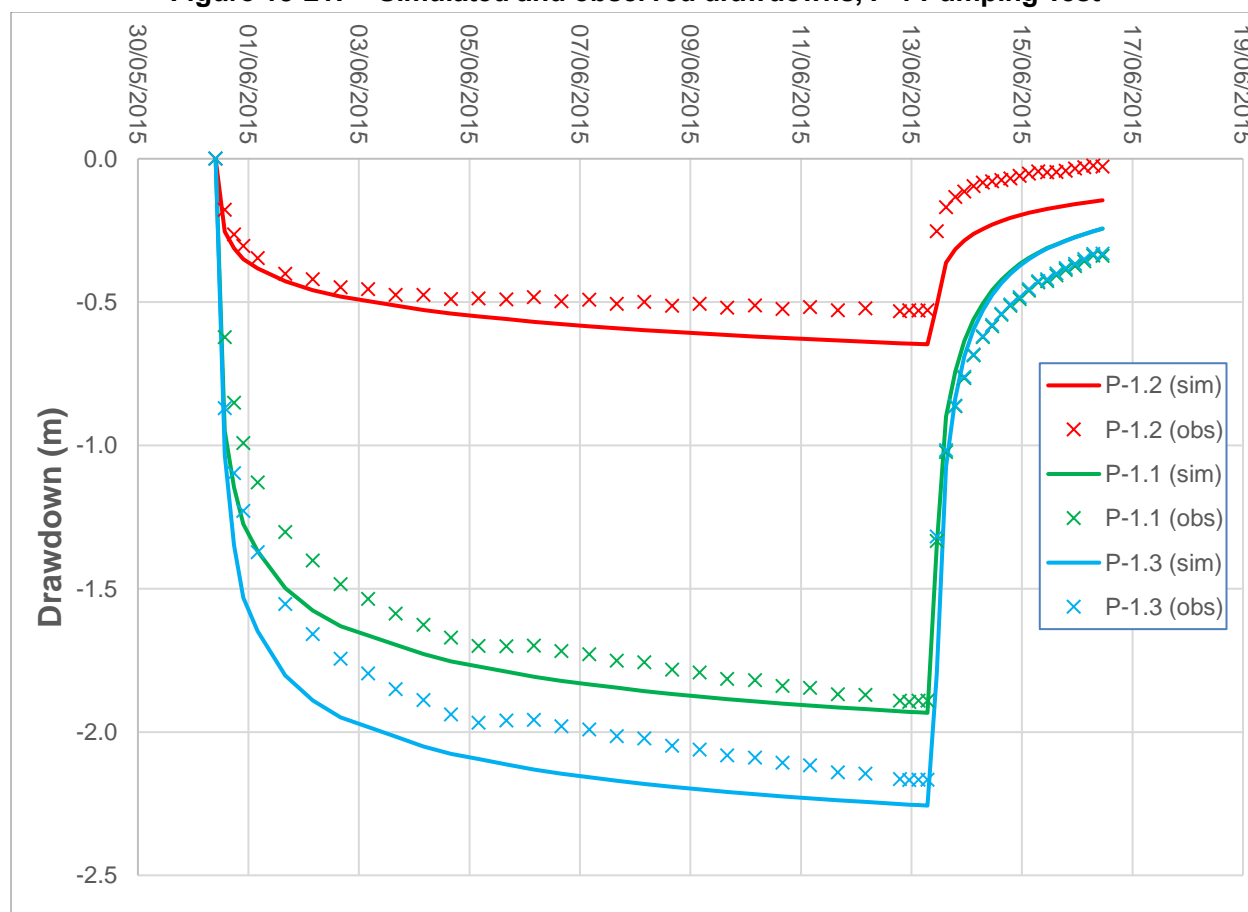
The magnitude of the drawdown in the two deeper observation wells, P-1.1 and P-1.3, is higher than expected for a low-hydraulic conductivity Clay Core unit. To fit the observed drawdowns at these two observation wells, a 400-m in diameter Sandy Clay zone was defined in Layer 8 of the model domain, in accordance with the detailed stratigraphy. Layer 8 in this location has an average thickness of 7 m. The calibrated horizontal hydraulic conductivity of the Sandy Clay zone is 2.75 m/d, with a vertical hydraulic conductivity of 1.19 m/d.

The well screen for pumping well P-1 extends through both the Upper Halite and the Clay Core. Even with the elevated hydraulic conductivity in the Sandy Clay, the large majority of the water extracted from P-1 during the pumping test, 92%, derives from the Upper Halite. The remaining 8% of the extracted brine derives from the Clay Core and Lower Alluvium units. This condition reflects the hydraulic conductivity contrast between the Upper Halite unit and the underlying units.

Table 15-14: Maximum simulated and observed drawdown values, P-1 Pumping Test

Pumping Well	Observation Well	Maximum Simulated Drawdown (m)	Maximum Observed Drawdown (m)
P-1	P-1.1	1.95	1.90
	P-1.2	0.65	0.53
	P-1.3	2.26	2.17

Figure 15-21: Simulated and observed drawdowns, P-1 Pumping Test



15.3.2.3 Pumping Test P-2

The drawdowns at 13 observation points were simulated during the P-2 pumping test and are compared to observed drawdowns on (Figure 15-22). Ten of the observation points (C2 to C6, P-1.1 to P-1.4 and P-3) were conceptualized to be not affected by pumping at P-2. The corresponding simulated drawdowns are less than 10 cm. The maximum simulated drawdown at observation well P-2.3 in the Upper Halite Unit is 11 cm more than the observed maximum drawdown (Table 15-15). The maximum simulated drawdown at P-2.4 in the Clay Core (UH-3) unit is 38 cm more than the observed maximum drawdown. The maximum simulated drawdown at P-2.5 in the Clay Core unit is 46 cm more than the observed maximum drawdown.

In general, the simulated drawdowns in the P-2-series observation wells are 5% to 17% higher than the observed drawdowns, a result that indicates that the hydraulic conductivity of the calibrated model are slightly lower than the field values. This result is conservative with respect to the reserve analysis, since a lower hydraulic conductivity will underestimate the ease with which pumping wells extract groundwater. The observed water levels at observation wells P-2.3 and P-2.4 recover more quickly than the simulated water levels. The quicker recovery indicates that the model may underestimate the storage properties of the sediments around P-2. An underestimate of storage is also conservative with respect to the reserve analysis.

The drawdown in the shallow observation well, P-2-3, was matched by the model using the same Upper Halite hydraulic conductivity that was required to fit the drawdown at the shallow monitoring point, P-1.2 in the P-1 pumping test. The drawdown at the other observation wells, P-2.4 and P-2.5 was accomplished by introducing the Clayey Sand and Clayey Gravel zones to the Clay Core, in accordance with the wells detailed geology. Both units have an isotropic hydraulic conductivity of 0.5 m/d. the Clayey Sand is present in Layers 10 and 11, and the Clayey Gravel is present in Layer 13. Both zones are larger than the Sandy Clay unit defined for the P-1 pumping test. The Clayey Sand zone has dimensions of approximately 600 m wide by 1000 m long by 9 m thick. The Clayey Gravel has dimensions of approximately 600 m wide by 1000 m long by 12 m thick.

In the P-2 pumping simulation, 92% of simulated pumping occurs in the Upper Halite, the remaining 8% of pumping were simulated to occur in the Clay Core and Lower Alluvium units. This reflects the hydraulic conductivity contrast between the Upper Halite and underlying units.

Figure 15-22: Simulated and Observed Drawdowns, P-2 Pumping Test

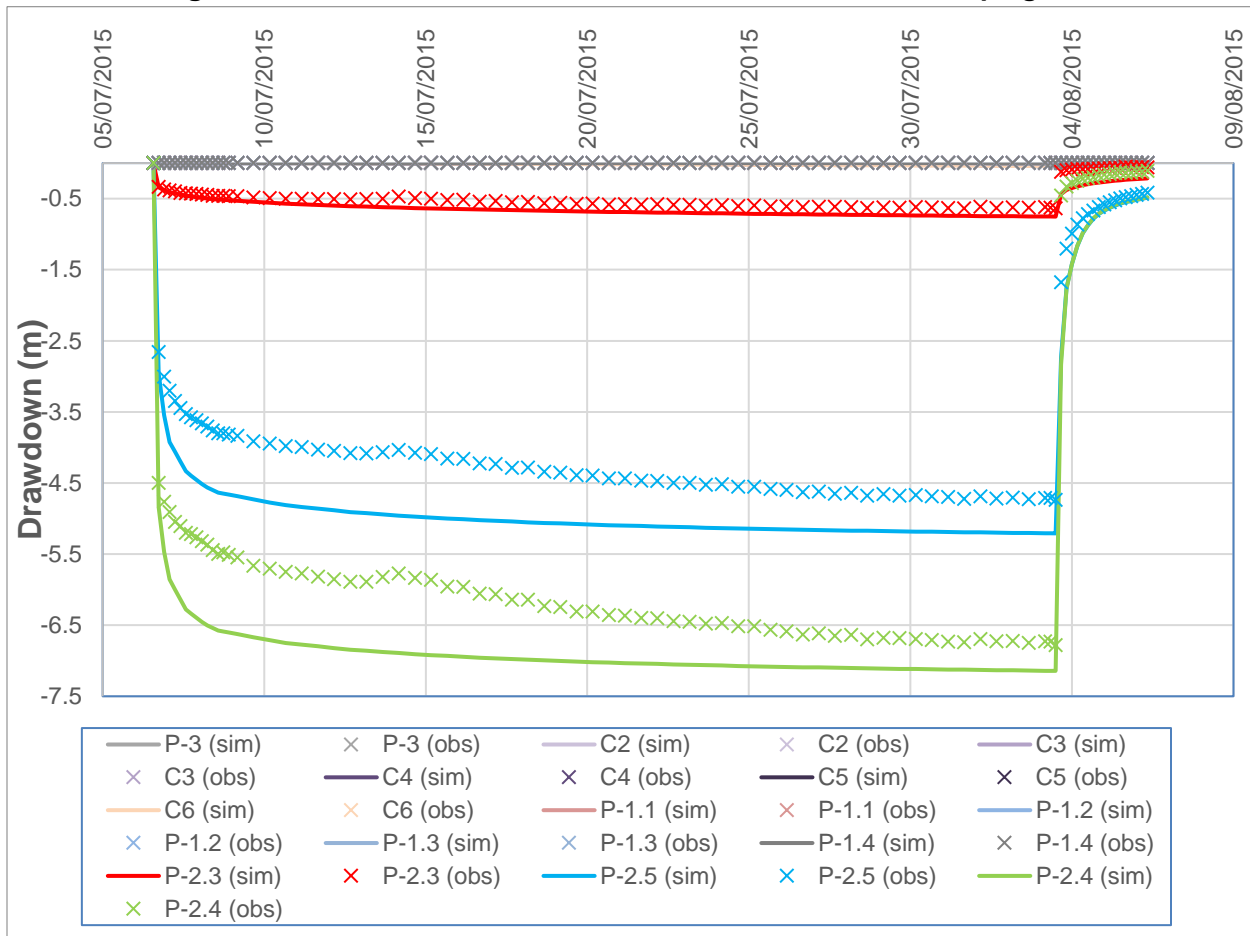


Table 15-15: Maximum simulated and observed drawdown values, P-2 Pumping Test

Pumping Well	Observation Well	Maximum Simulated Drawdown (m)	Maximum Observed Drawdown (m)
P-2	C2	0.00	0.00
	C3	0.01	0.00
	C4	0.03	0.00
	C5	0.04	0.00
	C6	0.05	0.00
	P-1.1	0.00	0.00
	P-1.2	0.00	0.00
	P-1.3	0.00	0.00
	P-1.4	0.00	0.00
	P-2.3	0.75	0.64
	P-2.4	7.14	6.78
	P-2.5	5.21	4.74
	P-3	0.01	0.00

15.3.2.4 Pumping Test P-4

The drawdowns at two observation points were simulated and are compared to observed drawdowns on Figure 15-23. The maximum simulated drawdown at observation well P-4.1 is 0.32 m, or 3%, less than the observed maximum drawdown. As conceptualized, the simulated hydraulic head changes at P-4.2, installed in the Upper Halite, are very small and less than 2 cm (Table 15-16). This is due to the disconnection that exists between the Upper Halite and the Lower Alluvium units, as a result of the presence of the low permeability Clay Core.

Therefore, the primary purpose of the P-4 pumping test was to test the integrity of the Clay Core (UH-3) unit as an aquitard separating the Upper Halite and Lower Alluvium. The P-4 pumping test shows that, even with lenses of higher hydraulic conductivity within the Clay Core, the unit as a whole forms a hydraulic barrier when pumping occurs in the Lower Alluvium.

On the other hand, the reserve model predicts a greater than zero drawdown in the Upper Halite observation well, P-4.2, and therefore slightly overestimates the connection between the Upper Halite and the Lower Alluvium. This overestimate of drawdown occurs because, although the numerical model would be better calibrated with a lower Clay Core hydraulic conductivity, the conservative, conceptual minimum hydraulic conductivity of the Clay Core is 0.01 m/d (see Table 15-1), and a lower value was not used in the reserve model. Note also that the three higher hydraulic conductivity Clay Core sand or gravel lenses occur at least 1 km south of the P-4 pumping test and are not responsible for the simulated hydraulic connection at P-4. The reserve

model is therefore conservative with respect to hydraulic connection between the two brine aquifers.

Figure 15-23: Simulated and observed drawdowns, P-4 Pumping Test

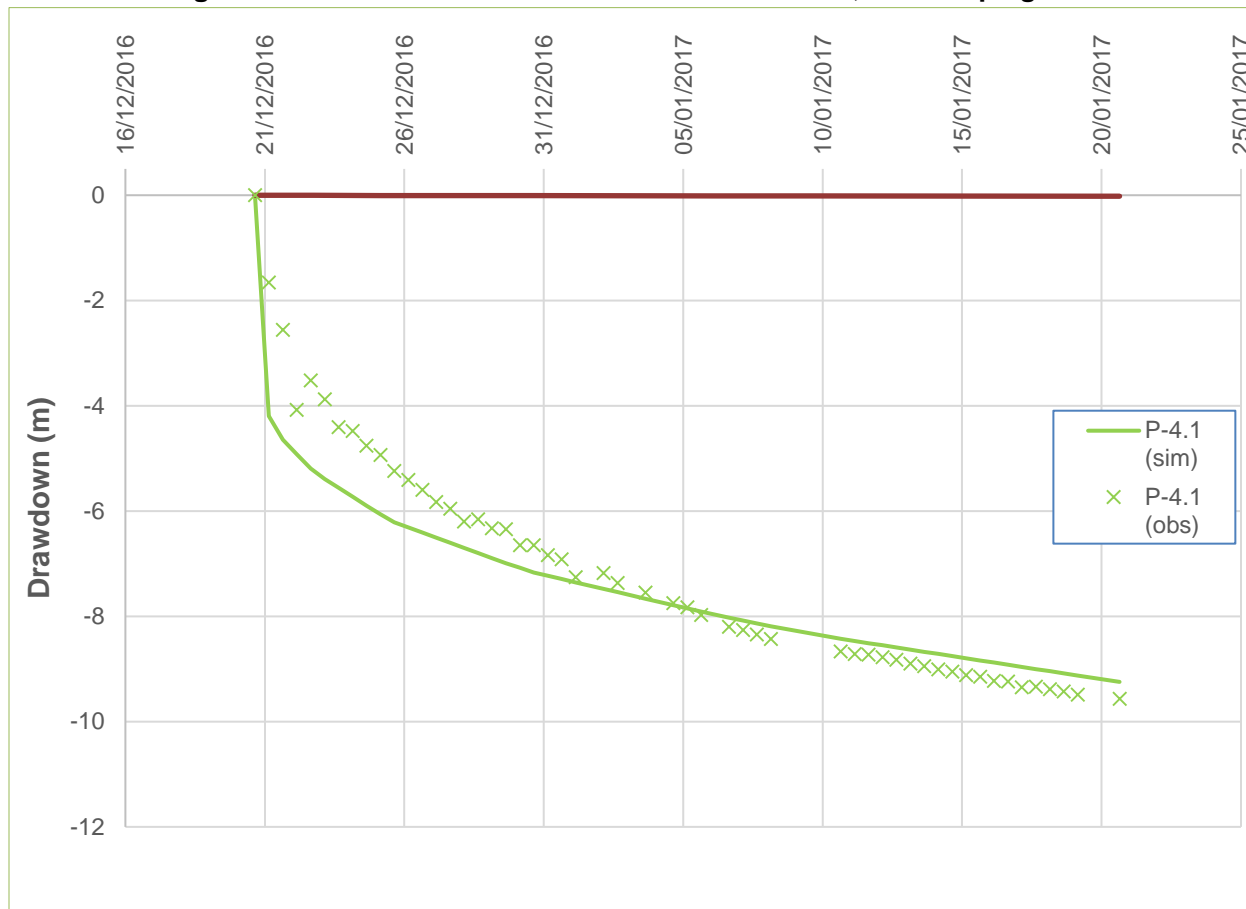


Table 15-16: Maximum simulated and observed drawdown values, P-4 Pumping Test

Pumping Well	Observation Well	Maximum Simulated Drawdown (m)	Maximum Observed Drawdown (m)
P-4	P-4.1	9.25	9.57
	P-4.2	0.02	0.00

15.3.3 Summary and conclusion

A multi-part calibration was completed using the available hydrogeological data. The pre-mining steady state groundwater model was calibrated to steady state heads at 73 monitoring points. The transfer coefficients used to simulate evapotranspiration were also calibrated to match the distribution of evapotranspiration based on field data and the conceptual model. In other words,

the steady state calibration was designed to simulate both heads and flows in the project area. The normalized root mean squared error for the steady state simulation is 5.9%, with a residual mean of -0.2 m. The simulated flows are consistent with the conceptual model.

The hydraulic conductivity for the stratigraphic units within the Salar were partly calibrated using pumping test data from three pumping wells, with a total of 18 observation wells. The pumping test analysis was also the basis of the calibrated specific storage values.

The P-1 and P-2 pumping tests—in which drawdowns were observed to be transmitted through the low-permeability Clay Core—indicate that localized higher-permeability units exist within the Clay Core aquitard. Of the higher-hydraulic conductivity zones defined based on the observed pumping test responses, the two larger zones associated with P-2 are upgradient (south) of the proposed brine extraction system. They will play a negligible role in the reserve analysis presented in Section 15.4. The smaller Sandy Clay zone associated with P-1 is within the area of proposed extraction system, but it is not a target of the reserve analysis due to its small size.

The P-4 pumping test shows that, even with localized zones of higher permeability evident from the P-1 and P-2 pumping test data, the Clay Core as a whole functions as an aquitard between the Lower Alluvium aquifer and the Upper Halite aquifer. In the reserve analysis, all of the extraction wells are either in the Upper Halite aquifer or the Lower Alluvium aquifer, and none of the wells is designed to target the small lenses of sand and gravel that exist within the Clay Core and were intercepted during the pumping tests.

15.4 BRINE RESERVE ANALYSIS

15.4.1 Approach

The numerical model, calibrated to steady state and transient flows and heads, was used for the Blanco Project reserve estimate in support of the DFS. The Blanco Project plans to produce 20,000 TPY of LCE over a 20-year project life. The Project's processing facilities (evaporation ponds and plant) are projected to have a lithium recovery efficiency of 58%. Therefore, average brine feed from the production wellfield to the evaporation ponds requires an LCE content of 34.6 kTPY.

Additionally, the numerical model was used to estimate the total reserves, by extending brine wellfield production beyond the 20 year DFS evaluation while restraining that less than 5% of the reserves come from outside of MSB concessions.

Water supply requirements for the Project (35 l/s) from the CAN-6 well located on the eastern margin of the Salar are included in the reserve model simulations.

The reserve simulations analysis takes the form of a transient groundwater flow and transport simulation, beginning with the initial steady state head distribution (Figure 15-17) and the initial

lithium concentration distribution equivalent to the M+I Resources described in Section 14 and at a more regional level shown in Figure 15-9. During brine production and for two years afterward, the model assumes that CAN-6 will pump freshwater at a rate of 35 L/s.

Prior to the 20 years of brine production, two years of freshwater extraction from Mantos de Oro wells MDO-23 and MDO-24, at a total rate of 66 L/s, is also included in the simulations. Pumping of the two Mantos de Oro wells continues for the first 7.5 years of the reserve model simulation.

The Blanco Project brine wellfield operations begin with the extraction of brine from the grandfathered concessions (Figure 15-24). The location and pumping rates of active brine production wells vary from year to year to optimize lithium concentrations and minimize the extraction of brines originating from outside the MSB concessions.

15.4.2 Wellfield Layout

Figure 15-24 shows the well locations in brine production wellfield. A total of 44 production wells are required over the 20-year Project life. Table 15-17 lists the coordinates of the brine production wells.

The proposed wellfield begins with 12 operating wells in Year 1 of the Blanco Project operations and ends with 11 operating wells during Year 20 of operations. Table 15-18 shows a detailed operating schedule for the wellfield over the 20 year Blanco Project life. Both the number of wells and the total extraction rate are predicted to decrease over the course of the Project life (Figure 15-25). The Year 1 of operations the total extraction rate is 300 l/s, compared to 158 l/s at the end of operations in Year 20 of operations. The wellfield total pumping rate in Years 1 and 2 of operations are higher due to the evaporation pond initial filling requirements.

The reserve simulations include an additional three years of brine production beyond the 20 year Project life at a combined pumping rate of 86.4 l/s from 5 production wells located in Litio 1-6 concessions.

Figure 15-24: Brine production wellfield layout

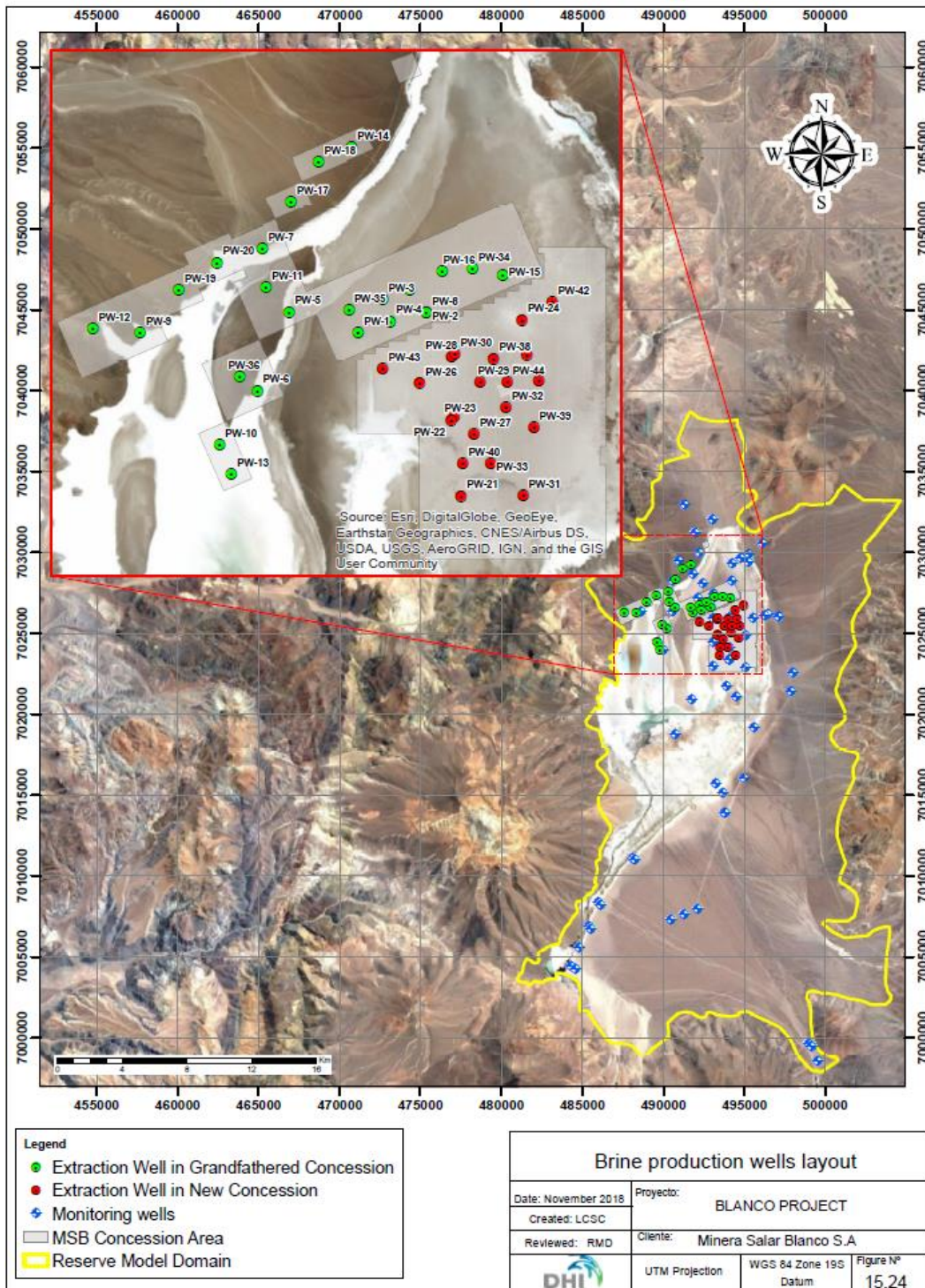


Table 15-17: Summary of production well construction details

Well	Concession	Geology	UTM Northing (m)	UTM Easting (m)	Total Depth (m) ¹	Initial Pumping Rate (l/s)	Final Pumping Rate (l/s)	Static Water Level (mbgs)	Pumping Water Level (mbgs) ²	Drawdown (m) ²
PW-1	Grandfathered	Lower Alluvial	491833	7026258	197	25	14	1.1	37.6	36.5
PW-2	Grandfathered	Lower Alluvial	492924	7026576	197	25	14	1.2	57.8	56.7
PW-3	Grandfathered	Lower Alluvial	492228	7026789	197	25	14	0.8	41.3	40.6
PW-5	Grandfathered	Lower Alluvial	490726	7026590	197	25	14	0.3	20.5	20.2
PW-6	Grandfathered	Lower Alluvial	490213	7025322	197	25	14	0.4	18.4	18.0
PW-7	Grandfathered	Lower Alluvial	490296	7027599	195	25	14	0.0	20.4	20.4
PW-9	Grandfathered	Lower Alluvial	488340	7026260	157	25	14	0.2	16.6	16.5
PW-10	Grandfathered	Lower Alluvial	489611	7024458	197	25	14	1.0	15.1	14.1
PW-11	Grandfathered	Lower Alluvial	490352	7026977	211	25	14	15.4	34.8	19.4
PW-12	Grandfathered	Lower Alluvial	487579	7026321	93	25	14	30.1	152.9	122.8
PW-13	Grandfathered	Lower Alluvial	489801	7023993	197	14	14	1.0	11.7	10.7
PW-14	Grandfathered	Lower Alluvial	491727	7029231	206	14	14	8.6	15.8	7.1
PW-15	Grandfathered	Lower Alluvial	494149	7027170	197	14	14	0.8	26.4	25.5
PW-16	Grandfathered	Lower Alluvial	493173	7027238	197	14	14	1.0	29.0	28.0
PW-17	Grandfathered	Lower Alluvial	490754	7028353	200	14	14	8.1	20.6	12.5
PW-18	Grandfathered	Lower Alluvial	491198	7028988	208	14	14	12.8	24.1	11.3
PW-19	Grandfathered	Lower Alluvial	488955	7026935	201	14	14	3.4	12.3	8.9
PW-20	Grandfathered	Lower Alluvial	489568	7027379	197	14	14	0.0	9.5	9.5
PW-34	Grandfathered	Lower Alluvial	493659	7027276	197	14	14	0.9	28.1	27.3
PW-35	Grandfathered	Lower Alluvial	491683	7026625	197	14	14	0.9	16.3	15.4
PW-36	Grandfathered	Lower Alluvial	489933	7025548	210	14	14	13.9	25.5	11.6
PW-41	Grandfathered	Lower Alluvial	492655	7026949	193	14	14	0.9	33.6	32.7
PW-21	New	Lower Alluvial	493475	7023638	196	14	14	0.7	46.4	45.6
PW-23	New	Lower Alluvial	493320	7024856	197	14	14	1.2	59.4	58.2
PW-24	New	Lower Alluvial	494452	7026460	197	14	14	0.9	42.9	42.0
PW-25	New	Lower Alluvial	494721	7025480	197	14	14	0.1	53.8	53.7

Well	Concession	Geology	UTM Northing (m)	UTM Easting (m)	Total Depth (m) ¹	Initial Pumping Rate (l/s)	Final Pumping Rate (l/s)	Static Water Level (mbgs)	Pumping Water Level (mbgs) ²	Drawdown (m) ²
PW-26	New	Lower Alluvial	492809	7025448	197	14	14	1.4	52.4	51.0
PW-27	New	Lower Alluvial	493682	7024633	197	14	14	1.0	72.8	71.9
PW-28	New	Lower Alluvial	493327	7025866	197	14	14	1.4	62.4	61.0
PW-29	New	Lower Alluvial	493786	7025455	196	14	14	0.5	63.3	62.8
PW-30	New	Lower Alluvial	493377	7025916	197	14	14	1.4	63.5	62.1
PW-31	New	Lower Alluvial	494470	7023648	197	14	14	0.9	118.7	117.8
PW-32	New	Lower Alluvial	494197	7025062	197	14	14	0.8	68.1	67.3
PW-33	New	Lower Alluvial	493953	7024161	196	14	14	0.6	91.1	90.5
PW-37	New	Lower Alluvial	494534	7025907	197	14	14	0.9	57.7	56.8
PW-38	New	Lower Alluvial	493995	7025840	197	14	14	1.3	59.5	58.2
PW-39	New	Lower Alluvial	494646	7024740	197	14	14	0.2	60.3	60.1
PW-40	New	Lower Alluvial	493501	7024156	196	14	14	0.6	51.5	50.9
PW-42	New	Lower Alluvial	494943	7026742	197	14	14	0.4	33.8	33.4
PW-43	New	Lower Alluvial	492223	7025683	195	14	14	1.2	38.0	36.8
PW-44	New	Lower Alluvial	494214	7025471	197	14	14	0.7	67.8	67.2
PW-4	Grandfathered	Halite	492346	7026436	19	25	14	1.4	4.4	3.0
PW-8	Grandfathered	Halite	492924	7026576	11	25	14	1.4	4.4	3.0
PW-22	New	Halite	493370	7024906	18	14	14	1.2	4.3	3.1

Note: ¹Well depth rounded to nearest 10 m.

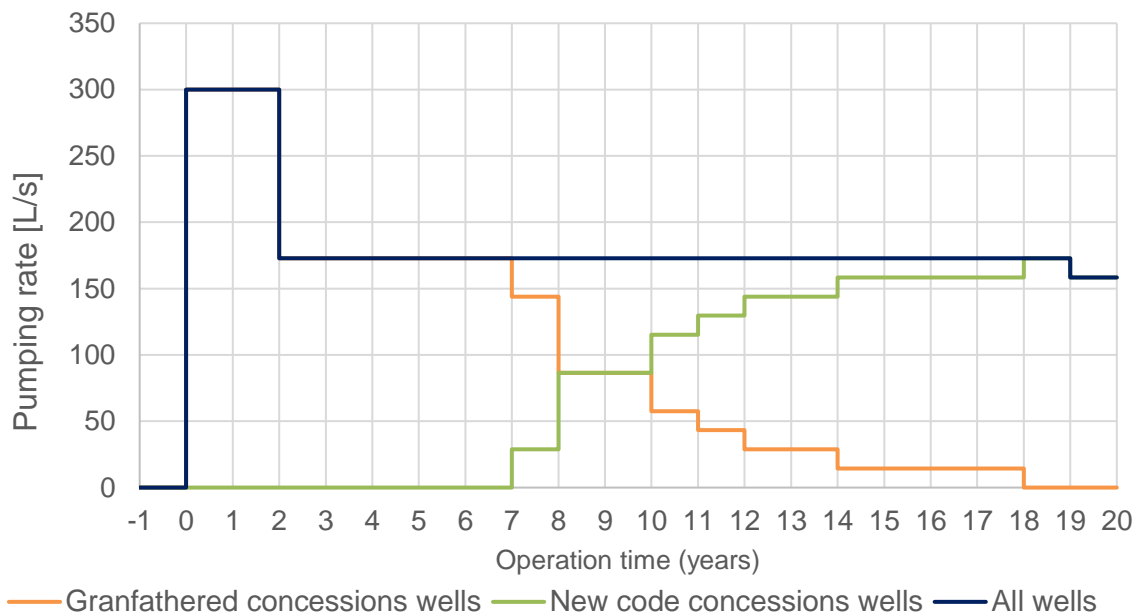
²The water level during pumping and drawdown computed for the aquifer around the well and does not include well losses.

Table 15-18: Simulated Blanco Project brine pumping schedule

Well	Average production rate per year (l/s)																			
	1	2	3	4	5	6	7	8	9	10	11	12	13	14	15	16	17	18	19	20
PW-1	25	25	14	14	14	14	-	-	-	-	-	-	-	-	-	-	-	-	-	-
PW-2	25	25	14	-	-	-	-	-	-	-	-	-	-	-	-	-	-	-	-	-
PW-3	25	25	14	14	14	14	14	14	-	-	-	-	-	-	-	-	-	-	-	-
PW-4	25	25	14	14	14	14	14	-	-	-	-	-	-	-	-	-	-	-	-	-
PW-5	25	25	14	14	14	14	14	-	-	-	-	-	-	-	-	-	-	-	-	-
PW-6	25	25	14	14	14	14	14	-	-	-	-	-	-	-	-	-	-	-	-	-
PW-7	25	25	14	-	-	-	-	-	-	-	-	-	-	-	-	-	-	-	-	-
PW-8	25	25	14	14	14	14	14	14	14	14	14	-	-	-	-	-	-	-	-	-
PW-9	25	25	14	14	14	14	14	14	14	14	14	14	14	14	14	14	14	14	-	-
PW-10	25	25	14	-	-	-	-	-	-	-	-	-	-	-	-	-	-	-	-	-
PW-11	25	25	14	14	14	14	14	14	14	14	-	-	-	-	-	-	-	-	-	-
PW-12	25	25	14	14	-	-	-	-	-	-	-	-	-	-	-	-	-	-	-	-
PW-13	-	-	-	14	-	-	-	-	-	-	-	-	-	-	-	-	-	-	-	-
PW-14	-	-	-	14	-	-	-	-	-	-	-	-	-	-	-	-	-	-	-	-
PW-15	-	-	-	14	14	14	14	-	-	-	-	-	-	-	-	-	-	-	-	-
PW-16	-	-	-	-	14	14	14	14	-	-	-	-	-	-	-	-	-	-	-	-
PW-17	-	-	-	-	14	-	-	-	-	-	-	-	-	-	-	-	-	-	-	-
PW-18	-	-	-	-	14	-	-	-	-	-	-	-	-	-	-	-	-	-	-	-
PW-19	-	-	-	-	-	14	14	14	-	-	-	-	-	-	-	-	-	-	-	-
PW-20	-	-	-	-	-	14	14	-	-	-	-	-	-	-	-	-	-	-	-	-
PW-34	-	-	-	-	-	-	14	14	14	14	-	-	-	-	-	-	-	-	-	-
PW-35	-	-	-	-	-	-	-	14	-	-	-	-	-	-	-	-	-	-	-	-
PW-36	-	-	-	-	-	-	-	14	14	14	14	14	14	14	-	-	-	-	-	-
PW-41	-	-	-	-	-	-	-	14	14	14	14	14	14	-	-	-	-	-	-	-
PW-21	-	-	-	-	-	-	-	14	14	14	14	14	14	14	14	14	14	-	-	-
PW-22	-	-	-	-	-	-	-	14	14	14	14	14	-	-	-	-	-	-	-	-
PW-23	-	-	-	-	-	-	-	-	14	14	14	14	14	14	14	-	-	-	-	-
PW-24	-	-	-	-	-	-	-	-	14	14	14	14	14	14	14	14	14	-	-	-
PW-25	-	-	-	-	-	-	-	-	14	14	14	14	14	14	14	14	14	14	14	14
PW-26	-	-	-	-	-	-	-	-	14	14	14	14	14	-	-	-	-	-	-	-
PW-27	-	-	-	-	-	-	-	-	-	-	14	14	14	14	14	14	14	14	-	-

Well	Average production rate per year (l/s)																			
	1	2	3	4	5	6	7	8	9	10	11	12	13	14	15	16	17	18	19	20
PW-28	-	-	-	-	-	-	-	-	-	-	14	14	14	14	14	14	14	14	-	-
PW-29	-	-	-	-	-	-	-	-	-	-	-	14	14	14	14	14	14	14	14	14
PW-30	-	-	-	-	-	-	-	-	-	-	-	-	14	14	14	14	14	14	-	-
PW-31	-	-	-	-	-	-	-	-	-	-	-	-	14	14	14	14	14	14	14	-
PW-32	-	-	-	-	-	-	-	-	-	-	-	-	-	14	14	14	14	14	14	14
PW-33	-	-	-	-	-	-	-	-	-	-	-	-	-	-	14	14	14	14	14	14
PW-37	-	-	-	-	-	-	-	-	-	-	-	-	-	-	-	14	14	14	14	14
PW-38	-	-	-	-	-	-	-	-	-	-	-	-	-	-	-	-	-	14	14	14
PW-39	-	-	-	-	-	-	-	-	-	-	-	-	-	-	-	-	-	14	14	14
PW-40	-	-	-	-	-	-	-	-	-	-	-	-	-	-	-	-	-	-	14	14
PW-42	-	-	-	-	-	-	-	-	-	-	-	-	-	-	-	-	-	-	14	14
PW-43	-	-	-	-	-	-	-	-	-	-	-	-	-	-	-	-	-	-	14	14
PW-44	-	-	-	-	-	-	-	-	-	-	-	-	-	-	-	-	-	-	14	14
Total (L/s)	300	300	173	173	173	173	173	173	173	173	173	173	173	173	173	173	173	173	173	158

Figure 15-25: Brine wellfield pumping rates



15.4.3 Lithium Production Simulations

For the pumping scheme described in Section 15.4.2, the model predicts that the wellfield will produce a brine feed to the evaporation ponds containing 692,000 t of LCE over the 20-year period. During the first two years of operation, the predicted production of LCE exceeds 53 kTPY, and during Years 2 to 20 of operations (Years 4 to 22 of the simulation), the production rate is generally between 25 kTPY and 38 kTPY (see Figure 15-26). An additional 50,000 t of LCE was produced over the 3-year period following the end of the 20 year Project life.

Over time, the lithium concentration of the brine will evolve as a response to the pumping. The average lithium concentration from the wellfield is predicted to remain above 1,000 mg/l throughout project operations, increasing slightly after Year 12 to above 1,100 mg/l (Figure 15-27). After 20 years of operation the projected lithium concentration remains above 1,100 mg/l.

The reserve model predicts that the concentration from the wells in the grandfathered concessions—from which 100% of the production will occur through the end of Year 7 of the operation (Table 15-18)—will drop over time. Thereafter, the wellfield production will switch to the new code concession starting in Year 8 of operations. Brine from the new code concession wells will have initially higher lithium concentrations, keeping the average lithium concentration above 1,100 mg/L.

With the continued extraction of brine from the Blanco Project, some brine from outside the property boundary may begin to migrate toward the wellfield. The Blanco Project reserve model separately tracks brine that originates outside of the property boundary. It predicts that a small amount, 4%, of the lithium produced by the wellfield may originate outside the Blanco Project property boundary over the 20-year Blanco Project operations. The pumping simulations for the 3 additional years beyond the 20 years Project life also predicts that less than 5% of the lithium produced may originate outside the MSB property boundary.

Figure 15-26: LCE contained in the brine wellfield production

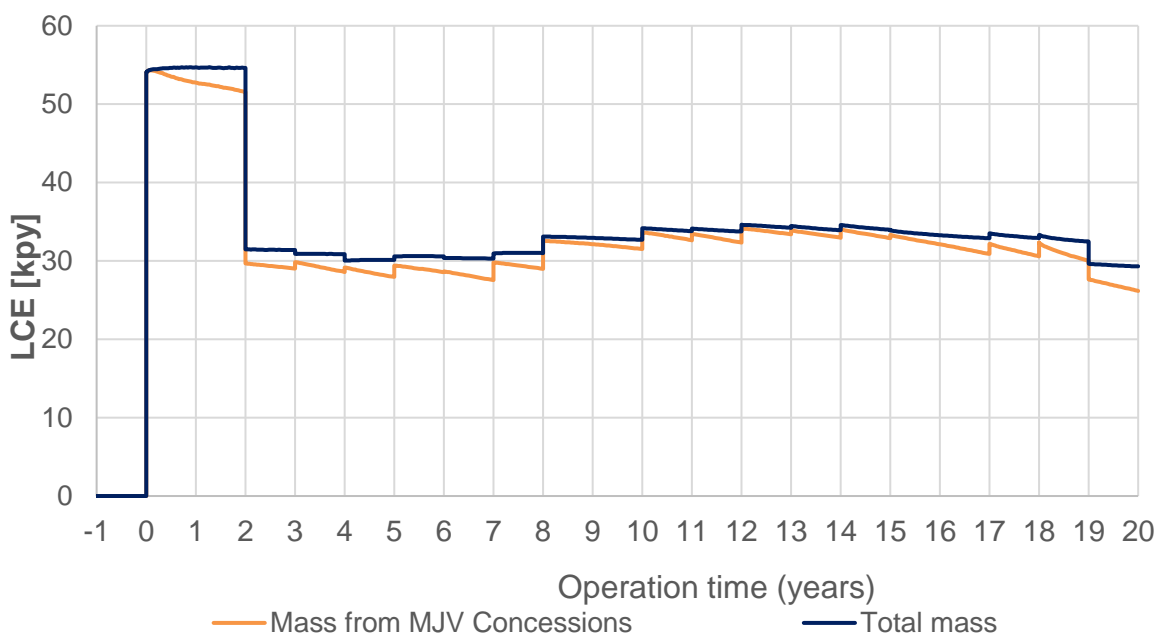
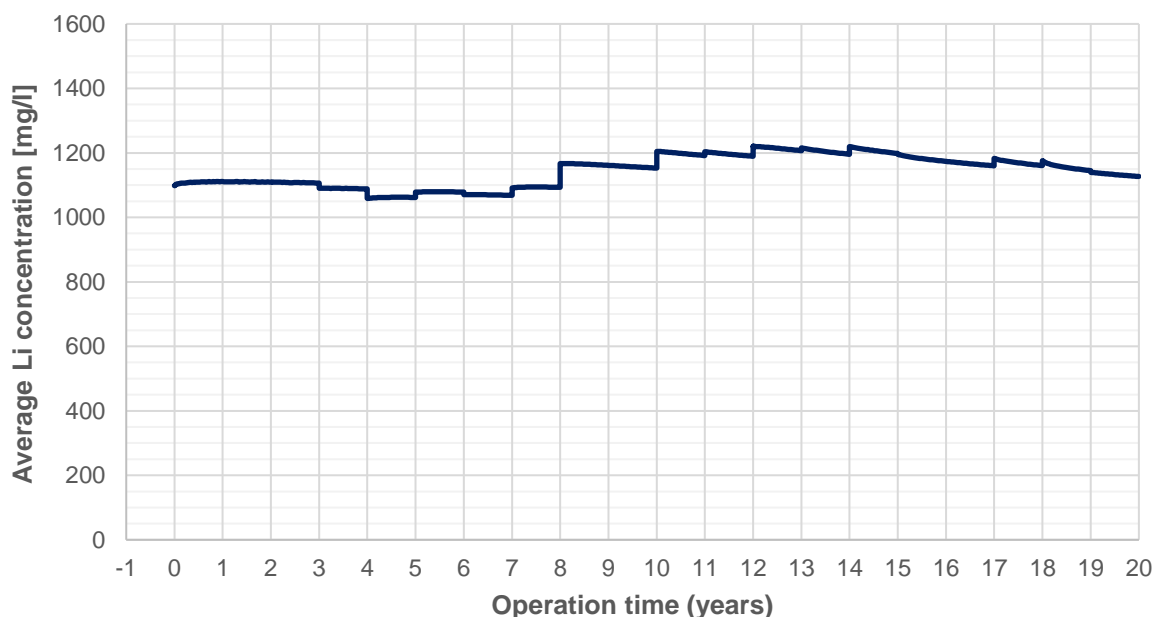


Figure 15-27: Average lithium concentration of wellfield production

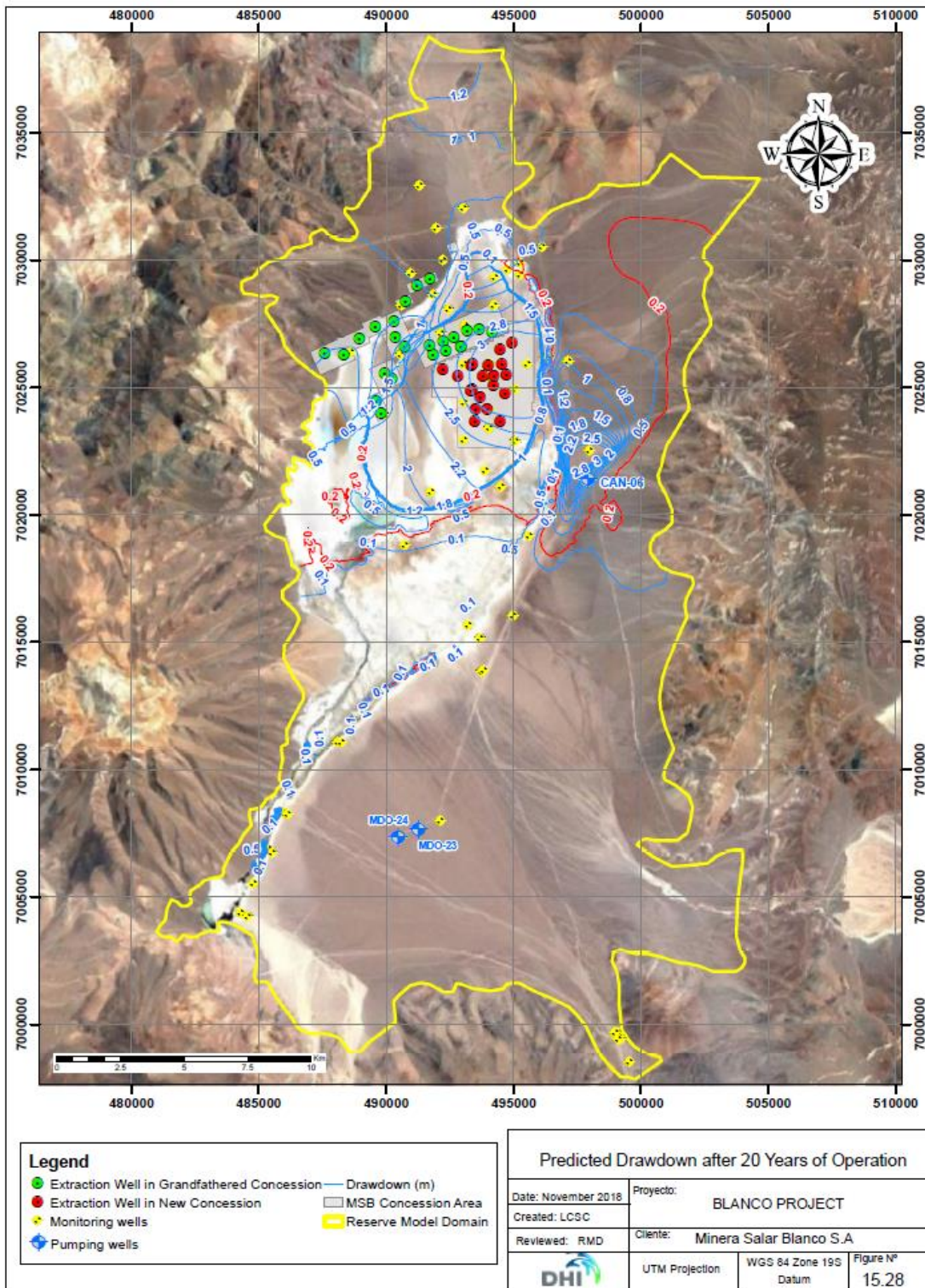


15.4.4 Water Table Predictions

As described above, the total inflow of groundwater to the Maricunga basin averages 1,409 l/s, most of which is lateral recharge from the Cordillera Claudio Gay, Río Lamas and Ciénaga Redonda catchments (see Section 15.3.1.3). Therefore, it is expected that 20 years of pumping between 300 l/s and 158 l/s of brine will lead to a depression of the water table. Maximum drawdowns for each pumping well are listed in Table 15-17. The maximum drawdown is predicted at 3 m in the Upper Halite wells and between 7 m and 123 m in the Lower Alluvial wells.

The predicted drop in the water table after 20 years of operations is shown in Figure 15-28. There are two water table depressions shown in the figure, one centered around the brine production wells in the Litio 1-6 concessions that are used in the later stages of the Project and one centered around freshwater supply well CAN-6. The maximum water table depression around either of the two pumping zones does not exceed 3.2 m. The water table depression is kept at a minimum by front-loading the pumping program, so that the pumping rate during the last 18 years of the wellfield remains less than 175 l/s; and by the use of pumping wells screened below the Clay Core, which acts as a hydraulic barrier between the deep well intakes and the shallow water table.

Figure 15-28: Predicted drawdown after 20 years of operation



15.4.5 Reserve estimate

The reserve estimate for the Blanco Project was prepared in accordance with the guidelines of National Instrument 43-101 and uses the best practices methods specific to brine resources. The lithium reserves are summarized in Table 15-19 and Table 15-20. The effective date for the estimate is January 15, 2019.

Table 15-19: Brine Mining Reserve for pumping to ponds

Concession area	Category	Year	Brine Vol (Mm3)	Ave Li conc (mg/l)	Li metal (tonnes)	LCE (tonnes)
Old code	Proven	1-7	21	1,051	22,000	115,000
	Probable	1-18	42	1,068	45,000	241,000
Litio 1-6	Proven	7-14	14	1,184	17,000	88,000
	Probable	14-23	48	1,170	56,000	298,000
Total 20y production	All	1-20	117	1,115	130,000	692,000
Mining Reserve	All	1-23	125	1,117	139,000	742,000

Table 15-20: Brine Production Reserve for Lithium Carbonate production (assuming 58% lithium process recovery efficiency)

Concession area	Category	Year	Brine Vol (Mm3)	Ave Li conc (mg/l)	Li metal (tonnes)	LCE (tonnes)
Old code	Proven	1-7	21	1,051	13,000	67,000
	Probable	1-18	42	1,068	26,000	140,000
Litio 1-6	Proven	7-14	14	1,184	10,000	51,000
	Probable	14-23	48	1,170	32,000	173,000
Total 20y production	All	1-20	117	1,115	75,000	401,000
Mining Reserve	All	1-23	125	1,117	81,000	430,000

Notes to the Reserve Estimate:

1. Blanco Project brine production initiates in Year 1 on the mining concessions constituted under old Chilean mining code and include the Cocina, San Francisco, Salamina, Despreciada concessions (the "Old Code concessions"). In Year 7 brine production switches to the Litio 1-6 concessions that were constituted under the 1983 ("new") Chilean mining code and require a special operating license (CEOL) from the Chilean government. It is the opinion of the author that there is a reasonable expectation that MSB will have obtained a CEOL by 2020, in advance of any brine production from the Litio 1-6 concessions.

2. The EIA for the Blanco Project was submitted to the Chilean Environmental Review Agency (SEA) in September 2018; it is the opinion of the author that there is a reasonable expectation that the final environmental approvals for the construction and operation of the Project will be obtained during 2019.
3. The Blanco Project Reserve Estimate includes an optimized wellfield configuration and pumping schedule to comply with environmental constraints and water level decline restrictions on the northeast side of the Salar over the total 23 year simulated brine production.
4. The total Mineral Reserves contain approximately four (4) percent of Li mass that is derived from outside of the Blanco Project property boundaries.
5. Lithium is converted to lithium carbonate (Li_2CO_3) with a conversion factor of 5.32.
6. The effective date for the Reserve Estimate is January 15, 2019.
7. Numbers may not add to due rounding effects.
8. Approximately 36 percent of the Measured and Indicated Resource are converted to Proven and Probable Reserves as brine feed from the production wellfield to the evaporation ponds without accounting for the lithium process recovery efficiency. The overall conversion from M+I Resources to Total Reserves including lithium process recovery efficiency is approximately 21 percent.

16. MINING METHOD – BRINE EXTRACTION

16.1 GENERAL DESCRIPTION

The production process starts with the brine extraction wells in the Salar.

Results of the pumping tests on the Blanco Project (as described in Section 10 above) indicate that brine abstraction from the Salar will take place by installing and operating a conventional brine production wellfield. Brine from the individual production wells will be fed into two collection/transfer ponds in the northwest of the Salar from where it will be boosted through the main trunk pipeline up to the evaporation ponds some 12 km to the north in the general plant area.

The brine composition and lithium concentrations of the Blanco Project indicate that a 20,000 TPY lithium carbonate production will require an average annual brine feed rate of 16,4120 m³/d. The predicted evolution of the lithium concentration over the life of the wellfield operation is shown in Figure 15-27. Seasonal fluctuations in the evaporation rate dictate that the required brine feed rate may be as low as 5,110 m³/d (59 l/s) during the winter months and will reach a maximum of 21,560 m³/d (250 l/s) during the summer months.

16.2 WELLFIELD LAYOUT

Results of the Blanco Project pumping tests and the reserve model simulations indicate that pumping rates of individual brine production wells will range between 14 l/s and 25 l/s. The detailed wellfield operation schedule is shown in Table 15-18. Well completion depths will vary between 40 m (upper brine aquifer) and 200 m (lower brine aquifer). The brine production wells will be completed with 12-inch diameter stainless steel production casing and equipped with 380 V submersible pumping equipment. Table 15-17 provides the planned location and construction detail of the production wells. It is projected that a total of 44 wells will be required over the life of the Project. However, no more than 15 wells will be operating at a single time. Permanent power will be delivered to the wellfield area through a mid-range power line.

Brine discharge from each wellhead will be piped through 8-inch diameter HDPE feeder pipelines to two central collection/transfer ponds in the northwest of the Salar. A 12 km length, 20-inch diameter steel / HDPE main trunk pipeline will be installed between the collection/transfer ponds and the evaporation ponds area. A booster pumping station will be installed at the bottom of the main trunk line adjacent to the collection ponds to pump the brine up to the evaporation ponds (130 m lift).

17. RECOVERY METHODS

17.1 OVERVIEW

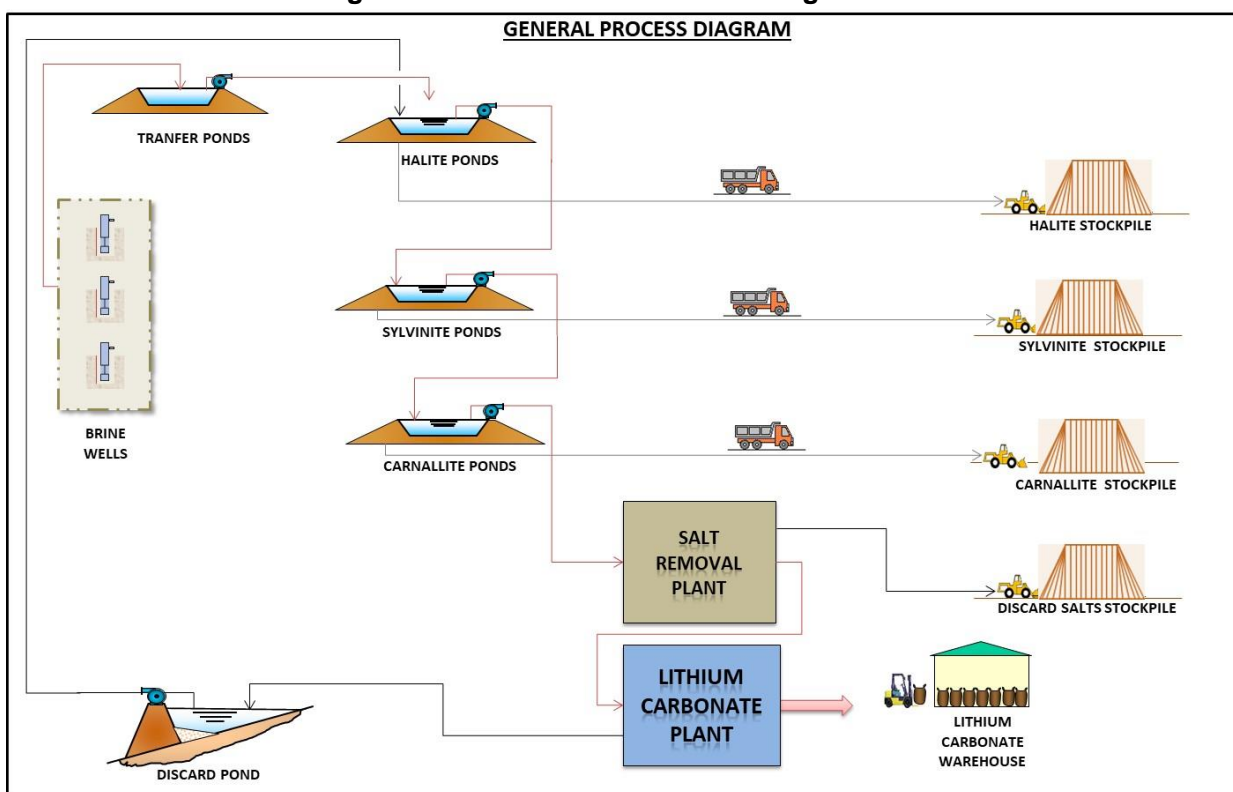
The objective of the Project is to produce 20,000 TPY of battery grade lithium carbonate (Li_2CO_3).

The raw material for both processes is the brine extracted from MSB's mineral properties in the salar. This brine is fed to evaporation ponds where various salts precipitate. Enriched Li^+ ion brine is obtained as a result of the evaporation stage.

This lithium-rich brine is fed to the Salt Removal Plant to remove most of the calcium and magnesium and further concentrate lithium in the brine. This brine is then pumped to the lithium carbonate production process, which consists of purification steps for boron, calcium and magnesium removal, a precipitation step for lithium carbonate, and steps for solid and liquid separation. Finally, there is a phase for drying, micronizing and packaging.

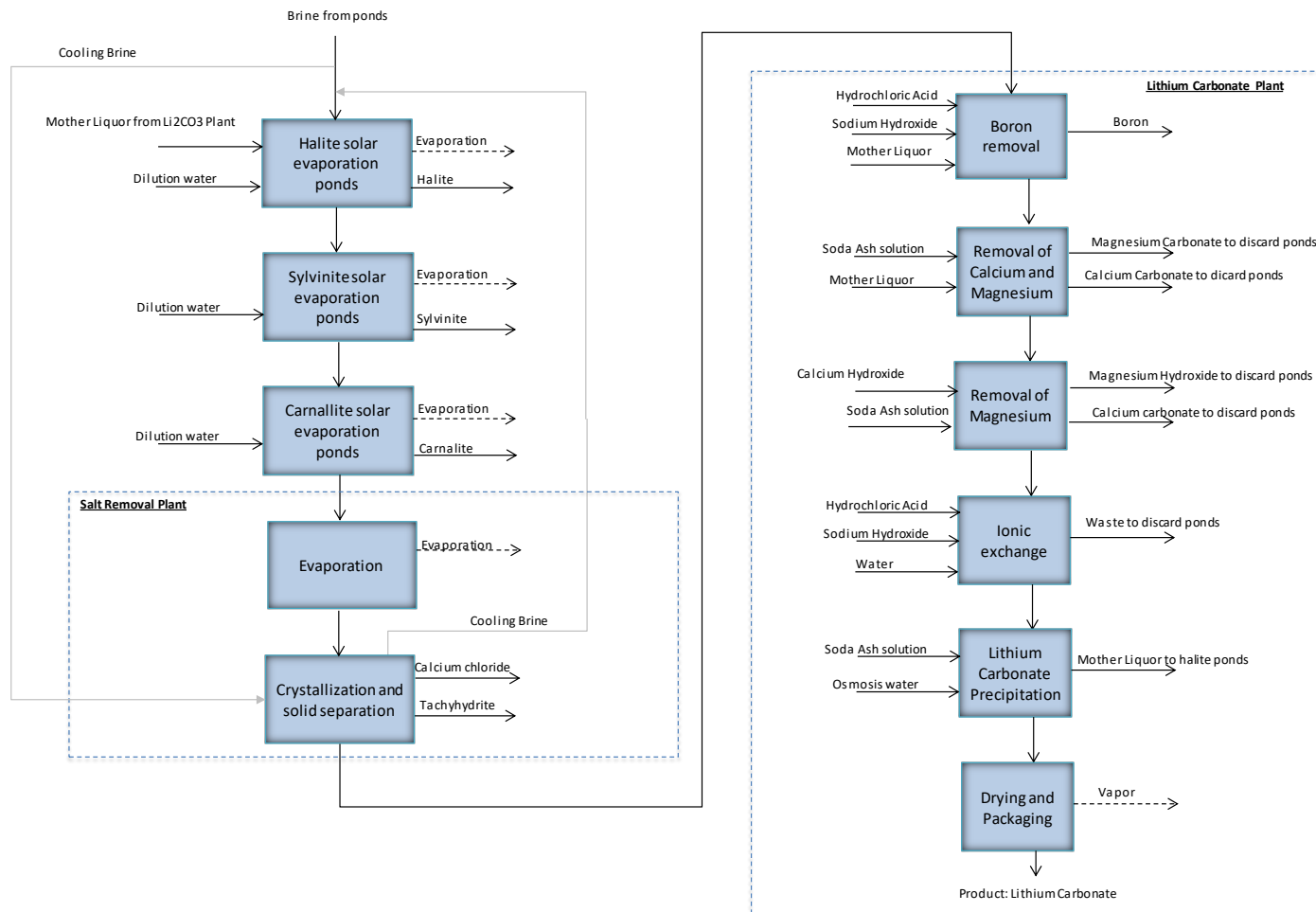
A general process diagram may be seen in Figure 17-1.

Figure 17-1: General Process Diagram



The complete process block diagram is presented in Figure 17-2.

Figure 17-2: Process Block Diagram



The complete process is described in the following chapters.

17.2 OPERATION OF THE SOLAR EVAPORATION PONDS

The solar evaporation ponds are a group of concentration facilities that take advantage of the natural water evaporation effect to concentrate the brine. They cover an extensive area. The evaporation rate depends on four main factors: solar radiation, the air's relative humidity, wind speed and temperature changes. These four factors are favorably present in the Salar de Maricunga area.

The solar evaporation ponds are simple structures of a very large size and low depth, located near the salt flat. Material from the area is used for their walls and platforms. They are

covered by a geomembrane to guarantee impermeability and avoid leakage. Ponds are fed with brine from the brine production wells.

Each solar evaporation pond is interconnected with the following ponds in a downstream series. Brine is transported from a pond to the next one, using a communicating vessel system, making the most of the gravitational energy to carry out the transportation. In the cases when this is not possible, pumping is used.

The system behaves like a crystallization or salt separation mechanism through precipitation, using the brine's natural saturation property. In this way, salts precipitate when the brine reaches its saturation point and the resulting brine, with a higher lithium concentration is transported to the next pond, as indicated previously. Precipitated salt must be harvested (extracted) from the ponds when it reaches pre-defined levels. Approximately 8,300,000 tonnes per year of brine are treated in the evaporation ponds annually.

The production of harvested salts is shown in Table 17-1.

Table 17-1: Annual generation of salts from evaporation ponds

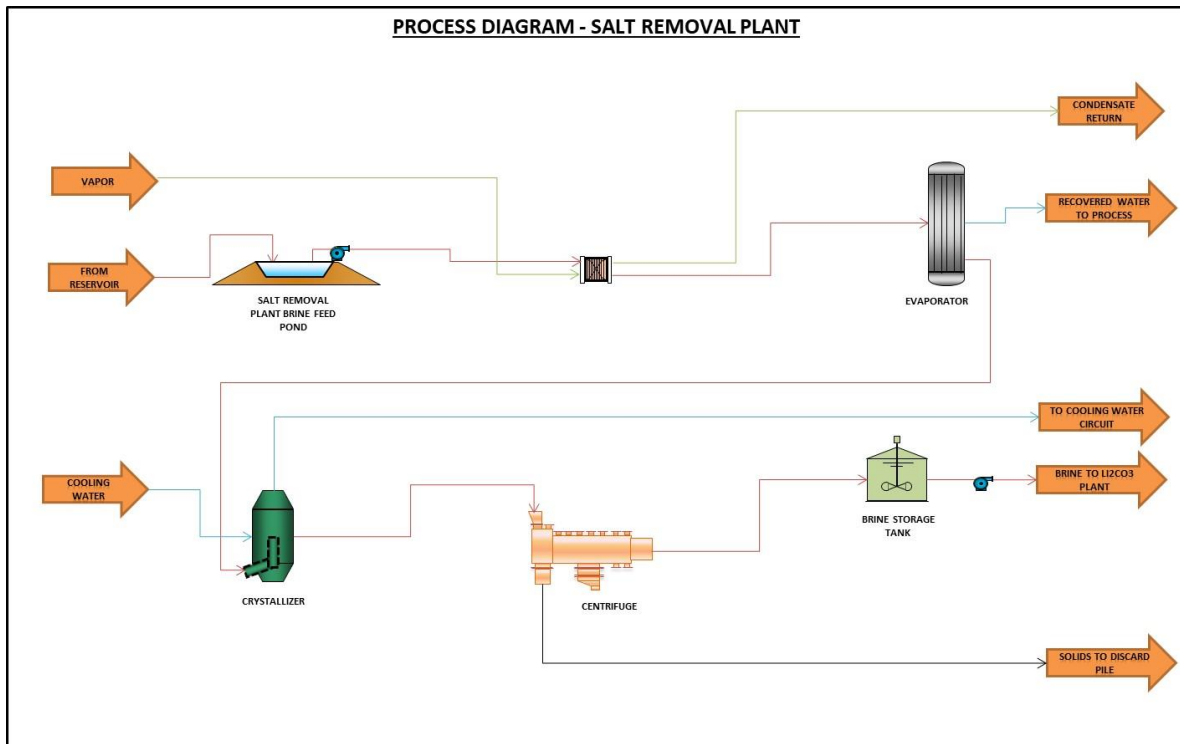
Compound/type	Annual production (TPY)
Pond Salts generated	
Halite (with 10% entrained brine)	1.722.394
Sylvinite (with 10% entrained brine)	142.023
Carnallite (with 10% entrained brine)	58.268

Harvested salts are deposited in authorized stocking areas and separated by the type of salt, depositing them directly on the stocking ground using the same backhoes that are used for harvesting. The floor of each stocking area will have a drainage system to recover the brine impregnated in the salts and other solutions that could be generated by rain or snow falls. This brine recovered will be sent back to the evaporation ponds.

17.3 SALT REMOVAL PLANT

The brine that comes from the ponds is in the first instance fed to the Salt Removal Plant, which, through the processes of evaporation and crystallization, allows increased concentration of the lithium contained in the brine. At the same time this plant enables the elimination of excess calcium and other impurities from the brine in the form of tachyhydrite and calcium chloride salts. This stage allows the of a more concentrated brine feed to the lithium carbonate plant, thus improving the plant's efficiency and producing a final product that will have improved market potential. It additionally generates water that is used in the process, thus reducing water consumption.

Figure 17-3: Simplified Salt Removal Plant Process Diagram



17.4 LITHIUM CARBONATE PLANT

The Lithium Carbonate Plant is a chemical plant that receives concentrated brine from the Salt Removal Plant. This lithium rich brine also contains concentrations of impurity elements. These impurity elements must be removed from the brine to generate a lithium carbonate product of high purity, in accordance with the international standards of the industry.

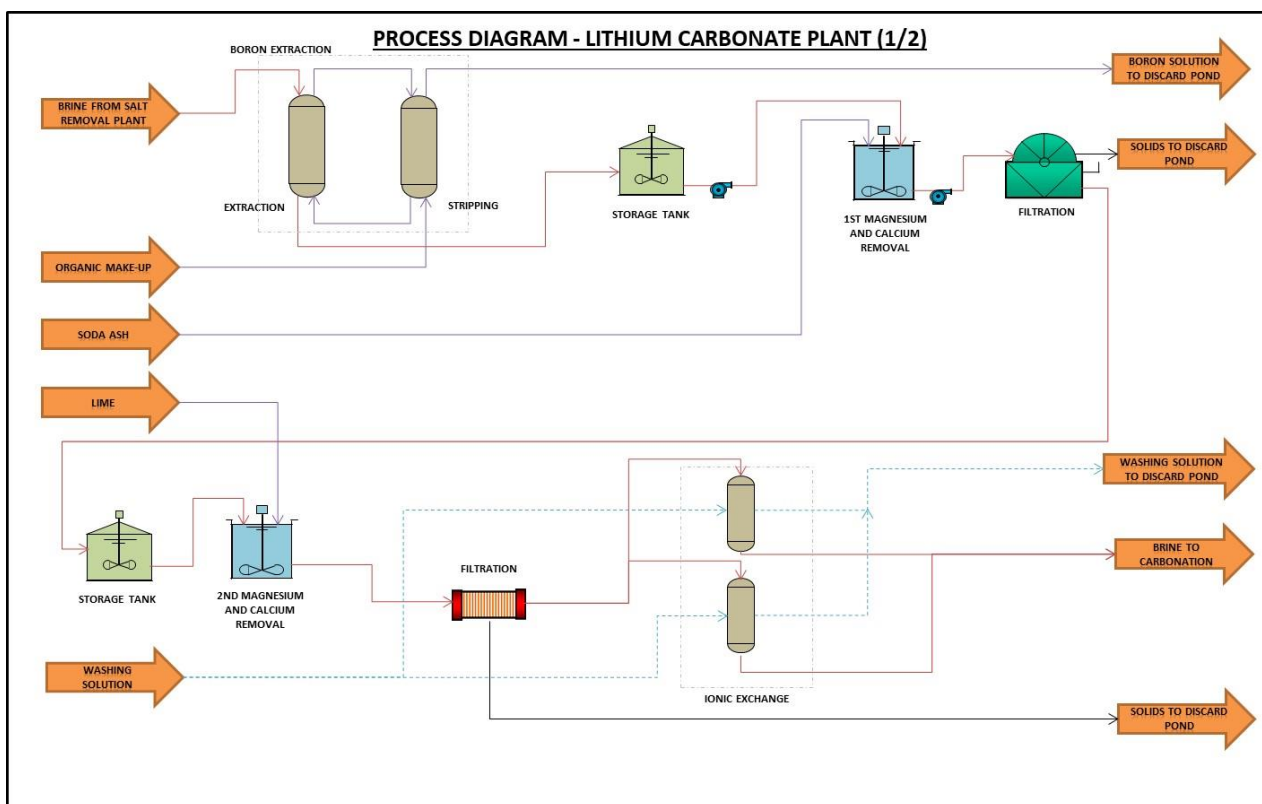
Boron extraction is carried out using a solvent extraction process. The boron extraction phase is carried out with an acidic pH and using a mixture of reagents (including diluent and extractant) to transfer the boron from the aqueous phase (boron free brine) to the organic phase. The phase of re-extraction (or stripping) to recover the organic phase is carried out in a basic pH, obtaining a boron rich solution to be sent to the discard pond, while the boron free brine is sent to the next stage.

For the elimination of other contaminants present in the brine, a primary reduction of calcium is carried out, using a recirculation of the mother liquor and a soda ash solution in a process at 40 °C to promote the formation and precipitation of calcium carbonate. All solids obtained from this stage are sent to discard ponds, and the solution with lower amounts of calcium is transferred to the next stage.

To assure the elimination of all contaminants, a second reduction stage for magnesium and calcium is carried out by mixture of soda ash solution with a slaked lime slurry, which allows the formation of calcium carbonate and magnesium hydroxide. The magnesium and calcium solids precipitated are filtered and later sent to the discard pond. The magnesium and calcium free brine is sent to an ionic exchange stage, to ensure that no contaminants are left in the brine.

The process stages mentioned above can be summarized in Figure 17-4.

Figure 17-4: Simplified Lithium Carbonate Plant Process Diagram (1/2)

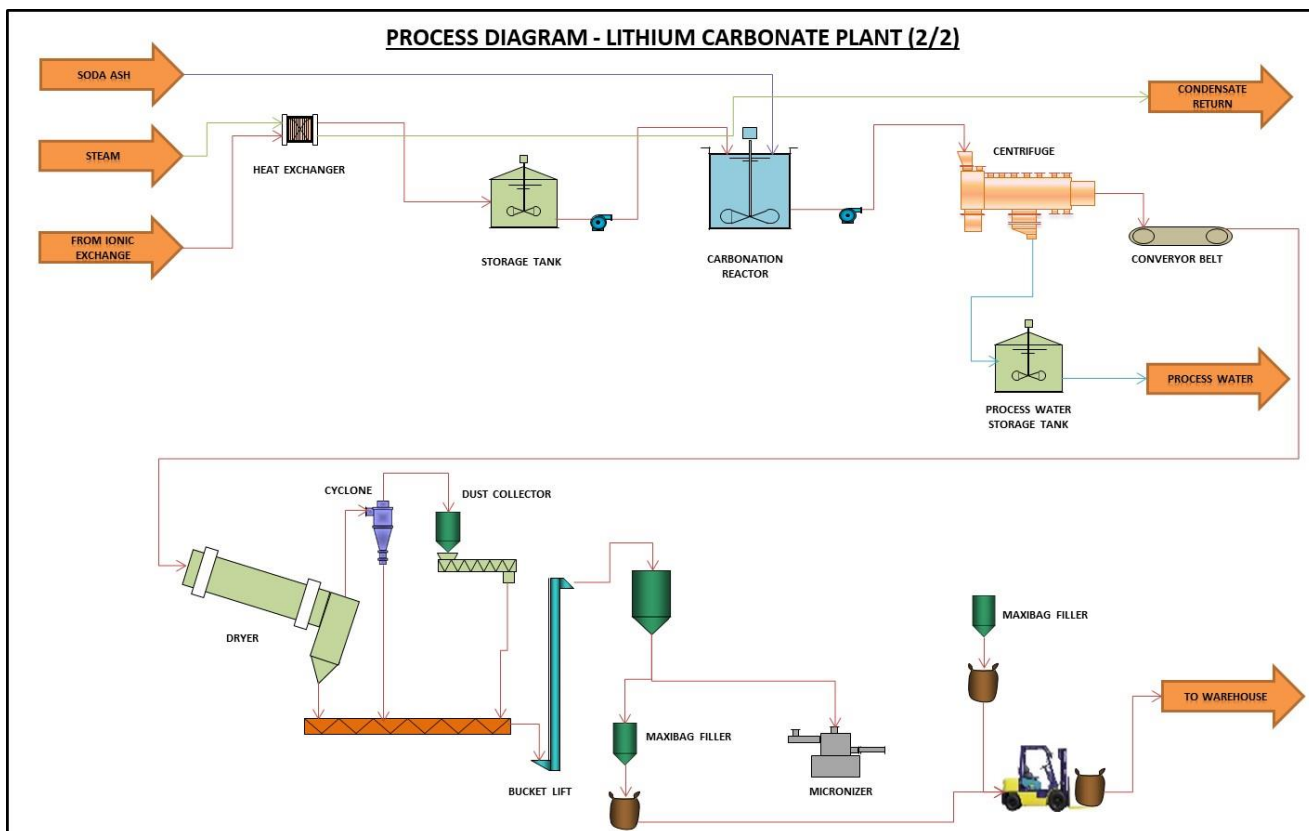


The contaminant free brine enters the carbonation stage, where it is placed in contact with a soda ash solution. The formation of lithium carbonate using soda ash is optimum at temperatures close to 80 °C, allowing the precipitation of the lithium carbonate in a solid state.

The pulp obtained from the carbonation stage is processed in solid/liquid separation centrifuges, and the product is also washed. Lithium carbonate obtained in the carbonation stage is transported to a dryer. After drying, some goes through size reduction in a micronizer. Finally, the dry, unmiconized and micronized lithium carbonate is packed into

separate maxi bags and stored in a final product warehouse and is later delivered to clients as required.

Figure 17-5: Simplified Lithium Carbonate Plant Process Diagram (2/2)



17.5 REAGENTS FOR THE PROCESS

The reagents to be used in the process, which includes the concentration in which reagent will be required, is shown in Table 17-2.

Table 17-2: Reagents used for the process

Reagent	Chemical formula	Annual consumption (TPY)
Lime	CaO	754
Soda Ash	Na ₂ CO ₃	46,886
Caustic Soda	NaOH (50%)	248
Sulphuric Acid	H ₂ SO ₄ (98%)	300
Hydrochloric Acid	HCl (32%)	6,559
Solvent extraction diluent	N/A	50
Solvent extraction extractant	N/A	20

The main reagents to be used are detailed in the following sections.

17.5.1 Preparation of Soda Ash solution

Soda ash is one of the main reagents used in the Lithium Carbonate Plant. A consumption of 46,886 TPY of this product is expected. This reagent is prepared in a plant specifically designed for this purpose, transforming it from the solid state in which it is purchased to a 28% concentrated solution, the concentration at which it is added to the process. For its preparation, recycled water from the process is mixed in a tank with soda ash solids. This tank contains an excess amount of soda ash, assuring a saturated solution. The temperature of the system is controlled by heating the recycled water. The solution is later transported to the soda ash storage tanks and is ready for use in the process.

17.5.2 Preparation of calcium hydroxide

The reagent used in the process is lime, which is slaked with water to calcium hydroxide and is used in the lithium carbonate plant for magnesium hydroxide precipitation. The process considers a total lime consumption of 754 TPY in the lithium carbonate plant. The liming system will be installed near the stage where it is applied.

17.6 WATER PURIFICATION

This process includes the re-utilization of process water at various points, but the injection of fresh clean water is still necessary in certain stages of the process. Process water is treated in a treatment plant which uses reverse osmosis to obtain the required water quality for the process. This is meant to avoid the entry of contaminants to the process.

17.7 EQUIPMENT CLEANING

The equipment of the Lithium Carbonate Plant needs to be periodically cleaned with a solution of sulfuric acid (H_2SO_4) at a concentration of 18 % to remove the accumulation of incrustations in their interior. This process is carried out at intervals defined by operations, and the neutralized solution obtained from cleaning is sent to the discard pond.

17.8 LITHIUM CARBONATE PLANT SOLID WASTE MANAGEMENT

Besides the solid salts generated in the evaporation ponds, there are also solid discards generated in the Salt Removal Plant and the Lithium Carbonate Plant. The main discards generated in the Salt Removal Plant are tachyhydrite and calcium chloride salts, while the main discards generated in the Lithium Carbonate Plant are calcium carbonate (CaCO_3), magnesium carbonate (MgCO_3), magnesium hydroxide ($\text{Mg}(\text{OH})_2$) at the Ca/Mg removal

stages. All discards generated from the Salt Removal Plant are sent, using trucks, to a discard pile, while all solids generated in the Lithium Carbonate Plant are pumped together with the mother liquor to a defined discard pond. In this pond solids decant and the liquid recovered is sent to the evaporation ponds to recover the lithium values. The total solids generated from both plants is presented in Table 17-3.

Table 17-3: Annual generation of solid discards

Discard type	Annual production (TPY)
Solids from Salt Removal Plant (with 15% brine entrainment)	434.023
Solids from Lithium Carbonate Plant (with 45% brine entrainment)	12.089

18. PROJECT INFRASTRUCTURE

18.1 OBJECTIVE

This section describes the infrastructure required for Blanco Project.

The project includes the following physical areas:

- Brine production wellfield in the Salar.
- Evaporation ponds area.
- Facilities area.

The brine production wells area will be located in the Salar de Maricunga, at 3,760 masl.

Figure 18-1: Location of Salar de Maricunga



The evaporation ponds area that MSB plans to build is located north of the Salar de Maricunga and will cover an area of 7.5 million m². These ponds will allow the brine to be concentrated in different steps. In addition, there will be approximately 30 million m³ of discards salt that will be stockpiled at site. These salts will be originated by the harvesting of the ponds and from processes plants.

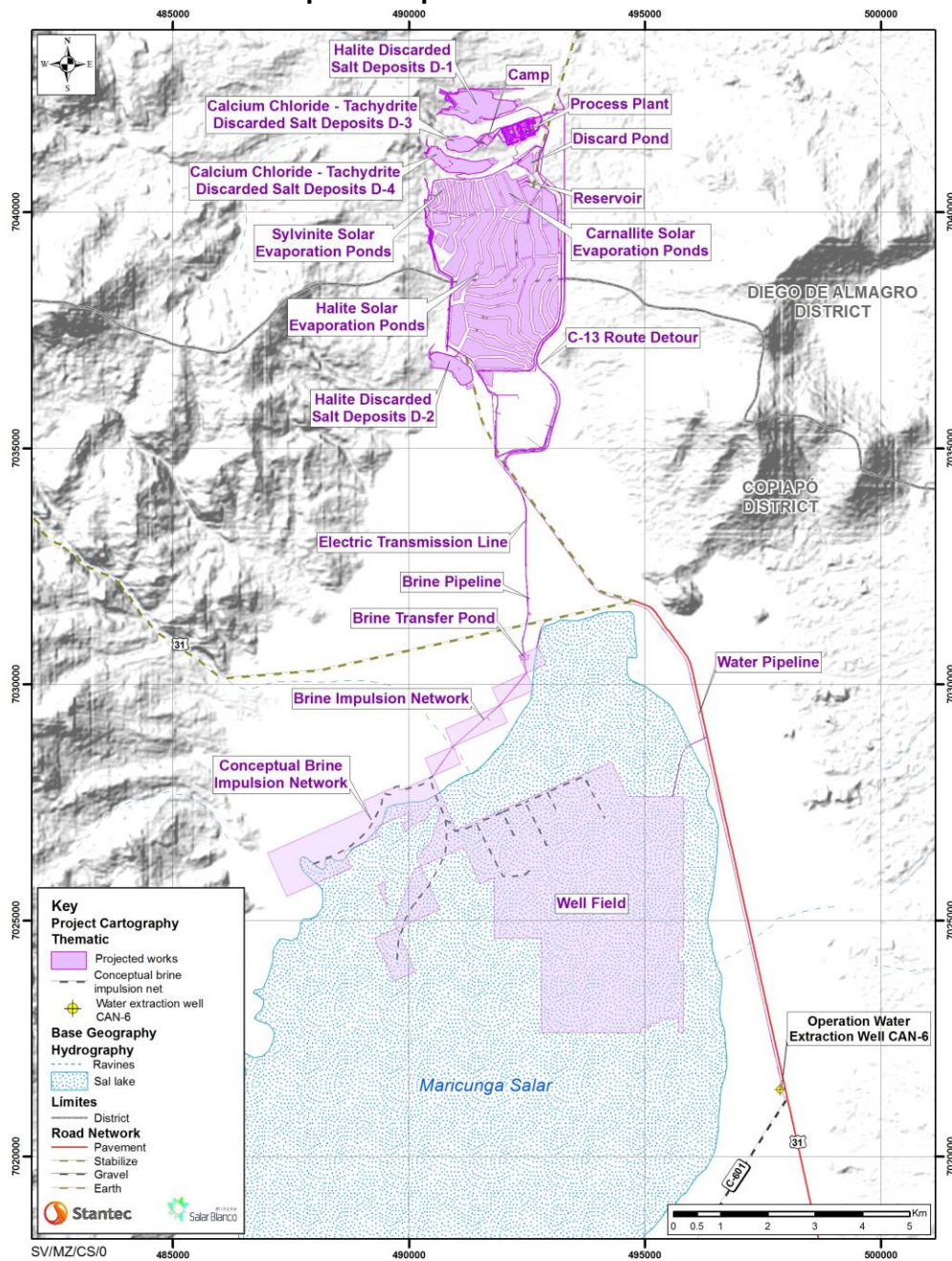
The facilities are located to the north of the ponds area, and include:

- Lithium carbonate process plant.

- Auxiliary services.
- Workers' camp.
- Temporary contractors' installations

Both areas (ponds and facilities) are shown in Figure 18-2.

Figure 18-2: Project location (magenta) showing the areas destined to the evaporation ponds and installation



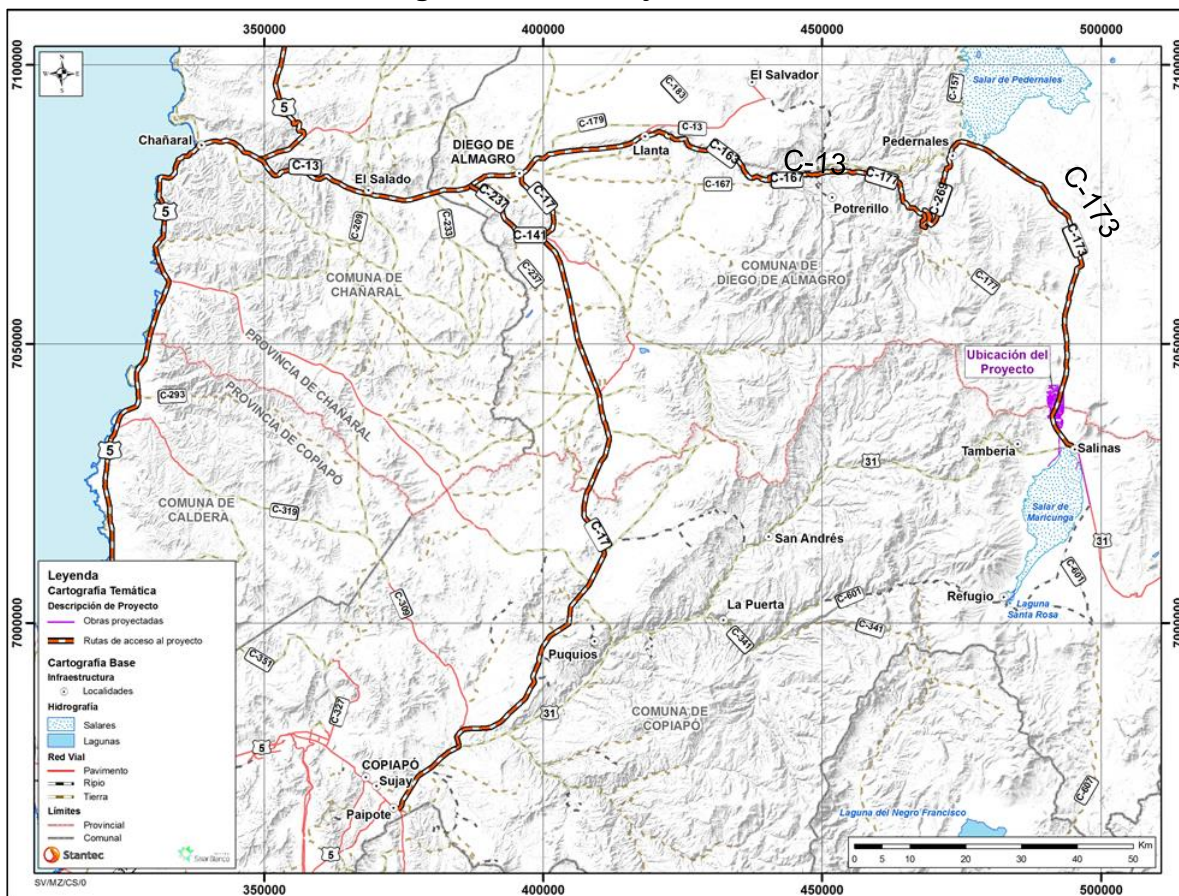
Source: Stantec Chile

18.2 PROJECT ACCESS

The main road access to the Project corresponds to Route C-173, which is an existing, well maintained, mining road. The Project includes a modification of this route, in an extension of approximately 8 km.

This route is accessed from Route 5 (Main North to South Highway) exiting to Diego de Almagro, and then taking Route C-13, then following Route C-163 East, until reaching Route C-173. The project location is 104 km south along this route.

Figure 18-3: Project Access



Source: Stantec Chile

18.3 TEMPORARY INSTALLATIONS

The project contemplates the execution of temporary and permanent facilities. In particular, the mining camp consists of temporary and permanent elements, according to the stage of the project's life cycle.

18.3.1 Contractors Installations

Temporary contractors' installations will be placed in different areas near working fronts for the main contractors. The temporary installations include:

- Offices
- Warehouses
- Workshops
- Storerooms
- Dining rooms
- Dressing rooms
- Sanitary facilities
- Concrete plant
- Aggregate plant
- Non-hazardous and domestic industrial waste management areas
- Hazardous waste area
- Other facilities

18.4 PERMANENT INSTALLATIONS

18.4.1 Brine production wellfields

The brine production wellfield considers 12 production wells that will be drilled in the Salar. The required average annual brine feed rate from the wellfield to the evaporation ponds is 16,416 m³/d to support an annual lithium carbonate production of 20,000 t. The brine production wellfield is described in detail in Section 16 above.

The extraction wells will be electrically fed with channeling at ground level, using isolated cable ducted in galvanized steel conduit.

18.4.2 Transfer Ponds and pumping station.

Two transfer ponds will be located at the northwest of the salar, including its pumping station which will receive brine from the production wells and pump it through a pipeline to the evaporation ponds area.

18.4.3 Evaporation Ponds

Their function is concentrating the brine extracted from the salar through solar evaporation. The construction of the ponds will be done by cut and fill as to level the ground and build the pond walls. The ponds will be lined with an HDPE or similar membrane for waterproofing.

Brine transfer from one pond to the next is mainly done by gravity. However, when this is not possible, a pumping station will be installed. In this case power supply is aerial.

All ponds will have access roads for monitoring and maintenance activities. In addition, contour channels will be constructed where required in order to divert the rain waters of the zone.

18.4.4 Process Plants

The process plant area includes the facilities described below:

18.4.4.1 Industrial Buildings

The buildings of the plant area are designed according to the weather conditions of the site. These buildings are classified as follows:

Salt Removal Plant

- Salt removal plant (includes evaporation and crystallization)

Lithium Carbonate Plant

- Solvent extraction building.
- Brine purification building (includes ionic exchange, magnesium and calcium removal).
- Lithium carbonate building (includes wet area, filtering, drying, micronizing, packaging and product storage).

Plant Services

- Reagent preparation building (includes SX reagents, hydrochloric acid and caustic soda preparation).
- Fuel station.
- Storage and distribution of sulfuric acid.
- Lime plant.
- Compressors room.
- Boilers room.
- Water conditioning plant.
- Storage and preparation of soda ash.

18.4.4.2 Electrical Rooms

Three electrical rooms are considered for the lithium carbonate plant, and one for the camp. In addition, backup generators will be available for critical equipment and the camp.

18.4.4.3 Control Rooms

One control room is considered and will be located in the interior of the industrial buildings.

18.4.5 Auxiliary Installations

18.4.5.1 Access Control Checkpoint

The control checkpoint at the main entrance will include the following facilities: admission control office, luggage control room, induction room, vehicles parking and toilets for visitors and internal plant staff.

18.4.5.2 Administration Building

The administration building includes the company's administrative offices, meeting rooms and a server room. This building will be located in the plant area with an approximate surface of 968 m². Construction will be in accordance with the rest of the existing buildings in the plant.

18.4.5.3 Laboratory

Within the plant there will be a Process Quality Control Laboratory, which will allow chemical analysis, grain-size analysis and moisture analysis in order to ensure the correct operation of the process and its quality.

18.4.5.4 Cafeteria-Dining Room

This will be located in the administration building with 128 m² of area.

18.4.5.5 Parking Areas

Two parking zones for buses, vans and pick-up trucks are considered, one of them prior to the access control, of approximately 2,200 m², and another by the administrative building, of approximately 1,643 m².

18.4.5.6 Weighing Station

The project includes a weighing trucks sector of 420 m².

18.4.5.7 Truck Workshop

The truck workshop includes the following facilities:

- Lubricants storage area

- Office area
- Truck washing area and water tank
- Electrical workshop
- Mechanical workshop
- Minor and major equipment workshop
- Sludge degreasing treatment plant
- Parking garage
- Waste yard

18.4.5.8 Waste Water Treatment Plant (WWTP)

A WWTP is considered for the project. For the construction phase, it will be able to service up to 1,200 persons and in the operation phase it will reduce to 400 persons.

18.4.5.9 Industrial waste yards and rooms

The project includes a temporary yard for non-hazardous waste and a closed area for the hazardous waste. Each type of waste will be transport to an authorize landfill.

18.4.5.10 Fire protection system

The fire system will consider a large storage water tank that feeds the fire protection wet network. It is also includes a pumping system (electric and diesel) to maintain a constant pressure in the fire network and guaranties the water supply, according to the National Fire Protection Association (NFPA).

A separate and special foam fire protection system will be installed in the solvent extraction plant and will also be constructed and maintained according to the National Fire Protection Association (NFPA).

18.5 MINING CAMP

The mining camp will have 2 platforms with a total area of 28,590 m². The facilities of the camp will be modular and will be connected by pedestrian and vehicular access.

18.5.1 Dorms

During construction phase there will be 8 dorm buildings with a capacity for 1,200 people. This will reduce to 220 people during the operation phase. All buildings will have a heating system, ventilation, power supply, networks, sanitary installations, fire detection and extinguishers according to DS594.

The dorms will have 3 types of bed rooms, one bedroom with an individual bathroom, double bedrooms with a shared bathroom and triple bedrooms with a shared bathroom.

18.5.2 Dining Room

It includes all the facilities for 400 people seated. It will have heating ventilation system, sanitary installations, fire detection and extinguishers according to DS594.

18.5.3 Recreation Areas

The camp includes recreation rooms equipped with TV, pool table and lounge area; a multisport court (baby soccer, basketball and volleyball) and a fitness center.

18.5.4 Polyclinic

The polyclinic is equipped with a reception room for first aid, beds, resuscitation equipment (defibrillation), utensils and medicines, bathrooms for patients and another for medical personnel, nursing office, dormitory for paramedics, and storage for cleaning supplies. It also includes an exclusive parking area for the ambulance.

18.6 SERVICES

18.6.1 Electrical Energy

The Blanco Project demand for 15 MW of electrical power. The Electric Coordinator already gave MSB the authorization to connect to an existing 23 kV transmission line. This existing line was originally built as a 66 kV by Kinross for future projects but is being operated at 23 kV. So, the MSB strategy is to change those transformers and increase the line capacity. Below, Figure 18-4, shows the existing line's route and the proposed location for MSB's connection to the line.

Figure 18-4: Transmission Line Route



18.6.2 Water

18.6.2.1 Potable Water

The supply of potable water for the construction phase will be carried out by tank trucks of 30 m³ capacity and distributed into storage tanks in the camp and in the industrial and administrative buildings.

During the operation phase the water of well CAN- 6 will be purified and will supply the water for the camp and plant.

For drinking water, bottles of water will be supplied.

18.6.2.2 Industrial Water

The project will require industrial water for the following purposes:

- Plant process
- Moistening the earthwork material
- Dust control in work fronts
- Water dilution for pumps that pump saturated brine.

The water will be pumped from the well CAN-6 nearby the salar to an industrial water storage pool. Industrial water will be treated in a reverse osmosis plant located inside the plant. This plant will feed tanks that will supply water to the process and purify the water for the camp. The waste stream from the reverse osmosis plant will be used as dilution water for the pumps in the evaporation ponds.

18.6.2.3 Diesel Fuel

The project includes diesel fuel storage and a loading facility. The fuel used by light vehicles, trucks, machinery and heavy equipment is estimated at approximately 67 m³ during operations. In the plants, diesel oil will be used in steam boilers and dryers. This consumption is estimated at approximately 2,100 m³/month. The diesel supply will be provided through tanker trucks that will feed a 700 m³ storage tank.

18.7 ENGINEERING DELIVERABLES

In order to develop CAPEX and OPEX values, procurement quoted main equipment, supplies, materials, freight costs, and construction contracts. For this purpose, quotations for each unit to be quoted were requested to three suppliers. Procurement also carried out a study of the conditions for imports of supplies and services to facilitate the purchases. Technical and commercial evaluations were made for all quotations received.

Critical equipment was defined, being those which have long delivery times and those that are required to begin construction.

The following table summarizes the work carried out by the engineering team of WP and GEA:

Table 18-1: WorleyParsons Engineering Deliverables

Area	Li ₂ CO ₃ Drawings	Li ₂ CO ₃ Documents	TOTAL
General	0	7	7
Process	12	4	16
Mechanics	30	26	56
Civil	34	6	40
Structural	47	4	51
Piping	43	7	50
Electricity	14	10	24
Instrumentation	16	5	21
Ac qof supply and/or Equip. Quotes	0	11*	11
Total	196	80	276

*More than 150 equipment/contract quotations

Table 18-2: GEA Engineering Deliverables

Code	Description	GEA Drawings	GEA Documents	Total
BFD	Block Flow Diagram	2		2
PFD	Process Flow Diagram	5		5
DIM	Data Sheet		71	71
DSC	Descriptions		8	8
EQL	Equipment List		2	2
LAY	Layout	8		8
LEW	Equipment List with Weights		2	2
PID	Piping & Instrumentation	2		2
PPL	Piping List		2	2
REP	Research Report Document		1	1
SLD	Project Time Schedule		1	1
SPC	Technical Specification		120	120
	Total	17	207	224

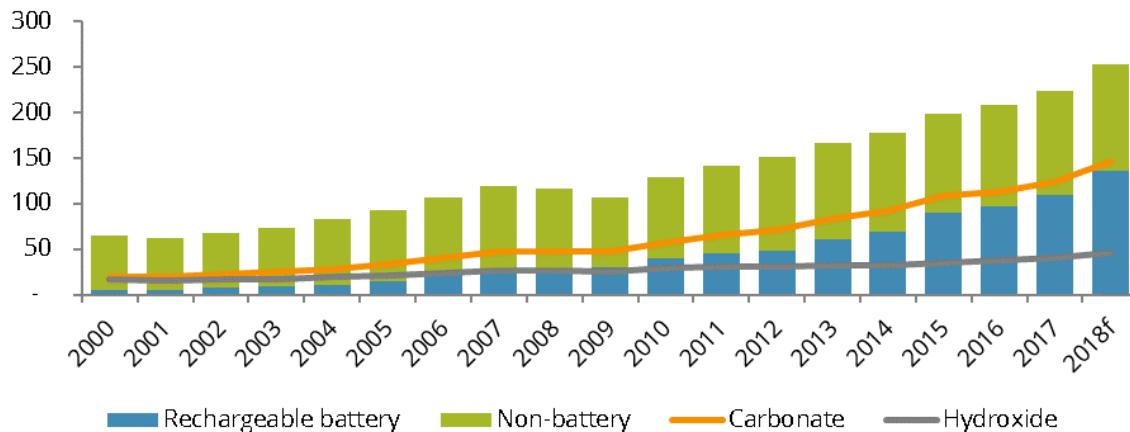
19. MARKET STUDIES AND CONTRACTS

19.1 CONSUMPTION

Consumption of lithium has grown by 7.4%py since 2000, increasing from just under 65,000t LCE to 224,000t LCE in 2017. In the mid-2000s, consumption grew even more strongly, by more than 10%py between 2004 and 2007. After an 8% fall in 2009, consumption recovered strongly in 2010 and the market has since grown by around 13,000tpy LCE, although 2015 witnessed a 12% rise (21,300t LCE) causing the market to become undersupplied and prices rose accordingly. Growth in 2016 was tempered by a stall in the portable consumer electronics market and the impact of availability and high prices on technical applications, despite the automotive industry absorbing yet more lithium in lithium-ion (Li-ion) batteries for electrified models. Consumption surged ahead again in 2017, increasing 7.2% or over 10,000t LCE year-on-year. It should be noted that procurement activities by consumers in 2016 and 2017, especially those in the battery supply chain, likely increased by closer to 7.0%py, ahead of future use. Therefore, demand in 2017 was over 10,000t LCE higher than consumption at over 237,000t LCE, ahead of an expected 13% rise in consumption in 2018 to 253,200t LCE.

Growth in consumption since 2000 has been led by the **rechargeable battery** market (within which Li-ion batteries account for 99% of lithium consumption and NiMH and NiCd the remaining 1%), which accounted for 110,230t LCE or 49% of total lithium consumption in 2017, a more than six-fold increase from a decade earlier and a growth rate of 20.2%py since 2000 (Figure 19-1). Consumption is expected to rise 24% in 2018 to almost 137,000t LCE. Consumption of Li-ion batteries has increased significantly because of rapid expansion in the portable consumer electronics sector through to 2014 and a growing market for batteries for automotive electrification since then. Li-ion batteries have also been gaining market share in other markets, including for use in power tools and electric bicycles, as performance increases and costs fall. Further technological advancement, together with the rise in installed renewable energy (wind and solar) capacity, has seen the use of Li-ion batteries extended to grid / off-grid energy storage systems (ESS). In 2018, the automotive market is expected to account for 51% of lithium consumption in rechargeable batteries, portables 39% and other applications 10%.

Figure 19-1: The rise of rechargeable batteries in lithium consumption, 2000-2018f (000t LCE)



Source: Roskill

When combined, **glass, ceramics and glass-ceramics** were the second largest market for lithium, accounting for 23% of total consumption in 2017, down from 28% in 2015 and 34% in 2012 when it was the largest consuming sector ahead of rechargeable batteries. These end-uses consume both lithium compounds and technical-grade lithium minerals, with the latter gaining market share due to more economical pricing and higher availability since 2016. Growth in consumption of lithium in ceramics and glass-ceramics has averaged 3.7 and 5.9%py since 2000, to reach 25,100t LCE and 23,600t LCE respectively, driven by a boom in construction in emerging and developed economies, especially in the mid-2000s and early 2010s. The glass market for lithium grew by 5.8%py between 2000 and 2017, to 9,100t LCE. The historical high growth rates mask more moderate growth since 2012, as construction activity has dwindled in the developed world and slowed in China.

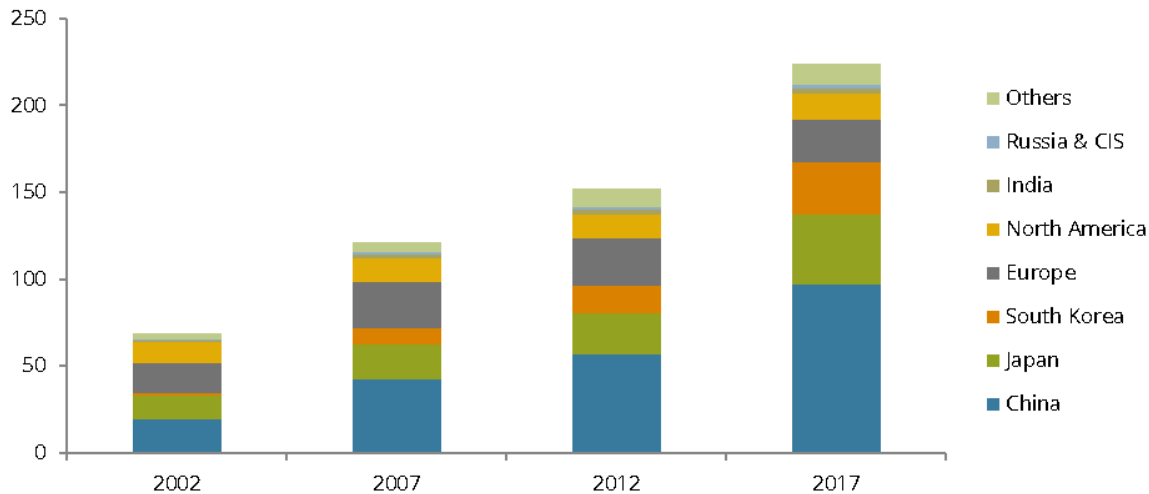
Rapid growth in construction and manufacturing output in emerging economies, particularly China, has also led to increased lithium consumption in **metallurgical powders**, used in the continuous casting of steel, and in the production of lithium-based **greases**. Lithium consumption in greases increased from 8,100t LCE in 2000 to 13,900t LCE in 2011, but has since plateaued. The metallurgical powders market peaked in 2014 at 8,800t LCE, but has since fallen slightly as the steel industry adjusts to a slowing China and more recently from higher lithium prices. These two markets use lithium hydroxide, and lithium carbonate and lithium minerals, respectively. The use of organolithium products for catalysing synthetic rubbers and thermoplastics has also provided strong growth, of around 5.0%py, in consumption of lithium in **polymers** since 2000 as tyres, tubes and rubber product demand grows.

The **air treatment** market for lithium includes absorption chillers, where lithium bromide is used as the absorption medium to produce chilled air from waste heat in large commercial and industrial complexes, desiccant dehumidifiers and air purification systems. Consumption of lithium bromide in absorption chillers, and also chloride and hydroxide used in desiccant dehumidifiers and carbon dioxide removal apparatus, has fallen 1%py since 2000 to around 4,600tpy LCE. While the market expanded rapidly in the mid-2000s as China's economy industrialised, the use of direct-fired chillers has waned in recent years and indirect-fired chiller sales have failed to replace the lost sales.

The **primary battery** industry has witnessed growth, albeit on a much smaller scale than for rechargeable batteries (8.6%py compared to 19.3%py) since 2000 to total 4,600t LCE in 2017. Primary batteries are used for memory back-up in portable electronics, in monitoring systems and in industrial equipment. Lithium metal is the main form used in these batteries. **Other** uses for lithium account for the remainder of consumption, at 17,000t LCE in 2017 and has grown by 1.2%py since 2000.

On a **regional basis**, China is the world's largest consumer of lithium (Figure 19-2), accounting for 43% of consumption in 2017, with domestic consumption having grown over five-fold since 2002, to 97,000t LCE. South Korea and China are the dominant Li-ion battery and battery material producers, and consumption has increased rapidly since 2000 on increased rechargeable battery cathode material output. Japan is also a major battery and battery material producer, especially for the automotive market, but has faced growing competition from its Asian neighbours in the portables market, partly due to lower manufacturing costs. Consumption in Japan has accelerated since 2012 with a shift to greater focus on the high value automotive sector for batteries, and it was the second largest consumer in 2017 at 40,000t LCE, compared to Korea at 30,000t LCE; 18 and 13% of the market respectively. Europe and North America consume lithium mainly in the manufacture of industrial and construction -related products, such as ceramics, glass-ceramics, greases, polymers and aluminium, as there is not a large Li-ion battery industry outside Asia as of 2017. Europe represented 11% of lithium consumption followed by North America at 7%. India, Russia/CIS and other countries account for the remaining 8%.

Figure 19-2: Consumption of lithium by country/region, 2002-2017 (000t LCE)



Source: Roskill

Lithium carbonate is the most widely consumed **product**, finding application in rechargeable batteries, ceramics, glass-ceramics, glass, metallurgical powders and other uses. Consumption of battery- and technical- grades exceeded 119,000t LCE in 2017, with battery-grade carbonate accounting for 41% of total lithium product consumption and industrial-grade 12%. Battery-grade carbonate consumption has doubled since 2012 and grown by 18.1%py since 2000. Technical-grade mineral concentrates (mainly spodumene, petalite and lepidolite) accounted for a further 18% of consumption and are used in similar ceramic, glass-ceramic, glass and metallurgical applications to lithium carbonate. Technical- and battery- grade lithium hydroxide together represented 13% of consumption, with battery-grade hydroxide showing high growth rates at 16.0%py since 2000. The growth in high-nickel battery cathode materials, in particular nickel-cobalt-aluminium (NCA), and alkali method lithium-iron-phosphate (LFP) production, for automotive and ESS markets has boosted battery-grade hydroxide consumption over recent years.

The **outlook** for lithium consumption has improved significantly since mid-2016, following much stronger forecasts for xEV requirements led by new government targets/mandates and automotive manufacturers' plans. Roskill now expects the total lithium market to exceed 1Mt LCE in 2026 in the base-case scenario; this represents a more than five-fold increase in consumption from 2017. Growth will, however, be more moderate in the short-term, with 19.0%py growth to 2022 when the market could reach 533,000t LCE, before accelerating in the mid-2020s. Consumption of lithium in volume terms will be driven by Li-ion battery use increasingly for automotive use, with rechargeable batteries forecast to register 22.7%py growth to 2032.

Other markets for lithium are also forecast to provide areas of growth for lithium consumption, but only at around 3.0%py in the base-case scenario. The volume of lithium consumption in rechargeable batteries, representing 49% of total consumption in 2017, will have much more impact on overall lithium consumption and this sector's influence will continue to increase with rechargeable batteries reaching 75% of total market demand in 2022.

There are, however, upside and downside risks to the outlook for growth in consumption of lithium to 2032. The low-case (pessimistic) scenario foresees slower global economic growth affecting consumption of basic products like ceramics, glass, aluminium, steel and rubber, as well as lower demand for portable consumer electronics, but most critically delays in the introduction of Li-ion battery powered xEVs. Despite lower growth levels, these will still be 14.3%py to reach 1Mt LCE by 2027. Meanwhile, in the high-case (optimistic) scenario, growth in consumption of lithium is forecast to increase by 21.4%py to reach just over 1.0MT LCE in 2022 and 4.1Mt LCE by 2032. The optimistic scenario is based on even higher penetration rates for xEVs as well as stronger demand for batteries in grid/off-grid ESSs, where they smoothen out power fluctuations of weather-driven renewable sources such as solar and wind, thus preventing the disruptions to transmission grid, and ensure stable power supply to industries, such as telecom towers, that are sensitive to electricity outage. portables and power & motive applications.

On a product level the greatest growth in demand will come from battery-grade lithium carbonate and hydroxide. To achieve higher energy density cells for longer range vehicles favoured by automakers and/or to meet incentive levels, as well as to reduce the use of expensive and volatile cobalt, high-nickel cathodes such as NMC622 (60% nickel), NMC811 (80% nickel) and NCA (>90% nickel) are increasingly being used. Processing and performance of high-nickel cathodes is improved by using battery-grade lithium hydroxide, meaning it is expected to outperform carbonate demand growth with close to 34%py volume growth going forward, with hydroxide surpassing carbonate as the main product used in the mid-2020s. Hydroxide growth could be higher if the switch to high-nickel cathodes accelerates. Lithium carbonate will still be in strong demand, albeit at growth rates closer to 17%py, led by use of lower-nickel cathode for xEVs, ESS, portable and power & motive applications. Although LFP has fallen out of favour with xEV manufacturers trying to reach ambitious goals for driving range and performance, it remains a key material for commercial, off-highway and two/three-wheel vehicles.

19.1.1 Lithium-ion battery market

The market for Li-ion batteries across all end-use applications reached 121GWh in 2017, increasing by 28%py since 2000 (Figure 19-3); intensity of lithium use was therefore 0.85kg LCE/kWh. What used to be an industry driven by demand for small batteries for portable electronics is now an industry experiencing rapid demand growth from electrified vehicles

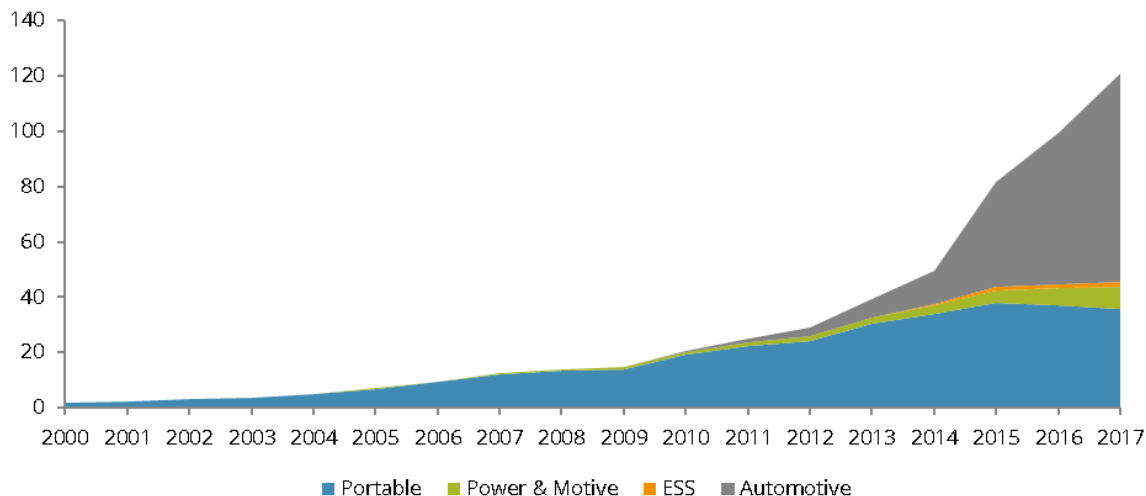


(xEVs) for the new energy sector. To keep up with growing demand, large capacity expansions across each segment of the battery supply chain started as early as 2007, although the largest expansions occurred in the early 2010s. The first mass-market electric vehicles, such as those from BYD, Nissan and Tesla, became commercially available from around 2011 and their impact on the Li-ion sector was substantial. The surge in electric car and bus sales in China in 2015 represented a clear tipping point in xEV demand.

The Li-ion battery supply chain comprises five different stages (Figure 19-4): raw material production; raw material synthesis; cell manufacturing; and, pack assembly and/or cell use. A Li-ion cell has two electrodes, one positive (cathode) and one negative (anode). Electricity is generated by the flow of ions from anode to cathode; however, it is the cathode that is lithiated prior to cell assembly because of lithium's ability to compound with transition metals to form the cathode structure rather than with carbon in the anode. The cathode and the typically carbon-based anode are pasted onto ultra-thin copper and aluminium foil respectively with a glue-like binder. The positive and negative electrodes are separated by a thin membrane, the separator. The electrodes and separator are rolled or folded together and inserted into a metallic cylinder, pouch or prismatic container. The cell is flooded with a liquid or polymer lithium-based electrolyte, which is made by dissolving fluorinated lithium phosphates in organic solution. Cells can be used singularly or combined in series and/or in parallel to form a pack.

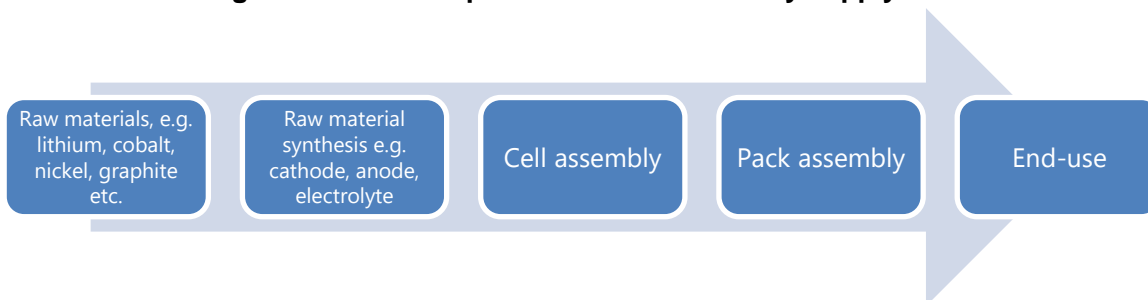
The companies occupying each segment of the Li-ion battery industry are not usually the same, although some integration has taken place – both horizontally and vertically. Synergies might appear between different stages in the battery business, but large corporations mostly integrate to diversify and reduce supply chain risks. The market leaders are already established, especially in China, Japan and Korea, and while they have several competitors in those same countries, the control of the top producers is high at most stages of the value chain (Table 19-1). The supply of lithium is the most consolidated part of the Li-ion battery value chain.

Figure 19-3: Li-ion battery consumption by end-use application, 2000-2017 (GWh)



Source: Roskill

Figure 19-4: Simplified lithium-ion battery supply chain



Source: Roskill

Table 19-1: Top five manufacturers in selected Li-ion battery components, 2017

Lithium	Market share	Cathode	Market share	Electrolyte salts	Market share	Small cells	Market share	Large cells	Market share
Albemarle	28%	Umicore	8%	Foosung	17%	Panasonic	23%	Optimum-Nano	14%
SQM	23%	Shanshan	8%	Tinci Materials	16%	Samsung SDI	22%	CATL	11%
Tianqi	17%	SMM	6%	Morita Chemical	15%	LG Chem	17%	BYD	11%
Ganfeng	17%	TODA-BASF	6%	DFD Chemicals	12%	ATL (TDK)	11%	Panasonic	10%
FMC	10%	Nichia	5%	Jiangsu Juijiujiu	10%	Murata (Sony)	8%	LG Chem	8%
Top-10	100%	Top-10	52%	Top-10	69%	Top-10	81%	Top-10	54%

Source: Roskill

Roskill's baseline **outlook** sees the total market for Li-ion batteries reaching 2,233GWh by 2027, growing at 33.9%py between 2017 and 2027. The automotive sector will have by far the largest impact on battery consumption. Changes in the transportation landscape will be mostly driven by regulatory forces and they will particularly relate to emissions control and the different legal instruments used by regulators to control supply and demand of certain vehicles. It is important to note that the regulatory trend is clear and seemingly irreversible, at least in two potentially very large markets. Transportation and energy sectors will need to become cleaner, and Li-ion batteries are currently the most suitable instrument to achieve that goal

In every scenario contemplated for xEV adoption, further battery cell manufacturing capacity will need to be added with profound implications across the whole battery supply chain. Battery cell manufacturing and some of its upstream components will expand outside Asia to efficiently supply local markets, signalling a trend towards a maturing market at the end of the next decade.

Li-ion technology still competes with other battery technologies, but the **level of competition** depends on the application. The portable electronics market is monopolised by Li-ion technology. In the power and motive market, Roskill has observed a different trend, with Li-ion technology claiming around 36% market share, while lead-acid has a 54% market share. This is because of the presence of lead-acid batteries in many electric scooters in Asia, and some use of NiCd in power tools. However, given the decreasing cost of Li-ion and the availability of suitable cathode chemistries, Li-ion technology is already an inevitable trend in these products.

The case of the ESS is more complex as there are many different substitutive technologies that cannibalise the share of electrochemical batteries in energy storage, leaving Li-ion batteries with a small share in terms of GWh – although this is growing rapidly. However, the share of Li-ion batteries in ESS also depends on the type of battery ESS system: grid (large-scale typically >1MW), off-grid (medium-scale, typically >100kWh) micro-grid (smaller-scale typically >10-100kWh and residential/commercial (small-scale typically 10s of kWh). The suitability of Li-ion depends on the cost, power rating, the discharge time, lifecycle and some other key technical parameters.

Finally, the case of the automotive market is relatively simple because the use of Li-ion technology primarily depends on the end-use (passenger or commercial) and the xEV category (pure electric, hybrid, plug-in hybrid, low speed, and so on). In passenger vehicles, plug-in options – battery electric vehicles (BEV) and plug-in hybrid electric vehicles (PHEV) – are nearly all based on Li-ion technology. However, other xEV categories still use non Li-ion battery types; notably low speed electric vehicles (LSEV) in China (lead-acid), and non-plug in hybrids (HEVs) that use NiMH, which lowers the total penetration figure for Li-ion technology in passenger vehicles to 73% in 2017. In the case of HEVs, this trend is rapidly

changing as automotive companies are opting to use Li-ion batteries in new models, for example Toyota choosing to use Li-ion for the Prius+ in Europe and Asia and now optioning it for the standard Prius. In commercial uses (buses and light commercial trucks) Li-ion technology is the absolute winner with hydrogen-powered buses taking a marginal share (2%).

Solid-state battery technology is not expected to be a serious commercial contender until later in the 2020s. Many working prototypes have shown performance improvements in energy density (solid-state typically has 3X the volumetric energy density of Li-ion because the internal components being thinner than Li-ion), charging speeds, safety and cost advantages. However most of these solid-state batteries lack balanced characteristics. For instance, they can have ultra-fast charging features but only last a few charging cycles. Thus, these batteries are far from commercial viability and additionally, most of the current battery supply chain is already geared towards the mass-manufacturing of existing Li-ion technologies and in automotive applications the testing and approval process can take many years meaning even if a mass-production-capable battery was available it would take several years to reach commercialisation in the main future market.

Given the uncertainty surrounding the acceleration of xEV and ESS battery consumption, it is not unrealistic to foresee greater downside risks to lithium consumption than upside. This has been the trend since EVs began to be talked-up in the mid-2000s. Nevertheless, if emissions (CO₂ and PM) emissions goals are to be met, unless new battery storage or alternative fuel technology appears, it is a case of when, not if, for high levels of lithium consumption in the future.

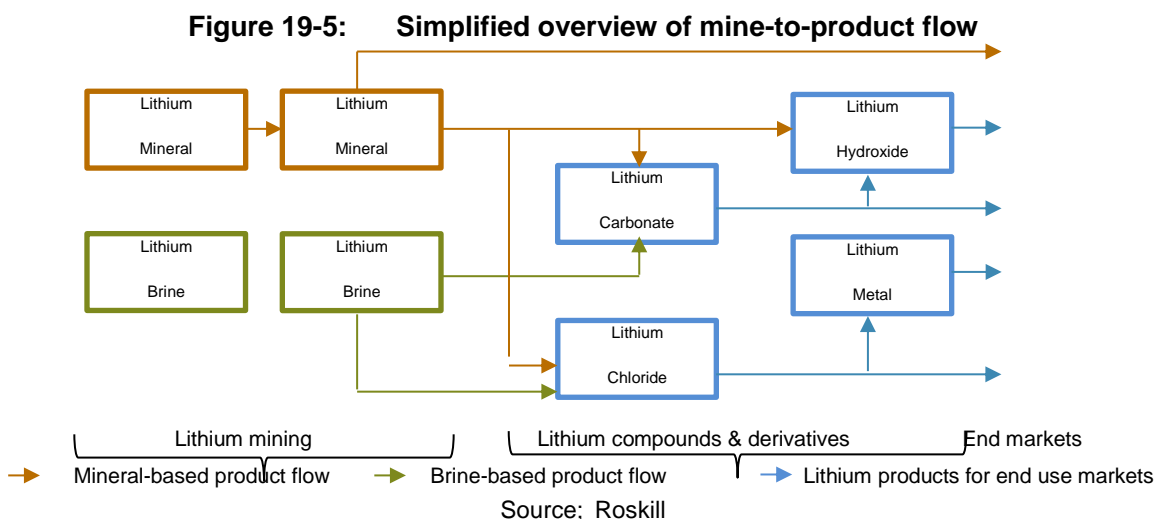
19.2 PROCESSING AND RESOURCES

There are five naturally occurring sources of lithium, but the only two commercial sources are currently lithium pegmatites and continental lithium brines. Other sources of lithium include oilfield brines, geothermal brines and clays, each of which have been subject to evaluation for, but have not yet reached, commercial production. Techniques used in the commercial mining and processing of lithium can be subdivided into two broadly different categories, dependent upon the nature of the lithium occurrence:

- Pegmatite “hard rock” occurrences produce lithium mineral concentrates including spodumene, petalite, lepidolite and amblygonite. Hard rock lithium ores are subject to beneficiation and typically some form of physical (normally dense or heavy media) concentration to produce a saleable or onward process-able mineral concentrate containing 4.0% Li₂O or above. Mineral concentrates may be consumed directly by industry or used for the production of downstream lithium compounds through mineral conversion.

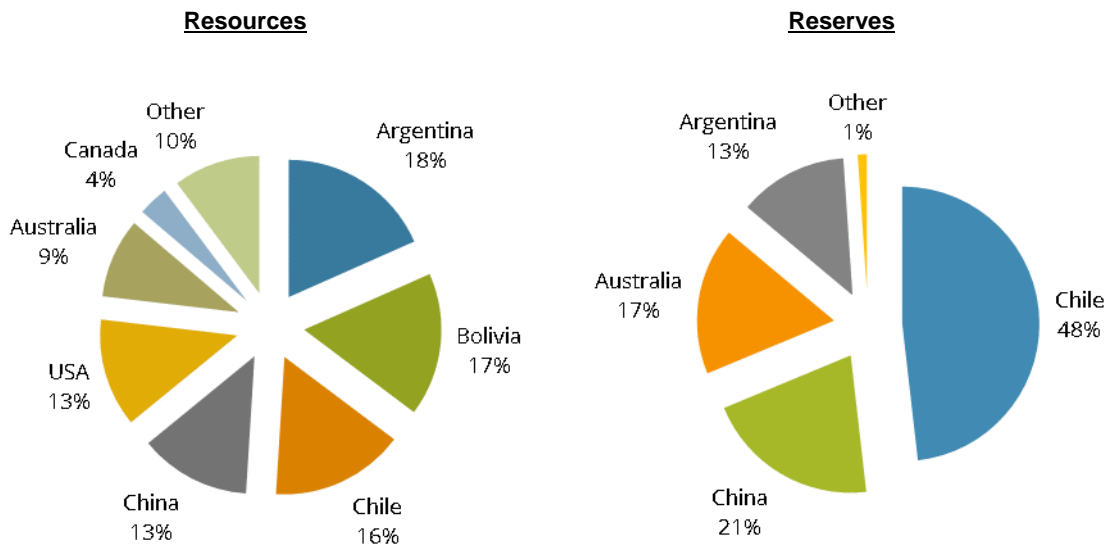


- Lithium-bearing brines occurring in salars (dried salt lakes) are pumped to the surface and typically undergo solar evaporation, ion-exchange or other upgrading technique to produce a concentrated lithium brine concentrate of 3.0-6.0% Li content, which can be processed further into lithium compounds.



In 2018, the USGS reported global lithium reserves, assembled from country geological survey and industry data, to be 16Mt Li (85Mt LCE). The majority of mineral reserves occur within Chile, China, Australia and Argentina; other major reserves exist in the USA, Brazil, Portugal and Zimbabwe (Figure 19-6). The USGS also reported lithium resources at 53Mt Li (282Mt LCE), identified in Argentina, Bolivia, Chile, the USA, China, Australia and Canada; other resources exist in the DRC, Russia, Serbia and the Czech Republic (each around 2%), and Zimbabwe, Spain, Mali, Brazil, Mexico, Portugal and Austria (each <1%). Increased exploration activity is adding to previously identified resources and reserves and they will continue to increase in future.

Figure 19-6: Global lithium reserves and resources by country, 2018



Source: USGS

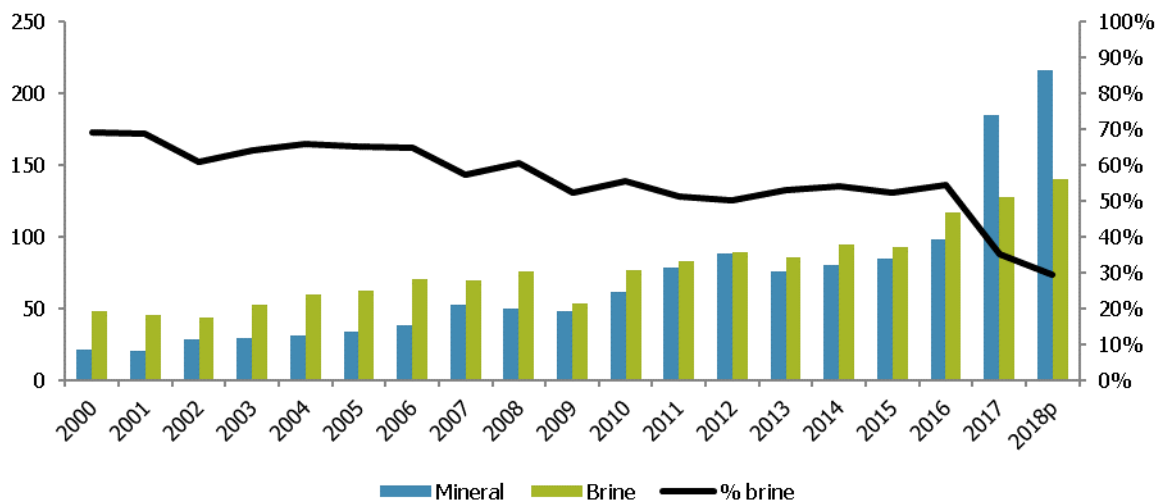
Note: Other Resources includes DRC, Serbia, Russia, Czech Republic, Zimbabwe, Spain, Mali, Brazil, Mexico, Portugal and Austria; Other Reserves includes Portugal, Brazil, USA and Zimbabwe

Global lithium resources are estimated by Roskill, from a review of all operations and projects where such data exists, at 156.3Mt LCE with reserves at 61.9Mt LCE. Argentina, Australia, Chile and China are the main locations of operating lithium assets exploiting these resources, with resources in Argentina, Chile and China largely brine-based and Australia mineral-based. Canada (mineral), the Czech Republic (mineral), Mexico (clay) and the USA (brine and clay) have large resources and hold promise as future potential new or larger sources of lithium supply.

19.3 PRODUCTION

Global lithium **mine production** increased by 10%py from 69,400t LCE in 2000 to almost 307,000t LCE in 2017 (360,250t LCE if including the contribution of direct shipped ore [DSO] from Australia) (Figure 19-7). Output in 2018 is expected to move significantly higher again, at over 472,000t LCE including DSO and 376,202 excluding DSO. Some DSO was processed in China in 2018 and therefore did contribute to mine supply. Lithium mineral production is dominated by output from Australia, accounting for over 50% of global mined output in 2017, with lesser amounts of minerals produced in Zimbabwe (2%) and Portugal (<1%). Spain and Brazil are minor producers. Brine output is dominated by Chile (25%) and Argentina (10%), with the USA a smaller contributor (2%). China is the only country where both minerals and brine are produced and together these accounted for 10% of the global total.

Figure 19-7: Mine production of lithium by source type, 2000-2018p (000t LCE)

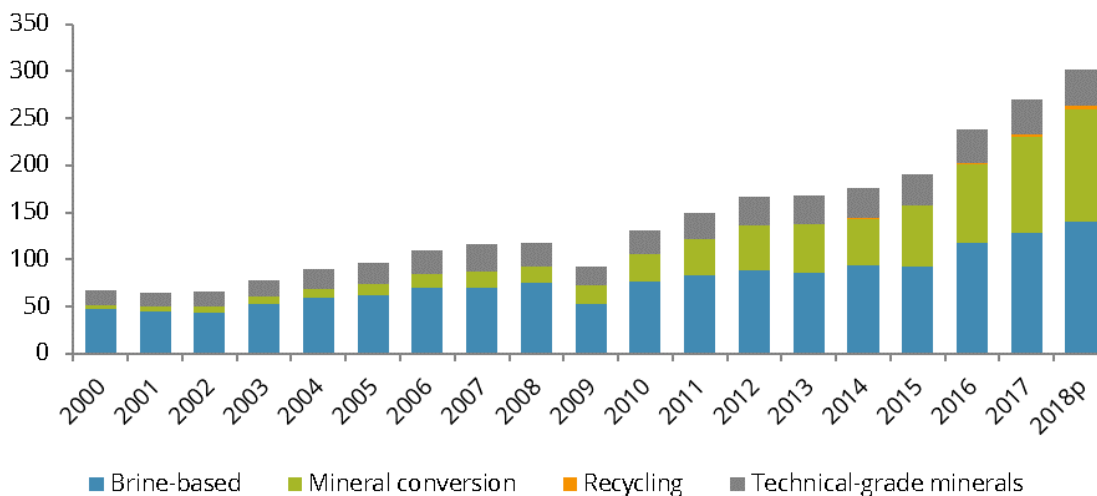


Source: Roskill estimates

Note: Mineral excludes DSO

Refined production (lithium compounds and technical-grade mineral concentrates) in 2017 totalled just over 238,050t LCE, increasing 13% year-on-year after a 22% increase in 2016. Output in 2018 is forecast to rise to almost 270,000t LCE. Brine-based output is predominately processed into lithium compounds (carbonate and chloride) at operations at or near to the brine source and accounted for 51% of refined product output in 2017. The balance of refined output comes either as technical-grade mineral concentrates (38,500t LCE) or as lithium compounds converted from chemical-grade lithium minerals (77,500t LCE). Recycling of end-of-life products contributed another 3,000t LCE. There are many mineral conversion plants in China processing mineral concentrate into refined lithium products, but some also reprocess low-grade lithium carbonate into marketable, higher-value, products, meaning their total output may appear higher than the actual refined output based on processing raw materials alone.

Figure 19-8: World: Refined production of lithium by type, 2000-2018p (000t LCE)



Note: Negligible impact of recycled output to 2018

Source: Roskill estimates

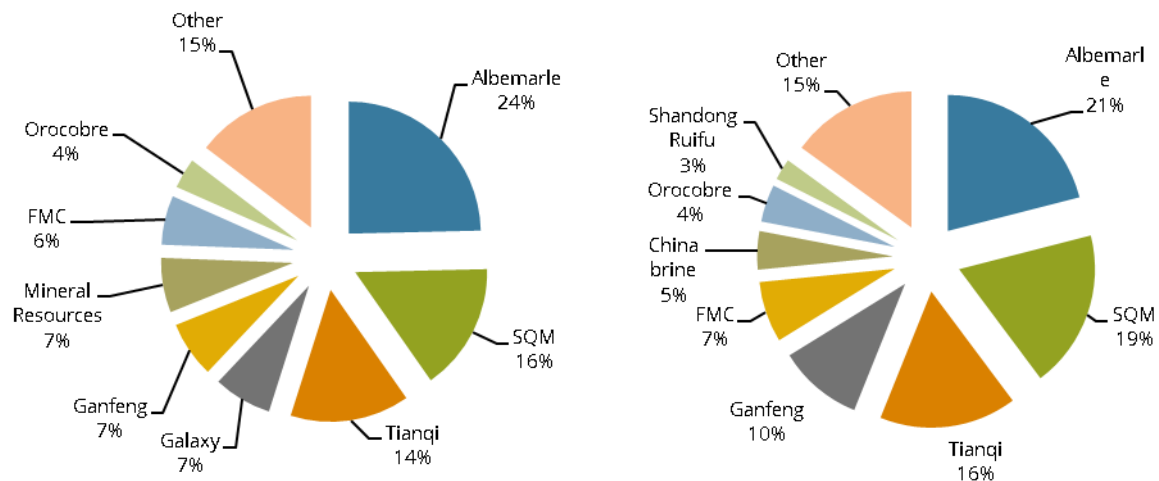
Lithium production has long been dominated by a small number of **producers**. Until the mid-2000s the “big-three”: SQM and FMC, which operate lithium brine operations in Chile and Argentina respectively, and Albemarle, which operates lithium brine operations in Chile and the USA, and more recently mineral conversion assets in China, accounted for the vast majority of mined and refined lithium output, in volume and value terms. Talison Lithium, a joint venture between Tianqi (51%) and Albemarle (49%), operates a hard rock lithium mine in Western Australia and has long been the largest supplier of both technical-grade and chemical-grade mineral concentrate to the market. In 2017, lithium mine production was dominated by Talison Lithium, SQM and Reed Industrial Minerals (a joint venture between Mineral Resources, Ganfeng Lithium and Neometals). If dividing Talison between its owners, the control of mine production was dominated by Albemarle, SQM and Tianqi Lithium, with Ganfeng, Mineral Resources, Galaxy Resources and FMC producing around half the volume of the former three (Figure 19-9).

With Tianqi’s acquisition of a majority 51% share in Talison, and Ganfeng with its share of Reed Industrial Minerals (43.1%), and both companies’ domestic expansion of downstream conversion facilities, they have displaced FMC into fifth place in terms of refined output by volume since 2014. When also dividing the output of technical-grade minerals (tech. min) produced by Talison at Greenbushes between Tianqi and Albemarle, five producers accounted for 75% of refined product output.

The production of downstream lithium chemicals and lithium metal is undertaken by several companies. Outside of China, Albemarle and FMC Lithium are the largest producers of

lithium chemicals and metal, at facilities in Germany, USA, Taiwan, India, France, the UK and Japan. Within China, several processors produce downstream added value lithium compounds, with Ganfeng Lithium the largest.

Figure 19-9: Mined and refined lithium output by producer, 2017 (%)
Lithium mine production **Refined lithium production**



Source: Roskill estimates and company data

Note: Mine production is shown by corporate control (Talison Lithium and Reed Industrial Minerals split by their equity owner shares)

Based on the average value of each of the main lithium products consumed, and the estimated volume used, the lithium market had a **value** of around US\$4Bn on a final lithium product basis in 2017. Value increases along the value chain, with a tonne of spodumene mineral concentrate costing around US\$6,000/t LCE compared to a tonne of lithium metal at US\$600,000/t LCE. Some specialist products such as lithium organics have an even higher value, but as lithium carbonate and lithium hydroxide accounted for around 65% of product consumption, when priced at around US\$12,000/t their value was US\$1.7Bn. Albemarle generated over US\$1Bn in lithium revenue in 2017, making it the largest lithium producer by value. Tianqi Lithium and Ganfeng Lithium were the second and third largest producers by revenue. The dominance of the “big-five” lithium producers above is down to their large-scale, low-cost, integrated mine-refined assets, experience and product quality.

With lithium consumption forecast to increase strongly in the years to 2027, the **outlook** for lithium production and producers is positive from a volume perspective. Mine production capacity in 2017 totalled 375,000tpy LCE and refined capacity 322,750tpy LCE, meaning producers are capable of meeting the base-case consumption forecast in 2018, based on an average industry utilisation rate of 80%. Additional capacity will therefore be required

and is expected to come from both expansion of existing operations, with a smaller contribution from new lithium projects.

At end-2017, global nameplate production capacity for mining lithium totalled almost 375,000tpy LCE (excluding 90,000tpy LCE of DSO at Mineral Resources Wodgina mine in Australia). Based on announced capacity expansions and new project schedules, lithium mine production capacity is forecast to increase to almost 1.0Mtpy LCE by 2022 and over 1.1Mtpy LCE by 2027. The largest additions to mine capacity are in Australia for mineral-based production and Chile for brine-based production. Additional mine capacity will be required from the mid/late-2020s. The majority of mined lithium output, with the exception of technical-grade mineral concentrates, will need to be converted to lithium compounds either through brine processing (typically captive) or mineral conversion. Beyond 2022, further expansion or other new operations might contribute additional capacity, but few producers have announced expansions beyond 1-3 years and the project pipeline remains uncertain. The current committed level of capacity is sufficient to meet base-case consumption, assuming an average 80% utilisation rate, until 2024 and potentially into 2025 with an increasing utilisation rate.

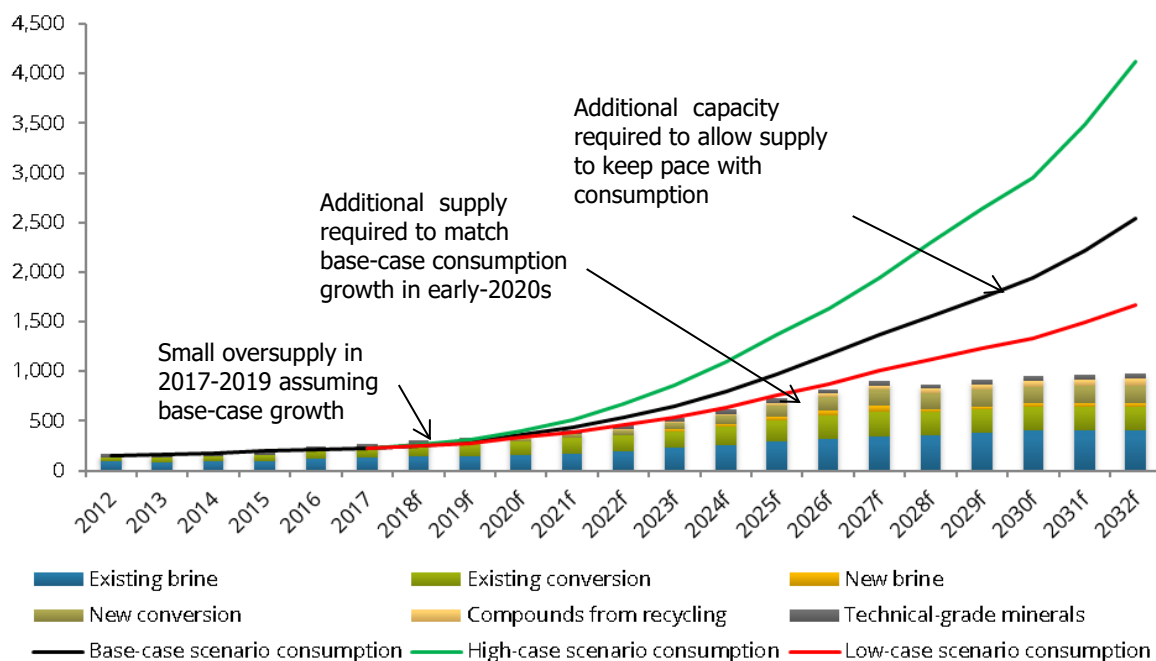
Refined capacity is expected to increase to 2022, but not quite as quickly as mine capacity, reaching around 710,400tpy LCE. Additional brine-based mine capacity will be matched by brine processing capability, but mineral conversion capacity currently lags mineral-based mine capacity.

Roskill assumes that the major producers above would account for 80-85% of mined output through integrated supply, or captive or off-take agreements with mine operators, in 2022, similar to their 80% share in 2017 but falling to 75% in 2027 with FMC losing some market share in the long-term unless they boost capacity further. Chinese brine and mineral producers currently enjoy around a 15% market share of mined output, but will likely lose market share, falling to 12.5% by 2022 and 5% by 2027. This means other suppliers currently accounting for 5-10% of mine supply increasing to 20% market share by 2027, supplying around 140,000t LCE.

The greatest uncertainty is the contribution to supply by the companies planning to enter the market in 2018-2022. In the long-term, their contribution is necessary unless further expansion occurs at existing producers above, but in the short-term, at the base-case consumption growth, they will contribute to a growing oversupply of spodumene concentrate. With the exception of Mineral Resources, Australian, Brazilian and Canadian mineral projects all have off-take contracts with companies operating or building conversion plants in China, or downstream consumers that could toll with their existing lithium compound suppliers. Their fortunes therefore largely rest on the ability of these off-takers to sell/use lithium compounds, which may be dependent on higher than forecast consumption growth, or an ability to compete for business against incumbent suppliers.

Roskill expects refined output will increase ahead of consumption as in a rapidly growing market, customer requirement (demand) often outpaces consumption, especially in the automotive market where there is a long lead time from raw material sourcing to the vehicle sale. Nevertheless, the market is at risk of oversupply in the late-2010s and early-2020s given the size of expansions and the number of new producers entering the market. Oversupply will be short-lived, however, as demand growth accelerates in the early 2020s, meaning undersupply unless producers effectively implement capacity expansions, have no delays to ramp-up, and produce product to specification. Additional capacity will be required later in the 2020s to ensure adequate supply to even higher consumption levels.

Figure 19-10: Forecast production and consumption, 2012-2032 (000t LCE)



Source: Roskill

19.4 PRICES

Lithium pricing has generally followed changes in the underlying cost position of producers (based on higher-cost mineral conversion until the mid-1990s, lower-cost brine production from the mid-1990s to mid-2000s, the re-emergence of higher-cost mineral conversion over the last decade, and the processing of lepidolite and DSO more recently), with market balance having a shorter-term impact. Price rises are generally elastic to increasing demand, and price falls to increasing supply.

Technical- and battery- grade lithium carbonate prices reached US\$6,500/t CIF and US\$6,250/t CIF in 2007 and 2008 respectively (Figure 19-11), after a period of strong

consumption growth and increasing reliance on mineral conversion plants in China, which had higher costs. In 2009, the global economic downturn saw producers and consumers run-down stocks and output fell below consumption. Prices fell to US\$4,600/t CIF in 2010 for industrial-grade carbonate and US\$4,850/t CIF in 2011. SQM, the leading carbonate producer, cut prices to stimulate demand. In 2010-2012 the market rebounded, as producers and consumers re-stocked, and with the expectation that demand would increase at similar rates to the mid-2000s.

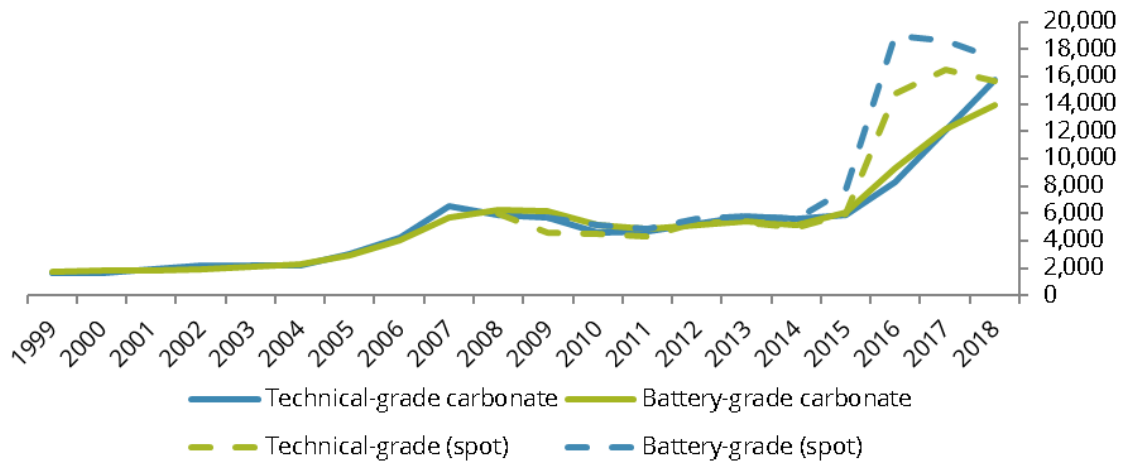
Overproduction between 2010 and 2012, on expectation for higher demand growth, was corrected in 2013 as producers cut-back output, and prices recovered further, but dipped again in 2014. The market further corrected itself through 2014 and on entering 2015 appeared to be heading back in approximate balance. Prices for both grades were back to around US\$5,600/t CIF in 2015. However, limited output growth in 2015 caused by: reduced availability of spodumene concentrate from Talison Lithium as more material was converted by Tianqi (or tolled by Albemarle); a surge in consumption caused by increased e-bus and xEV output in China; and, possible speculative activity with an expectation that market tightness would continue, meant spot prices in China for both technical- and battery- grade hydroxide and carbonate increased rapidly from mid-2015, and continued increasing through mid-2016 to US\$22,000/t ex. VAT for battery-grade carbonate and over US\$18,000/t ex. VAT for industrial-grade carbonate in Q2 2016. Lithium hydroxide spot prices witnessed even higher levels.

Contract pricing also rose in 2016, with technical- and battery- grade carbonate prices averaging 29% and 36% higher than 2015 and hydroxide grades 81% and 8% respectively. Spot prices in China started to fall from H2 2016 but staged a small recovery in H2 2017 while contract prices continued to climb. An increase in mine and refined output in 2016 helped restore market balance, at least numerically, but given the delay in final product reaching consumers and most producers remaining sold-out, the squeeze on the market continued into 2017 with contract prices rising further. Whilst refined output exceeded consumption in 2017, prices continued rising as strong demand for product to be consumed in 2018 met varying levels of output on a product basis: hydroxide supply improved, but battery-grade and industrial-grade carbonate remained tight, partly as more of the latter was used for hydroxide conversion.

The theory that battery-grade lithium carbonate typically carries a premium to industrial-grade of around US\$500-1,000/t, due to increased processing (micronization) and, depending on the exact product, the purification steps, is not borne out by average prices derived from the trade data. The trend is likely explained by the structure of contracts between producer and consumer benefitting battery-grade consumers, who have increasingly become the larger buyers, especially in the early 2010s when industrial-grade appears to have had a premium instead. Any premium may also be carried by the subsidiary,

agent or distributor supplying the product domestically, which is not shown when viewing prices on a CIF basis.

Figure 19-11: Average yearly contract and spot prices for lithium carbonate, 2000-2018 (US\$/t CIF)



Source: Roskill, based on trade data; Asian Metal

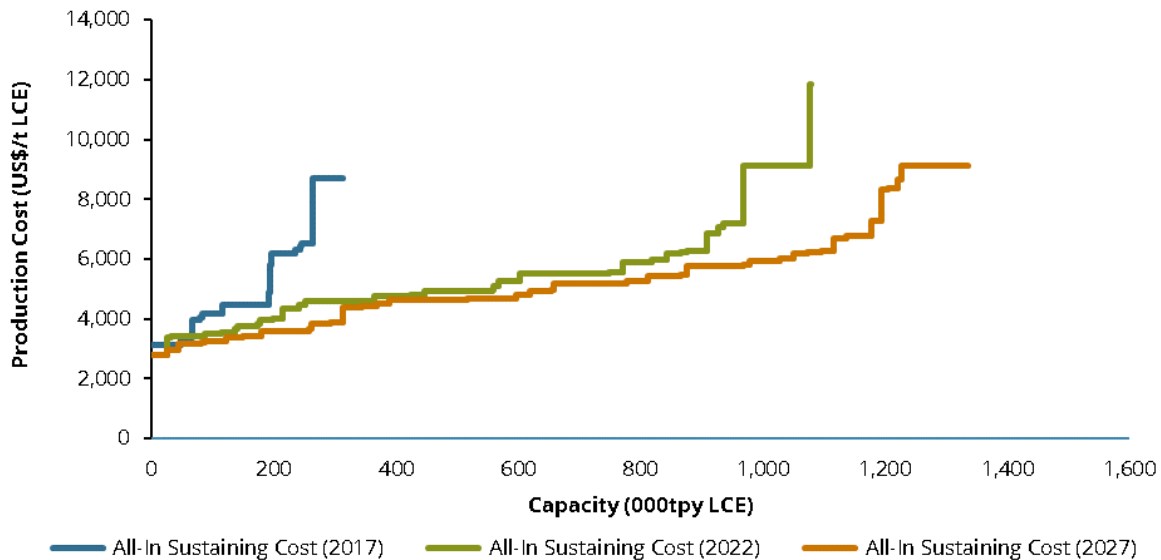
In 2018 to-date, contract prices for lithium carbonate continued rising, but spot prices in China fell. The latter is reportedly due to increased supply, as new/expanded conversion capacity comes on stream, additional brine-based production is available in the market, and lower consumption/demand is noted, partly driven by a change in Chinese NEV subsidies despite continued strong NEV sales. Major lithium producers SQM and Albemarle commented in their earnings that contract prices are expected to peak in 2018 following a peak for spot prices in late-2017.

Roskill's long-term price forecast methodology for lithium carbonate prices is based on the following:

- Future production/margin cost curve
- Incentive pricing for new capacity
- Supply/demand balance and trends

Roskill expects marginal **costs of production** to remain between US\$8,000-10,000/t LCE through 2027 (Figure 19-12), depending on whether the very high cost of lithium compound production from high cost lepidolite, spodumene or DSO-based concentrate at the upper end of the cost curve is justified by a lack of supply from other, cheaper, sources, or lower prices.

Figure 19-12: Lithium cost curve progression, 2017-2027



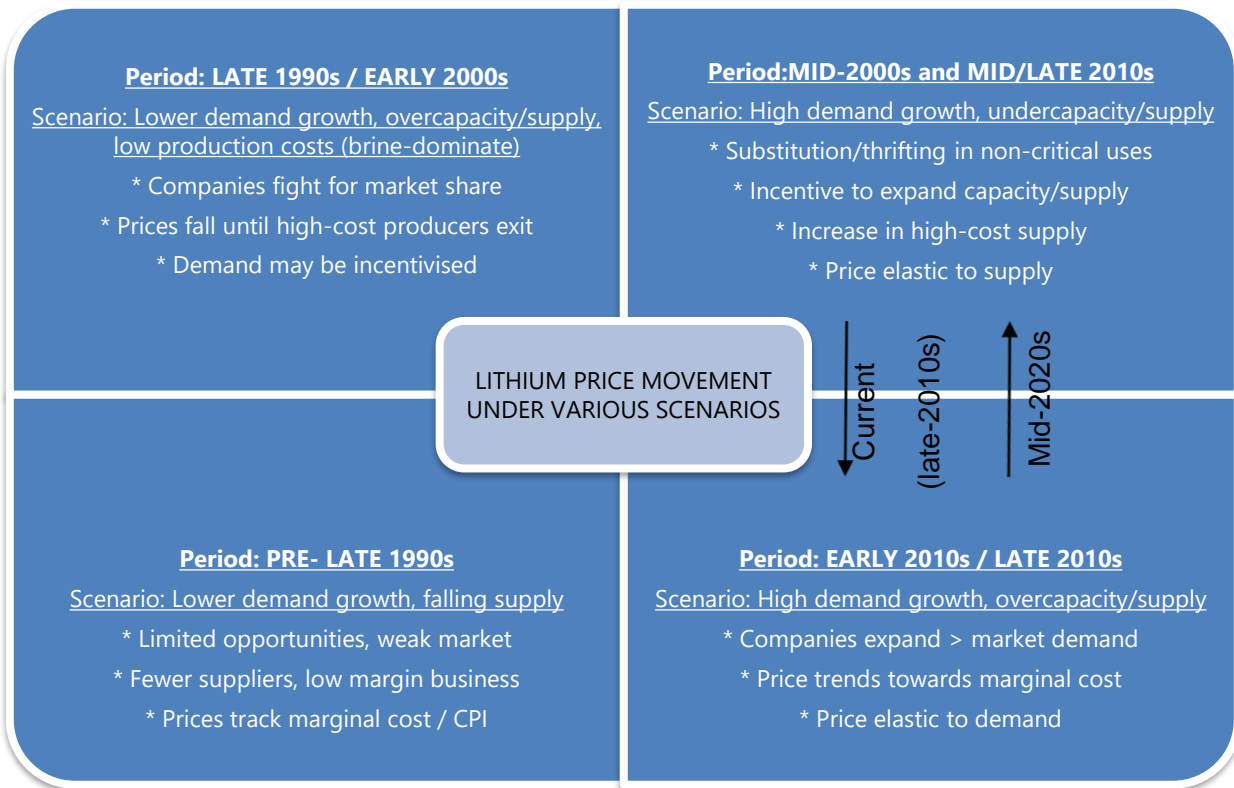
Source: Roskill Lithium Cost Model Service

Roskill has calculated the **incentive price** to bring online a typical brine-refining facility at almost US\$9,000/t LCE, meanwhile an integrated mineral-conversion capacity could be incentivised at a lower US\$7,750/t LCE.

Roskill expects refined output to outstrip consumption growth in the late-2010s and early 2020s (see above), and this **supply/demand imbalance** is expected to weigh on all lithium compound prices. A more significant oversupply of mined production in 2018 and 2019 could precede this and impact spodumene concentrate prices more severely, although as many off-take contracts are linked to the lithium compound price this is by no means certain. Approaching the mid-2020s, annual consumption growth becomes significantly higher in volume terms and will stretch available capacity, the growth of which is still unclear (although expected to track consumption) meaning renewed upside pressure on prices.

The lithium industry is currently adding mine and refined capacity ahead of short-term, but behind long-term, requirements, although the latter is less critical given additional capacity should be added as required in future. More worrying for the industry is that the experiences of 2010-2014 when new projects and expansions were announced and built, but subsequently failed or stumbled, compounded by a lower-price environment than envisioned, could repeat in 2018-2022, impacting longer-term industry development, effectively repeating the cycle.

Figure 19-13: Lithium price movement schematic



Source: Roskill

Despite surging mineral concentrate supply, there will not be such a significant increase in refined output in 2018, as refined producers remain more disciplined to market requirements, and there will be a lag in the processing of the additional mineral feedstock because of conversion capacity opening and ramp-up delays, stocking and qualification time. A large proportion of mineral-based capacity is also held by conversion facility owners; therefore, they will only produce to captive requirements. Roskill expects refined output will increase ahead of base-case consumption, but only slightly ahead of demand (which Roskill estimates equates to one year of the next year's consumption growth, i.e. demand is one year ahead of actual consumption in the lithium market) to restore balance to the market and return confidence after recent shortages.

If consumption and demand increase at the base-case scenario, there will be a small surplus of refined output to consumption in 2018 and 2019, with a potential undersupply situation arising as early as 2020.

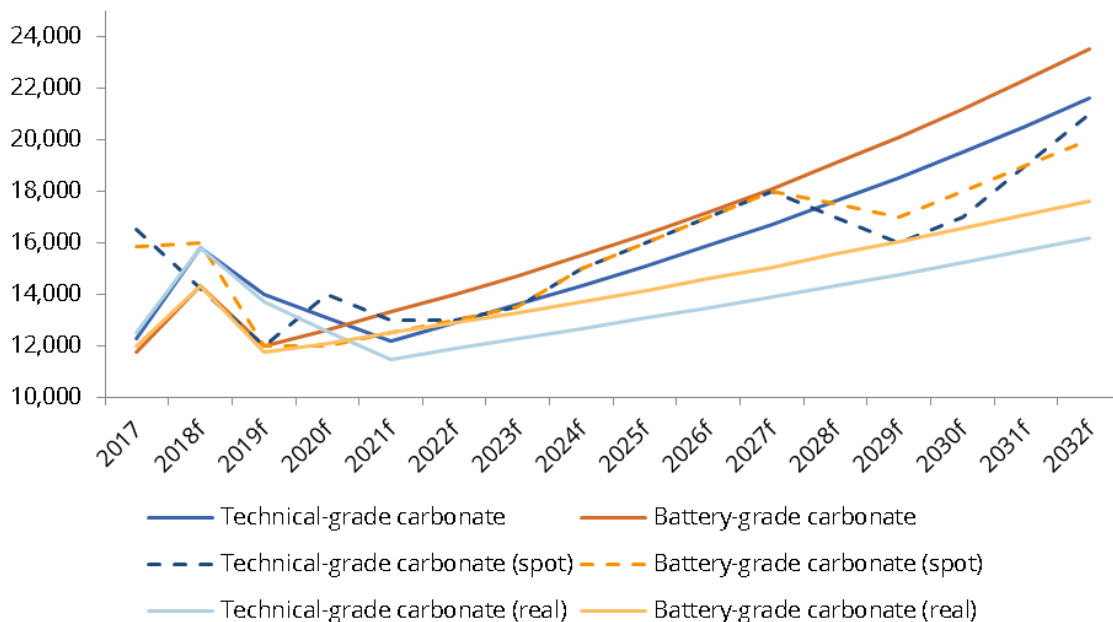
One downside risk is if Chinese converters aggressively process and supply product to the market; this has been a common theme in other mineral/metal products in China, but not yet seen in lithium. There is the potential for oversupply of lithium compounds in 2019-21 in

China as new and expanded mineral conversion and brine operations commission and ramp-up, but given previous delays in project delivery there can be no certainty to this. Any significant over or under supply of lithium compounds in the short-term will be quickly corrected, and into the mid-2020s rapidly increasing annual consumption and demand growth will again stretch capacity. If consumption proceeds at the high-case scenario, the additional supply will be necessary to balance the market.

Roskill forecasts average annual prices for lithium carbonate to remain above US\$10,000/t long-term on both a nominal and real (inflation adjusted) basis and rise to around US\$20-22,000/t in 2032 (around US\$16-18,000/t adjusting for inflation). This price level reflects the requirement for producers to invest in new capacity to satisfy future consumption and to incentivise the financing of new projects (see above). Roskill anticipates a premium re/emerging for battery-grade carbonate in the outlook period. In the short-term, after peaking in 2018, prices are expected to fall slightly to 2020 and then rise again in nominal terms out to 2032.

Note: The prices above and below are Roskill's assessment of where average annual contract prices will settle on a CIF basis. Delivered duty paid (DDP) prices may be higher depending on import duty, agent/distributor/trader premiums and delivery costs.

Figure 19-14: Forecast average yearly contract and spot price trend for lithium carbonate, 2017-2032 (US\$/t CIF)



Source: Roskill

Note: Real prices adjusted to constant 2018 US dollars using World GDP deflator data from the International Monetary Fund's World Economic Outlook Database.

Spot prices, which most typically are based on the Chinese domestic price, could diverge significantly from the average annual CIF contract price dependent upon market conditions, as evidenced by the trend in Asian Metal lithium carbonate prices rising more quickly, to higher levels, and falling in 2018 compared to the contract price since Q4 2015, but as the volume of spot-based sales is small, these quotations have minimal impact on the industry overall. Spot prices are expected to revert to a small premium of US\$500-1,000/t to contract prices over the longer-term.

Table 19-2: Average annual contract and spot price forecast trend for lithium carbonate, 2017-2032 (US\$/t CIF)

	Battery-grade				Technical-grade			
	Contract		Spot		Contract		Spot	
	Nominal	Real (inflation adjusted)	Nominal	Real (inflation adjusted)	Nominal	Real (inflation adjusted)	Nominal	Real (inflation adjusted)
2017	11,729	11,992	15,826	16,180	12,254	12,529	16,526	16,896
2018	14,321	14,321	15,970	15,970	15,805	15,805	14,248	14,248
2019	12,000	11,742	12,000	11,742	14,000	13,700	12,000	11,742
2020	12,600	12,086	12,000	11,510	13,100	12,565	14,000	13,429
2021	13,300	12,504	12,500	11,752	12,200	11,470	13,000	12,222
2022	14,000	12,894	13,000	11,973	12,900	11,881	13,000	11,973
2023	14,700	13,263	13,500	12,180	13,600	12,270	13,500	12,180
2024	15,500	13,699	15,000	13,257	14,300	12,639	15,000	13,257
2025	16,300	14,113	16,000	13,853	15,100	13,074	16,000	13,853
2026	17,200	14,589	17,000	14,419	15,900	13,486	17,000	14,419
2027	18,100	15,039	18,000	14,956	16,700	13,876	18,000	14,956
2028	19,100	15,547	17,500	14,244	17,600	14,326	17,000	13,837
2029	20,100	16,027	17,000	13,555	18,500	14,751	16,000	12,758
2030	21,200	16,560	18,000	14,060	19,500	15,232	17,000	13,279
2031	22,300	17,064	19,000	14,539	20,500	15,687	19,000	14,539
2032	23,500	17,616	20,000	14,992	21,600	16,191	21,000	15,742

Source: Roskill

Note: Nominal forecast rounded to nearest US\$500/t. Real prices adjusted to constant 2018 US dollars using World GDP deflator data from the International Monetary Fund's World Economic Outlook Database

Conditions that may cause the price to rise above the base-case trend include accelerating demand, tightness in market balance or undersupply, and the need to incentivise further, higher-cost, new supply sources. Prices could increase above the base-case especially towards the mid-2020s when significant new capacity will be required. Less predictable

conditions include force majeure at producing assets, a scenario potentially causing prices to go significantly higher over a short period.

There are also down-side scenarios to price, such as slower consumption growth, over-production (through new supply and/or aggressive marketing by new entrants), which could see the price move closer to the low-case forecast or below. Given prices are at, or approaching, historical highs, and balance is being restored to the market, prices are more likely to decrease below the base-case in 2018 and 2019, but with a return to the base-case in 2020.

Expansion potential at Atacama now that SQM and Albemarle have secured increased extraction licenses from CORFO has been cited as potentially creating an oversupply situation and causing prices to fall; however, this is unlikely to happen for a number of reasons:

1. Both companies have announced, and are installing, staged increases to capacity, in particular SQM has announced an expansion to 180,000tpy LCE in the mid-2000s but has only committed resources/investment to expanding to 100,000tpy LCE in 2019. As SQM's permit expires in 2030, the company is unlikely to commit to further capacity unless this timeframe is extended as the project payback may not be sufficient over less than 10 years, even to 180,000tpy LCE. Albemarle has recently suspended its Phase IV and V expansion plans limiting capacity to below 100,000tpy LCE.
2. Both companies are expected to show discipline in supply to prevent an oversupply position that significantly reduces prices and reduces profitability.
3. Brine operations are challenging to operate, and it is unclear at the scale potentially possible if they could be sustained. Roskill expects an upper limit of 100,000tpy LCE for each producer.
4. Both companies have committed to diversification of supply, with investments in Argentina (Albemarle at Antofalla) and Australia (SQM at Mt. Holland and Albemarle with Tianqi at Talison Lithium and Mineral Resources at Wodgina), and these are seen as reducing supply risk but also have longer development paths.

Other price risk factors include:

- **Global economic growth** – A global recession would negatively impact prices as demand, especially from industrial uses, would fall causing consumers to retreat from the market, and vice versa.
- **Changes to the cost of production (labour, energy, raw materials, freight)** – All could have an impact of prices.

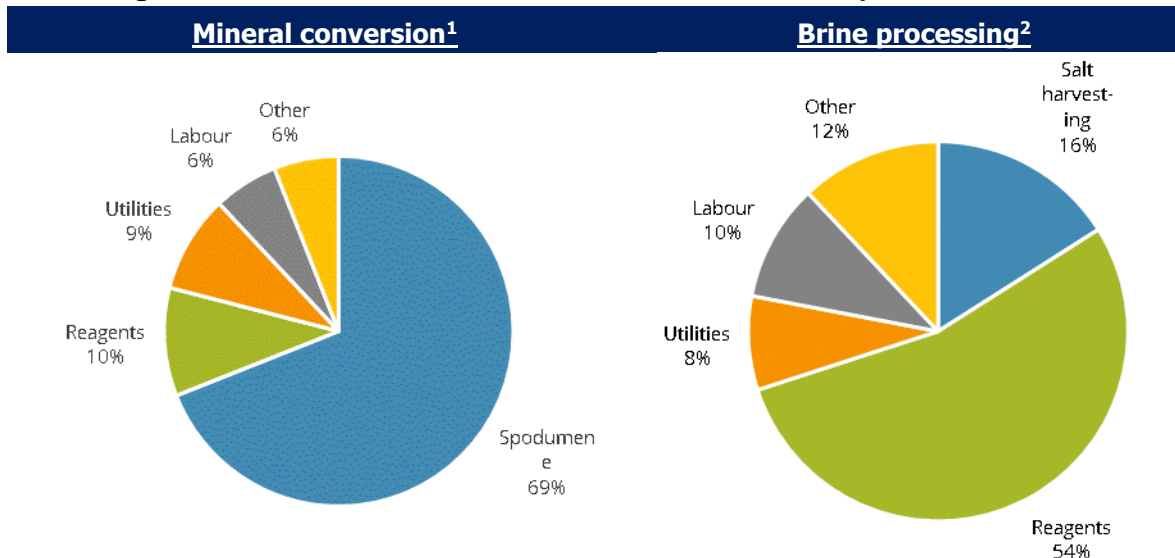
- **Changes to exchange rates** – A weakened RMB should favour domestic China producers and a weakened US dollar vice versa.
- **Capital availability** – Potential new lithium projects, exploration programs and expansion plans could sustain delays or cancellations if sentiment in the wider mining sector worsens for example as a result of another recession.
- **Stockpiling** – Stockpiling of commodities can lead to increases in prices through shortening the available supply to the market. Conversely, if large stockpiles are made available to the world market, prices are likely to fall owing to excess availability.
- **Technological developments** – Despite some new direct brine extraction technologies being developed, these have yet to be commercialised, and therefore the potential of them making a significant impact on lithium prices remain unknown. In the period to 2027 it is unlikely that enough lower cost capacity could come on stream to fundamentally change the cost position and therefore impact prices. On the demand side, new technological developments and products could impact lithium prices should they require large quantities of lithium. This is potentially the case if the automotive (EV) market or grid/off-grid storage (ESS) market expands rapidly and supply cannot keep pace.

19.5 COSTS

Production costs for refined lithium vary principally due to differences between the two main production methods to get to the main products (lithium carbonate and lithium hydroxide) consumed by the market: brine extraction and mineral conversion.

In the standard “Silver Peak” (or Atacama) method to achieve lithium carbonate product from brine, reagents are the main input cost at 54%. For the standard acid-roast mineral conversion route, reagents (sodium carbonate, calcium hydroxide, and calcium carbonate) account for only 11% of cash costs, and spodumene 69% (assuming an average feedstock cost of US\$608/t 6.0% Li₂O content in 2017). Labour costs are lower for mineral conversion, but this excludes the sunk labour cost of spodumene feedstock, ditto utilities and other costs at the mine site and its transport. Approximately eight tonnes of spodumene concentrate are required to produce one tonne of lithium carbonate equivalent.

Figure 19-15: Cash cost breakdown for refined lithium production, 2017



Source: Roskill; Hatch

Note: 1 – Standard acid roast conversion process using sulphuric acid and sodium carbonate in a continuous plant; US\$608/t spodumene concentrate cost

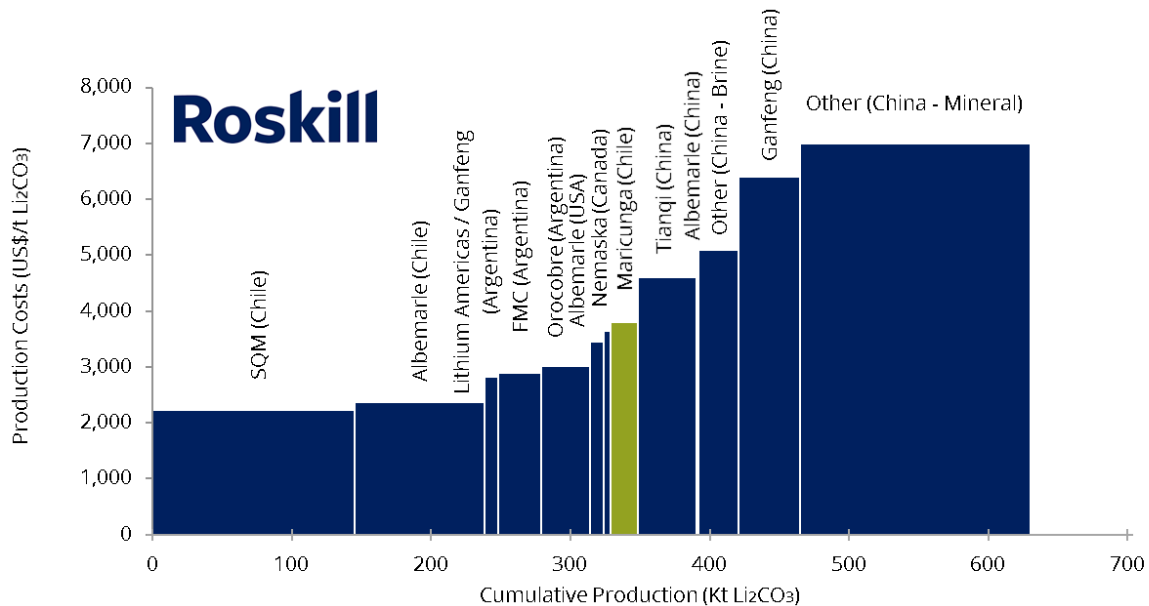
2 – Standard “Silver Peak” processing method using sodium carbonate in a continuous plant (e.g. Silver Peak or Atacama operations)

Americas brine producers (SQM, Albemarle, FMC and Orocobre) enjoyed the lowest lithium carbonate production cash costs in 2018 because of their lower energy intensity brine-based extraction methods and, for SQM and Albemarle, potash by/co-product revenue. Chinese brine producers had slightly higher costs than their Americas competitors. Chinese mineral converters, for example Ganfeng, have the highest costs as the price of their spodumene concentrate has risen to average around US\$900/t in 2018.

The shape of the cost curve for lithium carbonate production in 2027, and the position of various producers, is not expected to change dramatically from 2018 (Figure 16). Ganfeng and other mineral converters reliant on related-party or third-party spodumene concentrate will exhibit the highest costs, although their costs will fall from 2018 with a predicted decline in spodumene concentrate prices versus lithium carbonate prices.

Note: Production cash costs below show only include all direct and indirect operating costs related directly to the physical activity of producing a refined lithium compounds, including feedstock costs (either from external or internal sources measured using the total cash cost (but excluding royalty payments), refining, on-site general and administrative costs and selling expenses). They do not include costs associated with corporate-level administrative expenses, sustaining capital expenditure or royalties.

Figure 19-16: Lithium carbonate cash cost curve, excluding royalties, 2027 (US\$/t)



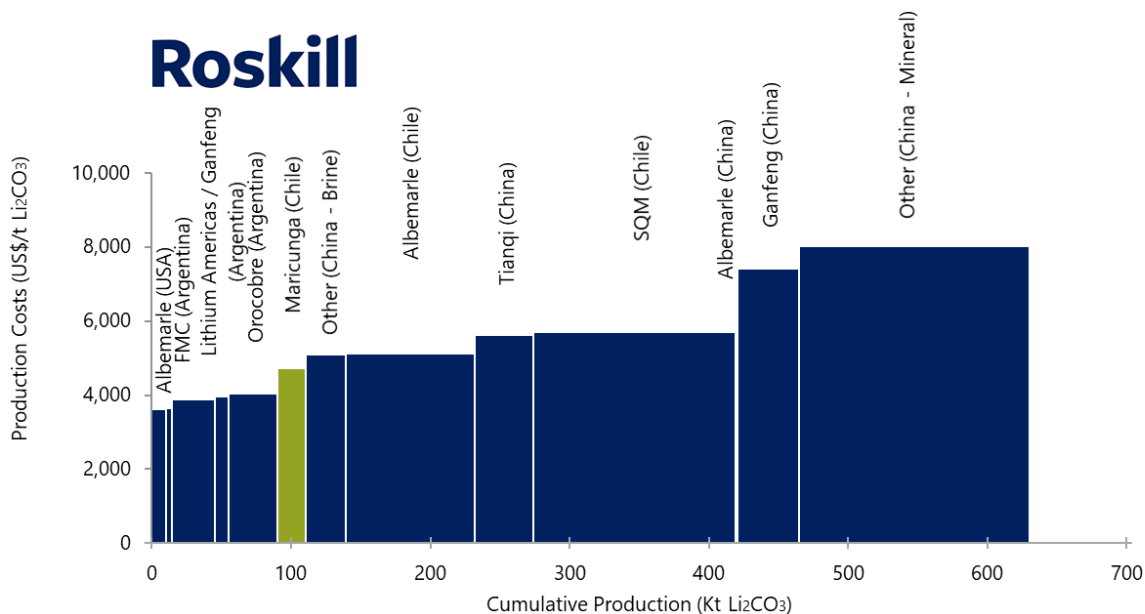
Source: Roskill - Lithium Cost Model Service

Notes: Battery and technical grades; SQM & Albemarle costs assume potash cost share methodology; Spodumene concentrate costs are based on those forecast by Roskill' for the respective years of the forecast; as such the cost presented here for Tianqi Lithium, Albemarle (China) and Ganfeng Lithium are inflated by the fact that a portion of the profit margin is incorporated within the spodumene feedstock cost which is sourced from their subsidiary mining companies.

SQM and Albemarle's total cash costs have increased in 2018 through the introduction of new royalty/leasing agreements with Corfo, since Corfo are the owners of the mining concessions they exploit. The royalty can reach up to 40% when the product sale price exceeds US\$10,000/t. With forecast prices above US\$10,000/t royalties for these producers will increase their overall cash costs and substantially flatten the cost curve making projects not subject to such high royalties elsewhere in Chile, Argentina and China more cost competitive (Figure 19-17 and Figure 19-18).

Blanco Project is the owner of the mining concessions in Maricunga and not subject to this Corfo royalty agreement.

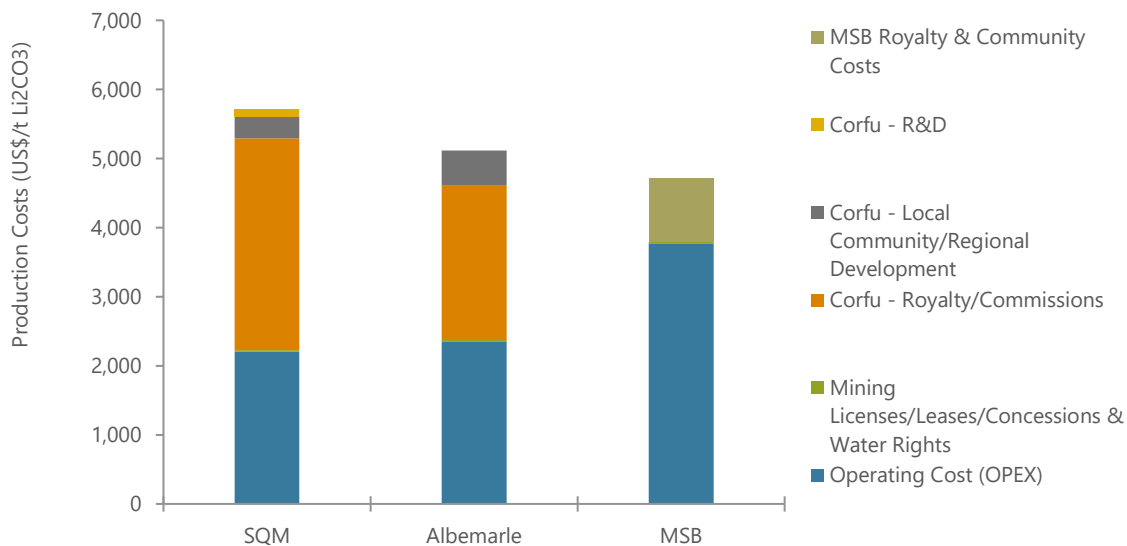
Figure 19-17: Lithium carbonate cash cost curve, including royalties, 2027 (US\$/t)



Source: Roskill - Lithium Cost Model Service

Notes: Battery and technical grades; SQM & Albemarle costs assume potash cost share methodology; Spodumene concentrate costs are based on those forecast by Roskill' for the respective years of the forecast; as such the cost presented here for Tianqi Lithium, Albemarle (China) and Ganfeng Lithium are inflated by the fact that a portion of the profit margin is incorporated within the spodumene feedstock cost which is sourced from their subsidiary mining companies.

Figure 19-18: Lithium carbonate production cost in Chile, including royalties, 2027 (US\$/t)



Source: Roskill - Lithium Cost Model Service

Notes: Battery and technical grades; SQM & Albemarle costs assume potash cost share methodology; Spodumene concentrate costs are based on those forecast by Roskill' for the respective years of the forecast; as such the cost presented here for Tianqi Lithium, Albemarle (China) and Ganfeng Lithium are inflated by the fact that a portion of the profit margin is incorporated within the spodumene feedstock cost which is sourced from their subsidiary mining companies.

20. ENVIROMENTAL STUDIES, PERMITTING AND SOCIAL OR COMMUNITY IMPACT

20.1 ENVIRONMENTAL STUDIES

MSB hired Stantec in November 2016 to carry out a Baseline Study of the project, including development of an environmental impact assessment report (“Estudio de Impacto Ambiental Proyecto Blanco” (EIA)), which was submitted to the Environmental Assessment Service (EAS) in September 2018 and is currently under evaluation.

The 2018 EIA also includes the construction and operation of a KCI plant, while this FS specifies a lithium carbonate plant only.

The baseline study covers the project site area and the main routes that will be used by the project during construction and operation.

The baseline study includes: climate and meteorology, air quality, noise and vibrations geology, geomorphology and natural risks, hydrology, hydrogeology, water balance, soil, flora, fauna, archaeology, landscape, tourism and facilities and human environment.

20.2 ENVIRONMENTAL BASELINE STUDY

A summary of the environmental baseline studies and monitoring activities are described as follows.

20.2.1 Climate and Meteorology

MSB installed a weather station at the site in November 2016 and continues to operate the station. The data generated by the weather station is as follows:

- Average temperature for the period January-December 2017 corresponds to 1.5°C, with maximum monthly average values around 10°C in summer, and minimum monthly average temperatures of -8°C in winter.
- The annual average atmospheric pressure is 481 mm Hg.
- Wind annual speed average is 5.6 m/s with predominant wind direction North and Northwest.
- Freshwater maximum evaporation is 11.3 L/m² (January).
- Saltwater maximum evaporation is 8.2 L/m² (January).
- Snow levels were recorded in the months of August and September of 2017, at depths of 8.6 cm and 4.3 cm, respectively.
- Average precipitation for all basins, at 3,890 m above sea level (asl), is 116.4 mm.

- Solar Radiation depends on the seasons, with average values over 300 W/m^2 between the months of October and March, reaching a maximum average of 385 W/m^2 during December and a minimum average of 170 W/m^2 in June.

20.2.2 Air Quality

Air quality was measured with MSB's air quality monitoring station, which was installed with the weather station (Figure 20-1). The air quality conditions in the area surrounding the Project site do not show any latency or saturation levels, as no emitting sources exist in the area. According to the measurements between January 2017 to December 2018, the average breathable particulate material (PM) in the project area are as follows:

- $\text{PM}_{10} = 12.3 \mu\text{g/m}^3\text{N}$.
- $\text{PM}_{2.5} = 2.3 \mu\text{g/m}^3\text{N}$.

Figure 20-1: Weather and Air Quality Monitoring Station – MSB



Source: MSB

20.2.3 Noise

Background noise levels were measured at the Project Site and at the roads that will be used by the project (Figure 20-2). Measurements for fauna sensitive receptors were conducted only at the site and the Salar. (Figure 20-3).

The potential sensitive noise receivers in the project area are the existing border crossing facility “Complejo Fronterizo San Francisco”, the project future camp and the communities that are adjacent to the routes that will be used by the project. Background noise levels were recorded for human receptors, as follows:

- Human receptors: During the day, the Continuous Sound Pressure Level (Leq) of background noise obtained fluctuates between 34 and 71 dBA and during the night, it fluctuates between 31 and 63 dBA.
- Fauna receptors: The measurements were lower than the referenced 85 dBZ, an international used reference to determine effects on wild fauna.

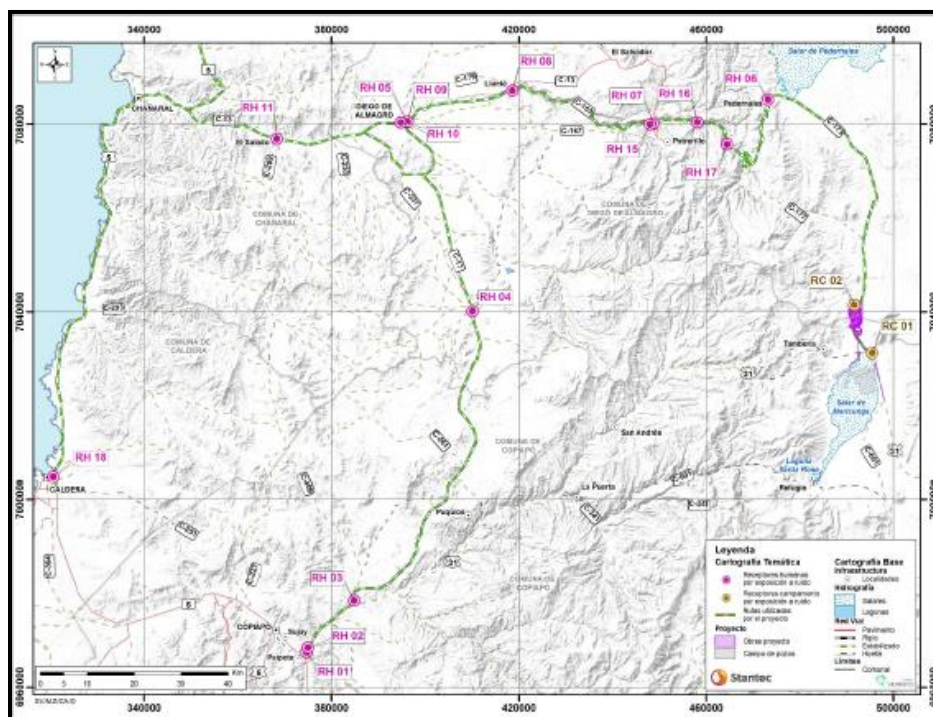
In addition, sound pressure level projections on sensitive receivers (both human and fauna) living in the area, were conducted for the EIA.

20.2.4 Vibrations

Background vibration measurements were conducted to obtain vertical acceleration. These measurements were recorded at the same measurement point for noise. All measurements were below the threshold of human perception.

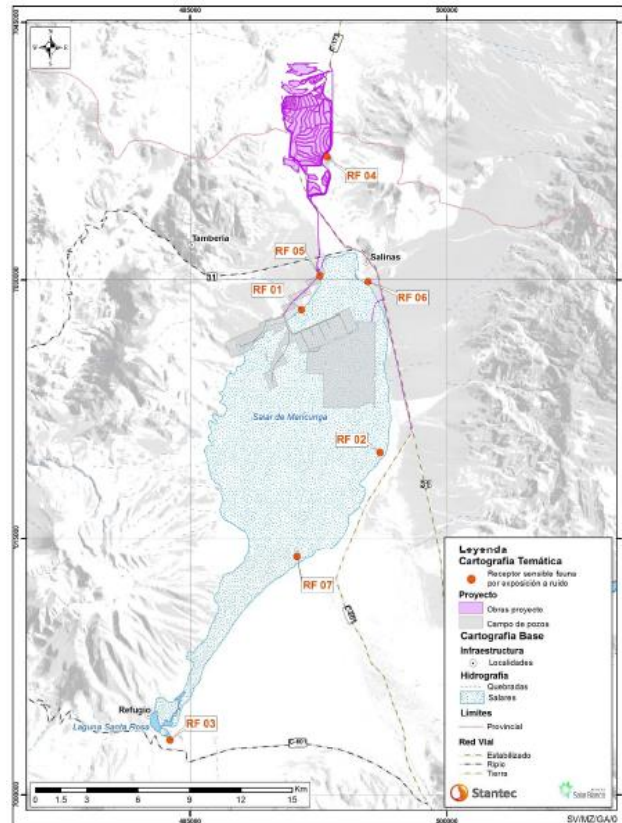
In addition, vibration projections that were recorded for the EIA, were below the threshold of human perception.

Figure 20-2: Measurement Locations for Noise and Vibration for Humans



Source: Stantec

Figure 20-3: Measurement Locations for Noise and Vibration for Fauna



Source: Stantec

20.2.5 Geology, Geomorphological and Geological Risks

The local geology of the Project area is comprised mainly of alluvial deposits from fans composed of gravels and blocks of low rounding. A detail description of the geology of the Salar is presented in section 7.2 Local Geology of this FS report.

The geomorphological pattern corresponds to the geomorphological unit called "*Salares Trench Prealtiplánicos*", in which forms of lithostructural modeling and water and fluvial modeling were identified, as well as forms of gentle slopes and the salar depression.

The geological risks identified include earthquakes, volcanic activity and morphodynamical processes, such as floods and mud or debris flows.

20.2.6 Soils

MSB conducted an edaphological study, which included the excavation of test pits to characterize the soil profile, texture and structure at the project site. It was determined that the soil is comprised mainly of sands with gravel from the alluvial fan. The gravels are mostly

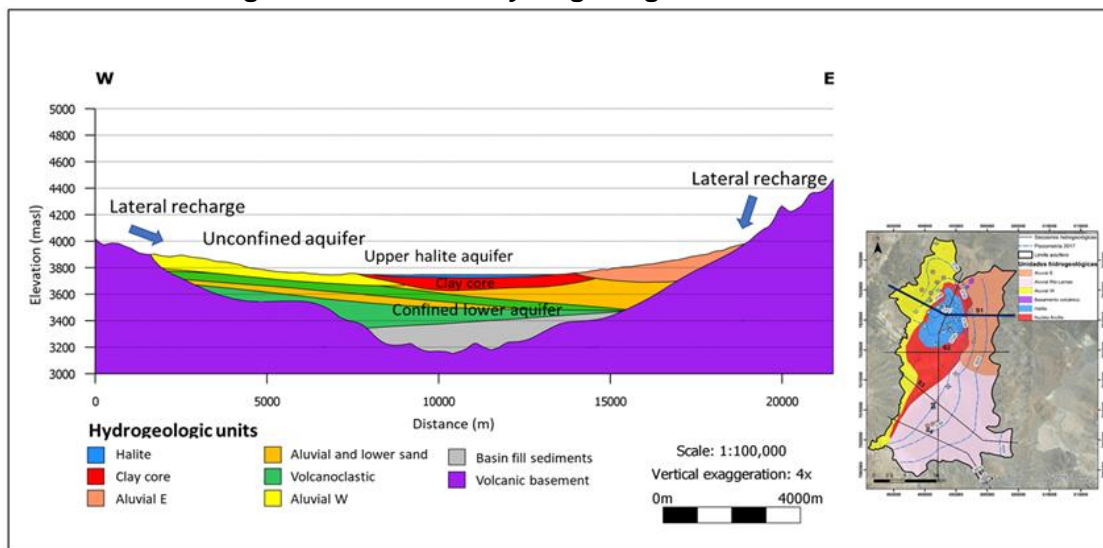
angular due to sand friction and erosion. Topsoil is minimal and therefore unable to support vegetation. There are, however, certain sectors located at the edges of the Salar de Maricunga which accumulate fine material and water due to poor drainage; these sectors do support endemic vegetation.

20.2.7 Hydrogeology and Water Balance

The Salar is the topographic low point within the Maricunga Basin and is surrounded by alluvial fans, which drain into the Salar. The floor of the Salar in the north and northeast is composed of chloride facies consisting of flat halite crust (more recently flooded) and coarse irregular and pinnacle shaped halite blocks (absence of recent flooding). The floor of the Salar in the southeast is composed of boric and sulphate facies. In the center of the Salar, the water table can be within approximately 5 cm of the surface.

The drilling and test results from previous explorations for freshwater resources in the Salar and surrounding alluvial fans, by MSB and other companies, suggests the occurrence of several hydrogeological units of importance. Figure 20-4 presents the hydrogeological cross-section of the Salar, showing the principal hydrogeologic units.

Figure 20-4: W-E Hydrogeological Cross-Section



Source: FloSolutions

20.2.8 Water Balance

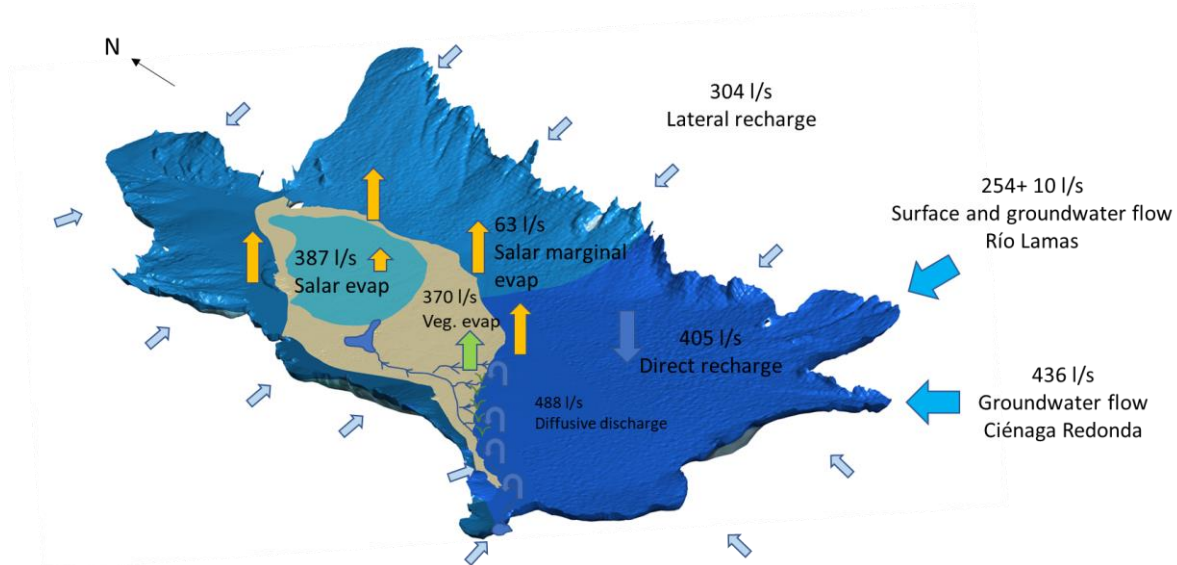
A water balance for Salar de Maricunga was prepared by FloSolutions, showing the general surface and groundwater flow patterns in the Salar de Maricunga watershed (Figure 20-5). Surface water flow generally occurs only at higher ground and infiltrates into the more permeable alluvial fan and sediments surrounding the Salar before reaching the Salar floor. The only surface water flow that occurs on the Salar floor is the natural discharge from

Laguna Santa Rosa, from the north towards the center of the Salar. There is no surface water outflow from the Maricunga watershed.

Groundwater flow patterns closely follow the surface water flow patterns. There are no known groundwater outflows from the Maricunga watershed. The majority of the recharge to the Salar de Maricunga basin occurs through the direct infiltration of precipitation. The total average annual recharge to the Salar de Maricunga basin is estimated at 1,409 L/s.

Discharge from the Salar de Maricunga basin is through evaporation, evapotranspiration and groundwater pumping. The total average annual discharge through evaporation has been estimated at 1,348 L/s.

Figure 20-5: Water Balance for the Maricunga Watershed



Source: FloSolutions

The hydrogeology and water balance of Salar de Maricunga have been described in detail in Sections 8 and 15 above.

20.2.9 Archaeological Heritage and Paleontology

A total of 51 archaeological monuments (AM) were detected during the baseline study, 12 of which were assigned to the pre-hispanic period, 8 to the historical period and 30 registered as indeterminate.

A paleontological desktop study was completed, resulting in the identification of a geological unit (*Los Chinchies formation*) with the potential for geological remains. During prospecting, no geological remains were discovered. This area has been classified as a susceptible zone.

In the geological unit of recent alluvial deposits, remains were identified that belong to a Jurassic marine unit that emerges approximately 10 km from the place of origin. This unit was classified as a fossiliferous unit.

20.2.10 Landscape

Two landscape units, UP1 and UP2, were identified (Figure 20-6). The visual quality of the UP1 landscape is highlighted in the Salar de Maricunga, with unique biophysical and structural attributes. The second landscape unit (UP2) is considered to be of average visual quality, since it presents more homogeneous characteristics and does not have any features that diminish the visual quality of the landscape. Based on the above analysis, the Project is considered to be in an area that has visual landscape value.

Figure 20-6: Landscape Units UP1 and UP2



Source: Stantec

20.2.11 Protected Areas and Natural Attractions

The area surrounding the project site is part of the main tourism circuit of the region, due to the interesting landscape and attractions. From a tourism perspective, several attractive areas were noted and classified into two groups by Sernatur, the Chilean government agency for tourism, as follows:

- Protected Areas and Priority Sites for Conservation
 - National Park Nevado Tres Cruces; and
 - Ramsar Complex Site Laguna del Negro Francisco and Laguna Santa Rosa.
- Natural or Cultural Attractions
 - Zones of Tourist Interest (ZOIT) - Salar de Maricunga and Ojos del Salado;

- Priority Tourism Areas (PTA) - Ojos del Salado in the Cordillera de Atacama and Desierto y Puna in the Atacama Desert.
- “Route of the Six Thousand” - a tourist Route developed by Sernatour that has more than twenty peaks above 6000 m asl and has the highest active volcano in the world (Ojos del Salado) at 6,893 m asl;
- Scenic Routes - A section of the Patrimonial Route N° 26 “El Derrotero de Atacama” and a section of the “Path of Chile”; and
- Hot Springs - Laguna Verde and Cascadas del Río Lamas.

20.2.12 Territorial Use and Planning

On a regional level, the majority of the territory does not have any current land use. The land use is categorized as follows:

- 50.88% of the land is categorized as “Use VIII”, which means it has no agricultural, livestock and/or forestry value; and
- 49.12% of the land is un-categorized.

The soil on the edges of the Salar de Maricunga was identified as Category V, which means it is very susceptible to flooding.

The Community Development Plans (PLADECOS) for the Copiapó and Diego de Almagro districts, highlight mining for Copper, Gold and Silver as part of the main economic activities for these districts. Mining is the main livelihood of the populated centers of Diego de Almagro and El Salado.

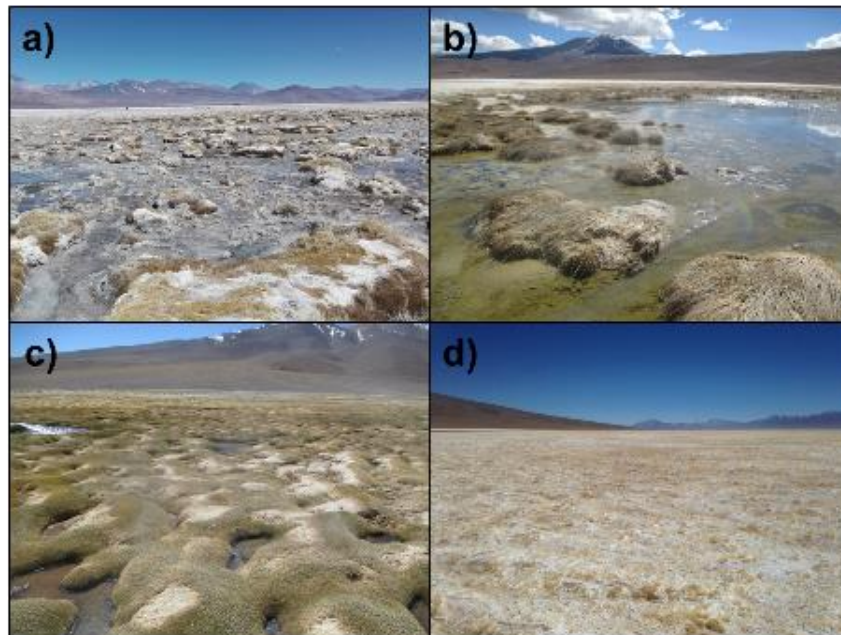
20.2.13 Flora and Vegetation

According to the flora and vegetation characterization results of the study area, 29 species were detected, of which 60% are grassy brush, 38.7% are bushes and 20.2% are endemic (grassy meadows and wetlands).

Most of the vegetation is found on the shore of the Salar de Maricunga. The most important are the endemic vegetation, of which 7.8 ha are grassy meadows and 12.4 ha are wetland vegetation (Figure 20-7). This 20.2 ha corresponds to 0.12% of the total study area.

Within the project area of influence, there are no flora or vegetation species under the official conservation category. Some protected species have been recorded near the Santa Rosa Lagoon, but they will not be disturbed by the project, as there will be no development activities close to this sector.

Figure 20-7: Endemic Vegetation on Shore of Maricunga Lake



a) Formation of isolated individuals and groups of species within the unit; b) Damaged wetlands formation surrounded by water; c and d) Homogenous formations of the vegetation coverings (bare soil, water and halite between the vegetation cover). Source: Stantec

20.2.14 Fauna

According to the fauna characterization results, a total of 37 species were recorded (two (2) reptiles, 25 birds and 10 mammals). Of these, 15 species are considered in some state of protection, as shown in Table 20-1.

Table 20-1: Endangered Species

<p>Critically Endangered: Supreme Decree No. 13/2013 of the MMA (Environment Ministry). <u>Mammalia</u> <i>Chinchilla Chinchilla</i></p>
<p>Endangered: Hunting Law Regulation (Supreme Decree No. 5/1998 of Minagri) and Supreme Decree No. 33/2012 of the MMA. <u>Mammalia</u> <i>Lama guanicoe</i> <i>Vicugna vicugna</i></p>
<p>Vulnerable category: Supreme Decree No. 33/2012; N°52/2014; N°16/2016, N°38/2015 of MMA and Supreme Decree No. 5/1998 of the Minagri. <u>Reptilia</u> <i>Liolaemus patriciaturrae</i> <i>Liolaemus rosenmanni</i> <u>Mammalia</u> <i>Ctenomys fulvus</i></p>

Birds

Tinamotis pentlandii
Chroicocephalus serranus
Phoenicoparrus andinus

Near threatened: Supreme Decree No. 42/2011 of the MMA

Mammalia

Puma concolor

Minor Concern category: Supreme Decree N° 33/2012 and. N°38/2015 MMA

Mammalia

Lycalopex culpaeus

Birds

Attagis gayi

Oressochen melanopterus

No immediate priority: pursuant to the Hunting Law Regulation (Supreme Decree No. 5/1998 of the Minagri):

Mammalia

Phyllotis xanthopygus

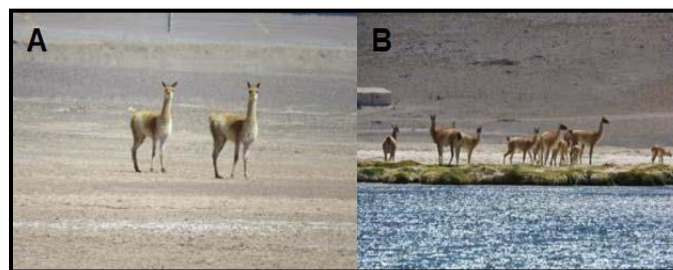
Abrothrix andina

Figure 20-8: Vulnerable Reptiles



A) *Liolaemus rosenmanni* (lagartija de Rosenmann)
B) *Liolaemus patriciaiturrae* (Lagartija de Patricia Iturra).

Figure 20-9: Endangered Mammals



A) *Vicugna* (vicuña); B) *Lama guanicoe* (guanaco);

20.2.15 Aquatic Continental Ecosystems

The following aquatic organisms are present in the lagoons of the Maricunga salt lake:

- Phytobenthos: Bacillariophyceae class;

- Zoobenthos: Harpacticoida class;
- Diatoms: 48 species recorded (Nitzschia, Amphora, Pseudostaurosira and Navicula class);
- Plankton: Harpacticoida; and
- Phytoplankton: Bacillariophyceae class.

20.2.16 Human Environment

The influence area of the Project for the human component includes the districts of Copiapó, Diego de Almagro, Caldera and Chañaral, in the region of Atacama and, the communities of Antofagasta, Mejillones and María Elena, in the region of Antofagasta.

At a local level three Indigenous Colla Communities were identified in the district of Diego de Almagro whose, relationship with the Project, is the use of existing roads that cross through the territories.

The Colla indigenous community mentioned above correspond to, Colla Chiyagua, Colla Quebrada El Jardín, and Colla Geoxcultuxial. The Colla communities use the pastures, flooded meadows and areas with plenty of potable water for pasturing their livestock. The Colla have traditionally built their homes adjacent to these areas, which include the road C-173 that is the main project road.

The main activities and ethnic group for each district can be summarized as follows:

Atacama Region:

- **Copiapó:** the primary and traditionally activities are mining, agriculture and artisanal fishing. Tourism is also becoming an important activity
- **Diego de Almagro:** the most important economic activities are mining of copper, silver and gold, and small commerce. In terms of identity, two elements identify this community, the first one is linked to the activity mining, the second the presence of the Colla ethnic group.
- **Chañaral:** the most important economic activities are mining and artisanal fishing. The largest group of indigenous communities are the Diaguita, which represent 3% of the communal population.
- **Caldera:** the most important economic activities are tourism and artisanal fishing.

Antofagasta Region:

- **Antofagasta:** The city of Antofagasta is closely linked to mining activity, being the primary major mining area of the country. The last decade has seen a steady

growth in the areas of construction, retail, hotel accommodations, population growth, and remarkable skyline development.

- **Mejillones:** is approximately 65 kilometers from the city of Antofagasta and has a close relationship with it.
- **Maria Elena:** stands out for being the last active nitrate office in the country.

20.3 WASTE AND TAILING DISPOSALS

Different types of precipitated salt will be harvested during the ponds evaporation process and transported to stockpiles for storage. Halite salts will be stored in a separate stockpile; whereas, sylvanite and carnallite will be stockpiled together for use in the future Potash Plant (not incorporate in this study).

Waste generated by the Salt Removal Plant includes calcium chloride-tachyhydrite salts, which are transported by truck from the salt removal plant and stockpiled.

The estimated amount of salt to be harvest during the entire Project operation phase is approximately 22,876,900 m³ of halite salt and 7,009,300 m³ of calcium chloride-tachyhydrite salts. For more information of the waste of the evaporation process and lithium production see Chapter 17.

The waste generated by the project (domestic, construction, maintenance, non-hazardous and hazardous waste) will be handled in accordance with the current regulations of Chile.

20.4 EVALUATIONS OF IMPACTS IDENTIFIED IN THE EIA

To predict and evaluate the impacts of the project it is necessary to quantify the direct and indirect changes to the elements described in the baseline study. Depending on the degree of change, it can result in non-impact, non-significant impact or significant impact.

The project has 23 non-significant impacts, which relate to the construction and operation phases, as follows:

- Construction (C): Air quality, Soil, flora and vegetation, fauna, archeology, paleontology, landscape, natural and cultural attractions, use of roads and human environment.
- Operation (O): Air quality, landscape, use of roads and human environment.

There are six (6) significant impacts. Each environmental component affected is linked to the phase of the project in which it occurs, as presented in Table 20-2.

Table 20-2: Significant Environmental Impacts

N°	Component	Phase	Name of Impact
1	Fauna	C	Loss of fauna specimens of low and medium mobility

2	Archeology	C	Alteration of archaeological monuments
3	Landscape	O	Visibility obstruction to an area with landscape value
4	Landscape	O	Attribute alterations of an area with landscape value
5	Human Environment	C	Alteration of livestock grazing; a traditional practice
6	Human Environment	O	Alteration of livestock grazing; a traditional practice

For these impacts, MSB has designed a Mitigation and a Compensation Plan that contains a total of 12 actions, as presented in Table 20-3.

Table 20-3: Mitigation and Compensation Plan

Component	Mitigation Plan
Fauna	<ol style="list-style-type: none"> 1. Relocation plan for reptiles and mammals 2. Restriction of habitat intervention areas 3. Controlled disturbance on low mobility fauna 4. Staff training plan
Archeology	<ol style="list-style-type: none"> 1. Staff training for protection of the archaeological heritage 2. Transitory protection of archaeological heritage 3. Permanent protection of some of the archaeological sites
Human Environment	<ol style="list-style-type: none"> 1. Multidisciplinary plan to mitigate effects on livestock grazing and traditional practices of indigenous communities
Archeology	<ol style="list-style-type: none"> 1. Archaeological Monuments Management Plan 2. Plan to inform communities of the archaeological cultural heritage
Landscape	<ol style="list-style-type: none"> 1. Construction of a site view point with parking and information panels

20.5 VOLUNTARY COMMITMENTS SPECIFIED IN THE EIA

The Project includes 22 voluntary commitments, as described in Table 20-4.

Table 20-4: Voluntary Commitments

Item	Voluntary Commitment	Description
Physical Environment		
1	Air Quality Monitoring	Air Quality will be monitored (MP10 and MP2.5) during Project construction and operation in Blanco Camp, Wetland extraction wells area, Pastos largos area, National Park Nevado Tres Cruces Limit, Santa Rosa Lagoon Sector.
2	Noise Level Monitoring	Noise will be monitored at the same locations that were monitored in the baseline study to compare the prediction with the real operation. These locations have human and fauna receptors that could possibly be affected by the project if the norm is exceeded.
3	Vibrations Monitoring	Vibration will be monitored at the same locations as the baseline to compare the prediction with the real operation. These locations have human and fauna receptors that could possibly be affected by the project if the norm is exceeded.
4	Hydrogeology Monitoring	A Sustainable Operation Program (SOP) will be implemented to verify the Hydrological Model pumping effects predictions. The SOP will enable

Item	Voluntary Commitment	Description
		actions to be implemented to correct any deviations in the model and optimize operation to avoid environmental impacts.
Terrestrial Ecosystems		
5	Ecosystems Monitoring in the wetlands area	Monitoring includes an analysis of the biodiversity of the aquatic biota and physical-chemical characterization of the aquatic (limnological characterization), flora and vegetation and fauna in the wetlands area
6	Ecosystems Monitoring in Laguna Santa Rosa	Monitoring includes an analysis of the biodiversity of the aquatic biota and physical-chemical characterization of the aquatic (limnological characterization), flora and vegetation and fauna in the Laguna Santa Rosa
7	Chinchilla Study	A Study of the Chinchilla habitat will be carried out to expand the knowledge of the habitat near the Project area.
Cultural Heritage Archeological		
8	Archeology monitoring	Permanent archaeological monitoring with supervision and surveillance during earthworks construction.
9	Archeological site protection	Physical protection of archaeological sites through the installation of perimeter fences and permanent signage, indicating and protecting their presence.
10	Paleontological protection plan	Staff training program about paleontological heritage and procedures.
11	Paleontological relocation plan	Paleontological monuments will be relocated to a museum in Atacama Region.
12	Paleontological monitoring	Permanent paleontological monitoring with supervision and surveillance during earthworks construction.
Roads and Traffic		
13	Staff training	Staff training on roads and security rules for driving the project routes.
14	Service level monitoring	It will be verified that road service levels do not decrease as a direct consequence of Project vehicle transit.
15	Road control	Strengthening of road signs and speed control in certain areas of the road.
16	Vehicles	Vehicles will include GPS and registration cameras.
Human Component		
17	Local communities	Share 0.3% of sales to the community in Diego de Almagro, Chañaral and Copiapo
18	Indigenous Communities	Share 0.3% of sales to the Indigenous Colla community.
19	Colla's territories	Installation of roadside signs with indigenous pertinence and improvement of settlements in Colla's communities.
20	Environmental monitoring	Flora, fauna, limnology, air and water quality will be monitored in Pastos Largos (relevance sector for the Colla Communities).
21	Support in infrastructure	Support infrastructure and laboratory equipment for the local schools: Liceo Polivalente Federico Varela in the municipality of Chagnaral and Liceo Manuel Magalhaes Medling in the district of Diego de Almagro
General		
22	Informative Plan	Develop informative material for the community related to the environmental component present in the area: flora, fauna, archeology

Item	Voluntary Commitment	Description
		and landscape and a brief explanation of the process of the lithium carbonate.

21. CAPITAL AND OPERATING COST

21.1 CAPITAL COST ESTIMATE

21.1.1 Capital Expenditures – CAPEX

Capital expenditures are based on an operating capacity of 20,000 tonnes of lithium carbonate per year. Potash production, which had been considered at the PEA stage has been put on-hold because current conditions in this particular market are not favorable, in addition enough sylvinite and carnallite salts to operate a potash plant are naturally produced in the ponds, and are harvestable from year 4 onwards, MSB will review the decision to build a potash plant a few years into the future. For this reason, at this stage all MSB efforts are being concentrated on lithium carbonate production, for which demand is expected to continue growing at a fast rate, as examined in Section 19 of this report.

Capital equipment and construction costs have been obtained from solicited quotes to equipment manufacturers and construction companies. As indicated on Sections 16 through 18, considerable engineering progress has been achieved both on plant design and infrastructure requirements. Given this, WorleyParsons give an accuracy of this estimate within a +/- 15% range.

Capital and operating costs estimates are expressed in fourth quarter 2018 US dollars. No provision has been included to offset future cost escalation since expenses, as well as revenue, are expressed in constant terms.

The capital costs estimate includes direct and indirect costs for:

- Brine production wellfields and pipeline delivery system.
- Evaporation ponds
- Salt removal plant
- Lithium carbonate plant
- General services
- Infrastructure

The capital investment for the Blanco Project, including equipment, materials, indirect costs and contingencies during the construction period is estimated to be US\$ 563 million. This total excludes interest expenses that might be capitalized during the same period. Out of this total Direct Project Costs represent US\$ 456 million; Indirect Project Costs represent US\$ 45 million, and the provision for Contingencies is US\$ 63 million. The former representing 8.0% of total project costs, while the latter is 11.1% of total project costs.

Working capital requirements over the project horizon averages US\$ 20 million; in addition, sustaining capital expenditures total US\$ 53 million over the 25-year evaluation period of the project, which includes a 3-year construction period and an operating life of 22 years.

Total capital expenditures are summarized in Table 21-1.

Table 21-1: Total Capital Expenditure

Area	1000 Brine Extraction Wells	Projected Budget 000 US\$
	Direct Costs	
1000	Brine Extraction Wells	39,374
2000	Evaporation Ponds	115,346
5000	Salt Removal Plant	66,438
6000	Lithium Carbonate Plant	71,622
8000	General Services	103,267
9000	Infrastructure	60,009
	Total Direct Cost	456,056
	Total Indirect Cost	44,831
	Contingencies (12,5%)	62,611
	Total	563,498

21.1.2 Brine production wellfield and pipeline delivery system

A brine production wellfield with a summer maximum production capacity of 330 l/s will be constructed in the Salar as described in Section 16. This wellfield will consist of 12 production wells each with a pumping capacity between 12.5 l/s and 27.5 l/s. Brine discharge from each wellhead is conveyed through a feeder pipeline system into two transfer ponds in the northwest of the Salar from where it is lifted through a 7 km average km pipeline up to the evaporation ponds.

The capital cost estimate for the brine production wellfield and pipeline delivery system considers the following main components:

- 12 production wells completed with 12-inch diameter stainless steel production casing and screen to an average depth of approximately 200 m and submersible pumping equipment
- 83 km of 8-inch diameter of HDPE feeder pipelines, from all wells to transfer ponds
- Two collection/transfer ponds
- Booster pumping station

- 3 main HDPE brine parallel delivery pipelines of 11 km each, with a 22-inch diameter, from the transfer ponds to the first halite pond.

Table 21-2: Brine production wellfields and pipeline delivery system Cost Estimate

1000 Brine Extraction Wells	Projected Budget 000 US\$
Drilling and wells construction	4,389
Concrete	307
Steel Structure	421
Mechanic Equipment	1,696
Piping	30,957
Electric	1,299
Instrumentation	305
Total	39,374

21.1.3 Evaporation Ponds

The evaporation ponds comprise 3 types, namely solar evaporation ponds proper, discard ponds and the lithium brine pool or reservoir.

The evaporation ponds are extensive low depth areas, reaching a maximum of approximately 2 m. The transfer of the brine from one pond to the next will be done by means of gravity overflow. In those sectors in which the topography of the sector is not favorable, transfer will be done by pumping.

Three lithium brine pool or reservoirs will be installed at the end of the circuit, where concentrated brine from the evaporation ponds will accumulate, for later transfer to the industrial area for further processing.

The solar evaporation ponds have a surface of approximately 7,500,000 m², the disposal ponds have an approximate area of 75,000 m² and the lithium brine reservoirs have a combined area of approximately 30,000 m².

All the ponds have a waterproofing system, which considers the incorporation of an HDPE or similar membrane, with resistance to impacts and punctures.

Table 21-3: Evaporation Ponds Cost Estimate

2000 Evaporation Ponds	Projected Budget 000 US\$
Earthworks	103,119
Concrete	491
Mechanic Equipment	1,417
Piping	4,971
Electric	722
Instrumentation	421
Harvesting equipment for evaporation ponds	4,204
Total	115,346

21.1.4 Salt Removal Plant

Given the temperature, wind solar radiation characteristics of the Salar de Maricunga, as well as its brine composition, brine process designers have reached the conclusion that in order to accelerate brine concentration and remove the high content of calcium, it is advisable to install a concentration plant, which will receive solar concentrated brine from the reservoir pool and will subject it to additional concentration by means of evaporation and crystallization. Input for the plant will be approximately 80 m³/h of concentrated brine. Output from the plant is directed to the Lithium Carbonate Plant.

The technology, equipment and construction supervision for the Salt Removal Plant is being provided by GEA Messo, part of GEA Aktiengesellschaft of Düsseldorf, Germany (GEA).

Table 21-4: Salt Removal Plant Cost Estimate

5000 Salt Removal Plant	Projected Budget 000 US\$
Earthworks	32
Concrete	7,496
Steel Structure	15,441
Architecture	40
Mechanic Equipment	33,074
Piping	718
Electric	1,559
Instrumentation	4,757
Water Cooling System	3,321
Total	66,438

21.1.5 Lithium Carbonate Plant

Concentrated brines from the Salt Removal Plant are sent to the Lithium Carbonate Plant, which by means of a series of continuous processes, such as solvent extraction, calcium and magnesium removal, ion exchange, filtering and washing, the remaining contaminants present in the brine, such as boron, magnesium and calcium, are removed. The purified lithium present in the brine is then precipitated through carbonation, after which it is dried, micronized and packaged, so that lithium carbonate is obtained as the final product.

The facilities that make up the plant comprise a total area of approximately 8,500 m² and include a solvent extraction building, a brine purification building which includes a magnesium and calcium removal section, as well as the lithium carbonate building which includes a wet area, filtering, drying, packaging and storage of the final product.

Table 21-5: Lithium Carbonate Plant Cost Estimate

6000 Li ₂ CO ₃ Plant	Projected Budget 000 US\$
Stripping - SX Plant	14,182
Calcium and Magnesium Removal	17,989
Ion Exchange	4,164
Carbonation	3,485
Filtering and Washing	7,764
Drying	14,459
Micronizing	884
Packaging and Storage	8,694
Total	71,622

21.1.6 General Services

The main auxiliary services required by the lithium carbonate and potassium chloride process plants are: water supply storage and distribution, fuel storage and distribution, electrical supply and distribution, and soda ash storage and preparation.

Table 21-6: General Services Cost Estimate

8000 General Services	Projected Budget 000 US\$
Fuel Storage and Distribution	7,243
Water Supply, Storage and Distribution	30,026
Electric Supply and Distribution	15,371
Acid Washing System (H ₂ SO ₄)	3,557
Thermal Unit	4,851
Fire Protection System	1,910
Plant and Instrumentation Air Supply	3,462
Reagents Storage and Distribution	23,900
Industrial water distribution	12,948
Total	103,267

21.1.7 Infrastructure and Equipment

- The project infrastructure and equipment include the following areas:
- Construction and Operation Camp
- Internal Roads and C-173 route by-pass
- Products warehouse.
- Auxiliary services.
- Workers' camp.
- Temporary contractors' installations

In addition, there will be approximately 30 million m³ of stockpiles and discards ponds, originating both from pond harvests and from processes plants.

Table 21-7: Infrastructure and Equipment Cost Estimate

9000 Infrastructure	Projected Budget 000 US\$
Plant buildings	5,757
Access control and Security	971
Camps and Facility	22,770
Truck Maintenance Workshop	8,920
Weighting Yard	218
Internal Roads (Plant)	11,181
Dangerous Waste Warehouse	635
Sanitary works	5,833
Piping Mains	3,724
Total	60,009

21.1.8 Exclusions

The following items are not included in this estimate:

- Sunk and legal costs
- Special incentives and allowances
- Owner's costs, including permitting and construction insurance
- Escalation
- Interest and financing costs
- Start-up costs beyond those specifically included
- Additional exploration expenses

21.1.9 Currency

All values are expressed in fourth quarter 2018 US dollars; the exchange rate between the Chilean peso and the US dollar has been assumed as CHP\$ 650 / US\$; no provision for escalation has been included since both revenues and expenses are expressed in constant dollars. A US dollar Euro rate of 0,85 has also been used in some calculations.

21.2 OPERATING COST ESTIMATE

This section presents the main elements of the estimated operating expenses for the Blanco Project.

An operating cost estimate for 20,000 TPY Li_2CO_3 facilities has been prepared. This estimate is based upon process definition, laboratory work, tests at equipment suppliers and reagents consumption rates all provided or determined by MSB. Vendor quotations have been used for reagents costs. Expenses estimates, as well as manpower levels are based on WP experience and information delivered by MSB. Energy prices -mainly electricity and diesel fuel- and chemicals prices correspond to expected costs for products delivered at the project's location.

21.2.1 Operating Expenses Summary – OPEX

Operating expenses are summarized on the following table:

Table 21-8: Operation Cost

Description - Operation Costs	US\$ / Tonne Li_2CO_3	Total 000 US\$
DIRECT COSTS		
Chemical Reactives and Reagents	1,040	20,799
Salt Removal	486	9,727
Energy	1,028	20,552
<i>Memo: - Electrical</i>	<i>370</i>	<i>7,398</i>
<i>- Thermal</i>	<i>658</i>	<i>13,154</i>
Manpower	458	9,160
Catering & Camp Services	105	2,100
Maintenance	295	5,899
Transport	237	4,740
DIRECT COSTS SUBTOTAL	3,649	72,977
INDIRECT COSTS		
General & Administration - LOCAL	123	2,702
INDIRECT COSTS SUBTOTAL	123	2,702
TOTAL PRODUCTION COSTS	3,772	75,679

Table 21-8 shows that chemical reagents are the major operating cost of the project, closely followed by energy costs, of which fuel consumed by the Salt Removal Plant is the major component. Over 90% of the chemical costs correspond to soda ash costs, of which over

46,000 t are required to produce 20,000 tonnes of Li_2CO_3 . Other important expense items are salt harvesting or removal, manpower and maintenance.

21.2.2 Ponds and Plants Reagents Costs

Table 21-9: Ponds and Plants Reagents Costs

Description	Formula	US\$ / Tonne Li_2CO_3	US\$ 000 / yr
Calcium Oxide	CaO	9	189
Soda Ash	Na_2CO_3	938	18.755
Sulphuric Acid	H_2SO_4	2	45
Hydrochloric Acid	HCl	77	1.541
Sodium Hydroxide	NaOH	5	99
Extractant	Iso-octanol	5	102
Diluent	SCAID	3	68
Reagents consumption total		1.040	20.799

21.2.3 Energy Cost

Major energy items are the electricity required by the wells, the ponds, and the processes plants. Electrical transmission tolls are also significant. Transmission tolls are relatively high, but this is since the project is planning to use an existing line, built by another mining company and which would be shared by both companies. MSB has had preliminary conversations with the line owner in this respect, but power line sharing is a well-regulated matter in Chile. At the PEA stage it was thought that there was enough capacity on the line to allow both companies to operate, but revised estimates of the Blanco Project power consumption indicate that it will be necessary to upgrade this line. The cost of this item has been included on the project's CAPEX. Transmission tolls have been estimated according to the prevailing methodology in Chile.

However, diesel fuel consumption on the Salt Removal Plant is by far the major component of energy expenses; these amount to over US\$ 13 million per year. Diesel fuel in this plant is used on boilers to produce steam required by the process.

Diesel fuel required by salt removal and transport equipment is included on item 21.2.5.

Table 21-10: Energy

Electric Energy Consumption	Consumed Energy US\$ / Tonne Li_2CO_3	Consumed Energy US\$ 000 / yr.
Wells	5	105
Transfer Ponds	34	674
Evaporation Ponds	23	465
Salts Removal Plant	157	3.145
Li_2CO_3 Plant	38	767
Camp	10	190
Truck Shop	6	124
Transmission Losses	6	119
Subtotal	279	5.588
Transmission Toll	91	1.810
Electric Energy Consump. Total	370	7.398

21.2.4 Maintenance Cost

Maintenance costs have been estimated by applying experience-based factors, to capital outlays for the different budget items. It is to note that maintenance of the salt harvesting equipment, which is a relevant amount, is included in the following salt harvesting cost sub section.

Table 21-11: Maintenance Cost

Description	US\$ / Tonne Li_2CO_3	US\$ 000 / yr.
Brine Extraction Wells	10	197
Evaporation Ponds	14	278
Salt Removal Plant	66	1.329
Lithium Carbonate Plant	49	974
General Services	80	1.603
Infrastructure	76	1.519
Total	295	5.899

21.2.5 Salt Harvest and Transport

This item corresponds to the costs incurred on harvesting the ponds and transporting discarded salts to their established dumping place, within MSB's surface property and according to the EIA expected to be approved. Material to be transported is approximately 2.4 million m^3/y . It should be noted that in Chilean mining operation, material transport of this type is usually sub contracted to third party operators, which provide the required equipment and personnel necessary for this operation, for an agreed fee. For this reason, in this item we have included all costs related to this operation.



In spite of the above, to maintain the full project basis for economic evaluation purposes, all equipment required in the operation, as well as the personnel involved on it have been assumed to be owned or employed directly for MSB.

Table 21-12: Salt Harvest and Transport Cost

Description	US\$ / Tonne Li_2CO_3	US\$ 000
Personnel Cost	216	4.316
Fuel & lubricants	128	2.566
Tires	46	915
Maintenance and spare parts	96	1.930
Total	486	9.727

21.2.6 Manpower, Catering and Camp Services Cost

Headcount for the plant was estimated based on experience in similar facilities, while personnel salaries and benefits were projected using data from actual costs for mining operations in the north of Chile, adjusted by relevant factors. Headcount increased substantially from that estimated at the PEA stage mainly due to a stricter interpretation of Chilean regulations concerning admissible personnel shifts.

Table 21-13: Manpower, Catering and Camp Services Cost

Description	# of people	US\$ / Tonne Li_2CO_3	US\$ 000 / yr.
Plant Operations	152	458	9.160
Catering and Camp Services	-	105	2.100
Total	152	563	11.260
Memo items:			
Ponds Harvesting (1)	51	154	3.078
Truck Workshop (1)	30	62	1.238
Management (2)	15	83	1.664
Total	248	862	17.240

Notes:

(1) Costs included in Salt Harvesting expenses

(2) Costs included in G & A expenses

21.2.7 Product Transportation Costs

Costs of all production supply items have been taken at the Maricunga plant, thus there no transport costs to add from the supply side.

However, product delivery expenses need to be included. Since prices for lithium carbonate shown in Section 19, and considered in the economic evaluation, correspond to CIF China prices, we need to include all costs items necessary to transport produced lithium carbonate to China. These costs include trucking the lithium carbonate to Antofagasta, or nearby Mejillones, both in Chile, and which are usual export locations for this product. Additional

costs to be considered correspond to port warehousing and handing fees, as well as ocean freight and insurance to a destination port in China. These costs are shown on following Table 21-14 Table 21-14..

Table 21-14: Product Transportation Costs

Description	Rate US\$ / Ton-km	Distance km	Origin	Destination	Rate US\$/Ton
Truck Transport	0,183	780	Salar de Maricunga	Mejillones	142.8
Port Storage Fees					23.5
Port Receiving and Dispatching Fees					40.7
Ocean Freight & Insurance					30
Total					237

21.2.8 Indirect Costs

Indirect costs include management compensation, office space rental, plant insurance, communications and other expenses.

Costs exclude Board of Directors compensation and expenses, and any other expenses above those corresponding to the company's local General Manager. These costs are shown on following Table 21-15.

Table 21-15: General & Administration

Description	US\$ / Tonne Li ₂ CO ₃	US\$ 000 / yr.
Management	83	1.664
Office Rental	7	130
Insurance	9	182
Personnel Transportation	21	420
Communications, office supplies & sundries	3	60
Total Local G & A Costs	123	2.456

22. ECONOMIC ANALYSIS

This section analyzes the economic feasibility of the MSB Blanco Project, which aims to produce 20,000 TPY of lithium carbonate.

To carry out the project's economic evaluation, WP developed a pre-tax and after-tax cash flow model. Inputs for this model were the capital and operating costs estimates presented in the previous sections, as well as an assumed production program and the pricing forecast included in Section 19.

Model results include the project's NPV at different rates, IRR and payback period. These parameters were calculated for different scenarios; in addition, a sensitivity analysis on the most important revenue/cost variables was performed.

22.1 EVALUATION CRITERIA

- Pricing has been obtained from Company calculations based on the Roskill Lithium Carbonate market study report prepared for MSB in November – December 2018, as indicated in Section 19.
- Long term lithium carbonate production rate has been assumed as 20,000 TPY, of which 90% will be produced as battery grade product and the remaining 10% will be technical grade product. Long term lithium carbonate production level is reached in the third year of operations. Production ramp up rates for technical grade lithium carbonate are higher than those assumed for battery grade lithium carbonate since the latter is a more technically demanding operation. Production ramp up rates and yearly output tonnages are shown on Table 22-4 and Table 22-5.
- Project horizon: Time allowed for engineering and permits is one year, and construction is 3 years, with commercial production starting on the fourth year. Projected operating period is 20 years at full lithium carbonate production, or 22 years from the start of operations.
- CAPEX and OPEX presented on Section 21 correspond to the process described on Section 17. However, since the evaporation and crystallization process has not yet been used commercially in lithium carbonate production, there is a risk that it may not turn out the expected quantity and/or required quality of Lithium Carbonate, or that it may result more expensive than expected. All other process steps are conventional and commonly used in the industry.
- Equity basis: For economic evaluation purposes, it has been assumed that 100 % of capital expenditures, including pre-production expenses and working capital are financed solely with owner's equity. Given the level of rates of return obtained,

considering leverage would further improve these rates of return. This is later done as part of the sensitivity analysis.

22.2 INCOME TAX AND ROYALTIES

The following tax assumptions and criteria have been considered in the project's evaluation:

22.2.1 Income Taxes

In accordance with the latest modification to the Chilean Income Tax Law (Ley N° 20.899, Reforma Tributaria, published on D.O. 02.08.16), income tax rate for corporations such as MSB has been set at 27 %. The new law left unchanged the provision for rapidly accelerated depreciation of capital goods. This provision results in losses for tax purposes in the early operating phase of project, losses which can be carried forward indefinitely. It has also been assumed that MSB projected total exploration and other capitalized project expenditures before construction, estimated as approximately US\$ 22.7 million can be used as amortization once the project starts operations, however this assumption has not been ratified by legal or tax advisors². It also should be mentioned that the Chilean Government is currently considering presenting to Congress a new Tax Reform Law, but this new reform is not expected to change corporate income taxes, as the reform is expected to be aimed at restoring full flow of tax credits of company paid income taxes to company owners or shareholders.

22.2.2 Value Added Tax (19 % flat on all items)

In the case of long lead projects, such as MSB's, Chilean VAT law allows for direct recovery from the government of VAT paid during the construction period. Additionally, in the case of companies that export all or nearly all their production, they can recover directly from the government VAT paid on all supplies. Considering that there are natural delays involved in this draw back system, the model considers that VAT payments are recovered six months after their payment.

22.2.3 Government Royalties

In the PEA we mentioned that this was an area of uncertainty for the project, given that there were no precedents for lithium carbonate exploitation in Chile, other than that carried out by SQM and Albemarle, at the Salar de Atacama, where in both cases the mining property belongs to CORFO -an arm of the Chilean Government- and the exploitation contracts have a relatively short termination date, and regulated rates of lithium brine extraction. In this economic and legal situation and given the buoyant condition of the lithium carbonate market, CORFO successfully renegotiated these agreements, with both producers receiving authorization for substantially increased lithium production rates, at the cost of accepting

² Some of these expenses may have been carried out by previous project owners, hindering their inclusion in tax allowable amortization.

considerably higher royalty rates for the authorized additional production. It must be noted though that the new royalty rates are on a sliding scale, depending on lithium carbonate realizations.

Given the above, there were some concerns that the Chilean Government might try to obtain similar conditions from other lithium producers in Chile. Nevertheless, there are several key factors that indicate that MSB's project should be subject to a significative lower royalty rate than that applied to Salar de Atacama producers:

Firstly, MSB has nearly 50% of its lithium mining properties registered under the old mining law, which according to MSB's interpretation of the relevant legislation, are exempt from any special royalties on lithium carbonate production and would be subject to royalties under the general mining regime, in which royalties to be paid depend on both lithium carbonate and copper prices. If this is the case, and if MSB were to produce 100 % of the brine required for the plant from the old properties -as it plans to do during the initial 12 years of the project life- we estimate yearly royalties would amount to approximately US\$ 3.8 million per year³. This is equivalent to about 1.3 % of yearly sales.

Secondly, in the lapse of time between publication MSB's PEA and this writing, the Government made public the conditions of CODELCO's "Contrato Especial de Operación de Litio (CEOL)" for its properties on the Maricunga Salar. Among them are the royalty conditions that would apply to this production, which would be from the so called "new mining concessions". Applying the same conditions to MSB's project results in a royalty payment of approximately US\$ 37.5 million per year, during the last nine years of the project, which is equivalent to 9.6 % of yearly sales. It is to note that this royalty is based mostly on the company's operating margin, thus it diminishes considerably in case the company's operating margin turn out to be below that included in our projections. Overall royalties⁴ to be paid during the full project horizon are equivalent 5.5% of total sales, with the advantage that the lower 1.3 % rate is the one that applies during the initial half life of the project. This compares very favourably with royalty rates agreed to by Albemarle and SQM⁵. Additionally, it must be pointed out that above royalty payment calculations for MSB have been done at the project's lithium price average of approximately US\$/Tonne 17,200. At this price level, royalties payable by both Albemarle and SQM should be well in excess of 20% of sales realizations, given that the maximum 40% royalty rate applies starting at a price of US\$/Tonne 12,000.

³ These royalties have been calculated at the projects expected lithium carbonate prices, and at a projected copper price of US\$/lb 3,0.

⁴ Royalties considered include agreed contributions to communities welfare funds. These contributions are related to lithium carbonate sales.

⁵ After MSB's PEA publication, CORFO and SQM reached an agreement on contract extension, increase allowable production and royalty rates very similar, if not the same, that apply to Albemarle.

Table 22-1: CORFO Albemarle Royalty Agreement Summary

	US\$/tonne LCE 8,000	US\$/tonne LCE 10,000	US\$/tonne LCE 12,000
Royalty Payable US\$/tonne LCE	872	1,372	2,172
Average Royalty Payable	10.9%	13.7%	18.1%

Source: Elaborated by WP from Albemarle published information.

Full table is included in Appendix 2 to this report.

Main reasons to expect a lower royalty rate for the MSB project than that applying to Salar de Atacama producers, as assumed in this report, are:

- MSB owns its mining property; thus, royalties will be due only to the Chilean government, and not to CORFO as a "rent or lease payment", for those properties, as is the case of Salar de Atacama producers.
- MSB has paid for initial exploration of its properties, which was not the case in Atacama,
- It is politically and legally difficult for the Chilean Government to set different economic conditions for MSB from those already granted to CODELCO, especially considering that the two companies would operate on the same salar.
- Objective conditions such as climate, location and brine grade and composition are not as favorable in Maricunga (or other salars) as in Atacama, and
- Expected risk and returns for greenfield projects are normally substantially higher than those for expansion projects.

It is also important to mention that the Chilean government is keenly interested in that further lithium production, beyond the Salar de Atacama, is established in the country. Thus, there is clear indications that royalty rates to be set for Maricunga will allow the project to proceed, at rates of return comparable with those available elsewhere in the mining industry, and consistent with particular project risks.

Finally, we add that given the above-mentioned situation, we have included the royalty rate in the parameters of the sensitivity analysis. The results are shown on Table 22-16, and the results indicate that the project can tolerate a higher royalty rate than that assumed in the base case, without undue impact on economic results.

22.2.4 Other Royalties

According to MSB no royalties, apart from those due to the Chilean Government are payable on this project. Still, there is a very small minority owner in some of the project's mining property, which for economic evaluation purposes is assumed to be bought out at production outset.

22.3 CAPITAL EXPENDITURES

As indicated in Section 21.1.1 and on Table 22-2, capital investment for the MSB project, including equipment, materials, indirect costs and contingencies during the construction period is estimated to be US\$ 563 million. As also indicated on the same section, working capital requirements are estimated to be US\$ 20 million and sustaining capital expenditures total US\$ 53 million, over the horizon of the project.

Table 22-2: Capex Schedule

Description	Capital Expenditures			
	US\$ 000			
	2020	2021	2022	Total
Brine Extraction Wells	20,943	18,431	0	39,374
Evaporation Ponds	20,761	55,189	39,396	115,346
Salt Removal Plant	3,140	46,533	16,765	66,438
Lithium Carbonate Plant	3,385	50,164	18,073	71,622
General Services	4,880	72,328	26,059	103,267
Infrastructure	2,836	42,030	15,143	60,009
Indirects	5,512	27,953	11,367	44,831
Contingencies	7,698	39,039	15,875	62,611
Total	69,155	351,666	142,678	563,498

22.4 LITHIUM CARBONATE PRODUCTION AND RAMP UP

As previously indicated, the economic evaluation considers that project long-term sustainable lithium carbonate production is 20,000 TPY, of which 90% is expected to be battery grade lithium carbonate and 10% technical grade lithium carbonate.

Table 22-3: Production Capacity

Production Capacity (TPA)	
Li ₂ CO ₃ Battery Grade	18,000
Li ₂ CO ₃ Technical Grade	2,000

Since it is known that start of lithium carbonate production is a difficult process, it has been assumed that full production design capacity is achieved during the third year of operations. Ramp up of technical grade product is somewhat faster, given its less strict specifications.

Table 22-4: Production Ramp Up %

Production Ramp Up % of Full Capacity			
Year	2023	2024	2025
	4	5	6
Battery Grade Ramp Up	30%	60%	100%
Technical Grade Ramp Up	50%	80%	100%

Given the above presented production ramp up table, expected quantities of battery grade and technical grade lithium carbonate to be produced are as follows:

Table 22-5: Production Ramp Up Tonnes

Year	2023	2024	2025	2029	2034	2039	2043	2044	Total
	4	5	6	10	15	20	24	25	
Battery Grade	5,400	10,800	18,000	18,000	18,000	18,000	18,000	16,600	358,600
Technical Grade	1,000	1,600	2,000	2,000	2,000	2,000	2,000	1,800	42,400
Total Production	6,400	12,400	20,000	20,000	20,000	20,000	20,000	18,400	401,000

22.5 OPERATING COSTS

As shown on section 21.2.1, Table 21-8, direct operating costs per tonne of lithium carbonate result to be US\$ 3,649. Indirect unit operating costs are estimated to be 123 US\$/tonne; thus, total estimated operating costs are 3,772 US\$/tonne.

22.6 PRODUCTION REVENUES

Production revenues result from projected product prices, shown on Table 19-2 and production quantities presented on Table 22-6. Results are as follows:

Table 22-6: Production Revenues


Revenues US\$ 000											
Year	2023	2024	2025	2026	2027	2028	2029	2034	2043	2044	Total
	4	5	6	7	8	9	10	15	24	25	
Battery Grade	71,618	147,953	254,031	262,594	270,703	279,837	288,487	317,081	317,081	297,420	6,277,844
Technical Grade	12,270	20,222	26,148	26,972	27,752	28,651	29,503	32,383	32,383	29,145	651,092
Total	83.888	168.175	280.179	289.566	298.455	308.488	317.989	349.464	349.464	349.464	6.928.935

22.7 CASH FLOW PROJECTION

Combination of assumptions on investments, revenues, costs, income taxes, royalties, amortization, depreciation, working capital, etc. combine to produce the cash flow projection shown on Table 22-7.

It should be mentioned that the cash flow projection shown on the above referred table, corresponds to the evaluation base case which, as mentioned, assumes full equity project funding.

Table 22-7: Project Summary Cash Flow Projection

<div> <div>SALAR BLANCO - SALAR DE MARICUNGA (20KTPA) PROJECT</div> <div>MINERA SALAR BLANCO S.A.</div> <div>DISCOUNTED CASH FLOW</div> </div> <div>  WorleyParsons resources & energy </div>																	
Year	2020	2021	2022	2023	2024	2025	2026	2027	2028	2029	2030	2031	2032	2039	2043	2044	Total
Period	1	2	3	4	5	6	7	8	9	10	11	12	13	20	24	25	
Revenues	-	-	-	83,888	168,175	280,179	289,566	298,455	308,488	317,989	328,537	338,523	349,464	349,464	349,464	321,564	6,928,935
L2CO3 Battery Grade	-	-	-	71,618	147,953	254,031	262,594	270,703	279,837	288,487	298,074	307,150	317,081	317,081	317,081	292,420	6,277,844
L2CO3 Battery Grade - OP	-	-	-	71,618	147,953	254,031	262,594	270,703	279,837	288,487	298,074	307,150	317,081	317,081	317,081	292,420	3,086,585
L2CO3 Battery Grade - NP	-	-	-	-	-	-	-	-	-	-	-	-	-	-	-	-	3,191,259
L2CO3 Technical Grade	-	-	-	12,270	20,222	26,148	26,972	27,752	28,651	29,503	30,463	31,373	32,383	32,383	32,383	29,145	651,092
L2CO3 Technical Grade - OP	-	-	-	12,270	20,222	26,148	26,972	27,752	28,651	29,503	30,463	31,373	32,383	32,383	32,383	29,145	325,895
L2CO3 Technical Grade - NP	-	-	-	-	-	-	-	-	-	-	-	-	-	-	-	-	328,434
Expenses	-	-	-	(31,211)	(46,328)	(79,395)	(82,062)	(82,516)	(83,027)	(83,512)	(84,050)	(85,619)	(85,611)	(94,927)	(96,229)	(90,224)	(1,856,231)
OPEX L2CO3 Battery Grade	-	-	-	(24,973)	(38,726)	(65,702)	(67,890)	(67,890)	(67,890)	(67,890)	(67,890)	(67,890)	(67,890)	(67,890)	(67,890)	(64,049)	(1,415,473)
OPEX L2CO3 Technical Grade	-	-	-	(3,285)	(5,257)	(7,543)	(7,543)	(7,543)	(7,543)	(7,543)	(7,543)	(7,543)	(7,543)	(7,543)	(7,543)	(6,995)	(158,860)
Royalties based on Sales	-	-	-	(2,000)	(985)	(4,117)	(4,539)	(4,939)	(5,391)	(5,818)	(6,293)	(8,002)	(7,729)	(17,044)	(18,346)	(16,899)	(232,483)
Communities	-	-	-	(600)	(1,009)	(1,681)	(1,737)	(1,791)	(1,851)	(1,908)	(1,971)	(2,031)	(2,097)	(2,097)	(2,097)	(1,929)	(41,670)
Mining Licenses & Water Rights	-	-	-	(352)	(352)	(352)	(352)	(352)	(352)	(352)	(352)	(352)	(352)	(352)	(352)	(352)	(7,744)
Operating Margin	-	-	-	52,678	121,847	200,784	207,504	215,939	225,461	234,477	244,487	252,704	263,853	254,537	253,236	231,340	5,072,704
Operating Margin %	-	-	-	61%	71%	72%	72%	72%	73%	74%	74%	75%	76%	73%	72%	72%	
Depreciation	-	-	-	(207,312)	(184,278)	(184,278)	-	-	-	(1,733)	(176)	(353)	(706)	(3,705)	(6,175)	(6,881)	(622,413)
Amortization	-	-	-	(4,000)	(4,000)	(4,000)	(4,000)	(4,000)	(4,000)	-	-	-	-	-	-	-	(20,000)
Remediation Allowance	-	-	-	(4,561)	(869)	(869)	(869)	(869)	(869)	(869)	(869)	(869)	(869)	(869)	(869)	(869)	(22,803)
Remediation Guaranty Cost	-	-	-	(91)	(109)	(126)	(143)	(161)	(178)	(195)	(213)	(230)	(248)	(369)	(439)	(456)	(6,020)
Operating Margin for Annual Royalty	-	-	-	(163,195)	(67,299)	11,637	202,635	211,070	224,592	231,876	243,442	251,483	262,279	249,964	246,192	223,591	4,407,488
Additional royalty based on Operating Margin	-	-	-	0	0	0	0	0	0	0	0	0	0	(10,357)	(10,378)	(10,357)	(110,780)
Profit Before Taxes	-	-	-	(163,286)	(67,407)	11,511	202,492	210,910	224,414	231,680	243,229	251,252	262,031	239,237	235,375	212,779	4,290,688
Income Taxes	-	-	-	-	-	-	-	(52,439)	(60,592)	(62,554)	(65,672)	(67,838)	(70,748)	(64,594)	(63,551)	(57,450)	(1,158,486)
Profit After Taxes	-	-	-	(163,286)	(67,407)	11,511	202,492	158,471	163,822	169,127	177,557	183,414	191,283	174,643	171,824	155,328	3,132,202
Depreciation, Amortization & Allowance	-	-	-	215,873	189,146	189,146	4,869	4,869	869	2,602	1,045	1,222	1,574	4,574	7,044	7,749	665,216
Operating After Tax Cash Flow	-	-	-	52,586	121,739	200,658	207,361	163,339	164,691	171,728	178,603	184,636	192,857	179,217	178,868	163,078	3,797,418
Non Operating Cash Flow	(80,239)	(382,627)	(126,947)	1,779	(5,969)	(11,517)	(875)	(113)	(128)	(650)	(664)	(1,501)	(1,007)	(4,596)	(7,103)	(6,080)	(653,516)
CAPEX & Sustaining Capital	(73,278)	(355,789)	(146,801)	-	-	(5,199)	-	-	-	(529)	(529)	(1,059)	(1,059)	(4,234)	(6,881)	(7,410)	(633,995)
Working Capital Variation	-	-	-	(10,404)	(5,039)	(4,406)	(667)	(113)	(128)	(121)	(134)	(442)	52	(362)	(222)	1,001	(15,037)
VAT (Net of refunds)	(6,961)	(26,839)	19,854	12,183	(930)	(1,912)	(208)	-	-	-	-	-	-	-	-	329	(4,484)
Cash Flow Before Interest and Tax	(80,239)	(382,627)	(126,947)	54,457	115,878	189,267	206,629	215,826	225,333	233,827	243,823	251,203	262,847	249,941	246,133	225,260	4,419,188
Remediation disbursement	-	-	-	-	-	-	-	-	-	-	-	-	-	-	-	(22,803)	(22,803)
Before Tax Cash Flow	(80,239)	(382,627)	(126,947)	54,457	115,878	189,267	206,629	215,826	225,333	233,827	243,823	251,203	262,847	249,941	246,133	202,457	4,396,385
Income Taxes (27%)	-	-	-	-	-	-	-	(52,439)	(60,592)	(62,554)	(65,672)	(67,838)	(70,748)	(64,594)	(63,551)	(57,450)	(1,158,486)
After Tax Cash Flow	(80,239)	(382,627)	(126,947)	54,457	115,878	189,267	206,629	163,387	164,741	171,273	178,152	183,365	192,098	185,347	182,581	145,007	3,237,900
Accumulated Cash Flow AfterTax	(80,239)	(462,866)	(589,814)	(535,357)	(419,479)	(230,212)	(23,583)	139,804	304,545	475,819	653,970	837,336	1,029,434	2,347,700	3,092,892	3,237,900	

22.8 ECONOMIC EVALUATION RESULTS

The cash flow projection shown on the Table 22-7 results in the following project economic metrics:

**Table 22-8: Base Case Economic Results
(full equity project funding)**

ECONOMIC RESULTS		BEFORE TAXES	AFTER TAXES
NPV 6%	MM US\$	1,738	1,248
NPV 8%	MM US\$	1,286	908
NPV 10%	MM US\$	949	653
IRR		23.8%	21.0%
PAYOUT		4 y, 1 m	4 y, 2 m

After tax cash flow results from the model can also be visualized on the graphs presented on the following page. These graphs indicate that the project generates substantial positive cash flow from the third year of operations onwards, and cumulative cash flow turns positive only four years after the start of operations.

Figure 22-1: Yearly Cash Flow

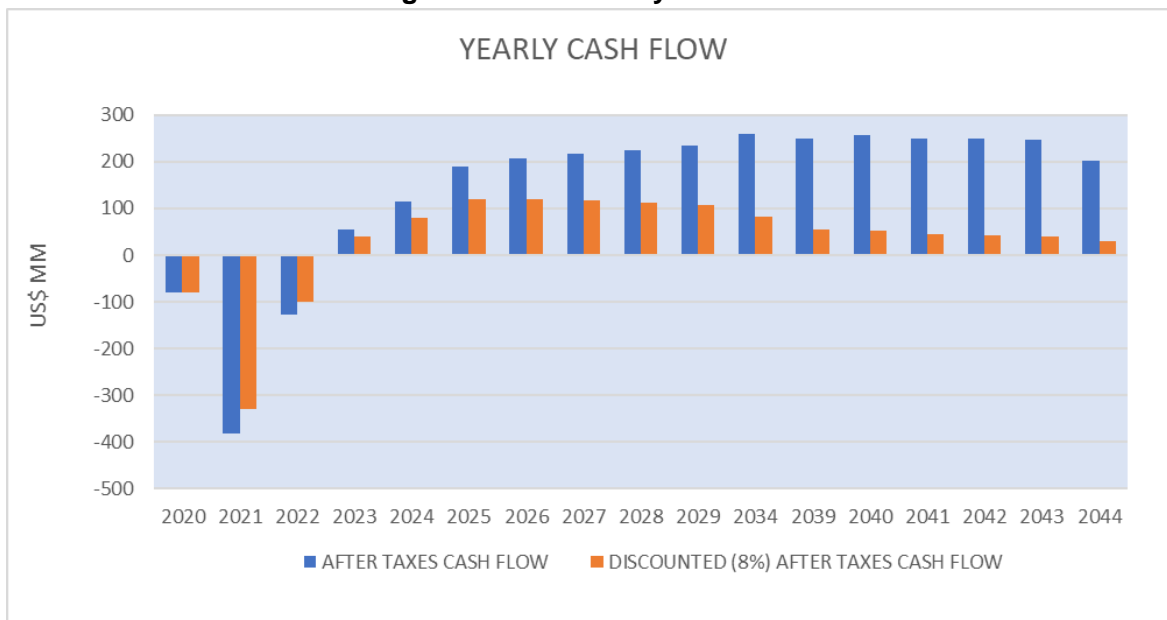
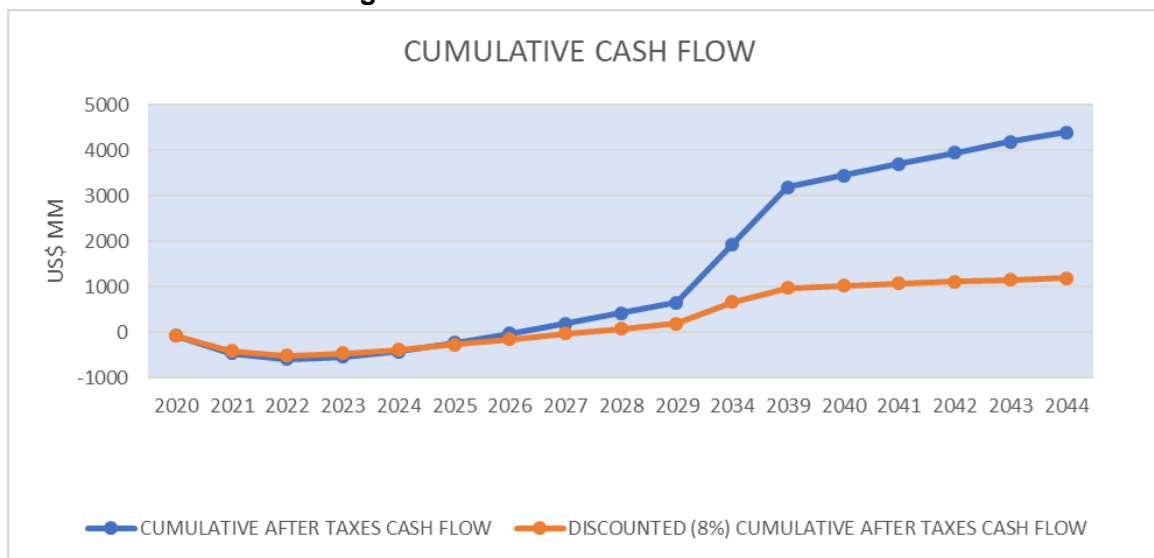


Figure 22-2: Cumulative Cash Flow⁶



⁶ Note that the slope change in cash flow shown in this graph between years 2029 and 2039 is only apparent. It is due to the elimination in the graph of in between years, to shorten its width. Actual cash generation is nearly even, as shown in figure 22-1.

22.8.1 Project Life

Project life, for evaluation purposes, as well as for environmental and other permit purposes, life of the project has been assumed as 20 years of lithium carbonate full production. Since the resource base seems to support a longer project life, consideration of further production years may uplift results if longer operation permits are obtained.

22.8.2 Sensitivity Analysis

22.8.2.1 Impact of Financing on Project's Owner returns

Since in practice a clear majority of large investment projects such as MSB's are financed with a variable mixture of debt and equity, it is very relevant to consider the impact on project owner's return of assuming the project is financed partly on credit.

For this purpose, we have assumed the project receives a loan amounting to 50% of total its expenditures during the first three years of construction (US\$ 295 million). This is equivalent to a 50/50 debt to equity ratio, without considering pre-construction expenditures. Other assumed conditions for the loan include a 6% annual rate, disbursements during the second and third year of construction, with repayment over a 10-year period, in equal yearly installments. While WorleyParsons believe these financial conditions to be realistic for a mining project in Chile, there is no assurances that these conditions will be available in the market for MSB's project.

Table 22-9: Loan Disbursement and Repayment

Financing Cash Flow - US\$ 000														
Year	2020	2021	2022	2023	2024	2025	2026	2027	2028	2029	2030	2031	2032	Totals
Period	1	2	3	4	5	6	7	8	9	10	11	12	13	
Beginning of Year Debt	-	-	172,998	317,942	293,821	268,252	241,149	212,420	181,967	149,686	115,469	79,199	40,753	
Debt Drawdown	-	167,960	126,947	-	-	-	-	-	-	-	-	-	-	294,907
Yearly Payment	-	-	-	43,198	43,198	43,198	43,198	43,198	43,198	43,198	43,198	43,198	43,198	431,982
Amortization (YE)	-	-	-	24,122	25,569	27,103	28,729	30,453	32,280	34,217	36,270	38,446	40,753	317,942
Interest	-	5,039	17,997	19,077	17,629	16,095	14,469	12,745	10,918	8,981	6,928	4,752	2,445	137,075
Year End Debt	-	172,998	317,942	293,821	268,252	241,149	212,420	181,967	149,686	115,469	79,199	40,753	-	
Financing Cash Flow	-	167,960	126,947	(43,198)	(43,198)	(43,198)	(43,198)	(43,198)	(43,198)	(43,198)	(43,198)	(43,198)	(43,198)	(137,075)

Considering the above financing conditions, project owner returns are as follows:

**Table 22-10: Economic Results
(50/50 debt / equity project funding)**

ECONOMIC RESULTS		BEFORE TAXES	AFTER TAXES
NPV 6%	MM US\$	1,726	1,256
NPV 8%	MM US\$	1,302	940
NPV 10%	MM US\$	987	706
IRR		29.8%	26.7%
PAYOUT		3 y, 5 m	3 y, 5 m

As expected, leveraged project returns improve substantially over the unleveraged case.

22.8.2.2 Sensibility Analysis - Main Drivers

To further investigate the impact on the project's economic results – NPV and IRR – for changes in key variables, a pre-tax⁷ and post-tax sensitivity analysis was carried out. This analysis considers separate variations in four project driver variables, these being project CAPEX, Lithium Carbonate prices and production level, and project OPEX.

Table 22-11: Driver Variable, Sensitivity Analysis

Driver variable	CAPEX	Price	Production level	OPEX
Li ₂ CO ₃	✓	✓	✓	✓

Results of this analysis are presented on the following tables and figures:

Table 22-12: Project Before Taxes – NPV 8% Sensitivity Medium Scenario

Driver Variable	Base Case Values		Project NPV (MUS\$)				
			75%	90%	100%	110%	125%
CAPEX	MUS\$	563	1,417	1,338	1,286	1,234	1,156
Price	US\$/tonne	17,280	671	1,040	1,286	1,532	1,901
Production	Tonne/yr	20,000	832	1,105	1,286	1,467	1,737
OPEX	US\$/tonne	3,772	1,440	1,348	1,286	1,225	1,133

⁷ In order to avoid text repetition, comments on these results are provided only in the after-tax cases.

Figure 22-3: Project Before Tax NPV 8% Sensitivity Medium Scenario

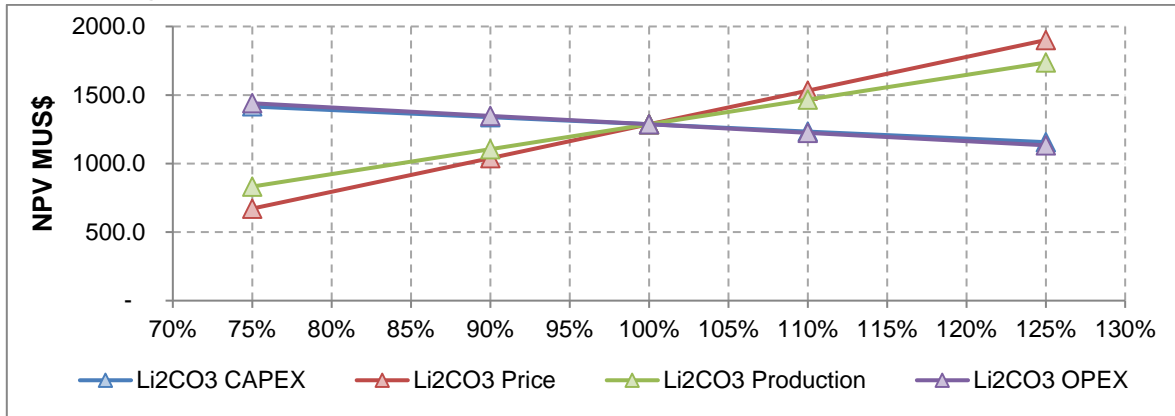


Table 22-13: Project Before Taxes – IRR Sensitivity Medium Scenario

Driver Variable	Base Case Values		IRR				
			75%	90%	100%	110%	125%
CAPEX	MUS\$	563	29%	26%	24%	22%	19%
Price	US\$/tonne	17,280	17%	21%	24%	26%	29%
Production	Tonne/yr	20,000	19%	22%	24%	25%	28%
OPEX	US\$/tonne	3,772	25%	24%	24%	23%	22%

Figure 22-4: Project Before Tax IRR Sensitivity Medium Scenario

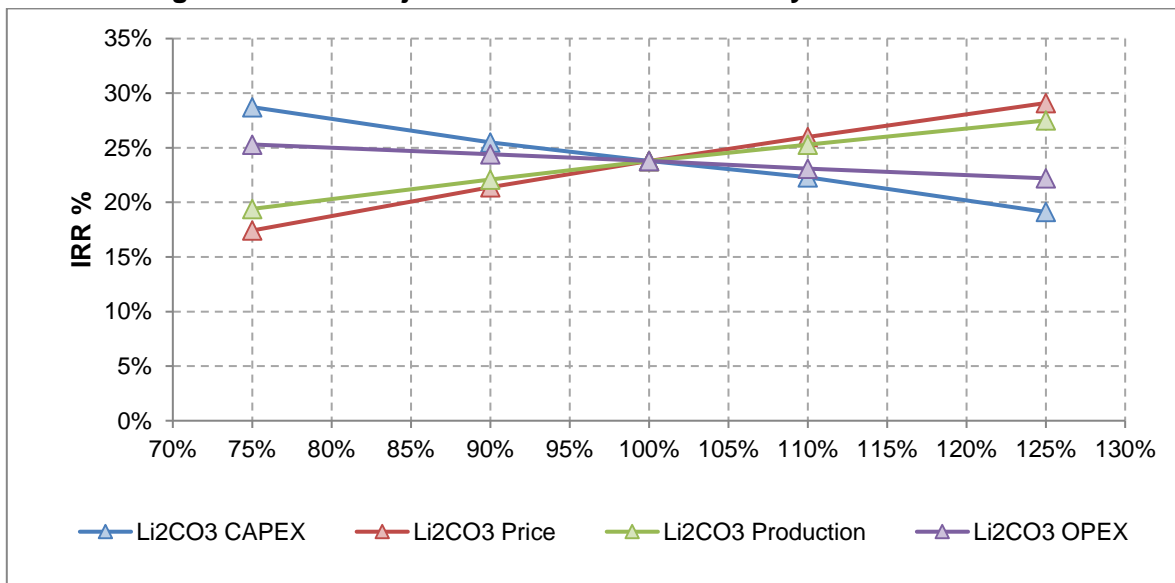


Table 22-14: Project After Taxes – NPV 8% Sensitivity Medium Scenario

Driver Variable	Base Case Values		Project NPV (MUS\$)				
			75%	90%	100%	110%	125%
CAPEX	MUS\$	563	1,014	950	908	864	800
Price	US\$/tonne	17,280	450	725	908	1,090	1,363
Production	Tonne/yr	20,000	572	774	908	1,041	1,239
OPEX	US\$/tonne	3,772	1,023	954	908	862	792

Conclusions that can be drawn from the above table and the following graph are that -as expected- the project's NPV results are quite sensible to the price level of lithium carbonate, since a 25% variation in this parameter causes a 50% variation in NPV. The project is slightly less sensible to variations in the production level since a 25% variation in this second parameter causes a 36% variation in NPV.

On the contrary, the project's NPV is not very sensible to variations in CAPEX or OPEX. In this manner, a 25% variation in these two parameters translates into an approximate 12% variation in NPV.

Figure 22-5: Project After Tax NPV 8% Sensitivity Medium Scenario

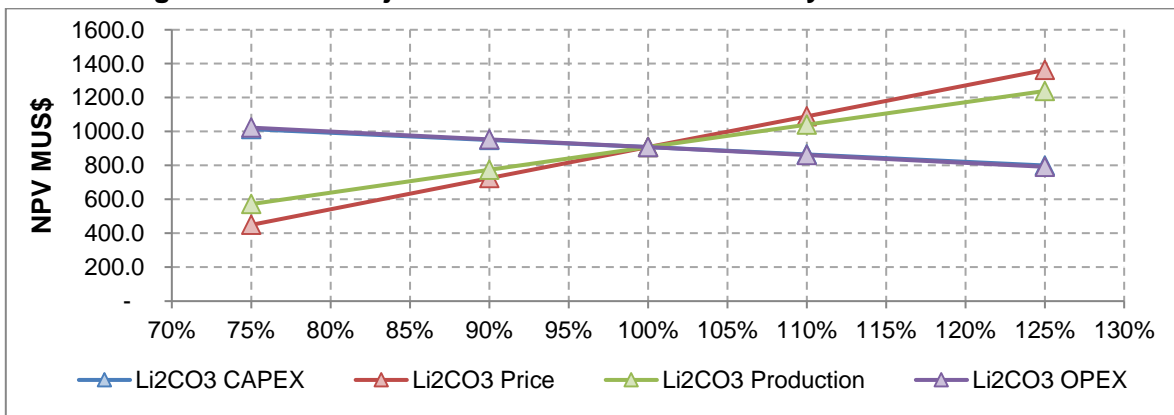


Table 22-15: Project After Taxes – IRR Sensitivity Medium Scenario

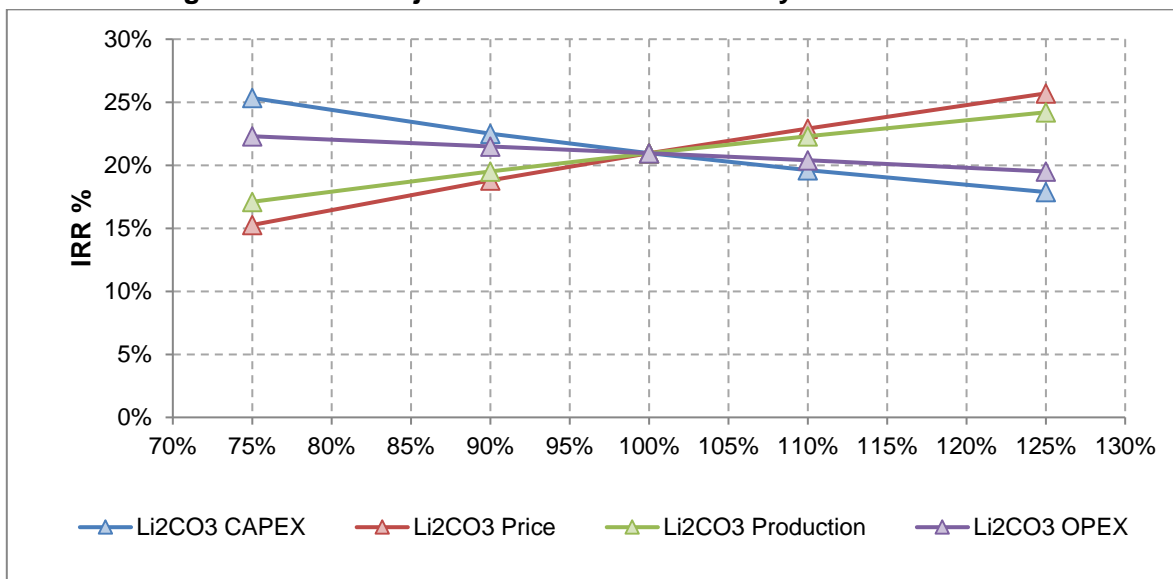
Driver Variable	Base Case Values		IRR				
			75%	90%	100%	110%	125%
CAPEX	MUS\$	563	25%	23%	21%	20%	18%
Price	US\$/tonne	17,280	15%	19%	21%	23%	26%
Production	Tonne/yr	20,000	17%	20%	21%	22%	24%
OPEX	US\$/tonne	3,772	22%	22%	21%	20%	20%

Conclusions to be drawn from the above table and the following graph are similar to those mentioned in the case of NPV sensitivity. This is that the project's IRR results are sensitive

to the price level of lithium carbonate and slightly less sensitive to variations in the production level.

Similarly to the NPV sensitivity, the IRR result is not very sensitive to variations in CAPEX or OPEX.

Figure 22-6: Project After Tax IRR Sensitivity Medium Scenario



22.8.2.3 Sensitivity to Royalty Rate

Since in Section 22.2.3 indicates that there is some uncertainty over the overall royalty rate that the project will face, in this point we investigate the project's economic results sensitivity to royalty rate variations. Results are presented on the following table:

Table 22-16: Sensitivity to Royalty Rate

PROJECT SENSITIVITY TO ROYALTY RATE BEFORE TAX RESULTS - BASE CASE				
Assumed Average Royalty Rate	NPV 6%	NPV 8%	NPV 10%	IRR
5.5 % (1)	1.738	1.286	949	23,8%
5.5 % (2)	1.671	1.228	899	23,1%
7.5 %	1.606	1.177	857	22,6%
10%	1.525	1.112	804	21,9%

**PROJECT SENSITIVITY TO ROYALTY RATE
AFTER TAX RESULTS - BASE CASE**

Assumed Average Royalty Rate	NPV 6%	NPV 8%	NPV 10%	IRR
5.5 % (1)	1.248	908	653	21,0%
5.5 % (2)	1.188	857	610	20,3%
7.5 %	1.140	819	579	19,8%
10%	1.080	770	539	19,3%

Notes:

- (1) **Base case**, with lower royalty rates for "old" properties
- (2) Assumes even 5.5% royalty over project life

Table 22-16 shows that the project is not very sensitive to the royalty rate, since increasing more than three⁸ times the royalty rate, which we do not expect, reduces the project's 8% NPV in approximately 15% and the IRR in less than two percentage points.

⁸ The base case 5.5% average rate is expressed in nominal terms. In discounted terms it is approximately equivalent to an even average 3% rate.

23. ADJACENT PROPERTIES

The MSB mining concessions (Litio 1-6, Cocina 19-27, San Francisco, Despreciada and Salamina) are located in the northern part of Salar de Maricunga. Other adjacent mining concessions in the Salar are held by SQM, Cominor and Codelco. SQM is a major lithium carbonate producer with operations at Salar de Atacama. Codelco is a Chilean government-owned copper producer. Codelco, Cominor and SQM have not undertaken any significant exploration work on their properties in the Salar. To date no lithium production is taking place from the Salar and the Blanco Project is at the most advanced stage of project evaluation.

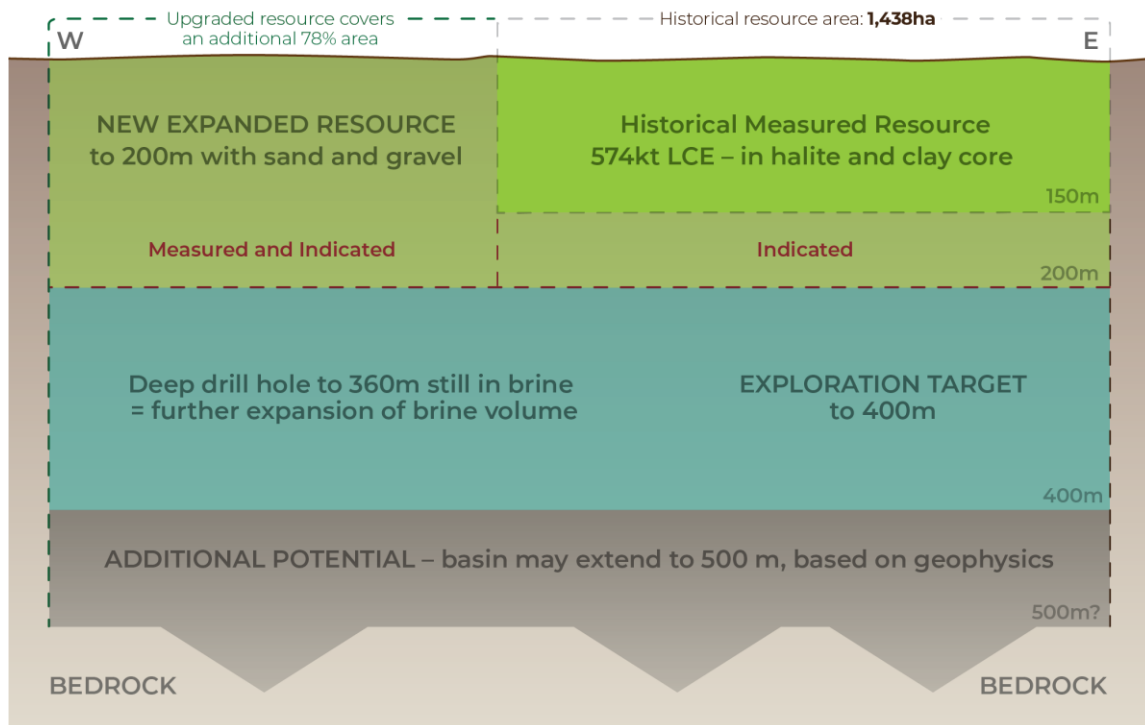


24. OTHER RELEVANT DATA AND INFORMATION

24.1 EXPLORATION POTENTIAL

The Measured and Indicated categories comprise 100 percent of the updated resource of the Blanco Project reported herein to a depth of 200 m. One deep borehole (S19) was drilled to 360 m depth by MSB in 2016. Borehole S-19 encountered a continuation of the lower brine aquifer in the Lower Alluvium and volcanoclastics units below 200 m depth with lithium concentrations above 900 mg/l. An exploration target is therefore defined below the base of the current resource to a depth up to 400 m as shown in Figure 24-1. Results of AMT and gravity surveys suggest that the Salar sediments may extend to over 500 m depth.

Figure 24-1: Schematic of the deep lithium exploration target (200-400 m)



Source: LPI 2018

The exploration target is where, based on the available geological evidence, there is the possibility of defining a mineral resource. The timing of any drilling with the objective of defining resources in the exploration target area has not been decided at this stage. In keeping with Clause 18 of the JORC Code and CIM requirements the exploration target defined at Maricunga is:

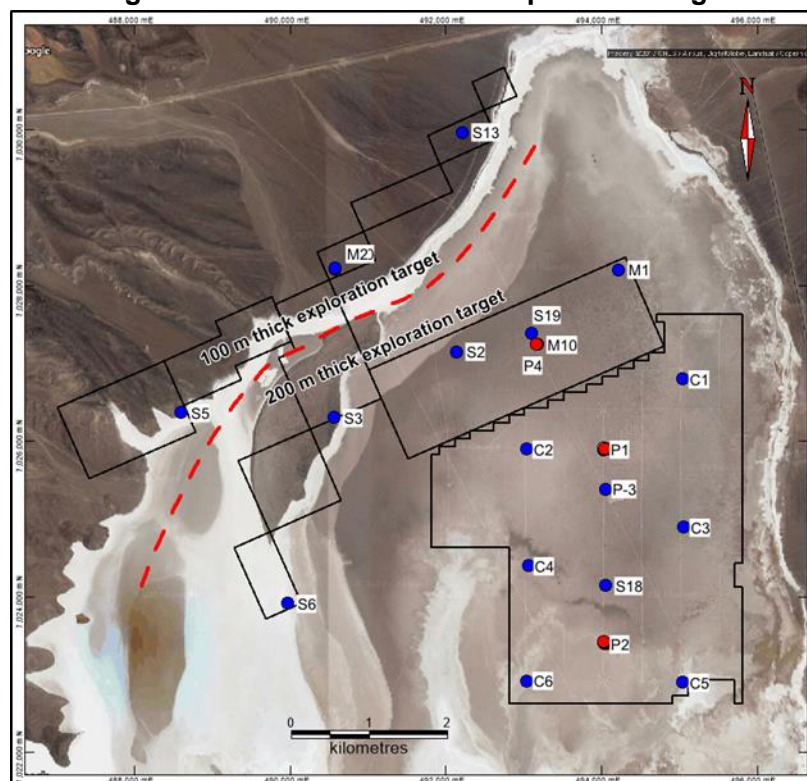
- Not to be considered a resource or reserve; and
- Based on information summarized below.

It is a requirement of stating an exploration target that it is based on a range of values, which represent the potential geological conditions. Values have been selected to present an upper and a lower exploration target size. It is likely that the lithium and potassium contained in the exploration target lies somewhere between the Upper and Lower Cases. The following parameters have been used to estimate an Upper Assumption and Lower Assumption case for lithium and potassium.

24.1.1 Area

The exploration target covers 25.63 km² (2,563 ha) beneath the area of all the exploration properties (effectively the area of the properties extending downward beneath the resource).

Figure 24-2: Outline of the exploration target



24.1.2 Thickness

- The western area of the exploration target is assigned a thickness of 100 m; and
- The central area of the exploration target is assigned a thickness of 200 m.

The difference in thickness is treated simplistically as a change from 200 to 100 m across the line shown in Figure 24-2.

24.1.3 Porosity

- For the Upper Assumption 10 % is used as the specific yield for the volcanoclastic unit in the western and eastern properties; and
- For the Lower Assumption 6 % is used as the specific yield, allowing for the presence of a much finer matrix, reducing the specific yield.

24.1.4 Lithium and Potassium Concentrations

- A value of 1,000 mg/l for lithium and 6,000 mg/l and 7,500 mg/l potassium (in the Western and Central parts) is used in the upside case for the central and western properties; and
- A value of 700 mg/l lithium and 5,500 mg/l potassium is used in the Lower Assumption case in the central area with 600 mg/l lithium and 5,000 mg/l potassium in the western properties.

Table 24-1: Blanco Project exploration target estimate

EXPLORATION TARGET ESTIMATE MARICUNGA										
Subarea	Area km ²	Thickness m	Mean drainable porosity %	Brine volume million m ³	Lithium Concentration mg/L	Contained Lithium tonnes	Lithium Carbonate LCE tonnes	Potassium Concentration mg/L	Contained Potassium tonnes	Potassium Chloride KCl tonnes
UPPER RANGE SCENARIO										
Western	4.23	100	10%	42.3	1,000	40,000	200,000	6,500	270,000	500,000
Central	21.41	200	10%	428.0	1,000	430,000	2,300,000	7,500	3,200,000	6,100,000
	Continues from directly below the resource					470,000	2,500,000		3,470,000	6,600,000
LOWER RANGE SCENARIO										
Western	4.23	100	6%	25.4	600	15,000	80,000	5,000	130,000	240,000
Central	21.41	200	6%	257.0	700	180,000	950,000	5,500	1,400,000	2,700,000
	Continues from directly below the resource					195,000	1,030,000		1,530,000	2,940,000

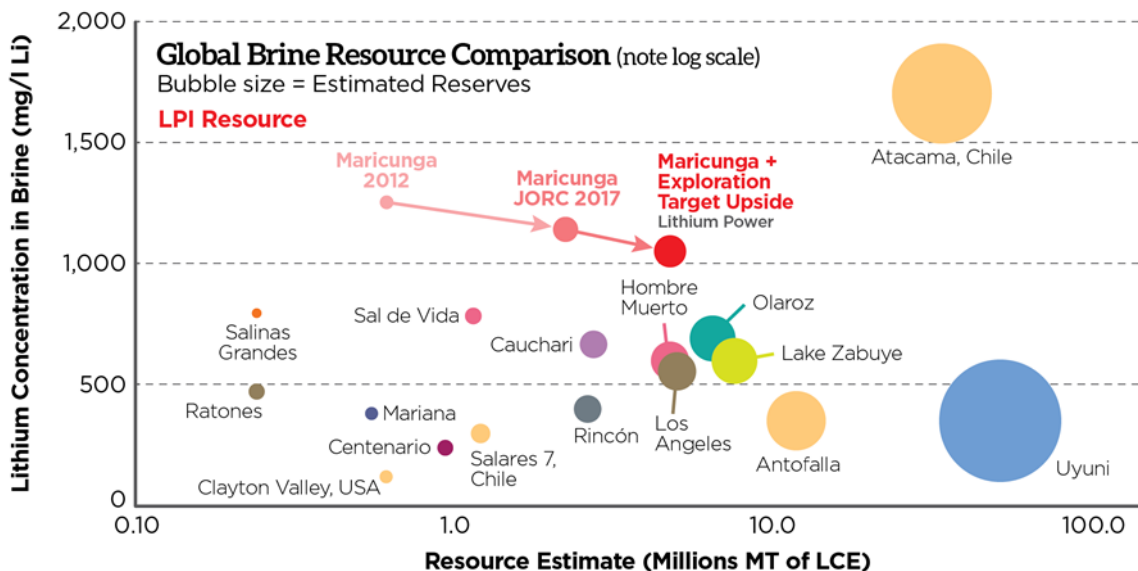
Lithium is converted to lithium carbonate (Li₂CO₃) with a conversion factor of 5.32. Numbers may not add due to rounding.

Potassium is converted to potassium chloride (KCl) with a conversion factor of 1.91

Source: LPI 2017

Figure 24-3 shows growth of the Maricunga resource and exploration target and how Maricunga, with high grades, compares to other lithium brine projects. It must be stressed that an exploration target is not a mineral resource. The potential quantity and grade of the exploration target is conceptual in nature, and there has been insufficient exploration to define a Mineral Resource in the volume where the Exploration Target is outlined. It is uncertain if further exploration drilling will result in the determination of a Mineral Resource in this volume.

Figure 24-3: Comparison of the Blanco Project with other lithium projects



Source: LPI 2017

24.2 GEA MESSO BASIC ENGINEERING

MSB has a signed contract with GEA Messo GmbH for engineering services involving the supply of process equipment and basic engineering for the Salt Removal Plant and for the Lithium Carbonate plant with a capacity of 20,000 mt/year of lithium carbonate. This is based on technology developed by GEA for the Salt Removal Plant and on commonly used technology for the lithium carbonate plant. These engineering inputs were used in this study.

Because the Salar de Maricunga brine has a very high calcium concentration, feeding the brine, after the conventional evaporation ponds, to the lithium carbonate plant is not technically practical. Therefore, a Salt Removal Plant design had to be developed that essentially removed most of the calcium from the brine before final treatment in the lithium carbonate plant. This is the novel aspect of the Blanco project.

GEA developed the Salt Removal plant design based on a series of evaporation and crystallization steps. The calcium is removed by crystallizing tachyhydrite (a calcium and magnesium chloride) and calcium chloride. The use of evaporators and crystallizers is a well-established technology and GEA is a leading supplier of this technology. The technology is used extensively in the global chemical industry and there are applications in lithium processing.

The application of evaporators and crystallizers to a lithium rich brine will be a first which is why GEA have conducted extensive testwork to prove the applicability of the process. MSB has been working for over two years with GEA in Germany developing the process to be used for the Blanco Project, initially with artificial brine and later with actual brine from this

salar. GEA has optimized this process and has been able to produce battery grade Lithium Carbonate from both artificial and actual brine. MSB and GEA are confident that the proposed process will produce battery grade lithium carbonate and GEA has agreed to provide process warranties.

According to the GEA - MSB agreement, GEA will provide a fixed price for the supply of the main process equipment for the Salt Removal Plant and for the lithium carbonate plant. Process Warranties will also be provided for lithium carbonate yield, capacity and product quality will be battery grade, based on an agreed “Design Feed” that will come from the evaporation ponds.

Product Quality: The Li_2CO_3 crystal product produced by the Plant will be “Battery Grade” and the impurities will not exceed the following ppm.

Table 24-2: Maximum Impurities in Li_2CO_3

Component	Unit	Note	Value
Na	ppm	max	600
Ca	ppm	max	100
SO_4	ppm	max	300
K	ppm	max	50
Cl	ppm	max	100
Mg	ppm	max	100
B	ppm	max	10
Fe	ppm	max	10
H_2O	wt%	max	0,2
Insol. in HCl	ppm	max	100

24.3 ENGINEERING DELIVERABLES

In order to develop CAPEX and OPEX values, Procurement quoted main equipment, supplies, materials, freight costs, and construction contracts. For this purpose, quotations for each unit to be quoted were requested to three suppliers. Procurement also carried out a study of the conditions for imports of supplies and services to facilitate the purchases. Technical and commercial evaluations were made for all quotations received.

Critical equipment was defined, being those which have long delivery times and those that are required to begin construction.

The following table summarizes the work carried out by the engineering team of WP and GEA:

Table 24-3: WorleyParsons Engineering Deliverables

Area	Li ₂ CO ₃ Drawings	Li ₂ CO ₃ Documents	TOTAL
General	0	7	7
Process	12	4	16
Mechanics	30	26	56
Civil	34	6	40
Structural	47	4	51
Piping	43	7	50
Electricity	14	10	24
Instrumentation	16	5	21
Ac qof supply and/or Equip. Quotes	0	11*	11
Total	196	80	276

*More than 150 equipment/contract quotations

Table 24-4: GEA Engineering Deliverables

Code	Description	GEA Drawings	GEA Documents	Total
BFD	Block Flow Diagram	2		2
PFD	Process Flow Diagram	5		5
DIM	Data Sheet		71	71
DSC	Descriptions		8	8
EQL	Equipment List		2	2
LAY	Layout	8		8
LEW	Equipment List with Weights		2	2
PID	Piping & Instrumentation	2		2
PPL	Piping List		2	2
REP	Research Report Document		1	1
SLD	Project Time Schedule		1	1
SPC	Technical Specification		120	120
	Total	17	207	224

24.4 PROJECT SCHEDULE

Table 24-5 presents the Level I Blanco Project Execution Schedule, covering from the detailed engineering phase, up to the production start-up for battery grade Lithium Carbonate. Table 24-6 presents a breakdown with the most important activities and milestones during this period. The schedule shows that load testing and first lithium carbonate production will occur during the first quarter of 2022, however, commercial operation is assumed to start by 2023.

Table 24-5: Summary for Blanco Project execution schedule

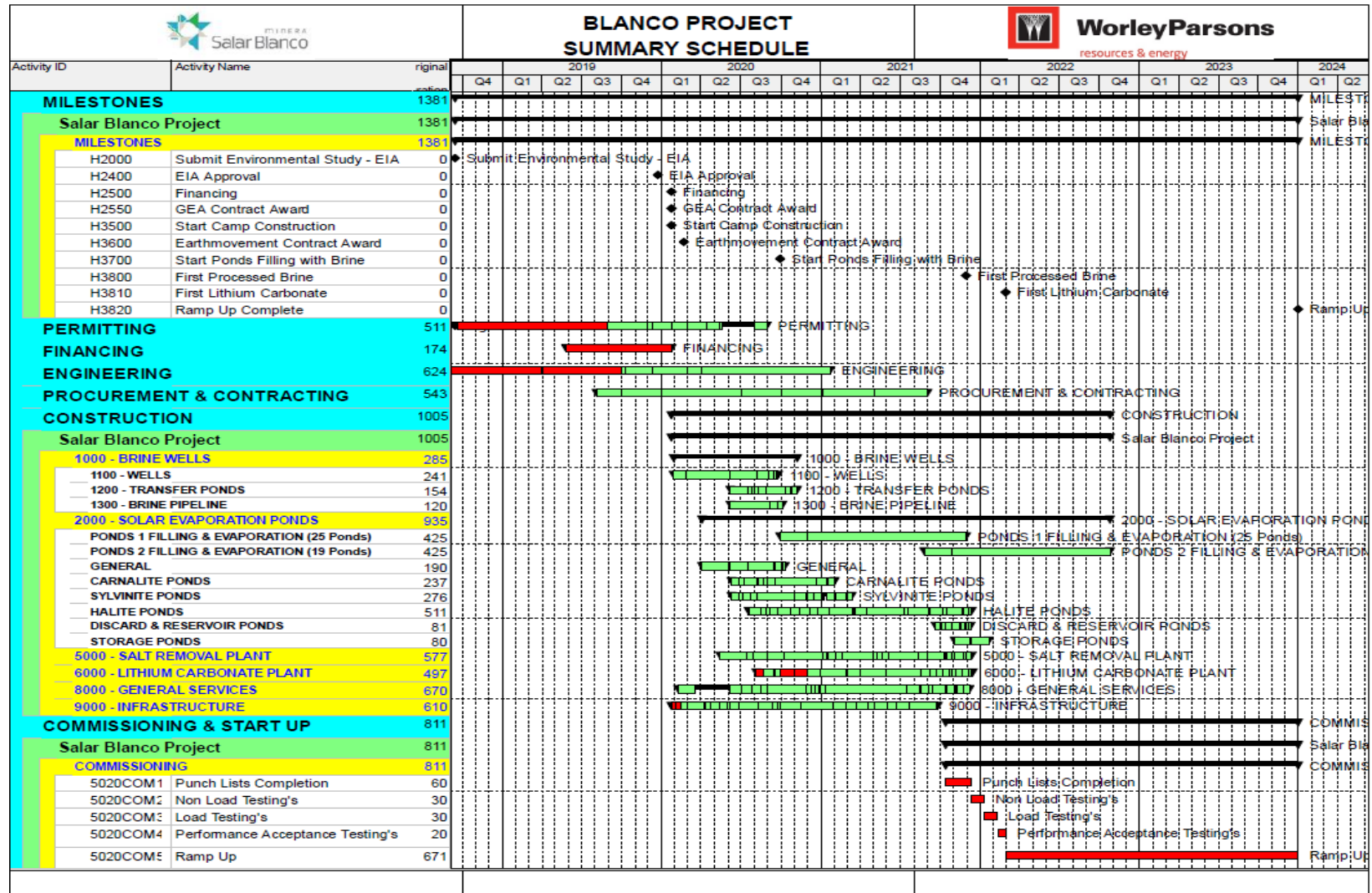


Table 24-6: Major Projects Milestones

Activity	Date
Submit Environmental Study – EIA (Actual date)	14-sept-18
Environmental Approval - RCA	23-dec-19
Financing in place	23-jan-20
GEA Contract Award	23-jan-20
Start Construction Camp	24-jan-20
Earthmovement Contract Award	21-feb-20
Start Pond Filling with Brine	30-sept-20
First Processed Brine	29-nov-21
First Lithium Carbonate	28-feb-22
Complete Production Ramp Up	31-dec-23

25. INTERPRETATION AND CONCLUSIONS

25.1 HYDROGEOLOGY, RESOURCE AND RESERVE ESTIMATE

Based on the analyses and interpretation of the results of the exploration work carried out by MSB in Salar de Maricunga between 2011 and 2018, the following concluding statements are prepared:

- The entire Blanco Project area has been covered by exploratory drilling between 2011 and 2018 at an approximate borehole density of one exploration borehole per 1.5 km²; it is the opinion of the authors that such borehole density is appropriate for the mineral resource estimate described herein.
- The results of the drilling (12 sonic boreholes 8 rotary/HWT boreholes, and 1,700 m of RC and other rotatory drilling) and the analysis of 651 primary brine samples identify favorable brine composition and grade at specific depth intervals, showing a relatively uniform distribution of lithium bearing brines throughout the Blanco project area to a depth of 200 m. The average brine composition is summarized in Table 25-1.

Table 25-1: Summary of the average Blanco Project brine composition (g/l)

K	Li	Mg	Ca	SO ₄	B	Mg/li	K/Li	(SO ₄ +2B)/(Ca+Mg)*
8.23	1.12	7.34	13.49	0.71	0.60	6.55	7.35	0.092

- The geology the Blanco Project consists of a permeable upper halite brine aquifer with a thickness of up to 34 m in the central part of the Project area. This upper aquifer is underlain for most parts by a low permeable clay core. Below the Clay Core occurs a lower brine aquifer hosted in relatively permeable sediments belonging to the Lower Alluvium and Volcaniclastics units. Permeable alluvial fans extend into the Salar on the western side of the Blanco Project. The fan material at depth grades into the Lower Alluvial and is underlain by the volcaniclastics.
- The results of four (4) pumping tests and 488 drainable porosity analyses suggest that the specific yield (or drainable porosity) for the Upper Halite unit averages 0.04; sediments of the lower brine aquifer have a drainable porosity between 0.06 to 0.18; and the Clay Core 0.02.
- It is the opinion of the authors that the Salar geometry, brine chemistry composition and the specific yield of the Salar sediments have been adequately defined to a depth of 200 m to support the Measured and Indicated Resource estimate described in Table 25-2.

Table 25-2: Measured and Indicated Lithium and Potassium Resources of the Blanco Project

	Measured (M)		Indicated (I)		M+I	
	Li	K	Li	K	Li	K
Property Area (km ²)	18.88		6.43		25.31	
Aquifer volume (km ³)	3.05		1.94		5	
Specific yield (Sy)	0.04		0.11		0.07	
Brine volume (km ³)	0.13		0.21		0.35	
Mean grade (g/m ³)	48	349	128	923	79	572
Concentration (mg/L)	1,175	8,624	1,153	8,306	1,167	8,500
Resource (tonnes)	146,000	1,065,000	244,000	1,754,000	389,000	2,818,000

Notes to the resource estimate:

- CIM definitions (2014) were followed for Mineral Resources.
- The Qualified Person for this Mineral Resource estimate is Frits Reidel, CPG
- No cut-off values have been applied to the resource estimate.
- Numbers may not add due to rounding.
- The Measured and Indicated Resources are inclusive of those Mineral Resources modified to produce the Mineral Reserves described in Section 15.
- The effective date is December 24, 2018

Table 25-3 shows the total resources of the Blanco Project expressed as lithium carbonate equivalent (LCE) and potash (KCl).

Table 25-3: Blanco Project resources expressed LCE and potash

	Measured and Indicated	
	LCE	KCL
Tonnes	2,070,000	5,380,000

- Lithium is converted to lithium carbonate (Li₂CO₃) with a conversion factor of 5.32.
- Potassium is converted to potash with a conversion factor of 1.9
- Numbers may not add due to rounding

The authors are of the opinion that the three-dimensional groundwater flow and transport model developed for the Blanco Project can adequately simulate the hydrogeological system of the Salar de Maricunga under steady-state and transient groundwater flow conditions for its use in the Project brine production simulations and the reserve estimate. The Blanco Project Lithium Reserve estimate is shown in Table 25-4.

Table 25-4: Brine Production Reserve for Lithium Carbonate production (assuming 58% lithium process recovery efficiency)

Concession area	Category	Year	Brine Vol	Ave Li conc	Li metal	LCE
			(Mm3)	(mg/l)	(tonnes)	(tonnes)
Old code	Proven	1-7	21	1,051	13,000	67,000
	Probable	1-18	42	1,068	26,000	140,000
Litio 1-6	Proven	7-14	14	1,184	10,000	51,000
	Probable	14-23	48	1,170	32,000	173,000
Total 20y production	All	1-20	117	1,115	75,000	401,000
Mining Reserve	All	1-23	125	1,117	81,000	430,000

Notes to the Reserve Estimate:

1. Blanco Project brine production initiates in Year 1 on the mining concessions constituted under old Chilean mining code and include the Cocina, San Francisco, Salamina, Despreciada concessions (the "Old Code concessions"). In Year 7 brine production switches to the Litio 1-6 concessions that were constituted under the 1983 ("new") Chilean mining code and require a special operating license (CEOL) from the Chilean government. It is the opinion of the author that there is a reasonable expectation that MSB will have obtained a CEOL by 2020, in advance of any brine production from the Litio 1-6 concessions.
2. The EIA for the Blanco Project was submitted to the Chilean Environmental Review Agency (SEA) in September 2018; it is the opinion of the author that there is a reasonable expectation that the final environmental approvals for the construction and operation of the Project will be obtained during 2019.
3. The Blanco Project Reserve Estimate includes an optimized wellfield configuration and pumping schedule to comply with environmental constraints and water level decline restrictions on the northeast side of the Salar over the total 23 year simulated brine production.
4. The total Mineral Reserves contain approximately four (4) percent of Li mass that is derived from outside of the Blanco Project property boundaries.
5. Lithium is converted to lithium carbonate (Li_2CO_3) with a conversion factor of 5.32.
6. The effective date for the Reserve Estimate is January 15, 2019.
7. Numbers may not add to due rounding effects.
8. Approximately 36 percent of the Measured and Indicated Resource are converted to Proven and Probable Reserves as brine feed from the production wellfield to the evaporation ponds without accounting for the lithium process recovery efficiency. The overall conversion from M+I Resources to Total Reserves including lithium process recovery efficiency is approximately 21 percent.

Based on results of exploration borehole S-19 to a depth of 360 m, it is the opinion of the authors that a significant exploration target exists below the current resource defined to 200 m depth as described in Section 24.

25.2 PERMITS

MSB was awarded a key regulatory license by the Chilean Nuclear Energy Commission (CChEN) to produce, market and export lithium products from Salar de Maricunga on March 9th, 2018. The CChEN license is for the production of an initial 88,885 t lithium metal or 472,868 t of LCE over a 30year term.

The permit is limited to the MSB's grandfathered mining concessions This permit allows MSB to request an increase on the initial quota under any of the following conditions:

- The current Indicated and Measured Mineral Resources are increased in grandfathered mining concessions
- The process recovery efficiency exceeds 40%.
- If MSB is awarded Special Operation Contract (CEOL) for the exploitation of lithium from the Litio 1-6 (new code) mining concessions. MSB is currently negotiating this contract with Chilean Government covering these mining concessions, i.e. those registered after 1979.

25.3 PROCESS AND ECONOMICS

Based on the engineering and economic analysis of the project, carried out both in the PEA and in this Definitive Feasibility Study, the following conclusions are presented:

- The Salar de Maricunga brine due to its high calcium concentration is not fully suitable for conventional processing. The Blanco Project process principally consists of solar evaporation of the brine to a suitable concentration such that the brine can be treated in a salt removal plant –an addition to the conventional process– and finally in a lithium carbonate production plant. The concentrated Maricunga brine will require a boron, calcium and magnesium removal stages.
- The CAPEX for the lithium carbonate 20,000 TPY Blanco Project is US\$ 563 million. This total is higher than for other similar size lithium carbonate projects due to the need to include a Salt Removal Plant. High calcium content in the Salar de Maricunga brine makes this plant necessary. However, it also must be mentioned that the above referred plant has the following advantages:
 - It allows ending the solar pond evaporation stage with a comparatively low lithium concentration brine (0.8% to 0.9%), given that in addition to Ca removal, substantial evaporation and concentration takes place at the above referred plant. Thus, if the Salt Removal Plant were not necessary, additional pond area

- would be required to obtain a concentrated brine suitable for the Lithium Carbonate Plant.
 - It allows recovery of part of the water contained in the brine, thus reducing the total water consumption.
 - It allows extracting impurities (mainly calcium) contained in the brine without the use of chemical reagents.
 - The above allows obtaining battery-grade lithium carbonate without adding a CO₂ purification stage.
- Total unit operating cost for the Project is US\$ 3,772 per tonne of lithium carbonate. Again, this is somewhat higher than some comparably sized brine lithium project, the main reason being the energy cost associated with the Salt Removal Plant, but which has the advantages pointed out in the previous commentary.
- The project's economic results are positive, with a full equity, after-tax base case that generates an IRR of 21,0 %, an NPV (8%) of over US\$ MM 908 and a pay out period of 4 years and two months. On a pre-tax basis, the NPV is US\$ MM 1,286 and providing a 23.8% IRR.
- Main reasons for the above results are the favourable outlook for lithium prices, as developed in Section 19, relatively low -27%- corporate income tax rate in Chile, as well as an expected low royalty rate regime for MSB, due mostly to the special "grandfathered" conditions affecting nearly half of the MSB mining properties.
- The project's sensitivity analysis carried out in sub section 22.8.2, analyzes its results when base case assumptions can deviate from expected values. The outcome of this analysis indicates that the project is quite sensitive to the expected price of lithium carbonate. In this way, if lithium prices were to be permanently only 75% of the base case projection⁹, the project's IRR drops to 15% and NPV after-tax (8%) declines to US\$ MM 450. Conversely, the project's results improve very substantially -IRR 26% and NPV after-tax (8%) US\$ MM 1,363- if lithium prices were to be permanently 125% of the base case projection.
- The project's sensitivity to other key variables, such as CAPEX and OPEX expenditures, is much less, with 25% changes in either variable causing only an 11% variation in NPV after-tax (8%). Variation in IRR is about 3.5 percentage points when CAPEX varies by 25%, while variation in IRR is only 1.5 percentage points when CAPEX varies by 25%. This indicates project resilience in face of possible negative CAPEX or OPEX scenarios.

⁹ Supplied by mineral prices specialist Roskill Ltd.

26. RECOMMENDATIONS

26.1 HYDROGEOLOGY AND RESOURCE ESTIMATE

There are several opportunities to increase the current Blanco Project resource base through

- 1) acquisition of adjacent mining claims and
- 2) further exploration at depth on the existing claims.

A work program should be initiated to continue expanding the Blanco Project resource estimate through the exploring of the deep exploration target as described in Section 24. It is recommended that the proposed work program includes the following components:

- Obtain the necessary permits from the regulatory agencies to carry out a deep drilling program on the MSB mining concessions.
- Deep drilling (7-10 holes) using a suitable drilling method to a depth of 400 m across the MSB properties. The drilling target will be the coarser grained sediments in the Lower Alluvium and Volcaniclastics.
- Sampling protocols need to be developed to properly characterize the hydraulic parameters and the brine chemistry of these deeper units.

The estimated cost for the above exploration program is approximately US\$ 7 million and is summarized in Table 26-1.

Table 26-1: Estimated costs for the deep exploration program

	Deep Exploration	000 US\$
1	Exploration drilling (7 holes)	3,500
2	Downhole geophysics	400
3	Laboratory analyses (porosity / brine)	300
4	Monitoring / pumping tests	700
5	Brine and process evaluation	500
6	Analyses, resource and reserve modeling, reporting	600
7	Camp operation	1,000
	Estimated Total Costs (000 US\$)	7,000

26.2 NEXT PHASE

MSB submitted the project's EIA to the environmental authorities in September 2018 and this presentation is currently undergoing the corresponding review process. Since the Project cannot proceed into the execution phase until the EIA is approved, it is recommended that, in the meantime, MSB examine and/or progress on the following items:

- Secure the financing of the project, conditional on EIA approval.

- Use an EPCM (Engineering, Procurement and Construction Management) contracting strategy for the project's next stage or a refundable type EPC (Engineering, Procurement and Construction) contract, with the support of an Owner's Engineer. In either case, experience in lithium projects of the engineer/contractor is recommended.
- Continue to work with GEA on a fixed price contract with process warranties for production of Battery Grade Lithium.
- Explore if it is feasible to procure from GEA only the Salt Removal plant, while maintaining the process guaranty. In this case, build the carbonate plant with a local EPC/EPCM contractor since the carbonate plant is better known process. This could lead to savings in the CAPEX, but in no case MSB should jeopardize the quality of the final product, Battery Grade Lithium.
- Continue immediately with the detail engineering of the evaporation ponds. This does not represent a significant cost but can reduce engineering time once the EIA is approved.
- Prioritise obtaining permits to modify the course of Highway C-173, given that solar evaporation pond construction is the most critical element in the project's construction plan and whose current routing runs through the project's pond farm.
- For the same reason and given the very large pond surfaces that need to be covered with plastic film, enter as soon as possible into a production contract with a reputable supplier of this critical material. This, considering that it may be possible that one, or more, additional lithium brine projects might be in construction at the same time, straining plastic film production capacity.
- Continue and accelerate tests of the flexible bituminous sheet that might be used instead of the plastic film for pond lining. The main advantage of the bituminous sheet is that it may be installed even in very cold weather during winter. This would constitute another way to shorten the critical pond construction time.
- Carry out Engineering Optimization in the project plant layout to minimize construction cost.
- Continue obtaining further climatic data of the area, especially, evaporation rates, rain and snow, records at the exact site of the project. Incorporate this data into final project design.
- In keeping with the PEA study recommendation, postpone the investment in a KCI plant for a few years, reconsidering the decision to build it, if there is a clear improvement of its expected long-term pricing outlook.

- Carry out a new risks evaluation workshop before the start of the detailed engineering. This workshop will address safety, environmental, brine production and process issues.
- Finally, and considering, on the one hand, that the Maricunga Salar is a mid size salar and considering on the other hand that the mineral property in the salar is divided among four large holders (MSB being the one of the largest) and many other small holders, there will be a material advantage to the party that is able to progress its project faster, because the resource might not support another competitively sized lithium carbonate plant. Thus, if MSB can proceed quickly with this project, it may become “dominant” in the salar and might be in position to acquire additional resources at favourable conditions.

26.3 ENERGY EXPENSES AND COGENERATION

The project’s energy expenses total approximately US\$ 17.2 million per year. Out of this total, US\$ 13.1 million corresponds to Diesel fuel used to generate vapor required at the Salt Removal Plant. This represents nearly 20 % of the project’s OPEX. For this reason, it is imperative to look for options to reduce this cost. The simplest one may be to switch the boilers to residual fuel oil, which is more complicated to handle than Diesel, and would surely require heating at Maricunga, but still considerable savings may be possible, even though there could be concerns about additional emissions.

As recommended in the project’s PEA, MSB carried out an economical evaluation into cogeneration. In this process, electricity and steam are produced jointly. This study concluded that the cogeneration alternative was not profitable. This, mainly due to the need of high energy steam in the salt removal plant, which requires that additional fuel be used in the boiler, over and above that required to produce electricity, thus partially negating the cogeneration advantage. Prices of electrical energy in the north of Chile have dropped substantially due to the plentiful availability of solar power, a situation that is not expected change in the short and medium term, making cogeneration difficult to justify.

Finally, given the project’s location, solar steam generation could be an attractive new technology to be investigated, in the future.

27. REFERENCES

Brüggen, J. 1950. Fundamentos de la Geología de Chile. Instituto Geográfico Militar (Chile), 378 p.

CORFO (1982): Informe Prospeccion Preliminar salar de Maricunga; Comite de Salas Mixtas CORFO, Santiago, Chile.

Cornejo, P., Mpodozis, C., Ramírez, C., y Tomlinson, A., 1993a. Estudio geológico de la región de Potrerillos y El Salvador (26°–27° lat. S): Santiago, Reporte registrado, IR-93–01, 2 volúmenes, 12 mapas escala 1:50000, Servicio Nacional de Geología y Minería.

Cornejo, P., y Mpodozis, C., 1996. Geología de la región de Sierra Exploradora (25°–26° Lat. S): Santiago, Chile, Reporte registrado, IR-96–09, 2 volúmenes, 8 Mapas, escala 1:50000, Servicio Nacional de Geología y Minería.

Cornejo, P., Mpodozis, C., y Tomlinson, A., 1998. Hoja Salar de Maricunga: Santiago, Servicio Nacional de Geología Minería, Mapa Geológico N°7, escala 1:100000.

Dirección General de Aguas, (DGA) 1987. Balance Hídrico de Chile.

DGA, 2006, Análisis de la Situación Hidrológica e Hidrogeológica de la Cuenca del Salar de Maricunga, III Región. DGA, Departamento de Estudios y Planificación (2006). S.D.T. N° 255.

DGA, 2009, Levantamiento Hidrogeológico para el Desarrollo de Nuevas Fuentes de Agua en Areas Prioritarias de la Zona Norte de Chile, Regiones XV, I, II, y III. Etapa 2 Sistema Piloto III Region Salares de Maricunga y Pedernales. Realizado por Departamento de Ingeniera Hidraulica y Ambiental Pontifica Universidad Catolica de Chile (PUC). SIT No. 195, Noviembre 2009.

EDRA, 1999, Hidrogeología Sector Quebrada Piedra Pómez- Placer Dome

Ehren-Gonzalez Limitada, 2015: Salar de Maricunga Desktop Study, Update of May, 2014 report, prepared for Minera Salar Blanco SPA, October, 2015

FloSolutions, 2018: Modelo Hidrogeológico Conceptual Salar de Maricunga; preparada para Minera Salar Blanco.

Flosolutions, 2015a: Proyecto Blanco, Programma 2015, Presentación de resultados, September 16, 2015

Flosolutions, 2015b: Proyecto Blanco, Informe Técnico: Programma de Pruebas de Bombeo 2015, Análisis y Resultados

Gabalda G., Nalpas T. y Bonvalot S., 2005. Base of the Atacama Gravels Formation (26°S, Northern Chile): first results from gravity data. ISAG YI, Barcelona.

García, F. 1967. Geología del Norte Grde de Chile. In Symposium sobre el Geosinclinal Yino No. 3, Sociedad Geológica de Chile: 138 p.

Gardeweg, M., Mpodozis, C., Clavero, J., y Cuitiño, L., 1997. Mapa Geológico de la Hoja Nevado Ojos de Salado, Región de Atacama, escala 1:100000: Santiago, Servicio Nacional de Geología y Minería.

Golder Associates, 2011, Linea Base Hidrogeologica y Hidrologica Marte Lobo y Modelo Hidrogeologico Cienaga Redonda – Kinross Gold Corporation.

González-Ferrán, O., Baker, P.E., y Rex, D.C., 1985. Tectonic-volcanic discontinuity at latitude 27° south, Yean Range, associated with Nazca plate subduction: Tectonophysics, v. 112, p. 423–441.

Hartley, A.J., May, G., 1998. Miocene Gypcretes from the Calama Basin, northern Chile. Sedimentology 45, 351–364.

Hidromas 2017, Informe Técnico Estudio Precipitación Eventos Extremos Proyecto Salar Blanco. 46 pp.

Houston, J, 2006. Evaporation in the Atacama desert: An empirical study of spatio-temporal variations and their causes. Journal of Hydrology, 330:402-412.

Houston, J., Butcher, A., Ehren, P., Evans, K., Godfrey, L. 2011. The Evaluation of Brine Prospects y the Requirement for Modifications to Filing Styards. Economic Geology, v. 106, pp. 1225–1239.

Isacks, B.L. 1988. Uplift of the Central Yean plateau y bending of the Bolivian orocline. Journal Geophysical Research, Vol. 93: 3211-3231.

Iriarte D., Sergio.,1999, Mapa hidrogeológico de la cuenca Salar de Maricunga: sector Salar de Maricunga, Escala 1:100.000, Región de Atacama. N° Mapa: M62. SERNAGEOMIN, 1999.

Iriarte, S, Santibáñez, I y Aravena, 2001. Evaluation of the Hydrogeological Interconnection between the Salar de Maricunga and the Piedra Pomez Basins, Atacama Region, Chile; An Isotope and Geochemical Approach

Kay, S.M., Coira, B., y Viramonte, J., 1994. Young mafic back-arc volcanic rocks as indicators of continental lithospheric delamination beneath the Argentine Puna plateau, central Andes: Journal of Geophysical Research, v. 99, p. 24,323–24,339.

Kay, S.M., y Mpodozis, C., 2002. Magmatism as a probe to the Neogene shallowing of the Nazca plate beneath the modern Chilean flat-slab: *Journal of South American Earth Sciences*, v. 15, p. 39–59.

Kay, S.M., y Copely, P., 2006. Early to middle Miocene back-arc magmas of the Neuquén Basin of the southern Andes: Geochemical consequences of slab shallowing and the westward drift of South America, en Kay, S.M. y Ramos, V.A., eds., *Evolution of an Andean margin: A tectonic and magmatic perspective from the Andes to the Neuquén Basin (35°–39°S lat.)*: Geological Society of America Special Paper 407, p. 185–213.

Lara L, Godoy E, 1998. Hoja Chañaral-Diego de Almagro, III Región de Atacama: Santiago, Chile. Servicio Nacional de Geología y Minería, Mapas Geológicos, escala 1:100000.

Maricunga Lithium Brine Project; 3.7 Fold Increase in Mineral Resource Estimate; JORC report dated 12 July 2017

Mercado, M., 1982. Hoja Laguna del Negro Francisco, Región de Atacama: Servicio Nacional de Geología y Minería, Carta Geológica de Chile, N° 56, p. 73.

Mortimer, C., 1980. Drainage evolution of the Atacama Desert of northernmost Chile. *Revista Geológica de Chile*, no. II, p. 3-28

Moscoso, R., MaksaeV, V., Cuitiño, L., y Díaz, F., Koeppen, R., Tosdal, R., Cunningham, C., McKee, E., y Rytuba, J., 1993. El complejo volcánico Cerro Bravos, región de Maricunga, Chile: Geología, alteración hidrotermal y mineralización, in *Investigaciones de Metales Preciosos en el complejo volcánico neógeno-cuaternario de los Andes Centrales: Bolivia*, Servicio Geológico, Banco Interamericano de Desarrollo, p. 131–165.

Mpodozis, C., Cornejo, P., Kay, S.M., y Tittler, A., 1995. La Franja de Maricunga: Síntesis de la evolución del frente volcánico oligoceno-mioceno de la zona sur de los Andes Centrales: *Revista Geológica de Chile*, v. 22, p. 273–314.

Mpodozis, C., y Clavero, J., 2002. Tertiary tectonic evolution of the southwestern edge of the Puna Plateau: Cordillera Claudio Gay (26°–27°S): Toulouse, *Proceedings of Fifth International Symposium on Andean Geodynamics*, p. 445–448.

Muntean, J.L., y Einaudi, M.T., 2001. Porphyry-epithermal transition: Maricunga belt, northern Chile: *Economic Geology and the Bulletin of the Society of Economic Geologists*, v. 96, p. 743–772.

Nalpas, T.; Dabard, M-P.; Ruffet, G.; Vernon, A.; Mpodozis, C.; Loi, A.; Hérail, G. 2008. Sedimentation and preservation of the Miocene Atacama Gravels in the Pedernales-Chañaral Area, Northern Chile: Climatic or tectonic control? *Tectonophysics* 459: 161-173.

NI 43-101 Technical Report, Lithium & Potassium Resource Estimate Maricunga Joint Venture, III Region, Chile. Prepared for: Minera Salar Blanco S.A. by: Frits Reidel, CPG, Murray Brooker, MSc, RPG, MAIG and Peter Ehren, MSc, MAusIMM, dated August 25, 2017.

Risacher, Alonso y Salazar, Geoquímica de Aguas en Cuencas Cerradas: I, II y III Regiones de Chile, Volumen I, Síntesis. S.I.T N° 51, Convenio de Cooperación DGA – UCN – IRD, 1999.

Risacher, F., Alonso, H. and Salazar, C. 2003. The origin of brines and salts in Chilean Salars: a hydrochemical review. *Earth Science Reviews*, 63: 249-293.

Riquelme, R., 2003. Evolution geomorphologique neogene de Andes Centrales du Desert d'Atacama (Chili): interaction tectonique-climat, Ph.D. Thesis, Université Paul Sabatier (Toulouse, France) y Universidad de Chile (Santiago, Chile), 258 p.

Salar de Maricunga Desktop Study, prepared for Minera Salar Blanco Spa by Peter Ehren, MSc., October 2015

SignumBOX Analysis – Lithium, Batteries and Vehicles – Perspectives and Trends. Issue N°14, August 2017.

Sillitoe, R.H., Mortimer, C; y Clark, A.H., 1968. A chronology of lyform evolution y supergene mineral alteration, southern Atacama Desert, Chile. *Institute of Mining y Metallurgy Transactions*, v. 77, p.

Sillitoe, R.H., McKee, E.H., y Vila, T., 1991. Reconnaissance K-Ar geochronology of the Maricunga gold-silver belt, northern Chile: *Economic Geology y the Bulletin of the Society of Economic Geologists*, v. 86,p. 1261–1270.

SRK Consulting, 2011, Hidrogeología Campo de Pozos Piedra - Compania Minera Casale.

Tassara, A. 1997. Geología del Salar de Maricunga, Región de Atacama. Servicio Nacional de Geología y Minería (SERNAGEOMIN). Informe Registrado IR-97-10.

Technical Report on the Maricunga Lithium Project, Region III, Chile. NI 43-101 Technical Report (update of 2012 NI 43-101 Technical Report) for Bearing Resources prepared by Don Hains March 20, 2017.

Technical Report on the Maricunga Lithium Project, Region III, Chile. NI 43-101 Technical Report for Li3 Energy Inc. prepared by Don Hains and Frits Reidel, CPG April 17, 2012.

Technical Report on the Salar de Maricunga Lithium Project, Northern Chile prepared for Li3 Energy Inc. NI 43-101 Technical report prepared by Donald H Hains, Amended May 26, 2011.

Tomlinson, A., Mpodozis, C., Cornejo, P., Ramirez, C.F., y Dimitru, T., 1994, El sistema de Fallas Sierra Castillo-Agua Amarga: Transpresión sinistral Eocena en la Precordillera de Potrerillos-El Salvador: Congreso Geológico Chileno VII, Actas, v. 2, p. 1459–1463.

Tomlinson, A., Cornejo, P., y Mpodozis, C., 1999, Hoja Potrerillos, Región de Atacama: Santiago, Servicio Nacional de Geología y Minería, Mapa Geológico no. 14, escala 1:100000.

Venegas, M.; Iriarte, S. y Aguirre, I., 2000, Mapa hidrogeológico de la Cuenca Salar de Maricunga: sector Ciénaga Redonda, escala 1:100.000, Región de Atacama. N° Mapa: M65. SERNAGEOMIN, 2000.

Vila, T., y Sillitoe, R.H., 1991, Gold-rich porphyry systems in the Maricunga belt, northern Chile: Economic Geology y the Bulletin of the Society of Economic Geologists, v. 86, p. 1238–1260.

Zentilli, M., 1974, Geological evolution y metallogenetic relationships in the andes of northern Chile between 26° y 29° south. Kingston, Ontario, Queen's University.

28. SIGNATURES PAGE AND QUALIFIED PERSONS CERTIFICATES

DATE AND SIGNATURE PAGE

This report titled "Definitive Feasibility Study of MSB Blanco Lithium Carbonate Project" for Minera Salar Blanco, Atacama Region, Chile, dated January 17th, 2019 was prepared and signed by the following authors:

(Signed and Sealed) "Frederik Reidel"
Dated at Santiago, Chile
Effective and signed January 17th, 2019



Frederik Reidel, CPG
Consulting Hydrogeologist

(Signed and Sealed) "Peter Ehren"
Dated at Santiago, Chile
Effective and signed January 17th, 2019



Peter Ehren, MSc, MAusIMM
Mineral Processing Consultant

(Signed and Sealed) "Marek Dworzanowski"
Dated at Santiago, Chile
Effective and signed January 17th, 2019



Marek Dworzanowski, Pr.Eng, BSc (Hons)
Mineral and Process Consultant



DATE, SIGNATURE AND CERTIFICATE OF QUALIFICATIONS

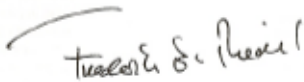
Frederik Reidel
Roger de Flor 2950, Piso 5, Las Condes, Santiago, Chile.
56 2 3245 0168
freidel@flosolutions.com

I, Frederik Reidel, CPG, as co-author of this report entitled "NI 43-101 Technical Report: Definitive Feasibility Study of the MSB Blanco Lithium Carbonate Project, Atacama Region, Chile, prepared for Minera Salar Blanco S.A., dated January 17, 2019 do hereby certify that:

1. I am employed as Principal Hydrogeologist and General Manager by FloSolutions-Chile, residing at: Roger de Flor 2950, Piso 5, Las Condes, Santiago, Chile.
2. I am a graduate of New Mexico Institute of Mining and Technology with a Bachelors of Science Degree in Geophysics in 1986.
3. I am registered a Certified Professional Geologist (#11454) with the American Institute of Professional Geologists.
4. I have worked as hydrogeologist for a total of 30 years since my graduation. My relevant experience for the purpose of the Technical Report is:
 - Qualified Person for the Cauchari JV Project, Salta Argentina for Advantage Lithium Corp. (2017 – to date).
 - Qualified Person for the Sal de los Angeles Project, Salta Argentina for LiX Energy Corp and Tibet Summit Resources (2016 – to date).
 - Qualified Person and Member of the technical committees of Li3 Energy Ltd and Minera Salar Blanco for the development of the Blanco Project in Chile (2011 – to date).
 - Co-author of the NI 43-101 Technical Reports on the lithium and potash resources in Salar de Maricunga for Li3 Energy Ltd (2012) and MSB (2017).
 - Evaluation of lithium and potash resources in Salar de Olaroz for Orocobre Ltd. in support of the project's DFS and NI 43-101 Technical Report (2010-2011).
 - Evaluation of lithium and potash resources in Salar de Cauchari for Lithium Americas Corporation; NI 43-101 Technical Report preparation; member of the company's Technical Advisory Panel (2009-2010).
 - Evaluation of brine resources in Salar de Hombre Muerto for FMC (1992-1993)
5. I have read the definition of "qualified person" set out in National Instrument 43-101 (NI 43-101) and certify that by reason of my education, affiliation with a professional association (as defined in NI 43-101) and past relevant work experience, I fulfill the requirements to be a "qualified person" for the purposes of NI 43-101.
6. I have visited the Salar de Maricunga and the Blanco Project area numerous times between August 2011 and to date. I was present on site on a regular basis during the 2011, 2015, 2016 and 2018 drilling and testing programs.
7. I have been involved as a QP with the property since 2011, but have no previous involvement with Minera Salar Blanco.
8. I have responsible for Sections 1-12, 14-16, and 24-27 of this report.
9. I am independent of the Issuer applying the test set out in Section 1.4 of NI 43-101.
10. I have read NI 43-101, and the Technical Report has been prepared in compliance with NI 43-101 and Form 43-101F1.

11. To the best of my knowledge, information, and belief, the Technical Report contains all scientific and technical information that is required to be disclosed to make the technical report not misleading.

Dated this 17th day of January, 2019



Frederik Reidel, CPG

DATE, SIGNATURE AND CERTIFICATE OF QUALIFICATIONS

Peter Ehren
Alberto Arenas 4005 112, La Serena, Chile
56 99883 7494
epitec.info@gmail.com

I, Peter Ehren, MSc., AusIMM (CP = Chartered Professional), do hereby certify that:

1. I am an independent consultant and owner of Ehren-González Limitada at Alberto Arenas 4005 112, La Serena, Chile.
2. I graduated with a Master of Science Degree in Mining and Petroleum Engineering, with a specialization in Raw Materials Technology and Processing Variant at the Technical University of Delft, The Netherlands in the year 1997.
3. I am an independent consultant, a Member of the Australasian Institute of Mining (AusIMM) and metallurgy and a Chartered Professional of the AusIMM.
4. I have practiced my profession for 21 years.
5. I have read the definition of “qualified person” set out in National Instrument 43-101 (“NI 43-101”) and certify that by reason of my education and past relevant work experience, I fulfill the requirements to be a “qualified person” for the purposes of NI 43-101. This report is based on my personal review of information provided by the Issuer and on discussions with the Issuer’s representatives. My relevant experience for the purpose of this report is:
 - 1997 Final Thesis of MSc.degree: “Recovery of Lithium from Geothermal Brine, Salton Sea”, BHP Minerals, Reno Nevada.
 - 1998-2001 Process Engineer, Salar de Atacama, SQM
 - 2001-2006 R&D Manager, Lithium and Brine Technology, SQM.
 - 2006 Process Project Manager, SQM
 - 2007 until today: Independent Lithium and Salt Processing Consultant, Ehren-González Limitada.

I have previously been involved in the several brine resource projects, where under:

- Salar de Olaroz for Orocobre, Argentina (2009-2019)
- Salar de Cauchari for Advantage Lithium, Argentina (2010-2018)
- Salar Salinas Grandes for Orocobre, Argentina (2010-2013)
- Salar de Maricunga for Li3 Energy and Minera Salar Blanco, Chile (2011-2018)
- Salar de Atacama and Silver Peak for Albermarle, Chile (2014 - 2016)
- Rann of Kutch, Archean Group, India (2015)

- Lake Mackay, Agrimin, Australia (2014-2016)
6. I am responsible for Chapter 13 of the technical report entitled “Definitive Feasibility Study of MSB Blanco Lithium Carbonate Project Atacama Region, Chile” prepared for MSB and dated effective January 17th, 2018. I also co-authored Chapters 17 of the same report. The latest site visit was for the duration of one day in May, 2018. I am independent of the Minera Salar Blanco.
 7. I have not had prior involvement with the properties that are the subject of the Technical Report.
 8. As of the date of this certificate, to the best of my knowledge, information and belief, the technical report contains all scientific and technical information that is required to be disclosed to make the technical report not misleading.
 9. I am independent of the issuer applying all of the tests in section 1.5 of National Instrument 43-101.
 10. I have read National Instrument 43-101 and Form 43-101F1, and the Technical Report has been prepared in compliance with that instrument and form.
 11. I consent to the filing of the Technical Report with any stock exchange and other regulatory authority and any publication by them for regulatory purposes, including electronic publication in the public company files on their websites accessible by the public, of the Technical Report.

Effective Date : January 17th, 2019

Date of Signing : January 17th, 2019



Signature of Qualified Person

Peter Ehren

Print name of Qualified Person

DATE, SIGNATURE AND CERTIFICATE OF QUALIFICATIONS

Marek Dworzanowski

39 Melrose Boulevard, Melrose Arch, Johannesburg, 2076, South Africa
+27832967432

marekdworzanowski.advisian@outlook.com

I am an independent qualified person responsible for supervising the preparation of the "Definitive Feasibility Study of MSB Blanco Lithium Carbonate Project, Atacama Region, Chile". I, Marek Dworzanowski, Pr. Eng. BSc (Hons), FSAIMM., do hereby certify that:

1. I am an independent consultant for WorleyParsons in Santiago, Chile, located at Av. Apoquindo 4501, Las Condes, Santiago, Chile and have been so since June, 2017.
2. I graduated from Leeds University, UK, with a BSc Honours in Mineral Processing in July 1980. In March 2016 I was appointed as a Visiting Adjunct Professor in Metallurgical Engineering, University of Witwatersrand, South Africa.
3. I became a Fellow of the Southern African Institute of Mining & Metallurgy (SAIMM) in 2006, membership number 19594. I became a registered Professional Engineer with the Engineering Council of South Africa (ECSA) in 1987, registration number 870480.
4. I have over 38 years' experience in the mining industry, during which time I gained a considerable amount of diverse experience in various roles within the areas of production, project execution, project studies, technical consulting and research & development. My commodity experience covers Diamonds, Gold, Iron Ore, Platinum Group Metals, Copper, Coal, Copper/Cobalt, Nickel, Chromium, Mineral Sands, Niobium, Phosphate, Zinc, Tin, Vanadium, Manganese, Lithium. I have worked in the following countries: South Africa, Australia, Botswana, Namibia, Zimbabwe, Zambia, Ghana, Chile, Brazil, Peru and Argentina. My experience gained in various roles, unit processes and commodities results in a unique skill set, including multidisciplinary due diligence studies, corporate governance, technical and project optimization reviews.
5. I have read the definition of "qualified person" set out in National Instrument 43-101 ("NI 43-101") and certify that by reason of my education, affiliation with a professional association (as defined in NI 43-101) and past relevant work experience, I fulfill the requirements to be a "qualified person" for the purposes of NI 43-101.
6. I visited the Blanco Project Salar Property, located in Maricunga, Chile on the 30th August 2017.

7. I am responsible for supervising the preparation of the Definitive Feasibility Study report titled "Definitive Feasibility Study of MSB Blanco Lithium Carbonate Project, Atacama Region, Chile", with an effective date of January 17th, 2019, relating to the Blanco Project Salar Property.
8. As of the date of this Report, to the best of my knowledge, information and belief, the Report contains all scientific and technical information that is required to be disclosed to make the Report not misleading.
9. I am independent of Minera Salar Blanco S.A, in accordance with the application of Section 1.5 of NI 43-101.
10. I have no prior involvement with the Property that is the subject of this Report.
11. I have read NI 43-101 and this Report has been prepared in compliance with that instrument.

Effective Date : January 17th, 2019

Date of Signing : January 17th, 2019



Signature of Qualified Person

MAREK DWORZANOWSKI

Print name of Qualified Person

29. APPENDIX 1 (LEGAL OPINION)

Philippi
Prietocarrizosa
Ferrero DU
& Uría

Santiago, (Chile) November 29, 2018

Minera Salar Blanco S.A.

ATT: Mr. Cristóbal García-Huidobro
(the “Recipient”)

Dear Sirs,

This opinion (the “Opinion”) is delivered to Minera Salar Blanco S.A. (“MSB” or the “Company”) in connection with the Maricunga project (the “Maricunga Project”) in Chile.

We have acted as counsel to in connection with the negotiation, execution and delivery of several agreements and instruments related thereto, as well as the proceedings for granting of new mining properties.

It is noted that the Mining Exploration Concessions (*Concesiones de Exploración*), Mining Exploitation Concessions (*Pertenencias*), whether fully granted or still under procedure (*pedimentos* or *manifestaciones*) are indistinctly and collectively referred to herein as the “Mining Concessions”. The Mining Exploitation Concessions subject to the Old Mining Chilean Legislation of 1932 are referred hereinbelow as the “Old Legislation Concessions” and the Mining Exploitation Concessions subject to the Current Mining Chilean Legislation of 1983 as the “1983 Exploitation Concessions”.

To deliver the present Opinion we have examined originals, or copies certified or otherwise identified to our satisfaction, of the documents of the Mining Concessions applied for by, granted to, and transferred to MSB, as applicable.

Where our Opinion relates to our knowledge, that knowledge is based solely upon our examination of the records, documents, instruments, and certificates listed or described above and the actual contemporaneous knowledge of attorneys in this firm who are currently involved in legal representation of MSB in connection with the Maricunga Project.

Subject to the foregoing, we are of the Opinion that:

1. MSB has been duly incorporated and is a validly existing company under the laws of Chile and is in good standing.
2. MSB owns 96% of the shares over six mining legal companies (*sociedades legales mineras*) Lito 1 up to Lito 6, which in turn are respectively the exclusive owners of six 1983 Exploitation Concessions, as is described in detail in **Schedule A** hereof.



3. The statutory capital of the Company is CH\$ 35,168,418,584.00¹ divided into 2,964,802,242 nominatives shares (the “Shares”), all of the same class and value.

4. The Shares have been fully subscribed as follows:

Shareholder	Shares and Stake
Minera Salar Blanco SpA	918,485,357.00 equivalents to 30.98%
Li 3 Energy Inc.	534,266,405.00 equivalents to 18.02%
Lithium Power Inversiones Chile SpA	1,512,050,480.00 equivalents to 51.00%
Total	2,964,802,242.00 – 100.00%

5. MSB has all necessary corporate faculties and authority to carry on its business as now conducted by it and to own its properties and assets.
6. MSB is duly licensed to carry on its business in Chile.
7. The Company currently has a portfolio of 12 Mining Concessions, as follows:
- 4 Old Legislation Concessions (*pertenencias*)
 - 6 1983 Exploitation Concessions (*pertenencias*)
8. All titles of the Mining Concessions set out on **Schedule A** are in good standing and there are no encumbrances on such Mining Concessions.
9. MSB is empowered to conduct exploration activities on the Exploration Concessions, and exploration and development activities on the Mining Claims.
10. By means of the Old Mining Chilean Legislation, MSB is entitled to explore and exploit lithium, fulfilling all legal requirements provided by the Chilean legislation.

The 1983 Exploitation Concessions do not allow to explore nor exploit lithium, unless a Special Operation Contract for Lithium, CEOL is obtained, but do permit the exploration and exploitation of any other mining substances, whether metallic or non-metallic, for example potassium, where lithium may be a sub product. In other words, the 1983 Exploitation Concessions, do not entitle to appropriate the extracted lithium, but only other concessible substances.

11. According to the legal documentation reviewed, the Mining Concessions are valid and in force.
12. The Mining Concessions have no marginal records evidencing mortgages, encumbrances,

¹ Approximately US\$52.5 million.

Philippi
Prietocarrizosa
Ferrero DU
& Uría

prohibitions, interdictions or litigations.

13. The Mining Concessions have all their last four periods of mining licenses duly paid.
14. All the Mining Concessions have preferential rights over the relevant area. There is no mining concession nor mining rights held or filed by third parties challenging the rights and preference of the Mining Concessions.
15. From a technical point of view and after having requested the review of the complete area by the expert in mining property Mr. Juan Bedmar, we can confirm that the location of the Mining Concessions is correct.

The foregoing opinions are subject to the following additional qualifications:

1. This Opinion does not refer to nor comprise any information or conclusion on the geologic potentiality of the Mining Concessions, technical matter which is beyond the scope of our review.
2. We are attorneys duly qualified to practice law in Chile and we express no opinion herein as to any laws other than the laws of Chile as in effect on the date hereof and thereof any references to applicable law and approvals are limited to the applicable laws of Chile and approvals by Governmental Agencies of Chile.
3. This Opinion is solely for the benefit of MSB and may not be relied upon or used by, circulated, quoted or referred to, nor may copies be delivered to any other person, without our prior written approval.
4. This Opinion is effective only as of the date hereof. We expressly disclaim any responsibility to advise you of any development or circumstance of any kind, including any change of law or fact that may occur after the date of this letter even though such development, circumstance or change may affect the legal analysis, a legal conclusion or any other matter set forth in or relating to this letter. Accordingly, any person relying on this letter at any time after the date hereof should seek advice of its counsel as to the proper application of this letter at such time.

Very truly yours,



Juan Paulo Bambach Salvatore
Philippi Prietocarrizosa Ferrero DU & Uría

30. APPENDIX 2: CORFO ALBEMARLE ROYALTY AGREEMENT

Table 30-1: CORFO Albemarle Royalty Agreement

Royalty Structure Table US\$/tonne		Royalty Rate %	Royalty Payable		
			US\$/tonne LCE 8,000	US\$/tonne LCE 10,000	US\$/tonne LCE 12,000
-	4,000	6.8	272	272	272
4,001	5,000	8.0	80	80	80
5,001	6,000	10.0	100	100	100
6,001	7,000	17.0	170	170	170
7,000	10,000	25.0	250	750	750
> 10,000		40.0	-	-	800
Royalty Payable			872	1,372	2,172
Average Royalty Payable			10.9%	13.7%	18.1%

Source: Albemarle